Uncertainty in hydrological scenario modelling: An investigation using the Mekong River Basin, SE Asia

Thesis submitted for the degree of Doctor of Philosophy at UCL

Amanda Jane Robinson

UCL Department of Geography

March 2018

I, Amanda Jane Robinson confirm that the work presented in this thesis is my own. Where information has been derived from other sources, I confirm that this has been indicated in the thesis.

28th March 2018

Abstract

This thesis investigates sources of uncertainty in hydrological scenario modelling. It quantifies the extent to which decisions made during the modelling process affect river flow projections under climate change. Sources of uncertainty explored include choice of: General Circulation Model (GCM) for generation of climate projections; hydrological model code; potential evapotranspiration (PET) method; spatial distribution of meteorological inputs within the hydrological model; and baseline precipitation dataset.

The Mekong River Basin is employed as a case study site. Initially a MIKE SHE model is developed for the Mekong using, where possible, the same data as an earlier model (SLURP). Climate scenarios investigated include a set based on a 2 °C increase in global mean temperature simulated by seven GCMs. There are considerable differences in scenario discharges between GCMs, ranging from catchment-wide increases or decreases in mean discharge, to spatially varying responses. Inter-GCM differences are largely driven by differences in precipitation, rather than PET or temperature. Results from MIKE SHE, SLURP and Mac-PDM.09 (a global hydrological model) are compared. Although inter-hydrological model uncertainty is evident and sometimes considerable, its magnitude is generally smaller than GCM uncertainty.

The MIKE SHE model is then recalibrated to provide five further models, each employing alternative PET methods. PET method impacts scenario changes in PET and hence scenario discharges. However, GCM-related uncertainty for change in mean discharge is on average ~3.5 times greater than PET method-related uncertainty. Additional MIKE SHE models are developed using alternative meteorological input spatial distributions and an alternative baseline precipitation dataset. These sources of uncertainty are comparable in magnitude; both are much smaller than PET- and GCM-related uncertainty.

Climate impact assessment using one MIKE SHE model and an ensemble of 41 CMIP5 GCMs for the RCP4.5 scenario provides further confirmation that GCM-related uncertainty is the dominant source of uncertainty for Mekong river flow projections.

Acknowledgements

I would like to thank my supervisor Dr Julian R. Thompson for his valuable support and guidance in carrying out this research and for enabling me to undertake this PhD in the first place. I am also very grateful for my Postgraduate IT Assistantship funding from the UCL Department of Geography, and my position as a part-time Research Assistant in the Department on a NERC funded project. Both these roles were valuable experiences.

I would like to acknowledge and thank Dr Daniel G. Kingston of the University of Otago for the advice, information and data that he provided me with. Daniel provided the results of the SLURP hydrological model of the Mekong River Basin and some of the data that were employed in the development of this model. He also provided some of the meteorological data for the Mekong that I use in Chapters 4 and 5 (more specifically the data distributed according to the sub-catchments originally used in the SLURP model of the Mekong).

I also thank Dr Simon N. Gosling of the University of Nottingham for his advice and for providing simulation results for the Mekong catchment from the Mac-PDM.09 global hydrological model.

Finally, I wish to thank my family and friends for their support, encouragement and patience. In particular, I am forever grateful to Alex (who over the course of my PhD has gone from being my boyfriend, to fiancé, to husband) and my parents. Without them I do not think I could have done this. I have also been very lucky to receive support and encouragement from a number of fellow PhD students (some of whom are already now Doctors), including Dr Charlotte Wheeler, Dr Miriam Fernandez-Nunez, Dr Luis Morales, Dr Darryl Price, Emily Alderton and Pooya Ghoddousi.

Table of contents

List of figures

List of tables

List of Acronyms and Abbreviations

AET	Actual Evapotranspiration
BC	Blaney-Criddle
CHMs	Catchment-scale Hydrological Model
CMIP	Coupled Model Intercomparison Project
CMIP3	Coupled Model Intercomparison Project Phase 3
CMIP5	Coupled Model Intercomparison Project Phase 5
CRU	Climate Research Unit, University of East Anglia
DEM	Digital Elevation Model
Dv	Deviation. Referring to deviation of the simulated mean from the observed mean (e.g. discharge)
ERFA	Ecological risk due to flow alteration
ESM	Earth System Model
ET	Evapotranspiration
ETo	Reference Crop Evapotranspiration or Reference Evapotranspiration
FAO	Food and Agricultural Organization of the United Nations
GCM	General Circulation Model
GHG	Greenhouse Gas
GHM	Global Hydrological Model
GIS	Geographic Information System
HM	Hamon
HRUs	Hydrologial Response Units
HS	Hargreaves-Samani
IPCC	Intergovernmental Panel on Climate Change
IPCC AR3	IPCC Assessment Report 3
IPCC AR4	IPCC Assessment Report 4
IPCC AR5	IPCC Assessment Report 5
LAI	Leaf Area Index
LN	Linacre
Mac-PDM.09	Macro-scale Probability Distributed Moisture Model
MRC	Mekong River Commission
NCDC GSOD	National Climate Data Centre, Global Surface Summary of the Day
NDVI	Normalized Difference Vegetation Index
NOAA-AVHRR	National Oceanic and Atmospheric Administration – Advanced Very High Resolution Radiometer
NSE	Nash-Sutcliffe coefficient
PET	Potential Evapotranspiration
PN	Penman
PT	Priestley-Taylor
QUEST-GSI	Quantifying and Understanding the Earth System – Global Scale Impacts
r	Pearson Correlation Coefficient
RCM	Regional Climate Model
RCP	Representative Concentration Pathway

RD	Root Depth
SLURP	Semi-distributed Land Use-based Runoff Processes
SRES	Special Report on Emissions Scenarios
SWAT	Soil and Water Assessment Tool
TOPAZ	Topographic Parameterization Tool
UDel	University of Delaware
UKMO	United Kingdom Met Office
USGS	United States Geological Survey
WBM	Water Balance Model
WMO	World Meteorological Organization

Chapter 1

Introduction, study aim and objectives

1.1. Introduction

Over recent decades, computer based hydrological models have been developed and applied at an ever increasing rate (Refsgaard, 2007). This has been aided by a number of factors, including considerable increases in computing power, advances in pre- and post-processing software such as Geographic Information Systems (GIS), improvements in scientific understanding of hydrological systems and wider availability of spatial datasets, such as topography and land cover data obtained through remote sensing (Singh and Frevert, 2002; Singh and Woolhiser, 2002; Mulligan, 2004; Liu and Gupta, 2007; Refsgaard, 2007; Döll *et al.*, 2008). Furthermore, much hydrological modelling research and application has been driven by the increasing pressure on water resources caused by rapid population growth, urbanization, climate change and agricultural, industrial and socio-economic development (Refsgaard, 2007; Rochester, 2010). The role of hydrological models in water resources planning and decision-making has become increasingly important, so that hydrological modelling is now an essential tool for water resources assessment and management (Singh and Frevert, 2002; Singh and Woolhiser, 2002; Loucks and van Beek, 2005; Henriksen *et al.*, 2008; McCartney and Acreman, 2009).

Surface and ground waters provide freshwater for domestic, agricultural and industrial consumers, as well as supporting numerous additional benefits and ecosystem services (Millennium Ecosystem Assessment, 2005; McCartney and Acreman, 2009). For example, rivers support productive and biodiverse riverine and floodplain ecosystems and provide food (notably fish and other aquatic organisms), opportunities for hydroelectric power production, routes for transporting bulk cargo and water-based recreational opportunities (Postel and Richter, 2003; UNEP, 2010). They also transport nutrient-rich sediments and deposit these onto their floodplains, helping to maintain agricultural productivity (Postel and Richter, 2003). Water resource planners and managers generally seek to maximise the benefits that people can obtain from water resources, whilst

planning for and minimising the negative impacts of the hydrological extremes of flooding and drought (Loucks and van Beek, 2005). Increasingly, it has been recognised that in order to maintain and enhance the benefits derived from water resource systems, effective management must take into account, protect and, where necessary, restore the environmental and ecological functioning of these systems (Loucks and van Beek, 2005).

Hydrological modelling can assist water resource managers in evaluating the quantity, quality, or spatial and temporal distribution of water resources (e.g. Henriksen *et al.*, 2003; García *et al.*, 2008; Henriksen *et al.*, 2008; Ouyang *et al.*, 2011). Moreover, hydrological models are widely used for assessing the potential impacts of a variety of scenario types on water resources. What-if scenario modelling is used to evaluate what hydrological conditions may be like in the future and can assist in the evaluation of different management scenarios. The results of such assessments can be potentially very useful for water managers, decision/policy makers, conservation organisations and other users of water resources, such as agriculture and industry (Thompson and Hollis, 1995; Burke, 2004; Thompson, 2004; Prudhomme and Davies, 2009a; Singh *et al.*, 2011). Scenarios typically explored include climate change (e.g. Prudhomme and Davies, 2009a; Västilä *et al.*, 2010; Thompson, 2012), land cover change (e.g. Thanapakpawin *et al.*, 2007; Choi and Deal, 2008; Wijesekara *et al.*, 2012) and a wide range of water management scenarios, from dam or barrage regulation in major river basins (e.g. Thompson and Hollis, 1995; Singh *et al.*, 2011; Räsänen *et al.*, 2012), to sluice control in small-scale catchments (e.g. Gasca Tucker and Acreman, 2000; Thompson, 2004).

Alongside the increasing use, number and importance of hydrological models, there has been a growing body of research and literature related to the identification and examination of sources of uncertainty in hydrological modelling and the scenario modelling process (e.g. Beven, 1993, 1996; Beven, 2002; Butts *et al.*, 2004; Beven, 2006; Pappenberger and Beven, 2006; Refsgaard *et al.*, 2006; Liu and Gupta, 2007; Todd *et al.*, 2011; Dobler *et al.*, 2012) and it is now widely recognised that uncertainty in hydrological scenario projections should be identified and communicated in a transparent manner. Uncertainty assessment is therefore an important aspect of hydrological modelling research. This thesis investigates a

series of issues associated with hydrological scenario modelling, focussing upon sources of uncertainty in climate change impact assessments.

1.2. Hydrological scenario modelling protocol

In order to introduce some of the key concepts and terms used in this thesis, this section outlines each of the stages that are typically taken during the hydrological scenario modelling process, as summarised in Figure 1.1. Of course, the actual stages will vary greatly from one application to another.

Purpose definition: At this stage, the aim of the modelling process is defined. This could, for example, take the form, 'The aim of this modelling study is to assess the potential impacts of scenario *x* upon catchment *y*', or 'The aim of this study is to assess the uncertainty in projections for scenario *x*, employing catchment *y* as a case study site'. The area to be modelled is therefore decided upon at this stage. This could, in fact, be the entire global land surface (e.g. Gosling and Arnell, 2011; Haddeland *et al.*, 2011; Arnell and Gosling, 2013; Hagemann *et al.*, 2013), or a particular region (e.g. Schuol and Abbaspour (2006) develop a model for a four million km^2 area in West Africa) or country (e.g. Henriksen *et al.* (2003) and Henriksen *et al.* (2008) describe the development and use of a national hydrological model for Denmark). Most commonly, however, modelling for scenario assessment is undertaken at the catchment or sub-catchment scale (e.g. Thompson and Hollis, 1995; Graham *et al.*, 2007a; Kingston and Taylor, 2010; Hughes *et al.*, 2011; Sultana and Coulibaly, 2011; Thorne, 2011). Sometimes, multiple case study catchments may be employed (e.g. Arnell, 2011).

The purpose definition stage also involves establishing which hydrological process(es) the study aims to determine the potential impacts of a particular scenario upon. Many scenario modelling studies focus on projected impacts upon river flow (e.g. Arnell, 2011; Nóbrega *et al.*, 2011; Xu *et al.*, 2011), but others assess potential changes in a range of hydrological processes, such as groundwater storage and wetland flood extents (Thompson and Hollis, 1995), groundwater depths and wetland ditch water levels (Thompson *et al.*, 2009) and overland and baseflow (Wijesekara *et al.*, 2012).

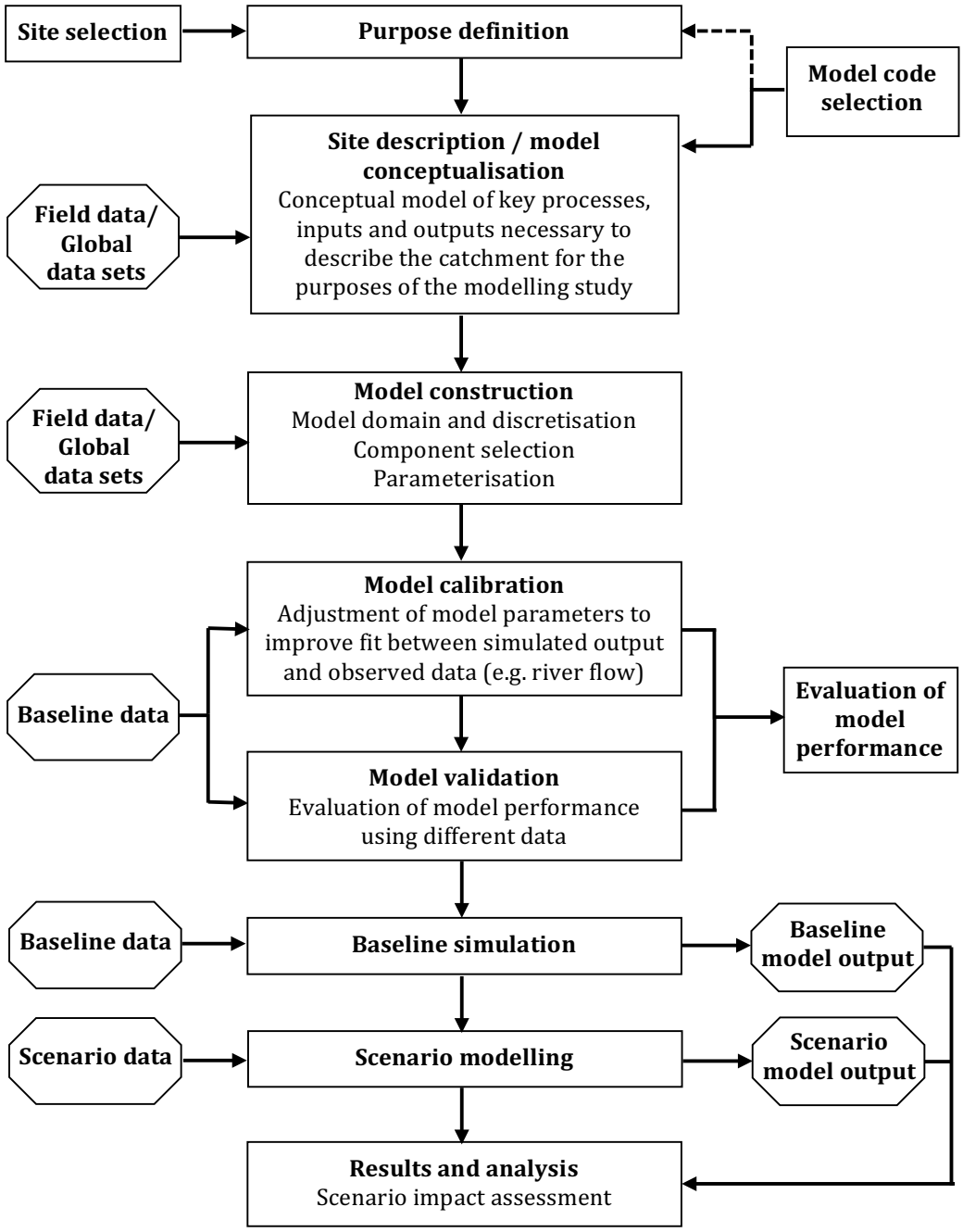

Figure 1.1. Hydrological scenario modelling workflow. Adapted from: Refsgaard (1997).

Most scenario assessments employ a pre-defined model code. If the aim of the study involves employing a specific model code, then the model code will be selected at this stage (e.g. if the aim is to demonstrate the application of a particular model code to a specific scenario modelling application). Following the terminology of Refsgaard and Henriksen (2004: 75) a model code is:

> 'A mathematical formulation in the form of a computer program that is so generic that it, without program changes, can be used to establish a model with the same basic type of equations (but allowing different input variables and parameter values) for different study areas.'

Conversely, the term 'model' is used to refer to a site-specific model developed for a particular study area (using, most commonly, a pre-defined model code), encompassing the site-specific input data and parameter values (Refsgaard, 2000; Refsgaard and Henriksen, 2004). Any changes to the input data or parameter values therefore results in the development of a new model.

Site description and model conceptualisation: Before developing a site-specific computerised model, it is essential that a conceptual (i.e. non-computerised) model of the hydrological system be established. This involves gathering information about the site to be modelled and deciding upon the key hydrological processes that need to be included within the computerised model for the particular objectives of the study, including the simplifications which are deemed acceptable for the purposes of the investigation (Refsgaard, 1997; Refsgaard and Henriksen, 2004). In addition, the conceptual model, and consequently the computerised model, is influenced by data availability, since the detail with which particular catchment attributes and processes can be described will be tempered by the information that is available about them (Wagener *et al.*, 2001). For example, if the study focuses upon river flow and/or there is a lack of data on subsurface hydrology, then a simplified groundwater model (compared to other model components) may be employed (e.g. Andersen *et al.*, 2001; McMichael *et al.*, 2006; Stisen *et al.*, 2008).

Model code development is not usually undertaken as part of a scenario modelling study. Instead, such studies tend to employ existing model codes. The model code(s) to be employed should normally be chosen following the establishment of the conceptual model. In this case, the decision will be strongly influenced by the need to match the model code to the model conceptualisation, including decisions pertaining to the simplifications to be made, as well as data availability and the required outputs, such as river flows or groundwater levels. Alternatively, if the aim of the modelling process involved the application of a specific model code (see

above), then the conceptual model itself is likely to be influenced by the type of model code that has already been selected. In either case, the model code selected should have previously undergone code verification that demonstrates that, for specific ranges of application, the equations that constitute the mathematical model are accurately solved by the program and that the code in some way accurately represents the theories and concepts behind the model (Anderson and Woessner, 1992; Refsgaard and Henriksen, 2004). All widely used model codes have undergone extensive code verification.

Model construction, parameterisation, calibration and validation: Site-specific model development involves converting the conceptual model into a computerised model of the study site. Model construction may involve definition of the model boundary, development of the model structure, including selection and set-up of the processes to be included within the model, and specification of required input data, such as meteorological, hydrogeological and land cover data. The model must also be parameterised (i.e. parameter values must be defined). Some, or even all, of the final parameter values may be defined through model calibration, whilst some values may be obtained from field, laboratory or remotely sensed data from the specific site, from a review of relevant literature, or from prior expert knowledge (Refsgaard, 2000).

Model calibration is the procedure whereby model parameters are adjusted in order to achieve as close a fit as possible between observed records of a given system response (e.g. river discharge) and the simulated system response of the model for the same period of time. Model performance is typically assessed using a combination of: i) qualitative techniques involving graphical plots of observations against simulated model output, such as river discharge and ii) statistical measures designed to assess the level of agreement (or disagreement) between observed and simulated time series (Refsgaard, 1997; Feyen *et al.*, 2000; Krause *et al.*, 2005; Moriasi *et al.*, 2007). Acceptable model performance should be defined prior to model calibration and validation. For example, Henriksen *et al.* (2003) and Moriasi *et al.* (2007) have developed rating threshold values for various performance statistics. A range of calibration procedures and model performance statistics are available and these are discussed in Section 2.6.5.

Once model performance over the calibration period is deemed acceptable according to predefined criteria, model validation is usually undertaken. This involves assessing model performance using datasets not used during model calibration. The most common approach is the split-sample approach (Klemeš, 1986), in which the available observed data record for a catchment is divided into parts for separate use in model calibration and validation. For example, validation is frequently undertaken by assessing model performance over a period of time not used in model calibration (i.e. by running the model with meteorological data from a different time period) (e.g. van der Linden and Woo, 2003a; Butts *et al.*, 2004; Thanapakpawin *et al.*, 2007; Poulin *et al.*, 2011; Wijesekara *et al.*, 2012).

Despite its wide use, validation is a controversial and contested term, with some arguing that models cannot be validated and that use of the term validation is erroneous (e.g. Konikow and Bredehoeft, 1992; Oreskes *et al.*, 1994). The arguments used include that demonstrating that a model performs well against observations in one instance does not mean that it will in another situation, that validation is often erroneously conflated with proving that a model is accurate or truthful (Oreskes *et al.*, 1994) and that models are embodiments of scientific theories, and therefore, following Karl Popper's philosophy, can only ever be falsified, never validated (Konikow and Bredehoeft, 1992). However, the use and usefulness of model validation is widely accepted within the environmental and hydrological modelling literature (e.g. Refsgaard, 1997; Andersen *et al.*, 2001; Mulligan and Wainwright, 2004; Refsgaard and Henriksen, 2004; Young *et al.*, 2004; French, 2010) and model validation is undertaken within the vast majority of hydrological modelling studies. Furthermore, Young *et al.* (2004) argue that model validation is an important falsification process, since poor model performance at the validation stage would mean that earlier stages of the modelling process, such as model parameterisation or model conceptualization, must be revisited (e.g. Henriksen *et al.*, 2003).

Baseline simulation: Following calibration/validation, the model is run for a baseline (historical) period. This may be the same as the model calibration and/or validation period. Following scenario modelling, model output under scenario conditions is compared with the baseline simulated model output. In non-scenario modelling studies, the aim may be to develop a model that provides a suitable

representation of hydrological conditions for a defined historical period, in which case this stage may be the end point of the study. In either case, baseline simulation results may be analysed to achieve further understanding of the system. For example, for variables for which observations are only available at discrete points, such as water table depths, the simulated spatial distribution of the variable over the baseline period may be analysed in order to gain understanding of the spatial variation in system behaviour (Dai *et al.*, 2010).

Scenario definitions – perturbation of baseline data or model parameterisation, or generation of new data: Scenario input data must be defined, such as scenario climate or land cover data. This may involve direct perturbation of baseline input data, or generation of new datasets. In some cases (e.g. land cover change; Wijesekara *et al.*, 2014), model parameters may require adjustment to reflect altered catchment conditions. Data may be generated for a range of alternative scenarios. For example, climate change scenarios might be developed through the perturbation of baseline meteorological inputs using projected changes in meteorology from a number of General Circulation Models (GCMs; a type of climate model) for different greenhouse gas emissions scenarios. Alternatively, projections of dominant land cover change processes may be used to develop alternative representations of land cover for future points in time. Tools and methods for generating climate scenarios are reviewed in detail in Section 2.5.

Scenario modelling: The hydrological model is forced with the scenario input data (which may replace some of the baseline input data), keeping all other components of the model the same as for the baseline simulation. For example, in the case of climate change scenario simulation, the baseline meteorological input time series are replaced with the scenario meteorological time series. If multiple scenarios are being investigated, multiple scenario simulations will be undertaken.

Results and analysis: Following scenario simulation runs, the simulated model output will be compared with the model output under baseline conditions. A range of graphical and statistical techniques are generally employed. Assessments most commonly focus on projected changes in river flow (e.g. Graham *et al.*, 2007a; McMichael and Hope, 2007; Prudhomme and Davies, 2009b; Thorne, 2011; Dobler

et al., 2012), but other variables may be analysed (depending upon the context, model used and study aims), such as groundwater levels (Goderniaux *et al.*, 2009), lake water levels (Singh *et al.*, 2010; Singh *et al.*, 2011), flood extent (Thompson *et al.*, 2009), evapotranspiration (Sultana and Coulibaly, 2011; Wijesekara *et al.*, 2012) and snow storage (Sultana and Coulibaly, 2011). Analysis can be undertaken to assess changes in average annual conditions (e.g. mean river discharge), mean monthly conditions (e.g. the river regime) or extremes (e.g. high or low flows).

In some cases, the hydrological projections may subsequently be employed in further assessment stages to evaluate the potential ecological, social or economic impacts of hydrological changes. For example, the range of variability approach (RVA) (Richter *et al.*, 1997) and a modified version of this called ecological risk to flow alteration (ERFA) (Laizé *et al.*, 2014) both use statistical techniques to generate indicators of hydrological alteration (IHAs) that quantify the degree of ecological risk posed by projected changes to the flow regime of a river.

1.3. Uncertainty in hydrological scenario modelling

As described above, the results of hydrological scenario assessments can be interesting and potentially useful for a wide number of stakeholders. However, uncertainty is inevitably introduced at each stage of the modelling process and is propagated through subsequent stages, leading to uncertainty in the scenario results. In the case of climate change impact assessments, this process has been described as a 'cascade of uncertainty' (Schneider, 1983; Wilby and Dessai, 2010), and is detailed in Sections 2.4–2.6. It is important to understand and quantify the various sources of uncertainty to allow better interpretation of results and to better establish the range of potential outcomes of a scenario. Furthermore, it is essential that policy makers, water resource managers and other stakeholders who are provided with hydrological projections are aware of the level of uncertainty they contain, so that this can be taken into account during decision-making (Pappenberger and Beven, 2006; Kay *et al.*, 2009). In addition, uncertainty assessment can sometimes help identify areas in which uncertainty can potentially be reduced, for example through additional field campaigns or improved modelling of a particular system component (Kay *et al.*, 2009). Uncertainty analysis is

therefore a vital component of hydrological scenario modelling. Various sources of uncertainty and the results of uncertainty assessments are discussed in Chapter 2.

1.4. Research aim and objectives

The overall aim of this thesis is to quantify the extent to which decisions made during the hydrological modelling process impact scenario results. More specifically, the study aims to assess sources of uncertainty in river flow projections under climate change.

The first objective of this research is to provide, through a review of the existing literature, a synthesis of the tools and approaches employed in hydrological climate change impact assessments and the sources of uncertainty introduced through the modelling process.

For climate change impact assessments, objectives two to six of this thesis are to investigate the following sources of uncertainty:

ii) choice of General Circulation Model (GCM) for the generation of climate scenario data (inter-GCM related uncertainty);
iii) use of alternative hydrological model codes (inter-hydrological model uncertainty);
iv) calculation of potential evapotranspiration (PET) data for baseline and scenario simulation using alternative methods (PET-related uncertainty);
v) spatial distribution of meteorological inputs within the hydrological model (this relates to both input data uncertainty and model structure uncertainty);
vi) use of alternative global gridded precipitation datasets for baseline simulation and the subsequent perturbation of these datasets to reflect climate change scenarios (precipitation input uncertainty).

The sources of uncertainty investigated in this thesis relate to multiple stages of the modelling protocol described in Section 1.2. For example, Objective (ii) relates to decisions made during scenario development, Objective (iii) relates to model code selection and objectives (iv–vi) relate to model construction and calibration, as well

as model code selection in the case of Objectives (iv) and (v). Objectives (iv –vi) are potential sources of both inter- and intra-hydrological model uncertainty.

1.5. Research design

Sections 1.5.1 and 1.5.2 describe the selection of an appropriate case study site and hydrological model code for the research undertaken within this thesis. Subsequently, the broad methodology for achieving the overall aim and objectives of the research is outlined in Section 1.5.3. It is necessary to first discuss the study site and model code selection, since the research design strongly relates to these.

1.5.1. Case study site selection

The 795,000 km^2 Mekong River Basin in Southeast Asia (see Figure 1.2) is employed as the case study catchment for this thesis. This catchment was selected for a number of reasons. Firstly, this study benefits from the opportunity to compare river flow projections for the Mekong generated as part of this research with those simulated by an earlier catchment model of the Mekong developed using the Semi-distributed Land Use-based Runoff Processes (SLURP) model code (Kite, 2000, 2001; Kingston *et al.*, 2011), allowing an assessment of inter-hydrological model uncertainty. Results from the Mac-PDM.09 global hydrological model (Gosling and Arnell, 2011) for the Mekong (Gosling *et al.*, 2011) for the same climate scenarios employed by Kingston *et al.* (2011) are also used. The research by Kingston *et al.* (2011) and Gosling *et al.* (2011) formed part of the QUEST-GSI (Quantifying and Understanding the Earth System – Global Scale Impacts) project, under a strand of the project that focused on assessing the potential impacts of climate on freshwater resources at the basin scale (Todd *et al.*, 2011).

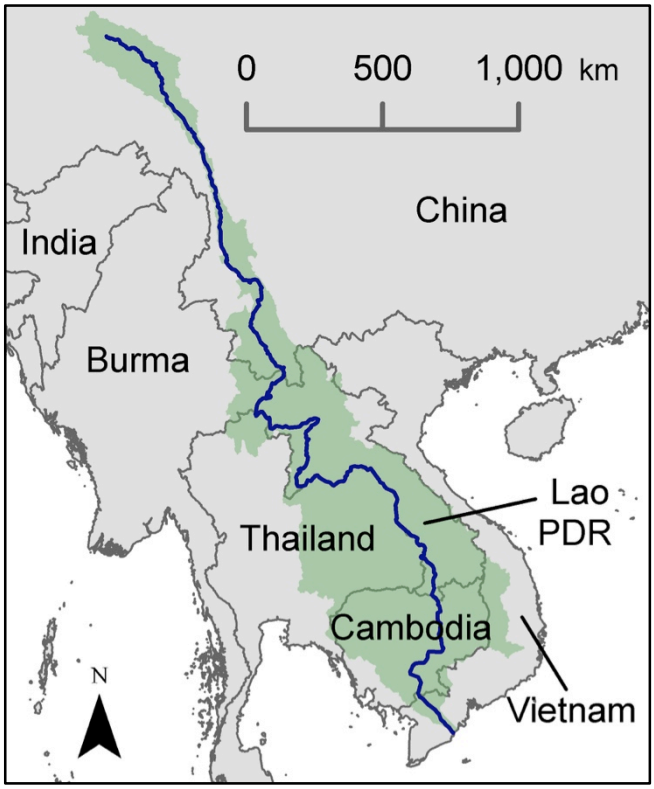

Figure 1.2. The Mekong River Basin.

Secondly, due to the large scale of the Mekong Basin, the catchment exhibits significant spatial variation in climate variables such as precipitation, temperature and PET. This is important since it means that decisions such as how meteorological inputs within the hydrological model are distributed may be expected to impact hydrological model results. Furthermore, it means that climate projections also vary across the catchment, as demonstrated in previous studies of the Mekong (e.g. Kiem *et al.*, 2008; Kingston *et al.*, 2011).

Thirdly, in large basins such as the Mekong, use of semi-distributed rather than gridded meteorological inputs may be particularly desirable in order to reduce hydrological model computation times, since it is widely acknowledged that higher model spatial resolutions and model input resolutions can lead to longer computation times (e.g. Vázquez *et al.*, 2002; Ajami *et al.*, 2004; Butts *et al.*, 2004; Vaze and Teng, 2007). It is therefore important to establish the extent to which the spatial distribution of meteorological inputs can impact scenario results.

Fourthly, there are long-term river discharge records available for multiple locations within the Mekong Basin. This is a significant advantage for enabling model calibration and validation against observed records. Finally, a large human population is dependent upon the Mekong for their water, food and energy requirements and for their livelihoods (MRC, 2010b). Assessing the potential impacts of climate change on Mekong River flow, including the associated uncertainty, has valuable practical implications for those responsible for managing the river basin's water resources, as well as the people who depend upon these resources. A more detailed overview of the Mekong River Basin is provided in Chapter 3.

1.5.2. Model code selection

The MIKE SHE model code was selected for use in this study primarily due to its flexibility, which means that it is most suitable to address the aims and objectives of this thesis. MIKE SHE is flexible in that it is capable of representing processes at different levels of complexity, with both physically-based and conceptual options available (Graham and Butts, 2005). MIKE SHE also allows processes and input data to be represented at different levels of spatial resolution, from lumped, to semi-distributed, to gridded at grid cell sizes ranging from square metres to square kilometres. This means that, in contrast to the earlier SLURP model of the Mekong, a model can be developed that is quasi-physically based and spatially distributed at the grid scale, whilst employing a conceptual, semi-distributed groundwater component. This method is particularly useful in large catchments with limited data available on subsurface hydrogeology (Andersen *et al.*, 2001; Stisen *et al.*, 2008). In addition, this flexibility is expedient for exploring the use of alternative meteorological input spatial distributions, whilst keeping the spatial distribution of other catchment processes unchanged.

MIKE SHE has been successfully used to model a wide range of hydrological systems, from small (<50 km^2) catchments in the UK such as the Elmley Marshes in southeast England (8.7 km^2) (Thompson *et al.*, 2004; Thompson *et al.*, 2009) and upland catchments in southwest Scotland (Thompson, 2012), through catchments of hundreds or thousands of km^2 (e.g. Singh *et al.*, 2010; Singh *et al.*, 2011), to major

transboundary river basins such as the 375,000 km^2 Senegal River Basin (Andersen *et al.*, 2002b; Stisen *et al.*, 2008). MIKE SHE has also been successfully employed in mountainous catchments that required use of the MIKE SHE snowmelt module (e.g. Smerdon *et al.*, 2009), an important consideration since snow accumulation and melting occurs in the upper reaches of the Mekong Basin. An overview of the MIKE SHE model code is provided in Section 2.6.3.1.

1.5.3. Research outline

In order to achieve the overall research aim and objectives given in Section 1.4, the following objectives were established:

i) a) To develop a MIKE SHE model of the Mekong River Basin using, where appropriate, the same input data as Kingston *et al*. (2011), who previously modelled the Mekong using SLURP. The MIKE SHE model should be capable of simulating historical observed discharges for the period 1961-1998, to at least the same level of performance as the SLURP model.

b) To use this model for climate change scenario simulation and compare the results with those of the earlier SLURP model of the Mekong and the global hydrological model Mac-PDM.09, in order to assess inter-hydrological model uncertainty and inter-GCM uncertainty. The two sets of scenarios to be used are those previously applied to SLURP and Mac-PDM.09. The first set is based on a 2 °C increase in global mean surface air temperature as simulated by seven GCMs (Todd *et al.*, 2011), enabling an exploration of the nature and magnitude of inter-GCM uncertainty. The second set is based on increases in global mean temperature of between 1–6 °C, as simulated by a single GCM.

ii) a) To develop additional MIKE SHE models, each employing PET input data derived using different PET methods to that of the first MIKE SHE model. The performance of each of these models following calibration and validation should be at least as good as the original MIKE SHE model of the catchment.

b) To investigate the implications of using alternative PET methods for discharge projections for the Mekong River by undertaking a comparison of baseline and scenario PET data produced using the alternative methods, and

comparing the river discharge projections simulated by the alternative MIKE SHE models.

iii) a) To develop two additional MIKE SHE models employing alternative meteorological input spatial distributions with finer spatial discretisation compared to that of the first MIKE SHE model.
b) To compare river discharge projections of the three hydrological models (employing alternative meteorological input spatial distributions) to explore uncertainty related to spatial distribution of meteorological inputs.

iv) a) To develop a MIKE SHE model that throughout model calibration and baseline simulation employs precipitation data derived from an alternative global gridded dataset to that used for the first MIKE SHE model and the earlier SLURP model.
b) To compare river discharge projections of the two hydrological models to explore uncertainty related to choice of baseline precipitation data.

v) To extend the analysis of GCM uncertainty by driving (a selected version of) the MIKE SHE model of the Mekong with climate scenario projections generated using scenarios and GCMs from the latest IPCC[1] report (the Fifth Assessment Report – AR5) and latest phase of the Coupled Model Intercomparison Project, phase five (CMIP5).

1.6. Thesis structure

This thesis is structured into a further six chapters. Chapter 2 provides a synthesis of the tools and approaches employed in hydrological climate change impact assessments and reviews the literature related to uncertainty in hydrological scenario modelling, with a focus on uncertainty in climate change impact assessments. This chapter therefore provides the background and rationale for this thesis. Chapter 3 provides an overview of the Mekong Basin and presents the data that are subsequently used in the construction of the MIKE SHE models.

[1] Intergovernmental Panel on Climate Change

Chapter 4 details the development of an initial MIKE SHE model of the Mekong, including model calibration/validation. This model is then used for climate change scenario simulation, the results of which are presented and compared to those of the SLURP and Mac-PDM.09 hydrological models, whose results have been made available for this research. Two climate change scenario sets are employed: the first based on a 2 °C increase in global mean temperature as simulated by seven GCMs, the second on prescribed warming of between 1–6 °C, as simulated by a single GCM. This chapter explores inter-hydrological model uncertainty and GCM-related uncertainty.

Chapter 5 focuses on uncertainty related to meteorological inputs, with three sources being investigated in turn: PET-related uncertainty, the spatial distribution of meteorological inputs and choice of baseline precipitation dataset. In each case, alternative versions of the initial MIKE SHE model of the Mekong described in Chapter 4 are developed, all requiring model recalibration due to the disparity between the different meteorological datasets specified in the models. In the case of PET-related uncertainty, five additional models are created, each with PET data derived using a different method to that of the initial model. To explore the effect that the spatial distribution of meteorological inputs can have upon model scenario results, two further versions of the model are created and calibrated, each employing a different meteorological input spatial distribution. In order to assess the impact that choice of baseline precipitation datasets can have on climate change impact assessments, a model is developed that uses precipitation derived from a different dataset to that used for the initial model. For each source of uncertainty in turn, following a description of model development and the generation of alternative baseline and scenario data, analyses of the alternative meteorological datasets are undertaken, and the calibration, validation and scenario results of the alternative models are presented and compared. The 2 °C, seven GCM climate change scenarios introduced in Chapter 4 are employed.

Chapter 6 extends the analysis of the potential impact of climate change on the Mekong Basin and GCM-related uncertainty through the use of scenario climate data generated using more up-to-date GCMs and scenarios from IPCC AR5 and CMIP5.

Those used in earlier chapters were based on scenarios and GCMs from IPCC AR4 and CMIP3.

Chapter 7 provides discussion, conclusions and recommendations for further research. This includes an overview and comparison of the nature and magnitude of the different sources of uncertainty investigated in the thesis.

Chapter 2

Hydrological modelling and uncertainty in climate scenario impact assessments

2.1. Introduction

As detailed in Sections 1.4 and 1.5, this thesis investigates themes related to uncertainty in hydrological climate change impact assessments. This chapter therefore provides an overview of the tools, stages and sources of uncertainty in such assessments.

2.2. Climate change and freshwater resources

It is unequivocal that anthropogenic emissions of greenhouse gasses have led to an enhancement of the greenhouse effect, and hence warming of the Earth's climate system (Myhre *et al.*, 2013; Stocker *et al.*, 2013). Furthermore, human induced changes in the Earth's climate system through the 21th century and beyond are seen as inevitable, even if it were possible to immediately stop all anthropogenic greenhouse gas emissions today (IPCC, 2013).

Climate change will have major consequences for the hydrological cycle. Since the saturation vapour pressure of air (and hence the amount of water vapour that air can hold) increases with temperature, as described by the Clausius-Clapeyron relationship, warming of the troposphere is expected to lead to increases in specific humidity (Huntington, 2006; Stocker *et al.*, 2013). Consequently, precipitation on a global scale is projected to increase, with the IPCC rating the likelihood of this occurring as 'virtually certain' (Collins *et al.*, 2013), equating to a probability of 99–100% (Stocker *et al.*, 2013). Similarly, global annual surface evaporation is projected to increase with increasing mean global surface temperatures (Collins *et al.*, 2013). These changes have been characterised as an intensification of the hydrological cycle (Huntington, 2006). However, changes at regional and local scales will be highly diverse, with the seasonality, rates, direction and magnitude of climatic changes showing great spatial variability, particularly in the case of precipitation (Todd *et al.*, 2011; Collins *et al.*, 2013; Kirtman *et al.*, 2013; Jiménez

Cisneros *et al.*, 2014). Regional changes in precipitation will be influenced by atmospheric circulation patterns and atmosphere-ocean interactions, which themselves will also be subject to anthropogenic forcing (Nijssen *et al.*, 2001).

At the land surface, changes in the fluxes of energy and water will impact river flows, wetland functioning, groundwater recharge and storage, soil moisture storage and water storage in snow and ice, therefore changing the distribution of freshwater resources in both space and time (Nijssen *et al.*, 2001; Bates *et al.*, 2008; Jiménez Cisneros *et al.*, 2014). In turn, the frequency and severity of flooding and drought will be impacted. These changes could have far-reaching implications for aquatic ecosystems and the human use of their water and related services (Gleick, 1989; Millennium Ecosystem Assessment, 2005; Gosling, 2013). These include food supply, energy production and domestic and industrial water supply.

2.3. Climate change impact assessments on freshwater resources

Due to their fundamental importance, there are strong socio-economic incentives to assess the potential impacts of climate change on water resources at the catchment scale, such as changes in river and wetland hydrological regimes and groundwater recharge (Buytaert *et al.*, 2009; Feyen and Vázquez Zambrano, 2011). The most common method for achieving this has been condensed by Arnell and Reynard (1996) into three broad stages, as follows:

1. Construct, calibrate and validate a hydrological model (or multiple hydrological models) of the system using observed (baseline) climate data.
2. Define/select climate scenarios and perturb the baseline input climate data accordingly. This typically involves the use of climate projections from one or more climate models, for one or more climate change scenarios.
3. Run the hydrological model(s) using the perturbed, future climate scenario input data and then compare the scenario results with the output of the model(s) simulated under baseline climatic conditions.

This three-stage assessment process is a succinct adaptation (i.e. for hydrological impact assessment) of the standard, non-hydrologically specific climate change

impact assessment approach outlined by Carter *et al.* (1994). This demonstrates that, as noted by Gosling *et al.* (2011), the broad stages of a climate change hydrological impact assessment are similar to those of other climate change impact assessments that employ different impact models (e.g. crop and ecosystem models; Olesen *et al.*, 2007; and temperature-mortality relationship modelling for assessing the risk of future temperature-related mortality; Gosling *et al.*, 2009).

2.4. Uncertainty in hydrological projections under climate change

Despite major improvements in both climate and hydrological modelling in recent years, a key caveat of all hydrological climate change impact assessments is that the projections provided are highly uncertain. In fact, uncertainty is introduced at every stage of the assessment process (Xu *et al.*, 2005), in what can be described as a 'cascade of uncertainty' (Schneider, 1983; Wilby and Dessai, 2010). This term has been used to describe climate change impact assessments in general, but is highly relevant to hydrological climate change impact assessments (Wilby and Dessai, 2010), as demonstrated in Figure 2.1. This schematic encapsulates the way in which additional sources of uncertainty are introduced at each stage, leading to an increasing number of permutations (in terms of greenhouse gas scenarios, GCMs, downscaling methods and hydrological models that could be used) and hence an expanding envelope of uncertainty (Wilby and Dessai, 2010).

It is important to note, however, that the schematic is by no means comprehensive; there are numerous other sources of uncertainty, such as potential changes in land use that would affect the hydrological response of a basin to rainfall events. Furthermore, the increasing number of triangles at each stage does not attempt to represent accurately the actual number of possible permutations, or the amount of uncertainty in the final results that is introduced at each stage. As emphasised by Hawkins (2014), the different layers of the pyramid are not equally important and, furthermore, their relative importance will depend upon factors such as the relevant climate variables and the impact, region and timescale of interest. An alternative visualization of the cascade of uncertainty is provided in Section 2.5.2.

As stated in Section 1.3, it is important to identify, characterise and quantify the different sources of uncertainty in hydrological projections in order to gain a more complete picture of the potential range of outcomes, allow uncertainty to be communicated to decision makers and other stakeholders and identify avenues of research that have the potential to close gaps in knowledge (Pappenberger and Beven, 2006; Kay *et al.*, 2009). Uncertainty analysis has therefore become a key aspect of many hydrological climate change impact assessments (e.g. Wilby and Harris, 2006; Minville *et al.*, 2008; Kay *et al.*, 2009; Prudhomme and Davies, 2009b; Poulin *et al.*, 2011; Todd *et al.*, 2011; Dobler *et al.*, 2012; Hagemann *et al.*, 2013).

The various stages and tools required in hydrological climate change impact assessments and some of the associated sources of uncertainty are outlined in Sections 2.5–2.6. Section 2.5 focuses on the generation of climate projections that can be used to drive hydrological models and the uncertainties introduced therein, whilst Section 2.6 focuses on sources of uncertainty introduced in the hydrological modelling stages of the impact assessment process.

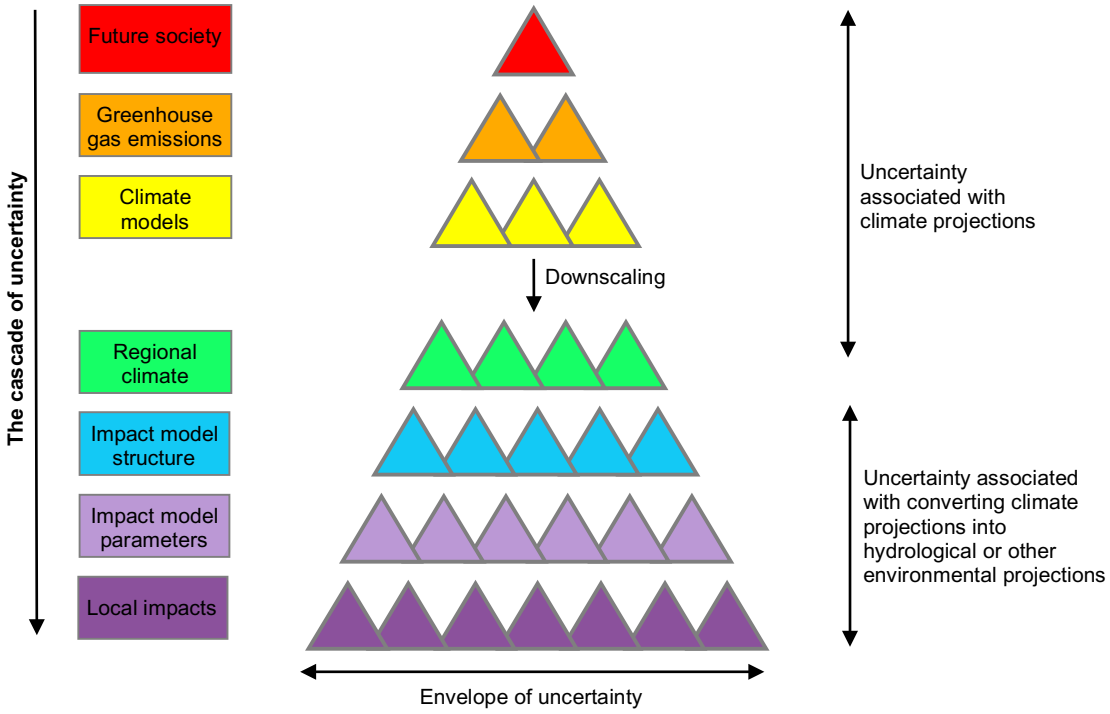

Figure 2.1. The cascade of uncertainty associated with climate change impact assessments that couple climate change projections from GCMs with an impact model, in order to project the potential impacts of climate change on environmental variables at the regional to local scale. In hydrological impact assessments, the impact model used would be a hydrological model. Adapted from: Wilby and Dessai (2010).

2.5. Climate projections

Essential to the impact assessment protocol outlined in Section 2.3 are projections for the climate variables that are required to drive a hydrological model, such as precipitation and temperature. Coupled atmosphere-ocean general circulation models (GCMs) are the primary tool for projecting future climate change (McGuffie and Henderson-Sellers, 2005). These GCMs contain mathematical representations of the atmosphere, ocean, land surface, cryosphere and biogeochemical processes (Randall *et al.*, 2007). However, the process of generating projections of future climate under anthropogenic forcing is inherently uncertain, as indicated by the top four tiers of the cascade of uncertainty (Figure 2.1) relating to the generation of climate projections. These sources of uncertainty are discussed in Sections 2.5.1–2.5.3.

2.5.1. Climate forcing uncertainty: Greenhouse gas scenarios and prescribed warming scenarios

Firstly, we do not know what the actions of humans (future society) will be in the future, what technological advancements there will be, or what legislation will be introduced. We therefore cannot know precisely what future anthropogenic climate forcing will be in terms of anthropogenic emissions of greenhouse gases (GHGs) and other radiative forcing agents. As it is impossible to know what the future will be, these are irreducible sources of uncertainty. However, to generate projections of future climate, scenarios of potential future radiative forcing agents, such as GHG and aerosol atmospheric concentrations, must be applied to a GCM (Meehl *et al.*, 2007b). Therefore, in order to allow plausible future emissions scenarios to be explored, the Intergovernmental Panel on Climate Change (IPCC) developed a range of emissions scenarios based on alternative 'storylines' of future demographic, socio-economic and technological development. These were outlined in the 'Special Report on Emissions Scenarios' (SRES) (Nakićenović *et al.*, 2000). To provide the time series of atmospheric concentrations of GHGs and other forcing agents required by GCMs, the emissions scenarios were run through simple climate models (Stocker *et al.*, 2013). Since their conception, six 'marker' scenarios (Figure 2.2) have been widely used to drive GCMs, in order to provide climate scenarios for specified

time periods (Figure 2.3). These SRES scenarios were employed in IPCC Assessment Reports 3 and 4 (AR3 and AR4).

a)

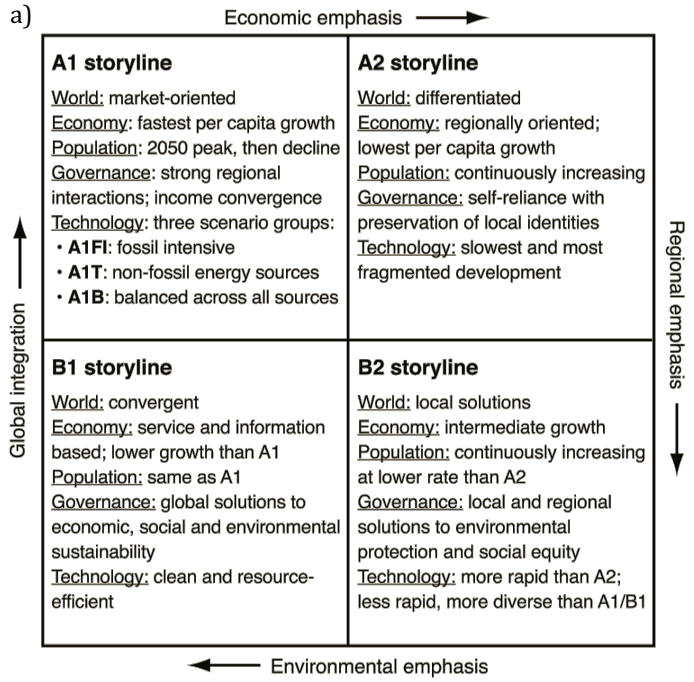

b)

SRES marker scenario	Description of emissions
A1F1	High end of SRES Range
A1B	Intermediate case
A1T	Intermediate/low case
A2	High case
B1	Low end of SRES range
B2	Intermediate/low case

Figure 2.2. a) 'Summary characteristics of the four SRES storylines (based on Nakićenović et al., 2000).' Each storyline represents different demographic, socio-economic and technological developments. From these, six scenario groups were developed: A1F1, A1T, A1B, A2, B1 and B2. Each scenario group has an illustrative marker scenario. b) The level of GHG and aerosol emissions associated with each marker scenario. a) Source: Carter et al. (2007: 147). b) Based on: Carter et al. (2007).

The SRES scenarios have been extremely useful for investigating the uncertainty in hydrological projections under climate change associated with future emissions (e.g. Arnell, 2003; Prudhomme *et al.*, 2003; Arnell, 2004; Hayhoe *et al.*, 2004; Zierl and Bugmann, 2005; Wilby and Harris, 2006; Graham *et al.*, 2007a; Prudhomme and Davies, 2009b; Bastola *et al.*, 2011). However, their use makes it difficult to assess the relationship between the magnitude of climate forcing and the nature of the hydrological response, or to infer the impacts at different levels of climate forcing (Arnell, 2011). In addition, the use of different emissions scenarios and time horizons (e.g. 2040–2069 or 2070–2100) in different studies reduces the ability to draw comparisons between the results of different studies (Arnell, 2011). In particular, the magnitude of different sources of uncertainty can vary considerably between different time horizons (Hawkins, 2014).

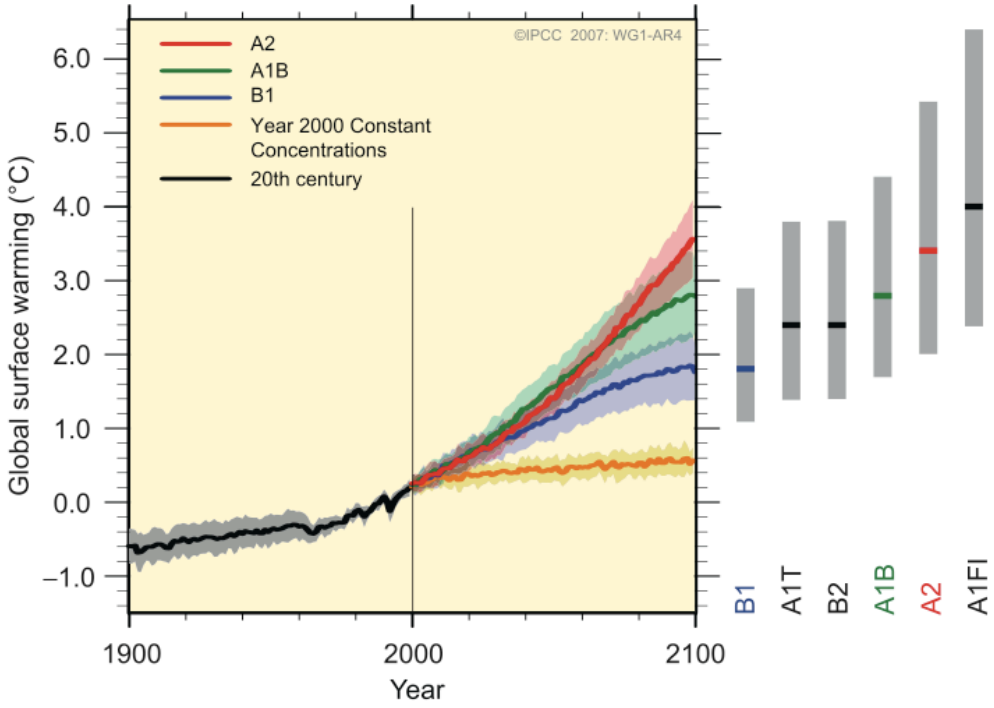

Figure 2.3. Multi-model projections of global average surface warming relative to 1980-1999 for the SRES A2, A1B and B1 emissions scenarios. Solid lines are multi-GCM averages of projected surface warming, shown as continuations of GCM hindcast simulations of the 20th century. Shading denotes the ±1 standard deviation range of individual model annual averages. The orange line represents simulations where atmospheric concentrations are held at year 2000 levels. Grey bars on the right indicate the range of plausible warming for each SRES marker scenario. Solid coloured line within each bar denotes the best estimate for 2100 for each marker scenario. Source: IPCC (2007).

An alternative approach involves firstly driving a GCM with an emissions (atmospheric concentrations) scenario and then 'rescaling' the response of each climate variable (e.g. precipitation), in order to obtain climate scenarios for prescribed increases in global mean air temperature (Todd *et al.*, 2011). Rather than exploring emissions uncertainty, climate scenarios of prescribed global warming allow the uncertainty associated with the magnitude of climate forcing/climate sensitivity to be assessed, as indexed by the increase in global mean air temperature (Arnell, 2011). This approach was used within the QUEST-GSI project, in which hydrological models for catchments around the world were driven with climate projections generated using a consistent methodology (Todd *et al.*, 2011). For example, this approach was employed by Kingston *et al.* (2011) in order to quantify the potential impacts of a prescribed increase in global mean temperature of between 0.5–6˚C relative to a baseline period of 1961–1990 (simulated by a single

GCM) on river discharge in the Mekong Basin, using the hydrological model SLURP. The climate scenarios used in this earlier investigation are amongst those employed in this study.

For each catchment in the QUEST-GSI project, the potential impacts of climate change on river flows, and the associated uncertainty, were assessed. Table 2.1 summarises the studies of the QUEST-GSI project, including the catchments, hydrological models and climate scenario sets employed, and some of the key findings. Figure 2.4 displays projected changes in low, mean and high river flows (Q95, Q50 and Q5, respectively, i.e. discharges equalled or exceeded 95%, 50% or 5% of the time, respectively) for six QUEST-GSI catchments for scenarios of 1–6˚C prescribed warming, generated using the HadCM3 (UK Met Office) GCM. Q95, Q50 and Q5 are important indicators of freshwater availability with implications for water management (Todd *et al.*, 2011). Although for some of the catchments the magnitude of changes in low, mean and high flows increase fairly linearly with increasing warming (e.g. increases in the case of the Rio Grande and decreases for the Okavango), other catchments show non-linear patterns of change (e.g. Mekong, Mitano; Todd *et al.*, 2011). This demonstrates the expediency of employing prescribed warming scenarios to assess the relationship between changing hydrological variables and increasing climate forcing, since it cannot be assumed that projected hydrological changes for a specific climate forcing can be linearly rescaled for different magnitudes of climate forcing. These non-linear discharge responses are attributed to the influence of spatially and temporally (through the year) variable changes in precipitation and temperature, and a shifting balance between increases in temperature (and hence evaporation) and changes in precipitation (Kingston *et al.*, 2010, 2011; Todd *et al.*, 2011). In support of this, Figure 2.5 demonstrates that for HadCM3, the Mekong and Mitano (which exhibit non-linear changes in mean discharge) show greater inter-annual variability in river flow changes compared to the Rio Grande and Okavango (linear response).

As indicated in Table 2.1, two of the QUEST-GSI studies (Nóbrega *et al.*, 2011; Xu *et al.*, 2011), in addition to using prescribed warming scenarios, employed four SRES marker emissions scenarios, as simulated by the HadCM3 GCM, in order to investigate emissions scenario uncertainty.

Table 2.1. Summary of studies and findings of the QUEST-GSI project.

Reference	Hydrological model	Catchment(s)	Scenarios sets employed*	Additional information / key findings
Kingston *et al.* (2011)	SLURP – conceptual, semi-distributed model.	Mekong River Basin, SE Asia (modelled area: 569,410 km^2)	i) HadCM3 GCM: 0.5–6 °C ii) Seven GCMs: 2 °C	Discharge response to progressive increases in mean global temperature (using HadCM3) found to be non-linear. Magnitude and direction of discharge changes highly GCM dependent, primarily driven by differences in projections of precipitation (not temperature). Parameterisation uncertainty investigated by varying most sensitive parameters by +/- 10% and re-running baseline and scenario simulations – found to impart little uncertainty.
Thorne (2011)	SLURP.	Liard River Basin, Canada (250,000 km^2)	i) HadCM3 GCM: 1–6 °C ii) Seven GCMs: 2 °C	Uncertainty associated with magnitude of prescribed warming high. Inter-GCM uncertainty also found to be high and driven by differences in precipitation, with changes in annual runoff ranging from -3% to +15%, despite projected increases in precipitation for all GCMs.
Hughes *et al.* (2011)	Pitman – conceptual, semi-distributed model.	Okavango, southern Africa (226,256 km^2)	i) HadCM3 GCM: 1–6 °C ii) Seven GCMs: 2 °C	Hydrological model parameter uncertainty investigated by undertaking 1000 member ensemble simulations designed to represent the uncertainty in key model parameters (for both the baseline and scenario runs). The ensemble results show large differences in the magnitude and direction of projected changes in flow across the seven GCMs. The magnitude of projected reductions in river flow for the HadCM3 GCM increase fairly linearly with prescribed warming. Parameter uncertainty not trivial (up to 10% in peak season magnitude), but inter-GCM uncertainty far greater.

* HadCM3 GCM: 0.5–6 °C = scenario set based upon a prescribed warming in global mean air temperature of 0.5, 1, 1.5, 2, 2.5, 3, 4, 5 and 6 °C relative to the 1961–1990 baseline, using the UKMO HadCM3 GCM.

HadCM3 GCM: 1–6 °C = scenario set based upon a prescribed warming in global mean air temperature of 1, 2, 3, 4, 5 and 6 °C relative to the 1961–1990 baseline, using the UKMO HadCM3 GCM.

Seven GCMs: 2 °C = scenario set for an ensemble of seven GCMs, based upon a prescribed warming in global mean air temperature of 2 °C relative to the 1961 – 1990 baseline. The seven GCMs: CCCMA CGCM3.1, CSIRO Mk3.0, IPSL CM4, MPI ECHAM5, NCAR CCSM3.0, UKMO HadGEM1 and UKMO HadCM3.

HadCM3 GCM: SRES A1B, B1, B2, A2 = scenario set based upon the IPCC SRES emissions scenarios, as simulated by HadCM3.

Seven GCMs: SRES A1B = scenario set based upon the IPCC SRES A1B emissions scenario, as simulated by the seven GCMs listed above.

Table 2.1 (cont.) Summary of studies and findings of the QUEST-GSI project.

Reference	Hydrological model	Catchment(s)	Scenarios sets employed*see above	Additional information / key findings
Nóbrega *et al.* (2011)	MGB-IPH – large-scale, distributed model.	Rio Grande, Brazil (145,000 km²)	i) HadCM3 GCM: 1–6 °C ii) HadCM3 GCM: SRES A1B, B1, B2, A2 iii) Seven GCMs: 2 °C iv) Seven GCM: SRES A1B	Using HadCM3 climate scenario data, mean annual discharge is projected to increase by 8% – 51% under the 1–6 °C prescribed warming scenarios, and 5% – 10% under the SRES emissions scenarios. The magnitude of uncertainty is much greater under the seven GCM scenario sets. Choice of GCM impacts the direction of changes in average, high and low flows, and pattern of intra-annual changes. Mean discharge changes by between -28% and +14% for the A1B scenario, and -20% and +18% for 2 °C warming.
Xu *et al.* (2011)	AV-SWAT-X 2005	Xiangxi (Yangzte tributary) and Huangfuchuan, (Yellow tributary) China	i) HadCM3 GCM: 1–6 °C ii) HadCM3 GCM: SRES A1B, B1, B2, A2 iii) Seven GCMs: 2 °C iv) Seven GCMs: SRES A1B	For the 1–6 °C HadCM3 scenarios, near-linear increases in mean annual river discharge are projected for both basins (~+10% per +1 °C). Increases are also projected for the seven GCMs under the 2 °C and SRES scenarios, with the exception of a -2% decrease for one GCM for the River Xiangxi. There are substantial disparities in the magnitude of projected changes in mean annual, mean monthly and high and low flows across the seven GCMs. e.g. for the River Xiangxi, changes in high flows of -1 to +41% for SRES A1B.
Kingston and Taylor (2010)	AV-SWAT-X 2005	River Mitano (Nile tributary), Uganda (2098 km²)	i) HadCM3 GCM: 0.5–6 °C ii) Seven GCMs: 2 °C	For the 0.5–6 °C scenarios, annual discharge shows a non-linear response to increasing warming. For the 2 °C scenarios, choice of GCM impacted the direction and mean monthly pattern of projected changes in rainfall and hence river discharge. Parameter uncertainty investigated by varying the ten most sensitive parameters by ±10% and re-running the model for the baseline and HadCM3 2 °C scenario – found to impart little uncertainty.
Arnell (2011)	Cat-PDM – conceptual model	6 UK catchments (from 74 to 1200 km²)	i) HadCM3 GCM: 0.5–6 °C ii) Scenarios for an ensemble of 21 IPCC AR4 GCMs, for 2 °C prescribed warming	Some catchments show non-linear changes in runoff with increasing warming. There is a large spread in runoff response across the 21 GCM scenarios, largely due to inter-GCM differences in rainfall projections. Parameter uncertainty investigated by identifying, for each catchment, 100 parameter sets with "good" fits for the calibration period and using these for the HadCM3 2 °C scenario. Impact on percentage changes in mean winter/ spring runoff was negligible; more of an effect seen in summer/ autumn.

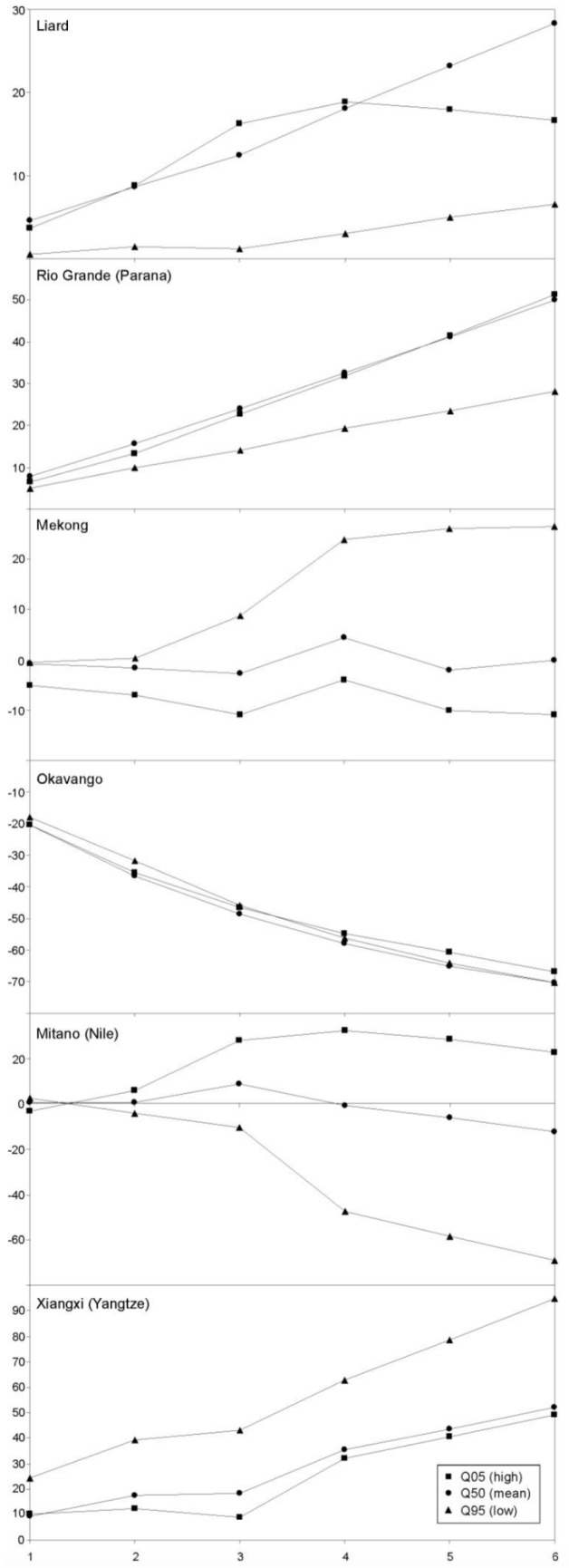

Figure 2.4. Projected 30-year change in river flow (% change from 1961–1990 baseline) for six QUEST-GSI study basins as a function of global mean temperature increase, with driving climate data from the HadCM3 GCM. Source: Todd et al. (2011).

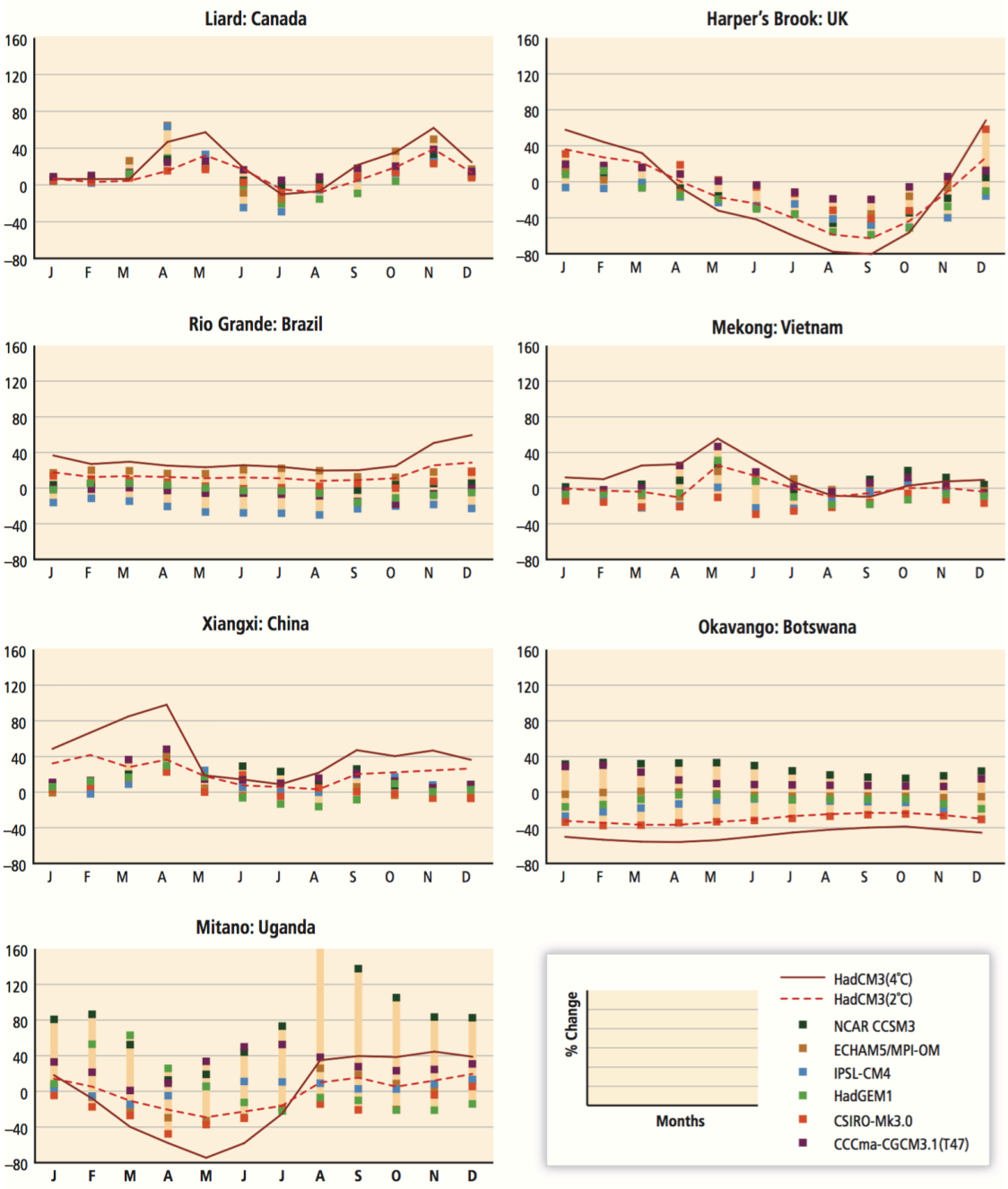

Figure 2.5. 'Change in mean monthly runoff across seven climate models in seven catchments, with a 2°C increase in global mean temperature above 1961–1990 (Kingston and Taylor, 2010; Arnell, 2011; Hughes et al., 2011; Kingston et al., 2011; Nobrega et al., 2011; Thorne, 2011; Xu et al., 2011). One of the seven climate models (HadCM3) is highlighted separately, showing changes with both a 2°C increase (dotted line) and a 4°C increase (solid line).' Source (figure and caption): Jiménez Cisneros et al. (2014: 245).

For the Rio Grande (Nóbrega *et al.*, 2011) and River Xiangxi (Xu *et al.*, 2011), differences in hydrological projections between the emissions scenarios were relatively minor (e.g. increases in mean discharge relative to the baseline of 5 to 10% and 13 to 17%, respectively).

Differences were more substantial for the River Huangfuchuan (Xu *et al.*, 2011), however (e.g. increases in mean discharge of 73 to 121%). This demonstrates that, as with other sources of uncertainty, the magnitude of emissions scenario uncertainty can vary considerably between catchments. Nevertheless, choice of GCM (for climate scenario generation) was found to be a greater source of uncertainty in all three catchments. This is generally consistent with the findings of other studies (e.g. Arnell, 2003; Prudhomme *et al.*, 2003; Arnell, 2004; Wilby and Harris, 2006; Graham *et al.*, 2007a; Prudhomme and Davies, 2009b), although some have found emissions- and GCM-uncertainty to be of a similar magnitude (e.g. Zierl and Bugmann, 2005). GCM uncertainty is discussed in the next section.

For IPCC Assessment Report 5 (AR5), a new generation of scenarios was developed, called Representative Concentration Pathways (RCPs) (Moss *et al.*, 2010; van Vuuren *et al.*, 2011; Stocker *et al.*, 2013). Four pathways were produced, each named according to their approximate radiative forcing level (in watts per square metre) in 2100: RCP2.6, RCP4.5, RCP6 and RCP8.5 (Figure 2.6a). For example, RCP8.5 has a radiative forcing impact of 8.5 watts per square metre in 2100. Data available for each RCP include: land-use data; emissions data for GHGs, aerosols and chemically active gases; and atmospheric concentrations of GHGs, aerosols and chemically active gases (van Vuuren *et al.*, 2011). RCP2.6 and RCP8.5 represent low and high emissions scenarios, respectively, whilst RCP4.5 can be considered an intermediate/mid-range emissions scenario (Moss *et al.*, 2010; van Vuuren *et al.*, 2011). Figure 2.6b provides projections for the global annual mean surface air temperature anomaly generated using the RCP scenarios.

Unlike the SRES scenarios, for which each emissions scenario was based upon a different socio-economic storyline, the RCP scenarios are not associated with unique socio-economic scenarios (Moss *et al.*, 2010). Instead, it is recognised that each radiative forcing trajectory could result from a range of different socio-economic, technological and policy futures (van Vuuren *et al.*, 2011). The four RCPs were selected to be both plausible and representative of the range of emissions and concentrations scenarios published in the existing literature (van Vuuren *et al.*, 2011).

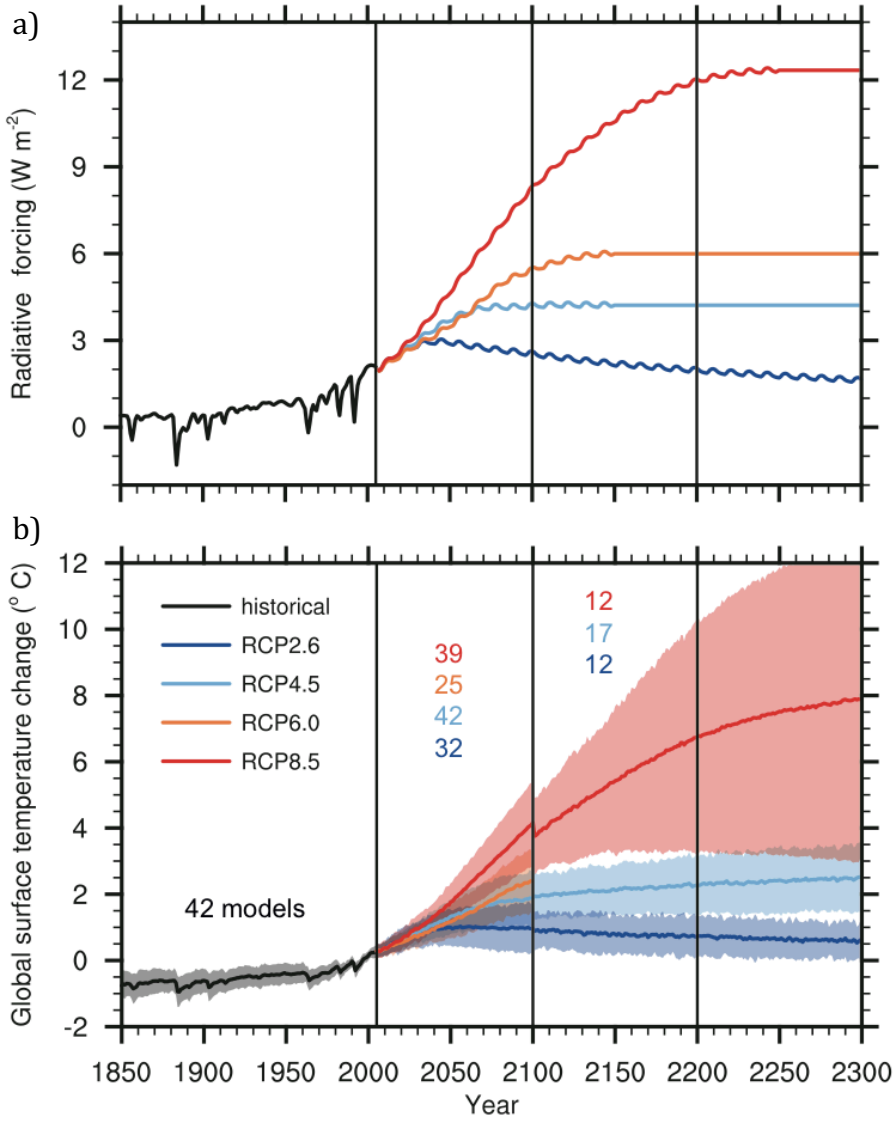

Figure 2.6. The RCP scenarios. (a) 'Total global mean radiative forcing for the four RCP scenarios based on the Model for the Assessment of Greenhouse-gas Induced Climate Change (MAGICC) energy balance model. Note that the actual simulated forcing differs slightly between models.' (b) 'Time series of global annual mean surface air temperature anomalies (relative to 1986–2005) from RCP concentration-driven experiments. Projections are shown for each RCP for the multi-model mean (solid lines) and ±1.64 standard deviation (5 to 95%) across the distribution of individual models (shading), based on annual means. The 1.64 standard deviation range based on the 20 yr averages 2081–2100, relative to 1986–2005, are interpreted as likely changes for the end of the 21st century. Discontinuities at 2100 are due to different numbers of models performing the extension runs beyond the 21st century and have no physical meaning. Numbers in the same colours as the lines indicate the number of different models contributing to the different time periods.' Source (figure and caption): Stocker et al. (2013: 89).

For running the current generation of climate models, the RCPs provide more detailed information than the SRES scenarios (van Vuuren *et al.*, 2011). In particular, the RCPs provide emissions and concentrations for a greater number of reactive gases and aerosol precursor compounds, and land use and emissions data are mostly available at a 0.5° × 0.5° spatial resolution (a coarser resolution is used for well-mixed gases) (van Vuuren *et al.*, 2011). In contrast, for the SRES scenarios, spatially explicit land cover scenarios were not developed and emissions were provided for four world regions (as well as in the form of global totals) (IPCC, 2000). This thesis makes use of the RCP4.5 climate scenario in Chapter 6.

2.5.2. GCM uncertainty

Although GCMs have improved considerably over the last two decades, they remain a major source of uncertainty in climate change impact assessments. Different GCMs represent the climate system in different ways, incorporating different components of the global climate system and using varied process descriptions, numerical equations, parameterisations and spatial resolutions (Meehl *et al.*, 2007b; Flato *et al.*, 2013). Consequently, climate projections for the same forcing differ between GCMs. Moreover, there is greater inter-GCM variation in projections of precipitation than for temperature (Meehl *et al.*, 2007b), with important implications for hydrological impact assessments (Todd *et al.*, 2011).

The evaluation and comparison of GCMs developed by modelling groups from around the world and the use of GCM outputs for climate impact and uncertainty assessments have been greatly aided by successive phases of the Coupled Model Intercomparison Project (CMIP; Meehl *et al.*, 2007a; Taylor *et al.*, 2012). CMIP was initiated in 1995 and is an international, co-ordinated effort to collate and analyse the output of numerous GCMs for a consistent set of climate model experiments (Meehl *et al.*, 2005). For each successive phase of CMIP, an increasing number of standard climate model experiments have been promoted and the number of GCMs taking part has increased. Whilst less than 30 models contributed to CMIP Phase 3 (CMIP3) (Meehl *et al.*, 2007a), over 50 models participated in CMIP Phase 5 (CMIP5) (Taylor *et al.*, 2012). The CMIP3 multimodel dataset (Meehl *et al.*, 2007a) provided the basis for model projections analysed in IPCC AR4, whilst both CMIP3 and CMIP5

(Taylor *et al.*, 2012) contributed greatly to IPCC AR5 (Flato *et al.*, 2013). The CMIP3 climate change experiments employed the SRES emissions scenarios (Meehl *et al.*, 2007a), whereas CMIP5 climate change projections are driven by concentration or emissions scenarios consistent with the RCPs (Taylor *et al.*, 2012). The models used to generate the RCP-driven temperature anomaly time series in Figure 2.6.b are therefore from CMIP5.

Some of the CMIP5 models include biogeochemical cycles such as interactive carbon cycles and are sometimes referred to as Earth System Models (ESMs) rather than GCMs (Taylor *et al.*, 2012). However, for simplicity in this thesis, the term GCM is used to encompass ESMs as well, a convention previously adopted by Ho *et al.* (2016).

Figure 2.7 provides a visualisation of the cascade of uncertainty in projections of global mean surface air temperature using simulations from CMIP5. It attempts to portray the time evolution and relative importance of different sources of uncertainty. The top layer indicates the uncertainty associated with choice of RCP scenario; the middle layer represents the different responses of the GCMs to the RCPs (Hawkins, 2014). The lowest layer illustrates the role of internal climate variability by displaying, for those GCMs where such results are available, multiple realisations of the same forcing pathway (Hawkins, 2014), produced using, for example, different initial conditions (Taylor *et al.*, 2012). Uncertainty in model response is more important in the near-term, but RCP uncertainty dominates by 2080–2099. The relative importance would likely differ for other climate variables.

Assessment of inter-GCM related uncertainty in hydrological projections under climate change is commonly undertaken by driving a hydrological model with climate projections derived from multiple GCMs for the same GHG or prescribed warming scenario(s), and then comparing the results (e.g. Maurer and Duffy, 2005; Buytaert *et al.*, 2009; Jackson *et al.*, 2011; Todd *et al.*, 2011). GCM structure has frequently been found to be a source of considerable uncertainty, and in studies that have investigated several sources, it has repeatedly been found to be the greatest (e.g. Prudhomme *et al.*, 2003; Wilby and Harris, 2006; Graham *et al.*, 2007a; Graham *et al.*, 2007b; Minville *et al.*, 2008; Prudhomme and Davies, 2009b; Arnell, 2011;

Crosbie *et al.*, 2011; Gosling *et al.*, 2011; Kingston *et al.*, 2011; Todd *et al.*, 2011). Choice of GCM has been found to impact the magnitude, intra-annual temporal pattern, and sometimes even the direction of projected changes in precipitation and, when climate projections are incorporated within hydrological models, in river discharge and other hydrological variables. Consequently, there is increasing recognition that a multi-model ensemble approach should be taken, in which the climate projections of several GCMs are used in order to provide a better indication of the range of potential future impacts.

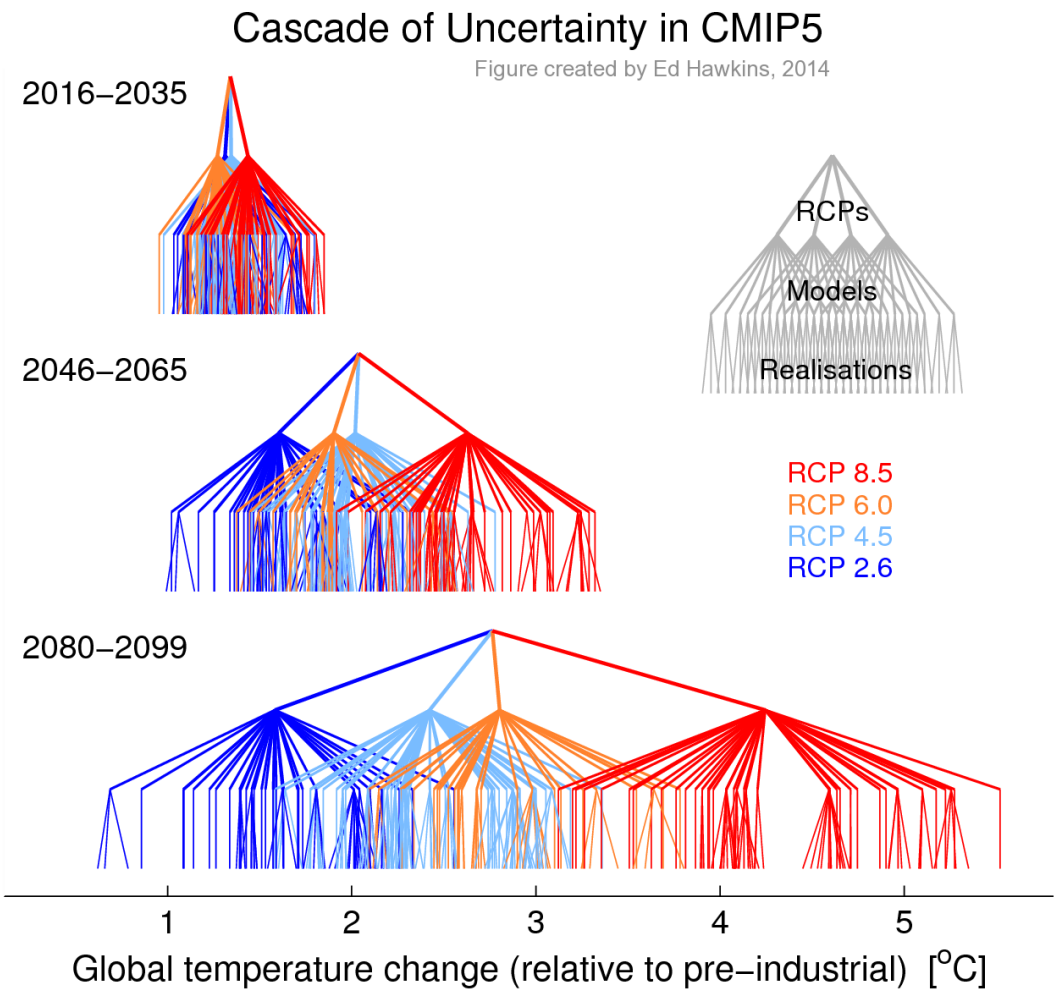

Figure 2.7. 'The 'cascade of uncertainty' in global mean surface temperature from the CMIP5 simulations for different time periods as labelled. The three levels of the pyramid highlight the uncertainty due to the choice of RCP, GCMs and realisation of climate variability. Unfortunately not all the simulations have multiple realisations, resulting in a vertical line in the lowest layer. The intersection on the top row for each time period is the multi-scenario, multi-model, multi-realisation mean.' Source (figure and caption): Hawkins (2014).

A multi-model approach was used within the QUEST-GSI project (Todd *et al.*, 2011). For each basin included in the project, climate scenarios were generated for a 2 °C increase in global mean air temperature (and in some cases also for the SRES A1B emissions scenario) for an ensemble comprising seven CMIP3 / IPCC AR4 GCMs (see Table 2.1). GCM-related uncertainty was found to be considerable and stemmed largely from inter-GCM differences in projections of precipitation (Todd *et al.*, 2011). For six of the study basins, Figure 2.8 demonstrates the variability in projected percentage changes in low, mean and high flows under 2 °C prescribed warming across seven GCMs. For several catchments (e.g. Mekong – SE Asia, Rio Grande – South America, and Okavango – Southern Africa) there was no consensus between the GCMs on the projected direction of change in mean annual precipitation, resulting in uncertainty in the direction of simulated change in mean river flow. For other catchments and regions, whilst there was more consistency in the direction of projected changes in mean annual precipitation, uncertainty in the magnitude of changes (both at an annual and intra-annual scale) remained high.

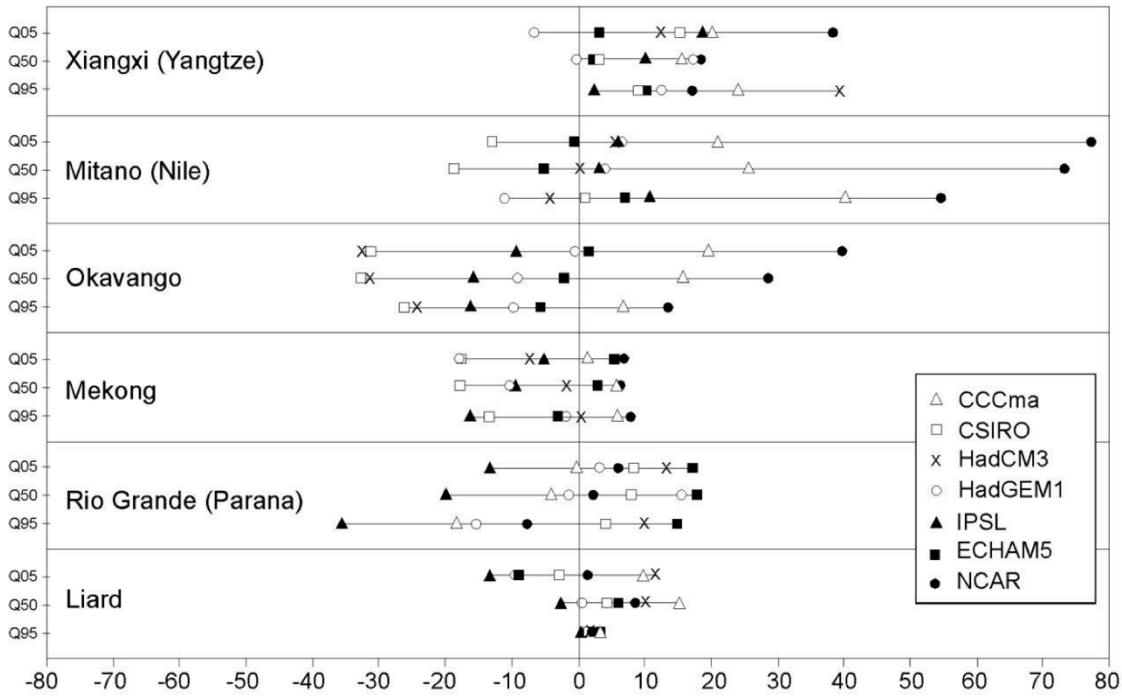

Figure 2.8. Envelope of projected changes (from the 1961–1990 baseline) in metrics of river flow for six QUEST-GSI study basins, for a scenario of 2 °C prescribed warming, as projected by seven GCMs. For each catchment, the top, middle and bottom lines represents Q5, Q50 and Q95 flows (i.e. exceedance in % of months over the simulated 30-year period). Source: Todd et al. (2011).

For example, for the Liard Basin (Canada), all GCMs projected increases in mean annual precipitation (ranging from 1% to 22%) and simulated changes in mean flow ranged from –3% to +15%. Furthermore, with the exception of Q95 for the Liard River, none of the Q5, Q50 or Q95 change indicators for the catchments in Figure 2.8 show a consistent direction of change across all GCMs. Figure 2.5 demonstrates notable inter-GCM differences in the projected magnitude and direction of changes in mean monthly discharge. The studies of the QUEST-GSI project therefore demonstrate the importance of using climate projections from multiple GCMs when assessing potential hydrological impacts of climate change.

2.5.3. Downscaling

In order to be used as input to a hydrological model, GCM climate projections must first be downscaled to a finer spatial (horizontal) and temporal resolution that is appropriate for hydrological modelling. Numerous downscaling techniques have been developed, all of which introduce additional uncertainty to climate impact assessment results. The main techniques can be divided into dynamical downscaling and empirical/statistical downscaling approaches (Prudhomme *et al.*, 2002; Bates *et al.*, 2008; Flato *et al.*, 2013). With dynamical downscaling, outputs from a GCM are applied to the lateral boundaries of a Regional Climate Model (RCM) that has a higher horizontal resolution and is applied over a smaller spatial domain that encompasses the area of interest (Xu *et al.*, 2005). For example, for the UK Climate Projections 2009 (UKCP09), the Met Office Hadley Centre HadRM3 RCM was driven by outputs from the HadCM3 GCM that had a horizontal spatial resolution of approximately 300 km × 300 km (Murphy *et al.*, 2009). This provided climate projections for the UK with a horizontal spatial resolution of approximately 25 km × 25 km, which is more amenable for use in hydrological (and other) impact assessments (e.g. Burke, 2004; Thompson, 2012). A limitation of dynamical downscaling is that it is computationally expensive, therefore limiting the ease with which data can be generated for multiple scenarios (Mearns *et al.*, 2003).

Conversely, empirical/statistical downscaling techniques are relatively computationally inexpensive (von Storch *et al.*, 2000; Mearns *et al.*, 2003; Wilby *et al.*, 2004). The simplest of empirical spatial downscaling techniques involve the

spatial interpolation of grid-based GCM outputs (Wilby *et al.*, 2004). More complex statistical downscaling techniques use statistical relationships between large-scale atmospheric variables and local climate in order to derive higher resolution (local-scale) data from GCM outputs (Prudhomme *et al.*, 2002; Prudhomme and Davies, 2009a). They rely on the unverifiable assumption that these relationships will remain the same under altered climate conditions in the future (Mearns *et al.*, 2003; Wilby *et al.*, 2004). Statistical downscaling techniques include the use of regression models, which employ linear and non-linear relationships to relate large scale and local climate variables, and weather generators, which replicate the statistical attributes of a local climate variable whilst introducing a stochastic element to the sequencing of events (von Storch *et al.*, 2000; Wilby *et al.*, 2004).

Downscaling may involve several stages. For example, one technique may be used for spatial downscaling, and then a different technique may be used for temporal downscaling (Prudhomme *et al.*, 2002; Todd *et al.*, 2011; Immerzeel *et al.*, 2012b). The downscaling process will often incorporate a form of bias-correction in order to correct for systematic biases in the GCM or RCM outputs. The simplest approach is to develop monthly change (or delta) factors between the GCM (or RCM) outputs for the baseline and outputs for the future scenario, and to then apply these change factors to the observed baseline data to form the scenario climate data (see for example Minville *et al.*, 2008; Dobler *et al.*, 2012). This is known as the 'change factor' or 'delta change' approach (Hay *et al.*, 2000; Dobler *et al.*, 2012). A variety of more complex techniques also exist, such as quantile-quantile mapping, in which cumulative distribution functions of observed and GCM or RCM simulated data for a historical period are used to develop transfer functions which are then applied to the simulated scenario climate data (see for example Goderniaux *et al.*, 2009; Dobler *et al.*, 2012).

Whilst the uncertainty in hydrological projections related to downscaling is not investigated within this thesis, it is important to acknowledge that downscaling method has previously been found to be a notable source of uncertainty by some studies (e.g. Wilby and Harris, 2006; Crosbie *et al.*, 2011), although others have obtained similar hydrological projections when using a range of statistical techniques and RCMs (e.g. Kay *et al.*, 2009).

2.6. Hydrological modelling of the impacts of climate change

As outlined above, the most common method for assessing the potential hydrological impacts of climate change is to run the downscaled climate output of one or more GCMs through a hydrological model and to compare the hydrological model output, such as river discharge, with that simulated by the model under baseline climate conditions. This section provides an overview of various sources of uncertainty associated with hydrological modelling in climate change impact assessments. Since these sources of uncertainty are relevant to hydrological modelling in general, they are discussed both in relation to the wider hydrological modelling literature and within the context of climate change impact assessments. Furthermore, whilst the concepts discussed below are provided specifically in the context of hydrological modelling, it is worth noting that some of the concepts, such as model structural uncertainty, parameterisation uncertainty, and input data uncertainty, are common to environmental models in general (e.g. Mulligan and Wainwright, 2004). Climate change impact assessments that employ other types of environmental impact model, such as vegetation models (e.g. Cramer *et al.*, 2001) and crop models (e.g. Olesen *et al.*, 2007), are therefore subject to some similar sources of uncertainty.

2.6.1. Hydrological model classification

As with many environmental models, such as climate models, the number and complexity of hydrological model codes available has increased substantially over recent decades alongside vast increases in computer power (Singh and Woolhiser, 2002; Mulligan, 2004; Beven, 2012). There is now a large number of hydrological model codes, with different capabilities, data requirements and computational requirements. The majority of hydrological model codes are designed for the development of catchment-scale hydrological models that employ a specified drainage area as the hydrological unit to be modelled. In contrast, macro-scale or global hydrological model (GHMs) simulate land surface hydrological dynamics over very large spatial domains, from the continental-scale to the entire global land surface (Arnell, 1999; Gosling and Arnell, 2011). Such models tend to use large grid sizes and simplified process descriptions.

In addition to distinguishing between model codes that are intended for catchment-scale or macro-scale modelling, hydrological models can be classified according to a number of factors (Figure 2.9), including: i) whether they are deterministic or stochastic, ii) the degree of process representation and iii) the degree of spatial representation (Refsgaard, 1996; Jones, 1997; Grayson and Blöschl, 2000; Ward and Robinson, 2000; Mulligan, 2004). Deterministic hydrological models will consistently simulate the same output for a given input (Grayson and Blöschl, 2000; Ward and Robinson, 2000; Mulligan, 2004). In contrast, stochastic models incorporate an element of randomness through taking the probability distribution of selected meteorological or hydrological variables into account (Grayson and Blöschl, 2000; Ward and Robinson, 2000; Mulligan, 2004; Aronica and Candela, 2007). As noted by Grayson and Blöschl (2000) and Singh and Woolhiser (2002), the majority of hydrological models, including those used for scenario simulation, are deterministic. The hydrological models employed in this study are deterministic.

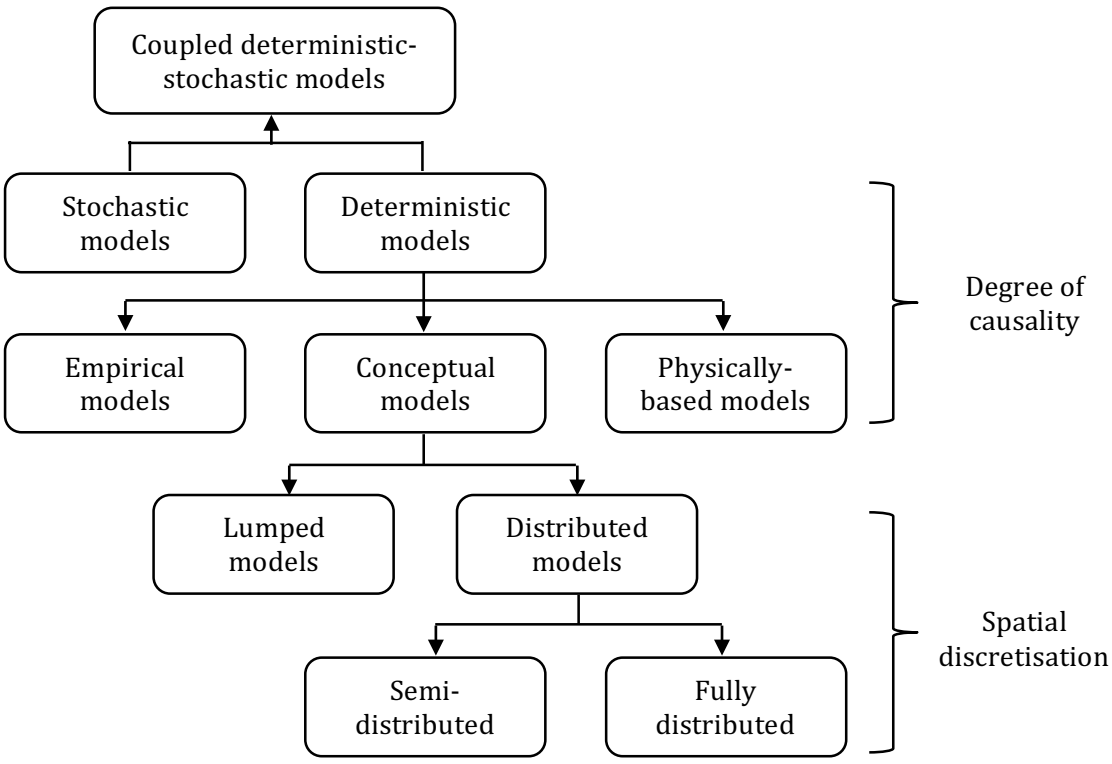

Figure 2.9. Classification of hydrological models. Adapted from: Jones (1997).

Based upon the degree to which hydrological processes are represented, hydrological models can be further classified into i) simple, empirical, black box models that take no account of physical processes, instead using patterns in observed data, ii) conceptual models, in which physical processes are represented in a simplified manner and iii) complex, physically-based models, in which hydrological processes are modelled through the use of fundamental scientific laws (Mulligan, 2004). Since empirical models rely upon relationships between observed catchment variables (e.g. the simple rainfall-runoff relationship), they have limited capability of simulating variables outside of the conditions under which the observed data were collected (Mulligan and Wainwright, 2004). They are therefore not widely used in hydrological scenario impact assessments, although examples do exist (e.g. Zeng *et al.*, 2012).

Instead, conceptual or physically-based hydrological models are much more widely used for scenario impact assessments. Conceptual hydrological models commonly represent a catchment using a series of stores or reservoirs, with simple mathematical equations governing the flows between stores. These are sometimes referred to as bucket models. Typical examples of conceptual models include the Stanford Watershed Model (Crawford and Linsley, 1966), HBV (Bergström, 1995), TANK model (Sugawara, 1995) and SLURP (Kite, 1995; Kite, 2007), the last of which is discussed in Section 2.6.3.2. Examples of some physically-based model codes include THALES (Grayson *et al.*, 1992), MODFLOW (a groundwater model; Harbaugh *et al.*, 2000), SHETRAN (Ewen *et al.*, 2000) and MIKE SHE (Refsgaard and Storm, 1995; Graham and Butts, 2005). SHETRAN and MIKE SHE were both based upon the Système Hydrologique Europeén (SHE) (Abbott *et al.*, 1986a, b). MIKE SHE, which actually incorporates both physically-based and conceptual approaches and is employed in this thesis, is described in detail in Section 2.6.3.1.

Hydrological models can also be classified according to their degree of spatial representation (Refsgaard, 1996). Lumped models treat the basin as a homogeneous whole, meaning that inputs, outputs and parameters are spatially averaged (Muzik, 1996; Refsgaard, 1996; Jones, 1997). Examples of lumped model codes, or at least those offering a lumped version, that are still in common use include HBV (Bergström, 1995), IHACRES (Jakeman *et al.*, 1990) and Sacramento

(Burnash *et al.*, 1984). In contrast to lumped models, semi-distributed models divide the catchment into lumped sub-units that have separate inputs and parameters, and for which flow contributions are calculated independently (Jones, 1997; Kite, 2007). For some models, the catchment may be divided into sub-catchments (sub-basins) based upon topography and hence drainage patterns (e.g. the DPHM-RS model; Biftu and Gan, 2001). In others, the catchment is divided into hydrologically similar units, sometimes referred to as Hydrological Response Units (HRUs), based upon a combination of factors, such as topography, land use and soil type (Kite and Pietroniro, 1996). For example, in the Soil and Water Assessment Tool (SWAT) model (Arnold *et al.*, 1998), a catchment is first divided into sub-basins based upon topography; each of these is then subdivided into a series of HRUs according to unique soil-land use combinations, with the possibility in later versions of SWAT of also taking land management and slope into account (Douglas-Mankin *et al.*, 2010). Within distributed models, the model domain is discretised horizontally into a network of grid squares or elements, each of which is assigned its own characteristics (Refsgaard, 1997; Grayson and Blöschl, 2000).

Empirical models are usually lumped, conceptual models are generally semi-distributed and physically-based models tend to be distributed (Mulligan, 2004). The development of physically-based, distributed models has been aided by improvements in data availability and computer technology (Refsgaard *et al.*, 2010). Some advanced hydrological models now offer the flexibility of being modular, with the option of including or excluding particular system components (modules) and the option of representing different processes at different levels of complexity and spatial resolution. These can be employed to reflect factors such as data availability and the processes of interest to a specific study. A typical example of such a model is MIKE SHE (Graham and Butts, 2005), which is discussed further in Section 2.6.3.1. A MIKE SHE model of the Mekong is developed in Chapter 4.

Table 2.2 provides a summary of some widely used hydrological model codes, demonstrating the variety available. All of these models were first developed more than ten years ago (and in some cases many more) and have undergone significant development over the years. The majority of these model codes have therefore had multiple versions, with some having several versions currently in common use.

Table 2.2. Summary of a selection of widely used hydrological models.

Model name	Key reference(s)	Process representation	Spatial representation	Further details
HBV	Bergström (1995); Lindstöm *et al.* (1997)	Conceptual.	Lumped and semi-distributed versions of HBV are available. The semi-distributed version employs sub-basin division. Each sub-basin is divided into elevation bands, vegetation and snow classes.	Used for runoff simulation. HBV comprises a snow routine, soil moisture function, response function (which controls flow between the soil and saturated zone stores) and routing routine.
Mac-PDM	Arnell (1999); Gosling and Arnell (2011)	Conceptual.	Mac-PDM.09 (the latest version) is a distributed, global hydrological model that operates on a gridded basis, usually a grid cell size of 0.5° × 0.5°.	Mac-PDM simulates runoff on a gridded basis. Calculations are undertaken for each grid cell for each time step. No river routing routine – runoff from relevant cells is aggregated for catchment-scale analyses.
		Greater detail provided in Section 2.6.3.3.		
MIKE SHE	Refsgaard and Storm (1995); Refsgaard *et al.* (1995); Graham and Butts (2005)	Physically based, but with conceptual options available for some model components.	Lumped, semi-distributed and distributed options for various modules. It is possible to employ different approaches for different components.	Modular structure with components for: interception/ evapotranspiration, overland flow, unsaturated zone, saturated zone and channel flow.
		Greater detail provided in Section 2.6.3.1.		
MODFLOW	McDonald and Harbaugh (1988); Harbaugh (2005)	Physically based – MODFLOW is a three-dimensional finite difference groundwater model.	Distributed on a gridded basis.	Developed by the US Geological Survey (USGS). MODFLOW has a modular program structure. According to Refsgaard *et al.* (2010) MODFLOW is the most widely used groundwater model for both research and practical applications.
Sacramento Soil Moisture Accounting (SAC–SMA)	Burnash *et al.* (1984); Burnash (1995)	Conceptual.	Both lumped and semi-distributed versions available (e.g. Ajami *et al.*, 2004). In the semi-distributed version, a basin is divided into sub-basins based on topography.	Used for operational forecasting by the US National Weather Service (NWS). SAC–SMA contains two soil layers: an upper and a lower zone. Each layer includes tension and free water storages.

Table 2.2 (cont.) Summary of a selection of widely used hydrological models.

Model name	Key reference(s)	Process representation	Spatial representation	Further details
SLURP	Kite (1995); (Kite, 2007)	Conceptual.	Semi-distributed. Basin first divided into sub-basins based on topography. Each sub-basin then divided into units of different land use.	Each land use unit in each sub-basin is represented by four stores/reservoirs: canopy storage, snow storage, fast storage and slow storage.
		Greater detail provided in Section 2.6.3.2.		
SWAT (Surface Water Assessment Tool)	Arnold *et al.* (1998); Douglas-Mankin *et al.* (2010)	Quasi-physical (e.g. Saraswat and Pai, 2011). Described as conceptual by Arnold *et al.* (1998), but physically-based by Douglas-Mankin *et al.* (2010). SWAT is also classed inconsistently within the wider literature and is sometimes called a conceptual, physically based model (e.g. El-Nasr *et al.*, 2005).	Semi-distributed. A catchment is first divided into topographically-based sub-catchments; these are then subdivided into Hydrological Response Units (HRUs) of uniform soil, land use and land management characteristics, as well as slope in later versions of SWAT.	As well as runoff modelling, SWAT can be used for sediment and nutrient modelling. SWAT can also simulate a variety of agricultural structures and practices, such as tillage, subsurface drainage and fertiliser/manure application.
TOPMODEL	Beven and Kirkby (1976, 1979); Beven *et al.* (1995); Beven and Freer (2001a)	Quasi-physical (e.g. Lamb *et al.*, 2000). Described by Beven and Kirkby (1976, 1979) (and subsequently others) as physically-based since its parameters could in theory be assessed in the field and it has some physical basis. However, also often classed as conceptual (e.g. Mulligan, 2004; Refsgaard *et al.*, 2010) since its process descriptions are more conceptual rather than physics-based.	Semi-distributed. TOPMODEL uses a distribution function approach. An index of hydrological similarity is used to emulate a spatially distributed response. The index is computed across the catchment based on topography and soil data; formulation of the index varies between model versions. Points with the same index value are treated as a response unit.	Used for runoff simulation. Beven *et al.* (1995) describe TOPMODEL as more of a collection of concepts than a single model structure.

2.6.2. Hydrological model structure uncertainty

As highlighted above, there are a large number of hydrological model codes, whose structures can differ greatly in terms of how they represent hydrological processes. Furthermore, when developing a model of a particular catchment using a selected model code, there will often be alternative model structures that could be adopted (Butts *et al.*, 2004; Booij, 2005). For example, in a semi-distributed or distributed hydrological model, there is no definitive discretisation for a given catchment; rather, the division of the catchment may be determined by a combination of subjective choices made by the modeller (and the software employed to aid discretisation, where applicable). Similarly, there may be a range of numerical engines available for a given model component, each with their own benefits and disadvantages (e.g. Graham and Butts, 2005). Different model codes and structures may perform satisfactorily during the calibration and validation stages of model development, when they are driven with past climate data and their simulated output (e.g. river discharge) is compared with observations. However, during climate change scenario modelling, different model structures may respond differently to the same climatic perturbations, and the results of several models may be equally plausible (Ludwig *et al.*, 2009).

The problem of there being multiple possible model structures (or parameter sets – see Section 2.6.5) that display acceptable performance against observations has been termed 'equifinality' (see for example Beven, 1993; Beven and Freer, 2001b; Beven, 2002). Beven (2001; 2002) emphasises that the problem of equifinality is different from that of non-identifiability, which relates to difficulty in trying to find an 'optimal' model according to specific model performance criteria. Instead, the concept of equifinality signifies the recognition that there will always be a range of model structures that could simulate acceptable representations of available observations (Beven, 2002). This source of uncertainty is particularly significant as many studies use only one model code and hence only one model structure.

A relatively small number of studies have investigated the uncertainty introduced into hydrological projections under climate change through the use of different model codes or structures. A selection of these are summarised in Table 2.3.

Table 2.3. Summary of a selection of studies that investigate inter-hydrological model uncertainty in climate change impact assessments.

Reference	Study area	Outline	Key findings
Wilby and Harris (2006)	River Thames, UK (8,600 km^2)	Assessed multiple sources of uncertainty in low flow projections. Used a Monte Carlo approach and an ensemble of four GCMs, two IPCC SRES emissions scenarios (A2 and B2), two statistical downscaling techniques, two hydrological model structures and alternative sets of hydrological model parameters.	GCM structure found to be the greatest source of uncertainty, followed by downscaling method, hydrological model structure, hydrological model parameters and emissions scenario. Systematic differences in results were found between CATCHMOD (a water balance model) and REGMOD (a simple linear regression model), attributed to inclusion of soil moisture accounting in CATCHMOD.
Jiang *et al.* (2007)	Dongjiang basin, South China (25,325 km^2)	Compared changes in hydrological conditions simulated by six conceptual water balance models (Thornthwaite–Mather, Vrije Universitet Brussel, Xinanjiang, Guo, WatBal and Schaake) under multiple hypothetical climate change scenarios.	All hydrological models performed well under historical climate conditions. However, under climate change scenarios, the models show considerable differences in simulated changes in soil moisture, evapotranspiration and runoff. The nature of these differences depends on the variable, climate scenario and season.
Ludwig *et al.* (2009)	Ammer watershed, Germany (709 km^2)	Compared the use of three hydrological models of varying complexity (PROMET, a spatially distributed model; HYDROTEL, a semi-distributed model and HSAMI a lumped, bucket-type conceptual model) in a climate change impact assessment for 2071–2100.	Under climate change, the HSAMI model produced runoff far below plausible values due to large overestimation of evapotranspiration. The other two models simulated plausible results and behaved comparably. However, there were some important differences in the spatial and seasonal patterns of change.
Bae *et al.* (2011)	Chungju Dam basin, Korea (6661 km^2)	Employed 13 GCMs, three emissions scenarios, three semi-distributed hydrological models (PRMS, SLURP and SWAT) and different potential evapotranspiration (PET) computation methods (detailed further in Section 2.6.6.1).	Although GCM structure was found to be the greatest source of uncertainty overall, monthly and seasonal runoff changes were significantly affected by choice of hydrological model and PET method. The range of relative changes (magnitude of uncertainty) was greater during the dry season (low flows) than the wet season.
Crosbie *et al.* (2011)	Three sites in Australia with contrasting hydro-meteorology	Quantified the relative uncertainty in groundwater recharge projections contributed by multiple GCMs (five), downscaling methods (three) and four hydrological models: WAVES-G (physically based with dynamic vegetation regrowth), WAVES-C (a simplified version of WAVES-G), HELP (multi-layered bucket model), SIMHYD (simple lumped conceptual).	Choice of GCM found to be the greatest source of uncertainty, with a median inter-GCM range (between the max. and min. future recharge projections) of 53% of the historical recharge for a given downscaling method and hydrological model. Downscaling method had a median range of 44%. The median inter-hydrological model range was 24%; differences between the models were not consistent across all sites.

Table 2.3 (cont.) Summary of a selection of studies that investigate inter-hydrological model uncertainty in climate change impact assessments.

Reference	Study area	Outline	Key findings
Najafi *et al.* (2011)	Tualatin River Basin, USA (1847 km^2)	Employed one semi-distributed (PRMS) and three lumped hydrological models (Thornthwaite-Mather, HYMOD, SAC-SMA), each calibrated using different objective functions to assess parameter uncertainty. These were driven with climate scenarios from eight GCMs and two emissions scenarios.	Uncertainties in river flow projections associated with choice of GCM are more significant than those associated with hydrological model structure and parameterisation. However, inter-hydrological model differences were notable during the summer (dry season). Choice of objective function also impacted the magnitude of dry season runoff changes.
Poulin *et al.* (2011)	Ceizur river basin, Quebec, Canada (6954 km^2)	Two climate scenarios are employed, as well as two hydrological model codes: HSAMI, a lumped, reservoir-based conceptual model and HYDROTEL, a spatially distributed, physically-based model code. Multiple (68) parameter sets are developed for each model code under recent past climate conditions and employed under modified climate conditions.	The impact of model structure uncertainty upon model projections (of streamflows, groundwater content and snow water equivalent) is greater than the effect of parameter uncertainty. Differences in results between the two model codes were larger than the largest envelope (spread of results) resulting from a single model code run with 68 parameter sets. Parameter uncertainty under modified climate is very similar to that obtained under recent past climate.
Gosling *et al.* (2011) (Part of the QUEST-GSI project)	Six QUEST-GSI catchments, including the Mekong Basin	Comparative analysis of projected impacts of climate change on river runoff simulated by Mac-PDM.09 (GHM, for global hydrological model) and six catchment-scale hydrological models (CHMs; each of a different catchment) for the consistent set of QUEST-GSI scenarios. Runoff from Mac-PDM.09 was aggregated over the relevant cells for each basin.	Differences in projected changes in mean annual runoff simulated by the GHM and CHM for a given GCM could be substantial, with GHM-CHM differences in high and low monthly runoff generally greater. However, inter-hydrological model uncertainty was relatively small compared to GCM-related uncertainty; the range of projections across the seven GCMs (for a given catchment / climate forcing) was consistently greater than GHM-CHM differences.
Hagemann *et al.* (2013)	Global land surface	Three GCMs and eight GHMs were used to assess the uncertainty in hydrological response to climate change at the global scale. All models were run at a 0.5° spatial resolution. Haddeland *et al.* (2011) previously found significant differences between the GHMs in simulated runoff and evapotranspiration under historical conditions.	The results show large differences in simulated runoff changes under climate change between the different GHMs. In some regions, the spread in projected changes resulting from choice of GHM is larger than the spread associated with choice of GCM, demonstrating that choice of impact model can be a considerable source of uncertainty. Inter-GHM differences can in part be attributed to different model formulations of evapotranspiration.

Table 2.3 (cont.) Summary of a selection of studies that investigate inter-hydrological model uncertainty in climate change impact assessments.

Reference	Study area	Outline	Key findings
Velázquez *et al.* (2013)	Two catchments: *au Saumon*, Canada (738 km^2); *Schlehdorf*, Germany (640 km^2)	For each catchment, an ensemble of four hydrological models (with varied spatial and temporal resolutions and differing levels of structural complexity) were employed to assess changes in river flow under climate change. These were: HSAMI (conceptual, lumped), HYDROTEL (conceptual, semi-distributed), WASIM-ETH (conceptual, fully-distributed) and PROMET (process-based, fully-distributed).	The largest relative difference between hydrological model outputs under climate change was seen in changes in low flows. For example, in the case of winter 2-yr return period 7-day low flow for *Schlehdorf*, median change values ranged from -20% to +20%, with two models projecting decreases and two models increases. Inter-model differences were statistically significant for most hydrological indicators in the case of *au Saumon* (including mean flow and summer low flow, when low flows are most severe).
Vansteenkiste *et al.* (2014)	Grote Nete catchment, Begium (385 km^2)	Five hydrological models with different spatial resolutions and process descriptions were employed to assess changes in river flows under dry, medium and wet climate scenarios. The models used were: NAM, PDM and VHM (all lumped, conceptual), WetSpa (intermediate detailed) and MIKE SHE (spatially distributed, physically-based). Impact of model calibration was assessed using manual and automatic calibration approaches for the VHM model.	All five models projected similar trends in peak flows changes, although PDM simulates systematically higher changes under wet winter scenario conditions. All models show reductions in low flows; however, the magnitude of reductions varies considerably between models. For example, under the dry scenario, reductions ranged from -60% (average decrease for return periods higher than 1 year) to -25%. Calibration approach for VHM did not significantly impact model results for peak flow, but low flow projections were highly influenced.

Results from these studies that are particularly worth drawing attention to include the finding that inter-hydrological model uncertainty is greater than parameterisation uncertainty (Wilby and Harris, 2006; Poulin *et al.*, 2011) and that choice of hydrological model can impact the magnitude and seasonal patterns of simulated changes in hydrological variables, sometimes substantially. These variables include river flow and surface runoff (e.g. Ludwig *et al.*, 2009; Gosling *et al.*, 2011; Velázquez *et al.*, 2013), groundwater recharge (Crosbie *et al.*, 2011) and soil moisture and evapotranspiration (Jiang *et al.*, 2007; Bae *et al.*, 2011). The majority of studies assessed either simulated changes at a single point (e.g. at a single gauging station in the case of river flow) or spatially averaged or lumped changes, for example in the case of changes in soil moisture and evapotranspiration (e.g. Jiang *et al.*, 2007). However, Ludwig *et al.* (2009) analysed the spatial patterns of changes in evaporation and runoff and found notable inter-hydrological model differences in spatial patterns of summer water shortages and spring flood intensity under climate forcing.

Several studies in Table 2.3 compared GCM uncertainty to inter-hydrological model uncertainty and found GCM uncertainty to be greater overall (e.g. Wilby and Harris, 2006; Bae *et al.*, 2011; Crosbie *et al.*, 2011; Gosling *et al.*, 2011; Najafi *et al.*, 2011). However, it is worth noting that usually a greater number of different GCMs than hydrological models are used. For example, Wilby and Harris (2006) employed four GCMs, whilst only two hydrological model codes were used. Similarly, for six study catchments, Gosling *et al.* (2011) used climate projections from seven GCMs, whilst the results of a single catchment model were compared to those of the Mac-PDM.09 GHM. The likely reason for this is that GCM outputs are routinely available, whereas hydrological model outputs are not and developing a new/alternative hydrological model can be a considerable undertaking. It is possible that the envelope of uncertainty associated with hydrological model structure would increase if further model codes were included in such inter-hydrological model comparisons. In support of this, in an intercomparison between eight GHMs using climate scenarios from three GCMs, Hagemann *et al.* (2013) found that the GHMs produced considerably different results, with the spread in the projected changes in runoff associated with the GHMs often comparable to that of the GCMs, and greater than that of the GCMs for some regions. Overall, the studies outlined in Table 2.3 highlight

that the impact of inter-hydrological model uncertainty can be notable and therefore merits further investigation, particularly considering that the majority of hydrological climate change impact assessments employ a single hydrological model.

2.6.3. Opportunity for an inter-hydrological model comparison

As outlined in Chapter 1, one objective of this study is to undertake an inter-hydrological model comparison between the climate change projections of river discharge/runoff for the Mekong River simulated by the pre-existing SLURP catchment model of the Mekong, the Mac-PDM.09 GHM and a MIKE SHE model of the Mekong developed specifically for this intercomparison. Section 2.6.3.1 provides an overview of the MIKE SHE modelling system. Development and details of the MIKE SHE model of Mekong are not provided here, however, but in Chapter 4. Sections 2.6.3.2 and 2.6.3.3 detail the SLURP and MacPDM.09 models, respectively.

As highlighted in Table 2.1, as part of the QUEST-GSI project, Gosling *et al.* (2011) undertook an inter-hydrological model uncertainty assessment. This included a comparison of the results of Mac-PDM.09 and SLURP for the Mekong River Basin under climate change. However, this analysis was limited to the outlet of each catchment, whilst several of the hydrological models, including the SLURP model of the Mekong, provided distributed responses in river flow from major sub-catchments. This thesis therefore extends this analysis for the Mekong through the inclusion of MIKE SHE in the intercomparison and by undertaking the intercomparison at multiple locations throughout the Mekong. This will provide an indication of the spatial variability in river flow changes and inter-hydrological model uncertainty under climate change.

2.6.3.1. MIKE SHE

The MIKE SHE model code was developed by DHI (formerly the Danish Hydraulic Institute) from the Système Hydrologique Europeén (SHE), which was created through a joint venture between DHI, the UK's Institute of Hydrology and the French environmental consultancy company SOGREAH (Abbott *et al.*, 1986a, b). In its

original formulation, MIKE SHE could be categorised as a deterministic, physically-based, distributed, hydrological model code (Graham and Butts, 2005). However, following extensive development since the late 1980s, it is now a highly flexible modelling system with the capability of representing processes at different levels of spatial resolution, and at different levels of complexity (Graham and Butts, 2005; Refsgaard *et al.*, 2010).

MIKE SHE has a modular programme structure, with components for each of the primary processes of the land phase of the hydrological cycle, including interception/evapotranspiration, snow melt, overland/channel flow, the unsaturated zone, the saturated zone and exchange between aquifers and rivers (Storm and Refsgaard, 1996). Channel flow is simulated using the MIKE 11 one-dimensional hydraulic model (Havnø *et al.*, 1995), with dynamic coupling between MIKE SHE and MIKE 11. Figure 2.10 provides a conceptual representation of the MIKE SHE model structure, including the processes that can be represented by the model. This schematic also shows the discretisation of a catchment horizontally into an orthogonal network of grid squares, as well as vertically into a series of horizontal layers below the ground surface when using a distributed process solution for groundwater simulation. However, it is also possible to employ a conceptual, semi-distributed process module for the saturated zone (as detailed in Section 4.2.5). Figure 2.11 depicts the numerical engines available for each module.

As demonstrated in Table 2.4, the MIKE SHE model code has been employed in a wide range of environments. The small (<50 km^2) catchments that MIKE SHE has been successfully applied to vary from low-lying wetland (Thompson *et al.*, 2004; Thompson *et al.*, 2009; House *et al.*, 2015) and upland catchments in the UK (Thompson, 2012), to a semi-arid shrubland catchment in California, USA (McMichael *et al.*, 2006), to a tropical, mountainous, flashy catchment in Hawaii (Sahoo *et al.*, 2006). The model code has also been applied to areas that are hundreds or thousands of square kilometres, in climates ranging from temperate (Henriksen *et al.*, 2003) to tropical monsoonal (Andersen *et al.*, 2001; Stisen *et al.*, 2008; Singh *et al.*, 2010; Singh *et al.*, 2011).

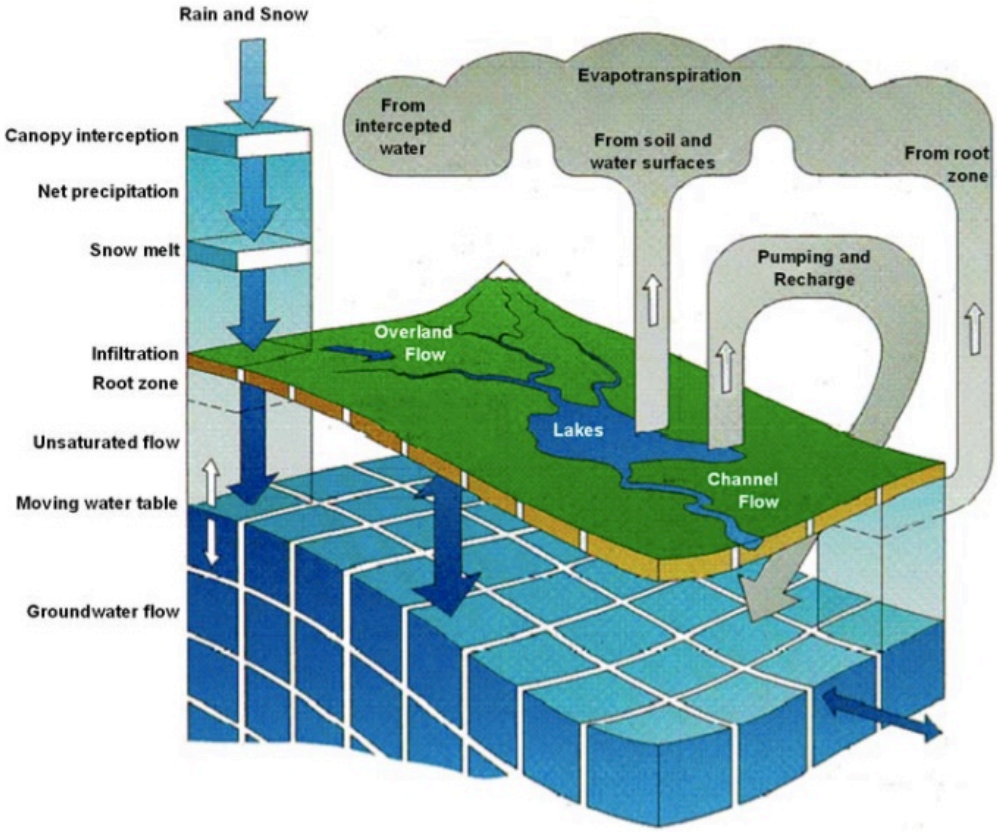

Figure 2.10. Conceptual representation of the MIKE SHE model structure. Source: Graham and Butts (2005).

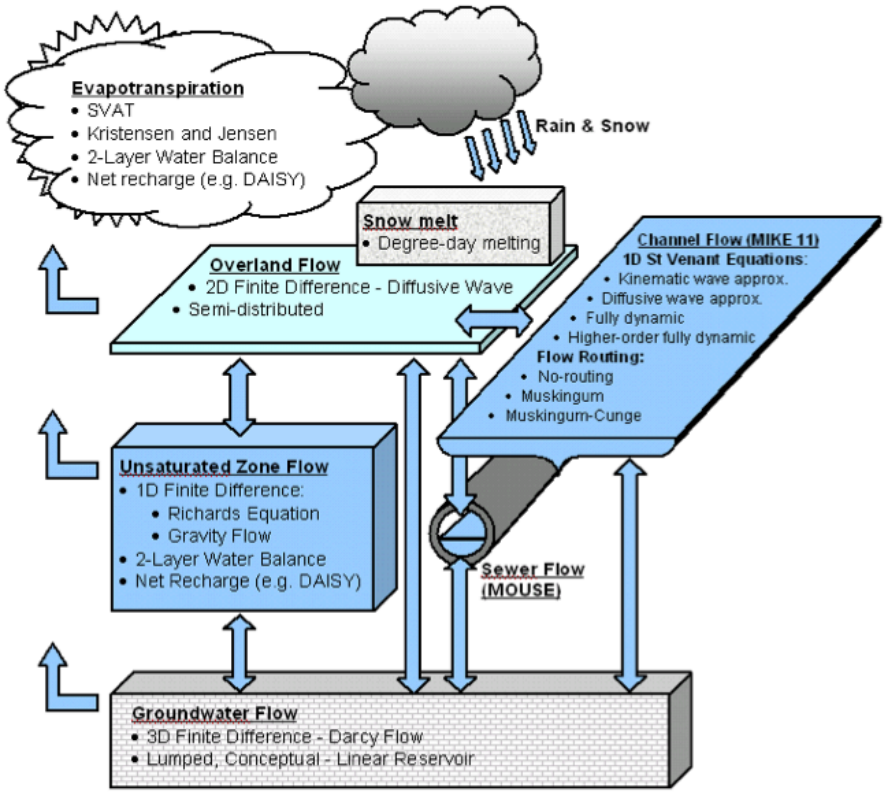

Figure 2.11. Schematic showing the processes in MIKE SHE, including the available numeric engines for each process. The arrows show the exchange pathways for water between the process models. Source: Graham and Butts (2005).

Table 2.4. Summary of a selection of studies employing the MIKE SHE model code.

Reference	Study catchment	Outline
Andersen *et al.* (2001)	Senegal Basin, West Africa (375 000 km^2)	Details the construction, calibration and validation of a model of the Senegal that employs the conceptual linear reservoir groundwater module.
Henriksen *et al.* (2003)	Island of Sjælland, Denmark (7330 km^2)	Part of a national-scale modelling project. Development of multiple model versions is described, highlighting methodological issues related to model parameterisation, establishment of performance criteria, calibration and validation. Snow accumulation and melt included in the models.
Thompson *et al.* (2004); Thompson *et al.* (2009)	Elmley Marshes, England (8.7 km^2)	1st paper: details the development of a model of the lowland wet grassland catchment, with calibration and validation against groundwater depths and ditch-water levels. 2nd paper: The model is used to assess potential impacts of climate change on the wetland. Drier conditions are simulated, with the magnitude of changes increasing with higher emissions scenarios.
Sahoo *et al.* (2006)	Manoa-Palolo stream system, Hawaii (24.6 km^2)	Successful application of MIKE SHE to a tropical, flashy, mountainous catchment on a 15 min time step, including model calibration and validation.
Stisen *et al.* (2008)	Senegal basin, West Africa (350 000 km^2)	A model is developed employing precipitation, PET and leaf area index (LAI) derived from remote sensing data. Saturated zone represented using the linear reservoir method.
Singh *et al.* (2010)	Three sub-catchments of Loktak Lake, India: Thoubal (963 km^2) Iril (1271 km^2) Nambul (178 km^2)	Following development, the three catchment models are driven with climate scenario data. Under 2 °C prescribed warming, six GCMs suggest overall increases in river flow to Loktak Lake, and one GCM a decrease. River discharges simulated by MIKE SHE then used as input to a water balance model to assess impacts on the lake's water level regime.
Singh *et al.* (2011)	As above.	The MIKE SHE models and (non-MIKE SHE) water balance model developed in Singh *et al.* (2010) are employed to assess the sustainability of operation options for the barrage which impounds the lake.
Sultana & Coulibaly (2011)	Spencer Creek, Canada (291 km^2)	Snow storage, ET and streamflow at multiple sites are generally well captured by the model over the calibration and validation periods. Model then used for climate impact assessment using a single GCM.
Thompson (2012)	Three sub-catchments of Loch Dee, SW Scotland (10.3 km^2)	Separate models of the three upland sub-catchments are calibrated and validated against observed discharge. These are then driven with climate data for various GHG scenarios. Most scenarios result in increased winter flows and reduced summer flows.
Wijesekara *et al.* (2012)	Elbow River Watershed, Canada (1238 km^2)	Following development, the model is used to assess the potential impacts of land-use change scenarios on hydrological processes in the catchment.

To the knowledge of this author, prior to its application to the Mekong, the largest basin to which the MIKE SHE model code had been applied was the 350,000 – 375,000 km^2 transboundary Senegal River basin in West Africa (Andersen *et al.*, 2001; Stisen *et al.*, 2008). Table 2.4 also demonstrates that MIKE SHE has been used for many different applications, including methodological studies exploring issues related to the construction, parameterisation, calibration and validation of distributed hydrological models, as well as climate and land cover change scenario impact assessments.

2.6.3.2. SLURP

The SLURP (Semi-distributed Land Use-based Runoff Processes) hydrological model code was developed by Kite (1995, see also Kite, 2007). It is a deterministic, conceptual, semi-distributed model in which the basin is divided into topographically-based sub-basins. These sub-basins are known as aggregated simulation areas (ASAs) since each one is further divided into different land cover types. Similar to HRUs in the SWAT hydrological model, each land cover type within each sub-basin acts as a sub-unit and is represented by four nonlinear reservoirs representing canopy storage, snow storage, interflow (fast storage) and groundwater flow (slow storage) (Figure 2.12). The model is driven with daily climate data and simulates the vertical water balance for each sub-basin/land cover element. At each time step, changes in storage are simulated and the outputs generated include evapotranspiration, surface runoff, interflow and groundwater discharge. Runoff from each element is first routed to the river and then down to the sub-basin outlet. Flows from each sub-basin are then routed downstream to consecutive sub-basin outlets until they reach the outlet of the basin. SLURP is also capable of simulating the effects of dams, reservoirs and water extractions/diversions.

SLURP has been applied to a variety of catchments that vary greatly in terms of both size and climate. These range from small catchments less than 1 km^2 in Canada, including a subarctic, subalpine hillslope catchment (Leenders and Woo, 2002) and a prairie wetland (Su *et al.*, 2000), through catchments hundreds of

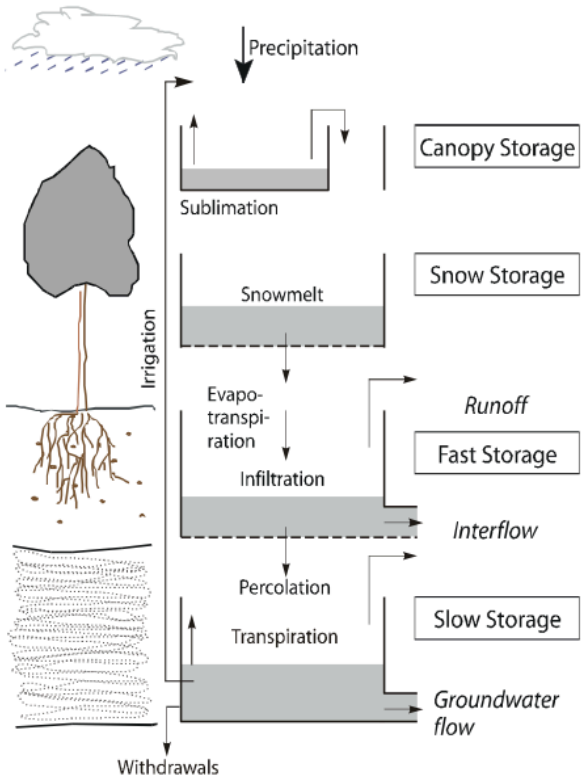

Figure 2.12. Conceptual representation of the structure of the SLURP hydrological model. The vertical water balance shown is calculated for each sub-unit within the SLURP model. Source: Kite (2000).

square kilometres in, for example, Germany (Breuer *et al.*, 2009) and Turkey (Apaydin *et al.*, 2006). Major river basins it has been applied to include that of the Mekong River (area modelled: 550 000 km^2; Kite, 2000, 2001; Kingston *et al.*, 2011), which flows through high altitude, sub-tropical and tropical climate zones; the Canadian Liard River (275 000 km^2; van der Linden and Woo, 2003a, b), which traverses Arctic and subarctic climatic zones and is a tributary of the Mackenzie River; and the Mackenzie River (1.6 × 10^6 km^2; Kite *et al.*, 1994).

Development of the original SLURP model of the Mekong is detailed by Kite (2000, 2001). The model was driven with daily meteorological data from the US National Climate Data Centre (NCDC) global surface summary of the day (GSOD) and a simulation period of 1994–1998 was employed. This model was subsequently adapted by Kingston *et al.* (2011) as part of the QUEST-GSI project. To ensure consistency with other modelling studies contributing to the project, climate inputs to the model were derived from gridded datasets and model calibration and validation were undertaken using the periods 1961–1990 and 1991–1998,

respectively. These data are described in detail in Sections 3.5.1–3.5.3 as they are also employed within the models developed as part of the current study.

2.6.3.3. Mac-PDM.09

Mac-PDM.09 ('Mac' for 'macro-scale' and PDM for 'probability distributed moisture model') is a GHM that simulates river runoff across the global land surface on a gridded basis, at a spatial resolution of 0.5° × 0.5° (Gosling *et al.*, 2010; Gosling and Arnell, 2011). The first version was developed by Arnell (1999), whilst the revised version, denoted Mac-PDM.09, was presented in Gosling and Arnell (2011).

Division of the global land surface into a 0.5° × 0.5° grid results in there being 65,000 cells. Mac-PDM.09 calculates the water balance for each cell on a daily basis. The model does not include river routing. For catchment-scale analyses, river runoff from relevant cells is therefore aggregated. Required input data include precipitation, temperature, net radiation or cloud cover and wind speed. The model can be provided with either daily or monthly data. In the case of the latter, some variables are disaggregated to a daily time step, and the number of wet days (daily precipitation greater than 0.1 mm) in a month is an additional required input. The model parameters employed within Mac-PDM.09 were based upon spatial datasets of soil texture and vegetation. Although basin-specific (catchment-scale) calibration of parameter values was not undertaken, parameter values were 'tuned' in order to improve model performance (Arnell, 1999; Gosling and Arnell, 2011). This involved a parameter sensitivity analysis and comparison of simulated and observed long-term annual runoff and inter-annual runoff patterns at multiple sites. Validation of Mac-PDM.09 simulated runoff against observed runoff was undertaken for 50 catchments (Gosling and Arnell, 2011). For the majority of catchments, observed annual runoff was reasonably well represented by the model (Figure 2.13), although Mac-PDM.09 displays a tendency towards overestimating annual runoff in dry catchments. This is a common issue in GHMs and may be due to omission of the following from Mac-PDM.09: i) transmission losses along rivers, ii) evaporation from wetlands and depressions and iii) phreatophyte evapotranspiration (Gosling and Arnell, 2011).

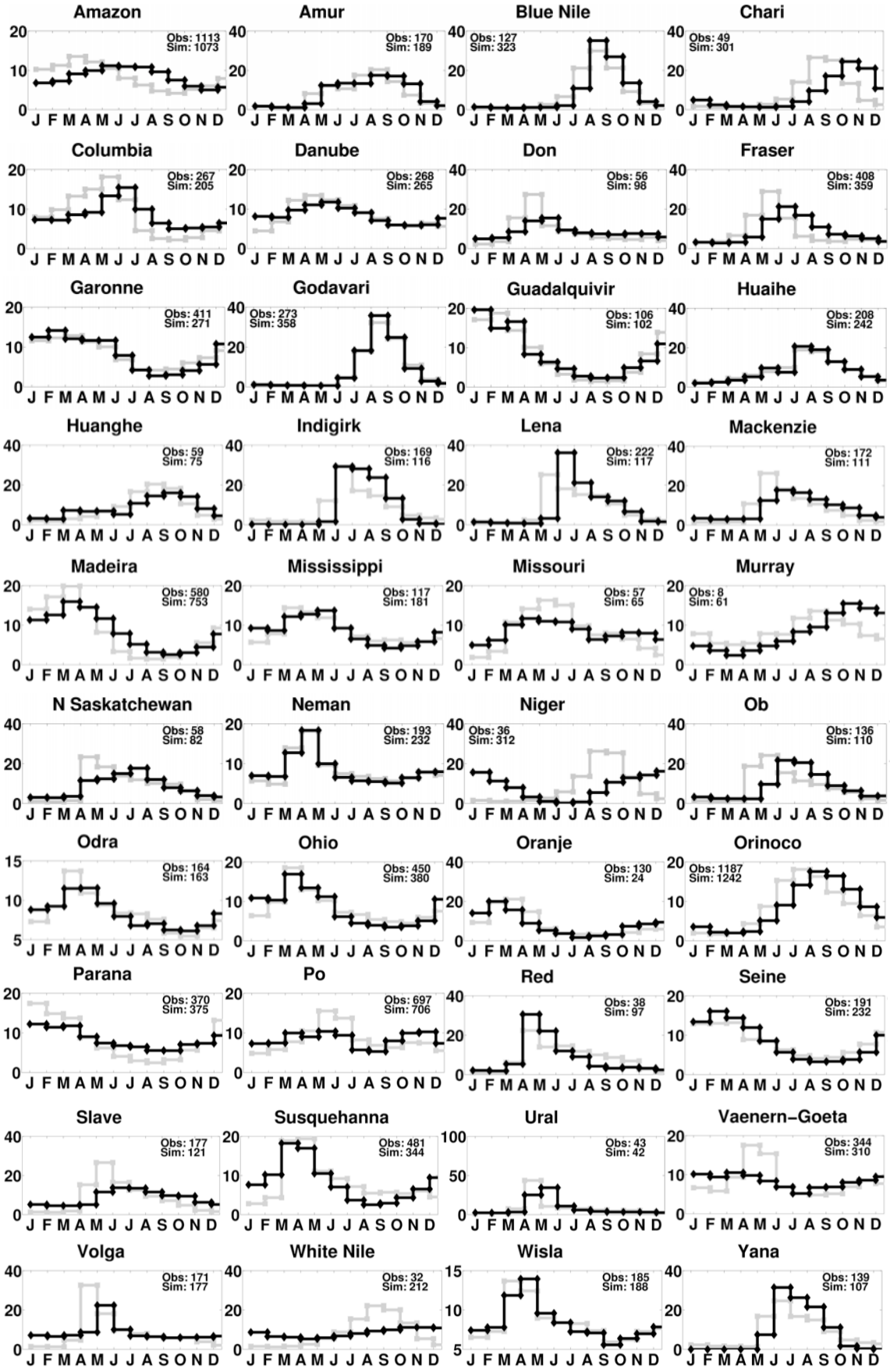

Figure 2.13. Observed (dark) and Mac-PDM.09 simulated (light) runoff regimes for 40 representative catchments (out of 50). The observed (Obs) and simulated (Sim) average annual runoff (mm) is shown for each. Source: Gosling and Arnell (2011).

The monthly runoff regimes were also generally well simulated by Mac-PDM.09, with both the magnitude and timing of monthly runoff very close to that observed for some sub-catchments. However, for the largest catchments, including the Amazon (4,640,300 km^2), Volga (1,360,000 km^2), and Ob (2,949,998 km^2), whilst the magnitude of simulated runoff matches the observed very well, the timing can be off, with the simulated runoff peak leading the observed peak by one month. This is attributed by Gosling and Arnell (2011) to the lack of river routing between grid cells within the model, which means that runoff generated by all the cells in a catchment is accumulated at each time step. The delay between peak upstream runoff generation and peak downstream river runoff is therefore not represented. The omission of river routing is not uncommon in GHMs, however. Furthermore, Mac-PDM.09 has been shown to perform as well as other GHMs in a model intercomparison study (Haddeland *et al.*, 2011).

2.6.4. Input data uncertainty

It is often remarked that a hydrological model is only as good as the input data used to create it (Verma, 1982; Ngigi *et al.*, 2007). This alludes to the issue of input data uncertainty, which arises due to the inevitable imperfectness of the input data used to construct and drive a hydrological model (Liu and Gupta, 2007; Matott *et al.*, 2009). This includes the observed climate data with which the model is driven during calibration and baseline simulations and the observed data (such as river discharge or groundwater levels) against which a model is calibrated. Errors can derive from the imperfect measurement of variables (instrument and observational errors) (Liu and Gupta, 2007; McMillan *et al.*, 2011). Representativeness issues also arise due to scale differences between the variable measured (e.g. point rain gauge measurement of precipitation) and the spatial or temporal extent to which the variable is applied within the model; the spatial/temporal sampling may be inadequate, unrepresentative, or even biased (Liu and Gupta, 2007; Villarini *et al.*, 2008; McMillan *et al.*, 2011). Errors or poor representativeness, and hence uncertainty, can be introduced through the generation of data, such as meteorological inputs, at a higher temporal or spatial resolution using stochastic or deterministic interpolation techniques (Mileham *et al.*, 2008). Similarly, the generation of input data at a lower spatial resolution also introduces uncertainty.

Examples include the up-scaling of gridded digital elevation model (DEM) data to a lower spatial resolution (Vázquez and Feyen, 2007), or area averaging of variables for input to a lumped or semi-distributed hydrological model (Ajami *et al.*, 2004; Patil *et al.*, 2014).

Furthermore, in many cases there may be alternative datasets available to a modeller for the same input variable. For example, several models (e.g. El-Sadek *et al.* (2011), Lauri *et al.* (2014), and the QUEST-GSI project models – Table 2.1) have used gridded meteorological datasets, of which there are a number of examples such as CRU (Mitchell and Jones, 2005) and UDel (Willmott and Matsuura, 2000). Although these are both derived from station records, the use of different numbers and distributions of stations (which may also change over time; Thompson *et al.*, 2016) can mean that over the same area there are differences between such datasets, with implications for their use in hydrological models.

For example, Kingston *et al.* (2011) and Hughes *et al.* (2011) found that adequate baseline hydrological model performance (of the SLURP model of the Mekong and Pitman model of the Okavango Basin, respectively) could not be achieved whilst using CRU rainfall data, suggesting that the data may be poorly representative for these regions. For the Okavango, extreme rainfall in 1967 and deficient rainfall in other years could be detected through identification of years with excessive and deficient simulated flows compared to observations, and comparison of the gridded precipitation with station-based records. For both basins, improved model performance was achieved by instead using UDel precipitation. This demonstrates that, whilst the imperfectness of input data is inevitable, some input data can be more erroneous than others. In many cases, however, determining which dataset is most representative of a basin, and hence the best to use, may be difficult or even impossible (El-Sadek *et al.*, 2011). For the specific case of precipitation data, the availability of alternative datasets is discussed further in Section 2.6.6.3.

Input data uncertainty leads to uncertainty in the results of hydrological climate change impact assessments, since different results might be obtained during scenario modelling if a model employed alternative input data during calibration and baseline simulation. Input data uncertainty is highly related to model

parameterisation, since the input data employed can impact optimized model parameter values. Model parameterisation and uncertainty are therefore discussed in the next section (2.6.5), before three specific sources of uncertainty related to meteorological inputs are introduced in Section 2.6.6.

2.6.5. Parameter acquisition and uncertainty

A further source of uncertainty in hydrological modelling relates to model parameterisation. In conceptual hydrological models, the majority of model parameters are usually (though not always) conceptual in nature (e.g. time constants that control flow between different storage reservoirs). This means that, rather than being based upon physical properties within a catchment that could in principle be established in the field, they relate to aggregated hydrological processes that are not explicitly represented within the model (Madsen, 2003; Wagener *et al.*, 2003). Such parameters cannot, for obvious reasons, be obtained from field measurements. Instead, parameter values are determined through model calibration, with model parameters being adjusted in order to improve the fit between simulated and observed phenomena, such as river discharge (Klemeš, 1986; Duan *et al.*, 1992; Gupta *et al.*, 1998). The variable(s) to be calibrated will depend upon the intended use of the model and the availability of observations.

Model calibration may be undertaken manually, in which case the modeller iteratively adjusts model parameters, re-runs the model and assesses model performance, in a form of trial-and-error process (Anderson and Woessner, 1992; Madsen and Jacobsen, 2001). As stated in Section 1.2, both qualitative and quantitative techniques can be employed to evaluate model performance in terms of the closeness of simulated model behavior to observations (Feyen *et al.*, 2000; Grayson and Blöschl, 2000; Krause *et al.*, 2005). Qualitative techniques involve the visual, and therefore subjective, comparison of graphical plots representing observed and simulated values of a hydrological variable, such as river flow (e.g. Masood *et al.*, 2015), wetland/lake water levels (e.g. Su *et al.*, 2000; Singh *et al.*, 2010) or groundwater levels (e.g. Thompson *et al.*, 2004; Jackson *et al.*, 2011). The plots may, for example, depict daily, monthly, or mean monthly data, or in the case of river flow, percentage exceedance / flow duration curves (i.e. showing the

percentage of time that a given flow is equaled or exceeded). Flow duration curves illustrate how well a model reproduces the observed distribution frequency of flows of a given magnitude (Moriasi *et al.*, 2007; Xu *et al.*, 2011).

Quantitative methods of model evaluation use statistical measures, which, according to Moriasi *et al.* (2007), generally fall within one of three major categories. These are as follows: i) standard regression statistics, which evaluate the strength of the linear relationship between observed and simulated data, ii) dimensionless techniques that provide a relative measure of model performance and iii) error indices that quantify the deviation of simulated values from those observed, in either the units of the data of interest (Moriasi *et al.*, 2007), or as a percentage. Table 2.5 provides an example of each type of statistical measure. The Pearson correlation coefficient (r) is a regression-based technique, the Nash-Sutcliffe Efficiency coefficient (NSE) is a dimensionless statistic and Dv (for deviation) represents percentage deviation of the simulated mean from the observed mean. Performance ratings (i.e. threshold values) for different statistical measures may be employed to categorise model performance (e.g. as poor, good or very good; Henriksen *et al.*, 2003; Moriasi *et al.*, 2007; Henriksen *et al.*, 2008).

As an alternative to manual calibration, autocalibration (automatic calibration) involves the use of a numerical optimisation routine. In this case, the search algorithm iteratively adjusts parameters (within bounds set by the modeller) and seeks to optimise model performance assessed against observed data using statistical measures (objective functions) (Duan *et al.*, 1992; Duan *et al.*, 1993; Madsen and Jacobsen, 2001; Madsen, 2003).

In physically-based, distributed hydrological models, model parameters should, in theory, have direct physical meaning, and it should therefore be possible to determine parameter values from field measurements, therefore negating the need for model calibration (Beven, 1996; Madsen, 2003; Silberstein, 2006). In practice, however, the parameters of physically-based models are often not gained directly from field data from the catchment being studied, and the models do frequently require calibration (Beven, 1996; Madsen, 2003; Silberstein, 2006). There are a

Table 2.5. Example statistics used to evaluate model performance during calibration and validation.

Statistic	Calculation
Dv (adapted from Henriksen *et al.*, 2003)	$Dv = 100\ \frac{\overline{Q_s} - \overline{Q_o}}{\overline{Q_o}}$, (%)
Dv (denoted F_{Bal} by Henriksen *et al.* (2003)) indicates the ability of the model to simulate the average conditions for a particular variable (e.g. river discharge) and is a measure of the percentage deviation of the simulated mean from the observed mean over the period simulated (Henriksen *et al.*, 2003). The closer to 0 this value is, the better the model performance according to this statistic. A positive value indicates over-estimation of the mean, whilst a negative value indicates under-estimation of the mean.	
Nash-Sutcliffe Efficiency (NSE) (Nash and Sutcliffe, 1970)	$NSE = \frac{(\sum_{i=1}^{n}(Q_{o,i} - \overline{Q_o})^2 - \sum_{i=1}^{n}(Q_{s,i} - Q_{o,i})^2)}{\sum_{i=1}^{n}(Q_{o,i} - \overline{Q_o})^2}$
NSE indicates the ability of the model to simulate the variation in the observed values (Henriksen *et al.*, 2003). NSE can range between 1, representing a perfect fit between observed and simulated data and - ∞. An NSE of 0 signifies that the model is no better a predictor than the mean of the observed time series, whilst a value below 0 indicates that the mean of the observed time series would have been a better predictor (Krause *et al.*, 2005).	
Pearson product moment correlation coefficient (r)	$r = \frac{(\sum_{i=1}^{n}(Q_{o,i} - \overline{Q_o})\,(Q_{s,i} - \overline{Q_s})^2}{\sqrt{\sum_{i=1}^{n}(Q_{o,i} - \overline{Q_o})^2}\ \sqrt{\sum_{i=1}^{n}(Q_{s,i} - \overline{Q_s})^2}}$
r is a measure of the linear relationship between observed and simulated values (Moriasi *et al.*, 2007). r can vary between -1 and 1. An r of -1 indicates a perfect negative linear relationship, 0 indicates no linear relationship and 1 indicates a perfect positive linear relationship. Values closer to 1 are therefore desirable. However, as r is a measure of co-variance between observed and simulated values, high r values can still be produced if observed discharge is systematically over or under predicted by the model (Legates and McCabe, 1999).	
where $Q_{o,i}$ is observed value (e.g. discharge) for time step i (e.g. one day or one month) $Q_{s,i}$ is simulated value for time step i Q_o is mean observed value over the period of evaluation. Q_s is mean simulated value over the period of evaluation. n is the number of data points evaluated (e.g. number of days/months in the simulated/observed period)	

number of reasons for this. Firstly, field measurements of parameters may not exist. Undertaking a field campaign for model parameterisation is likely to be costly in terms of both time and money, and so is often impractical, particularly in very large catchments (Andersen *et al.*, 2001; Mulligan and Wainwright, 2004; Stisen *et al.*, 2008). Where measurements do exist, there will likely be a discrepancy between the measurement scale (which is generally smaller) and model element scale (Beven, 1993; Blöschl and Sivapalan, 1995). Furthermore, as parameters are in fact lumped/homogenized at the grid scale, they cannot reflect the spatial heterogeneity found in reality (Beven, 1989). The problems related to parameterisation of a distributed model are eloquently summarised by Rosso (1994: 18–19):

> 'In principle, spatially distributed models can accept experimental data at each grid element or calculation node. In practice, because of heterogeneity of parameter values, differences between measurement scales and model grid scales, and experimental constraints, the specification of parameter values is very difficult.'

In order to reduce the number of different parameters within a distributed model, it is common practice to employ spatial patterns of classifiable catchment characteristics, such as soil types and land use / vegetation cover, to distribute parameter values (Refsgaard, 1997; Grayson and Blöschl, 2000). For example, soil class maps are commonly employed to distribute soil hydraulic properties (parameters), with a single parameter value being applied to each class for a given parameter type (such as saturated hydraulic conductivity).

Representative parameter values for different parameter classes may be based upon field data or remotely sensed data (e.g. Kite, 2000; Andersen *et al.*, 2002a) from the study site. Alternatively, parameter values, such as those for specific soil types or vegetation types, are commonly based upon values from the literature (i.e. studies of field or laboratory measurements). This approach has, for example, been taken in many studies that have employed the MIKE SHE model code, for sites ranging from an 8.7 km^2 area of lowland wet grassland in the North Kent marshes, UK (Thompson *et al.*, 2004; Thompson *et al.*, 2009), through sub-catchments of Loktak Lake in Northeast India ranging in size from 178 km^2 to 1278 km^2 (Singh *et al.*, 2010; Singh

et al., 2011), to the 350,000 km^2 Senegal River Basin (Andersen *et al.*, 2001; Stisen *et al.*, 2008). Literature-based parameter values may sometimes be subject to calibration within realistic bounds (again, based upon the literature), or may be fixed, since it is widely accepted that reducing the number of free parameters (those which are subject to calibration) is good modelling practice in order to prevent over-parameterisation (e.g. Refsgaard, 1997; Grayson and Blöschl, 2000; Andersen *et al.*, 2001; Henriksen *et al.*, 2003; Henriksen *et al.*, 2008; Stisen *et al.*, 2008). Over-parameterisation refers to a situation where too many parameters of a model were subject to calibration; although the fit between observed and simulated system behaviour may be very good over the calibration period, performance will likely be significantly reduced when the model is run for a period for which it has not been calibrated (Beven, 1996; Refsgaard, 1997).

Model parameterisation is a key source of uncertainty in hydrological modelling (e.g. Beven and Binley, 1992; Wagener *et al.*, 2003; Liu and Gupta, 2007), as well as for environmental modelling in general (e.g. Dubus *et al.*, 2003; Quinton, 2004; Refsgaard *et al.*, 2006; Ascough *et al.*, 2008; Matott *et al.*, 2009). Similar to equifinality of model structures, equifinality of model parameters also occurs; different parameter values (parameter sets) can perform similarly well during model calibration/validation according to particular statistical criteria (Beven, 1993; Rochester, 2010). However, during scenario modelling, the alternative models (with alternative parameter sets) may give varied but equally plausible results. It is worth noting that parameterisation uncertainty is still a potential issue for parameters that have not been subject to calibration, since the values employed will not be definitive, regardless of whether these are based on site-specific field data or the literature. If obtained from alternative datasets or literature, or if the parameter was varied during model calibration alongside other parameters, then it is quite likely that a different value would be employed, with the potential for the scenario results obtained to be impacted.

In general, however, parameterisation uncertainty has been found to be low in comparison to other sources of uncertainty in hydrological climate change impact assessments. For example, Poulin *et al.* (2011) (see Table 2.3) found the impact of hydrological model parameterisation on model outputs under climate change to be

less important than inter-hydrological model uncertainty. Wilby and Harris (2006) found model parameterisation to be less important than GCM, downscaling, and inter-hydrological model related uncertainty, but more significant than emissions scenario uncertainty. Dobler *et al.* (2012) quantified the uncertainty in projections for the Lech watershed (~1000 km^2), Austria, resulting from the use of three GCMs, three RCMs, three bias-correction techniques for the RCM outputs and a single hydrological model code with 20 parameter sets. Hydrological model parameter uncertainty was found to be the least important and had little impact on projections of mean annual runoff and a relatively small impact on changes in monthly runoff compared to other sources of uncertainty.

2.6.6. Uncertainty associated with meteorological inputs

Sections 2.6.6.1–2.6.6.3 discuss three specific sources of uncertainty associated with meteorological inputs to a hydrological model, namely PET estimation uncertainty, the spatial distribution of meteorological inputs to a hydrological model and input precipitation uncertainty. All three sources are relevant to hydrological modelling in general, since they have the potential to influence model calibration / parameterisation. They are therefore discussed in relation to the wider hydrological modelling literature, as well as in the specific context of climate change impact assessments.

2.6.6.1. PET estimation uncertainty

One potentially significant source of uncertainty in hydrological projections under climate change that has been relatively overlooked in uncertainty assessments is that associated with the method used in order to estimate potential evapotranspiration (PET). Evapotranspiration is a key component of the hydrological cycle and therefore a major factor in catchment water-balance equations (Oudin *et al.*, 2005b). Within many hydrological models, the rate of 'actual' evapotranspiration (AET) is calculated based on time-series of PET data and the amount of water available for evaporation from the soil or land surface (Kay and Davies, 2008). PET is a conceptual variable that represents the amount of evapotranspiration that would occur if water availability was not a limiting factor

(Kingston *et al.*, 2009). It is usually calculated empirically using measurable meteorological variables such as temperature (see below), although in some cases it is based on measurements of AET. In some hydrological models, such as SLURP (Kite, 2007) and Mac-PDM.09 (Gosling and Arnell, 2011), PET must be calculated internally. In such cases, either a single or multiple calculation schemes may be built into the model code. In other models, such as MIKE SHE, PET must be calculated externally and then applied as an input to the model. During the scenario simulation stage of climate change impact assessments, PET is calculated using meteorological variables generated by a GCM.

There are, however, more than 50 different methods for calculating PET (Lu *et al.*, 2005). These methods employ different meteorological variables and different empirical functions, sometimes as a result of being developed for specific regions, and so the PET time-series generated can vary considerably (Lu *et al.*, 2005; Kingston *et al.*, 2009). For some methods, temperature is the only meteorological variable required, whilst other formulae incorporate additional variables, such as net solar radiation or cloud cover, relative humidity and wind speed (Oudin *et al.*, 2005a). Table 2.6 provides a summary of six widely used PET methods that are employed in this thesis. A distinction is sometimes made between the term PET, which has been criticised for ambiguities in its definition, particularly the reference evaporation surface, and reference crop evapotranspiration or reference evapotranspiration (ET_0) (Allen *et al.*, 1998). ET_0 is the potential evapotranspiration rate from a strictly defined hypothetical grass reference crop (Allen *et al.*, 1998). However, for the purposes of the following discussions, the term PET is used to encompass both reference and non-reference evapotranspiration.

When developing a hydrological model, PET method selection may be influenced by a number of factors. Where a hydrological model calculates PET internally, the method will depend upon those incorporated within the model code (Bae *et al.*, 2011). Data availability may also exert an important influence since different PET methods require different meteorological variables. This may have important implications for climate change assessments since less confidence is placed in GCM

Table 2.6. PET methods employed in this thesis and their required inputs.

PET method	Inputs	Calculation for PET in mm/day*
Blaney–Criddle (1950) (BC), as expressed by Brouwer and Heibloem (1986)	Temperature, day length (latitude based)	$BC\ PET = p(0.46 \times T + 8)$
Hamon (1963) (HM), as expressed by Lu *et al.* (2005)	Temperature, day length	$HM\ PET = 0.1651 \times Dl \times e_s \times K$ where K (calibration coefficient) = 1.2
Hargreaves–Samani (1982) (HS), as expressed by Oudin *et al.* (2005a)	Temperature, extraterrestrial radiation	$HS\ PET = 0.0023\frac{R_e}{\lambda}(T_{max} - T_{min})^{1/2}(T + 17.8)$
Linacre (1977) (LN), as expressed by Dent *et al.* (1988). See Kite (2007).	Temperature, day length	$LN\ PET = \frac{Dl.700\ T_h/(100 - L) + u \times T_{diff}}{80 - T}$
Penman (1948) (PN), as expressed by Shuttleworth (1993)	Temperature, wind, vapour pressure, net radiation	$PN\ PET = \frac{\Delta A' + \Upsilon[6.43(1 + 0.536\ U_m)e_d]/\lambda}{\Delta + \lambda}$
Priestley–Taylor (1972) (PT), as expressed by Lu *et al.* (2005)	Temperature, net radiation	$PT\ PET = \frac{\alpha(\Delta/(\Delta + \gamma))(R_n - G)}{\lambda}$ where α (calibration constant) = 1.26

***Notation and units**

Δ is the slope of the saturation vapour pressure curve (in kPa °C^{-1}) at air temperature T

λ ($= 2.501 - 0.002361.T$) is the latent heat of vaporisation of water (in MJ kg^{-1})

γ is the psychometric constant (= $0.0016286\ P/\lambda$, in kPa), where P is the atmospheric pressure (in kPa)

L is the latitude (degrees)

A' is the measured or estimated energy available for evaporation from the free water surface expressed as an evaporated water equivalent (in mm day^{-1}) ($= 0.408\ Rn$)

Rn is net radiation (in MJ m^{-2} day^{-1}).

Dl is the daylight hours according to latitude divided by 12

e_d is the vapour pressure deficit (in kPa) at 2 m, i.e. the difference between the mean saturation vapour pressure (based upon mean daily maximum and minimum air temperature) and actual vapour pressure

p is the mean daily percentage of annual daytime hours according to latitude

R_e is extraterrestrial radiation (MJ m^{-2} day^{-1}) according to latitude

e_s *(= 216.7 × ESAT / (T + 273.3))* is the saturated vapour density (g/m^3) at T, where *ESAT* *(= 6.108 × EXP (17.26939 × T / (T + 237.3)))* is the saturated vapour pressure (mb) at T;

T is the mean air temperature (°C) for the period for which average daily PET is being calculated. This could, for example, be the mean for a single day or for a month.

$T_h = T + 0.0006\ h$, where h is the elevation (m)

u is a wind factor for the Linacre equation (often defaulted to 15)

T_{diff} is the difference between air and dewpoint temperatures approximated by:

$T_{diff} = 0.0023\ h + 0.37\ T + 0.53\ T_r + 0.35\ T_{hc} - 10.9$; where T_r is the mean daily or monthly range in temperature and $T_{hc}$is the difference between the mean temperatures of the hottest and coldest months of the year.

T_{max} is the mean daily maximum temperature (°C)

T_{min} is the mean daily minimum temperature (°C)

U_m is the wind speed at 2 m above soil surface (in m s^{-1})

G is the heat flux density to the ground (in MJ m^{-2} day^{-1})

simulations of some variables such as cloud cover and vapour pressure compared to others, most notably temperature (Randall *et al.*, 2007). Similarly, other variables, such as wind speed and net radiation, are typically less reliable in the gridded datasets often used for baseline simulations (e.g. Haddeland *et al.*, 2011) due to measurement difficulties and the relatively limited number of observations (New *et al.*, 1999). Although many large-scale (global) hydrological models use either the Penman–Monteith or Priestley–Taylor methods, these decisions are often based on the theoretically more realistic nature of these methods as opposed to a large-scale validation of their output (although Sperna Weiland *et al.*, 2012 is an exception).

Several studies have demonstrated the sensitivity of hydrological models to choice of PET method in a non-scenario modelling context. For example, Vörösmarty *et al.* (1998) compared the use of 11 different PET methods in the global-scale water balance model (WBM) applied to the USA. Model parameters were assigned *a priori* and recalibration of the model was not undertaken for the different PET methods. Across the USA, use of the different methods produced differences in simulated annual evaporation, and hence annual runoff, of between 0–400 mm. Similarly, Gosling and Arnell (2011) applied two well known and commonly used PET methods (Penman-Monteith and Priestley-Taylor) to the Mac-PDM.09 GHM. Simulated runoff was sensitive to choice of PET method, with differences in simulated annual runoff of up to 60% occurring for the USA.

Andréassian *et al.* (2004) make an insightful distinction between static and dynamic model input-related sensitivity studies. Studies that take a static sensitivity approach undertake a single model calibration and hence model parameters are optimized for a single set of model input time series. The sensitivity of model outputs to choice of input data, such as PET, is then assessed by comparing model outputs produced using alternative input datasets, without further model calibration. In dynamic sensitivity studies, separate model calibrations are performed for the alternative input data, and the sensitivity of both model outputs and parameters are analysed. With static sensitivity studies, there is an implicit assumption that the calibration parameter values are the 'true' catchment-specific parameter values; with dynamic sensitivity studies, there is explicit acknowledgement that the calibrated parameter values are dependent upon the

climatic input data (Andréassian *et al.*, 2004). The PET sensitivity assessments of Vörösmarty *et al.* (1998) and Gosling and Arnell (2011) therefore employed the static sensitivity approach.

In an example of a dynamic sensitivity study, Vázquez and Feyen (2003) developed three models of the 586 km^2 Gete catchment in Belgium using the MIKE SHE model code, each initially differing only in the method used to generate the input PET time series. Each model was then calibrated separately but using an identical procedure. Three Penman-type PET methods were employed. One method produced consistently higher PET estimates than the other two methods, as demonstrated in Figure 2.14. PET method was found to impact both the calibrated parameter values and model performance. As might be expected, the parameters related to the model water balance, such as vegetation properties that impact evapotranspiration rates (e.g. leaf area index, which impacts interception storage) were generally more significantly dependent upon the PET method employed than parameters related to water routing, such as horizontal and vertical conductivity. Variation in model performance for stream flow following calibration was notable. For example, the Nash-Sutcliffe coefficient of efficiency (where a value of 0 indicates that the mean of observations is as good a predictor as the model and 1 indicates that there is a

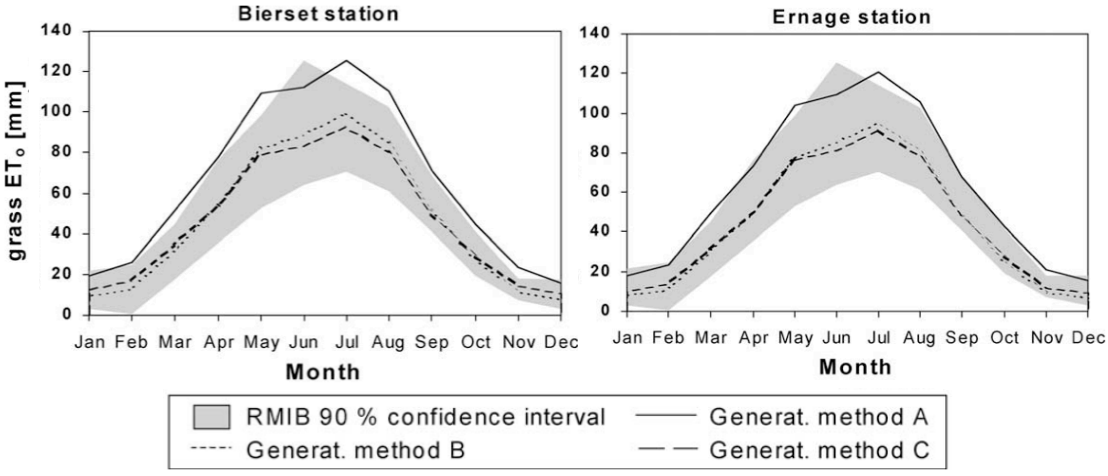

Figure 2.14. Mean PET (grass reference evapotranspiration) estimates for two meteorological stations compared to the station-based (RMIB) 90% confidence intervals, for the period 1967–1995. Source: Vázquez and Feyen (2003).

perfect match between simulated and observed values) for streamflow for a seven year period varied between 0.60 and 0.75. Andréassian *et al.* (2004) also report sensitivity of model calibration parameters to PET inputs. A sample of 62 watersheds in the Massiff Central highland of France was used. Rather than employing alternative empirical PET methods, this study compared the use of PET data generated using average regional estimates, data from the closest meteorological station to a given watershed, or regionalisation to provide improved PET estimates. Andréassian *et al.* (2004) demonstrated that, through adjustment of model parameters, the calibration process was able to compensate for differences (and therefore also potentially error) in PET input values, resulting in similar model performances despite the use of differing PET data.

Fewer studies have investigated the sensitivity of hydrological climate change impact results to the use of different PET methods. In a study that did not involve hydrological modelling, Kingston *et al.* (2009) investigated a scenario of 2°C increase in global mean temperature (relative to a 1961–1990 baseline). They reported large differences (over 100%) in PET climate change signals (scenario PET minus baseline PET) on a global basis produced using six different PET methods commonly used within hydrological models (Figure 2.15). Using a precipitation/PET aridity index, it was found that for some regions, namely East Africa and Southeast Asia, choice of PET method could influence the projected direction of change in water availability. Furthermore, PET-related uncertainty was sometimes of a similar magnitude or, in some cases, greater than GCM-related uncertainty.

The analyses undertaken by Kingston *et al.* (2009) indicate that PET method selection could be a notable source of uncertainty in hydrological model projections under climate change, a particularly important finding considering that the majority of modelling studies employ a single PET method. There are, however, some exceptions. Kay and Davies (2008) investigated the impact of uncertainty in changes in PET on the changes in river discharge under climate change simulated for three catchments in the UK, using climate scenario data from five GCMs and multiple RCMs. The three hydrological models were calibrated and validated using PET data derived using a single PET method. Monthly percentage changes between

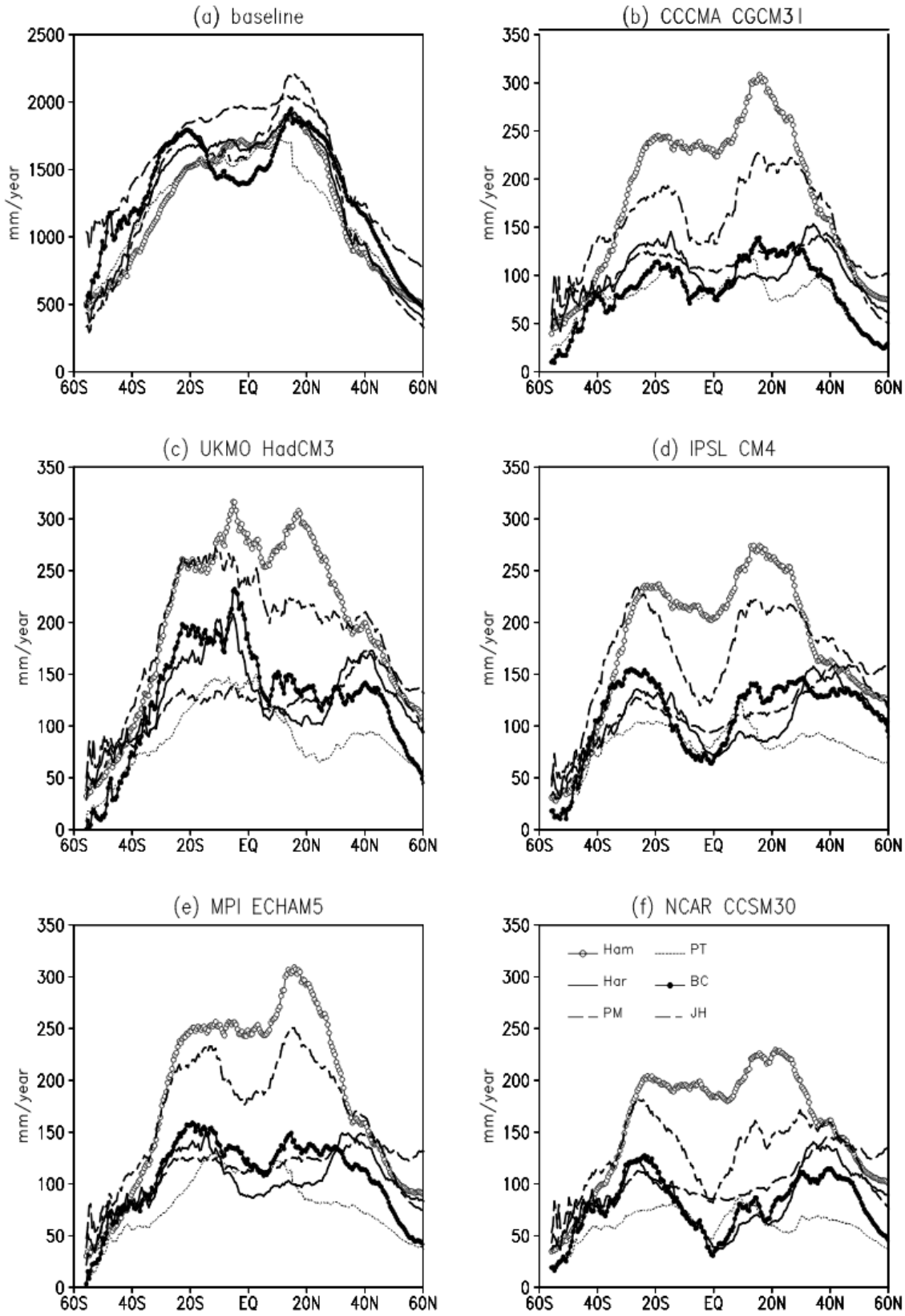

Figure 2.15. Latitudinally averaged annual PET for (a) 1961–1990 baseline and (b–f) 2°C climate change signal (scenario minus baseline for each method), grouped by GCMs (CCCMA, HadCM3, IPSL, MPI and NCAR). PET methods: Ham, Hamon; Har, Hargreaves; PM, Penman-Monteith; PT, Priestley-Taylor; BC, Blaney-Criddle; and JH, Jensen-Haise. Source: Kingston et al. (2009).

baseline and scenario PET for each of the climate models were then calculated using two different PET methods: Penman-Monteith PET and temperature-based PET (using a formula from Oudin *et al.*, 2005a), and these changes were applied to the baseline PET. This is known as the delta-change approach of downscaling and was also used to perturb baseline precipitation. The two PET methods produced very different changes in PET (Figure 2.16), with implications for modelled changes in flows under climate change for the three example catchments. Results showed that the method used to define changes in PET could influence the magnitude and sometimes even the direction of changes in low, medium and high flows, as exemplified in Figure 2.17 for the GCM scenarios. However, the uncertainty due to PET formulation was less than that due to GCM and RCM structure uncertainty.

Bae *et al.* (2011) used three alternative semi-distributed catchment models and different PET methods to simulate climate change scenarios for a medium sized catchment (c. 7000 km^2) in central South Korea. Hamon and Jensen-Haise PET were employed in the PRMS model, Penman-Monteith, Priestley-Taylor and Hargreaves PET in SWAT, and Penman-Monteith, Granger and Spittle-House Black in SLURP. Results showed that the different PET methods impacted runoff changes, with the magnitude of PET-related differences varying between hydrological models and season. The parameters of each of the hydrological models were optimized using a single internal PET method, and then different internal PET methods were applied without further optimization.

In an assessment of the potential impacts of climate change on the Elmley Marshes, UK, Thompson *et al.* (2009) explored the impact of using two different approaches for deriving scenario PET: one that assumed changes in temperature only, and one that incorporated perturbed temperature, radiation and wind speed data. Scenario water tables and ditch water levels were consistently lower when using the PET data calculated using perturbed temperature, radiation and wind speed. Although the alternative scenario PET time series were calculated using the same PET method (Penman-Monteith), this finding highlights that the incorporation of different meteorological variables in different PET methods could have important implications for climate change impact assessments.

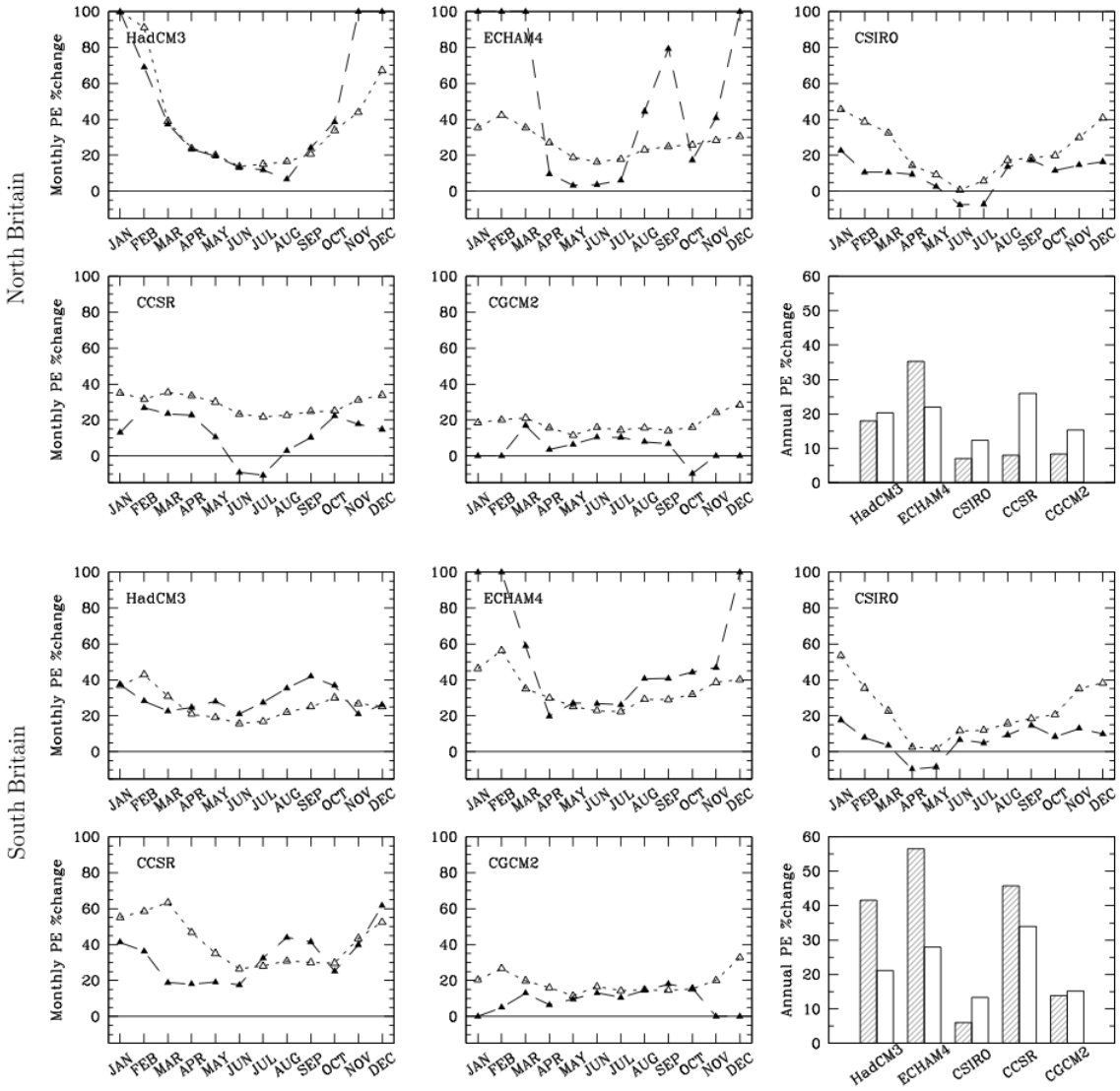

Figure 2.16. Plots comparing the potential changes (from the 1970s to the 2080s) in Penman–Monteith and temperature-based (T-based) monthly mean PET (PE) derived from five GCMs (respectively, filled triangles/dashed line and open triangles/dotted line), over regions covering North and South Britain. The final plot in each group of six for the two regions compares percentage changes in Penman–Monteith and T-based mean annual PET (respectively, hatched and open bars) for each GCM. Source: Kay and Davies (2008).

The studies outlined above indicate that PET formulation may be an important and yet understudied source of uncertainty in climate change impact assessments. Furthermore, these studies all used a static sensitivity approach. Consequently, whilst non-scenario modelling studies have demonstrated that PET method can impact model parameterisation when PET-specific calibration is adopted (Vázquez and Feyen, 2003; Andréassian *et al.*, 2004), very few climate change impact studies investigating PET-related uncertainty have explored the implications of undertaking a separate model calibration for each PET method.

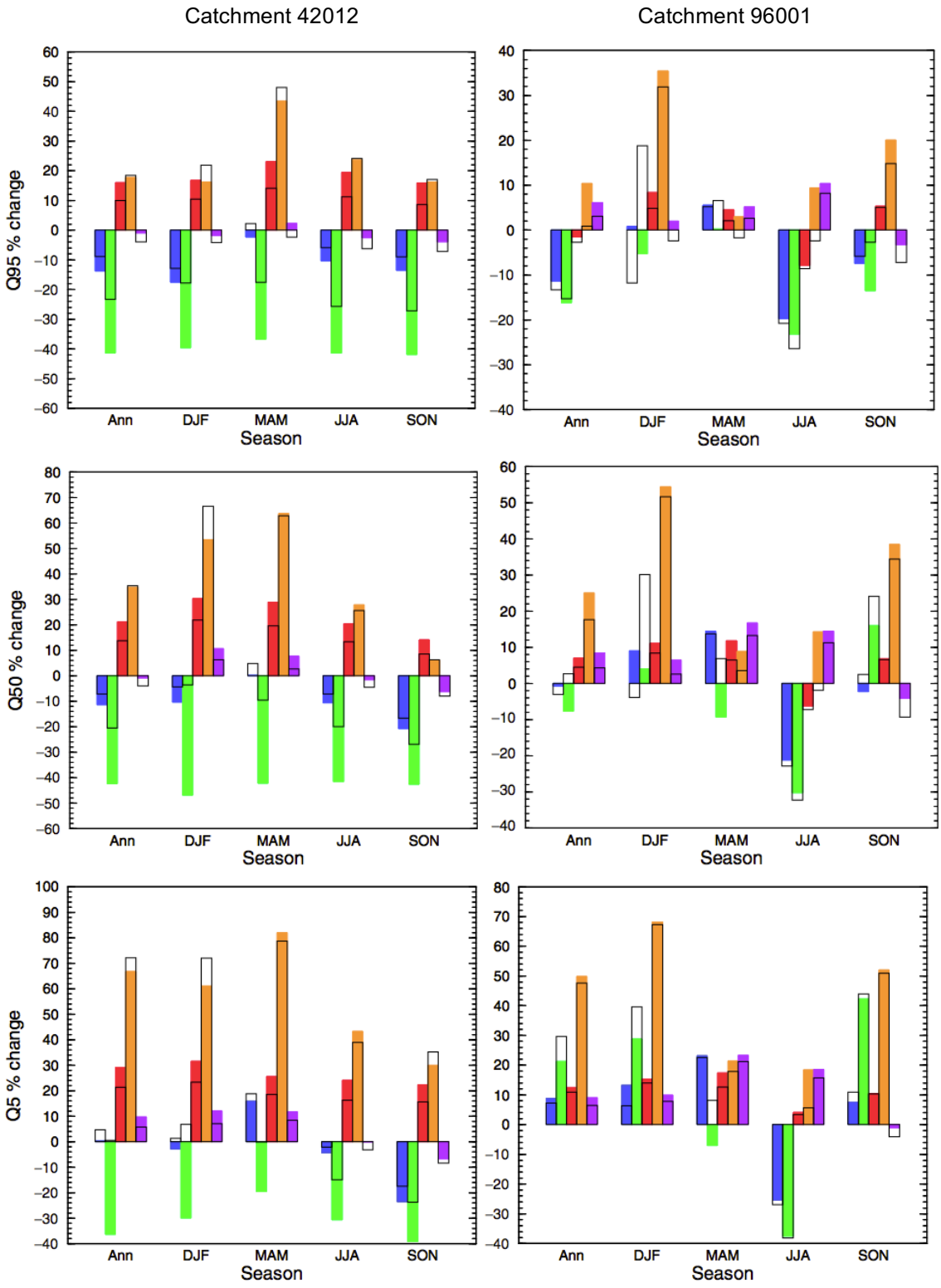

Figure 2.17. Bar charts showing modelled annual and seasonal percentage changes in low (Q95), median (Q50) and high (Q5) flows for two example catchments, for each GCM (left-to-right bar order: HadCM3; ECHAM4; CSIRO; CCSR; CGCM2). The solid bars indicate the results when the changes in Penman–Monteith PET are applied, whilst the outlined bars indicate the results when the changes in temperature-based PET are applied instead. Source: Kay and Davies (2008).

A notable exception is a study by Remesan and Holman (2015), which is discussed in Section 2.6.6.3 rather than here since it also explored uncertainty related to choice of baseline precipitation input data.

2.6.6.2. Spatial distribution of meteorological inputs

As well as there being alternative data sources for a given meteorological input, additional uncertainty may be associated with the meteorological input spatial distribution employed within the hydrological model (Mileham *et al.*, 2008; Vaze *et al.*, 2011; Patil *et al.*, 2014). For a given catchment, provided that sufficient hydrometeorological data are available, a model could be developed that employs a lumped, semi-distributed or gridded meteorological input spatial distribution, potentially using the same original data source. For example, weighted averaging of point-based observational data from multiple weather stations could be undertaken to provide input to a lumped or semi-distributed model, whilst the same data could also be interpolated to provide gridded inputs.

As an alternative to the direct use of station-based records, pre-gridded global datasets such as CRU (Mitchell and Jones, 2005) and UDel (Legates and Willmott, 1990) are freely available and can be easily sampled for specific regions of interest. Such datasets are particularly useful in cases where station records may be difficult to obtain (Thompson *et al.*, 2016). Pre-gridded data could be directly input to a gridded hydrological model, or it could be re-interpolated onto an alternative grid, spatially averaged to provide a single input time series for a lumped model, or spatially averaged to generate multiple input time series for a model with a semi-distributed meteorological input spatial distribution (see for example Ajami *et al.*, 2004; Kingston *et al.*, 2011). The meteorological input spatial distribution employed could potentially influence climate change scenario results through a combination of influencing i) model parameters resulting from calibration and ii) the spatial pattern of changes in meteorological inputs. This source of uncertainty relates to both input data representativeness issues and uncertainty associated with hydrological model structure.

Previous research has demonstrated that the spatial distribution of meteorological inputs within a hydrological model can impact simulated outputs and model parameterisation and calibration. For example, Mileham *et al.* (2008) investigated the impact of the spatial distribution of precipitation on the parameterisation and calibration of a soil-moisture balance model (SMBM) of the 2098 km^2 River Mitano catchment in Uganda. The SWMB model was first calibrated using station-based precipitation data distributed using Thiessen polygons. Gridded precipitation, produced through interpolation of the point-based station data, was then applied to the model. It was found that the subsequent discrepancy in model output necessitated recalibration, with substantial adjustment to model parameterisation being required.

To assess the impact upon simulated streamflow of using spatially uniform (lumped) or distributed meteorological inputs, Patil *et al.* (2014) compared the application of lumped and semi-distributed versions of the Exponential Bucket Hydrologic Model (EXP-HYDRO) to 41 meso-scale (500–5000 km^2) catchments in Northwest USA. Separate calibrations were undertaken for each model version, with spatially uniform parameter values being applied in each case. Results showed that the distributed model performed better in 38 catchments. In particular, model performance was superior in catchments with either low homogeneity (i.e. high heterogeneity) of moisture distribution (meaning that spatial variability of precipitation was important), or high spatial variability of precipitation phase (i.e. rain vs. snow, meaning that spatial variability of temperature was important).

Although many studies have investigated the impact of spatial variability of meteorological inputs, most commonly precipitation (Mileham *et al.*, 2008; Vaze *et al.*, 2011; Zhao *et al.*, 2011), to a hydrological model under non-scenario conditions, there is a paucity of such investigations for climate change impact assessments.

2.6.6.3. Input precipitation uncertainty

Precipitation is both a key input and major source of uncertainty in hydrological modelling. Uncertainties in rainfall input data based upon point rain gauge data derive partly from measurement errors, which are widely acknowledged. For example, errors may be introduced due to evaporation from the rain gauge or reduced catch due to wind effects (Rodda, 1967; Legates and Willmott, 1990; Sevruk, 1996; Sevruk *et al.*, 2009).

Uncertainties also arise through representativeness issues related to i) the adequacy (in terms of number and location of gauges) of the rain gauge network to capture the spatial variability in rainfall over a catchment, and ii) the methods and assumptions used to convert point data into areal precipitation estimates for input to a hydrological model, for example through the use of spatial averaging to provide sub-catchment average data or interpolation to provide gridded data (Mileham *et al.*, 2008; McMillan *et al.*, 2011).

The derivation of areal precipitation is often particularly problematic in mountainous regions (Frei and Schär, 1998; Frei *et al.*, 2003; Immerzeel *et al.*, 2012b; Duethmann *et al.*, 2013). Orography influences the spatial pattern and amount of precipitation through a wide variety of processes (Roe, 2005; Houze, 2012). Generally, these processes lead to an increase in precipitation with elevation, especially on windward slopes, with leeward slopes typically being drier due to the rain-shadow effect (Legates and Willmott, 1990; Duethmann *et al.*, 2013). Average precipitation rates therefore show greater spatial variability in mountainous regions compared to flatter regions (Legates and Willmott, 1990). Consequently, the spatial density of rain gauges should ideally be higher in mountainous areas in order to capture this variability, as recommended by the World Meteorological Organization (WMO, 2008). For example, for non-recording rain gauges, a density of 250 km^2 per station is recommended, compared to 575 km^2 per station on interior plains and 900 km^2 per station in coastal regions (WMO, 2008). Unfortunately, a high density of rain gauges in mountainous regions is often not achieved (Yu *et al.*, 2011; Immerzeel *et al.*, 2012b).

Furthermore, rain gauge networks (and meteorological station networks in general) in mountainous regions often display a bias towards having stations sited at lower elevations (i.e. valley bottoms) due to the logistical difficulties of operating stations at higher altitudes, which can lead to systematic underestimation of precipitation (e.g. Frei and Schär, 1998; Frei *et al.*, 2003). In some hydrological modelling studies, a precipitation lapse rate (elevation-based correction factor) is applied in order to address a perceived deficiency in rain gauge precipitation data (e.g. Immerzeel *et al.*, 2012b; Wijesekara *et al.*, 2014).

As an alternative to areal precipitation estimates based upon rain gauge data, remotely sensed rainfall derived from radar or satellite-based data may be employed as input to a hydrological model. Such datasets may be particularly valuable in regions with limited station-based records (e.g. Andersen *et al.*, 2002a; Su *et al.*, 2008; Lauri *et al.*, 2014). However, these datasets are inherently uncertain; errors arise from temporal and spatial sampling errors and uncertainty in the methods for estimating rainfall based on the remotely sensed data (Winchell *et al.*, 1998; Villarini *et al.*, 2008).

As highlighted above, when developing a hydrological model, there may be different precipitation datasets available, such as point- / station-based rain gauge data or alternative gridded datasets derived from interpolation of station-based data, remotely sensed rainfall data, or the merging of observational datasets (and sometimes climate model output) to form reanalysis datasets (see for example El-Sadek *et al.*, 2011; Lauri *et al.*, 2014 for studies comparing alternative precipitation datasets in specfic basins). Previous studies have found that recalibration of a model is often required after switching from one meteorological dataset to another. For example, the SLURP model of the Mekong developed by Kite (2000) required recalibration after switching from sub-catchment averaged climate inputs derived from station data for a simulation period of 1994–1998, to sub-catchment averaged data derived from gridded data (Kingston *et al.*, 2011). Similarly, Hughes *et al.* (2011) found that a pre-existing Pitman hydrological model of the Okavango Basin required recalibration when switching from station-based sub-catchment averaged precipitation to sub-catchment averaged precipitation derived from gridded data. In another example, Xue *et al.* (2013) found that recalibration of a hydrological

model of the Wangchu Basin of Bhutan specifically for satellite precipitation products provided significant improvements in model performance compared to forcing the rain gauge-calibrated model with the satellite products without recalibration.

Other studies have also reported improvements in model performance following precipitation-specific calibration (e.g. Stisen and Sandholt, 2010; Jiang *et al.*, 2012). Similarly, in a study exploring the impact of rain gauge sampling upon model performance and parameterisation, Andréassian *et al.* (2004) showed that through calibration of parameters, catchment models are able to cope with rainfall data of varying quality. These studies demonstrate that use of alternative precipitation datasets to drive a hydrological model can impact simulated runoff and model calibration. However, it is difficult to find studies that compare hydrological model projections under climate change simulated after using alternative precipitation datasets for model calibration/baseline simulation (and hence also for perturbing to generate scenario precipitation data), but keeping all other model components and inputs the same.

A notable exception is a study by Remesan and Holman (2015) that explored how use of two different baseline precipitation datasets (TRMM and APHRODITE) and three different reference evapotranspiration (ETo) methods (FAO Penman–Monteith, Hargreaves-Samani and Priestley-Taylor) impacted the baseline hydrological model calibration/parameterisation and uncertainty in simulated climate change impacts. The hydrological model used was HySim and the study area was the north western Himalayan Beas river catchment. Six models were developed using different combinations of the baseline input datasets. A key finding was that model calibration compensated for uncertainties in input data, enabling similar calibration performance for the alternative models. However, there were significant differences between the six models in simulated changes in mean, high and low river flows under scenario climate conditions. The level of inter-hydrological model uncertainty tended to be higher under scenario climate conditions compared to the baseline. This study demonstrates that choices made during model construction, including choice of baseline precipitation data and PET method, can have important implications for the simulated hydrological impacts under climate change. This

finding is particularly relevant for data-sparse regions (Remesan and Holman, 2015), where uncertainty in meteorological datasets will be higher.

2.7. Uncertainty in future freshwater resources due to multiple drivers of change

As highlighted above, climate change is a key driver of potential change in hydrological systems. However, freshwater resources are impacted by a myriad of non-climatic drivers of change. These include riverine and groundwater abstraction (e.g. for domestic, industrial and agricultural water use); land cover change; changing agricultural practices; the implementation or alteration of irrigation schemes; river engineering; and the construction and management of reservoirs, dams and other water control structures (Bates *et al.*, 2008; Praskievicz and Chang, 2009; Wilby and Dessai, 2010; Jiménez Cisneros *et al.*, 2014). These drivers are in turn influenced by a number of factors, such as population growth, water demand changes, economic development, technological advancements, changing scientific knowledge, evolving societal attitudes and the prevailing political and regulatory environment (Bates *et al.*, 2008; Praskievicz and Chang, 2009; Wilby and Dessai, 2010; Jiménez Cisneros *et al.*, 2014). Importantly, adaptation measures may be undertaken to reduce or ameliorate potential negative impacts of climate change on water resources and their human use (Stakhiv, 1997; Bates *et al.*, 2008; Wilby and Dessai, 2010; Bastakoti *et al.*, 2013; Jiménez Cisneros *et al.*, 2014). Non-climatic drivers of change (whether or not they are related to adaptation) will therefore interact with climatic drivers of change to impact future freshwater resources.

In many cases, hydrological climate change impact assessments do not take non-climatic drivers of change into account (i.e. only climate change scenarios are simulated). This is a justifiable and useful method as it allows the potential impacts of climate change to be explored in the absence of other changes. This approach is taken in this thesis. However, when reviewing the results of assessments that use this approach, it is important to recognise that future water resources will in fact be strongly influenced by interacting drivers of change, both climatic and non-climatic. This contributes to the uncertainty in water resource projections (e.g. river flow projections) under changing climate.

2.8. Summary

This chapter has provided an in-depth review of the tools and approaches employed in hydrological climate change impact assessments and various sources of uncertainty introduced through the modelling process. In addition, the pre-existing SLURP model of the Mekong and the Mac-PDM.09 GHM, both of which have been used for climate change impact assessment on the Mekong, have been introduced. The MIKE SHE model code, which will be employed subsequently in this thesis, has also been introduced.

Having discussed the key tools, concepts and issues relevant to this thesis, subsequent chapters investigate various understudied sources of uncertainty using the Mekong River Basin as a case study site. An overview of the Mekong and the data employed within the subsequent hydrological modelling investigations is therefore provided in the next chapter.

Chapter 3

The Mekong River Basin

3.1. Introduction

As described in Section 1.5.1, this thesis uses the Mekong River Basin as a case study catchment for the investigation of sources of uncertainty in modelled river flow projections under climate change. The trans-boundary Mekong River is located in Southeast Asia (Figure 3.1) between 8–34 °N and 93–109 °E and is the eighth largest river in the world in terms of discharge (ca. 475 km^3 $year^{-1}$; MRC, 2011), 12th longest (4350 km) and 21st largest by drainage area (795,000 km^2) (Kingston *et al.*, 2011). It originates on the Tibetan Plateau in China, where it is named the Lancang, at an elevation of over 5000 masl (meters above sea level) (Zhou *et al.*, 2006). The Mekong River flows in a generally southeasterly direction through China's Yunnan Province and then flows through or borders a further five countries: Burma, Laos, Thailand, Cambodia and Vietnam, before reaching the South China Sea. Major tributaries include the Chi and Mun, which drain the Khorat Plateau (also Korat) of eastern Thailand and join the Mekong upstream of Pakse, and the Se Kong, Se San and Sre Pok, which rise in Vietnam's Central Highlands and flow into the Mekong at Stung Treng. The Mekong Basin can be broadly divided into the Upper Mekong Basin, which is upstream of Chiang Saen and encompasses the part of the basin in China and eastern Burma, and the Lower Mekong Basin, which extends southeastwards of this point to the South China Sea.

The Mekong Basin has a population of over 65 million people (MRC, 2016), more than two-thirds of whom live in rural areas and are strongly dependent on the Mekong River and its tributaries for their food, water and livelihoods (MRC, 2010b). The Mekong River is highly biodiverse and its annual flood pulse is essential for the productivity of agriculture, wetlands and fisheries in the Lower Mekong Basin (south of China) (UNEP, 2006; MRC, 2010b; UNEP, 2010). In particular, flows of the Mekong are vitally important within the Mekong Delta in Vietnam, providing water and fertile silt to vast rice paddy fields, washing away acidic and salty water from soils and sustaining high levels of fish production and consumption from both capture fisheries and aquaculture (Hortle, 2007; Hoa *et al.*, 2008). As well as feeding

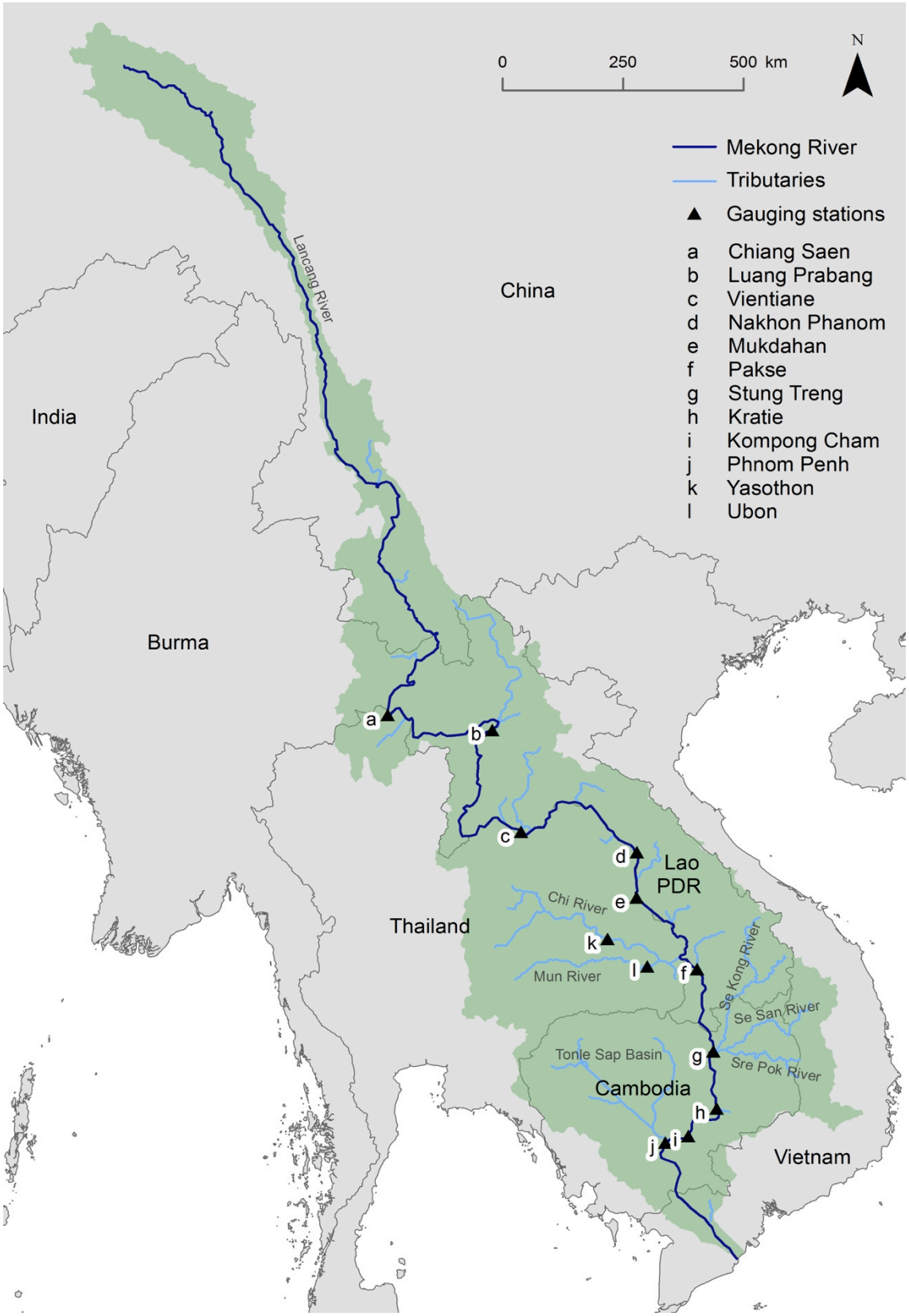

Figure 3.1. The Mekong catchment, including the river network and gauging stations employed during the development of a MIKE SHE model of the Mekong.

a large proportion of Vietnam's population, a large volume of the agricultural and fisheries outputs from the Mekong Delta are exported (Cosslett and Cosslett, 2014). Similarly, the hydrological regime, wealth of biodiversity and high productivity of the Tonle Sap Lake in Cambodia, which is the largest freshwater lake in Southeast Asia, are dependent upon wet season flows in the Mekong River downstream of Kratie (Sokhem and Sunada, 2006). The lake is connected to the Mekong River via Tonle Sap River, which flows towards the Mekong River in the dry season, but towards Tonle Sap Lake in the wet season, causing it to expand in area (Kummu *et al.*, 2006). The Tonle Sap plays a vital role in the food security and economy of Cambodia (Bonheur and Lane, 2002).

Climate change could have severe consequences for the Mekong River system and major concerns exist about the implications of changes in flood patterns associated with changes (e.g. in terms of magnitude or seasonality) in Mekong River flows (Eastham *et al.*, 2008; Penny, 2008; MRC, 2010b; Västilä *et al.*, 2010; Bastakoti *et al.*, 2013). Determining the potential impacts of climate change on the Mekong River is therefore highly important. However, climate change is by no means the only driver of change in the Mekong Basin. For example, a combination of rapid population growth, rural to urban migration and rising incomes are expected to lead to large increases in the demand for food and electricity, therefore increasing the pressure on its water resources (Pech and Sunada, 2008; MRC, 2010b). Economic development and population growth also continue to drive large-scale logging and the expansion of agriculture, leading to high rates of forest degradation and deforestation (MRC, 2010b). Furthermore, the basin is undergoing significant hydropower development, with numerous dams planned for the Mekong River and its tributaries, with the potential for huge negative impacts on downstream biodiversity, migratory fisheries and hence food security (Ziv *et al.*, 2012). Existing mainstream dams in upstream parts of the catchment, the first of which (Manwan) was only completed in 1993, have already been implicated in changes in flow regime, sediment flows and fisheries (Li and He, 2008; Kummu *et al.*, 2010; Wang *et al.*, 2011; Räsänen *et al.*, 2017).

Climate change will interact with these pressures (Pech and Sunada, 2008; MRC, 2011; Grumbine *et al.*, 2012; Räsänen *et al.*, 2012). Effective water resources

planning within the Mekong Basin must therefore take the potential impacts of climate change into account. For example, Grumbine *et al.* (2012) highlight that the planning of dams in the basin should take the potential impacts of climate change into account. Furthermore, the development and implementation of climate change adaptation strategies is identified by the Mekong River Commission (MRC) as a key regional priority (MRC, 2011).

This chapter provides an overview of the Mekong River Basin and presents the secondary data that are used within this thesis in setting up, parameterising, forcing and calibrating the hydrological models that are developed. In doing so, this chapter provides a conceptualisation of the basin, in terms of the key controls on the spatial and temporal variability of hydrological characteristics and processes within the catchment. This, and the sections of this chapter, are summarised in Figure 3.2.

3.2. Topography and physiography

Figure 3.3a shows the topography of the Mekong Basin and surrounding region. The 30 arc-second (approximately 1 km) resolution United States Geological Survey (USGS) GTOPO30 digital elevation model (DEM) (USGS, 1996) employed in the SLURP model of the Mekong (Kite, 2000, 2001; Kingston *et al.*, 2011) is utilised within this study. The basin extent is also indicated. This was defined by Kite (2000) through topographic analysis of the DEM using the United States Department of Agriculture / University of Saskatchewan digital terrain analysis tool TOPAZ (Topographic Parameterization tool; Garbrecht & Martz 1997). Figure 3.3b presents an elevation-area curve for the basin, derived from the USGS GTOPO30 DEM. This demonstrates that whilst parts of the catchment lie at over 5000 masl, the majority (over 70%) lies at less than 1000 masl, and over half the catchment is less than 500 masl. The basin can be divided into broad physiographic regions (MRC, 2003; UNEP, 2006; MRC, 2010b), as shown in Figure 3.3c. For the SLURP model, however, the basin was divided into 13 topographically-based sub-catchments using TOPAZ (Kite, 2000), as indicated in Figure 3.3d. These are subsequently referred to as SLURP sub-catchments, and their use is discussed further in Section 3.6. Table 3.1 provides elevation statistics for both the physiographic regions and SLURP sub-catchments, based on analysis of the DEM.

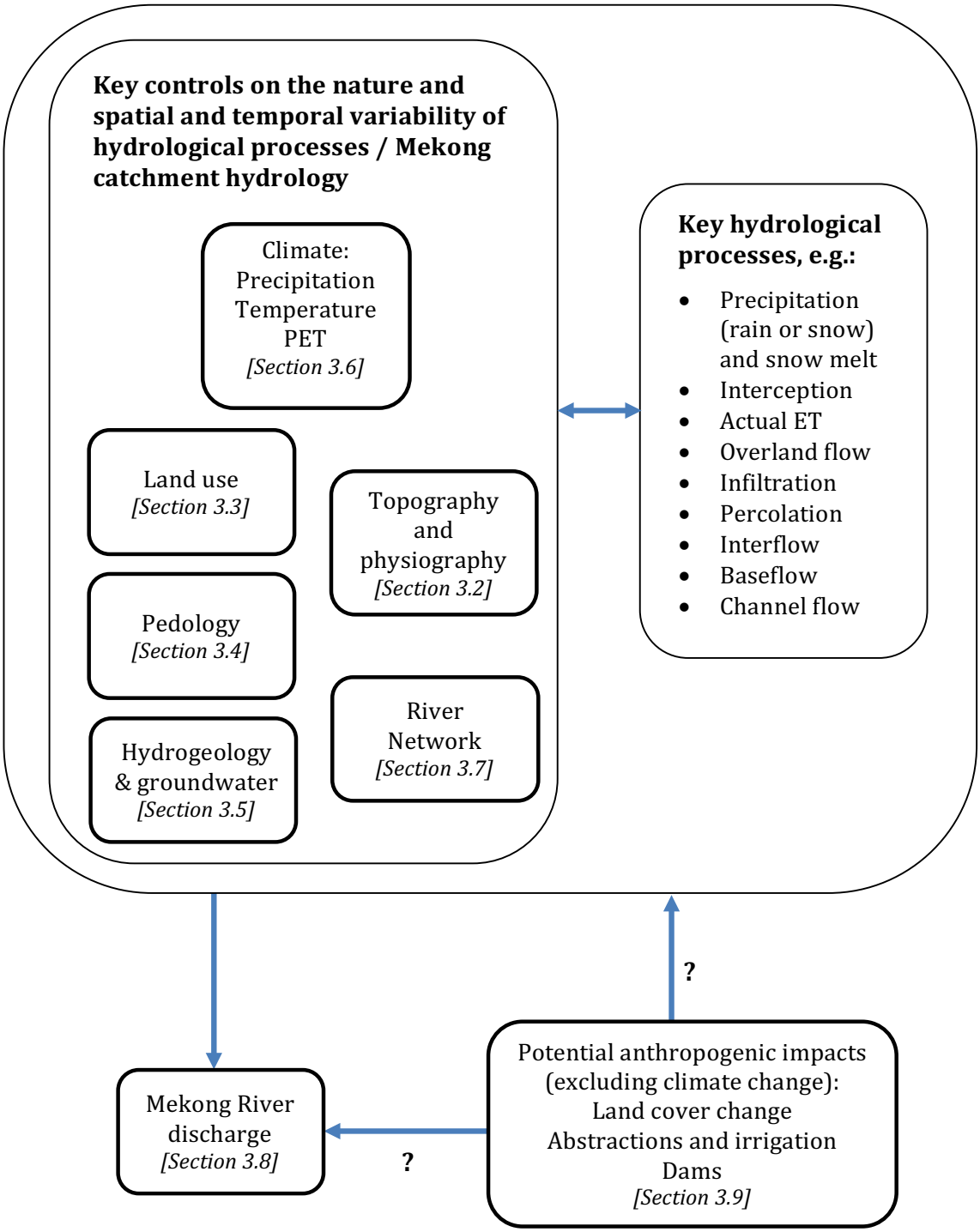

Figure 3.2. Conceptualisation of key controls on the nature and spatial and temporal variability of Mekong catchment hydrology. These influence, and are also influence by, key hydrological processes and associated characteristics. Combined, these influence Mekong river discharge. Anthropogenic activities also have the potential to impact catchment hydrology and Mekong river discharge. This diagram summarises the sections of this chapter (boxes with a thicker border). Arrows represent influence/impact.

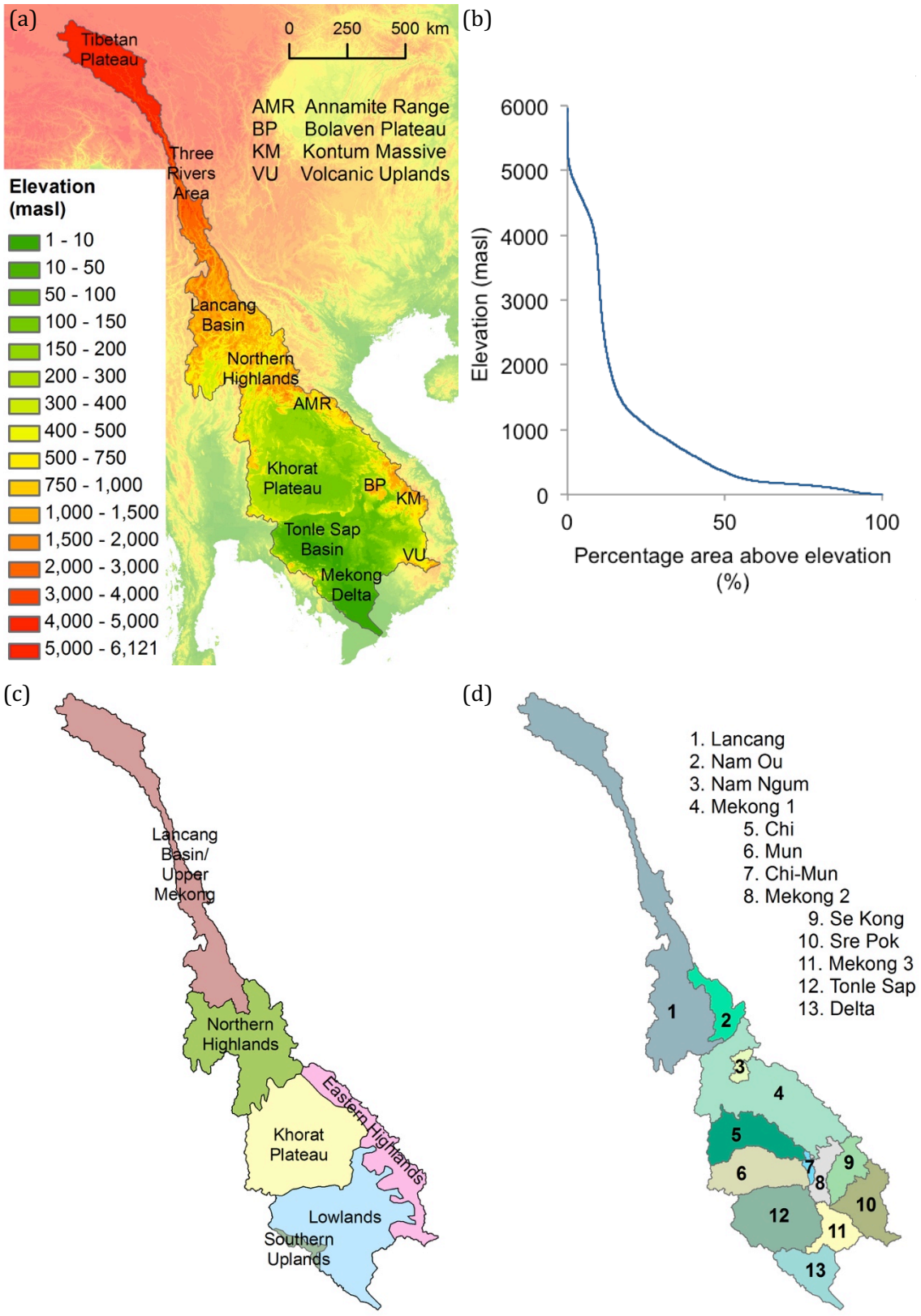

Figure 3.3. (a) USGS GTOPO30 DEM of the Mekong Basin and surrounding region. Labelling of regions and topographic features is based upon MRC (2010b). (b) Hypsometric curve for the Mekong Basin, derived using the basin DEM. (c) Physiographic regions of the basin, based on: UNEP (2006); MRC (2010b). (d) Sub-catchments used in the SLURP model of the Mekong (SLURP sub-catchments).

Table 3.1. Elevation statistics for the physiographic regions (top) and SLURP sub-catchments of the Mekong Basin (bottom), based on analysis of the GTOPO30 DEM.

Region	Area (km^2)	Min. elevation (masl)	Max. elevation (masl)	Median elevation (masl)
Lancang Basin	165530	483	5956	3099
Northern Highlands	155790	153	2706	784
Khorat Plateau	194360	96	1309	180
Eastern Highlands	91140	84	2207	571
Southern Uplands	8350	40	1680	305
Lowlands	188510	1	1404	70
SLURP sub-catchment	**Area (km^2)**	**Min. elevation (masl)**	**Max. elevation (masl)**	**Median elevation (masl)**
Lancang (1)	228,000	282	5956	1794
Nam Ou (2)	31,040	271	2009	930
Nam Ngum (3)	8,980	166	2601	1102
Mekong 1 (4)	158,250	96	2706	317
Chi (5)	56,590	103	1309	197
Mun (6)	61,570	97	1264	171
Chi-Mun (7)	4220	107	525	147
Mekong 2 (8)	20,780	61	1637	144
Se Kong (9)	28,910	58	2100	429
Sre Pok (10)	48,840	63	2250	336
Mekong 3 (11)	28,000	7	927	97
Tonle Sap (12)	87,530	1	1633	55
Delta (13)	40,930	1	1680	10

In comparison to the broad physiographic regions, the SLURP sub-catchments allow separate regions for some of the main tributaries of the Mekong, such as the Rivers Nam Ou, Nam Ngum, Chi, Mun, Se Kong, Se San and Sre Pok (both within the Sre Pok sub-catchment) and Tonle Sap sub-catchment.

In the upper Lancang, topography is mountainous and the Mekong (Lancang) and its tributaries flow through narrow gorges with steep sides and a steep channel gradient (Gupta *et al.*, 2002). In addition to the Mekong River, the eastern rim of the Tibetan Plateau is drained by the Salween and Yangtze Rivers. In the aptly named Three Rivers Area (see Figure 3.3a), these rivers run in approximately parallel valleys within relatively close proximity of each other (a few tens of kilometres), with the Salween to the west of the Mekong and the Yangtze to the east (MRC, 2010b). In this region, the basin of the Mekong is very restricted (in some places less

than 20 km wide) and the river flows through a deep ravine with no significant tributaries (MRC, 2010b). Downstream (to the southeast) of this region, the Mekong Basin widens as the paths of the three rivers diverge.

The Northern Highlands region, which is again mountainous, has elevations of up to 2700 m (Table 3.1) and encompasses the Burmese portion of the Mekong Basin, northern Thailand and northern Laos (MRC, 2003, 2010b). To the south of this region, a large proportion of the western Lower Mekong Basin (northeastern Thailand) is covered by the Khorat Plateau, a large saucer-shaped basin that is drained mainly by the Chi and Mun Rivers (FAO-Unesco, 1974b; Costa-Cabral *et al.*, 2008; MRC, 2010b). The majority of this region lies at elevations of between 150 masl to 300 masl (median: 180 m, Table 3.1), although some of the mountain ranges towards the boundary of this area reach altitudes of between 500 masl and 1300 masl (Floch and Molle, 2009).

The eastern rim of the Mekong Basin is bounded by a series of highlands that extend along the eastern border of Laos, eastern border of Cambodia and western border of Vietnam and have elevations of up to 2200 masl (Table 3.1). These are collectively known as the Eastern Highlands and include the Annamite Range, Bolaven Plateau and Kontum Massive (MRC, 2003, 2010b). The Se Kong, Se San and Sre Pok Rivers (see Figure 3.1) originate in this part of the basin.

The Lowlands comprise the floodplains of the Mekong in southern Laos and Cambodia, the Tonle Sap sub-basin in Cambodia and the Mekong Delta in Vietnam (MRC, 2003; UNEP, 2006). Although a small proportion (<0.05%) of the Lowlands reach elevations of over 500 masl, approximately two thirds of the area lies at less than 100 masl and over a quarter lies at less than 20 masl (median elevation: 70 m, Table 3.1). The Southern Uplands to the west of the Lowlands (in southeastern Cambodia) are extensions of the Northern Highlands (MRC, 2003).

3.3. Land use

To represent the spatial distribution of different land cover types and their associated characteristics (see Sections 4.2.2 and 4.2.3), this study employs a 1 km × 1 km land cover grid originally specified within the SLURP model of the Mekong (Kite, 2000). This was derived from the USGS Global Land Cover Characterization dataset (USGS, 1997), which was produced using NOAA-AVHRR (National Oceanic and Atmospheric Administration, Advanced Very High Resolution Radiometer) data covering a 12-month period from April 1992 to March 1993. The original 24 land cover classes of the USGS dataset (Figure 3.4a) were aggregated by Kite (2000) into nine categories (Figure 3.4b). Table 3.2 details the percentage coverage and dominant spatial distribution within the Mekong Basin of the nine aggregated land use classes and provides further information about the typical vegetation or land use of each class. It also indicates the constituting USGS classes (of the aggregated classes) and their percentage coverage. The dominant land uses are forest (42.6%), comprising evergreen (19.8%), mixed (13.7%) and deciduous forest (9.1%), and agriculture (39.1%).

Land cover change in the Mekong Basin is discussed in Section 3.9.1. In this study, land cover representation within the MIKE SHE model of the basin is kept the same throughout model calibration, validation and scenario modelling. Justifications for this include that there is a lack of studies that have demonstrated a clear impact of land cover change on river flows on the main Mekong (see Section 3.9.1) and that the vast majority of climate impact assessments adopt the same approach. Furthermore, this study aims to investigate only specific sources of uncertainty in Mekong River flows under climate change, such as GCM-related uncertainty and PET-related uncertainty. It does not aim to assess all potential sources of uncertainty. It is, however, worth recognising that land cover change is a potential driver of hydrological change and therefore another source of uncertainty when projecting Mekong river flows.

(a)

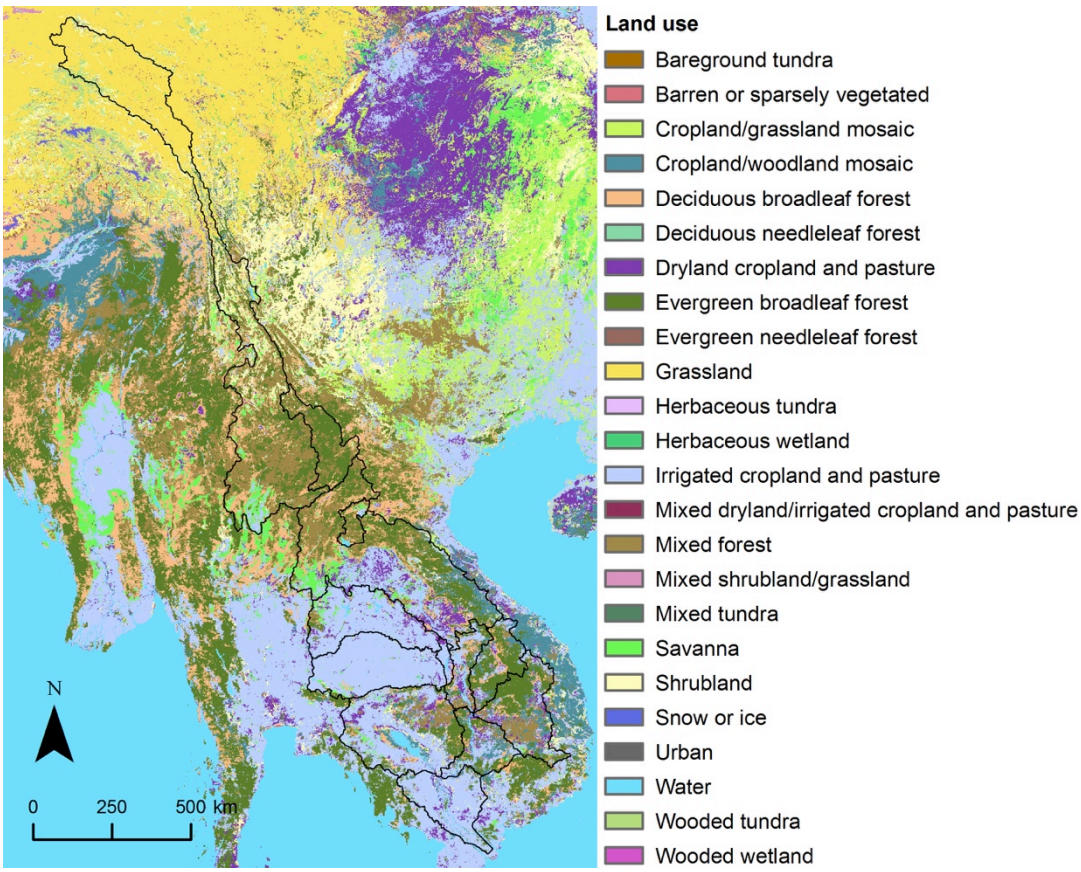

(b)

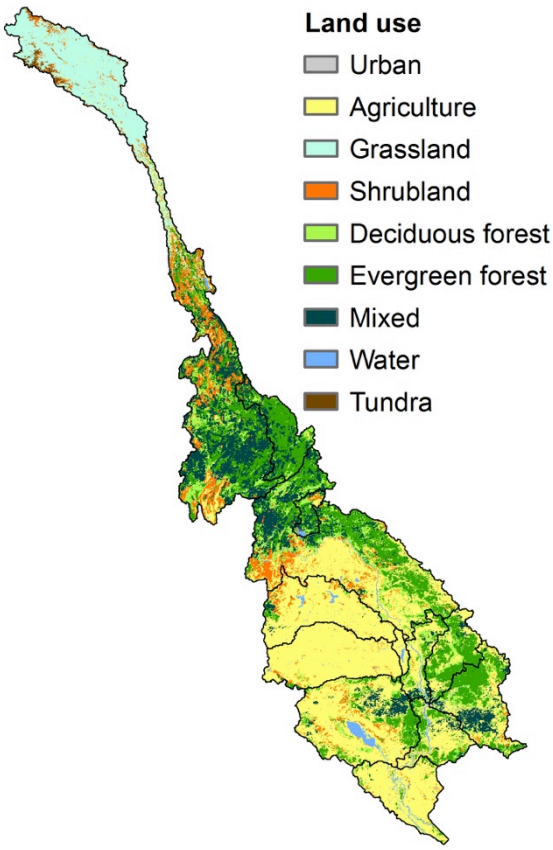

Figure 3.4. (a) USGS digital land cover map of the world. (b) Land cover map for the Mekong Basin derived from map a. SLURP sub-catchments shown to aid interpretation.

Table 3.2. Land use characteristics, including percentage coverage and dominant spatial distribution of nine aggregated USGS land use classes.

Land use class	Percentage coverage (%)	Dominant spatial distrubution	Constituting USGS land cover classes	Percentage coverage of constituting classes (%)	Further information / typical vegetation/land use*
Urban	0.1	Concentrated in major urban centres, e.g. Vientiane, Phnom Penh	Urban	0.1	Minimal vegetation, impervious surfaces. Much of the land is covered in structures or roads.[1]
Agricuture	39.1	Khorat Plateau and Lowlands of the Lower Mekong Basin	Cropland/grassland mosaic Cropland/woodland mosaic Dry cropland and pasture Irrigated cropland and pasture	0.3 4.7 5.4 28.7	Rice is the dominant crop and is both rainfed and irrigated. Others include maize, fruit, vegetables, oil crops, tea, coffee and sugar.[2]
Grassland	8.9	Concentrated largely in the upper and mid-Lancang	Grassland	8.9	Alpine grassland dominates on the Tibetan Plateau.[3]
Shrubland	7.5	Lower sections of the Lancang and northen parts of the Khorat Plateau	Shrubland Mixed shrubland/grassland Savanna	3.7 0.01 3.8	Dominated by grasses, shrubs and herbaceous plants <2 m tall, with canopy cover <60%.[5]
Deciduous forest	9.1	Small patches adjacent to other forest types	Deciduous broadleaf forest Deciduous needle leaf forest	9.1 0.0002	Broadleaved species dominate. From the Upper to Lower Mekong Basin there is a transition from temperate and subtropical to tropical forests. Montane forest is found at higher altitudes in both the Upper and Lower Basin.[4]
Evergreen forest	19.8	Lower Lancang, Northern and Eastern Highlands	Evergreen broadleaf forest Evergreen needle leaf forest	19.8 0.04	
Mixed forest	13.7	Lower Lancang and Northern Highlands	Mixed forest	13.7	
Water	1.4	Concentrated in the Tonle Sap Lake and along the Mekong and its tributaries	Water Herbaceous wetland Wooded wetland	1.4 0.0005 0.01	Seasonally inundated land is not included in this land use class. [1]
Tundra	0.4	Wholly in the upper Lancang	Wooded tundra Snow or ice	0.4 0.0001	Only sparse, predominantly low-lying vegetation.[1]

*Sources: [1]Anderson *et al.* (1976); [2]MRC (2010b); [3]Gao *et al.* (2010); [4]Rundel (2009); [5]FAO (2000).

3.4. Pedology

In order to characterise the spatial distribution of soil characteristics for the Mekong Basin, a methodology is adopted that was previously outlined by Andersen *et al.* (2001) for modelling the Senegal River Basin. Following their methodology, soil texture data for the Mekong Basin were extracted from the FAO Digital Soil Map of the World (FAO, 1998). Figure 3.5 presents a soil map for the Mekong Basin derived from the FAO soil map. The catchment is divided into 382 map units (polygons) that are categorised into 41 different FAO soil associations. Each soil association map code contains the abbreviation for the dominant soil unit (i.e. the soil unit occupying the largest area of the map unit). Soil unit here means soil type. This is followed by a number indicating the composition, including associated soils and inclusions, of the soil association (FAO-Unesco, 1974b). Associated soils are subdominant soils that cover more than 20% of the map unit. Inclusions refer to important soils that occupy less that 20% of the map unit (FAO-Unesco, 1974b). In the case of associations for which lithosols (abbreviation I) are dominant, the abbreviations for one or two of the associated soil units are additionally provided, and there is no composition number. Lithosols are soils 'which are limited in depth by continuous coherent hard rock within 10 cm of the surface' (FAO-Unesco, 1974a: 34). When information on soil texture is available, a hyphen and a second number signifying the textural class of the dominant soil follow the dominant soil unit and association code. There are three textural classes: (1) coarse, (2) medium and (3) fine. As summarised in Table 3.3, these represent the relative proportions of clay, silt and sand in the soil (FAO, 2003). The final part of each soil association map code is a letter indicating the slope class of the map unit.

The composition of each soil association in Figure 3.5 is provided in Table 4 of the FAO Soil Map report for Southeast Asia (FAO-Unesco, 1974b: 35:43). This information is not presented here since soil associations are not used in this thesis. Instead, the FAO soil texture classes are employed for the distribution of soil parameters in the MIKE SHE model of the Mekong (Section 4.2.4).

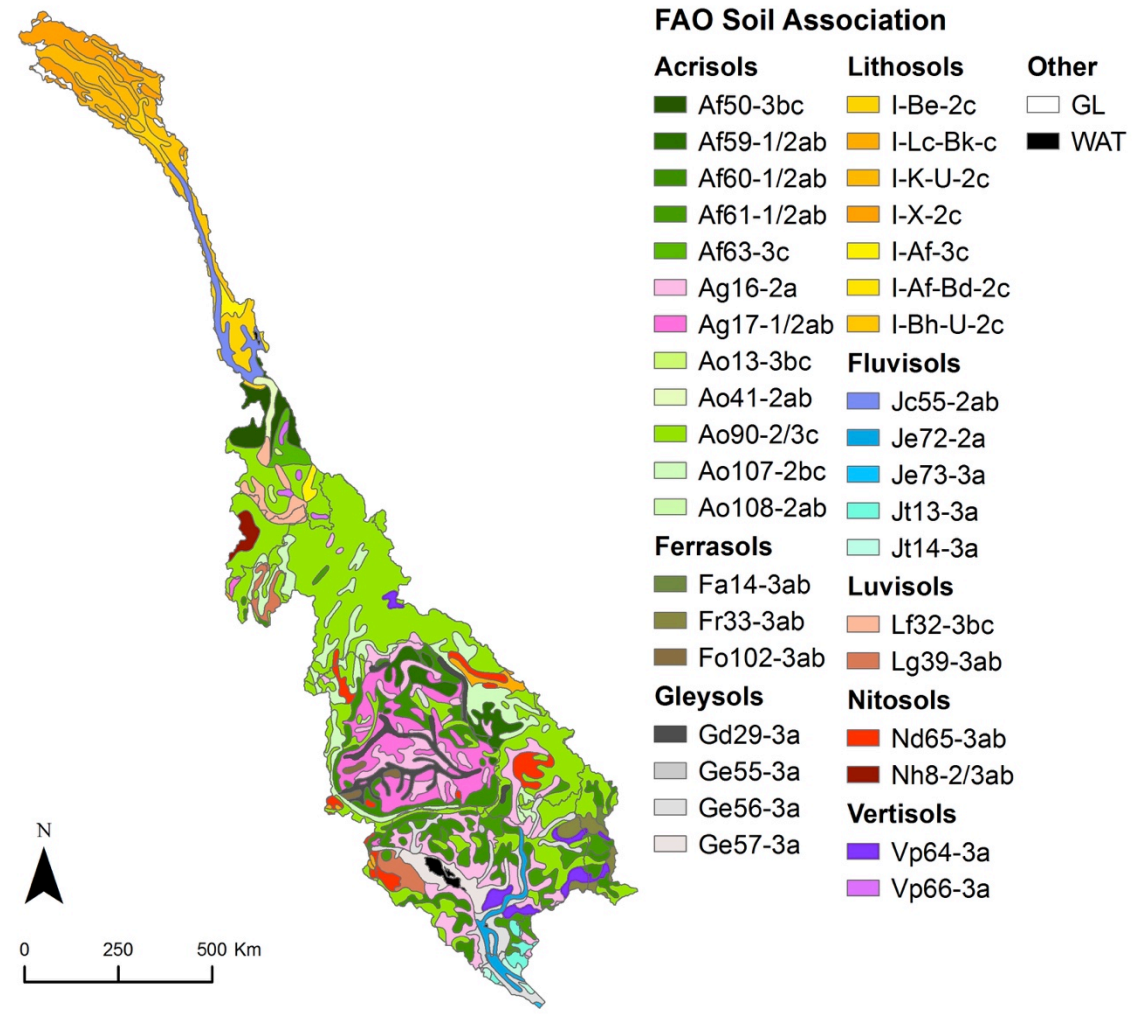

Soil Units

A	**ACRISOLS**	**G**	**GLEYSOLS**	**N**	**NITOSOLS**
Af	Ferric Acrisols	Gd	Dystric Gleysols	Nd	Dystric nitosols
Ag	Gleyic Acrisols	Ge	Eutric Gleysols	Nh	Hurric nitosols
Ao	Orthic Acrisols	**I**	**LITHOSOLS**	**V**	**VERTISOLS**
B	**CAMBISOLS**	**J**	**FLUVISOLS**	Vp	Pellic vertisols
Be	Eutric Cambisols	Jc	Calcaric Fluvisols		
Bh	Humic Cambisols	Je	Eutric Fluvisols		
F	**FERRALSOLS**	Jt	Thionic Fluvisols		
Fa	Acric Ferralsols	**K**	**KASTANOZEMS**		Other
Fr	Rhodic Ferralsols	**L**	**LUVISOLS**	GL	Glacier
Fo	Orthic Ferralsols	Lc	Chromic Luvisols	WAT	Water

Figure 3.5. Map of FAO soil associations within the Mekong Basin, derived from the FAO Digital Soil Map of the World (FAO, 1998).

Table 3.3. FAO soil texture and slope classes.

Texture class	**Description from (FAO-Unesco, 1974a: 5)**
Coarse soils (1)	'Sands, loamy sands and sandy loams with less than 18 percent clay and more than 65 percent sand'
Medium soils (2)	'Sandy loams, loams, sandy clay loams, silt loams, silt, silty clay loams and clay loams with less than 35 percent clay and less than 65 percent sand; the sand fraction may be as high as 82 percent if a minimum of 18 percent clay is present'
Fine soils (3)	'Clay, silty clays, sandy clays, clay loams, with more than 35 percent clay'
Slope class	
a	'level to gently undulating: dominant slopes ranging between 0 and 8 percent'
b	'rolling to hilly: dominant slopes ranging between 8 and 30 percent'
c	'steeply dissected to mountainous: dominant slopes are over 30 percent'

Figure 3.6 presents a soil texture map for the Mekong Basin derived from the FAO Digital Soil Map of the World (FAO, 1998). Using the approach adopted by Andersen *et al.* (2001) and Stisen *et al.* (2008), soils were aggregated into four broad categories based on textural classes: coarse/medium, medium, medium/fine and fine. The coarse/medium and medium/fine categories apply to soils where neither of the two component soil texture classes is dominant. Coarse soils do not occur as a stand-alone category within the Mekong catchment. Glaciers and water are two additional FAO classes within the catchment that represent permanently glaciated areas and permanent water bodies, respectively.

The upper Lancang and Three Rivers Area are dominated by medium-textured lithosols (shallow soils less than 10 cm deep), with relatively small permanently glaciated regions on the Tibetan Plateau. Glaciers cover just under 0.9% of the total catchment. In the Lancang Basin south of the Three Rivers Area, fine and medium/fine are predominant, whilst across the Northern and Eastern Highlands, medium/fine and medium are the prevalent texture classes.

On the Khorat Plateau, there are different terrace levels (FAO-Unesco, 1974b). The lower terrace levels (floodplain) adjacent to the channels of the Chi and Mun Rivers (and some of their tributaries) are inundated during the wet season. Fine-textured, poorly drained soils have developed here on old alluvium. Medium-textured and coarse/medium soils have developed on the old alluvium of poorly to moderately well drained higher terraces. The hills and mountains that border the Khorat Plateau

are characterised by coarse/medium and medium-textured soils (FAO-Unesco, 1974b).

A similar pattern can be seen over the Tonle Sap Basin, although the region of fine soils is larger. The area of water in this basin in Figure 3.6 indicates the dry season extent of Tonle Sap Lake, where soils would be permanently waterlogged. Adjacent to this, fine-textured soils have formed on the areas that would be inundated during the wet season. Medium-textured and coarse/medium soils dominate beyond this region. Downstream of Kratie and in the Delta region, medium-textured soils have developed from recent alluvial deposits on the natural levees along the Mekong River (FAO-Unesco, 1974b). Adjacent to these bands of medium-textured soils, fine textured soils dominate, with some areas of coarse/medium soils to the east and west of these bands of fine-textured soils.

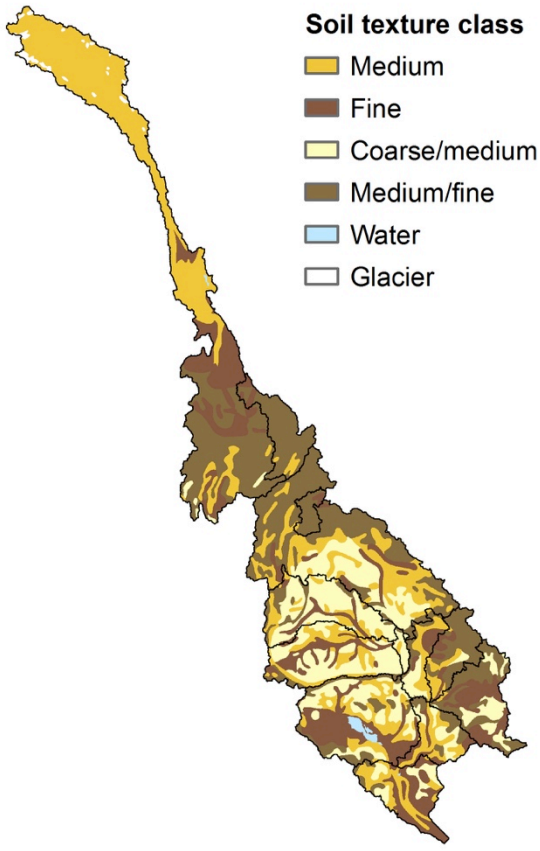

Figure 3.6. Soil texture map derived from the FAO Digital Soil Map of the World. SLURP sub-catchments shown to aid interpretation.

3.5. Hydrogeology and groundwater

As highlighted by University of Washington (2009), there isn't a coherent geological map for the Mekong Basin. Similarly, groundwater data for the Mekong region is very sparse (Johnston and Kummu, 2012). This helps explain why none of the models currently developed for the basin have a working, physically based groundwater model (Johnston and Kummu, 2012). Indeed, the MIKE SHE models developed in this study employ a conceptual saturated zone (see Section 4.2.5).

To provide a coarse overview of the hydrogeology of the Lower Mekong Basin, MRC (2010b) divided its aquifers into four broad categories based on lithology an connectivity. Figure 3.7 (from MRC, 2010b) presents the spatial distribution of these categories. It demonstrates that basement rocks, which support groundwater storage in weathered and fractured zones, but do not support a coherent subsurface flow regime, only cover a relatively small proportion of the basin. The other three categories are associated with porous, permeable aquifers with greater connectivity, and therefore make important discharge contributions to the Mekong and its tributaries (MRC, 2010b).

3.6. Climate

The dominant climatic influence on the Mekong is the Asian monsoon, which has two contrasting seasons; the wet southwest monsoon occurs between mid-May and mid-October, whilst the dry northeast monsoon occurs between October to March (Table 3.4; Adamson and Bird, 2010). Over 90% of annual precipitation falls within the wet season (Kite, 2001). Annual precipitation across the catchment varies considerably, ranging from under 1000 mm over large parts of the Khorat Plateau in Thailand (within the Chi and Mun river basins) to over 3200 mm in mountainous parts of Laos (MRC, 2010b). Precipitation falling as snow is limited to the northernmost parts of the catchment, since low enough temperatures do not occur over the lower Mekong. Snow covers approximately 5% of the basin between November–March and there is very little snow cover in the summer months of June–August (Kiem *et al.*, 2005), as shown in Figure 3.8. Maximum seasonal snow cover occurs in March (Savoskul and Smakhtin, 2013b).

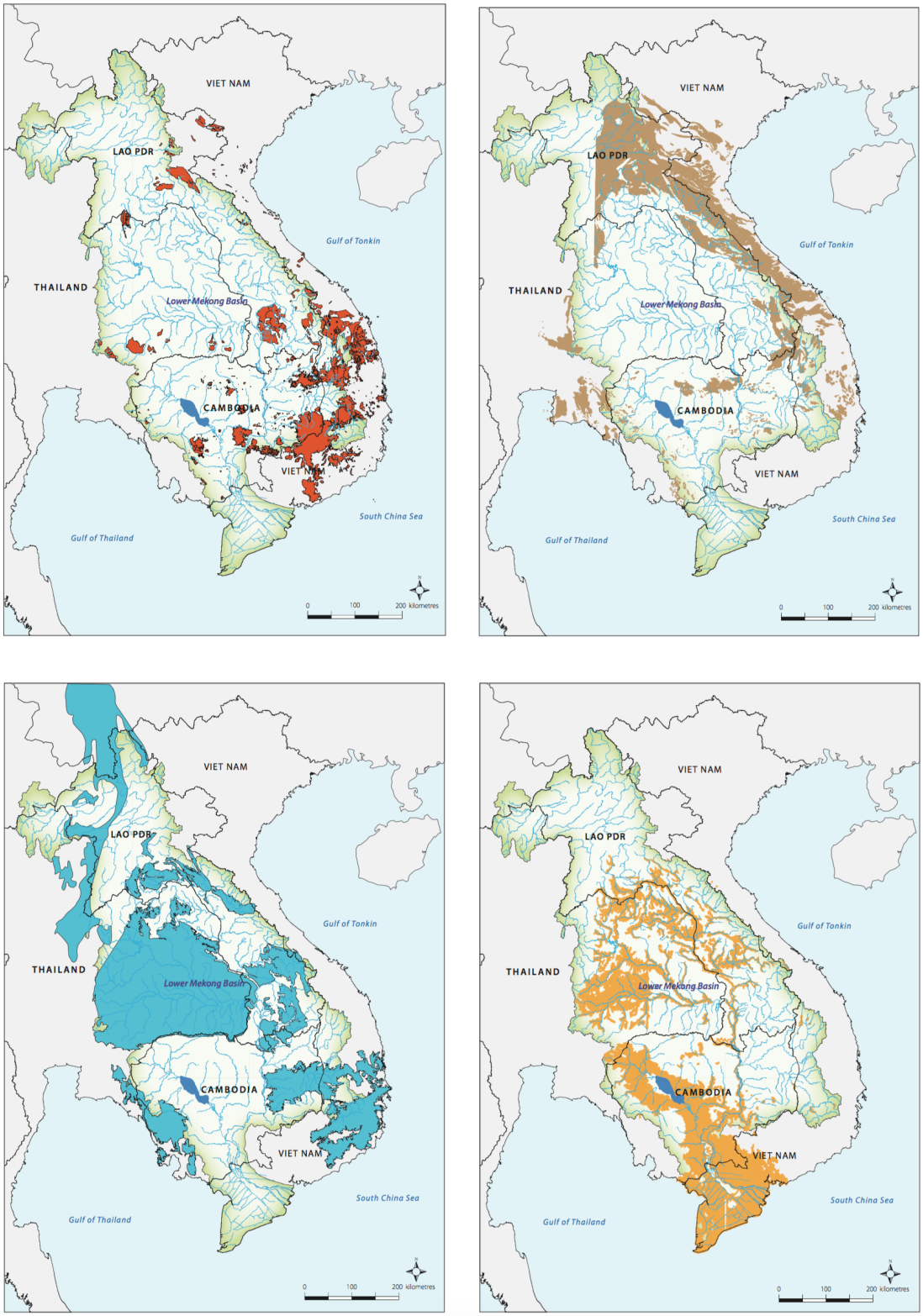

Figure 3.7. 'Types of aquifers in the Lower Mekong Basin: Top left: Basement rocks (granites and high-grade metamorphic rocks), groundwater storage in weathered and fractured zones. Top right: Late Paleozoic strata (sandstones and limestones), fragmented aquifers discharging to the Mekong mainstream and tributaries. Bottom left: Mesozoic strata (sandstones), regional aquifers, hosting the important groundwater flow regime in the Khorat Plateau. Bottom right: Alluvial/fluvial deposits in upstream areas and alluvial/deltaic/marine sediments of the Mekong Delta, important aquifers.' Source (figure and caption): MRC (2010b: 13).

According to Eastham *et al.* (2008), snow melt contributes approximately 8% of the mean annual discharge at Chiang Saen (station a, Figure 1.1) under historical climate (1951–2000). In contrast, the area covered by glaciers is much smaller (<0.001% of the basin) and glacier meltwater only accounts for 0.1% of mean annual discharge at Chiang Saen (Eastham *et al.*, 2008). Future climate-related changes in glacial meltwater will therefore have an insignificant impact on Mekong river flows and water availability (Eastham *et al.*, 2008; Savoskul and Smakhtin, 2013a).

Table 3.4. Generalised features of the seasonal climate in the Mekong Basin. Source: Adamson and Bird (2010).

Cooler		Hot/Dry		Wet					Hot/Dry		
Jan	Feb	Mar	Apr	May	Jun	Jul	Aug	Sep	Oct	Nov	Dec
NE Monsoon			Transition	SW Monsoon						NE monsoon	

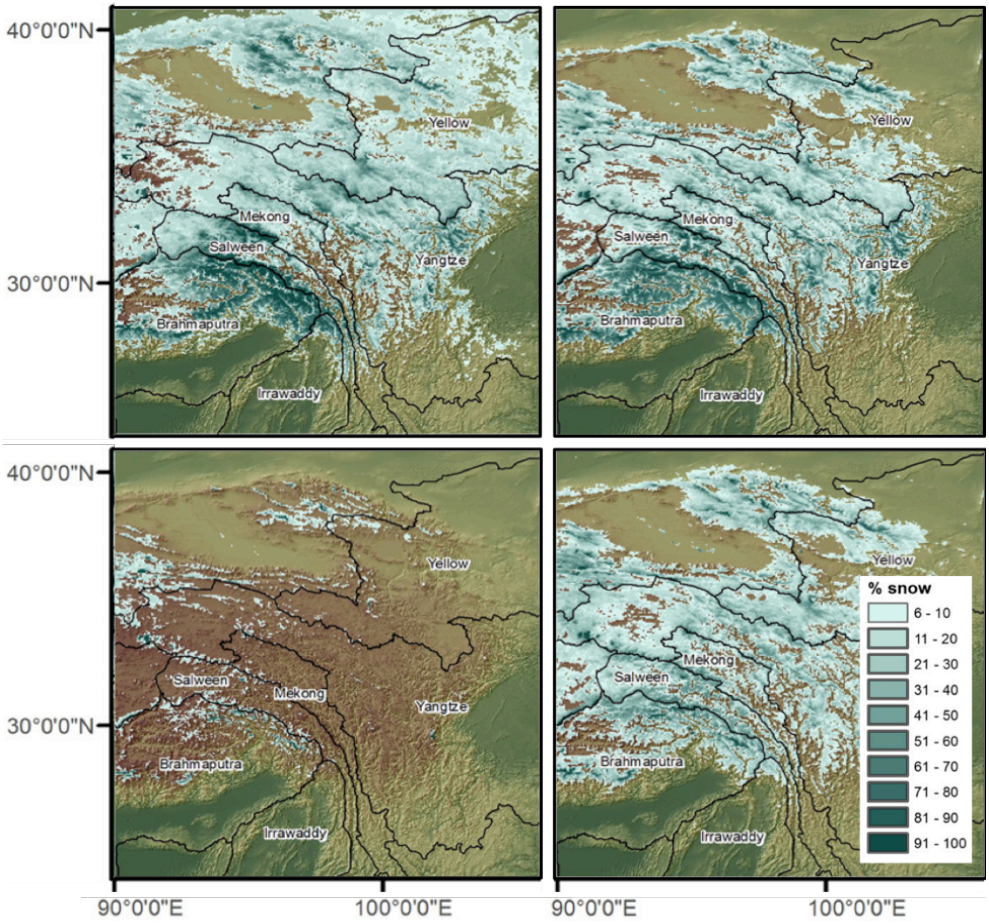

Figure 3.8. Seasonal snow cover (winter (top left), spring, summer, autumn (bottom right)) based on satellite snow cover time series from March 2000 to February 2008. The values show the percentage of time that a pixel was snow covered during the specified season within the entire time series. Adapted from: Immerzeel et al. (2009).

Sections 3.6.1 to 3.6.3 present observational climate data for the Mekong Basin from the specific secondary data sources employed in this thesis. Consistent with Kingston *et al.* (2011), this study uses the period 1961–1990 for model calibration and baseline simulation, and the period 1991–1998 for model validation. Climate data were therefore required for the period 1961–1998.

3.6.1. Precipitation

Precipitation data for the Mekong were obtained from two 0.5° × 0.5° spatial resolution, monthly gridded global datasets: the University of Delaware (UDel) dataset (Willmott and Matsuura, 2000) and the CRU TS 3.0 dataset (Mitchell and Jones, 2005). These datasets were selected to be consistent with Kingston *et al.* (2011). Furthermore, both are very widely used in the literature. Both datasets were generated through the interpolation of station based data onto a 0.5° × 0.5° (latitude/longitude) grid covering the global land surface (excluding Antarctica), with grid nodes centred on 0.25°. In both cases, monthly precipitation anomalies (differences compared to the climatological mean) for each station were interpolated onto a 0.5° × 0.5° grid. These were then combined with (added to) the corresponding fixed (i.e. time invariant) monthly gridded climatology to provide monthly gridded precipitation data. However, different interpolation techniques and sources of station records were employed for the two datasets (see Willmott and Matsuura, 2000; Mitchell and Jones, 2005). For the UDel data, Legates and Willmott's (1990) station archive was employed to generate the climatology (gridded average values), whilst data from the Global Historical Climatology Network (GHCN) version 2 (Vose *et al.*, 1992; Peterson and Vose, 1997) were used to generate the monthly precipitation anomalies and therefore temporal variability (Willmott and Matsuura, 2000; Kenji Matsuura, personal communication). For the CRU dataset, the CRU climatology (CL) version 1.0 (New *et al.*, 1999) provided the gridded normals (Mitchell and Jones, 2005; Harris *et al.*, 2014), whilst station records of precipitation were obtained from a wide variety of sources (see Mitchell and Jones, 2005; Harris *et al.*, 2014).

Figure 3.9 presents gridded mean annual precipitation derived from these datasets for the Mekong Basin. Data were obtained only for the 268 grid cells whose centre

coordinates fall within the catchment boundary. Some of the grid cells in Figure 3.9 that are adjacent to the catchment boundary therefore extend beyond the original UDel/CRU grid cell boundaries. The precipitation maps produced using the two different datasets exhibit similar general patterns. Both show lowest annual totals (<500 mm) over the upper Lancang on the Tibetan Plateau and a band of high annual precipitation totals (> 2000 mm) in the general region of the Eastern Highlands. Both datasets also depict annual precipitation totals of between 1250 mm and 1750 mm over the majority of the Lower Mekong Basin (e.g. over parts of the Northern Highlands, eastern Khorat Plateau and Lowlands), with a region of lower precipitation totals (1000 – 1250 mm) over the western Khorat Plateau.

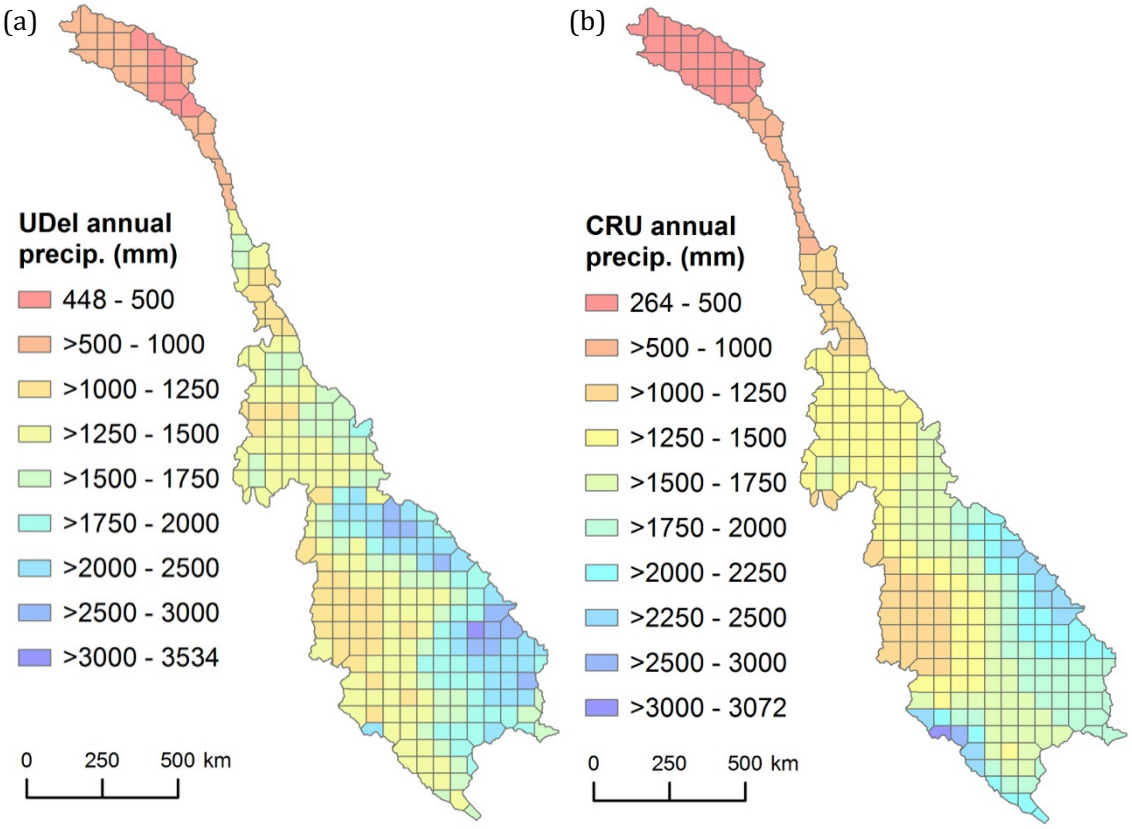

Figure 3.9. UDel (a) and CRU (b) mean annual total gridded precipitation, calculated for the period 1961–1998.

However, there are also some notable differences between the two datasets. In particular, UDel shows greater annual precipitation totals than CRU over parts of the upper Lancang (red region in Figure 3.9b) and Northern and Eastern Highlands. For example, UDel shows maximum totals of 589, 2441 and 3534 mm over these three regions, respectively, compared to values of 465, 1728 and 2352 mm for CRU. Conversely, UDel displays lower totals over parts of the western Tonle Sap Basin

(including the Southern Uplands) and Delta regions. For example, UDel shows a maximum precipitation total of 2300 mm over the Southern Uplands, compared to 3071 mm for CRU.

For the SLURP model of the Mekong (Kingston *et al.*, 2011), meteorological inputs were distributed according to the sub-catchments shown in Figure 3.3d. To provide a separate time series (for each meteorological input) for each sub-catchment, data were spatially averaged over the UDel/CRU grid cells whose centre coordinates fall within each respective sub-catchment. It is worth noting here that although, for completeness, data over the Tonle Sap and Delta regions/sub-catchments are presented for many of the datasets introduced in this chapter, hydrological model outputs from the Tonle Sap and Delta sub-catchments are not analysed in subsequent chapters. There are three reasons for this. Firstly, projections under climate change from the SLURP model of the Mekong (Kingston *et al.*, 2011) were not analysed below the Pakse gauging station. Secondly, there is a lack of observed discharge records for the purposes of model calibration/validation downstream of the Mekong 3 sub-catchment / Phnom Penh gauging station (see Section 3.8 for presentation of river discharge records). Thirdly, in order to model the bi-directional flow of the Tonle Sap River, a more computationally expensive numerical engine for the MIKE 11 river module (Section 4.3) would need to be used. Table 3.5 lists the number of CRU/UDel grid cells that fall within each of the 11 SLURP sub-catchments from which modelling results are analysed in subsequent chapters.

Table 3.5. Number of CRU/UDel grid cells per SLURP sub-catchment.

Lanc-ang (1)	Nam Ou (2)	Nam Ngum (3)	Mek. 1 (4)	Chi (5)	Mun (6)	Chi-Mun (7)	Mek. 2 (8)	Se Kong (9)	Sre Pok (10)	Mek. 3 (11)
83	10	3	52	18	18	1	7	9	16	8

Figure 3.10 displays mean monthly precipitation for both the SLURP sub-catchment average data and grid cell based data for five SLURP sub-catchments. These five sub-catchments were selected to encompass the four sub-catchments through which the Mekong River flows (Lancang and Mekong 1, 2 and 3) and one of the larger tributary sub-catchments (Mun). Plots are shown for both UDel-based (left) and CRU-based (right) precipitation. In each plot, the precipitation regime for each of the grid cells

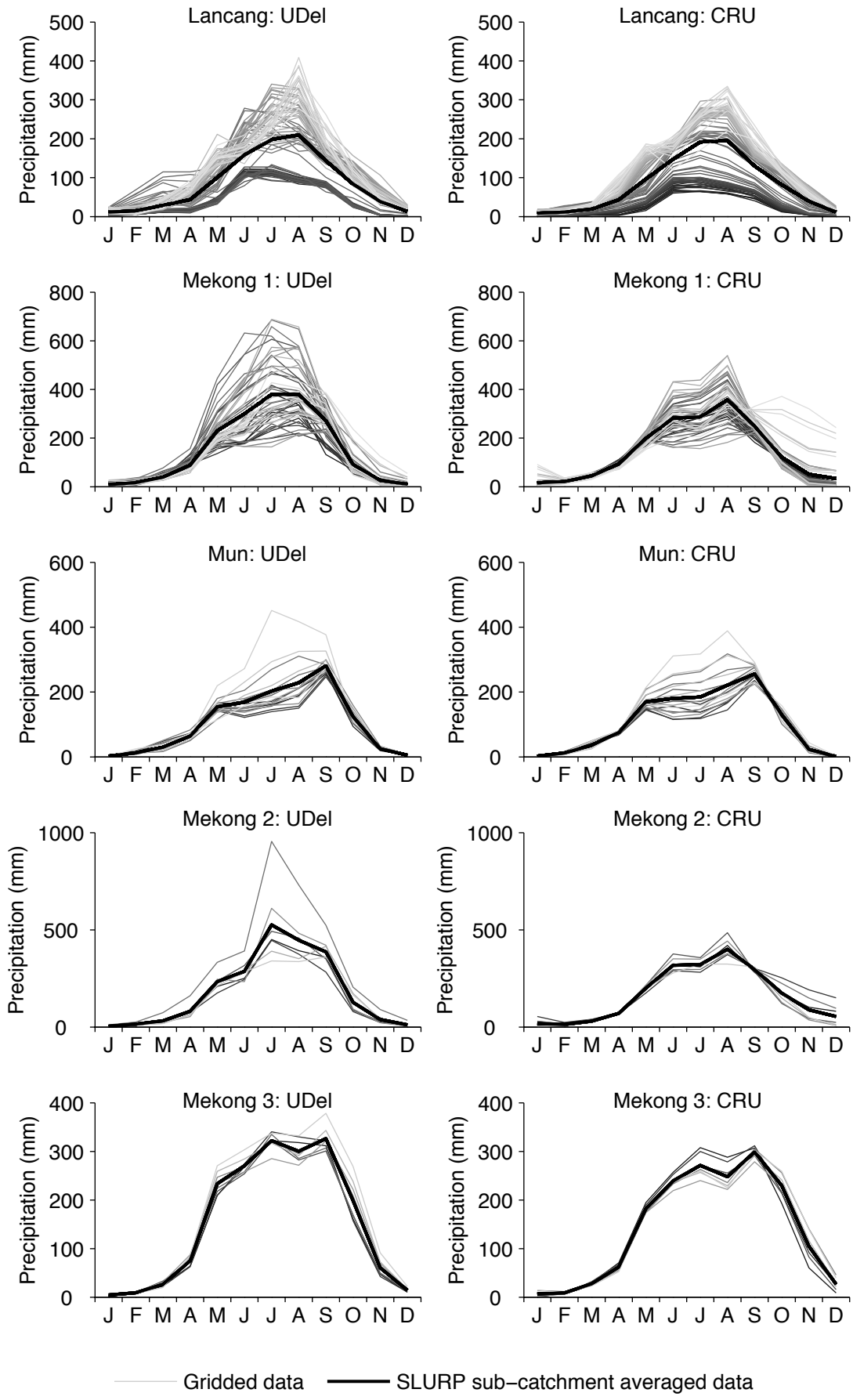

Figure 3.10. Grid based and sub-catchment average UDel and CRU mean monthly precipitation (for 1961–1998), presented for five SLURP sub-catchments. For each sub-catchment, grid cell based data are shown for the cells in that sub-catchment.

that falls within the named sub-catchment is shown, as well as the regime derived using SLURP sub-catchment average precipitation. These plots demonstrate that precipitation within the Mekong Basin is highly seasonal, with the highest mean monthly totals occurring between June and September.

In general, UDel and CRU display similar mean monthly precipitation patterns. However, in the case of gridded precipitation, over a given area (sub-catchment), UDel generally shows a greater spread of mean monthly precipitation values across the different grid cells for a given month. For both gridded and sub-catchment average precipitation, the temporal distribution of rainfall through the year can vary notably between UDel and CRU. For example, over the Mekong 1 sub-catchment, the month of peak precipitation varies between June and September for the gridded UDel data, leading to the sub-catchment average data showing approximately even mean monthly precipitation totals for July and August. In contrast, August is the month of peak precipitation for the majority of the CRU grid cells, leading to August being the month of peak precipitation for the sub-catchment average data. In addition, a small number of CRU cells in Mekong 1 display elevated mean monthly totals in October–December compared to both the other CRU cells in the same sub-catchment, and compared to the UDel data.

Monthly total precipitation and annual total precipitation are presented in Figure 3.11 for ten of the SLURP sub-catchments. Data are not shown for the smallest sub-catchment (Chi-Mun) or for sub-catchments downstream of Mekong 3, as this is (as discussed above) the furthest downstream catchment from which hydrological modelling results are extracted in subsequent chapters. In general, UDel and CRU display similar patterns of monthly total precipitation within each sub-catchment. However, it is apparent that peak monthly precipitation totals are frequently greater with UDel than with CRU, as are the annual precipitation totals. UDel and CRU annual totals are more consistently similar over the Lancang, Chi and Mun. For other sub-catchments, although the two datasets often show generally similar trends in terms of drier and wetter years, the disparity between the two datasets varies greatly from year to year. For example, despite showing a relatively small difference (<50 mm) in total annual precipitation for the Nam Ngum sub-catchment in 1986, there is a disparity of >350 mm for both 1985 and 1987.

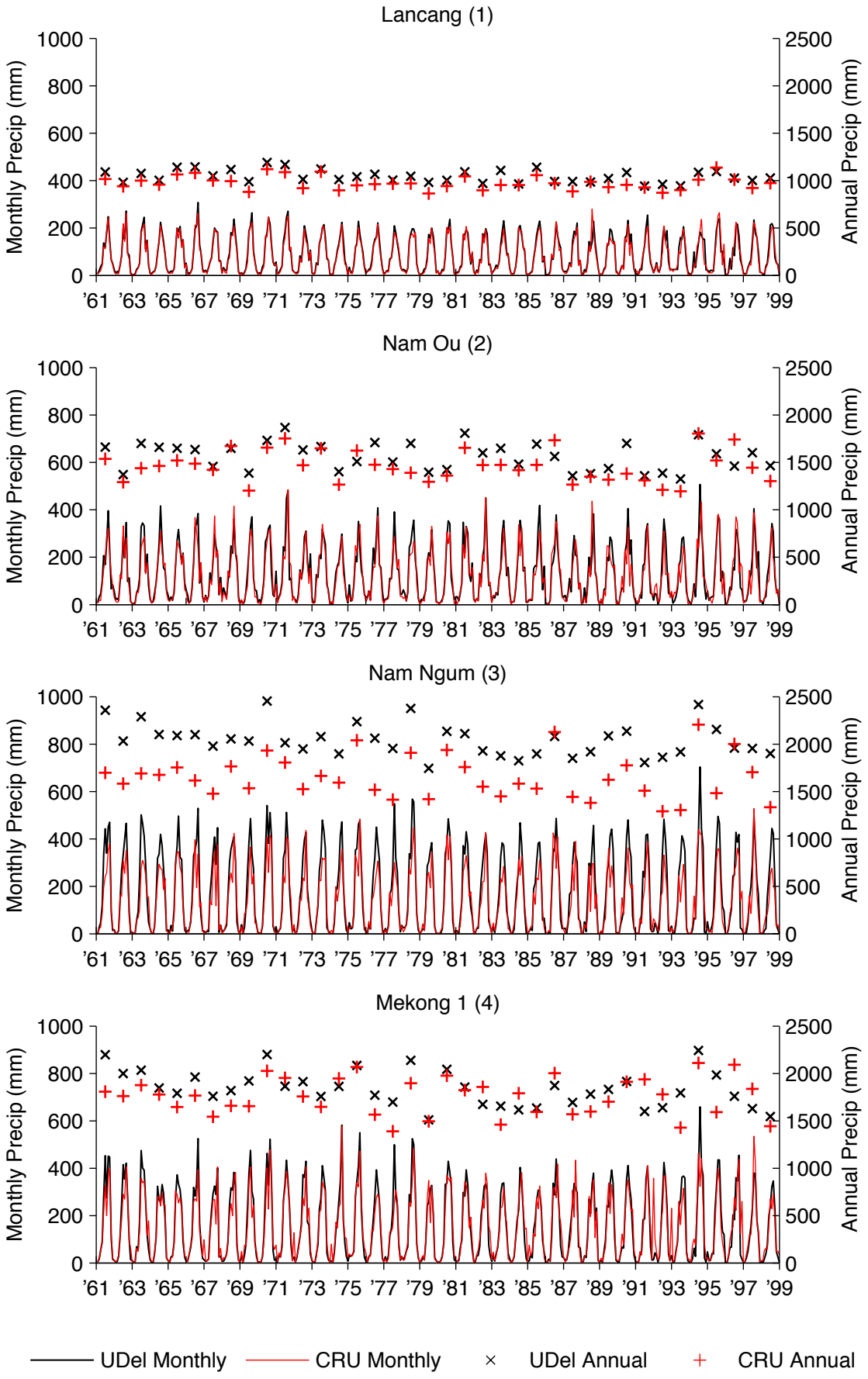

Figure 3.11. SLURP sub-catchment based UDel and CRU monthly total and annual total precipitation.

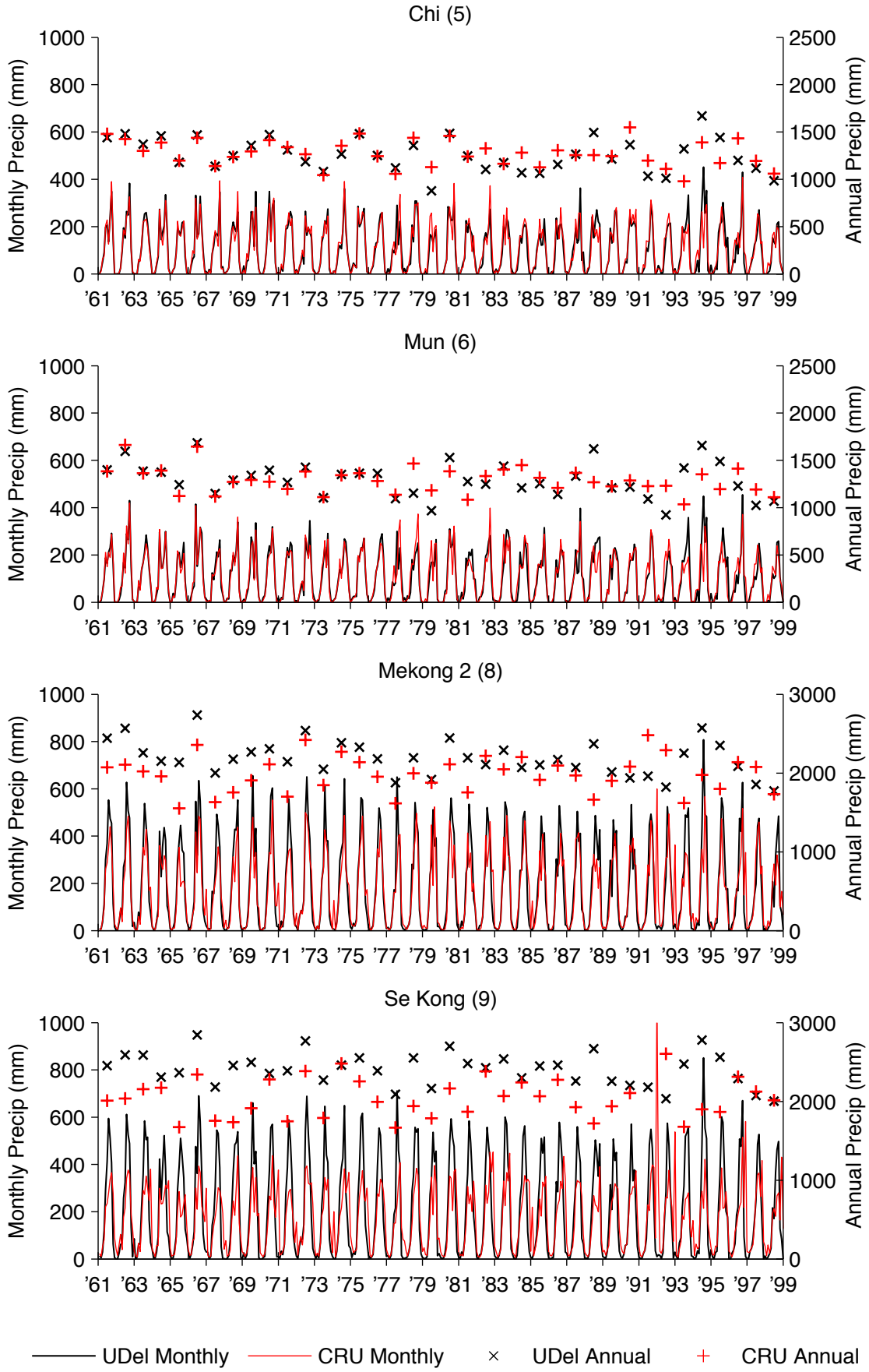

Figure 3.11. (cont.) SLURP sub-catchment based UDel and CRU monthly total and annual total precipitation. (Note different y-axis scales.)

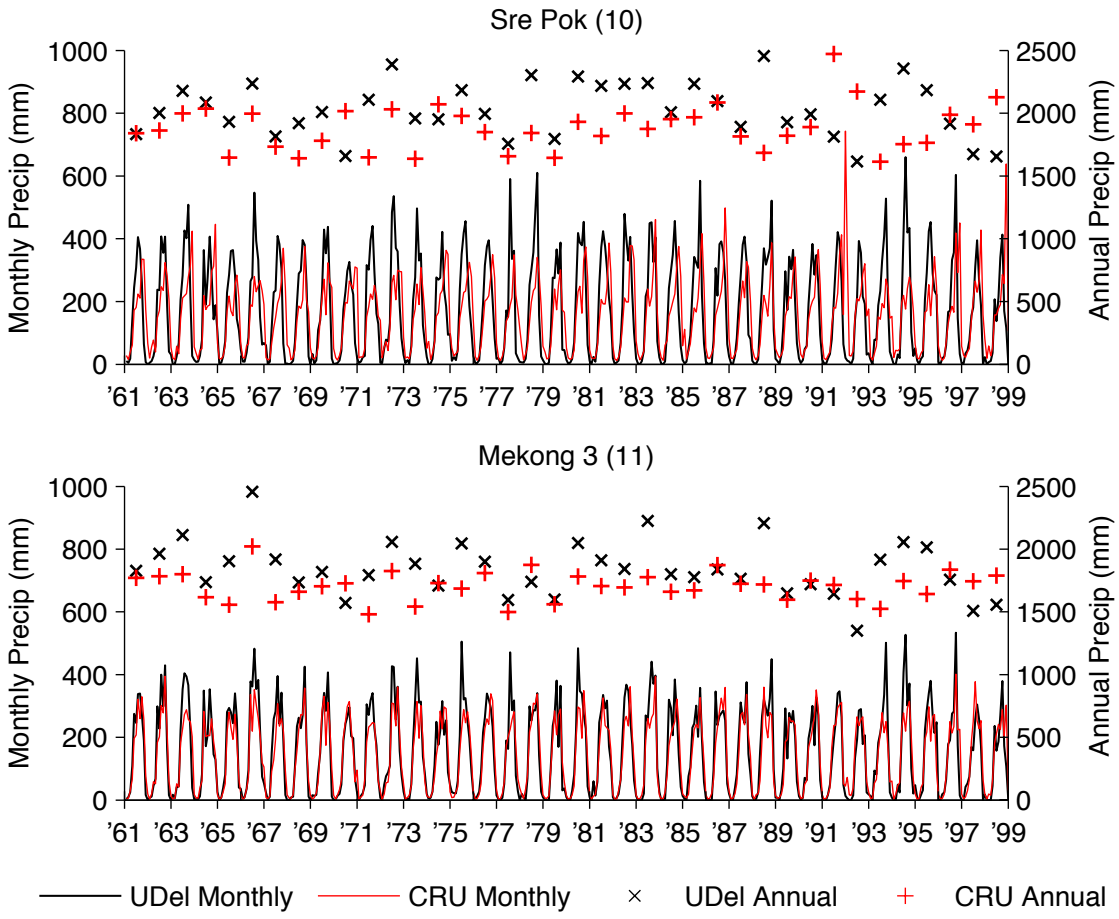

Figure 3.11. (cont.) SLURP sub-catchment based UDel and CRU monthly total and annual total precipitation.

Comparison of the minimum, mean and maximum mean annual precipitation totals across the grid cell based data for each SLURP sub-catchment (Table 3.6) further demonstrates that UDel is associated with higher annual values over the majority of the catchment. UDel produces the highest mean and maximum mean annual precipitation totals within all sub-catchments in Table 3.6 except the Chi sub-catchment in both cases. Across the ten sub-catchments there is an average difference between UDel and CRU in the grid-based mean and maximum values of 151 mm and 440 mm, respectively. The average range between the minimum and maximum grid cell-based mean annual precipitation values for UDel is 950 mm, compared to 521 mm for CRU, demonstrating that UDel generally shows greater spatial variability in gridded mean annual precipitation values. The range is greater for UDel in eight of the ten sub-catchments (the exceptions being the Lancang and Chi sub-catchments). UDel-derived precipitation was employed within SLURP, following initial difficulties in calibrating SLURP using CRU precipitation (Kingston *et al.*, 2011).

Table 3.6. UDel and CRU minimum, mean and maximum mean annual precipitation totals (mm) over the period 1961–1998 across the grid cells of the SLURP sub-catchments.

	Lanc-ang (1)	Nam Ou (2)	Nam Ngum (3)	Mek. 1 (4)	Chi (5)	Mun (6)	Mek. 2 (8)	Se Kong (9)	Sre Pok (10)	Mek. 3 (11)
UDel										
Min.	448.8	1341.5	1573.6	1185.3	1093.6	1092.9	1758.0	1893.8	1577.2	1729.3
Mean	1044.5	1567.3	2047.9	1844.3	1270.1	1301.5	2192.0	2410.6	2031.5	1845.5
Max.	1656.0	1810.7	2441.4	2936.2	1454.1	1985.5	3533.8	2693.5	2563.3	2121.6
CRU										
Min.	264.0	1353.4	1611.8	1188.2	1107.0	1052.9	1772.2	1846.2	1792.4	1588.3
Mean	976.9	1459.8	1648.1	1756.8	1274.1	1291.7	1983.4	2063.8	1883.0	1704.6
Max.	1529.7	1552.9	1704.0	2351.7	1550.9	1755.1	2203.8	2275.4	2090.6	1776.1

3.6.2. Temperature

Temperature data for the Mekong catchment for the period 1961–1998 were obtained from the 0.5° × 0.5° monthly gridded CRU TS 3.0 dataset, from which temperature data for the SLURP model were generated. Figure 3.12 presents gridded mean annual temperature for the Mekong Basin derived using this dataset.

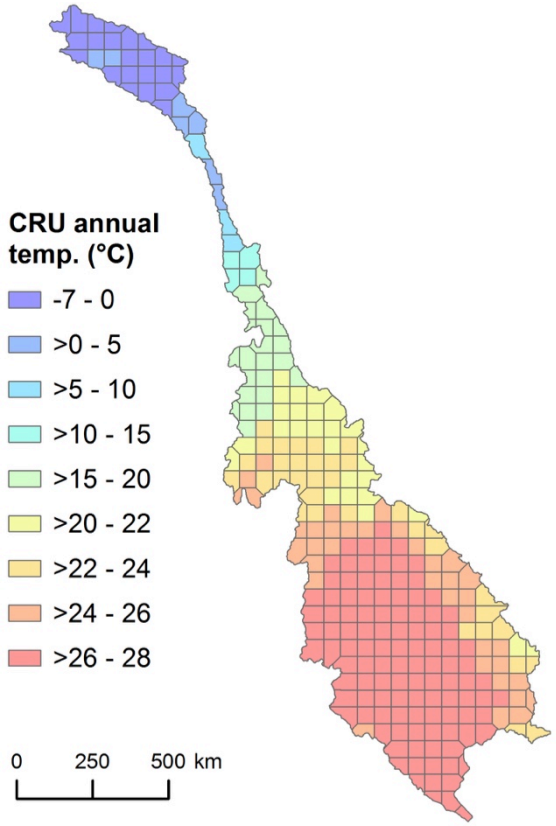

Figure 3.12. CRU gridded mean annual temperature calculated for the period 1961–1998.

Negative values of between –7 to 0 °C are seen over the Tibetan Plateau, with mean annual temperatures of between 0 to 15 °C in the Three Rivers area and between 15 to 20 °C over the lower Lancang Basin. Mean annual gridded temperatures lie between 26 and 28 °C over the majority of the Lower Mekong Basin (i.e. south of China), with values of between 20 and 24 °C over much of the Northern and Eastern Highlands. Mean monthly temperature derived for the period 1961–1998 is shown in Figure 3.13 for both the grid cell-based data and sub-catchment average data for ten SLURP sub-catchments. Mean monthly temperatures are highest between April and October. Whilst mean monthly temperatures peak in July–August over the upper Lancang, peak temperatures are seen in April over much of the Lower Mekong Basin. Negative mean monthly values are restricted to northerly grid cells within the Lancang sub-catchment.

Table 3.7 shows minimum, mean and maximum mean annual temperatures over the period 1961–1990 across the grid cells of ten of the SLURP sub-catchments. The sub-catchment means vary between 11.3 °C for the Lancang and 27.4 °C for the Mun sub-catchment. Across the sub-catchments, the grid cell based minimum mean annual temperatures range between –7.1 °C (Lancang) and 26.7 °C (Mun), whilst the maximum values within each sub-catchment range between 22.9 °C (Nam Ou) and 27.6 °C (Mun).

Table 3.7. CRU-based minimum, mean and maximum mean annual temperatures (°C) over the period 1961–1990 across the grid cells of the SLURP sub-catchments.

	Lanc-ang (1)	**Nam Ou (2)**	**Nam Ngum (3)**	**Mek. 1 (4)**	**Chi (5)**	**Mun (6)**	**Mek. 2 (8)**	**Se Kong (9)**	**Sre Pok (10)**	**Mek. 3 (11)**
Min.	–7.1	18.5	20.8	20.5	25.8	26.7	23.2	22.7	21.6	26.6
Mean	11.3	21.3	21.7	24.5	26.9	27.4	26.1	24.9	24.5	27.1
Max.	24.5	22.9	23.2	27.0	27.5	27.6	27.3	27.1	26.7	27.5

SLURP sub-catchment average monthly mean, annual mean and mean annual temperature for the period 1961–1998 are presented in Figure 3.14 for the same 10 sub-catchments. Annual mean temperatures for each sub-catchment vary between approximately 1 °C above or below their respective mean annual temperature.

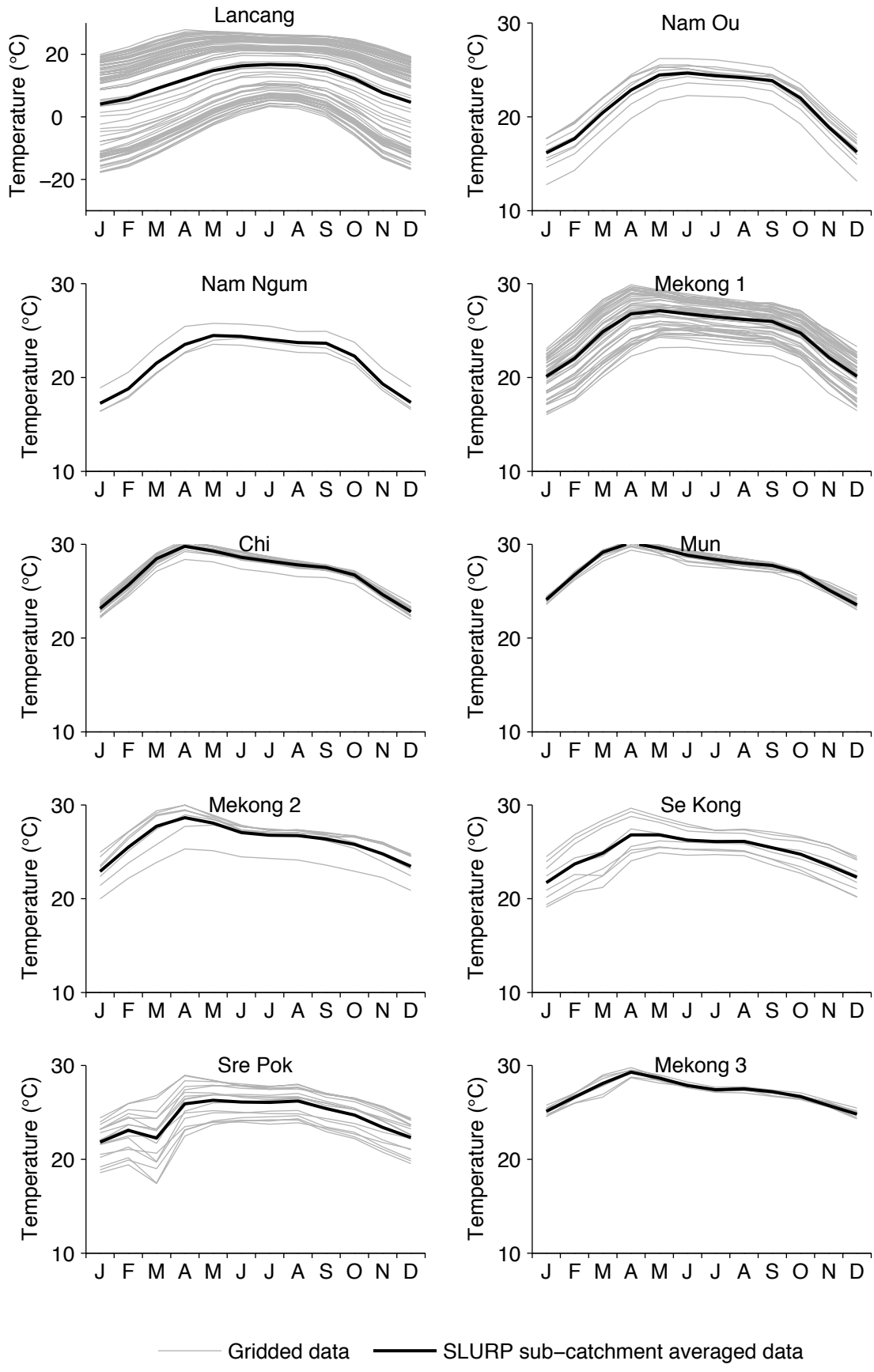

Figure 3.13. Grid based and sub-catchment average CRU mean monthly temperature (for the period 1961–1998), presented for 10 SLURP sub-catchments. For each sub-catchment, grid cell based data are shown for the grid cells that fall within that sub-catchment. (Note different y-axis scale for Lancang.)

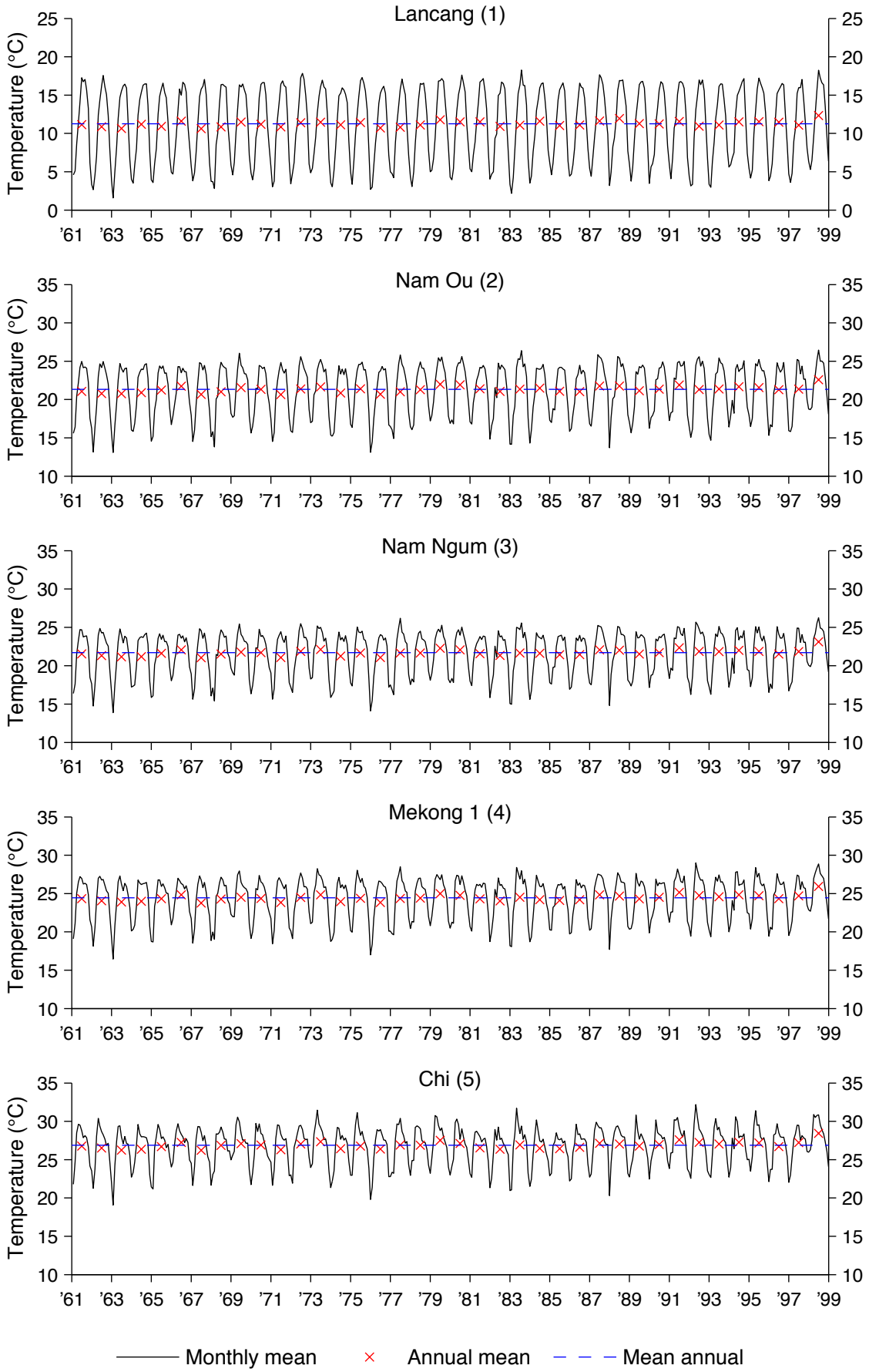

Figure 3.14. SLURP sub-catchment average CRU monthly mean, annual mean and mean annual temperature (1961–1998), presented for 10 sub-catchments. (Note different y-axis scale for Lancang.)

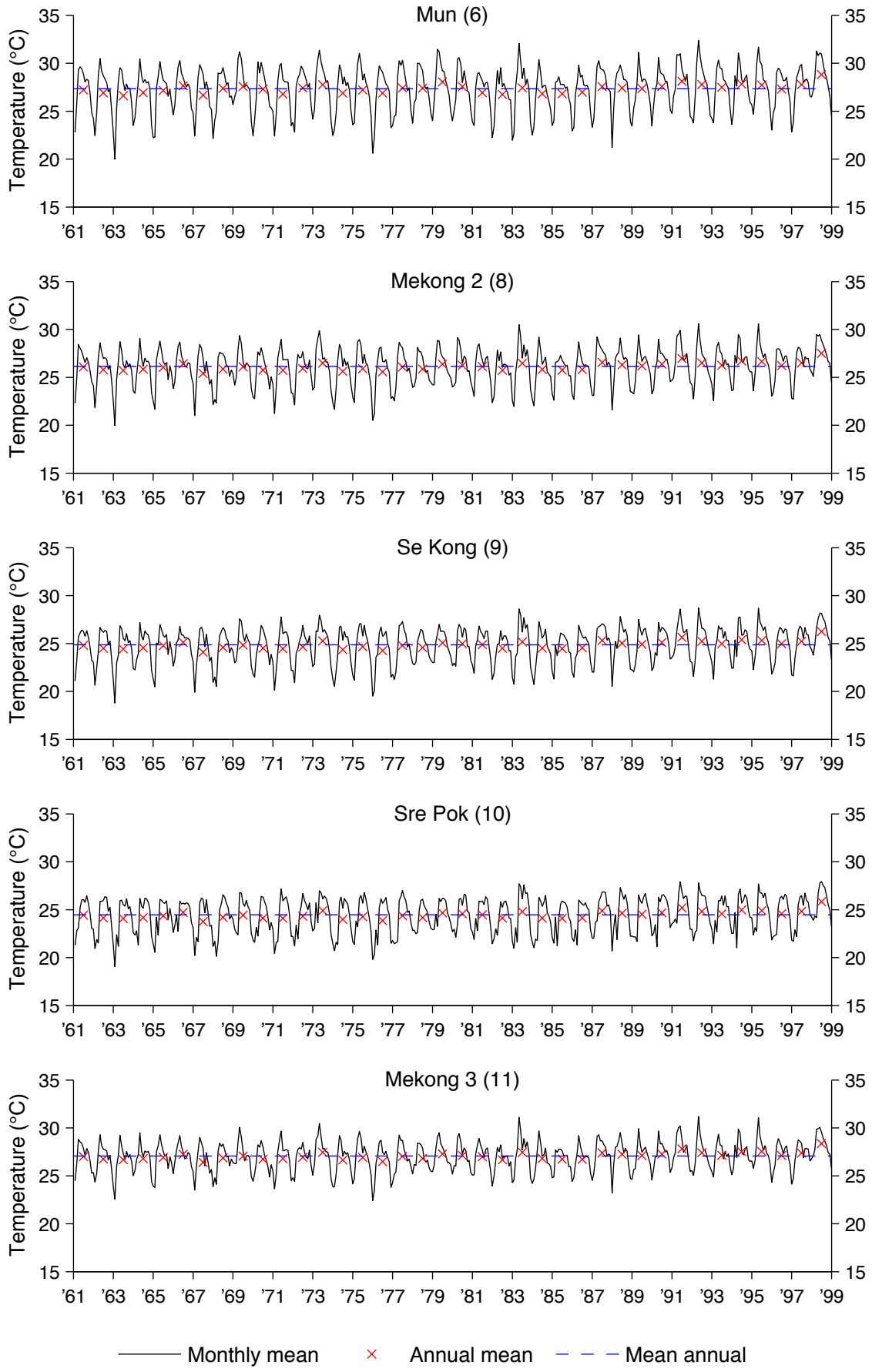

Figure 3.14. (cont.) SLURP sub-catchment average CRU monthly mean, annual mean and mean annual temperature (1961–1998), for 10 sub-catchments.

There is a general reduction in the range of monthly mean temperatures from north to south. For example, monthly mean temperatures for the Lancang vary between approximately 7 °C above and 9.7 °C below (range: 16.7 °C) the sub-catchment mean annual temperature, whilst for Mekong 3, monthly mean temperatures vary between 4.1 °C above and 4.7 °C below the mean (range: 8.8 °C). It is worth noting that the sub-catchment average monthly mean temperatures for the Lancang never go below 0 °C. Use of sub-catchment average data for hydrological modelling will therefore necessitate the use of a temperature lapse rate in order that snow accumulation and melting are simulated over the upper Lancang, as described in Section 4.2.6.3.

3.6.3. Potential evapotranspiration

As discussed in Chapter 2, evapotranspiration is a key component of a catchment's water balance and for the majority of hydrological models potential evapotranspiration (PET) time series must be either calculated externally (to the model) or internally. In Chapter 4, a model of Mekong Basin is developed using the MIKE SHE model code, in order to undertake an inter-hydrological model comparison between the newly developed model and the earlier SLURP model of the Mekong. In the SLURP model, the Linacre method (see Table 2.6) was employed to calculate PET internally, using CRU temperature time series as input. For the MIKE SHE model code, PET must be calculated externally and then specified as an input time series. Linacre PET is therefore calculated externally for the MIKE SHE model developed in Chapter 4. Whilst the use of alternative PET methods is explored in Chapter 5, only PET data calculated using the Linacre method are presented here in order to demonstrate spatial and temporal variations.

Figure 3.15 displays gridded mean annual total Linacre (LN) PET for the Mekong Basin calculated using CRU TS 3.0 temperature data. The lowest annual LN PET totals (<1600 mm) are found over the upper and mid-Lancang, whilst the highest values (>2300 mm) are seen over the Khorat Plateau. Excluding the Khorat Plateau, LN PET totals range between 1600 and 2000 mm over the majority of the Lower Mekong Basin.

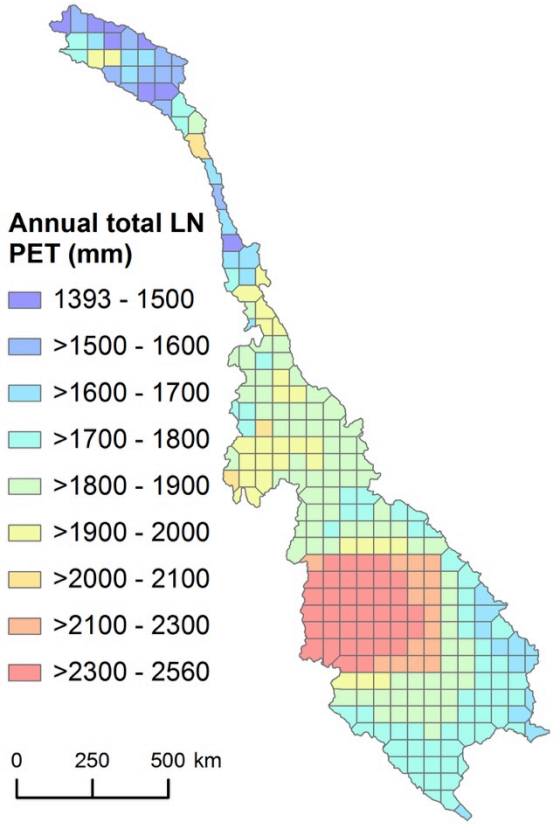

Figure 3.15. Mean annual total gridded PET for the period 1961–1998, calculated using CRU temperature following the Linacre PET method.

Mean monthly grid cell-based and sub-catchment average Linacre PET for the period 1961–1998 are presented in Figure 3.16 for ten SLURP sub-catchments. As might be expected considering that Linacre is a temperature based PET method, the seasonal distribution of PET totals through the year for each sub-catchment shows a similar pattern to that of mean monthly temperature. Peak mean monthly totals generally occur in April–May (July in the case of the Lancang) with lows in November–February.

Table 3.8 presents the minimum, mean and maximum mean annual Linacre PET totals across the grid cells for 10 SLURP sub-catchments. The Chi and Mun show the greatest sub-catchment average mean annual PET totals (2560.3 mm and 2432.4 mm, respectively), whilst the lowest mean totals are seen over the Sre Pok and Se Kong, (1710.3 mm and 1743.8 mm, respectively). Across the ten sub-catchments there is an average difference between the minimum and maximum grid cell-based mean annual PET totals of 244.6 mm. The equivalent values for UDel precipitation and CRU precipitation are 950.2 mm and 521.4 mm, demonstrating that gridded PET shows less variability within each sub-catchment.

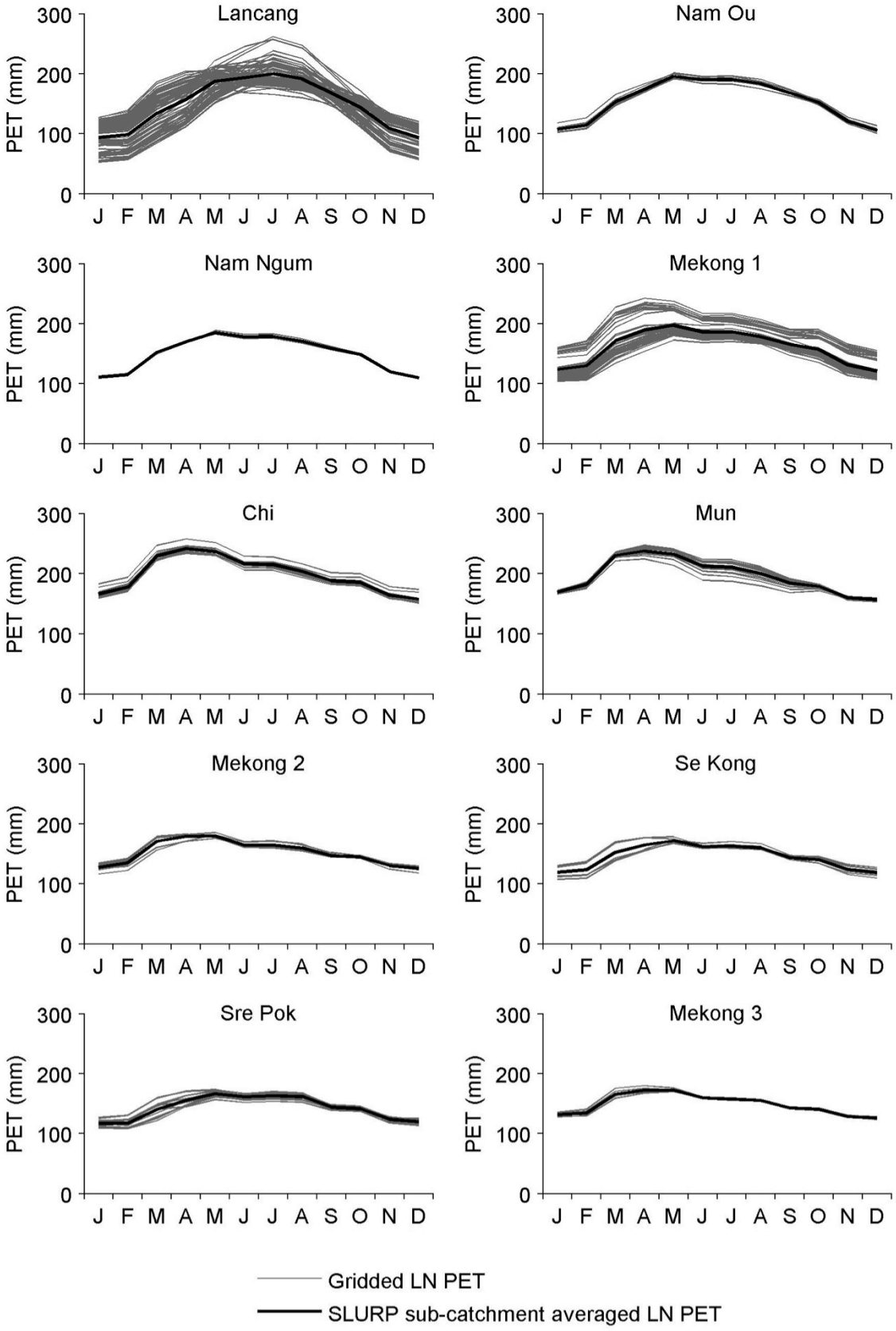

Figure 3.16. Grid based and sub-catchment average mean monthly Linacre PET (for the period 1961–1998), presented for 10 SLURP sub-catchments. For each sub-catchment, grid cell based data are shown for the grid cells that fall within that sub-catchment.

Table 3.8. Gridded minimum, mean and maximum mean annual PET totals (mm) over the period 1961–1998 across the grid cells of the SLURP sub-catchments.

	Lanc-ang (1)	**Nam Ou (2)**	**Nam Ngum (3)**	**Mek. 1 (4)**	**Chi (5)**	**Mun (6)**	**Mek. 2 (8)**	**Se Kong (9)**	**Sre Pok (10)**	**Mek. 3 (11)**
Min.	1393.8	1814.5	1782.3	1677.2	2303.6	2212.4	1789.6	1670.0	1635.9	1765.2
Mean	1769.1	1854.4	1796.3	1934.7	2382.5	2356.2	1829.4	1743.8	1710.3	1785.1
Max.	2097.5	1918.6	1810.3	2382.4	2560.3	2432.4	1852.9	1826.3	1785.5	1824.2

Monthly total, annual total and mean annual total Linacre PET are presented in Figure 3.17 for the same ten SLURP sub-catchments. Nam Ou and Nam Ngum display very similar pattern and magnitudes. Likewise, the Mun, Chi and Chi-Mun (not shown) sub-catchments, which have the highest PET totals, exhibit similar patterns to each other. Finally, the PET totals of sub-catchments 9–11 display comparable magnitudes and patterns. This figure demonstrates that in comparison to precipitation (Figure 3.11), PET shows less inter-annual variability. To illustrate this, across sub-catchments 1 to 11 there is a mean difference between the sub-catchment minimum and maximum annual PET totals (the red crosses in Figure 3.17) of 254.6 mm. In contrast, the equivalent values for sub-catchment average UDel and CRU precipitation are 785.5 mm and 751.9 mm, respectively.

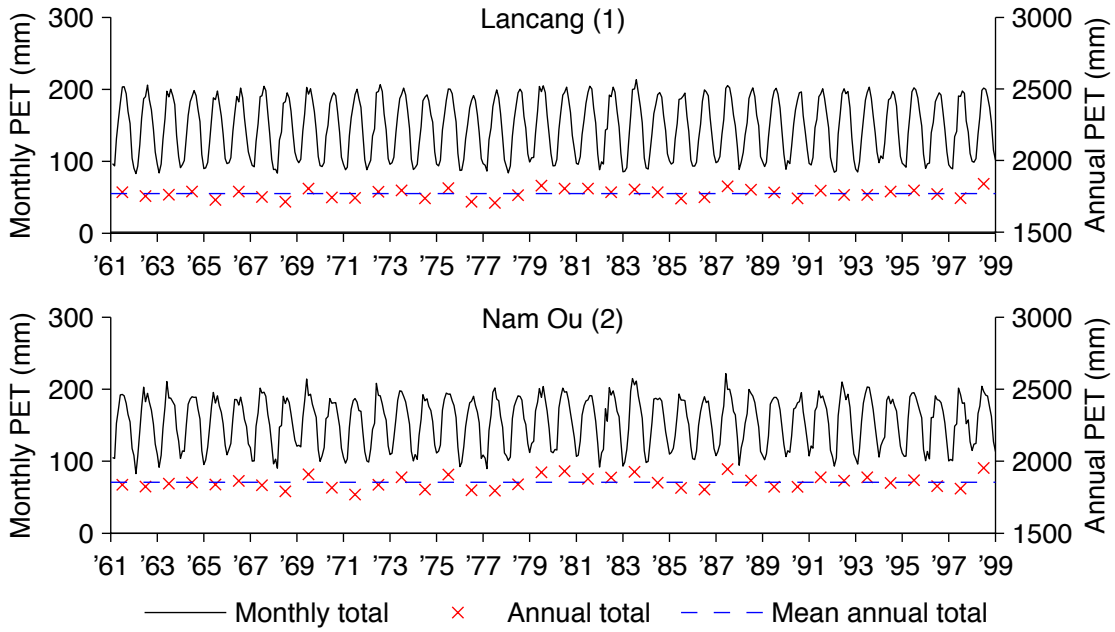

Figure 3.17. SLURP sub-catchment average monthly total, annual total and mean annual total Linacre PET (for the period 1961–1998), presented for six SLURP sub-catchments.

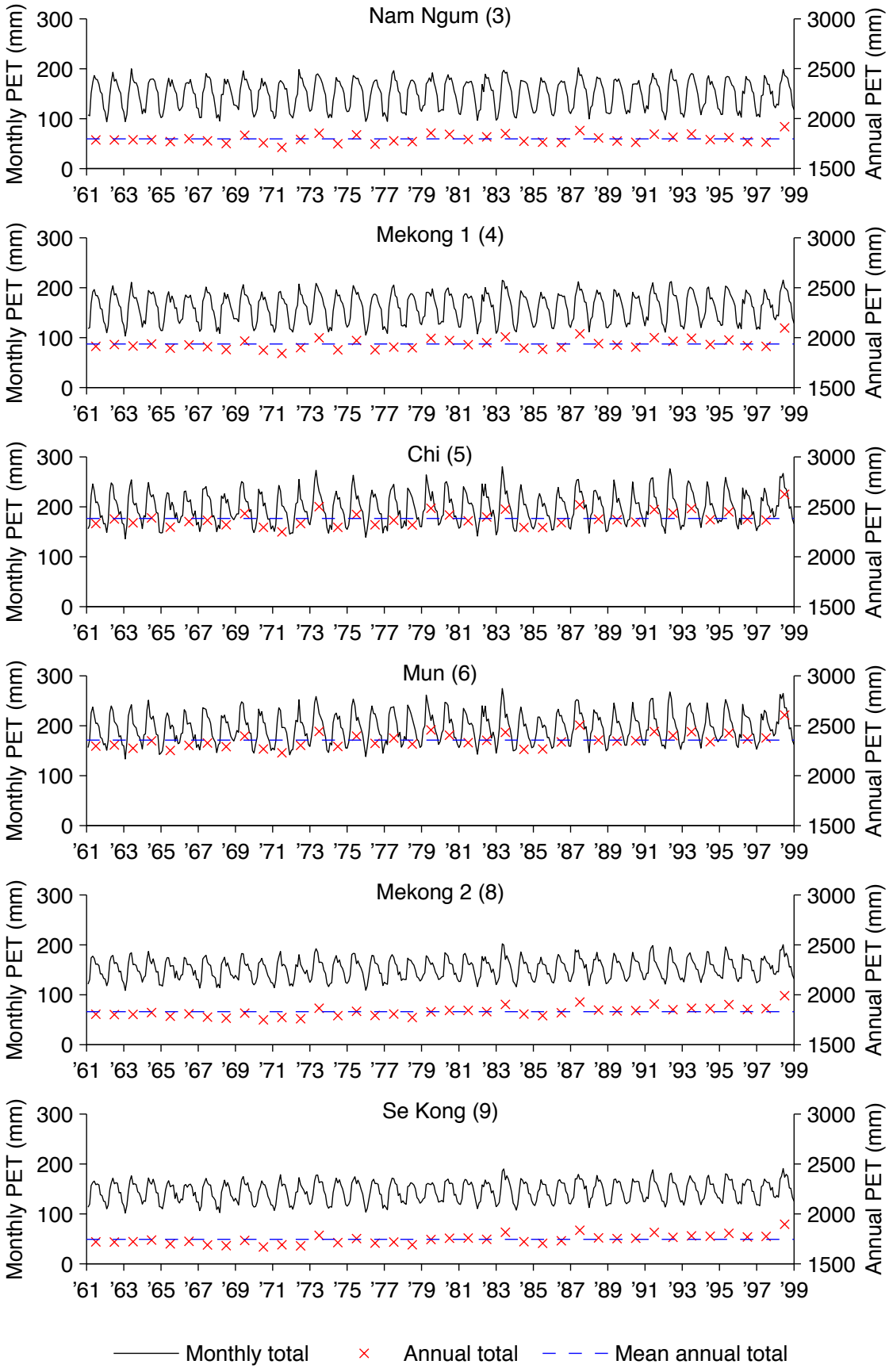

Figure 3.17. (cont.) SLURP sub-catchment average monthly total, annual total and mean annual total Linacre PET (for the period 1961–1998), presented for ten SLURP sub-catchments.

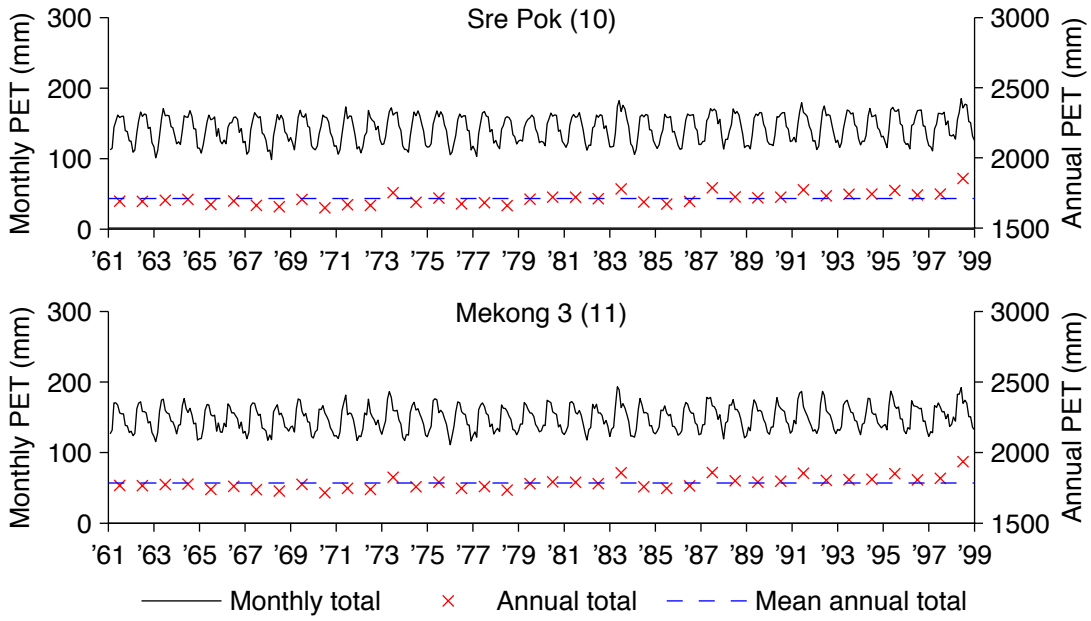

Figure 3.17. (cont.) SLURP sub-catchment average monthly total, annual total and mean annual total Linacre PET (for the period 1961–1998), presented for ten SLURP sub-catchments.

3.7. River network

The river network employed in this thesis is based on the network used in the SLURP model of the Mekong, which was derived by Kite (2000) through topographic analysis of the 1 km × 1 km USGS GTOPO30 DEM of the basin using the TOPAZ digital terrain analysis tool (Garbrecht and Martz, 1997). The river network derived by Kite (2000) was divided into five stream orders using Strahler's numbering system (Figure 3.18a). However, few (only four) of the stream order 1 (headwater/upper tributary) channels could be included in the MIKE 11 model developed in this thesis, due to a computational limit to the number of q-points (where river flows are calculated) that could be included within the model, and hence the number of channels that could be incorporated within the river model. The river network employed (Figure 3.18b) is therefore a reduced version compared to that used in the SLURP model. Development of the MIKE 11 river model that used this river network, including specification of channel cross-sections, is discussed in further detail in Sections 4.3.1 and 4.3.2.

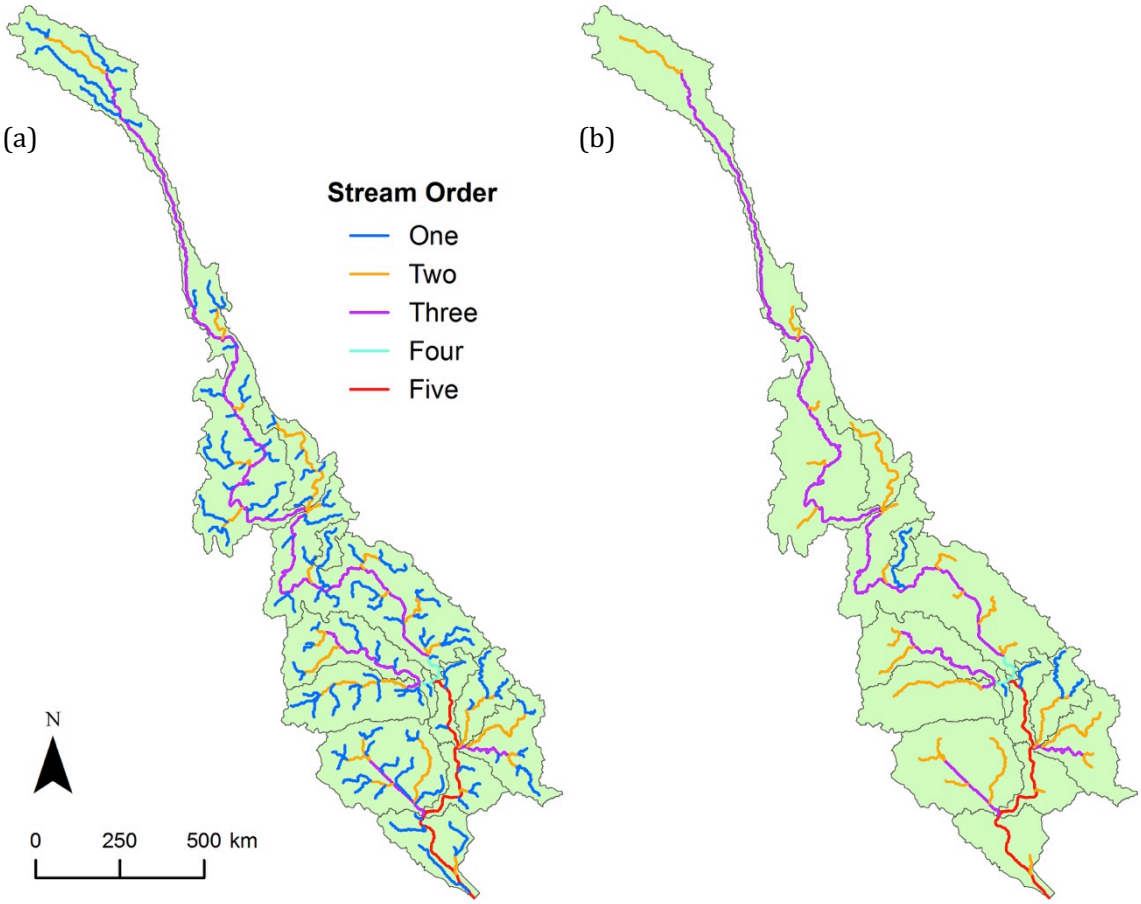

Figure 3.18. a) River network of the Mekong Basin derived by Kite (2000). b) Reduced river network, as used in the MIKE 11 river model. SLURP sub-catchments shown to aid interpretation.

3.8. River discharge

Discharge data from twelve gauging stations, as summarised in Table 3.9, are used in this thesis for the purposes of model calibration and validation. Daily data for eleven of these stations were compiled by the Mekong River Commission (MRC). Daily discharge data for Kratie were derived by Kite (2000) from daily records for Pakse using a simple linear regression model developed by the Institute of Hydrology (1988), due to limited data availability for this station. The model employs separate relationships for the wet and dry seasons. Ten of the gauging stations are located on the main Mekong (i.e. the main stem of the Mekong River), whilst the Yasothon and Ubon gauging stations are located on the Chi and Mun tributaries, respectively. Although daily discharge data were available for the full calibration period (1961–1990) for the majority of these stations, the records for Stung Treng, Kompong Cham and Phnom Penh were limited to January 1961–March

1970, January 1964–March 1974 and January 1961–March 1974, respectively. For the validation period (1991–1998), however, no observations were available for Kompong Cham or Phnom Penh, whilst availability for the remaining stations varies between the full eight years (Pakse and Kratie, albeit derived from Pakse records in the case of the latter) to only three (Stung Treng and Mun at Ubon).

Table 3.9. Gauging stations employed in this study, including their locations and the periods (relevant to this study) for which records are available.

Gauging station	Country	SLURP sub-catchment located in	Lat (Decimal degrees)	Long (Decimal degrees)	Data availability
Chiang Saen	Thailand	Lancang	20.273	100.083	1961–Jun 1997
Luang Prabang	Laos	Mekong 1	19.892	102.137	1961–1997
Vientiane	Laos	Mekong 1	17.928	102.620	1961–1996
Nakhon Phanom	Thailand	Mekong 1	17.398	104.803	1961–Nov 1995
Mukdahan	Thailand	Mekong 1	16.540	104.737	1961–1995
Yasothon (River Chi)	Thailand	Chi	15.782	104.142	1961–1995
Ubon (River Mun)	Thailand	Mun	15.222	104.862	1961–1993
Pakse	Laos	Mekong 2	15.117	105.800	1961–1998
Stung Treng	Cambodia	Top end of Mekong 3	13.545	106.017	1961–Mar 1970, 1991–1993
Kratie	Cambodia	Mekong 3	12.460	106.010	1961–1998*
Kompong Cham	Cambodia	Mekong 3	11.909	105.388	1964– Mar 1974
Phnom Penh	Cambodia	Mekong 3	11.837	105.039	1961– Mar 1974

*Observed' flows for Kratie for full period calculated from observed Pakse records – see text.

Driven by its monsoonal precipitation regime, the Mekong River exhibits a unimodal flow regime throughout the basin (Figure 3.19). River discharge begins to markedly increase in May and peak discharges are reached between August and September on the Mekong River itself, and in October on the Rivers Chi and Mun within the western Lower Mekong Basin. Peak flows are followed by the flood recession, with discharges reaching their lowest levels in March–April. Snowmelt within the upper catchment (Lancang) helps maintain dry season flows and also contributes to the initial rise of the annual flood within the Lancang (MRC, 2003; Kiem *et al.*, 2005). Estimates of mean annual total river discharge into the South China Sea vary, but values are frequently cited between approximately 460 km^3 (e.g. MRC, 2010b) and 475 km^3 (e.g. Kiem *et al.*, 2008).

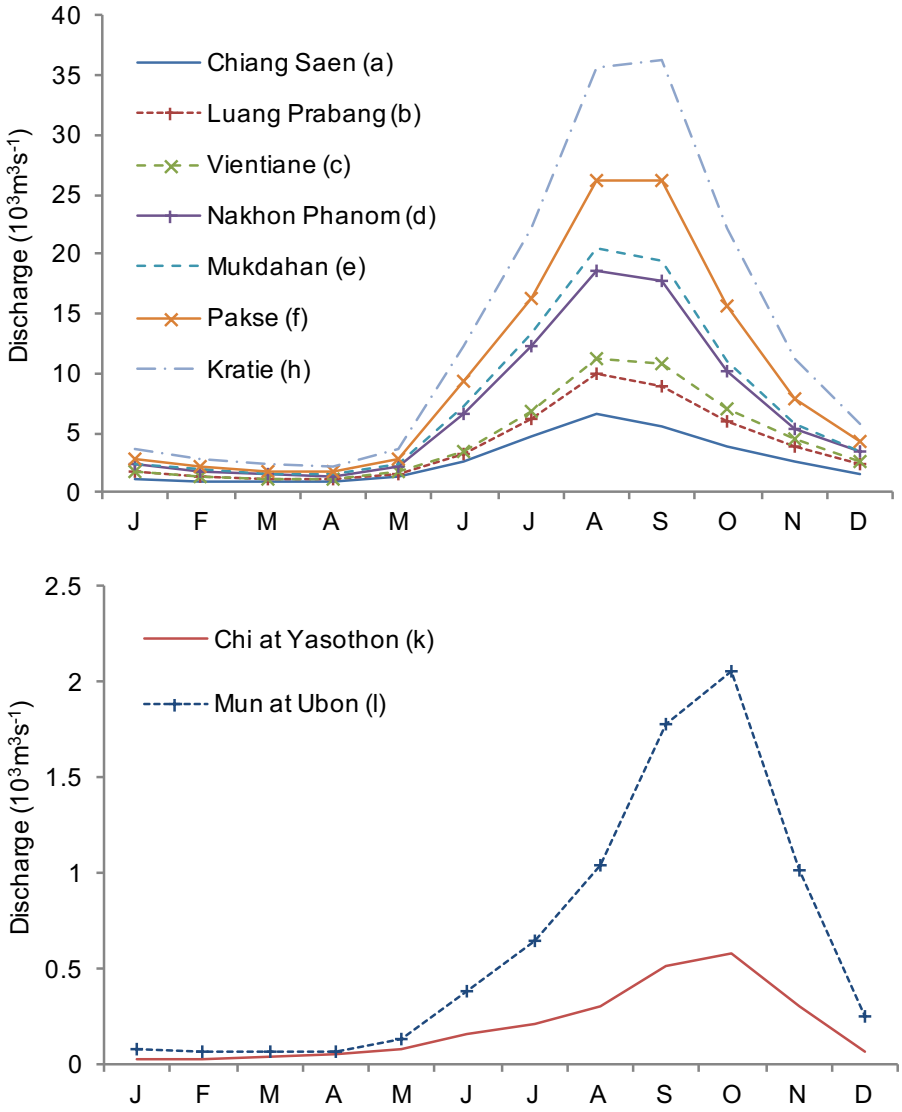

Figure 3.19. Observed river regime for the period 1961–1990, for the seven gauging stations on the main Mekong for which records are available for the duration of this period (top) and for two tributaries of the Mekong (bottom). Letters after gauging station names refer to the labels used in Figure 3.1. (Note different y-axis scales.)

Figure 3.20 shows daily observed discharge for the 12 gauging stations employed in this study for the period 1961–1998 and provides a good visual representation of the data availability (as indicated in Table 3.9) for each station throughout the calibration and validation periods. Although these plots demonstrate that the magnitude of flows in the Mekong Basin vary considerably from year to year, this is more clearly displayed in Figure 3.21, which displays annual mean discharge and mean discharge for six of the gauging stations (again, for the period 1961–1998). It is evident that stations on the main Mekong, particularly downstream of Chiang

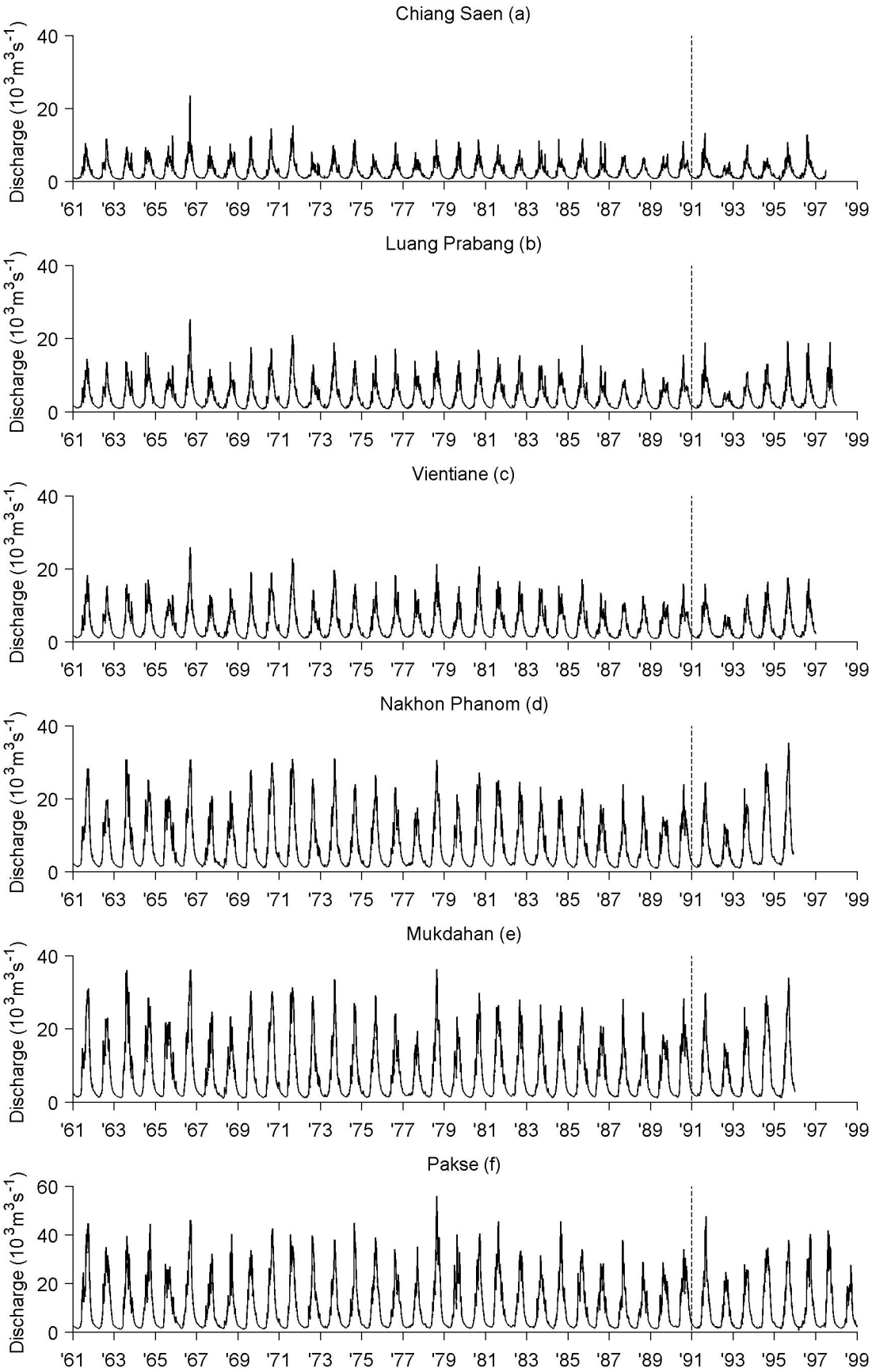

Figure 3.20. Daily observed discharge for 12 gauging stations in the Mekong Basin for the period 1961–1998 (subject to data availability). Dashed vertical line indicates the divide between the calibration and validation periods. (Letters in brackets refer to the gauging station labels used in Figure 3.1). (Note different y-axis scales.)

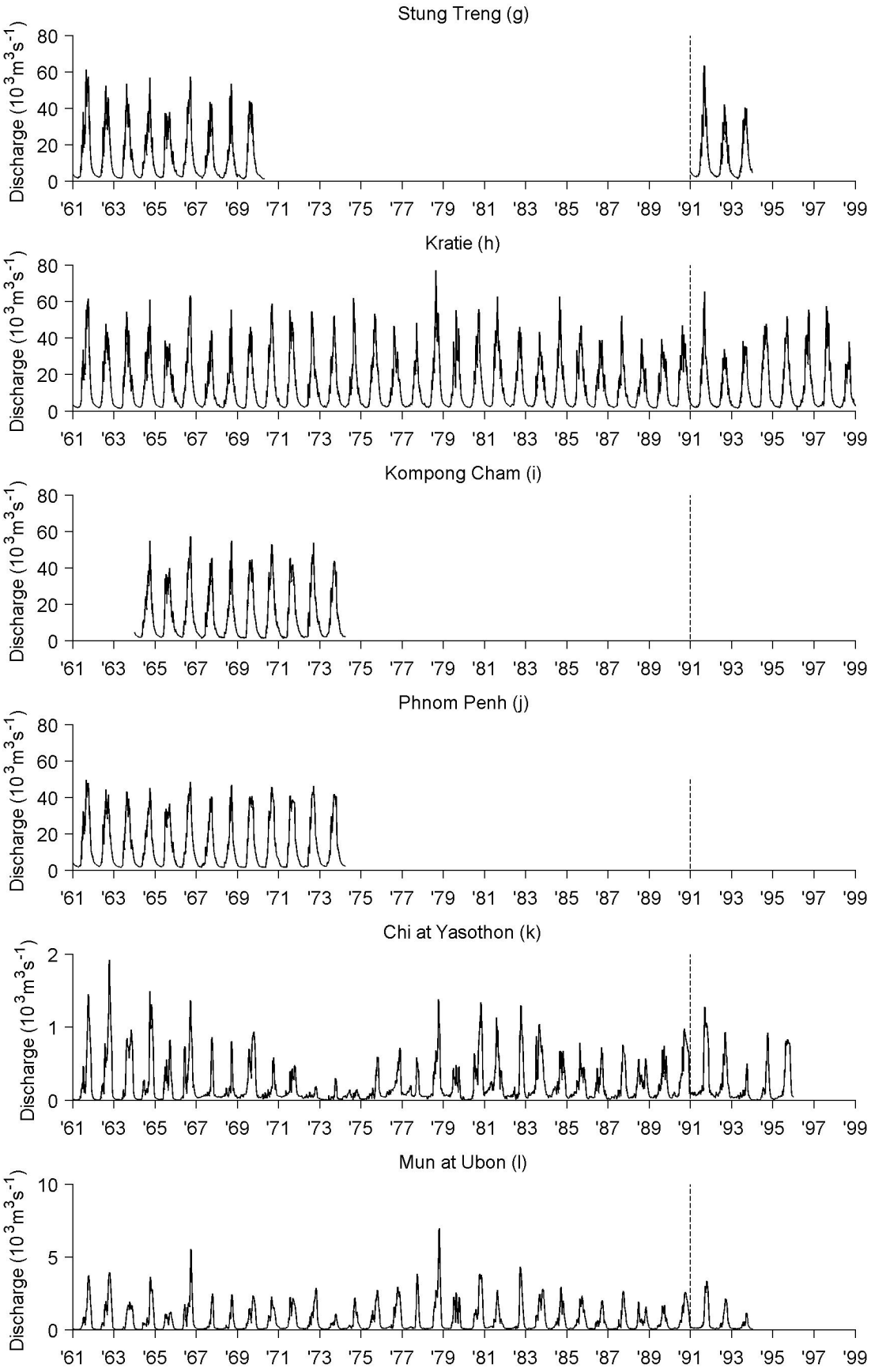

Figure 3.20 (cont.) Daily observed discharge for 12 gauging stations in the Mekong Basin for 1961–1998 (subject to data availability). Dashed vertical line indicates the divide between the calibration and validation periods. (Letters in brackets refer to the gauging station labels used in Figure 3.1). (Note different y-axis scales.)

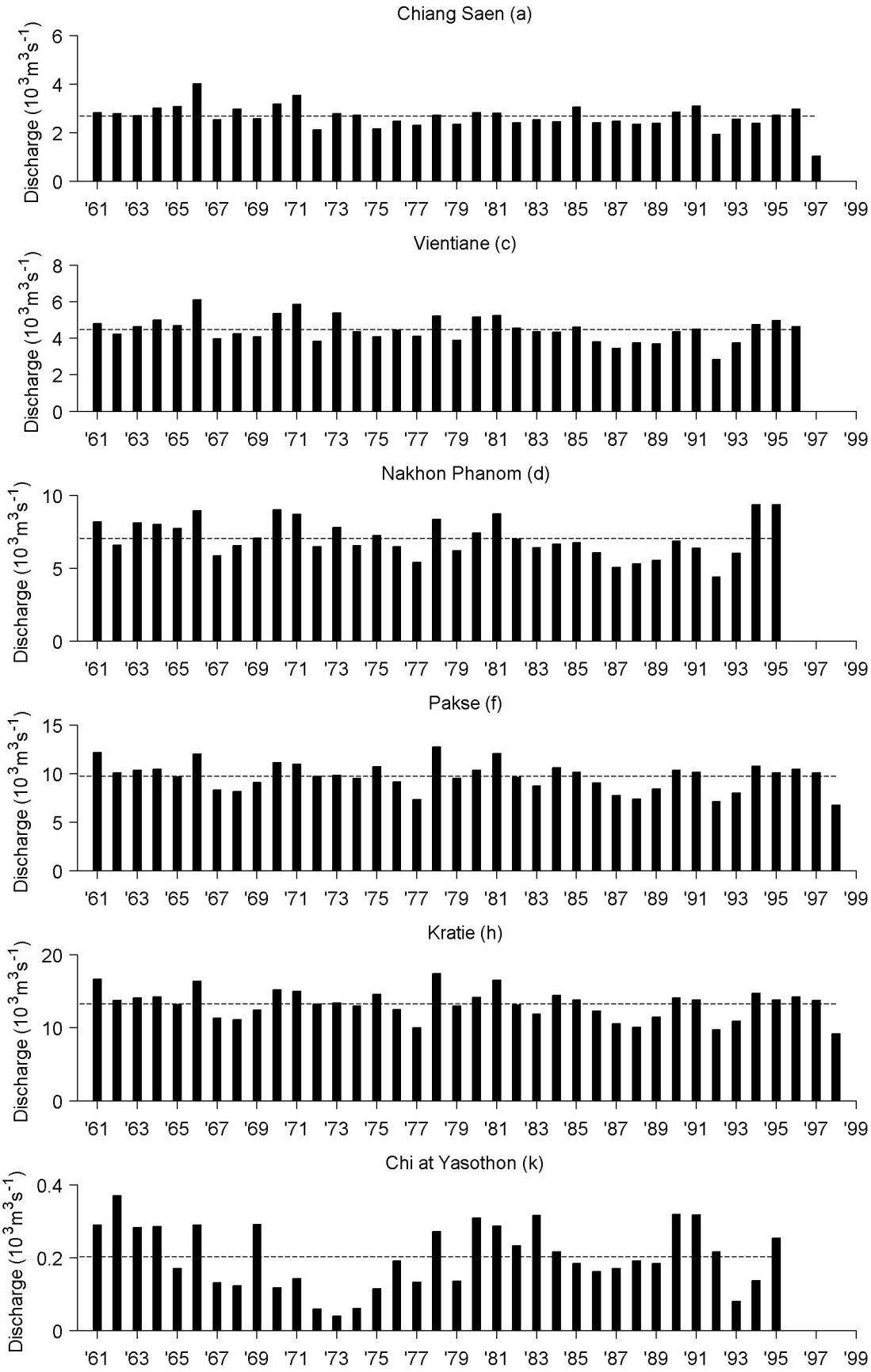

Figure 3.21. Observed annual mean discharge (solid line) for six gauging stations in the Mekong Basin, for the period 1961–1990. The dashed line represents the mean discharge for the available data for each station. (Note different y-axis scales.)

Saen, display a similar pattern of annual mean discharge, meaning that there is a good correspondence between stations in terms of the years with above and below average flows. For example, all of the stations display a spike of above average flows in 1966, whilst Nakhon Phanom, Pakse and Kratie show high annual mean discharge in 1978 and 1981. For stations downstream of Chiang Saen on the main Mekong, years with notable below average annual mean flows include 1967–1968, 1977, 1986–1989 and 1992. Despite close agreement in some years, there is generally less agreement between mean annual discharge on the River Chi at Yasothon and the stations on the main Mekong. Analysis shows that the Chi-Mun system contributes ~6.4% of mean annual discharge at Pakse on average over the period 1961–1993. This is consistent with a value of 6% given by MRC (2005b).

3.9. Anthropogenic influences on basin hydrology

Human activities have the potential to considerably impact the hydrological functioning of river basins. In order to provide a more complete overview of the key controls and influences on the Mekong's hydrology, this section discusses potential historical and future anthropogenic impacts on the basin's hydrology, other than through climate change. The three main interventions considered here are land cover change, water abstractions and dam building / river flow regulation.

3.9.1. Land cover change

The Mekong region has undergone significant land cover change since the 1960s, namely deforestation driven by agricultural expansion and demand for forest products and, in parts of the Lower Mekong Basin between 1960–1980, by conflict (Bernard and De Koninck, 1996; Nobuhiro *et al.*, 2008; Lacombe *et al.*, 2010; MRC, 2010b). Figure 3.22 provides an indication of the decline in forested area in the region between the 1970s and 1990s. Since the 1990s, forest loss has continued over much of Southeast Asia, including parts of the Lower Mekong Basin (Stibig *et al.*, 2014). Under these high rates of deforestation, it might be expected that the flow regime and rainfall-runoff relationships of the Mekong may have been altered. However, studies into whether there has been a discernible impact of land use changes on Mekong flows show conflicting results.

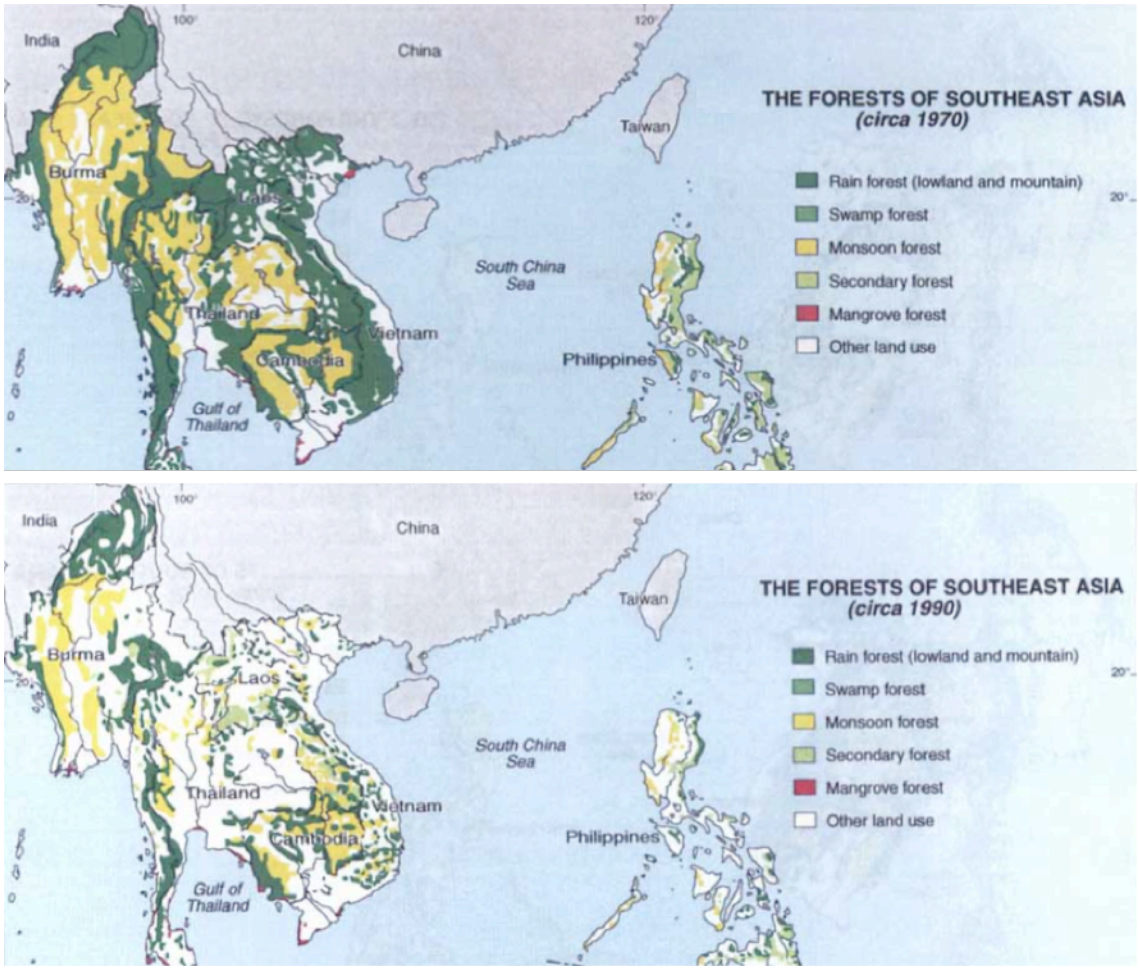

Figure 3.22. Forest cover in mainland Southeast Asia in circa 1970 (top) and 1990 (bottom). Source: Bernard and De Koninck (1996).

For example, Adamson (2006) undertook an analysis of percentage deviation of annual flows, annual maximum flows and mean dry season flows above and below their respective long-term means over the period 1960–2005 at Vientiane and Kratie. The study concluded that there were no systematic or statistically significant trends in these attributes (see Figure 3.23) and that land cover change has not yet had a detectable influence upon the Mekong's regime.

Lacombe *et al.* (2010) used a different approach by assessing, through hydrological modelling, the temporal variation in the rainfall-runoff relationship in two sub-catchments of the Mekong Basin over the period 1960-2004. The two sub-catchments had undergone contrasting land cover changes. In the northern sub-catchment (between Chiang Saen and Vientiane) conflict-induced depopulation

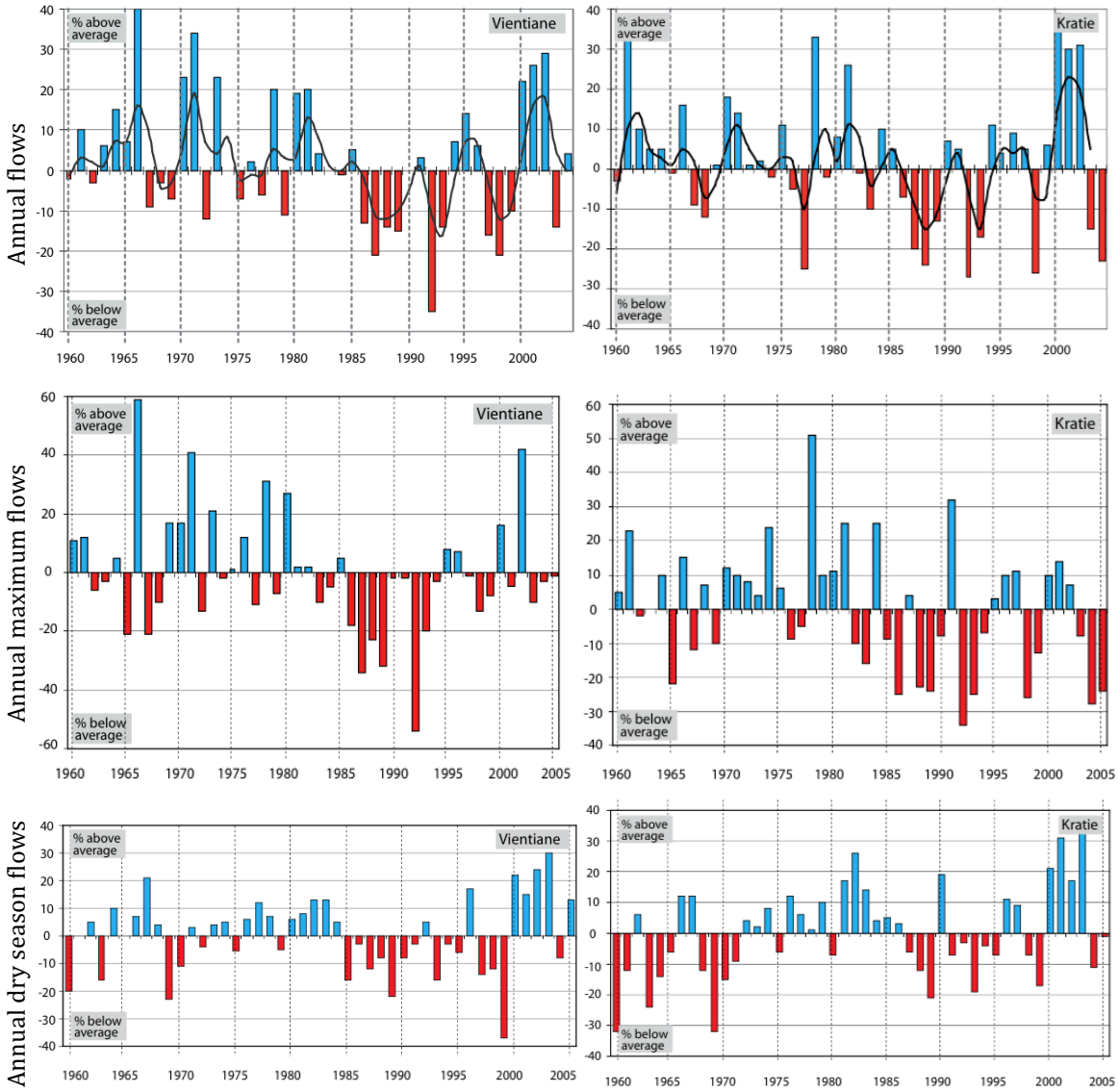

Figure 3.23. For the Vientiane (left) and Kratie (right) gauging stations on the Mekong River: Percentage deviation of annual flows (top), annual maximum flows (middle) and annual dry season flows above and below their long term mean values for the period 1960 – 2005. Source: Adamson (2006).

occurred over the period 1953–1985, leading to a shift towards forest regeneration. In contrast, the southern catchment (between Mukdahan and Pakse) experienced extensive deforestation in the early 1970s due to bombing by the United States Air Force during their military intervention in SE Asia as part of the Vietnam War. Lacombe *et al.* (2010) found changes in the rainfall-runoff relationships of the two sub-catchments that were consistent with the spatial distribution, magnitude and expected impact of changes in land cover. Expected flows in the absence of land cover change were established through hydrological modelling. Analysis indicated

a stable rainfall-runoff relationship in the northern catchment from 1961–1975 (Figure 3.24a). Runoff could not be estimated for the northern sub-catchment between 1976–1995, due to the interruption of discharge measurements. From 1995 onwards, the northern catchment displayed lower runoff production than would otherwise be expected in the absence of land cover change. This is consistent with the expectation of increased evapotranspiration rates following forest regrowth. Analysis of runoff from a nested sub-catchment (Nam Khan) of the northern sub-catchment suggested that the decline in runoff production occurred within the period 1976–1986. In contrast, runoff production in the southern catchment was higher than would otherwise be expected from the early 1970s (Figure 3.24b), consistent with the expectation of reduced evapotranspiration rates following forest clearance. These findings suggest that at a sub-catchment scale, changes in vegetation cover may have had a discernible influence on catchment hydrology, and hence Mekong flows, over recent decades.

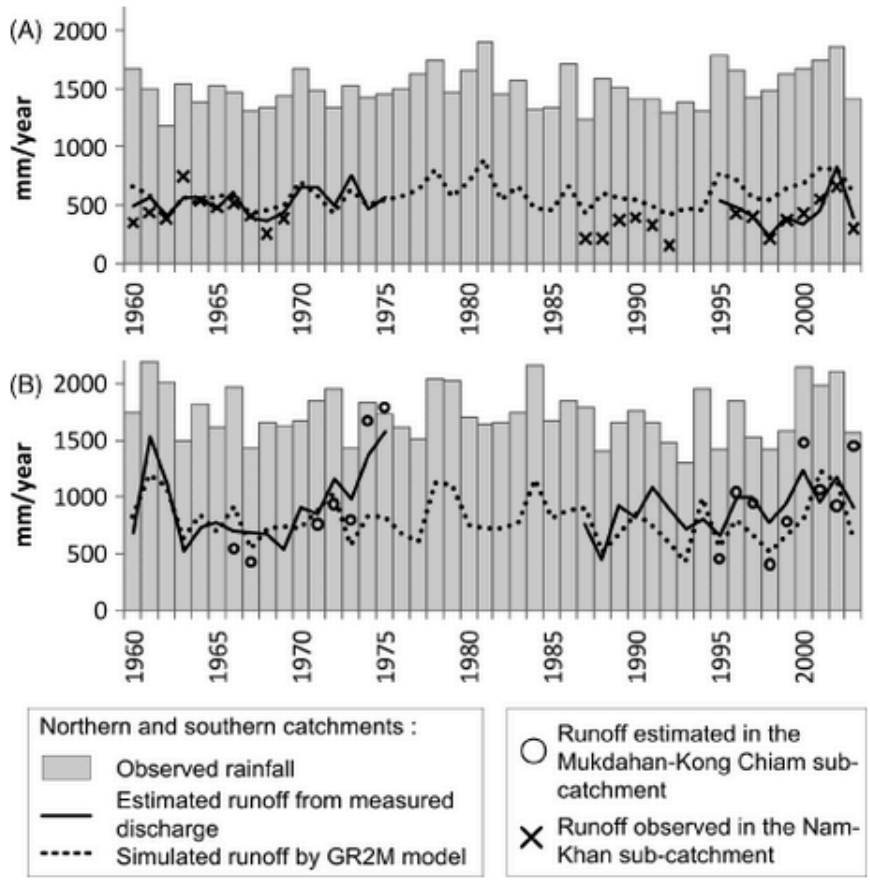

Figure 3.24. Observed rainfall and runoff and expected runoff (as simulated by GR2M hydrological model) for a northern (a) and southern (b) sub-catchment in the Mekong River Basin. Source: Lacombe et al. (2010).

During the baseline period used herein (1961–1990), the highest rates of forest loss in the Lower Mekong Basin occurred in Thailand, with the expansion of agriculture (MRC, 2005b). On the Khorat Plateau, forest cover decreased from 42% in 1961, to 13% in 1993 (MRC, 2005b). However, it is unclear how this has impacted the hydrological regime or extremes of the Chi and Mun rivers (MRC, 2005b; Kuntiyawichai, 2012). Analysis by Weesakul (2005, cited in Floch and Molle, 2009) on the impacts of deforestation on stream flow in nine sub-basins of the Chi-Mun found no coherent patterns to indicate that annual runoffs had been impacted by deforestation. Modelling of a 12,100 km^2 sub-catchment of the Chi basin by Wilk *et al.* (2001) could not detect any significant change in the water balance, despite a large reduction in the area classified as forest. Wilk *et al.* (2001) highlight that the land classification dividing forested and non-forested land masks the role that land cover is actually having on hydrology, effectively exaggerating perceived changes. Over large stretches of land, there is no clear-cut division between forest and non-forest. Swidden agriculture (rotational farming) is the most common method of agriculture in the region and these areas contain high numbers of shade trees, although they are classed as non-forest (Wilk *et al.*, 2001). Modelling undertaken by Goteti and Lettenmaier (2001) indicates that the increases in mean annual discharge in the Chi-Mun region that might be expected with conversion of forest to agriculture may have been offset by an increase in demand for irrigation. Furthermore, since the Chi and Mun only contribute <6.5% of mean annual flow at Pakse on average, hydrological changes on these tributaries are likely to have only a relatively small effect on the main Mekong.

To shed light on the issue of detecting the impacts of land use change on hydrology, it is important to consider the wider literature. According to Rust *et al.* (2014), amongst others (e.g. O'Connell *et al.*, 2007), whilst the impacts of land use change at local scales and in small catchments have been clearly demonstrated (Kirby *et al.*, 1991; Robinson, 1998), there is a lack of evidence that local scale effects aggregate to detectable impacts at larger scales, with studies unable to detect impacts on downstream flow records. This does not mean that impacts at the larger scale do not exist, but rather that changes at this scale may be complex and difficult to detect (O'Connell *et al.*, 2007; Rust *et al.*, 2014). Factors that may obscure the effects of land use change on catchment response include the overriding influence of climatic

variability on stream flow and the spatially and temporally heterogeneous nature of land use changes and land management practices (Rust *et al.*, 2014). Furthermore, the complex nature of land use influences upon catchment hydrology means that changes will occur at a range of different temporal scales (from rapid, e.g. hourly, to longer monthly, annual or multi-annual effects). Using a novel approach based on wavelet analysis (a statistical technique for decomposing time-series into various components of scale), Rust *et al.* (2014) were able to detect changes in flow records (of three UK catchments) that corresponded with changes in catchment land use. These changes occurred at a variety of temporal scales. However, the largest catchment studied was 67 km^2, and any influences on catchment hydrology are likely to have more notable/detectable impacts in smaller catchments.

For the Mekong River Basin, historical changes in land-use and land management will undoubtedly have impacted hydrological processes at the local scale, and on some of the Mekong's tributaries, the influence on river flows may be detectable. However, detecting the influence on river flows on the main stem of the Mekong with any confidence is likely to be very difficult due to a number of factors. These include: the huge size of the catchment; the temporally and spatially variable climate; the temporally and spatially heterogeneous nature of changes in land use and land management; and the confounding influence of other anthropogenic activities such irrigation and river flow regulation (see below). It follows that the same may be true of future changes in land use, with potentially significant impacts on some tributaries and at the local scale, but greater difficulty in disentangling the impacts of land cover change on Mekong river flows from other drivers of change and variability.

3.9.2. Abstractions and irrigation

Another human activity that has considerable potential to influence hydrology, and is also related to land use and management, is the abstraction of water for agriculture. Within the Lower Mekong Basin, agriculture is the biggest abstracter of freshwater (MRC, 2010b). For the four countries of the Lower Mekong Basin, water withdrawals for agriculture as a proportion of total annual withdrawals in the mid-2000s were estimated as follows: Cambodia: 94%, Lao PDR: 91%, Thailand: 90%

and Viet Nam: 95% (FAO, 2016). Withdrawals for domestic and industrial water supply represent only a small fraction of water withdrawals in the basin; as such, they are unlikely to have notable hydrological impacts except on a local scale (MRC, 2010b). Average total annual water withdrawals (across all sectors) are estimated to be around 60 km^3 or 12% of the Mekong's average annual discharge, with irrigation accounting for an estimated 41.8 km^3 (MRC, 2010b). A large proportion of this irrigation water use (26.3 km^3 or 43.8% of total annual withdrawals) takes place in the Mekong Delta (MRC, 2010b), which is outside of the area modelled in this study. This is followed by Thailand (9.5 km^3), Lao PDR (3 km^3), Cambodia (2.7 km^3) and the highlands of Viet Nam (0.5 km^3) (MRC, 2010b). However, not all of the water abstracted is completely lost from the system. For example, in a modelling study of the Lower Mekong Basin, Ringler *et al.* (2004) estimated that as a share of water withdrawals, return flows (to the river network) were 27% for agricultural and 35% for urban-industrial uses. It is worth noting that although return flows contribute to both groundwater and river discharge, they can present problems for water quality, such as high levels of dissolved salts, nutrients and pesticides in irrigation water return-flows (Johnston *et al.*, 2010). The irrigated area in the Lower Mekong Basin is about 1.2 million ha in the dry season, or 10% of the total agricultural area of 15 million ha, and 3.5 million ha in the wet season (MRC, 2010a, b). Rice is the main crop under irrigation (MRC, 2005a).

According to FAO (2012), groundwater use is modest throughout most of the basin, except in China, northeast Thailand and Viet Nam, where groundwater withdrawals are particularly important in the dry season when surface water is scarce. Groundwater is a key source of domestic water supply in some areas (MRC, 2010b). In terms of the area of the Lower Mekong Basin equipped for irrigation, 98% is supplied by surface water and 2% by groundwater (FAO, 2012).

As indicated in Figure 3.25, irrigation schemes are concentrated in northeast Thailand (on the Khorat Plateau) and on the Mekong Delta (outside of the area modelled herein). Of course, since the number of irrigation projects continues to expand over time (e.g. Cochrane *et al.*, 2014) more schemes are present today than shown in this figure from MRC (2005a). Furthermore, in terms of the baseline period used in this study (1961–1990) there would have been fewer irrigation schemes

than are shown in the figure, and water abstractions (both for irrigation and across other sectors) would have been lower than today.

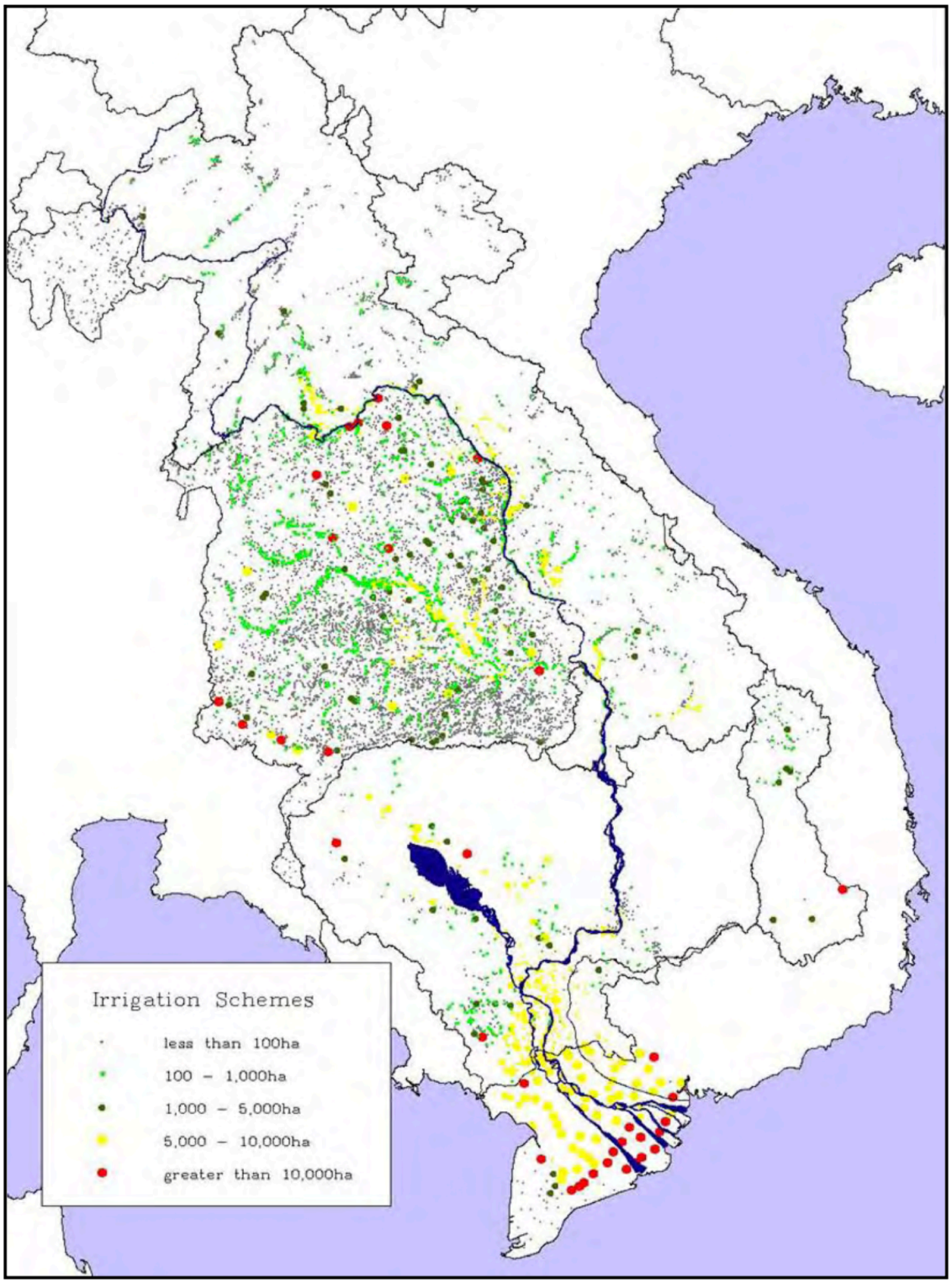

Figure 3.25. Irrigation schemes in the Lower Mekong Basin. Source: MRC (2005a).

The Chi-Mun Basin on the Khorat Plateau has experienced significant expansion of irrigation projects from the 1960s onwards (Floch and Molle, 2007, 2009). The types of irrigation projects range from small-scale measures (weirs, bunds, tanks and pumps) to large-scale schemes served by multi-purpose dams (Floch and Molle, 2009). However, according to Floch and Molle (2009) the basin has only experienced moderate reductions in runoff over this period. As discussed above, this basin also underwent significant forest to agriculture conversion from the 1960s onwards, and it is has been suggested that the associated reduction in evapotranspiration from natural vegetation has been offset by increased consumption from both rainfed and irrigated agriculture, including evapotranspiration from bunded agricultural areas (Goteti and Lettenmaier, 2001; Floch and Molle, 2009). Floch and Molle (2009) suggest that another factor limiting the impacts of irrigation in the basin, is that the majority of irrigation schemes in the region are primarily used for supplementary wet season irrigation, with only small areas irrigated in the dry season. According to Kite (2000), by the time flows from the Chi and Mun are merged and routed to the Mekong, the effects of irrigation cannot be detected.

Haddeland *et al.* (2006) undertook a hydrological modelling based study to assess the effects of irrigation on the water balances of the Mekong and Colorado river basins. Irrigated area, which was kept consistent for the simulation period, was based on a global gridded dataset that represents irrigation areas in around 1995 (Siebert *et al.*, 2002). Simulations performed for a 20-year period indicated that irrigation water requirements (with water assumed to be freely available) for the Mekong corresponded to a mean annual streamflow reduction of 2.3% at the basin outlet. When irrigation was restricted by available water, with two major reservoirs present, the value was 2.1%. This provides further indication that the impacts of irrigation on the main Mekong are likely to have been small historically.

Water abstractions are not included within the hydrological models developed within this thesis. The simulated discharge projections under climate change therefore give an idea of potential changes in the absence of abstractions. This is deemed justified as overall, it appears that water abstractions are unlikely to have had any major or widespread impacts on Mekong river flows, particularly on the

main Mekong over the baseline period used herein. However, since the number of irrigation projects and the area irrigated are expected to increase considerably in the future (MRC, 2016), this situation may change.

3.9.3. Dams and river flow regulation

Dams and river flow regulation have the potential to dramatically impact the hydrology and ecology of rivers. Up until very recently, the Mekong has been considered one of the few large river basins that has not been significantly and irreversibly impacted by large scale infrastructure (MRC, 2003; Sarkkula *et al.*, 2009; Lu *et al.*, 2014). However, the basin is undergoing rapid hydropower expansion and there are widespread concerns that existing and planned dams will have severe negative environmental consequences for the Mekong (International Rivers, 2017). Although the tributaries of the Mekong also face increasing hydropower development, it is the mainstream dams that are considered the greatest threat to the wetlands, fisheries and local livelihoods of the Lower Mekong Basin (MRC, 2010b).

There are currently at least six operational dams on the mainstem of the Mekong, all located in the Upper Mekong Basin on what is known as the Lancang cascade in China's Yunnan province (see Figure 3.26). The first of these, Manwan, was completed in 1993 and the largest (Nuozhadu) was only completed in 2014 (Räsänen *et al.*, 2017). Furthermore, there are several mainstream hydropower dams currently under construction in both the Upper and Lower Mekong Basin (International Rivers, 2017), with plans to build further large dams on the mainstream and tributaries (Figure 3.26). Many studies have considered the potential environmental impacts of existing and planned dams in the basin. Fan *et al.* (2015) provide a review of the literature related to the environmental impacts of the Lancang dams, focusing on those studies that have attempted to determine what changes have already occurred as a result of the existing dams. Key potential post-dam environmental impacts include hydrological changes, reservoir sediment trapping (with downstream consequences), changes in water quality and blocking of fish migration routes (Fan *et al.*, 2015). The focus here, however, is on hydrological impacts, in particular impacts on river discharge.

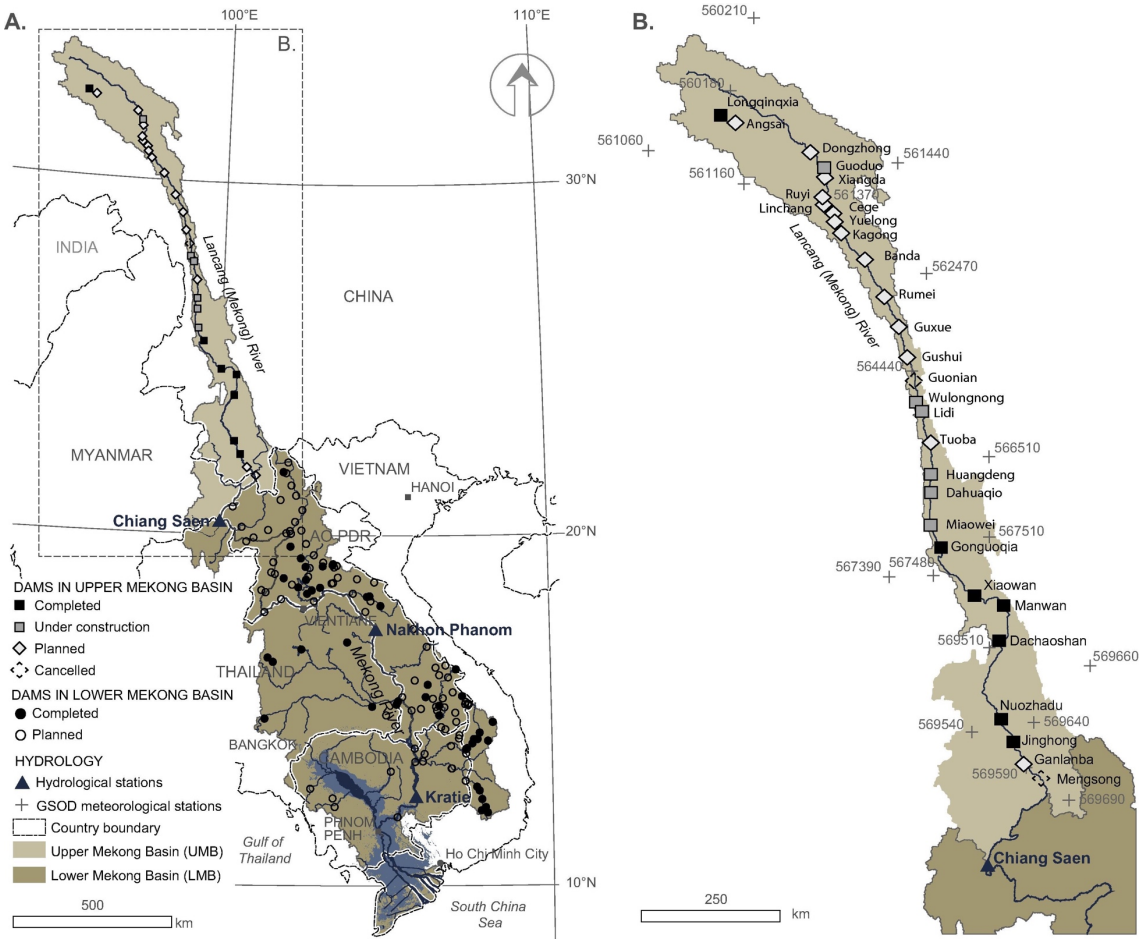

Figure 3.26. 'Map of (A) the large dams (height > 15 m) in the Mekong River Basin and the (B) existing, under construction and planned hydropower projects in the Upper Mekong Basin (UMB).' Source (figure and caption): Räsänen et al. (2017: 29).

Under increasing hydropower development, the amplitude of the annual flood pulse is expected to reduce, with a reduction in average monthly wet season discharges due to storing of water, and an increase in dry season discharges due to water releases from the reservoirs (Lauri *et al.*, 2012; Räsänen *et al.*, 2017). Several studies have sought to assess the hydrological impacts of Lancang cascade dams using observed discharge or water level records. A selection of these are summarised in Table 3.10. These demonstrate that several earlier studies found the impacts of the one or more existing dams were relatively small. For example, Lu and Siew (2006) found no significant change in mean discharge in the post-dam period, although dry season water level fluctuations increased considerably. Overall, the influence of Manwan dam on the Mekong's discharge regime was considered small and restricted to upper gauging stations closest to the dam.

Table 3.10. A selection of studies that have assessed recent hydrological impacts of the Lancang cascade dams on the Lancang-Mekong River using observed discharge or water level records.

Reference and Outline	Key findings
Lu and Siew (2006): Analysed discharge and sediment flux at several gauging stations on the Mekong downstream of Manwan dam (only completed mainstream dam at the time). Pre-dam period: 1962–1992. Post-dam period analysed: 1993–2000.	No significant change in mean discharge in the post-dam period. Annual minimum discharge showed a declining trend. Low mean annual discharge at several stations in 1992 potentially linked to infilling of the dam. Water level fluctuations in the dry season increased considerably in the post-dam period, with the contrast between the pre- and post-dam period largest at Chiang Saen, closest to Manwan dam. The impacts of the dam were largely restricted to the upper gauging stations closest to the dam. For the post-dam period analysed, it was concluded that although the discharge regime of the Mekong had been influenced by Manwan dam, the extent of the influence remained small.
Li and He (2008): Analysed water levels (1960–2003) at three sites on the Lancang.	Downstream effects of the two existing dams (Manwan; and Dachaoshan – under construction) on water levels were very limited in the case of annual mean and wet season mean levels and not apparent at the monthly & yearly times scales.
Lu *et al.* (2014): Used the Indicators of Hydrological Alteration (IHA) approach to examine the impacts of Chinese dams on river discharge at Chiang Saen. Compared discharge in the post dam period (1992–2010) to the pre-dam period (1960–1991).	No significant trend in annual water flow. Low discharge years of 1992, 2003 and 2010 were coincident with water infilling of the Manwan, Dachaoshan and Xiaowan reservoirs, respectively. 1992 was also a minimum precipitation year. At a mean monthly resolution (12 values for each period) hydrologic alteration in the post-dam period was classed as medium in March–April and low for other months, with the largest decrease in August (-9%) and largest increase in July (15%). Wet season discharge at a daily to weekly resolution (1-, 3- and 7-day maxima) was marginally lower in the post-dam period. Dry season discharge (1-, 3- and 7-day minima) was moderately lower in the post-dam period. Overall, the existing Chinese dams had altered river flow at Chiang Saen to a certain degree.
Räsänen *et al.* (2017): Analysed and compared observed discharge records (1960–2014) with hydrological model simulations in order to distinguish the likely impacts of dam operations on discharge.	Hydropower operations have considerably modified river discharges during the years 2011–2014. For these years, observed dry season discharges were considerably higher than simulated natural discharges. Observed wet season discharges were lower than simulated ones. Changes were largest at Chiang Saen, the most upstream station. However, discharge changes propagated downstream causing anomalies as far as Kratie in Cambodia. The largest impacts were in 2014 when discharge increased by 121–187% in March–May and decreased by 32–46% in July–August.

However, a recent study by Räsänen *et al.* (2017) indicates that since 2011, hydropower operations in the Upper Mekong Basin have considerably modified discharges on the Mekong River, even as far downstream as Kratie in Cambodia. Changes were characterised by increased dry season discharges and reductions in wet season discharges. In addition, Räsänen *et al.* (2017) found that hydropower operations on the Lancang could only partially explain observed discharge changes at Kratie, suggesting that river discharges may also be impacted by dam operations on tributaries in the Lower Mekong Basin.

A key barrier to assessing the potential future downstream impacts of hydropower dams in both the Upper and the Lower Mekong Basin is the lack of public information on their planned operation, such as reservoir operation and water releases (Lauri *et al.*, 2012; Räsänen *et al.*, 2012; Räsänen *et al.*, 2017). Several studies (e.g. Lauri *et al.*, 2012; Räsänen *et al.*, 2012; Piman *et al.*, 2013) have used a combination of a hydrological model and a reservoir cascade optimization model/algorithm to simulate the potential impacts of dams on the Mekong's discharge. However, the impacts of reservoir operations depend to a large extent on the operation rules applied (Lauri *et al.*, 2012; Piman *et al.*, 2013). Overall though, it is expected that dam and reservoir operations will, in general, lead to increases in dry season discharges and reductions in wet season discharges (Lauri *et al.*, 2012; Räsänen *et al.*, 2012; Piman *et al.*, 2013), although dry season increases may be offset by the impacts of expanded irrigation (Lauri *et al.*, 2012; Piman *et al.*, 2013).

Although it is clear that dams will play an important role in the Mekong's hydrology in the future, dams were not included in the MIKE SHE models developed herein for a number of reasons. A key reason is that the focus of this thesis is in assessing sources of uncertainty that are inherent in the climate change impact assessment process. Although the impacts of dams are a source of uncertainty in future river flows, dam impact assessment is not inherent to the climate impact assessment process. Related to this, the aim is not to try to project future Mekong river flows and how they might be impacted by all anthropogenic activities, but to assess a selected set of sources of uncertainty, using the Mekong as a case study catchment. Another justification is that at the time of initial model development (2012) and up until recently, the hydrological impacts of the mainstream dams were generally

considered to be relatively small. Furthermore, during the baseline period of 1961–1990 that is used throughout this thesis, many of the now existing dams in the basin were yet to be constructed, with none on the main Mekong (Kite, 2000; Cochrane *et al.*, 2014).

3.10. Summary

This chapter has provided an overview of the Mekong River Basin and the secondary data that are employed in this thesis, including topographic, soil, land use and hydrometeorological data. The data presented herein are subsequently employed in Chapter 4 in the development of a hydrological model of the Mekong using the MIKE SHE/MIKE 11 model code.

Chapter 4

Inter-hydrological model uncertainty in river flow projections under climate change and development of a MIKE SHE model of the Mekong

4.1. Introduction

As described in Chapter 1, one of the aims of this research is to assess inter-hydrological model uncertainty in river flow projections under climate change, using the Mekong River Basin as a case study site. Sections 4.2–4.4 of this chapter describe the development of a MIKE SHE hydrological model of the basin. This model was developed for the purpose of undertaking an inter-hydrological model comparison between the river flow climate change projections of the MIKE SHE catchment model, an earlier SLURP catchment model of the Mekong (Kingston *et al.*, 2011), and the Mac-PDM.09 global model (Gosling and Arnell, 2011; Gosling *et al.*, 2011). The MIKE SHE model therefore employs the same data as SLURP as far as possible. Section 4.2 describes the construction of the MIKE SHE model, whilst Section 4.3 describes the MIKE 11 model of the Mekong Basin's river network. The MIKE SHE and MIKE 11 models are dynamically linked. Model calibration and validation are described in Section 4.4. Following this, the development of climate change scenario data and use of these data for hydrological climate change scenario simulation is outlined in Section 4.5. Two scenario sets are employed, one representing a 2 °C increase in mean global air temperature as simulated by seven GCMs, the other a 1–6 °C increase as simulated by the HadCM3 GCM.

Section 4.7 is an extensive results section in which the calibration (Section 4.7.1) and validation (Section 4.7.2) results of the MIKE SHE model are first presented and compared to those of the earlier SLURP model. For the 2 °C, seven GCM climate scenario set and the 1–6 °C HadCM3 scenario set, respectively, result sections 4.7.3 and 4.7.4 each present the GCM simulated changes in climate, the MIKE SHE simulated changes in river flow, and a comparison of the projections simulated by MIKE SHE, SLURP and Mac-PDM.09. Finally, Sections 4.8–4.9 provide a discussion and summary. Some of the work in this chapter was incorporated within Thompson

et al. (2013) [1] and has been developed further herein to provide a more comprehensive presentation and analysis of results. The MIKE SHE model in this chapter is an improved version of that used in the paper. In particular, the new model produces better representation of seasonal accumulation and melting of snow (upper basin) and uses a different river routing method (Muskingum-Cunge) that provided better downstream attenuation of the flood pulse. Modelling results therefore differ to those previously presented, although they are very similar.

4.2. Model Construction: The MIKE SHE model

Table 4.1 summarises the components of the MIKE SHE model of the Mekong, including the data employed and the selected numerical solution method for each module. During model construction, each component was added and parameterised in turn. The graphical user interface framework within which MIKE SHE is operated is called MIKE Zero.

4.2.1. Model domain, grid and topography

The basin extent was defined using that derived by Kite (2000) for use in the SLURP Mekong model using the digital terrain analysis tool TOPAZ (Topographic Parameterization tool; Garbrecht & Martz 1997) and the USGS GTOPO30 DEM of the basin (see Section 3.2, Figure 3.2a). The USGS GTOPO30 DEM used for the SLURP model was employed to define the basin topography. This defines both the upper boundary of the MIKE SHE model and the drainage surface for overland flow (DHI-WE, 2009b). The model time step was set to a maximum of 48 hours. Initially, the model grid size was set to 1 km × 1 km. This was increased to 10 km × 10 km once the model had been constructed, following experimental runs that showed little change in simulated river discharge for grid sizes between 1 km and 20 km. During model runs, MIKE SHE interpolates input data onto the model grid of 10 km × 10 km (giving a total of 8034 cells). This compromise between computation time and representation of catchment characteristics is common with distributed hydrological models (e.g. McMichael *et al.*, 2006; Singh *et al.*, 2010).

[1] My contribution to this paper was the development of the MIKE SHE model of the Mekong and a sizeable proportion of the data processing and analysis. I contributed ~45% of the text.

Table 4.1. Summary of key data employed within each component of the coupled MIKE SHE/MIKE 11 model of the Mekong.

Model component	**Key inputs**	**Data sources / derivation**
Model domain	Catchment extent	Derived using the USGS GTOPO30 DEM (Kite, 2000).
Topography	Topography	Extracted from the USGS GTOPO30 DEM.
Land use/ vegetation	Vegetation distribution	Spatial distribution of nine land cover classes derived from the USGS Global Land Cover Characterization dataset.
	Leaf Area Indices	Kite (2000)
	Root depths	Jackson *et al.* (1996); DHI (2009) vegetation properties file; Rochester (2010).
Overland flow: modelled using the 2D finite-difference method	Manning's M for overland flow resistance	Spatially distributed according to land cover. Values taken from the literature (Chow, 1959; Vieux, 2004; Sahoo *et al.*, 2006; Thompson, 2012)
Unsaturated zone: modelled using the two-layer water balance method	Soil textural classes	Spatial distribution of four textural classes derived from the FAO Digital Soil Map of the World (FAO, 1998).
	Soil hydraulic properties	Clapp and Hornberger (1978); Marshall *et al.* (1996); Norman and Dixon (1995).
Saturated zone: modelled using the conceptual, linear reservoir method	Spatial distribution of sub-catchments	The catchment was divided into 17 groundwater sub-catchments based on: the locations of 12 gauging stations used for model calibration / validation, major tributaries and topography.
	Spatial distribution of interflow reservoirs	Each sub-catchment was divided into three interflow reservoirs, based on topography.
	Spatial distribution of baseflow reservoirs	Each sub-catchment was divided into an upper (faster) and a lower (slower) baseflow reservoir.
Catchment meteorology: Precipitation, evapo-transpiration and snowmelt modules.	13 meteorological (SLURP) sub-catchments	Derived through topographic analysis of the USGS GTOPO30 DEM (Kite, 2000) .
	Precipitation, PET and temperature data.	See text for meteorological data sources.
MIKE 11 one-dimensional hydraulic model for simulating channel flow, with Muskingum-Cunge routing	Plan of the main river channels	Derived through topographic analysis of the USGS GTOPO30 DEM (Kite, 2000).
	Cross-sections for different stream orders	Established using surveyed cross-sections (Shopea (2003); Mekong River Commission: http://ffw.mrcmekong.org/) and stream width measurements taken in Google Earth Pro.
	Manning's n for bed resistance	Chow (1959)

However, hypsometric curves for the resampled and original topography are very similar (Figure 4.1) whilst percentage coverage values for the different soil and land use classes (see below) are altered by <0.1% in all cases, suggesting that the larger grid size retains a good representation of catchment characteristics.

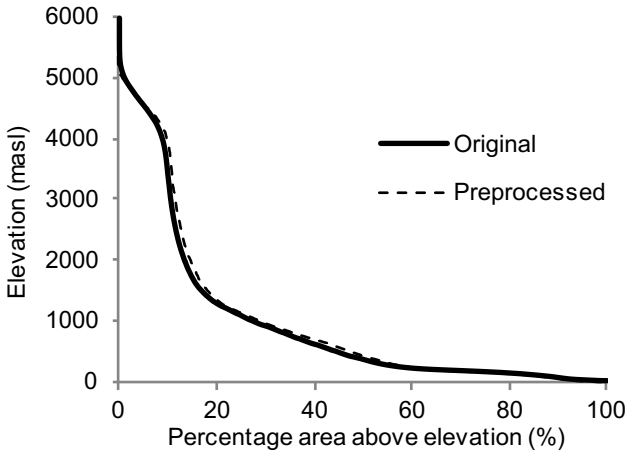

Figure 4.1. Hypsometric curve derived for the original (approximately 1 km × 1km) and MIKE SHE pre-processed (10 km × 10 km) DEMs of the Mekong Basin.

4.2.2. Land cover

Land cover / vegetation was spatially distributed within MIKE SHE using the 1 km × 1 km land cover grid specified within the SLURP model (Kite, 2000). As described in Section 3.3, this was derived from the USGS Global Land Cover Characterization dataset (1992/1993) through aggregation of the original 24 land cover classes into nine categories. For each land use, two vegetation attributes were defined: Leaf Area Index (LAI) and Root Depth (RD). These parameters are used in the calculation of interception and evapotranspiration. Variation in LAI through the year for each land cover class was obtained from Kite (2000). Using equations developed by Running *et al.* (1989) and Kite and Spence (1994), Kite (2000) derived these LAI values using NDVI (Normalized Difference Vegetation Index) images for the Mekong Basin generated from NOAA-AVHRR satellite imagery. Figure 4.2 depicts the LAI values employed; the same temporal patterns were used in each year. For the 'Water' land cover category, a constant LAI value of zero was specified. RD values are not required in SLURP and so were taken from the literature (Jackson *et al.*, 1996) and an existing DHI (2009) vegetation properties file. The values employed are shown in Table 4.2.

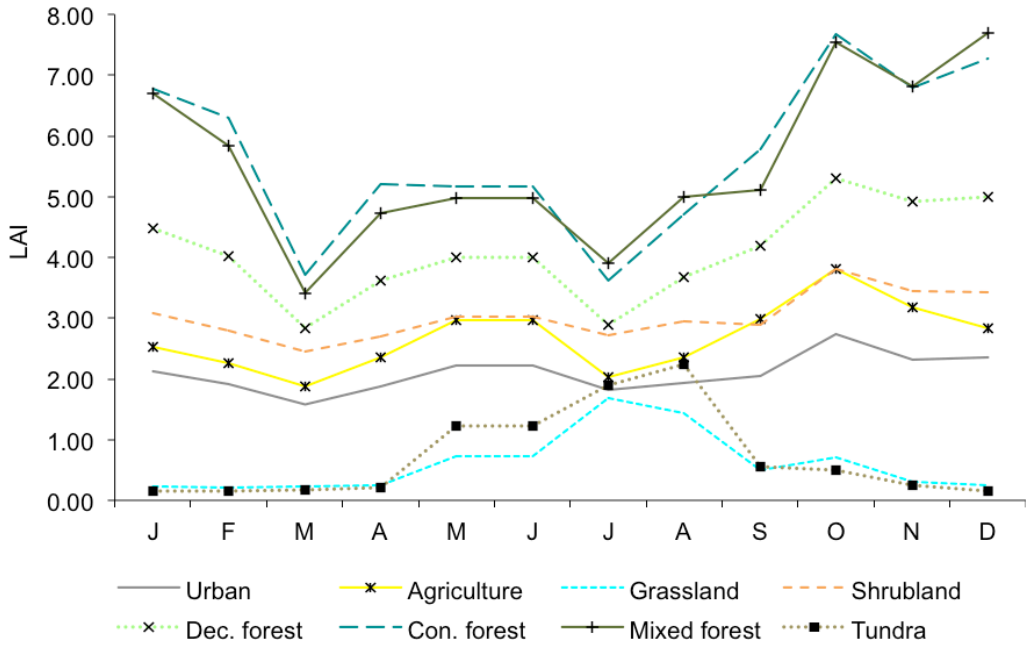

Figure 4.2. Variation in LAI through the year for different land cover categories.

Table 4.2. Root depth and Manning's M values employed for each land use class.

Vegetation class	Root depth (mm)	Manning's M
Urban	Constant value of 100	40
Agriculture	300 Dec–Jun, 450–600 Jul–Nov	13
Grassland	Constant value of 300	16
Shrubland	Constant value of 500	10
Deciduous forest	Constant value of 1000	8
Coniferous forest	Constant value of 800	8
Mixed forest	Constant value of 900	8
Water	Constant value of 0	35
Tundra	Constant value of 300	20

As discussed in Section 3.9.1, the Lower Mekong Basin underwent considerable changes in land cover from the 1960s to 1990s. However, temporally consistent land cover based on data from the early 1990s is used throughout baseline and scenario modelling. Consequently, the land cover employed is more representative of land cover towards the end of the baseline period than the early baseline period, and the potential impacts of future changes in land cover are not explored. This is, however, deemed justifiable for a number of reasons. In particular, there is a lack of evidence that land cover change has had any sizeable impacts on Mekong river flows (see

Section 3.9.1). In addition, some of the highest rate of land cover change occurred in the Chi-Mun Basin, which only contribute a relatively small proportion of discharge on the main Mekong. Furthermore, use of temporally consistent land cover is very common in climate change impact assessments and this approach was also adopted for both the SLURP and Mac-PDM.09 simulations against which MIKE SHE results are compared in this Chapter. Finally, this thesis only aims to assess specific sources of uncertainty in river flow projections under climate change; uncertainty associated with land cover change is not explored.

4.2.3. Overland flow

Overland flow in the MIKE SHE model is calculated using a finite-difference approach to solve the two-dimensional Saint-Venant equations (Graham and Butts, 2005). Overland flow resistance within MIKE SHE is defined using Manning's M, the inverse of Manning's n roughness coefficient (DHI-WE, 2009b). The higher the Manning's M value, the lower the resistance, and hence the faster overland flow is routed to the nearest river branch (Sahoo *et al.*, 2006). Values were spatially distributed using a modified version of the land cover map, in which all forest types were combined into one category. Each land cover was attributed an appropriate roughness coefficient (Table 4.2) using values taken from the literature (see Table 4.1), with a hierarchy from urban (least resistance and therefore highest Manning's M) to forest (greatest resistance).

4.2.4. Unsaturated zone flow

Obtaining detailed and representative soil profiles for the whole of the Mekong Basin would be infeasible. The simple two-layer water balance method (Yan and Smith, 1994), which does not require such information, was therefore selected for modelling the unsaturated soil zone. This approach also reduces computation time compared to more physically-based options and is more appropriate given the large model grid size. This method divides the unsaturated zone into an upper root zone, from which evapotranspiration can occur, and a zone below this where evapotranspiration does not occur (Graham and Butts, 2005). This component of the model is responsible for the calculation of interception, infiltration, surface

ponding, actual evapotranspiration (AET) and recharge to the saturated zone (DHI-WE, 2009b). Such calculations require the specification of several soil characteristics: water content at saturation, at field capacity and at wilting point, as well as saturated hydraulic conductivity. In order to characterise the spatial variation in these properties, a 1 km × 1 km soil texture grid map based on the FAO Digital Soil Map of the World (Figure 3.8) was specified. As detailed in Section 3.4, using the approach adopted by Andersen *et al.* (2001) and Stisen *et al.* (2008), soils were aggregated into four broad categories based on textural classes: Coarse/Medium, Medium, Medium/Fine and Fine.

Soil characteristics for each class are presented in Table 4.3. These were based on the literature (Clapp and Hornberger, 1978; Norman and Dixon, 1995). For the 'Glaciers' FAO class, an infiltration rate of 0 m s^{-1} and a uniform 100% soil moisture water content were applied. However, since this category is restricted to small areas in the Lancang and only covers just under 0.9% of the total catchment, the model results were insensitive to these parameter values.

Table 4.3. Soil class-based parameter values.

Soil class	**Water content at saturation (cm^3/cm^3)***	**Water content at field capacity (cm^3/cm^3)+**	**Water content at wilting point (cm^3/cm^3)+**	**Saturated hydraulic conductivity (m s^{-1})***
Coarse/ Medium	0.43	0.25	0.09	3.5e-005
Medium	0.45	0.3	0.15	7e-006
Medium/Fine	0.47	0.34	0.18	2.5e-006
Fine	0.48	0.38	0.22	1e-006

* Based on Clapp and Hornberger (1978)
+ Based on Norman and Dixon (1995)

4.2.5. Saturated zone flow

Although the majority of the MIKE SHE model of the Mekong uses physically-based solutions and is distributed at the grid scale of 10 km × 10 km, the conceptual, semi-distributed, linear reservoir method was selected for modelling groundwater flow. This method is more appropriate given the large model grid size. In addition, advantages of this method include a reduction in data requirements and reduced complexity compared to physically based solutions, and hence reduced execution time. This method is therefore particularly useful in large catchments where hydrogeological data are lacking and when the focus is on simulating river flow (e.g. Andersen *et al.*, 2001; Stisen *et al.*, 2008).

The linear reservoir method requires that the entire basin be divided into groundwater sub-catchments or linear reservoirs. Figure 4.3 depicts the conceptual structure of the linear reservoir saturated module for a single groundwater sub-catchment. Within each sub-catchment there are three adjacent, interdependent, shallow interflow reservoirs (I_1 I_2 and I_3 in Figure 4.3) and a deep baseflow reservoir. The baseflow reservoir is further divided into an upper (B_1) and a lower (B_2) reservoir, which can be used to differentiate between fast and slow components of baseflow storage (DHI-WE, 2009b). The interflow and baseflow reservoirs are linear in the sense that their output (and hence the rate of exchange between reservoirs, and ultimately with the MIKE 11 hydraulic model) is linearly related to their storage, as defined by time constant calibration parameters (Andersen *et al.*, 2001). During calibration, these time constants can be varied in order to modify, to a certain extent, the shape of the hydrograph.

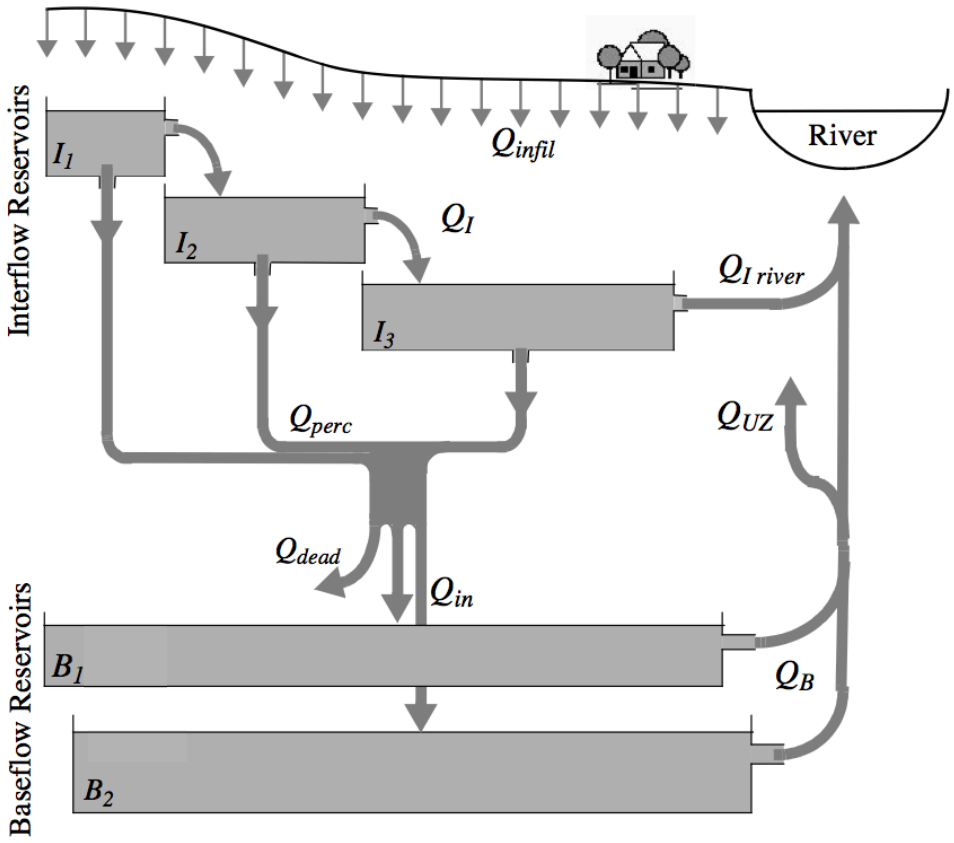

Figure 4.3. Conceptual structure of the sub-catchment based linear reservoir saturated zone module for a single groundwater sub-catchment. Adapted from: DHI-WE (2009b: 368).

As described by DHI-WE (2009b), water enters the interflow reservoirs from the unsaturated zone, which gains its water from vertical infiltration (Q_{infil}). It then flows laterally (Q_I) from the interflow reservoirs in the higher topographic zones to those in lower topographic zones (sequentially from I_1 to I_2 to I_3), before discharging into the river network ($Q_{I\ river}$) or percolating vertically (Q_{perc}) into the deeper baseflow reservoirs, each of which receive a fraction of the percolating water (Q_{in}). Water from the baseflow reservoirs is also able to discharge into the river network (Q_B).

Precipitation, temperature and PET in the MIKE SHE Mekong model are spatially distributed according to the 13 sub-catchments employed within the SLURP model (see next section). It would in theory have been possible to use this same sub-catchment division for the groundwater sub-catchments. However, in order to aid calibration of the model, the Mekong was instead divided into 17 groundwater sub-catchments using the ArcSWAT Watershed Delineation tool on the DEM of the basin (Figure 4.4). These were based on the locations of (i) the 12 gauging stations used

for model calibration / validation, (ii) major tributaries and (iii) large changes in topographic characteristics. Ensuring that each gauging station forms the terminus of a sub-catchment aids calibration as it means that during sequential calibration (starting at the most upstream gauging station and working downstream), it is possible to vary only the linear reservoir parameters for sub-catchments between the gauging station being calibrated and the previously calibrated upstream station. The only stations that do not form a terminus are Kratie and Kompong Cham, both in the Mekong to Phnom Penh groundwater sub-catchment. Due to the relatively close proximity of the Kratie, Kompong Cham and Phnom Penh stations, it was considered that calibration of all three stations should be possible through adjustment of the linear reservoir time constant parameters within the Mekong to Phnom Penh sub-catchment. It is worth reiterating here that simulation results from the Tonle Sap and Delta sub-catchments are not analysed (see Section 3.6.1).

The spatial extent of the interflow reservoirs was defined by dividing each linear reservoir sub-catchment into three interflow reservoirs of approximately equal area based on topographic analysis of the DEM. As noted above, two parallel baseflow reservoirs, representing faster and slower baseflow storage, are located within each groundwater sub-catchment. The linear reservoir parameters within each sub-catchment that were subject to calibration were the two time constants (interflow and percolation) for each interflow reservoir and the baseflow time constant for each baseflow reservoir (i.e. eight for each sub-catchment). In some cases, a dead storage proportion was included for the lower baseflow reservoir. The model calibration and validations procedures are outlined in Section 4.4.

4.2.6. Catchment meteorology

Since an objective of the current study is to compare results between the MIKE SHE model and those from SLURP (Kingston *et al.*, 2011), it was considered appropriate to maintain the original, sub-catchment based spatial distribution of meteorological inputs (Figure 4.4). Climate input data are therefore provided to MIKE SHE in

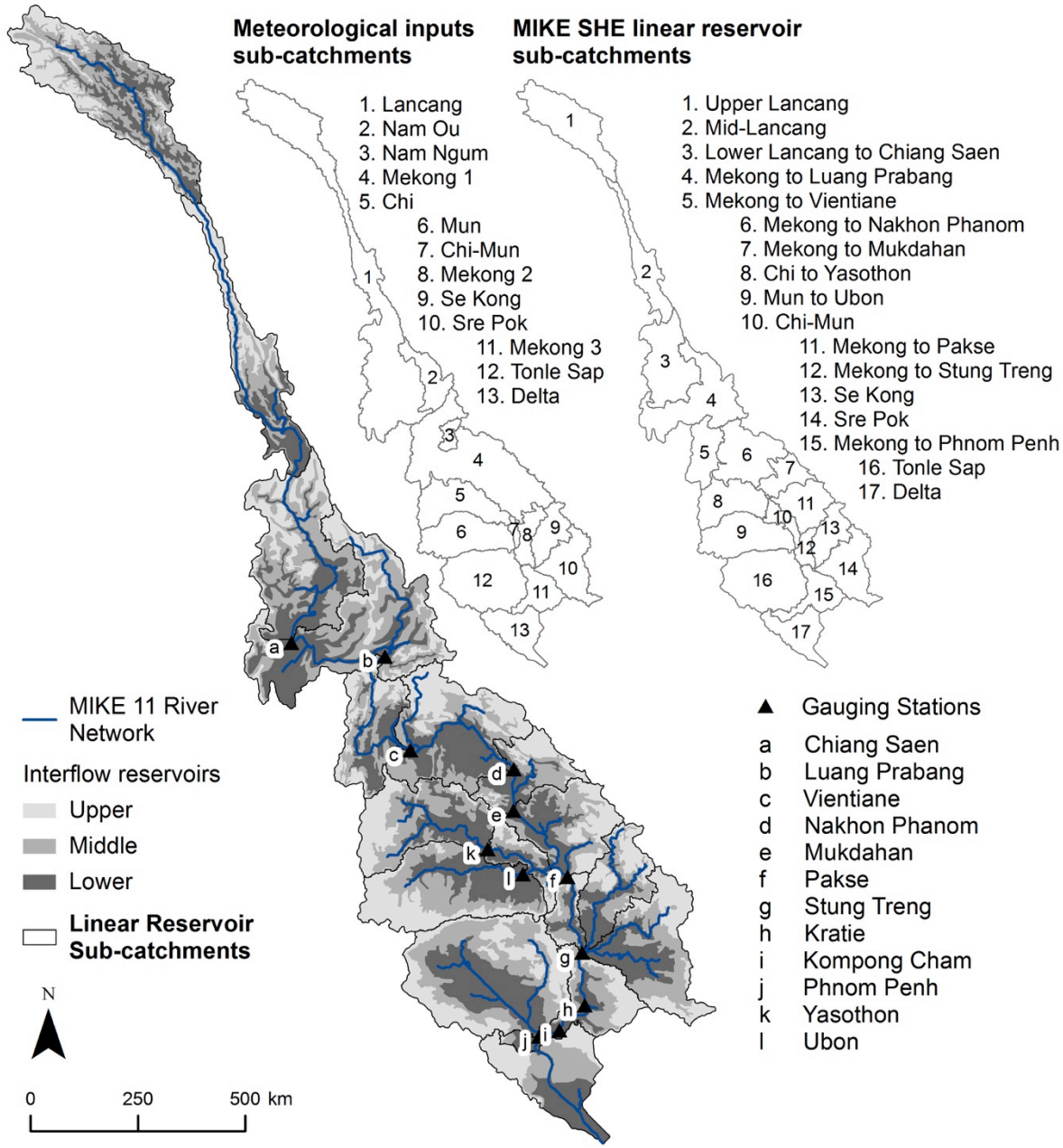

Figure 4.4. The Mekong catchment and its representation within the MIKE SHE model including the distribution of linear reservoir sub-catchments, interflow reservoirs and meteorological inputs. The gauging stations within the MIKE 11 river network that were used for calibration and validation are also indicated.

the form of daily sub-catchment averages, as with the SLURP model. Furthermore, the same precipitation and temperature data and the same PET method as employed in the SLURP model of the Mekong are used in the MIKE SHE model. Whilst only the eight northernmost sub-catchments were modelled by Kingston *et al.* (2011), all 13 sub-catchments were modelled in this study, although results are not extracted from the Tonle Sap and Delta sub-catchments. Setup of the MIKE SHE precipitation,

evapotranspiration and snowmelt modules, including the procedures used for the generation of meteorological data, are detailed in Sections 4.2.6.1–4.2.6.3.

4.2.6.1. Precipitation

The same precipitation data were used as employed in the SLURP Mekong model as part of the QUEST-GSI project (Kingston *et al.*, 2011). As described by Kingston *et al.* (2011), monthly precipitation totals were first obtained from the 0.5° resolution University of Delaware global precipitation dataset (UDel; Willmott and Matsuura, 2000; Section 3.6.1). Data from UDel V (Version) 1.01 were used for the period 1961–1996. Data from V1.02 were used for 1997–1998 (V1.01 only extends to 1996). The monthly precipitation totals from the 268 UDel grid cells covering the Mekong catchment were averaged over the meteorological input sub-catchments and subsequently stochastically disaggregated to a daily resolution using a weather generator extracted from the Mac-PDM hydrological model (Gosling and Arnell, 2011), following the procedures of Todd *et al.* (2011), which were based on those of Arnell (2003). The weather generator assumes that daily precipitation follows a gamma distribution. The coefficient of variation of daily precipitation for the Mekong was obtained from daily station-based data from the NCDC GSOD dataset which was previously employed by Kite (2001), and wet days data were obtained from the CRU TS 3.0 dataset (Mitchell and Jones, 2005). The occurrence of precipitation is described by a simple two-state Markov model with transitional probabilities fixed and the weather generator rescales the daily disaggregated data to ensure that the correct (i.e. input) monthly totals are maintained (Arnell, 2003; Todd *et al.*, 2011).

Within MIKE SHE, it was necessary to apply a precipitation lapse rate within sub-catchments with a large range in elevation, in the form of percentage increase in precipitation with an increase in height of 100 m (percent/100 m). These values were subject to calibration (see Section 4.4). The application of precipitation lapse rates is common practice when modelling mountainous regions (e.g. Fontaine *et al.*, 2002; van der Linden and Woo, 2003a; Immerzeel *et al.*, 2012a; Wijesekara *et al.*, 2014).

As acknowledged by Kingston *et al.* (2011), the use of daily meteorological inputs (and in particular precipitation) generated through stochastic disaggregation of monthly meteorological data means that there will be a disconnect between the daily meteorological inputs and simulated daily discharges. Consequently, simulated river discharges should be analysed at a monthly, or lower, temporal resolution, throughout model calibration, baseline and scenario modelling.

4.2.6.2. Evapotranspiration

MIKE SHE uses PET data to constrain the maximum amount of AET that can occur in each model time step. In contrast to SLURP, MIKE SHE does not calculate PET internally. Monthly PET for each of the sub-catchments employed to distribute meteorological data were therefore calculated externally to MIKE SHE using the Linacre method[1], the same PET scheme employed by Kingston *et al.* (2011) within SLURP (see Table 2.6 for the Linacre equation). Mean monthly temperature for the calculation of Linacre PET was obtained from the CRU TS 3.0 dataset (Mitchell and Jones, 2005), since this is the dataset from which the temperature data applied to SLURP were derived. Following calculation, PET was distributed on a daily basis evenly throughout the month, following initial experiments that showed model results to be insensitive to this method compared to the application of daily estimates of PET derived through stochastic disaggregation of monthly PET totals using a weather generator.

4.2.6.3. Snowmelt

As described previously (Section 3.6), snow is a regular feature in the upper Lancang from November–March. The MIKE SHE snowmelt module was therefore included in the model. In common with SLURP, this uses the degree-day method. Use of this component required that time-series of air temperature be provided for the Lancang sub-catchment. It also required two further parameters: a threshold melting temperature, at and above which melting occurs and below which precipitation accumulates as snow, and a degree-day coefficient (mm snow/day/˚C), which defines the amount of snow that melts per day, per every degree that the air

[1] The Linacre PET data were generated by Dr Daniel Kingston, University of Otago.

temperature is above the threshold melting temperature (DHI-WE, 2009b). The standard threshold melting temperature of 0˚C was used, whilst the degree-day coefficient was subject to calibration. The temperature data, (from the SLURP Mekong model), were derived from the 0.5° resolution CRU TS 3.0 mean monthly temperature dataset (Section 3.5.2; Mitchell and Jones, 2005). The monthly data were spatially averaged for each of the meteorological input sub-catchments and stochastically disaggregated to a daily resolution using the Mac-PDM weather generator (Kingston *et al.*, 2011). The standard deviation of daily temperature for application within the weather generator was derived from the NCDC GSOD dataset. A temperature lapse rate was applied over the Lancang to ensure annual snow accumulation and melting and was subject to calibration.

4.3. Model construction: The MIKE 11 model

MIKE SHE uses the 1D MIKE 11 hydraulic model (Havnø *et al.*, 1995) to simulate channel flow. This section describes the construction of the MIKE 11 model of the Mekong river network that was coupled to the MIKE SHE hydrological model.

4.3.1. MIKE 11 river network

The main channels and tributaries of the Mekong were manually digitised in the MIKE 11 Network Editor, using a shapefile of the river network used in SLURP as an underlay. This network was derived through processing of the basin DEM using TOPAZ (Kite, 2000) and was divided into five stream orders using Strahler's numbering system. Although all branches were originally digitised, it was necessary to only model stream orders two to five, due to a computational limit within the MIKE 11 model (see Section 3.7). This gave a total of 45 river branches. A zero flow boundary was specified at the upstream end of each open branch (i.e. ends not connected to other branches). Consistent with previous modelling studies using MIKE SHE/MIKE 11 (e.g. Singh *et al.*, 2010; Thompson, 2012) a uniform channel resistance was applied to the river network, with the value taken from Chow (1959). A Manning's M value of 30 was used (equivalent to a Manning's n roughness coefficient of 0.033).

All MIKE 11 river branches were coupled to the MIKE SHE model, and so received exchanges from MIKE SHE in the form of overland flow, interflow from adjacent interflow reservoirs, and baseflow. Flows from the interflow and baseflow reservoirs were specified as being equally distributed along the lengths of the river branches within the relevant sub-catchment. All river branches were set to the Muskingum-Cunge routing method. This method is computationally efficient, enables the use of large time steps and approximates the diffusion of a natural flood wave (DHI-WE, 2009a). The MIKE 11 time step was set to 24 hours. This was considered to be reasonable since simulated river flows throughout model calibration, baseline and scenario modelling were to be analysed at a monthly temporal resolution or lower (see Section 4.2.6.1). As discussed and justified in Section 3.9.3, dams are not included within the model.

4.3.2. Chanel cross-sections

In order to define channel dimensions, at least three cross-sections should be specified for each MIKE 11 river branch: one at the upstream end, one at the downstream end and one ~3 km upstream of each confluence. This is because MIKE 11 uses the cross-sections to interpolate cross-section dimensions along the length of each river branch. Synthetic cross-sections were generated, each in the form of depth relative to the bank at 10, 20, 30, 40, 50, 60, 70, 80, 90 and 100% of the cross-section width. A uniform width was assigned to each stream order within each meteorological input sub-catchment. These widths were determined using averages calculated from over 3500 river width measurements taken manually from satellite images in Google Earth Pro whilst using the channel network as an overlay. Cross-sections from Shopea (2003) and the MRC (http://ffw.mrcmekong.org/) were used to establish representative maximum cross-section depths and cross-section profiles for different stream orders. Estimated bank elevations for each cross-section were extracted from the GTOPO30 DEM. On each branch, the furthest upstream and penultimate cross-sections were given the uniform dimensions of the stream order of that branch, whilst the furthest downstream cross-section was given the width of that stream order, but the depth assigned to the branch that it is joining. This allows interpolation between the two depths, and so prevents a sudden drop in bed elevation, which would cause numerical instability during simulations.

4.4. Model calibration and validation

A split sample approach (e.g. Klemeš, 1986; Henriksen *et al.*, 2003) was adopted in order to calibrate and validate the MIKE SHE model. Following the methodology of Kingston *et al.* (2011), the baseline period of 1961–1990 was used for calibration and the shorter 1991–1998 period for validation. Whereas SLURP was only calibrated using three stations (Chiang Saen, Pakse and Ubon), data from a further nine gauging stations were used for MIKE SHE, giving a total of 12 stations (Figure 4.4). As described in Section 3.8, ten of these are on the main Mekong and two are on tributaries (the Chi and Mun, which both drain the Khorat Plateau in the western part of the basin). The length of records for three stations did not cover the complete calibration period, whilst discharge for Kratie was derived from records for Pakse using a linear regression model developed by the Institute of Hydrology (1988). Table 3.9 provides the data availability for each station.

4.4.1. Model performance criteria

During manual calibration and subsequent validation, performance of the model at each gauging station in terms of the agreement achieved between observed and simulated discharge was assessed visually (qualitatively) using plots of observed and simulated daily, monthly and mean monthly (the river regime) discharge. Performance was also assessed quantitatively, using the Nash–Sutcliffe coefficient (NSE; Nash and Sutcliffe, 1970), Pearson correlation coefficient (r) and percentage deviation in simulated mean flow from the observed mean flow (Dv; Henriksen *et al.*, 2003). The equations and significance of these statistical measures are outlined in Table 2.5. As stated above and acknowledged by Kingston *et al.* (2011), there is a disconnect between the daily meteorological input data and daily discharge as a result of generating the daily meteorological data from monthly values using a stochastic weather generator. This means that it is more appropriate to assess model performance at a monthly resolution. NSE and *r* were therefore calculated using monthly mean discharges (i.e. 12 values per year, so 360 values (30×12) for the 30-year calibration period). Additionally, during calibration of Chiang Saen, the furthest upstream gauging station, simulated snow extents were compared to the literature (e.g. Kiem *et al.*, 2005; Immerzeel *et al.*, 2009; Savoskul and Smakhtin,

2013b) and it was ensured that extensive snow cover was only present during the period November–May, with maximum accumulation occurring around March.

4.4.2. Selection of calibration parameters and model sensitivity analysis

A guiding principle that influenced model parameterisation was that the number of 'free' parameters subject to adjustment during the calibration stage of a distributed model should be kept to a minimum (Refsgaard and Storm, 1995; Refsgaard, 1997; Andersen *et al.*, 2001). Table 4.4 summarises which parameters were selected for calibration and which parameters were instead based on the literature without being calibrated. Justification and further information is also provided.

Two sets of parameters whose values, by necessity, had to be obtained through calibration were the time constants of the saturated zone's interflow and baseflow reservoirs. These parameters are conceptual in nature and so cannot be based on field measurements. They also cannot be obtained from the modelling literature.

The snowmelt degree-day coefficient and temperature lapse rate were selected for calibration of the Lancang at Chiang Saen, this being the one sub-catchment with significant snow cover. Although the values of these parameters could potentially be based on the literature or, in the case of the temperature lapse rate, on analysis of station based data (if available), they can also be obtained through calibration. Sensitivity analysis was undertaken in order to gauge the sensitivity of the model to these parameter values. They were manually varied within realistic bounds based on the literature and the impacts on model performance assessed using the criteria described in the section above. Snow depths and extents were found to be relatively sensitive to these parameters, with the average values from the literature providing weaker performance compared to that which could be obtained. These parameters were therefore subject to calibration. Similar sensitivity testing was undertaken for the other parameters in Table 4.4.

In a small number of sub-catchments with large elevation ranges, a precipitation lapse rate was applied. As described in Section 4.2.6.1, it is common for precipitation lapse rates to be required when modelling mountainous regions. In the absence of

Table 4.4. Selection of parameters for calibration.

Parameter(s)	Spatial distribution	Cal?*	Further notes / justification
Precipitation lapse rate (%/100 m)	Distributed according to meteorological input sub-catchments. Only applied over a handful of sub-catchments.	✓	As described in Section 4.2.6.1, it is common for precipitation lapse rates to be required when modelling mountainous regions. It is also not uncommon for them to be derived through calibration.
Temperature lapse rate (°C/100 m)	Only relevant over the upper Lancang, where snow cover occurs.	✓	Varied during calibration of the Lancang at Chiang Saen. Use of sub-catchment average temperature means a lapse rate is necessary to ensure annual build up and melting of snow. Subject to calibration as seasonal snow patterns found to be relatively sensitive to this parameter.
Degree-day snowmelt factor (mm/°C/day)	Only relevant over the upper Lancang, where snow cover occurs.	✓	Varied during calibration of the Lancang at Chiang Saen. Subject to calibration as seasonal snow patterns found to be relatively sensitive to this parameter.
Soil hydraulic parameters (see Table 4.3)	Distributed according to soil texture class	✗	Soil hydraulic parameter values associated with different soil texture classes available from the literature. Sensitivity analysis found that adjustment of model parameters did not provide any notable improvement in model performance compared to initial values based on the literature. Values from the literature therefore used.
LAI	Distributed according to land cover.	✗	LAI values were obtained from Kite (2000). See Section 4.2.2 and Table 4.2. Not subject to calibration because: i) they were based on remote sensing data for the Mekong, ii) these were the same values used in SLURP, iii) sensitivity analysis demonstrated that model performance was relatively insensitive to LAI values within realistic bounds for each land cover class.
RDs	Distributed according to land cover.	✗	RDs based on a DHI (2009) / MIKE Zero vegetation properties file and the literature. Not subject to calibration in order to reduce the number of free parameters.
Manning's M for overland flow	Distributed according to land cover.	✗	Values obtained from the literature. See Section 4.2.3 and Table 4.2. Sensitivity analysis found that model performance was relatively insensitive to these parameter values when values were varied within bounds based on the literature.
Saturated zone interflow and baseflow reservoir time constants	Distributed according to sub-catchments and linear reservoirs defined through topographic analysis. See Figure 4.4.	✓	These parameters are conceptual in nature, with no standard values available in the literature. These values were therefore subject to calibration. Sensitivity testing was undertaken to gauge how these parameters affected model performance.
Dead storage fraction in the baseflow reservoirs	Only applied to two groundwater sub-catchments	✓	Discussed in Section 4.7.1.

*Parameter subject to calibration? ✓ = Yes. ✗ = No.

station records on which to base these values, this parameter was selected for calibration, as done so by other studies (e.g. Luo *et al.*, 2013). Testing of the other parameter values whilst no precipitation lapse rates were applied revealed that in a small number of sub-catchments, adjustment of these other parameters could not provide satisfactory model performance. For example, in order to reduce evapotranspiration over the Lancang region, reduction of the vegetation RDs was tested, within realistic bounds based on the literature. Since this could not alter the water balance sufficiently, the RD values were returned to their original non-calibrated values. This adds support to the assumption that underestimation of discharge in the absence of a precipitation lapse rate may be due, at least in part, to underestimation of precipitation within the input data.

Sensitivity analysis indicated that model results were relatively insensitive to Manning's M for overland flow, and so values for this parameter were obtained from the literature, rather than subject to calibration. The model was more sensitive to RD values. However, consistent with other MIKE SHE studies that have derived RD values from the literature (e.g. Rochester, 2010; Singh *et al.*, 2010; Wijesekara *et al.*, 2012), the decision was made to not calibrate RDs in this study, in order to reduce the number of free parameters. As outlined in Table 4.4, LAI values were not selected for calibration for a number of reasons. Instead, remote sensing-based LAI values for different land cover classes in the Mekong Basin were obtained from Kite (2000). These were the same values used in SLURP. During calibration of a limited number of sub-catchments (two), a dead storage proportion for the baseflow reservoirs was applied and subject to calibration. Since these dead storage fractions were introduced during model calibration, rather than during the initial sensitivity testing, they are discussed in Section 4.7.1, where the calibration results and calibrated parameter values are presented.

Use of crop coefficients to modify PET was considered as an alternative or additional means of calibrating the model. However, crop coefficients in the literature (e.g. Allen *et al.*, 1998) are intended for use with reference evapotranspiration (Allen *et al.*, 2005), whereas the Linacre method provides PET. In addition, crop coefficients in the literature are associated with specific crop types (e.g. rice, maize, soybeans), rather than the broad land cover classes specified in the MIKE SHE model of the

Mekong. The establishment of effective crop coefficients for different land cover classes could not, therefore, be guided by values from the literature. Furthermore, neither SLURP nor the Mac-PDM.09 model of the Mekong employed crop coefficients.

4.4.3. Calibration procedure

Calibration was undertaken for each gauging station in a downstream sequence, beginning at Chiang Saen and progressing to Mukdahan. The Yasothon and Ubon gauging stations (on the Chi and Mun tributaries, respectively) were then calibrated before continuing the calibration for stations between Pakse and Phnom Penh. In each case, only those model parameters for sub-catchments between the previously calibrated upstream station and the current station were varied.

For each gauging station, a preliminary autocalibration was undertaken using MIKE Zero's in-built parameter optimisation tool, AUTOCAL. The Shuffled Complex Evolution (SCE) algorithm was employed, which uses Monte Carlo sampling (Duan *et al.*, 1992; Madsen and Jacobsen, 2001; Madsen, 2003). During autocalibration, parameters were permitted to vary between specified upper and lower bounds. Two equally weighted calibration criteria, the absolute value of the average error and the root mean square error, were employed (Butts *et al.*, 2004). These were aggregated into one measure using a transformation that compensates for differences in the magnitudes of the criteria (Madsen, 2003). The autocalibration routine evaluated the two calibration criteria at the model time step (defined as a maximum of 48 h).

According to Madsen and Jacobsen (2001), autocalibration is both more efficient and more objective than trial-and-error manual calibration. It would therefore have been desirable for autocalibration to achieve a satisfactory model performance at each gauging station. However, In the version of MIKE Zero which was employed (Version 2009, Service Pack 5), the observed and simulated discharge comparison statistics (objective functions) computed by MIKE Zero during autocalibration can only be calculated on model output at the time step of the model (48 hours in this case). Consequently, whilst model performance (at a monthly resolution) following autocalibration was generally good, it was possible to improve it through manual

modification of model parameters, with observed and simulated discharge being aggregated to monthly mean flows for calculation of performance statistics, an approach also used by Kingston *et al.* (2011). Following calibration, the model was run for the shorter 1991–1998 period for validation.

4.5. Simulation of climate change

In order to allow comparison between the scenario results of MIKE SHE and SLURP, the same revised meteorological inputs as used by Kingston *et al.* (2011) were employed to simulate potential impacts of, and uncertainty associated with, climate change. Monthly resolution climate scenarios for precipitation and temperature were generated using the ClimGen pattern-scaling approach (Mitchell, 2003; Arnell and Osborn, 2006; Osborn, 2009; Todd *et al.*, 2011). This technique allows the pattern of climate change simulated by a GCM to be downscaled to a finer spatial resolution and rescaled to produce climate data for a given increase in global mean air temperature (Kingston *et al.*, 2011; Todd *et al.*, 2011). ClimGen employs the assumption that the spatial pattern of climate change simulated by a GCM and associated with a particular change (increase) in global mean temperature can be linearly rescaled to produce the change pattern for a different increase in global mean temperature. Linear interpolation allows the change pattern to be downscaled to a spatial resolution of 0.5° × 0.5°. The change pattern for each climate variable is then used to perturb historical / observed climate data (in this case, those used in baseline hydrological simulation), using a delta-change approach. For precipitation, year-to-year variation is altered according to GCM-derived changes in the shape parameters of the gamma distribution describing year-to-year variation in monthly precipitation (Arnell and Osborn, 2006; Todd *et al.*, 2011). The initial change patterns for each variable for each month (January–December) were based upon the change in 30-year mean for the period 2070-2099 relative to the 1960-1990 reference period. However, rescaling these patterns to represent a prescribed increase in global mean temperature means that the scenario meteorological datasets, and hence the river flow projections, are for an arbitrary 30-year period.

Monthly resolution, 0.5° × 0.5° gridded precipitation, wet days and temperature scenario data were generated for a prescribed warming of 2 °C, the hypothesised

threshold for 'dangerous' climate change (Todd *et al.*, 2011), for seven CMIP3 GCMs (see Table 4.5). These were selected from the CMIP3 database (Meehl *et al.*, 2007b) for use in the QUEST-GSI project to encompass a range of different but plausible global climate futures (Todd *et al.*, 2011). In addition, the UKMO HadCM3, a widely employed GCM previously used for uncertainty analysis (e.g. Booij, 2005; Buytaert *et al.*, 2009; Kay *et al.*, 2009; Prudhomme and Davies, 2009b), was selected to derive scenarios for prescribed warming of global mean temperature of 1, 2, 3, 4, 5, and 6 °C. The monthly gridded datasets were subsequently spatially averaged at the meteorological input sub-catchment scale and disaggregated to daily resolution using the Mac-PDM weather generator, following the approach used for the baseline data. For each scenario, monthly Linacre PET was calculated for each sub-catchment using scenario temperature and then distributed evenly through each month at a daily time step, again replicating the steps used for the baseline data. The two resulting scenario sets are subsequently referred to as the 2 °C, seven GCM and 1–6 °C, HadCM3 scenario sets.

Table 4.5. CMIP3 GCMs used in this thesis.

CMIP3 GCM	Abbreviation in Chapters 4 and 5	Institute
CCCMA CGCM3.1	CCCMA	Canadian Centre for Climate Prediction and Analysis
CSIRO-Mk3.0	CSIRO	CSIRO Atmospheric Research
UKMO HadCM3	HadCM3	UK Met Office Hadley Centre for Climate Prediction and Research
UKMO HadGEM1	HadGEM1	
IPSL-CM4	IPSL	Institut Pierre Simon Laplace
MPI-ECHAM5	MPI	Max Planck Institute for Meteorology
NCAR-CCSM3	NCAR	National Centre for Atmospheric Research

4.6. Inter-hydrological model comparison

Following climate change scenario simulation, an assessment of inter-hydrological model uncertainty was undertaken through comparison of MIKE SHE model results with those of the SLURP catchment model of the Mekong (Kingston *et al.*, 2011) and Mac-PDM.09 GHM (Gosling *et al.*, 2011), for the same two sets of climate change scenarios. Table 4.6 summarises the key attributes of these three hydrological models.

Unlike the MIKE SHE and SLURP catchment models, Mac-PDM.09 does not contain river routing. Furthermore, Mac-PDM.09 was not specifically calibrated for the Mekong; instead, the model was calibrated at the continental scale by 'tuning' it to help define parameter values, as described in Section 2.6.3.3. This involved tests of precipitation datasets and potential evaporation calculations and comparisons with long-term average runoff and within-year runoff patterns for a small number of major river basins and for a large number of small basins, with simulated runoff being aggregated over the cells falling within the basins (see Arnell, 1999; Gosling and Arnell, 2011). Gosling and Arnell (2011) evaluated the performance of Mac-PDM.09 by validating simulated runoff against observed runoff for 50 catchments across the globe, and the model was found to perform well (see Section 2.6.3.3).

Results from SLURP for the same climate change scenarios were available for three stations from Kingston *et al.* (2011): Chiang Saen, Pakse and Ubon (although results for the latter station were not presented in the earlier study). For comparison with results from MIKE SHE and SLURP, simulated runoff (mm) from Mac-PDM.09 for each climate scenario was aggregated at a monthly time step for all the model grid cells within the boundaries of the catchments of six gauging stations: Chiang Saen, Vientiane, Nakhon Phanom, Pakse, Phnom Penh and Ubon (Figure 4.4). These were selected in order to provide a comparison of results for the three stations for which results are available for all three hydrological models (Chiang Saen, Pakse and Ubon). Vientiane and Nakhon Phanom were selected as stations in the middle of the catchment upstream of the two major tributaries draining the Khorat Plateau (the Chi and Mun), whilst Phnom Penh is the lowest station on the river and upstream of the ecologically and economically important Mekong Delta. Comparisons of results for these additional stations are limited to MIKE SHE and Mac-PDM.09. This analysis extends the preliminary inter-model comparison undertaken by Gosling *et al.* (2011) that was limited to a comparison of SLURP and Mac-PDM.09 for Pakse alone.

As indicated above, results (e.g. percentage change in mean annual flow/runoff compared to the baseline) for Mac-PDM.09 are based on runoff (i.e. mm) values, whilst results for MIKE SHE and SLURP are based on routed river discharge (m^3s^{-1}). It is worth noting, however, that converting runoff values into discharge (or vice versa) does not affect relative/percentage change values compared to the baseline.

Table 4.6. Summary of key attributes of the MIKE SHE, SLURP and Mac-PDM.09 hydrological models of the Mekong.

Attribute	MIKE SHE	SLURP	Mac-PDM.09
Model type	Distributed (10 km × 10 km grid), physically based model, with semi-distributed conceptual saturated zone component	Semi-distributed vertical water balance model	Gridded conceptual water balance global hydrological model
River routing	Muskingum-Cunge (MIKE 11)	Muskingum	None
Time step	Variable – max. 48 hours	Daily	Daily
Meteorological inputs+	P, T, PET	P, T	P, T, W, SH, LW_{net}, SW
PET method	Linacre PET calculated externally	Linacre PET calculated within the model	Penman-Monteith PET calculated within the model
Snow scheme	Degree-day	Degree-day	Degree-day
Meteorological inputs spatial distribution	Distributed according to 13 sub-catchments from SLURP (Figure 4.4)	Distributed according to 13 sub-catchments (Figure 4.4)	0.5° × 0.5° grid
Spatial distribution of catchment characteristics	Topography, land cover and soil: based on 1 km × 1 km gridded data resampled to a 10 km × 10 km computational grid	Topography, land cover and soil: based on a 1 km × 1 km gridded data	Land cover and soil: 0.5° × 0.5° grid
Spatial resolution of process computation	All model components except the saturated zone: distributed according to 10 km × 10 km grid. Saturated zone: distributed according to 17 sub-catchments, each comprising three interflow and two baseflow reservoirs (Figure 4.4).	13 sub-catchments divided into 98 elements for water balance calculations based on land cover . Results for each element aggregated based on relative cover within each sub-catchment.	0.5° × 0.5° grid
Calibration parameters*	k_i, k_p, k_b, DZ_{frac}, P_{lapse}, T_{lapse}, DD	RC, M, FC, U	Not calibrated for the Mekong (see text)

+ P: precipitation, T: air temperature, PET: potential evapotranspiration, W: wind speed, SH: specific humidity, LW_{net}: net longwave radiation flux, SW: shortwave radiation flux (downward)

* k_i: interflow time constants for saturated zone interflow reservoirs, k_p: percolation time constants for saturated zone interflow reservoirs, k_b: time constants for baseflow reservoirs, DZ_{frac}: dead storage in the baseflow reservoirs, P_{lapse}: precipitation lapse rate, T_{lapse}: temperature lapse rate, DD: snow melt degree-day coefficient, RC: retention constants and capacities of the fast and slow soil stores, M: Manning's n roughness coefficient for overland flow, FC: soil field capacity coefficients, U: wind factor used in computation of Linacre PET

4.7. Results

In this Section, calibration results from the MIKE SHE model (and from SLURP for three stations) are first presented (Section 4.7.1), followed by model validation results (4.7.2). Then in Sections 4.7.3 and 4.7.4, results of the hydrological climate change impact and uncertainty assessments for the 2 °C, seven GCM climate change scenario set and 1–6 °C, HadCM3 are presented, respectively. Throughout, numbering of the meteorological input sub-catchments and the letters used to refer to gauging stations follow those shown in Figure 4.4.

4.7.1. Model calibration

Table 4.7 summarises the calibrated parameter values of the precipitation lapse rates (in sub-catchments with large elevation ranges), baseflow reservoir time constants and baseflow reservoir dead storage proportions (for two sub-catchments only – discussed below). The interflow and percolation time constants of the interflow reservoirs, of which there are three in each groundwater sub-catchment (see Section 4.2.5 and Figure 4.4) were also subject to calibration, and the final parameter values varied between 1 and 50 days.

Table 4.7. Calibration parameter values. Numbers in the column headings refer to the MIKE SHE linear reservoir sub-catchments.

Parameter	1	2	3	4	5	6	7	8	9	10	11	12	13	14	15
Precipitation lapse rate (%/100 m)	1.80	4.80	4.80	5.35	0.00	8.49	0.00	0.00	4.47	0.00	0.00	0.00	0.00	0.00	0.00
Time constant for BR1* (days)	115	115	115	70	90	55	85	175	105	55	55	30	20	20	105
Time constant for BR2+ (days)	740	645	880	520	600	90	120	530	190	135	80	300	110	110	390
Dead storage fraction for BR2	0.00	0.00	0.00	0.00	0.30	0.00	0.00	0.90	0.00	0.00	0.00	0.00	0.00	0.00	0.00

* BR1: Baseflow reservoir 1; + BR2: Baseflow reservoir 2.

The use of single or multiple precipitation lapse rates as a calibration term has been adopted elsewhere (e.g. Yu *et al.*, 2011; Ji and Luo, 2013). In addition, the values employed in the model are within the range of those previously reported in mountainous regions (e.g. in the Upper Indus Basin, Pakistan, and in a headwater

catchment in the Himalayas, Immerzeel *et al.*, 2012a,b). A lower precipitation lapse rate was applied over the upper Lancang because analysis of the gridded UDel precipitation data revealed that annual precipitation rates over this region are considerably lower (by >30%) than over the mid to lower Lancang (see Figure 3.9). This is consistent with data presented in the literature (UNEP, 2006; Kiem *et al.*, 2008). Therefore, although precipitation lapse rates were required to address the perceived underestimation of precipitation over the Lancang region, a lower lapse rate over the upper Lancang was deemed appropriate in order to avoid excessive precipitation, and hence enhanced build up and melting of snow. Over the Lancang meteorological input sub-catchment, the temperature lapse rate was calibrated to -0.51 °C/100 m and the degree-day snowmelt factor to 1.75 mm/°C/day.

Table 4.8 presents model performance statistics for the 1961–1990 calibration period for the 12 stations used in model calibration. As previously discussed, NSE and *r* are derived from monthly mean discharges. For Stung Treng, Kompong Cham and Phnom Penh, statistics are based upon the reduced periods of observed discharge. In the case of Chiang Saen, Pakse and Ubon, the values of Dv and NSE reported by Kingston *et al.* (2011) for the SLURP model of the Mekong are also provided. Figure 4.5 shows the observed and simulated monthly mean flows for the 10 gauging stations for which data are available for both the calibration and validation periods (albeit with gaps).

According to the classification scheme of Henriksen *et al.* (2008) for Dv and NSE, the performance of the MIKE SHE model can generally be classed as ‘‘excellent’’ (21 out of the 24 model performance statistics; Table 4.8). It is worth noting that this scheme was originally based upon daily, rather than monthly, observed and simulated discharge. Higher NSE values are to be expected when aggregating to monthly mean discharges. However, increasing the lower boundary of the “excellent” class for NSE to 0.90 still results in eight stations (previously ten) retaining an “excellent” rating. The remaining stations on the main Mekong have an NSE of 0.88–0.89. Although an equivalent classification scheme is not employed for *r*, values are close to or above 0.95 at 10 of the 12 stations, reflecting a strong positive correlation between observed and simulated discharges.

Table 4.8. MIKE SHE model performance statistics for 12 gauging stations within the Mekong Basin for the calibration period (1961–1990 unless stated otherwise). Corresponding statistics from Kingston et al. (2011) for SLURP are shown in brackets for three stations. Model performance indicators are taken from Henriksen et al. (2008).

Station	Obs Mean (m^3s^{-1})	Sim Mean (m^3s^{-1})	Dv (%)+	NSE*	r#
Mekong at Chiang Saen (a)	2711.3	2818.0	1.56 ☆☆☆☆☆	0.88 ☆☆☆☆☆	0.94
		(2931.6)	(+8.12) (☆☆☆☆☆)	(0.78) (☆☆☆☆☆)	
Mekong at Luang Prabang (b)	3980.2	4138.1	2.57 ☆☆☆☆☆	0.89 ☆☆☆☆☆	0.94
Mekong at Vientiane (c)	4521.1	4741.7	3.65 ☆☆☆☆☆	0.90 ☆☆☆☆☆	0.95
Mekong at Nakhon Phanom (d)	7031.6	7135.6	0.69 ☆☆☆☆☆	0.91 ☆☆☆☆☆	0.95
Mekong at Mukdahan (e)	7602.4	7681.3	0.31 ☆☆☆☆☆	0.90 ☆☆☆☆☆	0.95
Mekong at Pakse (f)	9836.8	9653.2	-2.44 ☆☆☆☆☆	0.90 ☆☆☆☆☆	0.95
		(9925.3)	(+0.90) (☆☆☆☆☆☆)	(0.89) (☆☆☆☆☆☆)	
Mekong at Stung Treng (g) (1961–1969)	13381.0	13382.2	-0.42 ☆☆☆☆☆	0.93 ☆☆☆☆☆	0.97
Mekong at Kratie (h)	13418.9	13016.9	-3.41 ☆☆☆☆☆	0.91 ☆☆☆☆☆	0.95
Mekong at Kompong Cham (1964–Mar 1974) (i)	13409.5	13758.2	2.19 ☆☆☆☆☆	0.93 ☆☆☆☆☆	0.96
Mekong at Phnom Penh (j) (1961–Mar 1974)	13022.3	14132.2	8.07 ☆☆☆☆	0.93 ☆☆☆☆☆	0.97
Chi at Yasothon (k)	202.3	203.7	0.68 ☆☆☆☆☆	0.49 ☆☆	0.71
Mun at Ubon (l)	636.3	619.1	-2.70 ☆☆☆☆☆	0.55 ☆☆☆	0.74
		(899.5)	(+41.36) (☆)	(0.44) (☆☆)	

Performance indicator	Excellent ☆☆☆☆☆	Very good ☆☆☆☆	Fair ☆☆☆	Poor ☆☆	Very poor ☆
Dv	< 5%	5–10%	10–20%	20–40%	>40%
NSE	>0.85	0.65–0.85	0.50–0.65	0.20–0.50	<0.20

+ percentage deviation in simulated mean flow from observed mean flow (Henriksen *et al.*, 2003), * Nash-Sutcliffe coefficient (Nash and Sutcliffe, 1970), # Pearson correlation coefficient

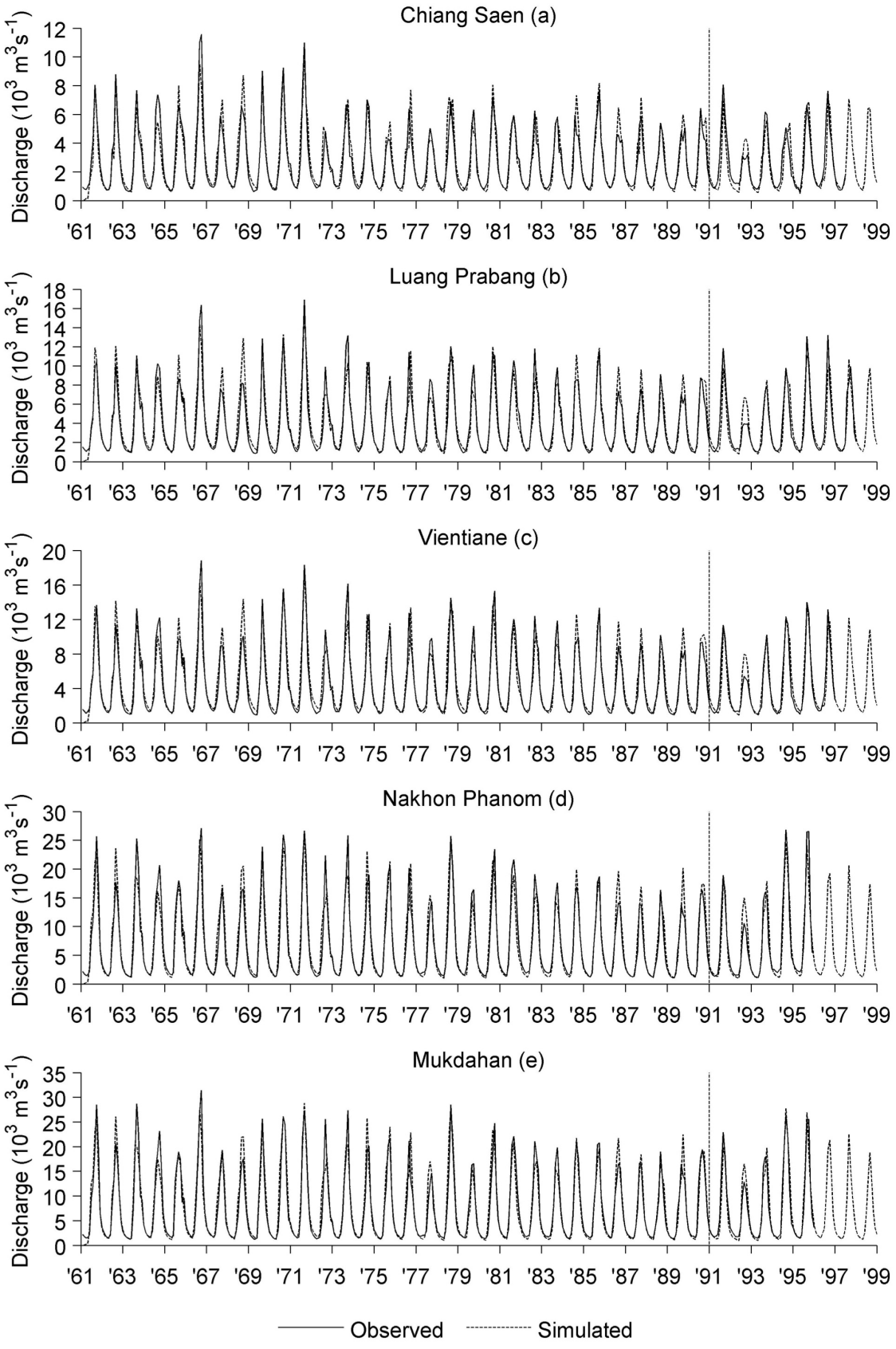

Figure 4.5. Monthly mean observed and simulated discharge for ten gauging stations in the Mekong Basin for the calibration (1961–1990) and validation periods (1991–1998). (Note different y-axis scales.)

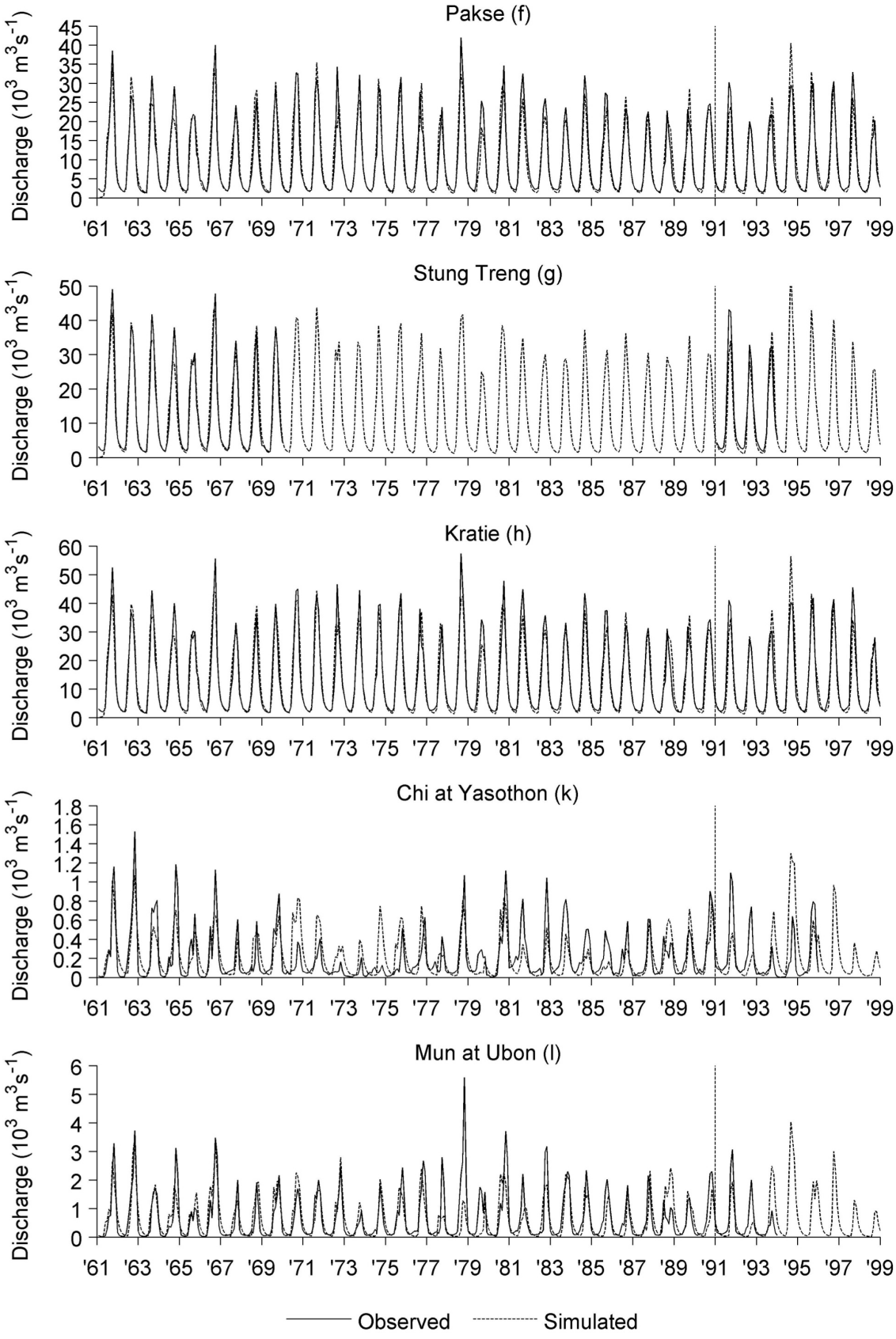

Figure 4.5. (cont.) Monthly mean observed and simulated discharge for ten gauging stations in the Mekong Basin for the calibration (1961–1990) and validation periods (1991–1998). (Note different y-axis scales.)

Good sequencing of the annual monsoon flood pulse is achieved at all gauging stations and on the main Mekong (i.e. excluding Yasothon and Ubon) the rising and descending limbs and the timing of the peak of the annual flood are well represented (Figure 4.5). However, magnitudes of the annual peaks are less well captured at Ubon and, in particular, Yasothon on the Rivers Mun and Chi, respectively. Figure 4.6 shows that for the calibration period there is an excellent fit between the observed and simulated river regime (mean monthly discharges) at the majority of gauging stations using the MIKE SHE model. However, there is a tendency towards underestimation of peak mean monthly discharges (August and September), particularly at downstream stations (e.g. by around 7–8% at Pakse and Kratie). At Phnom Penh, the most downstream gauging station, overestimation of the ascending limb results in a higher Dv value than elsewhere (>5%; Table 4.8), although this is based on a shorter calibration period (1961– March 1974).

River regimes simulated by the SLURP model are also displayed in Figure 4.6 for the stations for which they are available. These reveal that the river regimes simulated by MIKE SHE more closely match the observed than those of the SLURP model. At Chiang Saen, the SLURP model overestimates recession discharge (following the annual peak) between October–January. In contrast, discharges simulated by MIKE SHE at this time of year more closely follow the observed. The slightly poorer performance of SLURP at Chiang Saen compared to the MIKE SHE model is also reflected in the performance statistics (Table 4.8), with Dv and NSE for SLURP classed as "good" rather than "excellent". However, at Pakse, Dv and NSE are classed as "excellent" for both models, although the seasonal peak discharges (August and September) shows slightly greater underestimation by SLURP (up to 11.4% in September compared to 7.6% for MIKE SHE).

MIKE SHE model performance is relatively weak for the Chi and Mun tributaries, with peak seasonal discharge being underestimated and simulated flows deviating further from the observed compared to other gauging stations (Figures 4.5 and 4.6). This is reflected in lower r values (<0.75) and NSE being classed as "poor" and "fair" at Yasothon and Ubon, respectively (Table 4.8). During manual calibration, it was not possible to raise peak discharges without causing overestimation of the

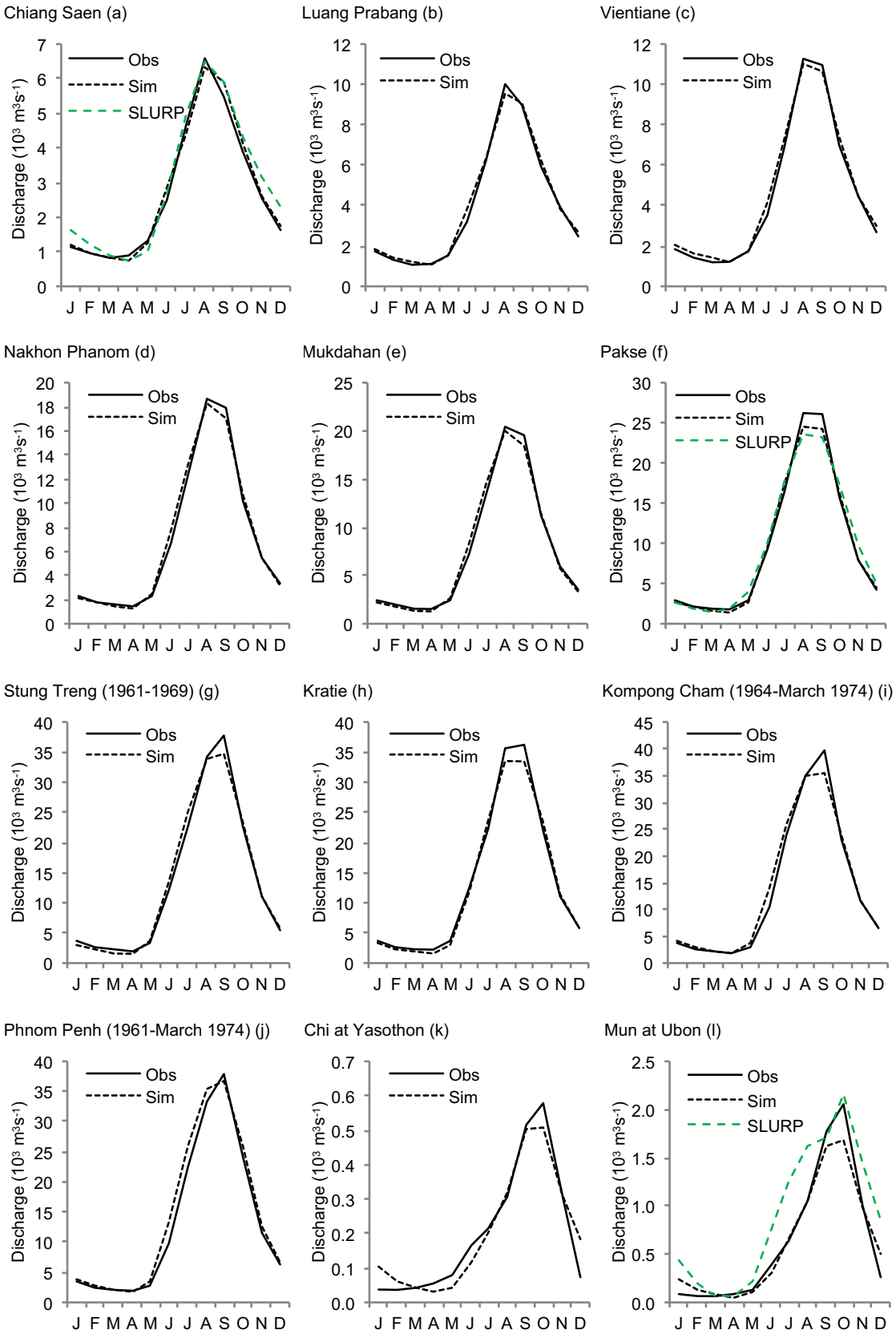

Figure 4.6. Observed and MIKE SHE simulated river regimes for all 12 gauging stations within the Mekong catchment for the calibration period (1961–1990 unless indicated otherwise). Regimes simulated by SLURP for three gauging stations are also shown. (Note different y-axis scales.)

rising and descending limbs of the annual river regime, which currently follow the observed reasonably well. This trade-off is evident in SLURP performance at Ubon, where the magnitude of the simulated annual peak corresponds well with the observed (Figure 4.6), but overestimation of discharge through most of the rest of the year causes Dv to be classified as ''very poor''. The NSE value for this station for MIKE SHE is a class above that of SLURP (''fair'' compared to ''poor'').

In the case of the Chi, a dead storage term was applied to baseflow reservoir 2 to prevent overestimation of flows (Table 4.7). Overestimation of flows in the absence of dead storage was also experienced in the calibration of the Mekong at Vientiane (linear reservoir sub-catchment 5), adjacent and to the north of the Chi sub-catchment. A possible explanation for large overestimations in flow without dead storage could lie with the precipitation input data; there could be anomalies within the station data used in its derivation. Such issues have been highlighted in previous modelling studies that have used gridded precipitation datasets, as discussed in 2.6.6.3. For example, whilst attempting to calibrate a hydrological model of the Okavango catchment, Southern Africa, Hughes *et al.* (2011) identified geographically isolated extreme rainfall within the CRU TS 3.0 precipitation data as the cause of excessive simulated flows. This issue was addressed, at least in part, by using UDel precipitation. However, this dataset did not produce as good a model performance as when using local rain gauge data (Hughes *et al.*, 2011). This suggests that the gridded datasets may have contained unrepresentatively high precipitation, due to either i) anomalies in the station data used in their derivation, or ii) stations from beyond the catchment with higher precipitation having too great an influence on gridded values within the catchment, as a result of the interpolation process.

In this study, discharge overestimation on the Chi tributary prior to implementation of dead storage could result from elevated precipitation within the UDel dataset. Supporting this theory, mean annual UDel precipitation values of 1273.1 mm and 1314.5 mm (Table 4.10, next section) for the Chi and Mun, respectively, exceed reported estimates of less than 1000 mm over parts of the Khorat Plateau (e.g. Kite, 2001; MRC, 2010b). However, dead storage was not required for the Mun sub-catchment to achieve an "excellent" Dv value (i.e. close mean discharge to the observed), and in fact, a small precipitation lapse rate was applied.

Alternatively, or in combination with the meteorological data issues, poorer reproduction of discharge on the Chi and the Mun (leading to the application of dead storage in the case of the Chi) may also be related to land use and/or dam operation. Of all the sub-catchments, these two experienced the highest rates of land cover change (forest to agriculture) and irrigation development (see Section 3.9) over the calibration period (Kite, 2000; Floch and Molle, 2007). Irrigation, changes in land cover and dams are not represented within the MIKE SHE model and this could help explain differences between observed and simulated discharge in the Chi-Mun.

In the relatively small linear reservoir sub-catchment above Vientiane (sub-catchment 5), elevated input precipitation over this region could explain the requirement for dead storage. In support of this, the Mekong to Vientiane linear reservoir sub-catchment falls within the large Mekong 1 meteorological input sub-catchment (Figure 4.4). The latter has a mean annual precipitation total of over 1850 mm (Table 4.10, next section), whereas Figure 3.9a demonstrates that the gridded UDel dataset displays lower annual precipitation totals over the Mekong to Vientiane region (between 1000–1750 mm). Furthermore, gridded CRU precipitation (Figure 3.9b) shows generally lower totals over this area compared to UDel and Kiem *et al.* (2008) present data that suggest annual totals of around 1200–1500 mm over this region. As with the Chi-Mun, water abstractions for irrigation, particularly in the part of the sub-catchment located in north-east Thailand, may also be a contributing factor for the requirement of a dead storage term.

Without detailed information on the representativeness of the gridded precipitation dataset and on irrigation abstractions, the application of dead storage in these few sub-catchments was considered justified in order to match observed and simulated annual contributions to the main Mekong. Further issues associated with the calibration of the Chi and Mun were revealed when calibrating additional MIKE SHE models of the Mekong that employ PET data derived using alternative methods. These are discussed in Section 5.2.4.2.

The generally good to excellent performance of the MIKE SHE model at the majority of gauging stations is confirmed by comparison of observed and simulated flow duration curves based on monthly discharges (Figure 4.7).

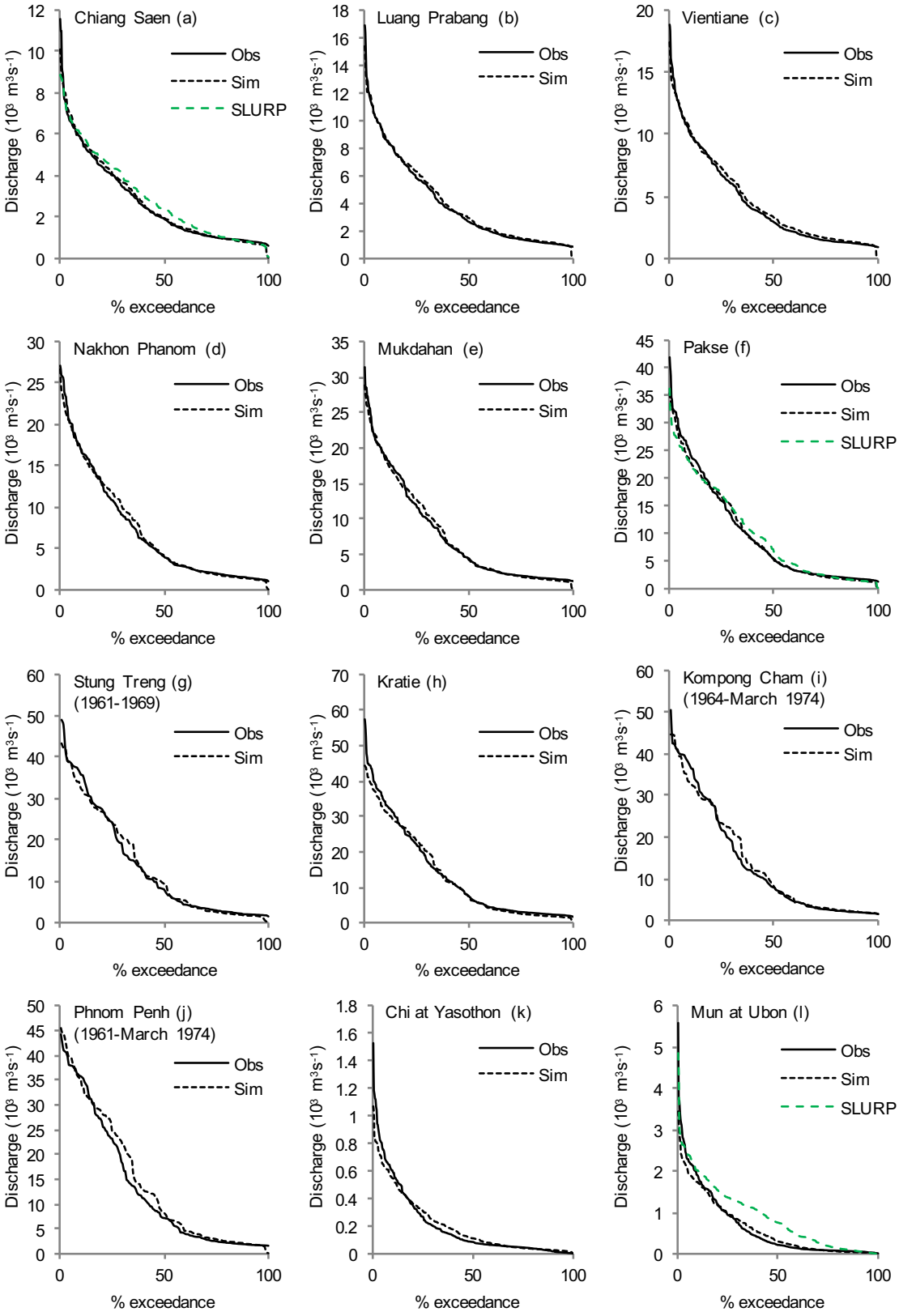

Figure 4.7. Observed and MIKE SHE simulated flow duration curves for all 12 gauging stations within the Mekong catchment for the calibration period (1961–1990 unless indicated otherwise). Flow duration curves simulated by SLURP for three gauging stations are also shown. (Note different y-axis scales.)

4.7.2. Model validation

Model performance statistics for the 1991–1998 validation period are shown in Table 4.9. Statistics for the SLURP model at Chiang Saen and Pakse, as reported by Kingston *et al.* (2011), are also provided. Values for Ubon were not reported in this earlier study. Good performance of the MIKE SHE model is indicated, although for some gauging stations it is inferior to the calibration period. Out of the eight stations on the main Mekong, five retain the "excellent" classification for both NSE and Dv. Performance according to NSE at Chiang Saen and Luang Prabang, previously classed as "excellent", is classed as "very good", as is Dv at Chiang Saen. At Stung Treng, Dv is classed as "fair". However, this is based on only three years of data due to limited observations. Compared to the SLURP model, MIKE SHE shows similar to slightly poorer performance at Chiang Saen and superior performance at Pakse, with an NSE of 0.89 ("excellent") compared to 0.77 for SLURP ("very good").

Lower NSE values at Chiang Saen and Luang Prabang for the validation period compared to the calibration period may potentially relate to the construction of the Manwan Dam on the Lancang in China. This dam was filled in 1992–1993 (Lu and Siew, 2006). Further downstream, poorer representation of flows for the validation period at some stations might relate to the use of unchanging land cover through time, an approach that was adopted in the SLURP model (Kingston *et al.*, 2011), but which is not completely realistic given the land cover changes which have occurred, especially in the lower part of the catchment.

However, Figure 4.5 demonstrates that at stations on the main Mekong, good sequencing of the annual flood pulse was achieved during the validation period. Similarly, Figure 4.8 indicates that there is generally a good fit between the observed and MIKE SHE simulated river regimes for these stations. At Chiang Saen, SLURP shows overestimation of discharge in November–January, and underestimation in August, whilst MIKE SHE simulated discharges follow the observed more closely.

Table 4.9. MIKE SHE model performance statistics for 10 gauging stations within the Mekong Basin for the validation period (1991–1998 unless stated otherwise). Corresponding statistics from Kingston et al. (2011) for SLURP are shown in brackets for two stations. Model performance indicators are taken from Henriksen et al. (2008).

Station	Obs Mean (m^3s^{-1})	Sim Mean (m^3s^{-1})	Dv (%)+	NSE*	r#
Using UDel V1.01 precipitation for 1991–1996, UDel V1.02 for 1997–1998					
Mekong at Chiang Saen (a) (1991–Jun 1997)	2490.3	2342.8	-5.92 ☆☆☆☆	0.77 ☆☆☆☆	0.89
		(2550.0)	(+2.40) (☆☆☆☆☆)	(0.81) (☆☆☆☆)	
Mekong at Luang Prabang (b) (1991–1997)	3749.7	3735.5	-0.38 ☆☆☆☆☆	0.84 ☆☆☆☆	0.91
Mekong at Vientiane (c) (1991–1996)	4241.7	4362.7	2.85 ☆☆☆☆☆	0.90 ☆☆☆☆☆	0.95
Mekong at Nakhon Phanom (d) (1991–Nov 1995)	7063.2	6859.9	-2.88 ☆☆☆☆☆	0.91 ☆☆☆☆☆	0.95
Mekong at Mukdahan (e) (1991–1995)	7434.4	7398.2	-0.49 ☆☆☆☆☆	0.92 ☆☆☆☆☆	0.96
Mekong at Pakse (f) (1991–1998)	9168.4	9033.0	-1.48 ☆☆☆☆☆	0.89 ☆☆☆☆☆	0.94
		(8783.4)	(-4.20) (☆☆☆☆☆)	(0.77) (☆☆☆☆)	
Mekong at Stung Treng (g) (1991–1993)	12569.5	10507.1	-16.41 ☆☆☆	0.87 ☆☆☆☆☆	0.95
Mekong at Kratie (h) (1991–1998)	12505.7	12048.0	-3.66 ☆☆☆☆☆	0.88 ☆☆☆☆☆	0.94
Chi at Yasothon (k) (1991–1995)	200.4	240.8	20.16 ☆☆	-0.39 ☆	0.41
Mun at Ubon (l)	486.8	468.1	-3.83 ☆☆☆☆☆	0.14 ☆	0.55
Using UDel V1.02 precipitation only					
Chi at Yasothon (k) (1991–1995)	200.4	162.8	-18.74 ☆☆☆	0.44 ☆☆	0.68
Mun at Ubon (l)	486.8	337.7	-30.63 ☆☆	0.55 ☆☆☆	0.78

Performance indicator	Excellent ☆☆☆☆☆	Very good ☆☆☆☆	Fair ☆☆☆	Poor ☆☆	Very poor ☆
Dv	< 5%	5–10%	10–20%	20–40%	>40%
NSE	>0.85	0.65–0.85	0.50–0.65	0.20–0.50	<0.20

+ percentage deviation in simulated mean flow from observed mean flow (Henriksen *et al.*, 2003), * Nash-Sutcliffe coefficient Nash and Sutcliffe, 1970), # Pearson correlation coefficient

At Pakse, mean monthly discharges in July–September are considerably underestimated by SLURP (by between 20% and 30% of the respective observed mean monthly discharges). In contrast, MIKE SHE simulated mean monthly discharges at this time of year differ from those observed by no more than 11%. Poorer performance by MIKE SHE is observed at Stung Treng, with underestimation of mean monthly discharges by up to 40% in January–April and up to 22% in in August–September. However, as noted previously, this is based on only three years of data.

Using UDel V1.01 precipitation, model performance for the Chi and Mun tributaries is poor, with low *r* values and NSE values classed as "very poor", whereas NSE was classed as "poor" and "fair", respectively, for these stations for the calibration period. There is also large overestimation of mean discharge at Yasothon (Dv: 20.26%). In order to investigate whether this poor performance may be in part related to the precipitation inputs, model performance at these two stations was also assessed when using UDel V1.02 precipitation for the Chi and Mun sub-catchments. Although use of UDel V1.02 leads to improved NSE and *r* values, it also causes large underestimation of discharge at both stations (Dv at Yasothon: -18.74%, Dv at Ubon: -30.63%). This demonstrates the influence of uncertainty in precipitation data for this region and adds support to the assertion that issues identified during calibration of these stations may lie, at least in part, with the meteorological data for this part of the catchment. The use of an alternative gridded precipitation dataset (CRU) is investigated in the next chapter.

Generally good performance by MIKE SHE for the validation period is supported by comparison of observed and simulated flow duration curves (Figure 4.9), although the match is slightly poorer at some stations compared to the calibration period. However, in light of the relatively short validation period and given an emphasis of the current study to compare alternative models of the catchment using the same input data, the overall performance of the MIKE SHE model is considered appropriate.

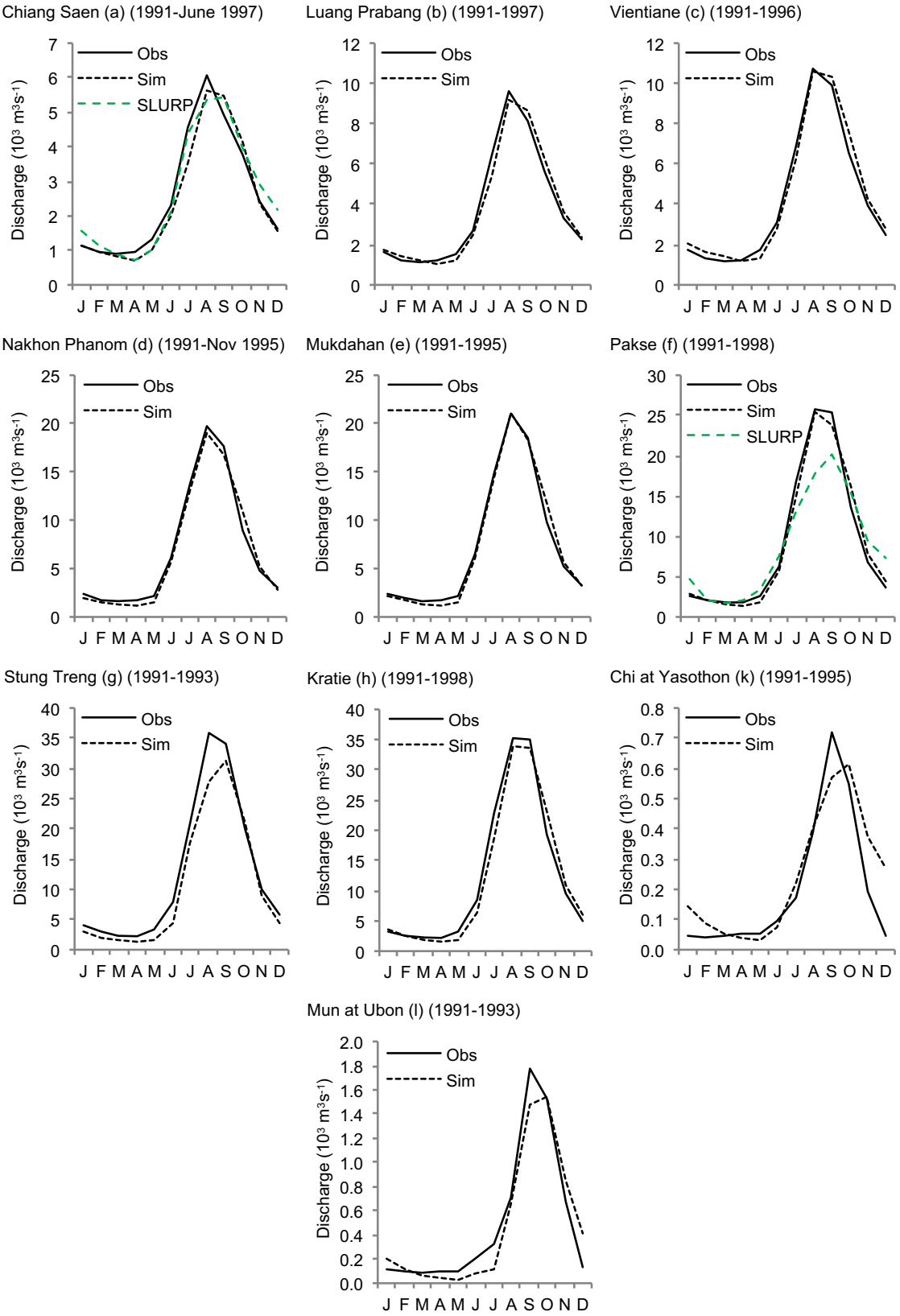

Figure 4.8. Observed and MIKE SHE simulated river regimes for 10 gauging stations within the Mekong catchment for the validation period (1991–1998 unless indicated otherwise). Regimes simulated by SLURP for three gauging stations are also shown. (Note different y-axis scales.)

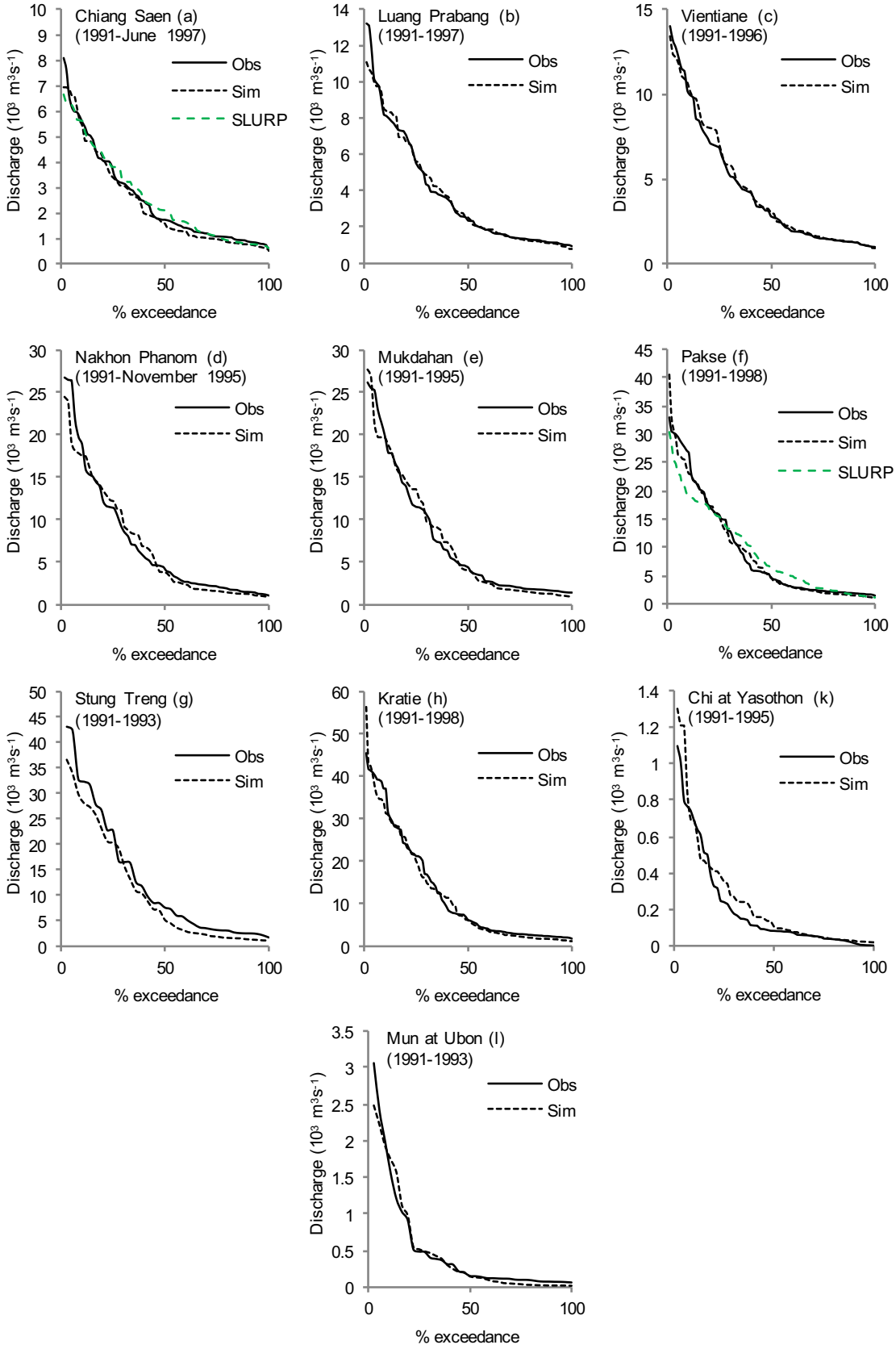

Figure 4.9. Observed and MIKE SHE simulated flow duration curves for 10 gauging stations within the Mekong catchment for the validation period (1991–1998 unless indicated otherwise). Flow duration curves simulated by SLURP for two gauging stations are also shown. (Note different y-axis scales.)

4.7.3. Climate change scenarios: 2 °C increase using seven GCMs

4.7.3.1. Changes in climate

Baseline annual precipitation, temperature and PET, and percentage changes (change in °C for temperature) from these values for each of the 2 °C seven GCM scenarios, are shown for eight sub-catchments in Table 4.10. Results for the other sub-catchments are not shown as they are relatively small and changes are represented by one or more of those in the table. However, Figure 4.10 presents changes in mean annual precipitation, temperature and PET for each of the 2 °C, seven GCM scenarios for all 11 meteorological input sub-catchments upstream of the most downstream gauging station (Phnom Penh) from which scenario flow results are extracted. Projected changes in climate for the Tonle Sap and Delta sub-catchments are not presented since, as discussed in Section 3.6.1, simulated flows are not extracted from these sub-catchments.

Projected changes in precipitation vary greatly between GCMs in terms of the spatial pattern, direction and magnitude of change. Annual precipitation is projected to increase in all sub-catchments according to CCCMA, MPI and NCAR. Increases are greatest for upstream (northern) sub-catchments for NCAR and northern and western sub-catchments for CCCMA, as displayed in Figure 4.10. CCCMA produces increases in mean annual precipitation of between 8.4–12.3% for sub-catchments to the north and west of Mekong 2 and increases of only 1.9–5.3% for the three southernmost sub-catchments in Table 4.10. NCAR shows an even greater variation between northern and southern sub-catchments, with increases of between 9.2–15.6% in the four northernmost sub-catchments (Lancang to Mekong 1) and ≤5.3% elsewhere. In contrast, for MPI, the smallest increases (≤4.4%) are projected for the three northernmost sub-catchments, with the greatest increases exhibited in southern sub-catchments (6.6–12.2%). Conversely, CSIRO simulates reduced annual precipitation across all sub-catchments, with the greatest reductions occurring in northerly sub-catchments (-6.1%, -4.6% and -4.5% in Nam Ou, Lancang and Mekong 1, respectively), and decreases of ≤3.3% elsewhere.

Table 4.10. Mean annual precipitation, temperature and PET for the baseline and changes (% / °C) for the 2 °C, seven GCM climate change scenarios for eight representative SLURP sub-catchments. Shaded cells indicate negative changes compared to the baseline.

Parameter/ Scenario		Lanc. (1)	Mek. 1 (4)	Chi (5)	Mun (6)	Mek. 2 (8)	Se Kong (9)	Sre Pok (10)	Mek. 3 (11)
Precipitation	Baseline (mm)	1053.4	1856.9	1273.1	1314.5	2214.6	2434.1	2056.6	1871.5
	CCCMA (% change)	10.1	10.2	12.3	10.2	8.4	5.3	1.9	5.3
	CSIRO (% change)	-4.6	-4.5	-3.3	-2.9	-2.8	-2.8	-2.9	-1.2
	HadCM3 (% change)	10.1	1.0	-0.1	-0.4	-1.1	-2.1	-4.5	-3.0
	HadGEM1 (% change)	6.0	-3.7	-6.1	-4.8	-1.2	2.9	3.9	1.0
	IPSL (% change)	-5.2	-1.1	-0.1	-0.1	0.6	-0.4	1.3	-0.4
	MPI (% change)	3.6	7.1	10.2	10.3	8.8	6.6	7.7	12.2
	NCAR (% change)	8.6	9.2	5.0	3.5	1.9	3.5	3.7	5.3
Temperature	Baseline (°C)	11.2	24.3	26.8	27.2	26.0	24.7	24.3	26.9
	CCCMA (change, °C)	2.3	1.9	2.0	2.0	1.8	1.9	1.9	2.0
	CSIRO (change, °C)	2.7	2.3	2.3	2.2	2.1	2.0	2.0	2.1
	HadCM3 (change, °C)	2.6	2.4	2.4	2.4	2.3	2.3	2.3	2.3
	HadGEM1 (change, °C)	2.5	2.0	1.8	1.8	1.9	2.0	2.0	2.0
	IPSL (change, °C)	2.9	2.3	2.2	2.1	2.1	2.0	1.9	2.0
	MPI (change, °C)	2.7	2.2	2.1	2.1	2.0	2.0	2.0	2.1
	NCAR (change, °C)	2.4	1.9	1.9	1.8	1.8	1.7	1.7	1.7
PET	Baseline (mm)	1766.7	1924.3	2365.1	2338.0	1814.2	1729.6	1697.0	1771.5
	CCCMA (% change)	11.7	12.3	13.2	12.7	12.5	12.7	12.4	12.5
	CSIRO (% change)	14.7	15.7	15.9	15.2	15.2	14.9	14.2	14.4
	HadCM3 (% change)	12.9	13.9	13.3	13.2	14.7	14.8	14.8	15.1
	HadGEM1 (% change)	12.5	12.1	10.4	10.3	12.4	13.0	12.7	12.5
	IPSL (% change)	15.9	15.8	15.3	14.2	14.3	13.9	12.8	13.2
	MPI (% change)	13.6	13.6	13.3	12.9	13.4	13.5	13.1	13.2
	NCAR (% change)	11.3	10.9	11.1	10.7	11.4	11.1	10.7	10.3

The remaining GCMs exhibit a spatially variable direction of change in mean annual precipitation. For IPSL, reductions occur across all but three south-central sub-catchments (Chi-Mun, Mekong 2 and Sre Pok), with the greatest decreases occurring over upstream sub-catchments (maximum reduction of -5.3% in Nam Ou). Changes in annual precipitation of less than 2% occur in meteorological input sub-catchments 4–11. HadCM3 projects increased annual precipitation in the four northernmost sub-catchments (Lancang to Mekong 1), peaking at 11.2% in Nam Ou, and decreased precipitation in the remaining sub-catchments, with a maximum reduction of -4.5% for Sre Pok. Finally, for HadGEM1, increases in annual

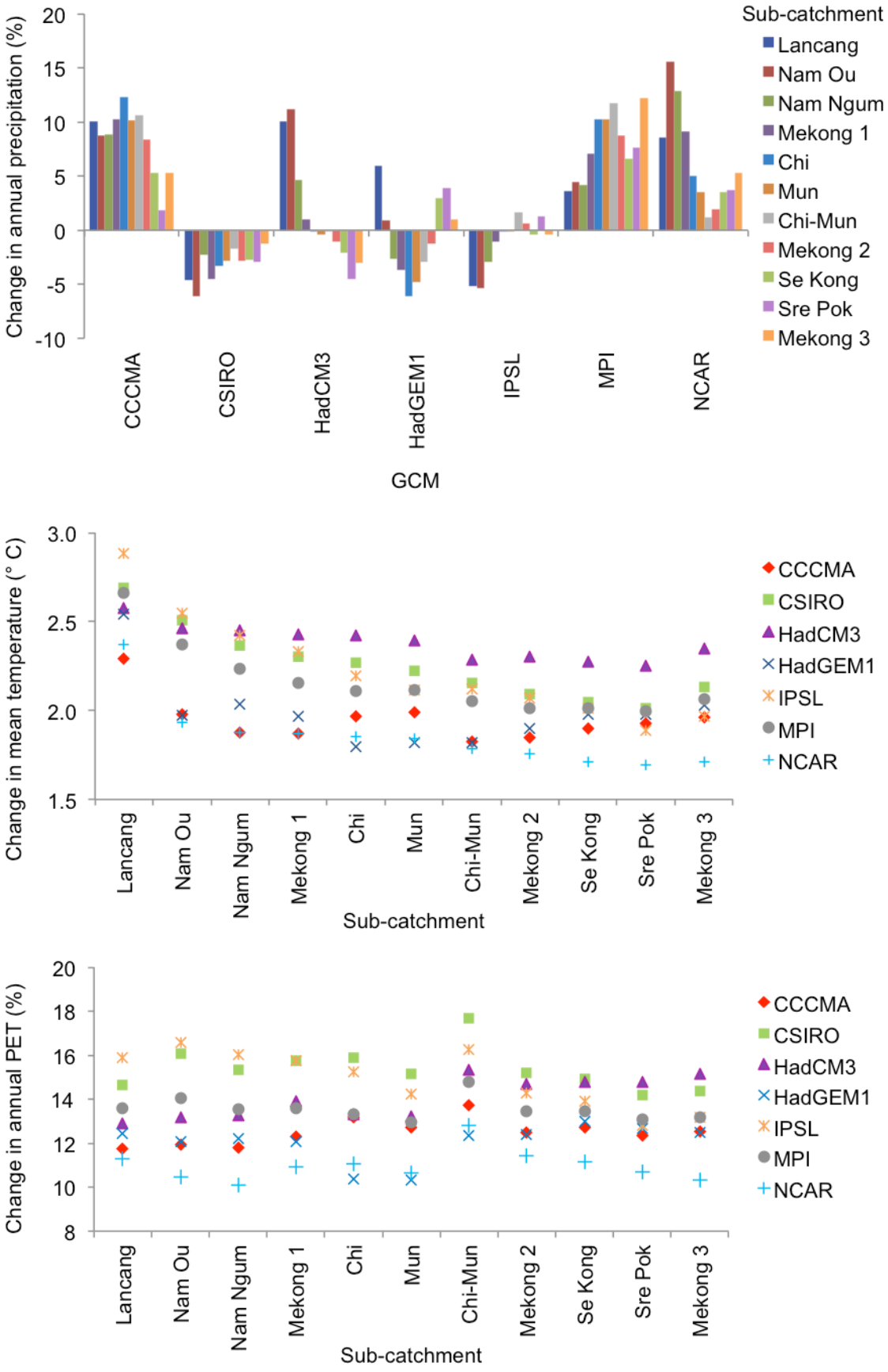

Figure 4.10. Projected changes in mean annual precipitation (%), temperature (°C) and Linacre PET (%) for eleven SLURP sub-catchments for the 2 °C, seven GCM climate change scenarios.

precipitation are restricted to the two most northern sub-catchments (Lancang and Nam Ou) and three southern sub-catchments (Se Kong, Sre Pok and Mekong 3), with declines projected over the central Mekong. The maximum projected increase is 6.0% for the Lancang, whilst the greatest decrease is -6.1% for the Chi sub-catchment.

Mean monthly precipitation and PET for the baseline and each scenario are shown for four representative sub-catchments in Figure 4.11. Absolute changes (mm) in mean monthly precipitation are presented in Figure 4.12 for the same four sub-catchments. Changes for each sub-catchment are plotted in separate graphs in order that differences in the pattern of change through the year for different parts of the catchment can be clearly seen. Lancang shows similar patterns of change to Nam Ou, Mekong 1 is representative of Nam Ngum, Mun is representative of the Chi, Mun and Chi-Mun sub-catchments, whilst Mekong 3 shows similar patterns of change to Mekong 2, Se Kong and Sre Pok.

As with changes in mean annual precipitation, the intra-annual pattern of precipitation change also varies considerably between GCMs, with the levels of similarity between sub-catchments also varying. For example, although the seasonal pattern of change does vary between sub-catchments, CCCMA exhibits a distinctly bi-modal pattern of change in the majority of sub-catchments (those upstream of and including Mekong 2), with peak absolute increases in mean monthly precipitation concentrated around April–June and August–September, and minimum increases, or decreases, concentrated in July and November–February/March. In some northerly and southerly sub-catchments, NCAR also displays peak increases around April–June and August–September, with the position of the peak being dependent upon the sub-catchment. Other sub-catchments in the middle of the basin (e.g. Mekong 1, Mun) show a unimodal peak centred on August or September. HadCM3 and HadGEM1 show a predominantly bimodal seasonal pattern of precipitation change, with peak increases occurring in May and September/October, or sometimes in November in downstream sub-catchments for HadGEM1 and reductions concentrated around March–April and in August. The pattern is not, however, consistent across all sub-catchments. For

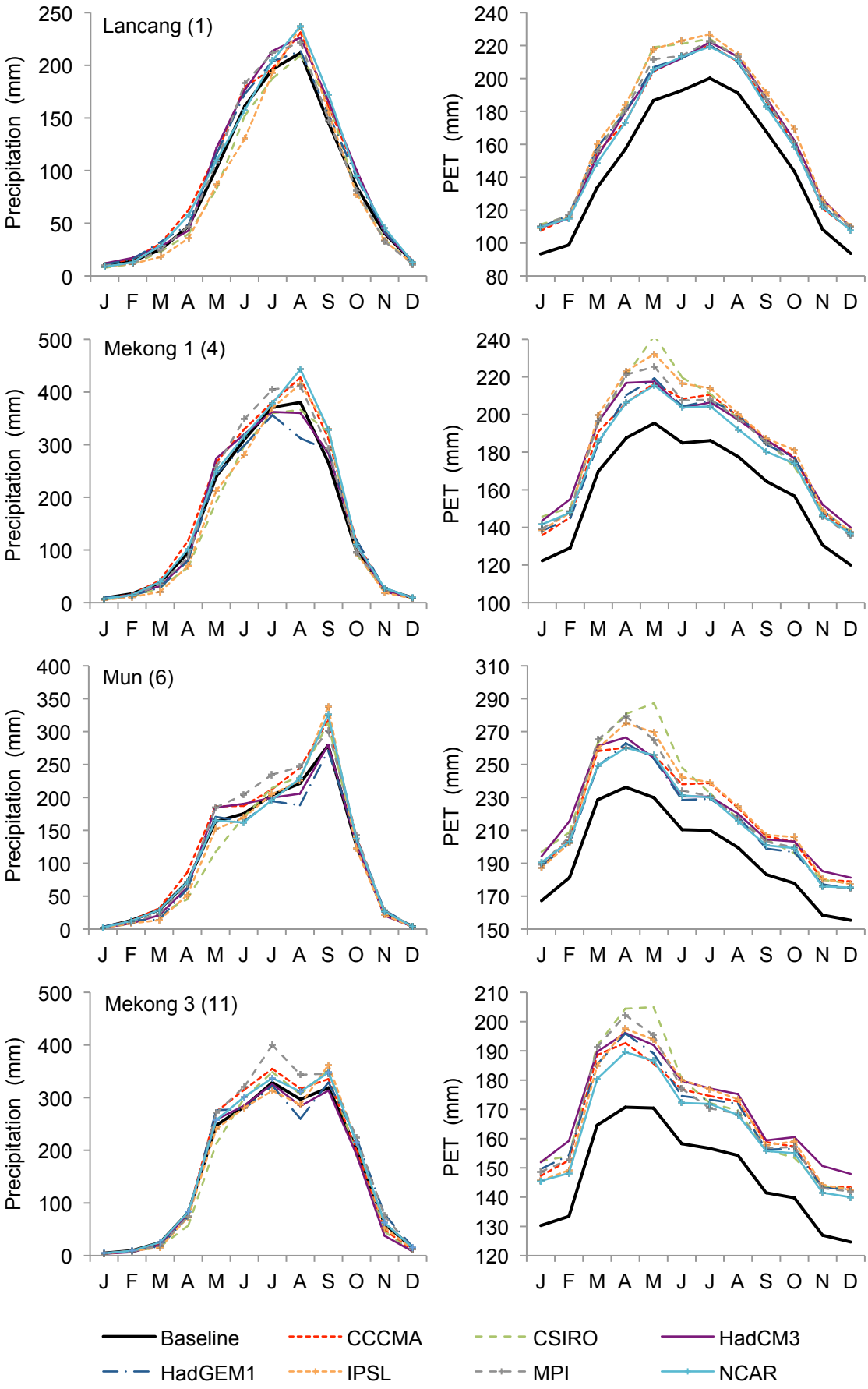

Figure 4.11. Mean monthly precipitation and PET for the baseline and the 2 °C, seven GCM climate change scenarios for four representative sub-catchments. (Note different y-axis scales.)

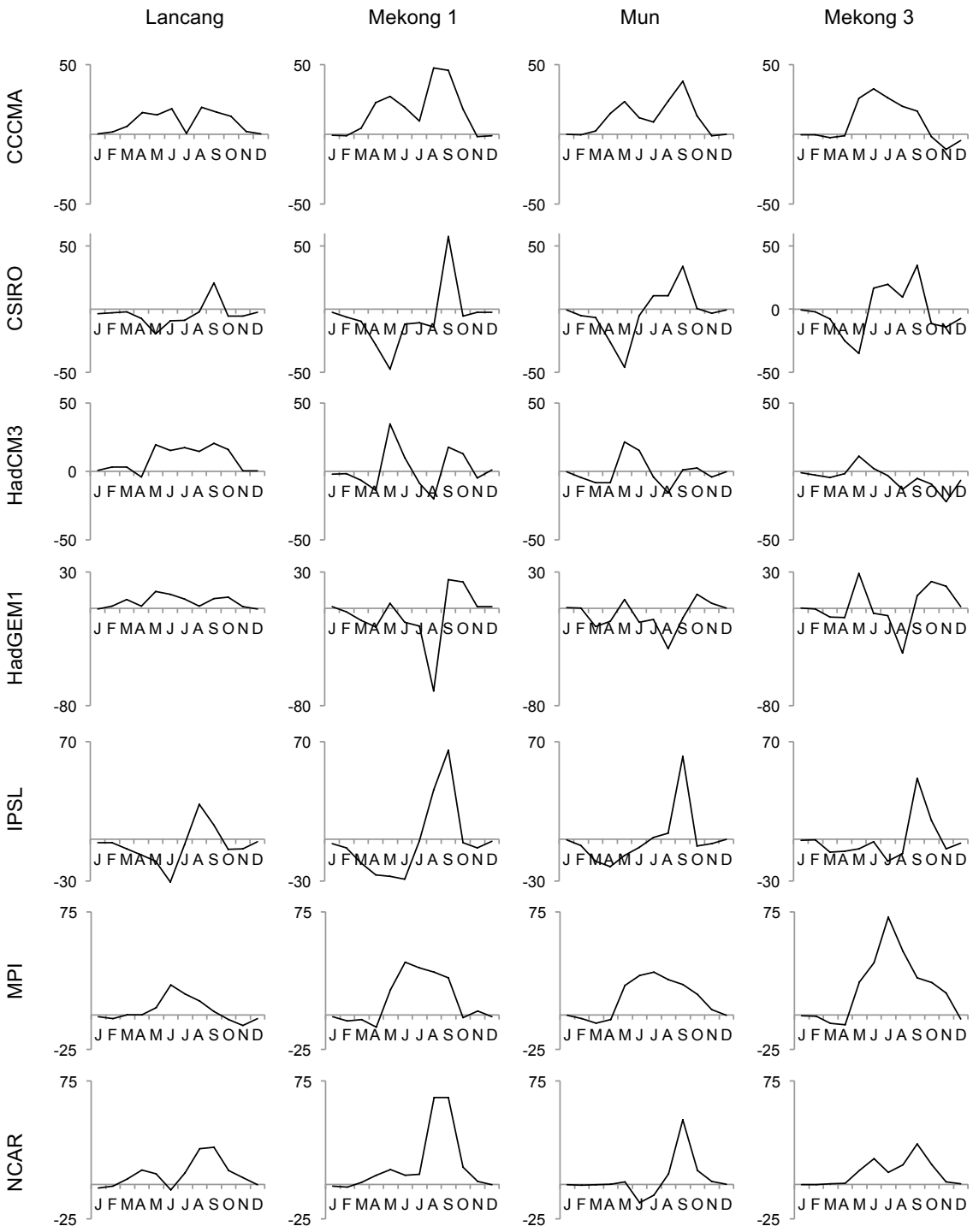

Figure 4.12. Change in mean monthly precipitation (mm for all y axes) for four representative SLURP sub-catchments for the 2 °C, seven GCM climate change scenarios. (Note different y-axis scales.)

example, for the Lancang sub-catchment for HadGEM1, there are three distinct peaks in the pattern of absolute change in mean monthly precipitation, in March, May-June and September-October.

In contrast, CSIRO, IPSL and MPI exhibit a predominantly unimodal pattern of change. For CSIRO, increases in precipitation are limited to September over upstream sub-catchments (Lancang to Mekong 1). This period expands to June–September in the far south (e.g. Mekong 3). However, some southerly sub-catchments (e.g. Mekong 2 and Se Kong) only display increases in June and September and decreases throughout the rest of the year. The distribution of change through the year for IPSL is also unimodal, with increases largely limited to August–September and, in the far south, September–October. For MPI, increases are concentrated in May-November, although the number of months over which increases extend differs between sub-catchments.

Monthly changes in temperature are not presented here since, within the MIKE SHE model of the Mekong, temperature inputs are only directly relevant to the Lancang, the one sub-catchment in which snow and its seasonal melt influences runoff. For all sub-catchments, the effect that changes in temperature (from the baseline to the scenario simulations) would have on evaporation rates is instead reflected in modified PET inputs. All GCMs show slightly higher increase in mean annual temperature over the Lancang, ranging from +2.3 °C (CCCMA) to +2.9 °C (IPSL), with increases of around 1.7–2.5 ˚C elsewhere (Table 4.10; Figure 4.10). Of the eight sub-catchments in Table 4.10, the smallest increase in mean temperature is associated with NCAR in five, HadGEM1 in two and CCCMA in one. HadCM3 produces the largest increases in the majority of sub-catchments, followed by CSIRO. For all sub-catchments, mean monthly temperatures increase throughout the year in all scenarios. For CCCMA, HadCM3, HadGEM1 and NCAR, the largest changes (up to +3.5 °C) tend to occur between October and March, whilst summer temperature increases are on average lower (+2.0–2.3 °C). In contrast, for the majority of sub-catchments, CSIRO and MPI show a distinct peak of maximum increases in May and April, respectively. Finally, IPSL produces peak increases between March and June, with a secondary (smaller) peak in October.

Differences between the seven GCMs in the temperature climate change signals, and therefore also in the PET climate change signals, are smaller than those for precipitation (Table 4.10; Figure 4.10; Figure 4.11). Similarly, the spatially variability (inter-sub-catchment differences) in the PET climate change signal is much lower than it is for precipitation. As with temperature, annual and mean monthly PET increases across the Mekong for all GCMs. With the exception of three sub-catchments (Chi, Mun and Chi-Mun), the smallest increases in annual PET are associated with NCAR (average across sub-catchments 1–11: +11.0%). In the three sub-catchments where this is not the case, the lowest PET increases result from HadGEM1, although these are only slightly (≤0.7%) lower than those of NCAR. HadGEM1 and CCCMA produce the second smallest increases in three and five sub-catchments (out of 11), respectively. There is a systematic geographical pattern for the GCMs that produce the largest increases in annual PET. In the four most northerly sub-catchments (1–4, Figure 4.4), IPSL produces the largest changes (mean: +16.0%), followed by CSIRO (mean: +15.4%). In the middle Mekong (sub-catchments 5–9), the largest changes are associated with CSIRO (mean: +15.7%), followed by IPSL or HadCM3, whilst in the lower part of the catchment (sub-catchments 10–11), HadCM3 produces the largest increase in PET (mean: +15.5%), followed by CSIRO. Many of the GCMs show a relatively constant climate change signal throughout the year. Notable exceptions are peak increases in May for CSIRO and in April for MPI and IPSL.

4.7.3.2. Changes in River Flow (MIKE SHE)

This section presents changes in river flow simulated by the MIKE SHE model of the Mekong for the 2 °C, seven GCM climate scenarios. Following the standard methodology for assessing climate change impacts on river flow (Arnell and Reynard, 1996), the scenario river discharge simulated by MIKE SHE is assessed relative to discharge simulated by the model for the baseline period (1961–1990).

Table 4.11 presents the values of the mean discharges and monthly Q5 and Q95 discharges (monthly[1] discharges exceeded 5% and 95% of the time, respectively)

[1] Consistent with SLURP and Mac-PDM, Q5 and Q95 are calculated from monthly discharge data. This method is used consistently throughout this and subsequent chapters.

for the baseline and the percentage changes in these discharges for each of the 2 °C, seven GCM scenarios. These are provided for eight gauging stations that are representative of changes at the other four stations used in model calibration/validation. Mukdahan represents the changes at Nakhon Phanom approximately 100 km upstream. Similarly, discharge at Stung Treng, which is not shown, responds in the same way as Kratie (c. 150 km further downstream), whilst Phnom Penh is representative of the changes in simulated discharge at Kompong Cham (c. 90 km upstream). Results for the Mun at Ubon represent those in the smaller catchment of the Chi at Yasothon. The simulated baseline and scenario river regimes for the same eight gauging stations are shown in Figure 4.13.

Table 4.11. Mean, Q5 and Q95 discharges (m^3s^{-1}) simulated by MIKE SHE for the baseline and changes (%) for the 2 °C, seven GCM scenarios at eight gauging stations within the Mekong catchment. Shaded cells indicate negative changes compared to the baseline.

Q	Scenario	Chiang Saen (a)	Luang Prabang (b)	Vientiane (c)	Mukda-han (e)	Pakse (f)	Kratie (h)	Phnom Penh (j)	Ubon (l)
Mean	Baseline	2753.7	4082.6	4686.2	7626.0	9597.3	12961.7	13332.8	619.1
	CCCMA	3.4	4.2	5.0	6.8	7.8	6.2	6.1	11.1
	CSIRO	-25.1	-24.4	-23.5	-19.4	-18.0	-15.7	-15.4	-11.6
	HadCM3	7.4	7.3	5.5	2.3	0.4	-2.5	-2.8	-8.3
	HadGEM1	-3.3	-5.9	-7.7	-9.9	-11.6	-10.0	-9.8	-20.9
	IPSL	-23.2	-20.6	-19.0	-14.1	-12.0	-10.4	-10.3	-3.0
	MPI	-6.1	-3.6	-2.1	1.1	3.7	4.8	5.0	16.7
	NCAR	4.7	9.6	10.1	11.2	10.2	7.4	7.2	3.1
Q5	Baseline	7016.5	10395.7	12385.4	21993.9	27232.0	37128.6	37806.9	2019.6
	CCCMA	-3.3	1.3	-0.9	7.9	10.8	4.4	4.8	17.3
	CSIRO	-18.2	-18.5	-18.3	-15.3	-12.2	-12.8	-13.4	-3.9
	HadCM3	8.0	10.5	3.1	-3.7	-2.3	-8.4	-8.6	-4.1
	HadGEM1	-4.1	-6.8	-10.8	-13.7	-14.8	-16.6	-16.7	-12.4
	IPSL	-11.6	-5.6	-9.8	-6.7	-3.8	-3.8	-4.8	9.6
	MPI	0.5	2.0	0.3	0.5	6.4	5.3	5.0	18.7
	NCAR	8.3	13.0	8.1	9.5	7.6	2.4	0.8	12.0
Q95	Baseline	692.2	1017.9	1148.4	1226.1	1314.3	1544.8	1630.2	29.1
	CCCMA	5.8	6.5	7.5	10.9	13.2	10.1	10.0	15.7
	CSIRO	-29.3	-29.6	-27.9	-21.5	-18.0	-18.6	-19.0	-11.2
	HadCM3	7.5	8.4	4.0	8.2	10.3	5.6	6.0	-6.7
	HadGEM1	-5.3	-9.7	-10.6	-7.2	-5.1	-6.1	-5.1	-15.7
	IPSL	-27.9	-27.1	-24.9	-21.2	-18.3	-18.3	-16.8	-7.7
	MPI	-10.0	-8.7	-7.0	-7.0	-3.4	-4.5	-2.1	9.6
	NCAR	8.0	10.7	11.6	17.0	18.6	12.5	14.8	3.4

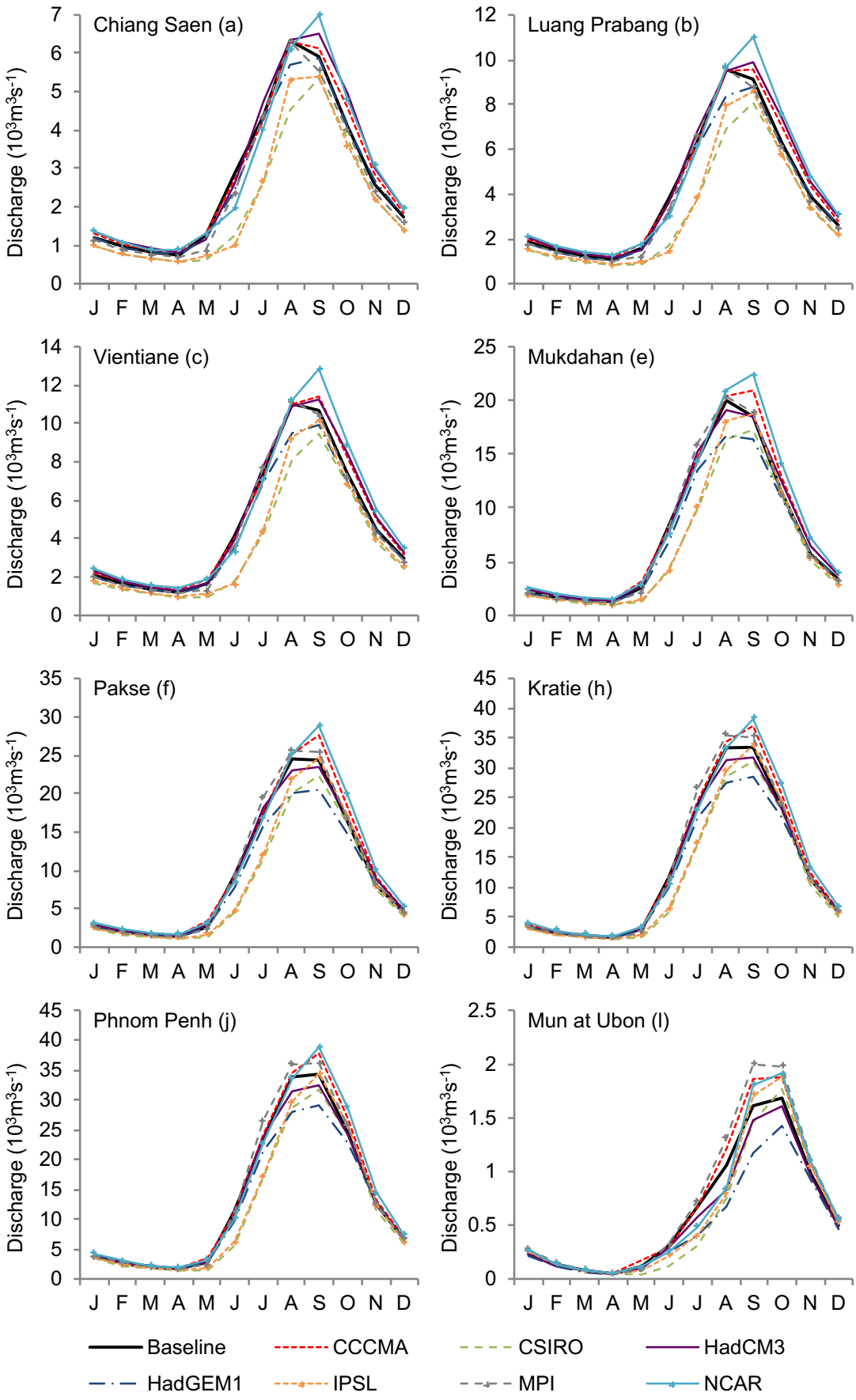

Figure 4.13. River regimes simulated by MIKE SHE for the baseline and 2 °C, seven GCM climate change scenarios for eight gauging stations within the Mekong catchment. (Note different y-axis scales.)

Of the three GCMs for which precipitation increases in all sub-catchments, two (CCCMA and NCAR) result in increases in mean discharge for all gauging stations. For CCCMA, the magnitude of the changes increases in a downstream direction from Chiang Saen (3.4%) to Pakse (7.8%). Downstream of Pakse, changes are consistently between 6.1–6.2% (Table 4.11). The larger increase in mean discharge of the Mun at Ubon is indicative of other sub-catchments in this part of the catchment, which results in enhanced flows from these tributaries to the Mekong, although absolute magnitudes are relatively small compared to those on the main Mekong. In the upper catchment (Chiang Saen), peak flow increases occur during the annual recession and low flow period, when increases in precipitation over the Lancang are greatest (Figure 4.12). Higher flows (up to +14.2%) during the initial rise in discharge (April–May; Figure 4.13) could be partially attributable to enhanced snowmelt. Peak annual discharge is, however, slightly (<0.5%) lower and still occurs in August. Q5 shows reductions of 3.3% and 0.9% at Chiang Saen and Vientiane, respectively, but increases at all other stations. Q95 consistently increases at all stations (Table 4.11). At Luang Prabang and stations further downstream, due to an increase in September discharge, mean discharge is higher in September than August, the opposite to baseline river regimes. This is due to the large increases in precipitation in August and September (Figure 4.12).

A similar pattern of change occurs for NCAR, although in most cases changes are larger than those associated with CCCMA, particularly in the middle section of the Mekong Basin between Luang Prabang and Pakse (Table 4.11; Figure 4.13). Figure 4.10 shows that whilst increases in mean annual precipitation over this part of the catchment are smaller for NCAR compared to CCCMA, increases over Nam Ou and Ngum are larger and PET rises by smaller amounts for NCAR, accounting for the enhanced river flow. NCAR shows a relatively consistent change in the river regime at all stations in Figure 4.13. Baseflows are higher than the baseline, as demonstrated by consistent increases in Q95 (up to 18.6%; Table 4.11), but mean monthly discharge shows reductions in June–July at all stations. Peak absolute increases occur in September, whilst peak percentage increases occur during the recession. The month of highest mean discharge shifts from August to September, although at stations between Luang Prabang and Pakse mean discharge in August also increases.

Precipitation increases in all sub-catchments for MPI. However, the magnitude of these changes is relatively small in upstream parts of the catchment compared to CCCMA and NCAR, whilst increases in PET are larger than for these two GCMs (Table 4.10). Mean annual flows between Chiang Saen and Vientiane therefore decline for MPI (by between -6.1% and -2.1%, Table 4.11), with the magnitude of change declining in a downstream direction. Below these stations, gains in precipitation are larger and mean discharge increases, with an increase in magnitude in a downstream direction, although changes are smaller than for CCCMA and NCAR (maximum: +5.0%, Phnom Penh). Consistent reductions during the low flow period result in Q95 experiencing declines at all gauging stations on the main Mekong. In contrast, Q5 shows small (up to +2.0%) changes between Chiang Saen and Mukdahan, but increases of between 5.0%–6.4% at and downstream of Pakse. Mean monthly discharge for MPI displays year-round reductions at Chiang Saen, but the number of months displaying increased mean discharge increases in a downstream direction, from two (July and August) at Luang Prabang to nine (July–March) at Phnom Penh. With the exception of May at Ubon, the Rivers Chi and Mun show increases in mean monthly discharge throughout the year, with higher percentage increases than at other stations. Both Ubon and Yasothon therefore show percentages increases in mean, Q5 and Q95 discharges that are of a much greater magnitude than at other stations (e.g. an increase in mean discharge of 16.7% at Ubon).

The patterns of change in mean, Q5 and Q95 discharge for the CSIRO and IPSL GCMs are broadly similar (Table 4.11). All three discharge measures decline at stations on the Mekong (Q5 increases at Yasothon and Ubon for IPSL) for both GCMs. CSIRO results in consistently larger reductions in mean discharge and Q5, and larger reductions in Q95 most cases. The magnitude of percentage reductions in mean flow and Q95 show a general (although not wholly consistent) decrease in a downstream direction for both GCMs. In the case of Q5 for CSIRO, the magnitude of change is relatively consistent between Chiang Saen and Vientiane, decreases in a downstream direction from Vientiane to Paske, and is again relatively consistent between Pakse and Phnom Penh. Departure from the downstream trend is even greater in the case of Q5 for ISPL, with a relatively small reduction at Luang Prabang compared to Chiang Saen and Vientiane, likely attributable to greater increases in

precipitation in August over the Nam Ou sub-catchment. The river regimes from both GCMs display a delayed response in the annual rise in river discharge, with the greatest reductions occurring during the annual rise and peak (between May–August), whilst discharge during the post-peak recession and the dry season (September–April) are less affected (Figure 4.13). Mean monthly discharge declines throughout the year at all stations on the Mekong for CSIRO and through most of the year (9–12 months) for IPSL. For both GCMs, there is a shift from August to September for peak flows. On the Mun and Chi tributaries, Q95 declines for both GCMs, but peak discharge, which occurs in October, exceeds the baseline. For ISPL on the Mun at Ubon, precipitation increases in August–September (Figure 4.12) cause mean discharges in September–October to exceed those of the baseline, resulting in an increased Q5.

Increases in annual precipitation in the upper Mekong (Lancang to Mekong 1) for HadCM3 result in increases in mean discharge on the Mekong down to Pakse. Following the pattern of precipitation change, these increases display a downstream reduction in magnitude (Table 4.11). Further downstream (i.e. at Stung Treng and onwards), in response to declining precipitation and higher PET, mean discharges decline. Increases in mean monthly discharge in the upper catchment occur in all months except May–June and August, resulting in increases in Q5 as far downstream as Vientiane. From Mukdahan and further downstream, mean discharges in both August and September are below the baseline (by -6.4% and -5.4%, respectively at Phnom Penh). Increases in dry season discharge are common to all gauging stations on the main Mekong and result in higher Q95 discharges (Q95 declines for Yasothon and Ubon).

In contrast to HadCM3, increases in annual precipitation in the upper Mekong are restricted to the Lancang and Nam Ou sub-catchments for the other UK Met Office GCM, HadGEM1, and are smaller in magnitude. This results in reductions in mean discharge at all stations, with the magnitude of reductions increasing with movement downstream until Pakse (Table 4.11). Modest increases in annual precipitation over the lower catchment (Table 4.10; Figure 4.11) stop this trend, with reductions in mean discharge for the stations between Stung Treng and Phnom Penh of 9.8–10.1%. Q5 and Q95 also decline at all stations. The most notable changes

in the river regimes are reductions in discharge concentrated in August and September, the period of peak flow (Figure 4.13). Between Stung Treng and Phnom Penh, mean discharge in these months declines by on average 17.4% and 14.8%, respectively.

Figure 4.14 summarises the percentage change in mean annual discharge at four representative gauging stations for each of the 2 °C, seven GCM scenarios. For each scenario, the corresponding changes resulting from the alternate specification of scenario time series for one meteorological input (precipitation, PET and temperature), whilst using baseline time series for the other two, are also shown. It is apparent that the inter-GCM differences are largely driven by differences in precipitation. As a result of the consistent increases in annual PET for the seven GCMs, mean discharge at all 12 stations declines if only scenario PET is specified. These declines occur in each month and the range of change in mean discharge at individual gauging stations (across the GCMs) is narrow (between a range of 3.8% for Phnom Penh and 6.3% for Yasothon), reflecting the relatively small inter-GCM differences in PET discussed in Section 4.7.3.1.

In contrast, the much larger differences in precipitation between the GCMs ensure that the specification of scenario precipitation with baseline PET and temperature enhances the inter-GCM differences in discharge. The smallest range of change in mean discharge for gauging stations on the main Mekong (21.9%, between -3.2% and 18.7%) is for Phnom Penh compared to the largest (35.2%, between -7.7% and 27.5%) for Chiang Saen. The average range on the main Mekong is 27.5%. Inter-GCM differences are larger on the two tributaries (e.g. 42.7%, between -10.1% and 32.6% for the Mun at Ubon).

Figure 4.14 demonstrates relatively small changes from the baseline when scenario temperature is employed with baseline precipitation and PET. Within the MIKE SHE model, the effect of changes in temperature on potential evapotranspiration are incorporated within the alternative scenario PET, so that temperature only directly influences snow accumulation and melting. However, over the upper Lancang, scenario temperatures result in reduced build-up of snow, which favours enhanced actual evapotranspiration rates, and an earlier, lesser snowmelt that provides

smaller contributions to river runoff. Consequently, the largest (but still fairly small) changes in mean flow occur at Chiang Saen (reductions in mean discharge of between 3.9% and 4.4%), closest to parts of the catchment that experience snow cover. The magnitude of these changes declines downstream, and for tributaries in which snow is not a feature (e.g. the Mun), changes in temperature alone have no impact on discharge. Small changes in the river regime at Chiang Saen are associated with a slight increase in April due to earlier snowmelt and peak reductions in May–June, but variability between the different GCMs is small. For example, the reduction in May discharge ranges from 15.5% to 20.2% (although absolute discharge is small), whilst August discharge declines by between 2.3% and 2.6%.

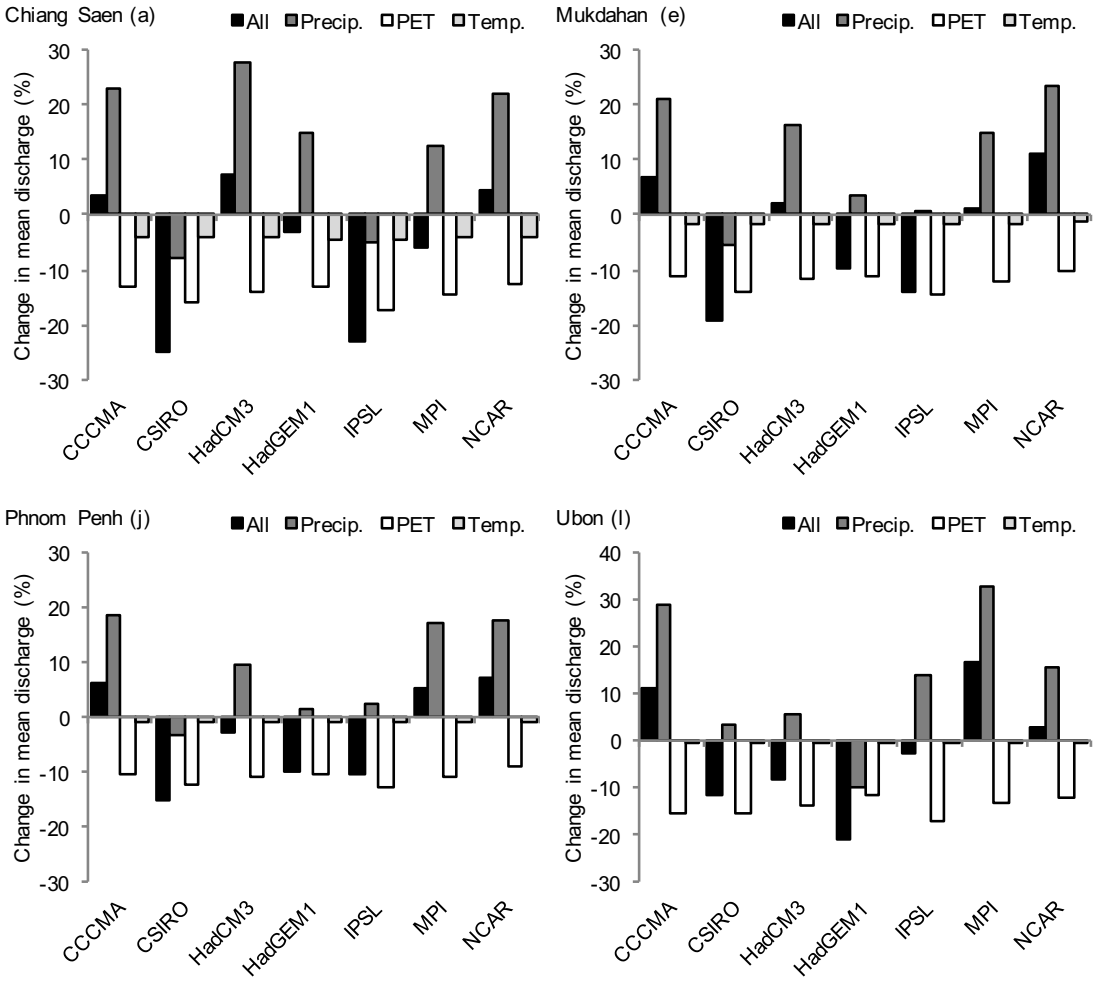

Figure 4.14. Percentage change in mean annual discharge simulated by MIKE SHE for four gauging stations within the Mekong catchment resulting from combined and individual modifications to precipitation, PET and temperature for the 2 °C, seven GCM climate change scenarios. (Note different y-axis scale for Ubon.)

4.7.3.3. Comparison of MIKE SHE results with SLURP and Mac-PDM.09

Figure 4.15 shows percentage changes in mean discharge (runoff for Mac-PDM.09 – see Section 4.6) at six gauging stations for each of the 2 °C, seven GCM scenarios, as simulated by the three hydrological models. As described above, results are only available for three stations for SLURP.

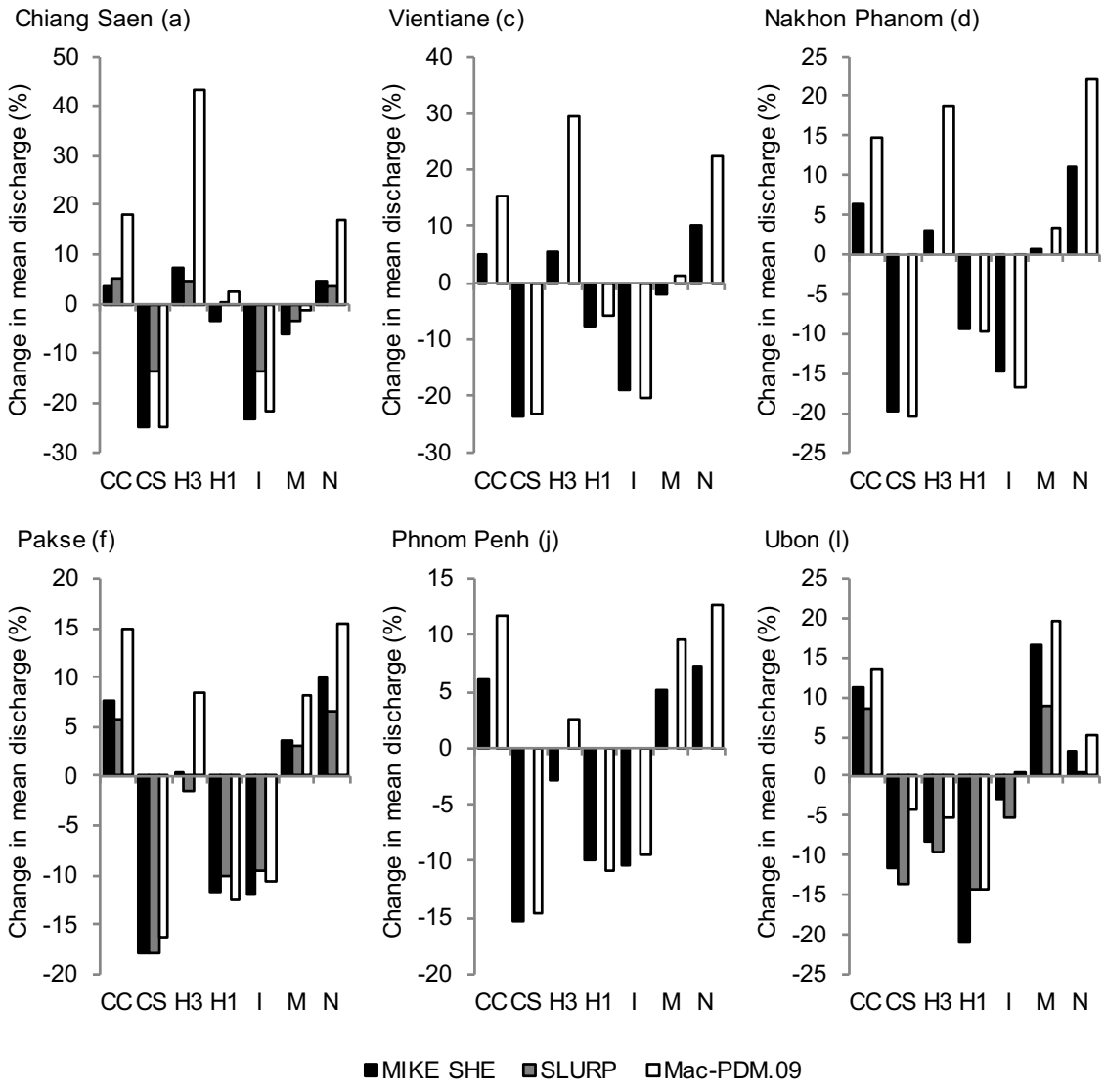

Figure 4.15. Change from baseline mean annual discharge (runoff for Mac-PDM.09) for the 2 °C, seven GCM climate change scenarios for six gauging stations within the Mekong catchment, as simulated by the three hydrological models. CC: CCCMA; CS: CSIRO; H3: HadCM3; H1: HadGEM1; I: IPSL; M: MPI; N: NCAR. (Note different y-axis scales.)

Direction of change in mean dischargerunoff) for a given GCM and station is predominantly the same for all the hydrological models. For example, all three hydrological models simulate increased annual discharge at all stations when for the CCCMA and NCAR GCMs and decreased annual flow for CSIRO. Of the 42 gauging station/GCM combinations (six stations × seven GCMs), only five exhibit changes in mean discharge (runoff) that differ in sign (+/-) between hydrological models. At Chiang Saen for HadGEM1, MIKE SHE produces a reduction (-3.3%), whereas SLURP and Mac-PDM simulate small increases (0.5% and 2.3%, respectively). At other stations for HadGEM1, all three models simulate reductions in mean discharge that increase in a downstream direction on the main Mekong, reaching a maximum at Pakse. For HadCM3 at Pakse, SLURP shows a reduction in mean discharge of 1.6% and MIKE SHE shows a small (0.4%) increase. In contrast, Mac-PDM.09 runoff increases by 8.4%. At Phnom Penh, this same GCM is associated with a reduction in MIKE SHE mean discharge of 2.8%, whilst Mac-PDM.09 runoff increases by 2.5% (SLURP results are not available). Similarly, for MPI at Vientiane, MIKE SHE is associated with a reduction of 2.1%, whilst Mac-PDM.09 displays a small increase of 1.2%. Finally, for the IPSL GCM at Ubon, both MIKE SHE and SLURP simulate reductions in mean discharge (-3.0% and -5.1%, respectively), whilst mean runoff from Mac-PDM.09 increases by a very small amount (0.5%). Beyond these differences, at each station there is general agreement between the different hydrological models on the order of magnitude of changes for the seven GCMs. At most stations, when listed in order of increasing change in mean discharge, the GCMs appear in the same order for both MIKE SHE and Mac-PDM.09, with the exception, in most cases, of a single pair of GCMs.

Where mean discharge (runoff) at a gauging station increases for an individual GCM for all three hydrological models (MIKE SHE and Mac-PDM.09 where SLURP results are not available), the greatest percentage changes are consistently associated with Mac-PDM.09 (Figure 4.15). This is particularly apparent at upstream stations. For example, at Chiang Saen, for the CCCMA, HadCM3 and NCAR GCMs (all associated with increased mean river flow) the percentage increase in mean runoff for Mac-PDM.09 ranges between 3.4 and 9.4 times (for CCCMA and HadCM3, respectively) as large as those of SLURP, and between 3.7 and 5.8 times (for NCAR and HadCM3, respectively) as large as those of MIKE SHE. HadCM3 stands out as a GCM for which

differences between the catchment and global hydrological models are particularly large, especially in upstream parts of the Mekong. Further downstream, inter-hydrological model differences in the magnitude of increases in discharge/runoff (when they occur for all the models) are smaller. This is exemplified in results for Ubon, where the increases in runoff for Mac-PDM.09 for the three GCMs with higher river flow for all three hydrological models are, on average, less than 1.4 times as large as the increases in MIKE SHE discharge. Mac-PDM.09 increases are still 4.6 times as large as those simulated by SLURP.

For GCMs associated with reductions in annual flow at gauging stations on the main Mekong for all three/two hydrological models, inter-model differences in the magnitude of change, in particular between MIKE SHE and Mac-PDM.09, are smaller than for those GCMs where annual flow increases (Figure 4.15). From the 15 instances on the main Mekong where both MIKE SHE and Mac-PDM.09 simulate a decline for a given GCM, the average inter-hydrological model range of percentage change in mean flow is only 1.3%, compared to 11.3% for the 16 instances where both models simulate an increase. At Ubon, reductions in the mean discharge, when they occur, are larger for MIKE SHE than for Mac-PDM.09 (and, as discussed above, for IPSL MIKE SHE mean discharge declines whilst mean runoff for Mac-PDM.09 increases slightly). For SLURP at Ubon, in most cases, reductions in mean discharge are larger (when they occur) than for the other two models. Differences between MIKE SHE and SLURP are relatively small. The exception is HadGEM1, where both SLURP and Mac-PDM.09 simulate a decline of 14.2%, and MIKE SHE is associated with a reduction of 20.9%.

Figure 4.16 shows mean monthly runoff for five (three in the case of SLURP) gauging stations simulated by the three hydrological models for the baseline and each of the 2 °C, seven GCM scenarios. Mean monthly runoff for MIKE SHE and SLURP was calculated by converting mean monthly discharge to volume of water and then dividing this by the catchment area upstream of the respective gauging station. This enables a comparison with the runoff results from Mac-PDM.09 that were originally provided in this form. Results for Vientiane (not shown in the interests of clarity), are similar to those for Nakhon Phanom. One notable inter-hydrological model difference is that the runoff values for Mac-PDM.09 at upstream gauging stations for

the baseline are lower than those of MIKE SHE and SLURP. This is likely the result of Mac.PDM.09 not being calibrated specifically for the Mekong, and therefore not using precipitation lapse rates over upstream areas, unlike MIKE SHE and SLURP. In addition, the amplitude of the annual cycle is generally greater for Mac-PDM.09 compared to the two catchment models, with a greater proportion of the total annual runoff occurring in the wet season (and a lesser proportion in the dry season).

In terms of the direction of changes in monthly runoff for the scenarios compared to the baseline, the most notable inter-hydrological model differences occur at Chiang Saen. For example, SLURP consistently simulates an earlier rise in the annual hydrograph, and so increased runoff in May (all GCMs) and June (five GMs, i.e. excluding CSIRO and IPSL), followed by reductions in July–September (the months of peak flows, with the exception of an increase in September for NCAR). Kingston *et al.* (2011) attributed this to earlier snowmelt and a subsequent smaller proportion of the annual total discharge occurring in peak months for all the scenarios. These consistent changes do not occur with MIKE SHE and Mac-PDM.09. For example, in contrast to SLURP, for CCCMA, HadCM3 and NCAR, increased runoff in September is evident for MIKE SHE and in both August and September for Mac-PDM.09. Furthermore, Mac-PDM.09 simulates year-round increases in runoff for CCCMA and HadCM3. Conversely, both MIKE SHE and Mac-PDM.09 simulate year-round reductions in runoff with CSIRO and IPSL. The magnitude of increases simulated by Mac-PDM.09 for the HadCM3 GCM in June–October and for NCAR and CCCMA in August–September are notably greater than increases simulated by MIKE SHE.

At Vientiane and Nakhon Phanom, for each GCM, MIKE SHE and Mac-PDM.09 display broad agreement on the months in which the greatest increases and reductions occur. For CSIRO, HadGEM1 and IPSL, reductions occur through the majority of the year, with the greatest reductions concentrated around June–August. Conversely, for CCCMA and NCAR, increases in runoff occur through the majority of the year, with the greatest increases concentrated around September.

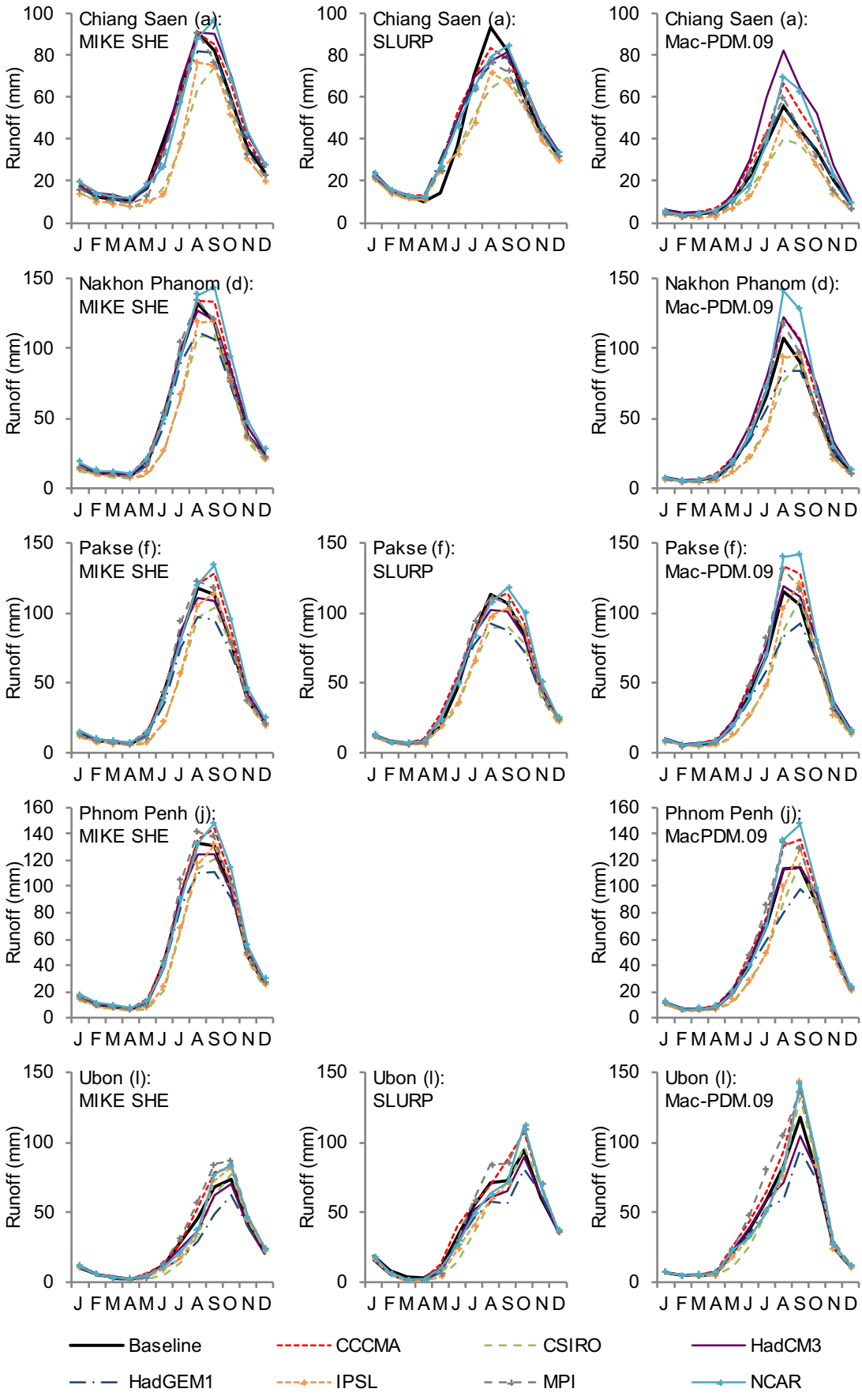

Figure 4.16. Mean monthly runoff for the 2 °C, seven GCM climate change scenarios for five gauging stations, as simulated by the three hydrological models. (Note different y-axis scales.)

However, the magnitude of the projected increases, in both absolute and percentage terms, is consistently greater with Mac-PDM.09. In addition, MIKE SHE shows the month of greatest flows shifting from August (for the baseline) to September for NCAR at Chiang Saen and downstream, a pattern that is displayed by SLURP for several scenarios at Chiang Saen, but not repeated for MacPDM.09. Increases are also simulated for the majority of months with the HadCM3 GCM. However, although Mac-PDM.09 simulates an increase in peak (August) runoff at Nakhon Phanom, MIKE SHE simulates a reduction. As at Chiang Saen, monthly runoff remains relatively unaltered between January to April.

The broad agreement between MIKE SHE and Mac-PDM.09 continues for the other two gauging stations (Pakse and Phnom Penh) further downstream on the main Mekong. However, in August–September, Mac-PDM.09 displays greater increases in runoff for GCMs including NCAR, CCCMA and MPI, and also displays increases for HadCM3 at Pakse whilst MIKE SHE simulates reductions. Figure 4.16 shows that for Pakse the influence of the earlier rise in discharge simulated by SLURP has diminished. In addition, SLURP does show some consistency with the results of the other two models, such as the shift of peak runoff from August to September for several GCMs (CCCMA, CSIRO, IPSL and NCAR), increases during the annual recession with CCCMA and NCAR and peak reductions during August–September with HadGEM1 and HadCM3 (the latter being consistent with MIKE SHE).

Results for Ubon show a general agreement between the three hydrological models. For example, all three models show only small changes in runoff between January–April. Both MIKE SHE and SLURP simulate increased runoff in October for all the GCMs except the two Hadley Centre GCMs (HadCM3 and HadGEM1). For Mac-PDM.09, the month of peak flows occurs a month earlier, in September rather than October, for both the baseline and all scenarios. Increased runoff is simulated for all but HadCM3 and HadGEM1 in September, and all but HadGEM1 in October.

4.7.4. Climate change scenarios: 1–6 °C increase using HadCM3

4.7.4.1. Changes in climate

Table 4.12 presents changes in mean annual precipitation, temperature and PET for eight representative meteorological input sub-catchments for each of the 1–6 °C, HadCM3 scenarios. These changes are also presented for 11 sub-catchments in Figure 4.17, whilst mean monthly precipitation and PET for the baseline and each scenario are shown for four sub-catchments in Figure 4.18. As in Figure 4.10, results for the Tonle Sap and Delta sub-catchments are not shown since they are downstream of the furthest downstream point at which river discharge is analysed. As described previously, temperature inputs to MIKE SHE are only directly relevant to the Lancang where snowmelt occurs. Changes in temperature are, however, reflected in the modifications to PET.

Table 4.12 and Figure 4.17 demonstrate that the relationship between prescribed warming and changes in annual precipitation projected by HadCM3 exhibits a distinct spatial pattern. Within the four northernmost sub-catchments, annual precipitation increases linearly with increasing global mean temperature. The magnitude of these increases declines in a downstream direction (e.g. Lancang versus Mekong 1; Table 4.12). Conversely, downstream parts of the Mekong (sub-catchments 9–13) show near linear decreases in annual precipitation with prescribed warming, with the magnitude of reductions increasing in a downstream direction. In the central Mekong (sub-catchments 5–8), annual precipitation responds in a non-linear way to increased prescribed warming, as a result of differing linear seasonal trends (see following paragraph and Figure 4.18). However, changes in precipitation on an annual basis for these sub-catchments are consistently low (≤1.5%) for all scenarios.

Due to the nature of the ClimGen technique for generating scenario precipitation, for any given sub-catchment and month, precipitation changes linearly with increasing global mean temperature (Figure 4.18). This means that for a given sub-catchment, increases / decreases in precipitation are produced in the same

Table 4.12. Mean annual precipitation, temperature and PET for the baseline and changes (% / °C) for the 1–6 °C, HadCM3 climate change scenarios for eight representative SLURP sub-catchments. Shaded cells indicate negative changes compared to the baseline.

Parameter/ Scenario		Lanc. (1)	Mek. 1 (4)	Chi (5)	Mun (6)	Mek. 2 (8)	Se Kong (9)	Sre Pok (10)	Mek. 3 (11)
Precipitation (% change)	Baseline (mm)	1053.4	1856.9	1273.1	1314.5	2214.6	2434.1	2056.6	1871.5
	1°C	5.0	0.4	-0.1	-0.3	-0.6	-1.3	-2.7	-1.7
	2°C	10.1	1.0	-0.1	-0.4	-1.1	-2.1	-4.5	-3.0
	3°C	15.2	1.7	0.1	-0.3	-1.3	-2.6	-5.6	-4.2
	4°C	20.3	2.4	0.4	-0.2	-1.3	-3.0	-6.3	-5.1
	5°C	25.3	3.3	0.9	0.1	-1.3	-3.1	-6.7	-6.0
	6°C	30.3	4.3	1.5	0.5	-1.1	-3.2	-6.9	-6.7
Temperature (change, °C)	Baseline (°C)	11.2	24.3	26.8	27.2	26.0	24.7	24.3	26.9
	1°C	1.3	1.2	1.2	1.2	1.1	1.1	1.1	1.1
	2°C	2.6	2.4	2.4	2.4	2.3	2.3	2.3	2.3
	3°C	3.9	3.7	3.7	3.6	3.5	3.4	3.4	3.6
	4°C	5.1	4.9	4.9	4.8	4.7	4.6	4.6	4.8
	5°C	6.4	6.1	6.1	6.0	5.9	5.8	5.7	6.0
	6°C	7.7	7.4	7.4	7.3	7.1	6.9	6.9	7.2
PET (% change)	Baseline (mm)	1766.7	1924.3	2365.1	2338.0	1814.2	1729.6	1697.0	1771.5
	1°C	6.3	6.8	6.4	6.2	7.4	7.4	7.3	7.2
	2°C	12.9	13.9	13.3	13.2	14.7	14.8	14.8	15.1
	3°C	19.8	21.3	20.6	20.6	22.4	22.5	22.6	23.5
	4°C	26.9	29.1	28.2	28.3	30.5	30.5	30.8	32.2
	5°C	34.4	37.3	36.3	36.5	39.0	39.0	39.4	41.4
	6°C	42.2	45.9	44.8	45.2	47.9	47.9	48.3	51.1

number of months for each of the 1–6 °C scenarios. There is, however, a downstream trend in the inter-seasonal pattern of precipitation change, as the number of months in which precipitation increases displays a reduction from north to south. For example, over the Lancang, precipitation increases in every month except April (Figure 4.18). The largest absolute increases occur in May-October, whilst the largest percentage changes occur in February and in May–June and September–October, either side of the wettest months. By Mekong 1, increases in precipitation are limited to 5 months (in particular May–June but also September–October and December). Precipitation in the wettest baseline months (July–August) is reduced, although the extension of the wet season on either side of these two months results in an overall increase in annual precipitation, albeit of a much smaller magnitude compared to the Lancang (e.g. an increase of 1% rather than 10.1% for the 2 °C scenario).

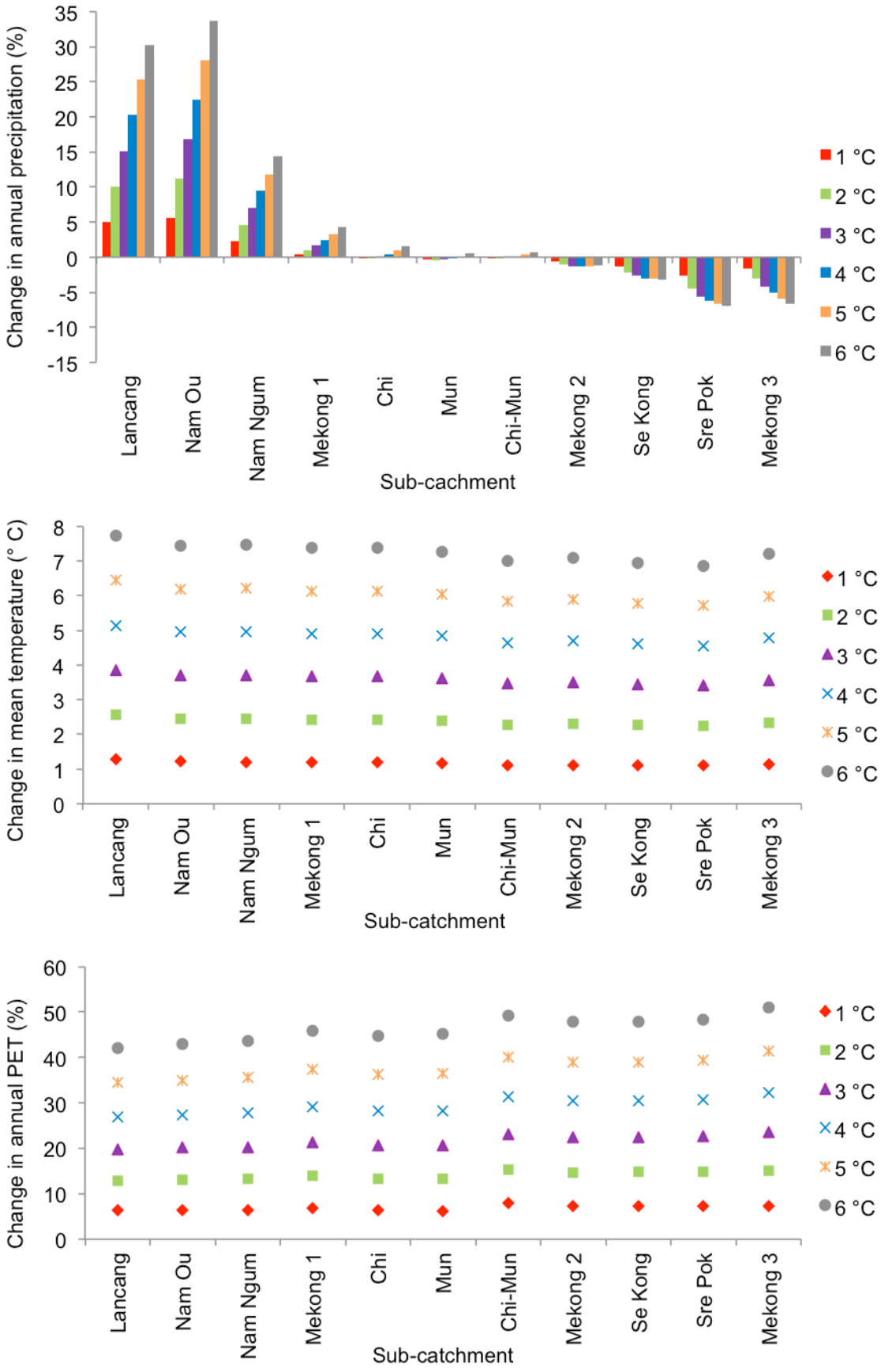

Figure 4.17. Projected changes in mean annual precipitation (%), temperature (°C) and Linacre PET (%) for eleven SLURP sub-catchments for the 1–6 °C, HadCM3 climate change scenarios.

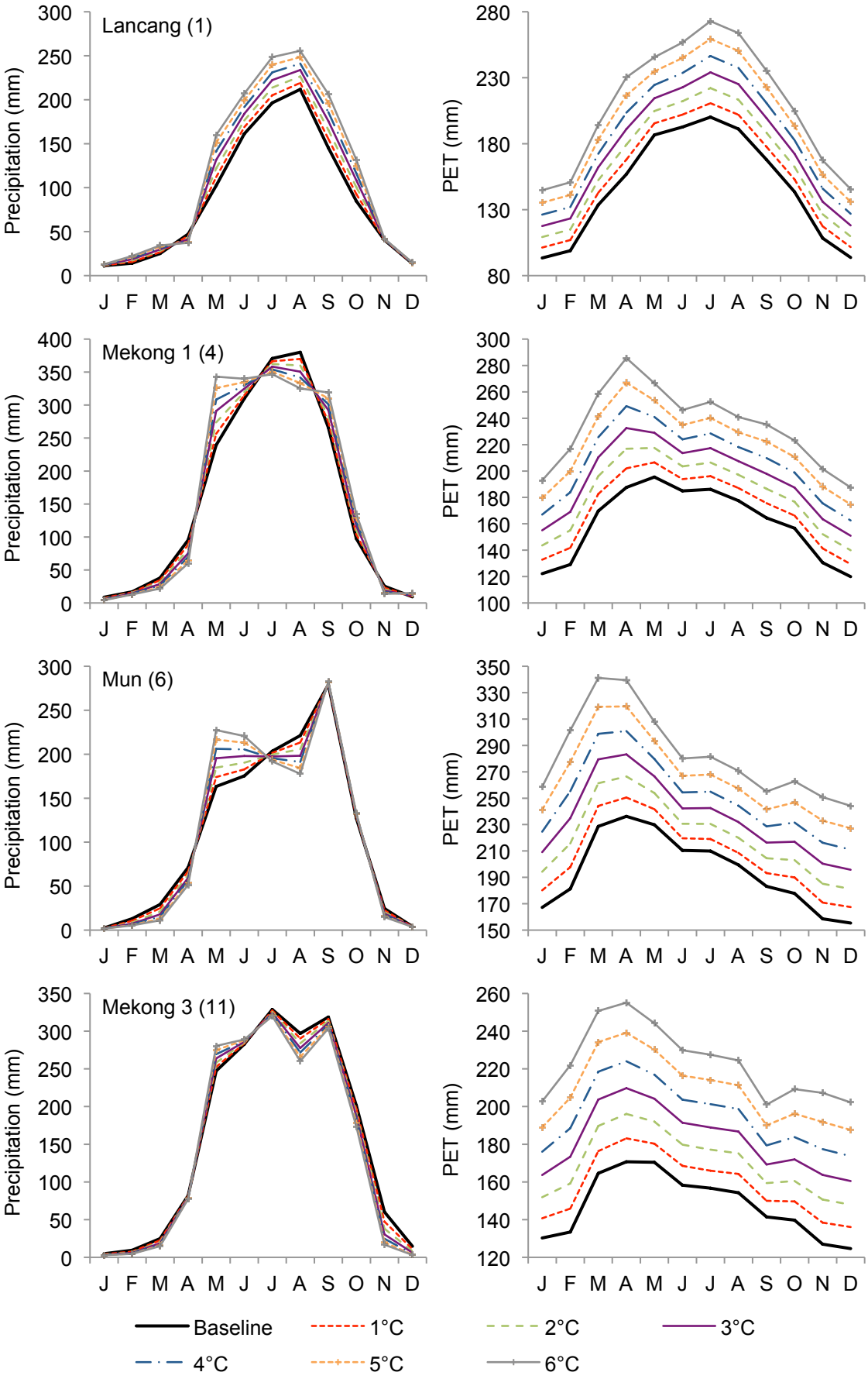

Figure 4.18. Mean monthly precipitation and Linacre PET for the baseline and the 1–6 °C, HadCM3 climate change scenarios for four representative sub-catchments. (Note different y-axis scales.)

For the four central sub-catchments (5–8), increasing precipitation is restricted to 4 months. Relatively large gains in precipitation are concentrated in the early part of the monsoon season (May–June). By Mekong 3, increases in mean monthly totals are limited to two months (May–June), with decreases projected throughout the rest of the year. The magnitudes of these increases are considerably smaller than those experienced in these months further upstream. For example, May increase for the 1 °C and 6 °C scenarios are 2.2% and 13.4% for Mekong 3, respectively, compared to 9.5% and 56.2% for the Lancang, respectively.

Throughout all the sub-catchments, both mean annual temperature and PET increase linearly with prescribed warming (Table 4.12; Figure 4.17). The Mekong Basin is projected to experience elevated increases in air temperature relative to the global mean (e.g. 2.3–2.6 °C across the sub-catchments for the 2 °C scenario, 6.9–7.7 °C for the 6 °C scenario). Both temperature and PET increase throughout the year with, in most cases, a relatively constant climate change signal through the year, particularly in comparison to precipitation changes. However, percentage changes in PET early and late in the year (between November to April) are generally larger than those in the summer, due to larger temperature increases occurring between November to April. Over sub-catchments 2–4 (including Mekong 1; Figure 4.18), greater increases in April compared to May result in April PET totals exceeding those of May for the higher prescribed warming scenarios (3–6 °C). Changes in PET are, in general, larger in the southern (warmer) part of the catchment compared to the northern (cooler) sub-catchments.

4.7.4.2. Changes in river flow (MIKE SHE)

Values of the mean annual and monthly Q5 and Q95 discharges for eight gauging stations for the baseline and the percentage changes in these discharges for each of the 1–6 °C, HadCM3 scenarios are shown in Table 4.13. Figure 4.19 provides the corresponding baseline and scenario river regimes. The eight gauging stations are the same as those used to present results for the 2 °C, seven GCM scenarios, and are representative of gauging stations for which results are not shown.

Table 4.13. Mean, Q5 and Q95 discharges (m^3s^{-1}) simulated by MIKE SHE for the baseline and changes (%) for the 1–6 °C, HadCM3 scenarios at eight gauging stations within the Mekong catchment. Shaded cells indicate negative changes compared to the baseline.

Q	Scenario	Chiang Saen (a)	Luang Prabang (b)	Vientiane (c)	Mukda-han (e)	Pakse (f)	Kratie (h)	Phnom Penh (j)	Ubon (l)
Mean	Baseline	2753.7	4082.6	4686.2	7626.0	9597.3	12961.7	13332.8	619.1
	1 °C	3.2	3.3	2.5	1.1	0.1	-1.4	-1.5	-5.2
	2 °C	7.4	7.3	5.5	2.3	0.4	-2.5	-2.8	-8.3
	3 °C	11.6	10.6	7.9	3.0	0.2	-3.7	-4.0	-14.4
	4 °C	16.5	15.3	11.5	4.8	1.1	-4.0	-4.4	-15.1
	5 °C	21.4	19.7	15.0	6.6	1.7	-4.6	-5.2	-21.9
	6 °C	27.5	24.6	18.9	8.4	2.6	-4.7	-5.4	-24.4
Q5	Baseline	7016.5	10395.7	12385.4	21993.9	27232.0	37128.6	37806.9	2019.6
	1 °C	2.1	2.4	-2.4	-4.5	-3.3	-5.3	-5.2	0.4
	2 °C	8.0	10.5	3.1	-3.7	-2.3	-8.4	-8.6	-4.1
	3 °C	9.8	9.6	1.6	-3.8	-4.7	-7.0	-6.9	-11.9
	4 °C	16.9	16.1	6.2	-5.1	-5.8	-10.5	-10.7	-9.8
	5 °C	20.5	19.0	9.9	-0.4	-1.6	-7.0	-6.3	-13.0
	6 °C	26.0	21.4	11.7	0.0	-3.8	-8.8	-8.8	-11.8
Q95	Baseline	692.2	1017.9	1148.4	1226.1	1314.3	1544.8	1630.2	29.1
	1 °C	3.2	3.4	2.7	3.1	5.7	1.6	2.8	-4.4
	2 °C	7.5	8.4	4.0	8.2	10.3	5.6	6.0	-6.7
	3 °C	12.5	11.4	9.8	9.0	12.7	5.9	5.2	-12.7
	4 °C	16.9	14.1	11.0	11.1	12.0	6.1	5.1	-19.4
	5 °C	19.4	18.0	13.4	13.1	14.7	8.8	7.0	-37.2
	6 °C	26.5	24.4	17.4	19.7	19.2	12.0	8.5	-38.4

Changes in mean discharge for the 1–6 °C, HadCM3 scenarios display a similar geographical pattern to changes in annual precipitation. The three northernmost (and furthest upstream) gauging stations (Chiang Saen to Vientiane; Table 4.13) exhibit near linear increases in mean discharge with prescribed warming, with the magnitude of percentage increase declining in a downstream direction under each scenario. These increases signify that increases in precipitation more than compensate for higher PET. Mean monthly discharge increases through most of the year, with the magnitude of the increase rising with degree of prescribed warming (Figure 4.19). Exceptions include reductions in May–June (up to 10%) for the 1–2 °C scenario and small decreases (<2.0%) in August for the 1–2 °C scenarios for all three stations. These decreases are indicative of increases in evapotranspiration outstripping enhanced precipitation, whilst for Vientiane, August decreases can

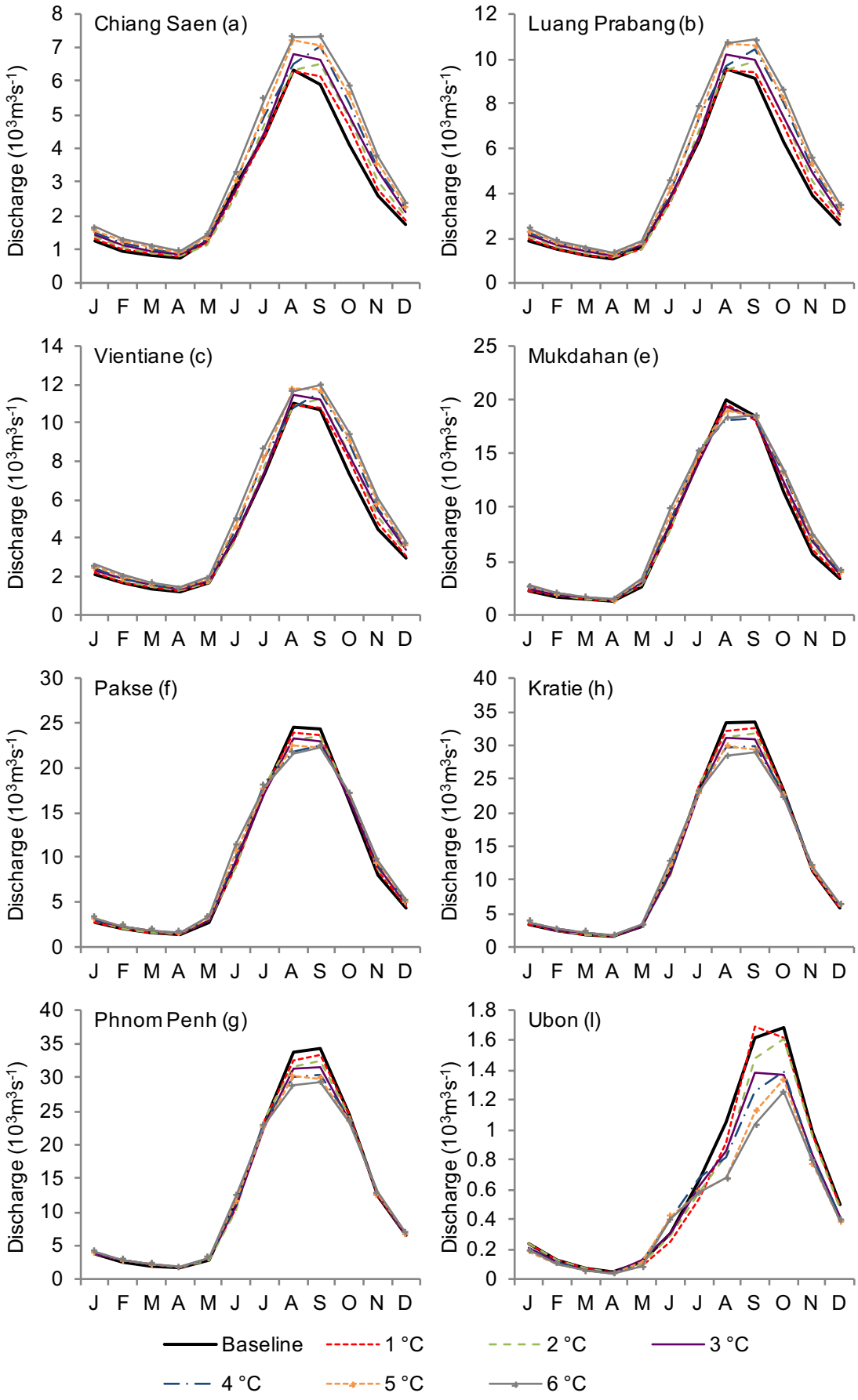

Figure 4.19. River regimes simulated by MIKE SHE for the baseline and 1–6 °C, HadCM3 climate change scenarios for eight gauging stations within the Mekong catchment. (Note different y-axis scales.)

also be attributed to reductions in precipitation for this month over Nam Ngum and Mekong 1. Table 4.13 shows that at Chiang Saen and Luang Prabang, in general, Q5 increases with the degree of prescribed warming, an exception being a slightly smaller increase for the 3 °C scenario compared to the 2 °C scenario at Luang Prabang. This is repeated at Vientiane, where there is also a modest decrease for the 1 °C, but Q5 increases with the degree of prescribed warming for the 4–6 °C scenarios. August characteristically remains the month of peak flows, although for the 4 °C scenario at all three stations and the 6 °C scenario at Luang Prabang and Vientiane, the highest mean monthly discharge occurs a month later. The higher dry season flows that are simulated cause Q95 to generally increase with the magnitude of prescribed warming. Percentage changes are higher at Luang Prabang than Chiang Saen for the two lowest scenarios, but consistently decrease in a downstream direction from Luang Prabang to Vientiane.

Results for Mukdahan (and Nakhon Phanom, not shown) also indicate larger mean flows as the magnitude of prescribed warming increases (Table 4.13). However, whilst discharges during the annual rise and recession increase with prescribed warming, peak flows in August and September are lower than the baseline (Figure 4.19). These reductions are not related linearly to degree of warming, with the largest associated with the 4 °C scenario. This reflects the balance between lower precipitation and higher PET in these months. Q5 declines for all but the warmest scenario (no change), with the smallest reduction resulting from the 5 °C scenario. Higher dry season flows cause Q95 to increase under all scenarios, although not consistently with prescribed warming. These increases are sustained by flows from upstream rather than local runoff, as precipitation over the Mekong 1 sub-catchment declines during the dry season, as PET increases (Figure 4.18).

At Pakse, the opposing effects of small increases in discharge through most of the year and larger reductions in August–September (Figure 4.19) result in little change (+0.1–0.4%) in mean discharge for the 1–3 °C scenarios, and small increases in mean discharge for the remaining scenarios, ranging from +1.1% to +2.6% (for the 3 °C and 6 °C scenarios, respectively Table 4.13). Following the pattern of reduced magnitude of increases with distance downstream, changes are an order of magnitude lower than those further upstream (e.g. a maximum of +2.6% for the

warmest scenario, compared to +24.9% at Chiang Saen). Increases in mean monthly discharge are still projected during the annual rise and recession, but these changes are relatively small in magnitude (Figure 4.18). Decreases are simulated for August and September, the months of peak flows, for all six scenarios. Changes in mean monthly discharge for each month do not always follow a linear pattern with prescribed warming. The modest increases in dry season discharge result in higher Q95 discharges, whilst the reductions in August–September result in lower Q5 discharges. Both show a non-linear pattern of change with prescribed warming.

Results for the Mun at Ubon, which flows into the Mekong just upstream of Pakse, are representative of the impacts of modest changes in annual precipitation coupled with large increases in PET over this part of the catchment. Mean flow declines consistently as prescribed warming increases (Table 4.13). In percentage terms, changes are of a similar magnitude to those experienced at upstream stations, albeit in the opposite direction. Particularly large reductions in discharge occur in months with the highest baseline flows (Figure 4.19), contributing to reductions in peak flows on the Mekong at Pakse. Small increases in mean monthly discharge are limited to September for the 1 °C scenario and one or two months around May–June for the 3–6 °C scenarios. Declines in discharge throughout most of the year, including during the annual recession and dry season, demonstrate that increases in discharge within the main Mekong at this time are dependent upon enhanced flows from upstream.

The four most downstream stations on the lower Mekong (Stung Treng–Phnom Penh) display similar patterns of change. Mean discharge declines with prescribed warming, with the magnitude of reductions increasing with distance downstream. The magnitude of percentage changes are smaller in comparison to increases further upstream, with a maximum change in mean discharge of -5.4% at Phnom Penh for the 6 °C scenario. However, it is important to note that since baseline mean discharges at the furthest downstream gauging stations are an order of magnitude higher than baseline mean discharges at the furthest upstream gauging stations (Table 4.13), a change of 5.4% at Phnom Penh equates to an absolute change (722.5 m^3s^{-1}) that is comparable to the absolute change (756.5 m^3s^{-1}) at Chiang Saen for the 6 °C scenario, which corresponds with a percentage change of 27.5%. The largest

reductions in mean monthly discharge at each of the four downstream stations (in both absolute and percentage terms) occur in August and September, the months of peak flows, with decreases also occurring in one or two months either side of this, dependent upon the scenario and gauging station. Q5 therefore declines (Table 4.13), but there is no consistent pattern with prescribed warming. Mean monthly discharge increases throughout November–May at all four gauging stations, although changes over this period are relatively small. This is reflected in increases in Q95 for all scenarios for the four stations. These increases are largely maintained by enhanced runoff in upstream parts of the catchment, rather than increases in local runoff.

Figure 4.20 shows percentages changes in mean annual discharge for four gauging stations resulting from the 1–6 °C, HadCM3 scenarios as well as those which result when one of each of the three meteorological inputs are modified in turn whilst retaining baseline values for the other two. It confirms the dominant influence of change in precipitation over upstream parts of the catchment (e.g. Chiang Saen). Consistent increases in precipitation with prescribed warming far outweigh increases in PET and are responsible for progressive increases in mean discharge. Further downstream, changes in discharge due to precipitation alone are smaller and, in terms of magnitude, begin to approximate those due to PET (e.g. Mukdahan and especially Phnom Penh). For tributaries in the south of the catchment in which discharge is not dominated by flows from upstream parts of the main Mekong, changes in PET exert a much larger influence (e.g. the Mun at Ubon). Results show that mean discharge is relatively insensitive to changes in temperature (excluding its influence upon PET), especially in lower parts of the catchment.

4.7.4.3. Comparison of MIKE SHE results with SLURP and Mac-PDM.09

Percentage changes in mean discharge (runoff for Mac-PDM.09) at six gauging stations (three for SLURP) for each of the 1–6 °C, HadCM3 scenarios, as simulated by the three hydrological models, are shown in Figure 4.21. Just as MIKE SHE

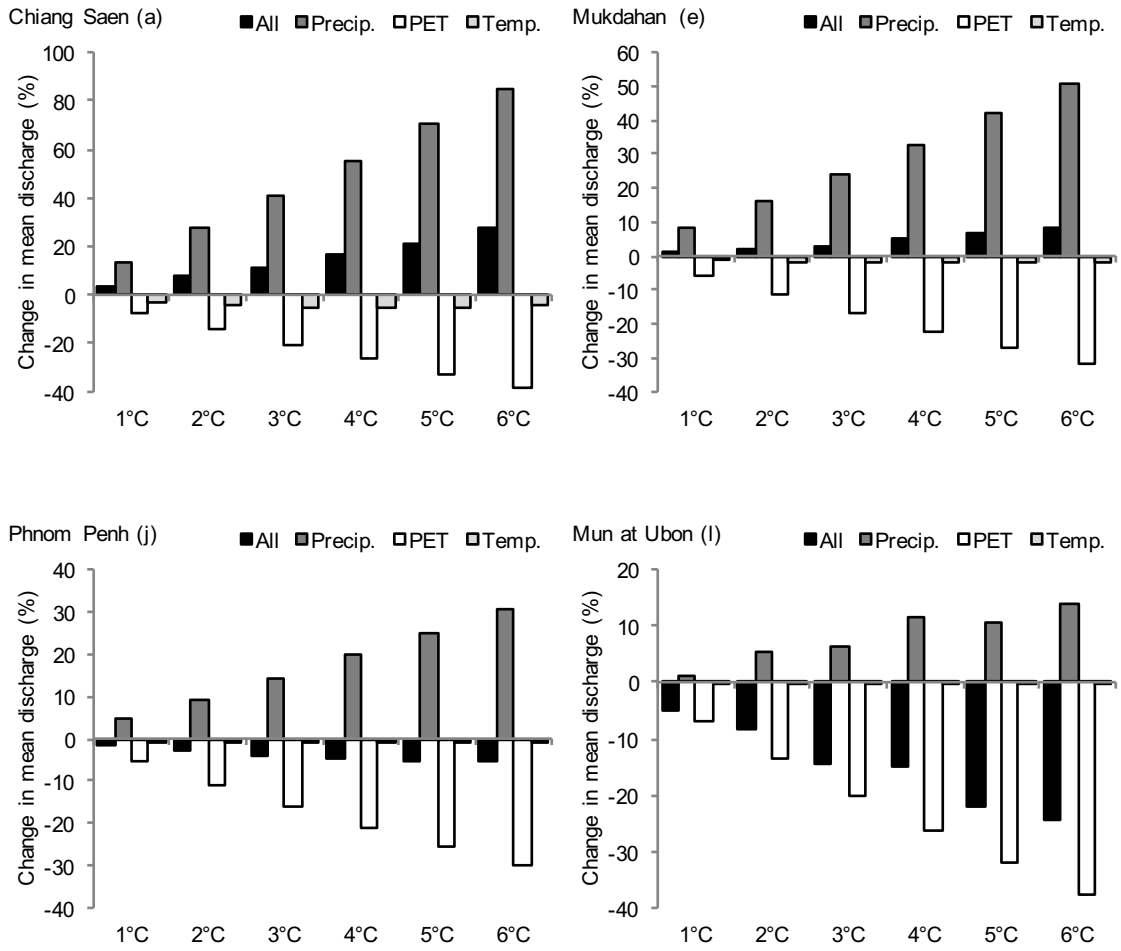

Figure 4.20. Percentage change in mean annual discharge simulated by MIKE SHE for four gauging stations, resulting from combined and individual modifications to precipitation, PET and temperature for the 1–6 °C, HadCM3 climate scenarios. (Note different y-axis scales.)

demonstrates a spatially variable response of river flow to these scenarios, the inter-model differences in the discharge (runoff) climate change signal also vary throughout the catchment. The systematic increase in mean discharge with magnitude of warming that occurs from Chiang Saen to middle parts of the catchment (Nakhon Phanom) for MIKE SHE are repeated for Mac-PDM.09 and probably SLURP, although results are limited to Chiang Saen. However, the magnitude of these changes varies between hydrological models. The smallest changes are associated with SLURP, at Chiang Saen ranging between +1.6% and +19.8% for the 1 °C and 6 °C scenarios, respectively. On average, the changes simulated by MIKE SHE are 45% higher than those for SLURP, although the very small change for the 1 °C scenario for SLURP skews this value. In contrast, much larger increases in mean runoff are simulated by Mac-PDM.09 (range for Chiang

Saen: +21.1% to +120.4%). On average, changes are 5.4 and 8.0 times as large as those simulated by MIKE SHE and SLURP, respectively. The same pattern is repeated at Vientiane and Nakhon Phanom. The magnitude of increases in runoff declines in a downstream direction for Mac-PDM.09, just as they do for MIKE SHE (from a 120.4% increase for the 6 °C scenario at Chiang Saen to 48.5% at Nakhom Phanom).

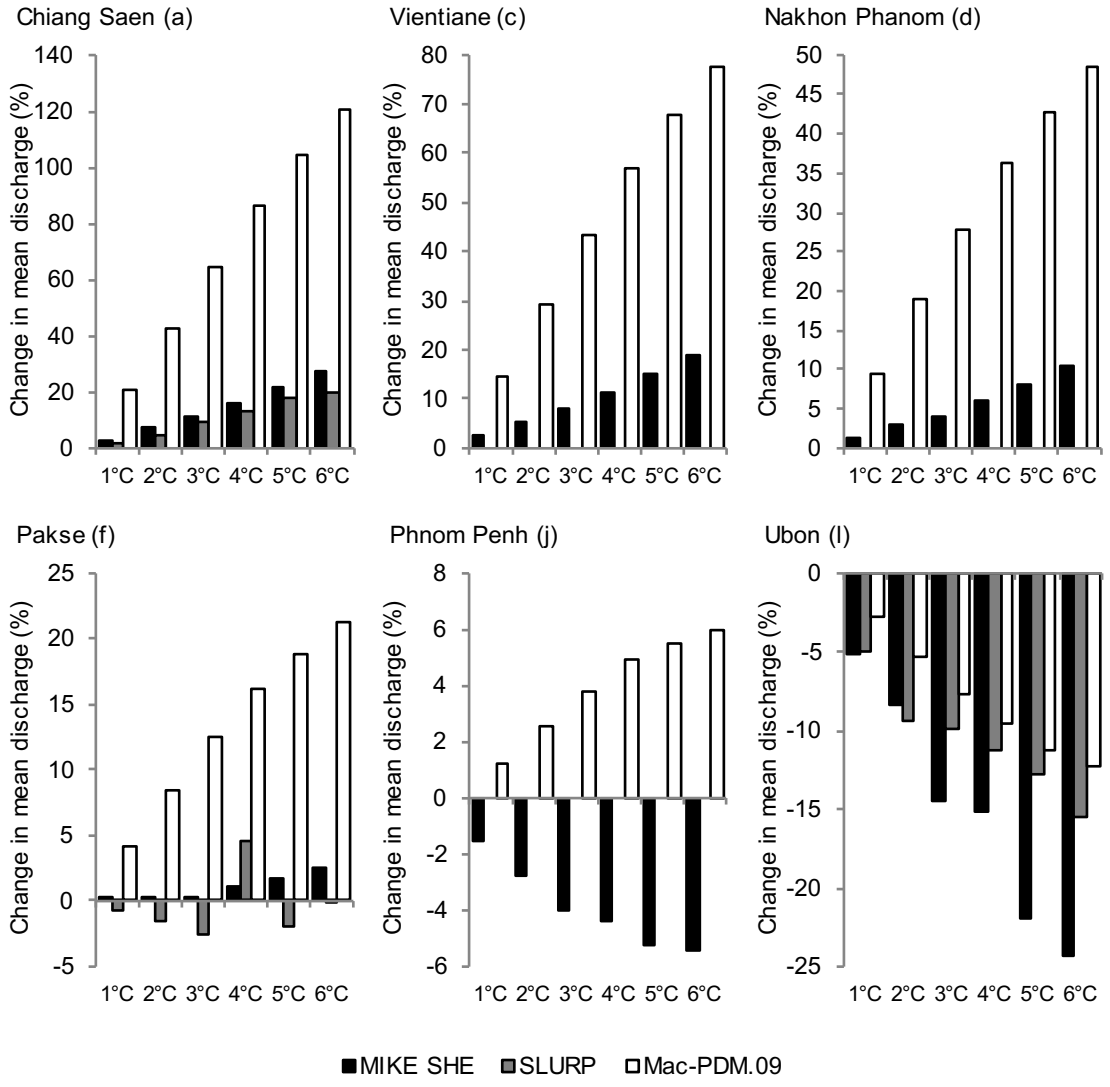

Figure 4.21. Change from baseline mean annual discharge (runoff for Mac-PDM.09) for the 1–6 °C, HadCM3 climate change scenarios for six gauging stations within the Mekong catchment, as simulated by the three hydrological models. (Note different y-axis scales.)

Results for Ubon on the Mun River demonstrate that all three hydrological models respond in a similar way to the generally lower precipitation and consistently higher PET over this part of the catchment as prescribed warming increases (Figure 4.21). The order of magnitude of the resulting declines in mean discharge (runoff) is,

however, different to the increases in the upper Mekong. MIKE SHE produces the largest reductions, whilst the smallest result from Mac-PDM.09, with the exception of the 2 °C scenario (SLURP > MIKE SHE). Reductions simulated by MIKE SHE are, on average, just under twice as large as the declines from Mac-PDM.09. The discharge reductions for SLURP are between those of these two models and are generally closer to those of Mac-PDM.09.

Differences between the three hydrological models in the magnitude and temporal distribution of flow changes in the upper and middle sections of the Mekong are responsible for the contrasting responses of the hydrological models at downstream gauging stations on the Mekong (Figure 4.21). At Pakse, whilst mean discharge simulated by MIKE SHE continues to increase (maximum: +2.6%), albeit not consistently with prescribed warming, results for SLURP demonstrate a variable response. Mean discharge declines for all but the 4 °C scenario (+4.5%). However, the largest decline is associated with the 3 °C scenario and the smallest with the 6 °C scenario. In contrast, the much larger increases in runoff upstream which are simulated by Mac-PDM.09 ensure that mean runoff at Pakse continues to exhibit a consistent increase with prescribed warming, despite reductions in runoff from downstream sub-catchments such as the Chi and Mun. The magnitude of the increases in mean runoff does, however, continue to decline in a downstream direction. The largest increase (6°C scenario) is 21.3% compared to 48.5% for Nakhom Phanom. This trend continues further downstream so that whilst Mac-PDM.09 runoff at Phnom Penh increases with prescribed warming, the largest increase is only 6.0%. In contrast, the smaller increases in discharge from upstream catchments, coupled with the largest declines in discharge from southern sub-catchments, results in the previously reported declines in mean discharge at Phnom Penh that are simulated by MIKE SHE. The magnitude of these declines almost mirrors the increases simulated by Mac-PDM.09.

Mean monthly runoff is shown in Figure 4.22 for five (three for SLURP) gauging stations for the baseline and each 1–6 °C, HadCM3 scenario. Results for Nakhon Phanom are representative of those for Vientiane (not shown).

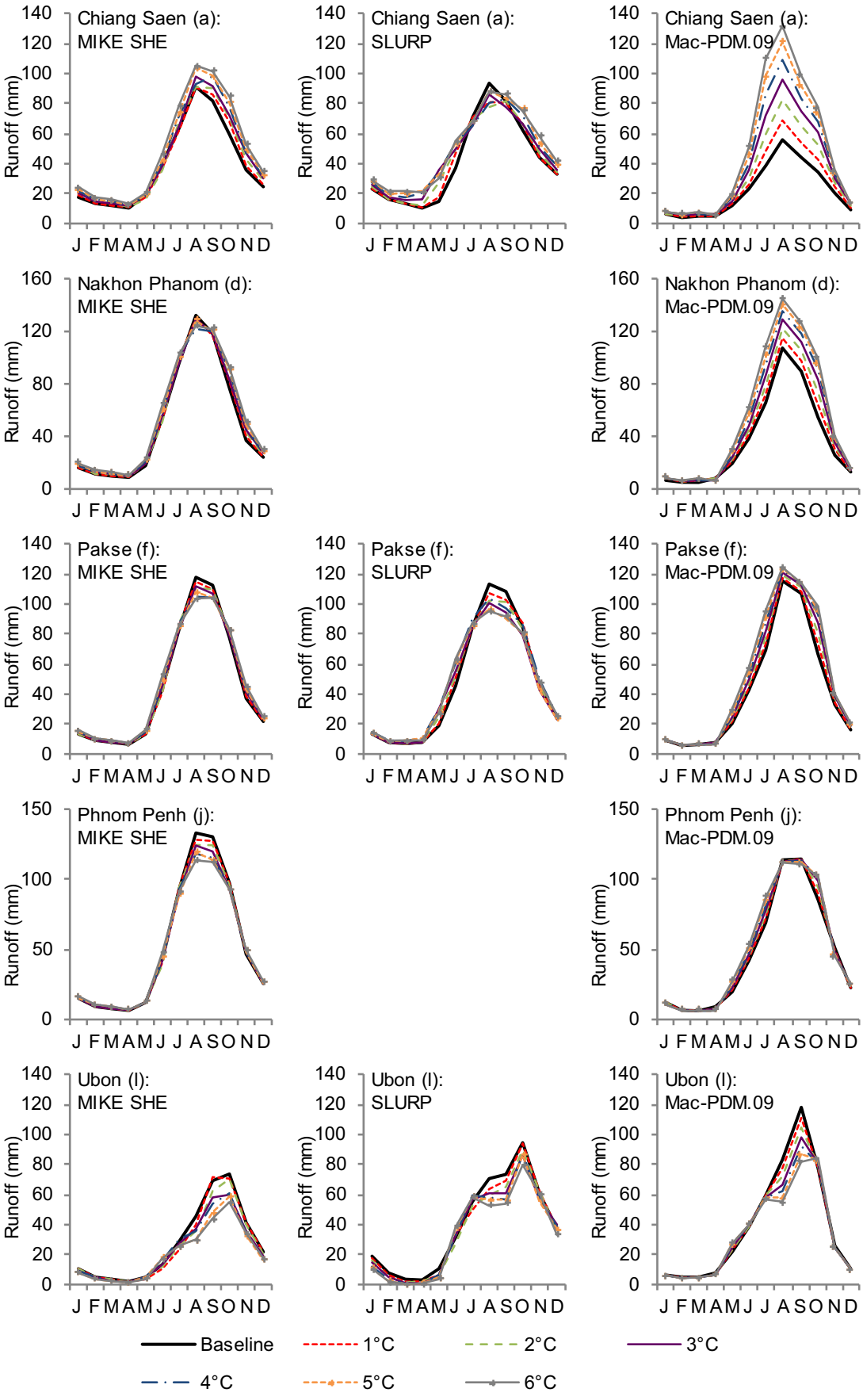

Figure 4.22. Mean monthly runoff for the 1–6 °C, HadCM3 climate change scenarios for five gauging stations, as simulated by the three hydrological models.

At Chiang Saen, Mac-PDM.09 shows increased runoff in all months for all six scenarios. Conversely, although MIKE SHE simulates year-round increases for the 3–6 °C scenario, minor reductions (up to 4 mm) are simulated for between 1–4 months (in May–August) for the other scenarios. In addition, the magnitude of increases simulated by Mac-PDM.09 between June–October are considerably greater. For example, whilst MIKE SHE simulates increases in runoff of up to 26 mm between June–October for the 6 °C scenario, Mac-PDM.09 simulates increases of between 28 mm and 76 mm. Unlike MIKE SHE and Mac-PDM.09, SLURP projects reductions in runoff of up to 15.7 mm in July–September for the 1–3 °C scenarios, and in July–August for the 4–6 °C scenarios. Simulated increases in September are more similar in magnitude to MIKE SHE, but are greater than those of both MIKE SHE and Mac-PDM.09 during April–May.

At Nakhon Phanom, results for MIKE SHE and Mac-PDM.09 show less agreement. Both models show increases during the annual rise and recession, with the magnitudes of changes generally increasing with prescribed warming. However, whilst Mac-PDM.09 simulates consistent increases in runoff for August and September, MIKE SHE simulates reduction in August for all scenarios and in September as well for the 1–3 °C scenarios.

Broad agreement is evident between MIKE SHE and SLURP at Pakse. Both show reductions in August and September for all scenarios and smaller changes through the rest of the year. Increases in May–June are larger for SLURP (Figure 4.22). Whilst Mac-PDM.09 shows comparable increases in May–June and only small changes between November–April, unlike MIKE SHE and SLURP, it simulates increases in August–September for the 1–6 °C scenarios. October increases simulated by Mac–PDM.09 are also notably greater. By Phnom Penh, Mac-PDM.09 also simulates reductions in peak season (August–September) runoff, although the magnitude of change is less than that of MIKE SHE and enhanced runoff is still simulated in October by Mac-PDM.09.

Results for Ubon for the three models display some similarities. For example, all show increasing reductions in runoff for August and September for most scenarios. Whilst MIKE SHE and SLURP also suggest a reduction for October, Mac-PDM.09

simulates small increases for October that are replicated at gauging stations on the main Mekong.

4.8. Discussion

4.8.1. MIKE SHE model development and performance

The MIKE SHE model of the Mekong uses a combination of physically based process descriptions that are spatially distributed using a 10 km × 10 km grid, and relatively simple conceptual, semi-distributed approaches appropriate for such a large catchment. This model can therefore be considered quasi-physically based. Much of the data employed were taken from the earlier SLURP model of the catchment (Kingston *et al.*, 2011) in order to reduce input-related uncertainty, ensuring that differences in climate impact results from the two catchment hydrological models can largely be attributed to model-structure related uncertainty with greater confidence.

Although the SLURP model was calibrated at only three gauging stations, the MIKE SHE model was calibrated at 12 stations. This allowed a more robust calibration and assessment of model performance throughout the catchment, and also enabled calibration and scenario assessments to be extended further downstream compared to the SLURP model. Model performance for the 1961–1990 calibration period is consistently classed as "excellent" on the main Mekong down to Kompong Cham, according to Dv and NSE values derived using monthly mean discharges. Further downstream at Phnom Penh, model performance is slightly weaker, with Dv classed as "very good". This may be related to the shorter calibration period employed at this stations (13 years), due to the shorter duration of observed discharge records. NSE is still classed as "excellent", however. In contrast, model performance on the two tributaries that drain the Khorat plateau, the Chi and the Mun, is notably poorer, with NSE classed as "poor" and "fair", respectively. This echoes the poor performance of SLURP at Ubon. Performance at ten stations for the validation period is, again, generally classed as "very good" to "excellent" on the main Mekong, with weaker performance at the most downstream stations, but poor performance on the Mun at Ubon and Chi at Yasothon. Overall, the performance of the MIKE SHE model

is superior to that of SLURP and compares very favourably with previous models of the Mekong (e.g. Hapuarachchi *et al.*, 2008; Västilä *et al.*, 2010).

Slightly reduced performance according to NSE for some gauging stations for the validation period compared to the calibration period may be due to changes in the catchment not represented within the model. For example, a number of dams have been constructed. The Manwan hydropower dam on the Lancang was completed in 1993 (Wang *et al.*, 2011). This could help explain the slightly lower NSE values at Chiang Saen and Luang Prabang during model validation. Lu and Siew (2006) examined the effects of the Manwan Dam from 1992 (year the reservoir was filled) to 2000. They showed that whilst the dam had some impacts on seasonality of flows, there was no consistent impact on annual discharges since the hydropower dams are non-consumptive (apart from relatively small evaporative losses).

The weaker performance of the MIKE SHE model at Ubon and Yasothon, particularly for the validation period, could be related to the precipitation data employed, which, in common with SLURP, were derived from the UDel 0.5° × 0.5° gridded precipitation dataset. However, as reported by Kingston *et al.* (2011), calibration of the SLURP model was initially attempted using data derived from the CRU TS 3.0 0.5° × 0.5° gridded precipitation dataset. With this alternative dataset it was even more difficult to obtain adequate performance at all the gauging stations that were considered. This led to the use of UDel precipitation data, which facilitated improved model performance. The impact on scenario results of employing CRU TS 3.0 precipitation and temperature data during MIKE SHE model calibration, validation and baseline simulation is explored in Chapter 5.

Alternatively, weaker performance at Yasothon and Ubon and for some downstream gauging stations may be partly related to land cover change. Considerable conflict-related (and post-conflict) changes in land cover occurred during the 1960s to 1980s (Lacombe *et al.*, 2010) and in recent decades deforestation within the Mekong has resulted from rapid economic development (Nobuhiro *et al.*, 2008). In the absence of time series of vegetation cover for the historic period, land cover within the model remains constant through the calibration and validation periods, an approach also adopted by Kingston *et al.* (2011). Land cover change can, however,

significantly impact runoff by altering evapotranspiration rates (Brown *et al.*, 2005). Large-scale forest clearance can increase runoff (Bruijnzeel, 2004), and over parts of the Mekong variations in rainfall–runoff relationships have been attributed to land cover modifications (Lacombe *et al.*, 2010).

Using the same data within the MIKE SHE model as those employed in the SLURP model inevitably resulted in the adoption of some approaches that may have differed if the new model had been developed in isolation from this earlier study. In particular, an alternative meteorological input spatial distribution may have been used. For example, in the MIKE SHE model different sub-catchments defined the meteorological inputs and saturated zone linear reservoirs (the former taken from SLURP and the latter being influenced by gauging station location and catchment topography). The same spatial distribution for both might instead have been used. This could have advantages for the Lancang, which extends over a relatively large latitudinal range and has a wide range of elevations, but is represented by one meteorological input sub-catchment (and three saturated zone linear reservoirs). Similarly, the area between the Chiang Saen and Mukdahan gauging stations encompasses two meteorological sub-catchments: the Mekong 1 sub-catchment that covers a large area and the relatively small Nam Ngum sub-catchment. The same stretch of the Mekong is represented by four groundwater sub-catchments whose areas are more comparable. Precipitation and temperature lapse rates result in some spatial variation in meteorological inputs within some sub-catchments, but the division of the largest sub-catchments into smaller units could more properly account for this variation. Alternatively, meteorological inputs could be distributed using the 0.5° × 0.5° grid employed within the datasets from which sub-catchment average inputs were derived. This would be analogous to changing inputs from station-based records (a single time series applied to a relatively large area) to gridded datasets and would enable the inclusion of smaller scale variations in meteorological inputs under both baseline conditions and the climate change scenarios. Previous research has demonstrated that a change such as this (i.e. in the model inputs employed) commonly requires model recalibration (e.g. Mileham *et al.*, 2008; Xu *et al.*, 2010). The impact on scenario results of employing the alternative spatial distributions of meteorological inputs described above is also investigated in Chapter 5.

4.8.2. Climate change impacts on river flow simulated by MIKE SHE

The use of climate scenarios associated with a prescribed 2 °C increase in global mean air temperature generated through rescaling the output from seven different GCMs reveals that there is great disparity in the spatial pattern, direction and magnitude of changes in mean and intra-annual discharges simulated by MIKE SHE when using the output of different GCMs. Choice of GCM is therefore a large source of uncertainty in projected river flow. Results for the different GCMs range from catchment-wide increases in mean discharge (CCCMA and NCAR GCMs), to decreases (CSIRO, HadGEM1 and IPSL) to spatially variable responses in the direction of change (HadCM3 and MPI). The seasonal pattern of changes also varies between GCMs. Differences are largely driven by inter-GCM differences in projections of precipitation, for which the spatial pattern, seasonality and magnitude of change shows great variability across GCMs. Across the gauging stations, the average absolute inter-GCM range of percentage change in mean discharge is ~31%. This is the average difference between the maximum (highest increase or lowest decrease) and minimum (lowest increase or highest decrease) change at each station. The equivalent values for changes in Q5 and Q95 are ~27% and ~37%, respectively.

With the HadCM3 GCM, increases in mean discharge are simulated for upstream gauging stations and extend to Pakse, whilst decreases are projected for downstream gauging stations on the main Mekong and on the two tributaries in the southwestern part of the catchment (the Chi and the Mun). This spatial pattern is evident for scenarios associated with increases in global mean temperature of between 1 °C and 6 °C, with the magnitude of changes in either direction generally increasing with greater prescribed warming except in central parts of the catchment. Across the gauging stations, the average inter-scenario range of percentage change in mean discharge is ~11%. The equivalent values for changes in Q5 and Q95 are ~13% and ~23%, respectively. These values demonstrate that the magnitude of uncertainty in changes in river discharge associated with the choice of prescribed warming scenario (of between 1–6 °C) generated using the HadCM3 GCM is considerably less than that associated with choice of GCM (out of

seven) for the 2 °C scenario. These findings reaffirm the importance of using an ensemble of GCMs to assess potential climate change impacts on hydrology.

Changes to the Mekong's river regime could have significant consequences for the ecological functioning of the Mekong, and therefore the ecosystem services it provides (e.g. Dugan *et al.*, 2010; Grumbine *et al.*, 2012). The assessment of Mekong River flows has been extended by Thompson *et al.* (2014b)[1] to evaluate associated uncertainty in "environmental flows". This term denotes the flow regime of a river required to sustain the freshwater ecosystem and related services. A modified version of the ecological risk due to flow alteration (ERFA) screening method (Laizé *et al.*, 2014) was applied to results of the 2 °C, seven GCM scenario set from an earlier version of the MIKE SHE Mekong model (presented in Thompson *et al.*, 2013). This statistical technique is based on the range of variability (RVA) approach (Richter *et al.*, 1997) and compares the natural and altered flow regimes to provide indicators of hydrological alteration (IHAs). The results reveal considerable inter-GCM differences in the risk of ecological change.

4.8.3. Comparison of climate change impacts between hydrological models: GCM- versus hydrological model-related uncertainty

Comparison of climate change scenario results from MIKE SHE with those from an alternative catchment hydrological model (SLURP) and the Mac-PDM.09 GHM provides an opportunity to assess the magnitude of uncertainty associated with the use of alternative hydrological model codes. This study demonstrates that, in accordance with other investigations (e.g. Jiang *et al.*, 2007; Ludwig *et al.*, 2009; Poulin *et al.*, 2011), hydrological model-related uncertainty should not be ignored. However, results suggest that, in general, climate model uncertainty is larger than that associated with the choice of hydrological model. Although results for the different GCMs demonstrate both increases and decreases in mean discharge (runoff for Mac-PDM.09), the direction of change simulated by each of the hydrological models for a particular gauging station and scenario is predominantly the same (differing for only five out of 42 gauging station/GCM combinations).

[1] My contribution to this paper was the development of the MIKE SHE model of the Mekong which provided the discharge projections to which the ERFA method was applied. I contributed some of the text, a table summarising the MIKE SHE model and general editing.

Where the direction of the mean river flow climate change signal differs between hydrological models, the magnitude of change is relatively small. Where increases occur, the largest changes are consistently associated with Mac-PDM.09. This is most evident at upstream gauging stations. The HadCM3 GCM, in particular, results in much larger changes for the GHM compared to the two catchment models.

Despite these differences, there are similarities in the distribution of runoff changes through the year simulated by the three hydrological models for each of the seven GCM scenarios. Many of the changes in these distributions simulated by MIKE SHE for the climate change scenarios are replicated by Mac-PDM.09. Similarities in the seasonal flow changes from the SLURP model and both MIKE SHE and Mac-PDM.09 are also evident. In particular, common features occur in the results for lower gauging stations, where the influence of the earlier rise in the annual hydrograph in the far north that is simulated by SLURP, but less so by MIKE SHE and Mac-PDM.09, has diminished.

Quantification of the relative uncertainty associated with choice of GCM and hydrological model can be provided using the approach of Gosling *et al.* (2011), which involves calculating the absolute differences in projected percentage change in mean discharge between the different GCMs and hydrological models. For five gauging stations, Table 4.14 summarises the inter-GCM range in percentage change in mean discharge from each of the hydrological models, as well as the maximum inter-hydrological range for any GCM for each of the three model pairings. The greatest absolute differences in the mean annual discharge (runoff) climate change signal between any two GCMs for the 2 °C scenarios for Pakse as simulated by MIKE SHE, SLURP and Mac-PDM.09 are 28.1%, 24.3% and 31.6%, respectively. In comparison, the largest absolute MIKE SHE–SLURP difference in the climate change signal for this station for any GCM is 3.6%. The corresponding figures for MIKE SHE–Mac-PDM.09 and SLURP–Mac-PDM.09 comparisons are 8.1% and 10.0%, respectively. This suggests that the maximum GCM-related uncertainty is around three times larger than that associated with choice of hydrological model. However, if Mac-PDM.09 is excluded from the analysis, the maximum GCM-related uncertainty at this station is more than six times larger than the maximum inter-hydrological model uncertainty.

Table 4.14. Summary of inter-GCM and inter-hydrological model related uncertainty in projected percentage change in mean discharge for the 2 °C, seven GCM scenarios. Top: absolute inter-GCM range of simulated percentage for each of the three hydrological models at five stations. Bottom: Maximum inter-hydrological model range for any GCM, for each of the three model pairings. The average column is the average taken across the stations in the respective row.

Results from the three hydrological models, for the 2 °C prescribed warming scenario, from seven GCMs							
Units: %		Chiang Saen (a)	Vientiane (d)	Pakse (f)	Phnom Penh (j)	Ubon (l)	Average
Inter-GCM range of change in mean Q:	MIKE SHE	32.5	33.6	28.1	22.5	37.6	30.9
	SLURP	18.8	-	24.3	-	23.0	22.0
	Mac-PDM.09	68.2	52.2	31.6	27.1	33.9	42.6
Max. inter-hydrological model range for a single GCM:	M.SHE–SLURP	11.8	-	3.6	-	7.9	7.8
	M.SHE–Mac	35.7	23.7	8.1	5.7	7.3	16.1
	SLURP–Mac	38.6	-	10.0	-	10.9	19.8

The analysis of Gosling *et al.* (2011) was limited to Pakse, the furthest downstream gauging station simulated by SLURP. By extending the inter-hydrological model analysis to other stations, it is possible to identify spatial differences in the relative uncertainty due to choice of GCM and hydrological model. For downstream gauging stations (Phnom Penh and Ubon), the absolute differences in the climate change signal for the different hydrological models for any GCM are similar to those for Pakse. Further upstream, however, differences between results for the two catchment models and Mac-PDM.09 are larger. At Chiang Saen, the largest absolute MIKE SHE–SLURP difference in the climate change signal for any GCM is 11.8%. The corresponding figures for comparisons between MIKE SHE–Mac-PDM.09 and SLURP–Mac-PDM.09 are 35.7% and 38.6%. These are larger than the absolute differences in climate change signal between any two GCMs simulated by MIKE SHE and SLURP (32.5% and 18.8%, respectively), but less than the largest inter-GCM range for Mac-PDM.09 (68.2%). Inter-hydrological model range in climate change signal when comparing catchment and global models is therefore sometimes of a similar or even larger magnitude than that associated with different GCMs. This result is predominantly due to the large increases in mean runoff simulated by Mac-PDM.09 for three scenarios, and in particular HadCM3. Excluding this GCM from the inter-hydrological model comparisons lowers the largest absolute difference in

mean discharge climate change signal for any GCM to 11.1% and 13.6% for MIKE SHE–Mac-PDM.09 and SLURP–Mac-PDM.09, respectively. Exclusion of HadCM3 also lowers the inter-GCM range of change for Mac-PDM.09 to 43.3%. As noted above, the direction of change for each GCM is, in most cases, the same for the three hydrological models. On average (across the gauging stations), GCM-related uncertainty for percentage change in mean discharge is more than five times greater than inter-hydrological model uncertainty.

Differences between results of Mac-PDM.09 and the two catchment models are especially evident for the 1–6 °C, HadCM3 GCM scenarios and has implications for direction of change in mean runoff. Both MIKE SHE and Mac-PDM.09 simulate increases in mean discharge/runoff at upstream gauging stations (with increases also predicted by SLURP at Chiang Saen). Towards the downstream end of the catchment, the two models display the opposite direction of change, with the magnitudes almost mirroring one another (small increases for Mac-PDM.09, declines of equal magnitude for MIKE SHE). The much larger upstream increases simulated by Mac-PDM.09 effectively drown out the influence of declining contributions from tributaries in the southern part of the catchment that are common to all three hydrological models. As such, differences between the downstream results for the two catchment hydrological models and Mac-PDM.09 for HadCM3 are a result of the spatially variable changes in projected climate: relatively large (compared to other GCMs) upstream increases in precipitation and progressively larger reductions in precipitation in a downstream direction. Inter-hydrological model differences in the temporal pattern of monthly runoff changes are also notable for the 1–6 °C, HadCM3 GCM scenarios. Whilst both MIKE SHE and Mac-PDM.09 display increases in peak monthly runoff (as well as through most of the year) at Chiang Saen, MIKE SHE displays reductions in peak flows at and downstream of Nakhon Phanom. This pattern is also exhibited by SLURP at Pakse. In contrast, Mac-PDM.09 only simulates reductions in peak flows at Phnom Penh, the most downstream gauging station. Similar to changes in mean runoff, this is a result of the much larger increases in peak runoff simulated by Mac-PDM.09 upstream. This counteracts the effect of reductions in precipitation during the height of the wet season over much of the Lower Mekong Basin.

In contrast to the HadCM3 scenarios, differences in the spatial and seasonal pattern of changes between the catchment models and the GHM are smaller where a predominantly uniform change in climate is projected by a GCM (increasing precipitation across the catchment: e.g. CCCMA, MPI and NCAR; declining precipitation over all, or most, sub-catchments: e.g. CSIRO, ISPL). Results from this study suggest that although the GHM may provide a useful tool in assessing likely changes in runoff at the individual catchment scale, care should be taken in situations such as those presented by the HacCM3 scenarios where spatially variable climate change signals are projected for a catchment. Differences in modelled hydrological response from linear changes in monthly climate introduce uncertainty into the identification of thresholds for ''dangerous climate change''.

Although a precise identification of the reasons for the differences in climate change signals from the three hydrological models is difficult due to their inherently different structures and process representations (Table 4.6), it is possible to highlight some factors that may influence the different responses of simulated discharge/runoff. For example, the previously noted greater amplitude of the annual runoff cycle simulated by Mac-PDM.09 for the baseline and each scenario when compared to results from MIKE SHE (and, where available, SLURP) is probably partly due to the absence of routing of runoff between cells within Mac-PDM.09 (Gosling and Arnell, 2011). Consequently, runoff generated in the far north of the catchment is included within the total runoff for that month at a gauging station that may be hundreds or thousands of kilometres downstream. In addition, the absence of a catchment-specific calibration of Mac-PDM.09 will most likely have impacted results.

Other differences may result from the spatial resolution and distribution of process computation. For example, the MIKE SHE model undertakes process calculations, with the exception of the saturated zone (for which the linear reservoirs are employed), for all cells within the 10 km × 10 km computational grid. The spatial distribution of catchment characteristics at this scale is therefore represented, and there is the potential for exchange between grid cells though processes such as overland flow. Similarly, water balance calculations within Mac-PDM.09 are undertaken for each 0.5° × 0.5° cell although, as described above, each cell is treated

as an independent catchment and there is no exchange between neighbouring cells. SLURP, in contrast, evaluates vertical balances for a relatively small number of elements, with results being aggregated at the sub-catchment scale.

Linked to the approach used to distribute process calculations and catchment characteristics is the distribution of meteorological inputs. MIKE SHE and SLURP employed the same sub-catchments to define the distribution of meteorological inputs (albeit with spatial variation in both models being induced through the inclusion of lapse rates), whereas Mac-PDM.09 employed the 0.5° × 0.5° grid used within the gridded meteorological datasets. As discussed above, the latter is more likely to represent true spatial variability over the catchment, especially for large sub-catchments such as the Lancang. The application of alternative approaches to distribute meteorological inputs is investigated in Chapter 5.

A potential cause of Mac-PDM.09 simulating larger increases in mean runoff at upstream gauging stations for the HadCM3 1–6 °C scenarios, as well as for the 2 °C scenarios for other GCMs for which such increases occur, may be related to the PET methods employed by the three hydrological models. Mac-PDM.09, which was not specifically calibrated for the Mekong, uses Penman–Monteith PET. In contrast, Kingston *et al.* (2011) selected Linacre PET for the SLURP model and so this method was employed in the MIKE SHE model developed herein. Linacre PET was used in SLURP following unsuccessful calibration attempts using Penman–Monteith PET. The use of the latter PET method resulted in significant over-estimation of discharge. Evaluation of mean annual Penman–Monteith PET using the CRU TS 3.0 dataset for meteorological input sub-catchments 1–11 shows that on average baseline Penman–Monteith PET is 69.4% of Linacre PET. The mean increase in annual Linacre PET for the 2 °C HadCM3 scenario for these sub-catchments is 14.0% compared to 8.4% for Penman–Monteith. This pattern is repeated for the other scenarios. Therefore, although Mac-PDM.09 is responding to the same changes in precipitation, PET scenario increases are smaller. It is likely that this results in larger increases in mean Mac-PDM.09 runoff for those scenarios in which precipitation increases. Alternative MIKE SHE models of the Mekong using different PET methods are developed and used in Chapter 5 to evaluate this additional source of uncertainty in climate change projections of Mekong River discharge.

Other factors that may contribute to the greater increases in runoff simulated by Mac-PDM.09 could relate to omissions from the model that are identified by Gosling and Arnell (2011). For example, as with other GHMs, Mac-PDM.09 does not simulate evaporation of water from overland flow that infiltrates downslope and does not account for evaporation from ponded water/depressions. The fact that the most exaggerated discharge increases occur at the most upstream gauging station (Chiang Saen) could indicate that they partly relate to the simulation of snow accumulation/melting, or the partitioning of snowmelt into runoff or evapotranspiration. Differences between MIKE SHE and SLURP in the seasonal pattern of discharge changes are also greatest at Chiang Saen, again indicating that this may relate to the simulation of snow accumulation and melting.

Overall, this part of the thesis has demonstrated that GCM-related uncertainty in climate change projections for the Mekong is predominantly larger than that related to the use of three alternative hydrological models. The latter, however, is not negligible, and in some cases hydrological model related-uncertainty is of a similar magnitude to GCM-related uncertainty.

4.9. Summary

In this chapter, a MIKE SHE model of the Mekong has been developed using, where appropriate, the same data as the earlier SLURP model of the catchment. This model was subsequently employed for climate change simulation using the same scenarios as those employed in a previous investigation featuring the SLURP model. Inter-GCM uncertainty was explored using of a set of climate scenarios based on a 2 °C increase in global mean temperature as simulated by seven GCMs. Prescribed warming uncertainty was investigated using a scenario set based on increases of 1–6 °C for a single GCM. Inter-hydrological model uncertainty was assessed through comparison of river flow projections simulated for the same two sets of climate change scenarios by MIKE SHE, SLURP and Mac.PDM.09.

Overall, GCM structure was found to be the dominant source of uncertainty with a prevailing influence on the direction, magnitude and spatial pattern of changes

simulated. However, results demonstrate that hydrological model-related uncertainty should not be ignored. Although the direction of change in mean runoff for any GCM from the 2 °C scenario set is predominantly the same across the hydrological models, choice of hydrological model can have a considerable impact upon the magnitude of simulated changes. Furthermore, choice of hydrological model can affect the seasonality of projected changes. Results of the prescribed warming scenarios demonstrate that spatial differences and different patterns of changes in climate variables through the year can result in non-linear patterns of change in discharge with the magnitude of climate forcing. The magnitude of inter-hydrological model differences, and hence uncertainty, generally increased with the magnitude of climate forcing.

GHMs such as Mac-PDM.09 are a useful tool for assessing impacts of climate change on runoff at the global to regional scale (e.g. Hagemann *et al.*, 2013; Gosling and Arnell, 2016). They can also be applied at the catchment scale, as demonstrated here and, may be particularly useful for quantifying climate model uncertainty in situations where a catchment model is not available and time or resources are inadequate to develop such a model. However, in the case of the Mekong, larger increases in upstream runoff for Mac-PDM.09 have implications for the direction of change further downstream, especially for scenarios (in particular HadCM3) where the nature of projected changes in climate varies across the catchment. This indicates that care should be taken in some circumstances such as the application of the model to individual sub-catchments with large distinct spatial variations in baseline or projected future climate. Moreover, the application of any GHM to the sub-catchment scale should be approached carefully, since these models are inherently intended for application across larger spatial domains and tend not to be calibrated for specific catchments.

In the next chapter, alternative MIKE SHE models of the Mekong are developed from the model described in this chapter, in order to investigate sources of uncertainty in hydrological climate change projections associated with: i) choice of PET method, ii) spatial distribution of meteorological inputs and iii) use of alternative precipitation data during model calibration/validation and baseline simulation.

Chapter 5

Uncertainty associated with meteorological inputs

5.1. Introduction

This chapter explores several sources of uncertainty in hydrological projections under climate change associated with the meteorological inputs used to drive the hydrological model. The first source of uncertainty that is investigated is the choice of PET method (Section 5.2). The second source of uncertainty is that associated with the spatial distribution of meteorological inputs within the hydrological model (Section 5.3). The third source of uncertainty considered in this chapter is the use of different precipitation data during hydrological model calibration, validation and baseline simulation (and which is also perturbed for climate scenario simulations; Section 5.4). All three sources of meteorological input uncertainty are investigated using the 2 °C, seven GCM climate scenario set employed in the previous chapter. Use of this consistent scenario set enables an assessment of the relative magnitude and nature of these different meteorological input-related sources of uncertainty, as well as GCM-related uncertainty and inter-hydrological model uncertainty, which were investigated in Chapter 4.

5.2. An assessment of PET method-related uncertainty

In order to assess the nature and magnitude of uncertainty in discharge projections under climate change associated with the use of alternative PET methods, the MIKE SHE model developed in the previous chapter was recalibrated for five additional PET methods. Section 5.2.1 details the PET methods employed, whilst Section 5.2.2 describes the model calibration/validation procedure. The generation of climate scenario data for each of the models is described in Section 5.2.3. Finally, Section 5.2.4 presents the results of this uncertainty impact assessment. Some of the work undertaken for this section was incorporated in Thompson *et al.* (2014a).[1] However, consistent with the MIKE SHE model developed in the previous chapter, the models

[1] My contribution to this paper was the recalibration of three MIKE SHE models for alternative PET methods. I undertook ~45% of the analysis and contributed ~45% of the text.

have subsequently been revised, and the modelling results therefore differ from those presented in the paper, although they are very similar. A more comprehensive analysis is provided herein.

5.2.1. Alternative PET methods – model development

In addition to the temperature-based Linacre (LN) PET (Dent *et al.*, 1988; Schulze, 1989), five alternative methods were employed to calculate PET. These were selected to represent a sample of the methods commonly used within hydrological models and reflect varying data requirements. Table 2.6 summarises the data requirements of each method and also provides the equation and corresponding reference used for each PET method.[1] Blaney–Criddle (BC) and Hamon (HM) are both based on temperature and day-length, with the latter being employed within the WBM global hydrological model (Vörösmarty *et al.*, 1998). Hargreaves–Samani (HS) uses mean, minimum and maximum temperature and extra-terrestrial solar radiation, which can be calculated based on latitude rather than requiring observed data. HS PET is often used in situations where data are insufficient to calculate Penman or Penman–Monteith (Allen *et al.*, 1998). These last two methods incorporate the meteorological variables that control evapotranspiration (net radiation, temperature, wind speed and vapour pressure) and are used in many hydrological models including the Mac-PDM global model (Arnell, 1999). In the absence of detailed land cover information required to calculate crop reference ET according to the FAO-56 Penman–Monteith equation (Allen *et al.*, 1998), the Penman (1948) PET (PN) method was used. Finally, Priestley–Taylor (PT) provides a simplification of the Penman/Penman–Monteith method based on net-radiation and temperature and is used in the WaterGAP hydrological model (Alcamo *et al.*, 2007).

Data for each PET method for the calibration/validation period (1961–1998) were derived from the CRU TS 3.0 dataset with the exceptions of cloud cover, for which CRU TS 2.1 was used and wind speed, for which climatological values were used (as done so by Kingston *et al.*, 2009), since wind speed data are not available within the CRU dataset. As with Linacre PET (Section 4.2.6.2), monthly PET data were derived

[1] Sub-catchment averaged PET data for the Mekong were generated by Dr Daniel Kingston.

for each SLURP meteorological input sub-catchment and then evenly distributed through each month to provide daily data.

Using the MIKE SHE model of the Mekong that employed LN PET as a base model, time series of PET from each method were specified within separate MIKE SHE models so that, including the original model employing LN PET, six hydrological models were defined. The other baseline meteorological inputs (precipitation and temperature) were not changed from those employed in the LN PET MIKE SHE model which formed the basis of the research described in Chapter 4.

5.2.2. Model calibration and validation

The same calibration/validation procedures as described in Section 4.4 for the LN MIKE SHE model were employed for each of the additional models, with the exception that only manual parameter optimisation was employed. Automatic calibration was not undertaken prior to manual calibration, since it was found for the LN model that automatic calibration was unable to achieve as good a model performance as manual calibration. The same gauging stations and performance measures were employed. Likewise, calibration of each model was undertaken in a downstream sequence, with observed and simulated discharge being aggregated to monthly mean flow for the calculation of NSE and *r*, due to the disconnect between daily meteorological inputs derived from monthly totals (mean for temperature) using the Mac-PDM weather generator and observed daily discharge. The aim of calibration was to achieve equally good performance for each model.

The calibration parameters were the time constants of the saturated zone's baseflow reservoirs, and in sub-catchments with large elevation ranges, the precipitation lapse rate. As with the LN MIKE SHE model, it was necessary to incorporate a dead storage proportion for the baseflow reservoirs in a limited number of sub-catchments (discussed below). The interflow reservoir time constants were kept the same as in the LN model, since this permitted the achievement of satisfactory model performance. The same degree-day snowmelt coefficient (1.75 mm/°C/day) and temperature lapse rate over the Lancang (-0.51 °C/100 m) employed in the LN model were used in the five other models.

Separate calibration of each of the six MIKE SHE models is a noteworthy aspect of this investigation. As discussed in Section 2.6.6.1, previous studies of uncertainty in climate change impacts on discharge associated with PET method have avoided the issue of different baseline PET values affecting model performance and parameterisation by developing a baseline hydrological model calibrated using a single PET method. The model may subsequently be forced using PET data derived through perturbation of the baseline PET using delta factors obtained using different PET methods (e.g. Kay and Davies, 2008). Other studies (e.g. Bae *et al.*, 2011) have optimized their baseline hydrological model to a single PET method and then implemented different PET methods without further optimization. Both methods necessitate the selection of a particular PET method for the baseline, with choice of that method over another representing a further source of uncertainty. Although this has the advantage of meaning that baseline-scenario changes in discharge can not be influenced by differences in parameter values, it means that a non-optimal hydrological model is used for all but one of the PET methods investigated. Furthermore, this approach, termed a static input-related sensitivity approach by Andréassian *et al.* (2004), involves the implicit assumption that the calibration parameter values obtained using a single PET method are the 'true' catchment-specific values. Conversely, the dynamic sensitivity approach employed here explicitly acknowledges that calibrated parameter values are dependent upon choice of baseline PET data. This approach has been less commonly employed, although there are exceptions (e.g. Remesan and Holman, 2015).

5.2.3. Simulation of climate change

For climate scenario simulation, the sub-catchment averaged precipitation and temperature data generated for the 2 °C, seven GCM scenarios described in the previous chapter were again employed in the six MIKE SHE models employing alternative PET data. Scenario PET datasets for the five new methods were generated using the same technique as previously employed for LN PET, using the method-specific meteorological variables derived using the ClimGen spatial scenario generator. As for the baseline period, PET data were spatially averaged at the meteorological input sub-catchment scale and evenly distributed on a daily basis through each month. Scenario PET was subsequently specified within the MIKE SHE

models calibrated using the respective PET method. In this way a total of 42 scenario model runs were simulated (seven GCMs for each of the six hydrological models).

5.2.4. Results

This section presents the results of the investigation into the implications of using alternative PET methods for discharge projections for the Mekong River. Section 5.2.4.1 presents sub-catchment average baseline PET for the Mekong catchment produced using the six alternative PET methods. Calibration and validation results of the six MIKE SHE models each employing a different PET method are provided in Sections 5.2.4.2 and 5.2.4.3, respectively. In Section 5.2.4.4 the scenario climate data are presented. Finally, in Section 5.2.4.5, the climate change discharge projections of the six MIKE SHE models are presented for comparison.

5.2.4.1. Baseline PET

Mean annual PET for the 1961–1990 baseline period for the six PET methods is shown for eight representative sub-catchments in Table 5.1 and for 11 sub-catchments in Figure 5.1. The relative magnitude of PET from the different methods follows a general, but not wholly consistent, pattern in each sub-catchment. PT PET is the lowest in all sub-catchments except the Lancang, for which it is the second lowest (and HM the lowest). In upstream sub-catchments LN produces the largest annual PET followed by BC. Further downstream (from Mekong 2) this order is reversed (Figure 5.1), whilst for the lowest sub-catchment (Mekong 3), HM PET is the second highest. With the exception of the Lancang, Nam Ou and Mekong 3, HM PET provides the third highest totals in all sub-catchments. Annual HS PET is generally very similar to PN PET (average absolute difference: 17.7 mm), which is to be expected given that HS is the preferred alternative to PN (or Penman-Monteith, Allen *et al.*, 1998). With the exception of the three uppermost sub-catchments (Lancang, Nam Ou and Nam Ngum) HS and PN are both lower than BC, HM and LN, but higher than PT PET.

Table 5.1. Mean annual baseline potential evapotranspiration for each PET method for eight representative SLURP sub-catchments within the Mekong catchment.

PET method	Lanc. (1)	Mek. 1 (4)	Chi (5)	Mun (6)	Mek. 2 (8)	Se Kong (9)	Sre Pok (10)	Mek. 3 (11)
Blaney-Criddle (BC)	1339	1923	2034	2059	2003	1944	1924	2042
Hamon (HM)	779	1633	1862	1907	1778	1656	1620	1868
Hargreaves-Samani (HS)	1131	1517	1696	1727	1565	1490	1478	1654
Linacre (LN)	1767	1924	2365	2338	1814	1730	1697	1771
Penman (PN	1112	1511	1715	1716	1586	1508	1481	1693
Priestley-Taylor (PT)	955	1353	1469	1489	1393	1375	1389	1576

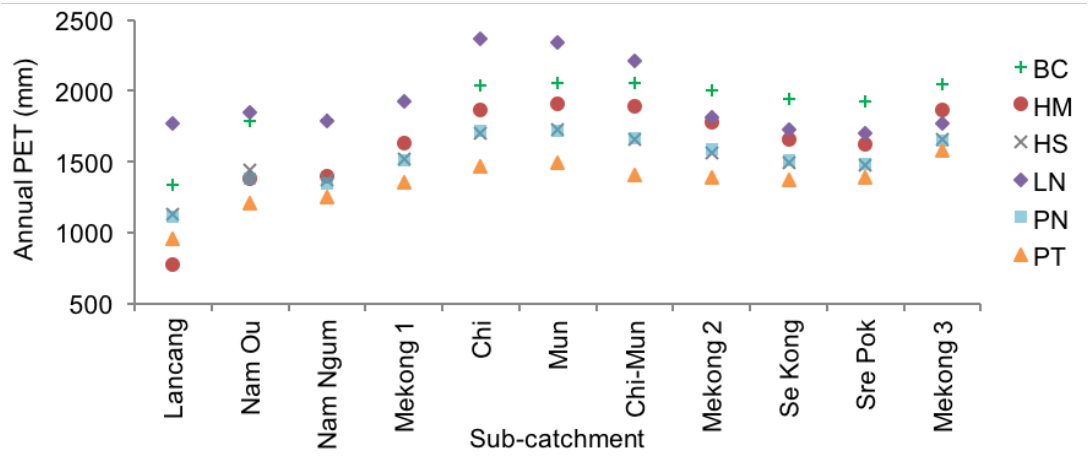

Figure 5.1. Mean annual baseline potential evapotranspiration for each PET method for 11 SLURP sub-catchments within the Mekong catchment.

There is a relatively consistent spatial pattern in annual PET. With the exception of LN PET, the lowest totals occur over the Lancang. This is unsurprising given its higher elevation and lower temperatures (mean temperature is 11.2 °C compared to 24.3 °C for Mekong 1). Annual PET increases along the Mekong (Lancang – Mekong 1 – Mekong 2 – Mekong 3) for all methods except LN (highest PET is for Mekong 1). Increasing PET in this direction echoes higher temperatures, although beyond Mekong 1 temperature variations are relatively small, with a mean temperature of 26.0 °C for Mekong 2 and 26.9 °C for Mekong 3 (see Table 4.10). The Chi and the Mun, which out of all 11 sub-catchments display the highest mean monthly temperatures throughout March–October, experience comparable mean annual PET totals to the Mekong 3 sub-catchment for most methods. The range in annual PET totals for a given sub-catchment varies between 988.1 mm (for Lancang) and 466.6 mm (Mekong 3).

Mean monthly PET derived for 1961–1990 using the six methods is shown in Figure 5.2 for four representative sub-catchments. Generally higher PET for three of the temperature-based methods (BC, HM and LN) is demonstrated, except for the Lancang in the case of HM. Lower PET occurs for the HS, PN and PT methods. Some methods (BC, HM) have a consistent June–August peak whilst in others (e.g. PN, PT) the seasonal peak is earlier (March–April). Seasonality declines in a downstream direction. For the Lancang, maximum monthly PET is, on average, 2.4 times the minimum. This reduces to 1.6 for Mekong 1 and 1.4 for Mekong 3.

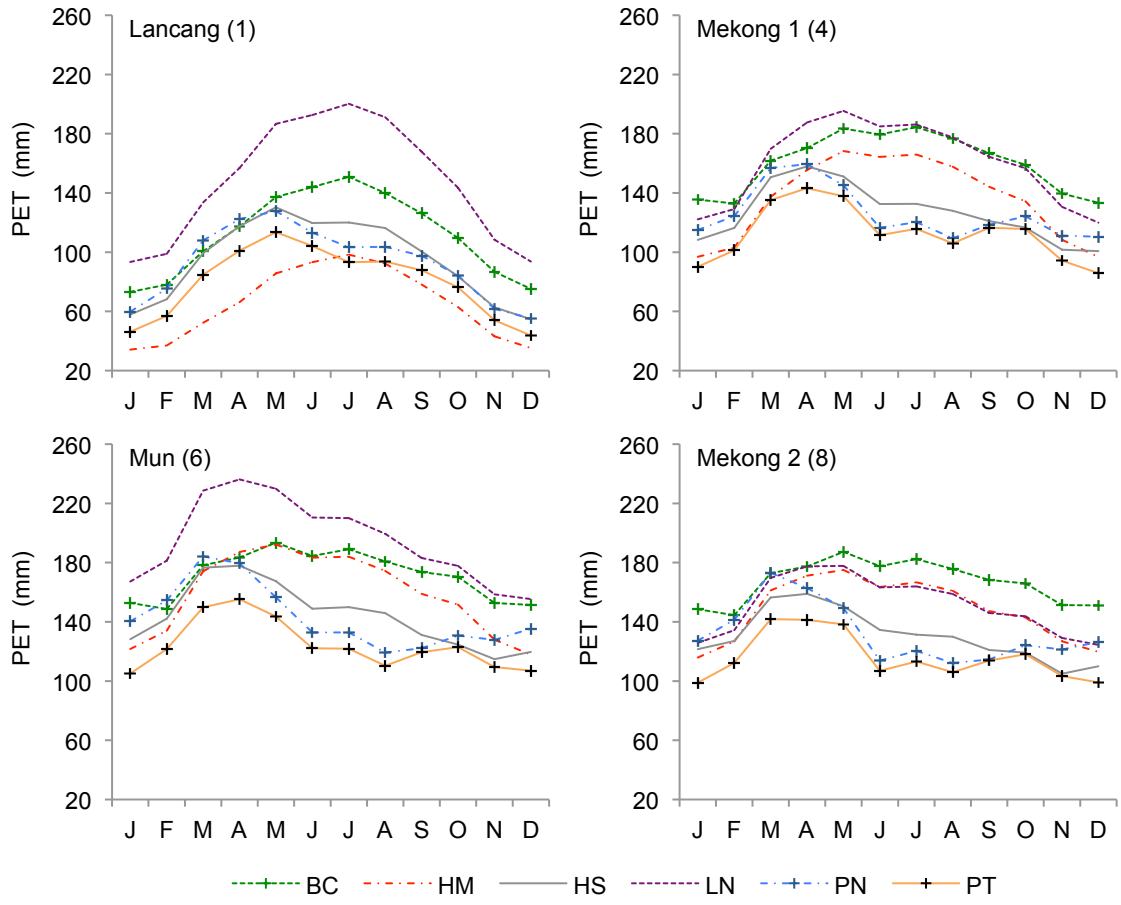

Figure 5.2. Mean monthly baseline (1961–1990) potential evapotranspiration for each PET method for four representative sub-catchments.

5.2.4.2. Model calibration

For the six hydrological models employing different PET methods, Table 5.2 summarises the optimised values of the baseflow time constants, precipitation lapse rates in sub-catchments with large elevation ranges and, for some sub-catchments, dead storage proportions.

Table 5.2. Final calibration parameter values for the six MIKE SHE models employing different PET methods. Numbers in column headings refer to the MIKE SHE linear reservoir sub-catchments identified in Figure 4.4.

Parameter	PET	1	2	3	4	5	6	7	8	9	10	11	12	13	14	15
Precip. lapse rate (%/100 m)	BC	1.15	3.00	3.00	3.95	0.00	9.90	0.00	0.00	1.82	0.00	0.00	0.00	0.00	0.00	0.00
	HM	0.21	0.57	0.57	0.51	0.00	8.20	0.00	0.00	0.00	0.00	0.00	0.00	0.00	0.00	0.00
	HS	0.71	1.90	1.90	0.70	0.00	5.95	0.00	0.00	0.00	0.00	0.00	0.00	0.00	0.00	0.00
	LN	1.80	4.80	4.80	5.35	0.00	8.49	0.00	0.00	4.47	0.00	0.00	0.00	0.00	0.00	0.00
	PN	0.61	1.63	1.63	0.00	0.00	4.60	0.00	0.00	0.00	0.00	0.00	0.00	0.00	0.00	0.00
	PT	0.40	1.10	1.10	0.00	0.00	3.60	0.00	0.00	0.00	0.00	0.00	0.00	0.00	0.00	0.00
Time constant for baseflow reservoir 1 (days)	BC	120	120	120	60	110	65	110	175	135	70	20	40	20	20	140
	HM	100	100	100	55	130	50	120	180	130	60	30	50	30	30	100
	HS	100	100	100	55	125	70	100	170	135	55	50	55	65	70	115
	LN	115	115	115	70	90	55	85	175	105	55	55	30	20	20	105
	PN	115	115	115	75	125	45	120	180	140	85	65	55	60	60	120
	PT	105	105	105	85	140	43	122	185	145	70	65	50	60	60	110
Dead storage fraction for baseflow reservoir 1	BC	0.00	0.00	0.00	0.00	0.00	0.00	0.00	0.08	0.00	0.00	0.00	0.00	0.00	0.00	0.00
	HM	0.00	0.00	0.00	0.00	0.00	0.00	0.00	0.20	0.00	0.00	0.00	0.00	0.00	0.00	0.00
	HS	0.00	0.00	0.00	0.00	0.00	0.00	0.00	0.37	0.00	0.00	0.00	0.00	0.00	0.00	0.00
	LN	0.00	0.00	0.00	0.00	0.00	0.00	0.00	0.00	0.00	0.00	0.00	0.00	0.00	0.00	0.00
	PN	0.00	0.00	0.00	0.00	0.00	0.00	0.00	0.46	0.00	0.00	0.00	0.00	0.00	0.00	0.00
	PT	0.00	0.00	0.00	0.00	0.00	0.00	0.00	0.44	0.00	0.00	0.00	0.00	0.00	0.00	0.00
Time constant for baseflow reservoir 2 (days)	BC	750	640	880	580	640	160	130	400	190	140	60	350	120	120	450
	HM	725	630	890	530	600	150	200	440	190	120	70	500	100	100	400
	HS	760	655	900	580	850	150	180	300	195	135	90	550	160	170	600
	LN	740	645	880	520	600	90	120	530	190	135	80	300	110	110	390
	PN	745	690	890	550	610	160	230	380	180	200	100	330	285	285	380
	PT	770	680	910	545	650	170	240	450	155	220	110	400	300	300	450
Dead storage fraction for baseflow reservoir 2	BC	0.00	0.00	0.00	0.00	0.38	0.00	0.00	1.00	0.00	0.00	0.00	0.00	0.00	0.00	0.00
	HM	0.00	0.00	0.00	0.00	0.55	0.00	0.00	0.96	0.05	0.00	0.00	0.00	0.00	0.00	0.00
	HS	0.00	0.00	0.00	0.00	0.55	0.00	0.00	0.96	0.44	0.00	0.00	0.00	0.00	0.00	0.00
	LN	0.00	0.00	0.00	0.00	0.30	0.00	0.00	0.90	0.00	0.00	0.00	0.00	0.00	0.00	0.00
	PN	0.00	0.00	0.00	0.00	0.80	0.00	0.00	0.93	0.59	0.00	0.00	0.00	0.00	0.00	0.00
	PT	0.00	0.00	0.00	0.00	0.95	0.00	0.00	1.00	0.72	0.00	0.00	0.00	0.00	0.00	0.00

There is no consistency in the relative magnitudes of the baseflow time constants between the models. In contrast, models employing PET methods associated with the highest baseline PET required the largest precipitation lapse rates. For example, LN and HM PET provide the largest and smallest mean annual baseline PET over the Lancang and result in the largest (4.8%/100 m for sub-catchments 2 and 3) and smallest (0.57%/100) optimal precipitation lapse rates, respectively. As previously stated for the LN MIKE SHE model (Section 4.7.1) the precipitation lapse rates values in Table 5.2 are within the range of those previously reported in the literature (e.g. Immerzeel *et al.*, 2012a,b). Variable lapse rates for sub-catchments with large elevation ranges mitigate the differences between PET methods. It was ensured that

for each model, the ratio between the precipitation lapse rate over the upper Lancang and over the mid to lower Lancang was kept the same as in the LN MIKE SHE model.

Observed and simulated mean monthly discharges from the six calibrated MIKE SHE models for the baseline period are shown in Figure 5.3. The very narrow range of simulated river regimes illustrates the very similar performance of the models. Good model performance, especially for the ten gauging stations on the main Mekong, and similarity between the six models is further demonstrated in Table 5.3, which summaries the model performance statistics for the calibration (and validation – discussed below) period.

Across the six models, out of the 24 Dv and NSE model performance statistics for each model, between 18 (for the PT model) and 21 (for BC, HM and LN) are classified as ''excellent'' according to the scheme of Henriksen *et al.* (2008). As described in Section 4.7.1, this scheme was originally based on comparisons of daily observed and simulated data and higher NSE values are to be expected when aggregating to monthly mean discharges. Increasing the lower boundary of the ''excellent'' class for NSE to 0.9 still results in two of the models (PN and PT) being classified as ''excellent'' for all the stations on the main Mekong, with the remaining models having eight or nine stations classed as "excellent". At Phnom Penh, a station with a shorter observed discharge record, NSE is classified as ''excellent'' for all six models. However, the overestimation of mean discharge results in Dv being classed as ''very good'' (two models) or ''fair'' (four models). For all six MIKE SHE models, r is ≥ 0.94 for ten of the 12 stations (i.e. those on the main Mekong), indicating strong correlation between observed and simulated monthly discharges.

The two stations with lower values of r (Yasothon and Ubon) also have lower values of NSE that are, in most cases, classified as ''fair'' (''poor'' for Yasothon for LN). Issues experienced during calibration of these stations in the LN model (Section 4.7.1) were repeated for the five furthers models; in each case, it was not possible to raise peak discharges for these stations without also raising discharge

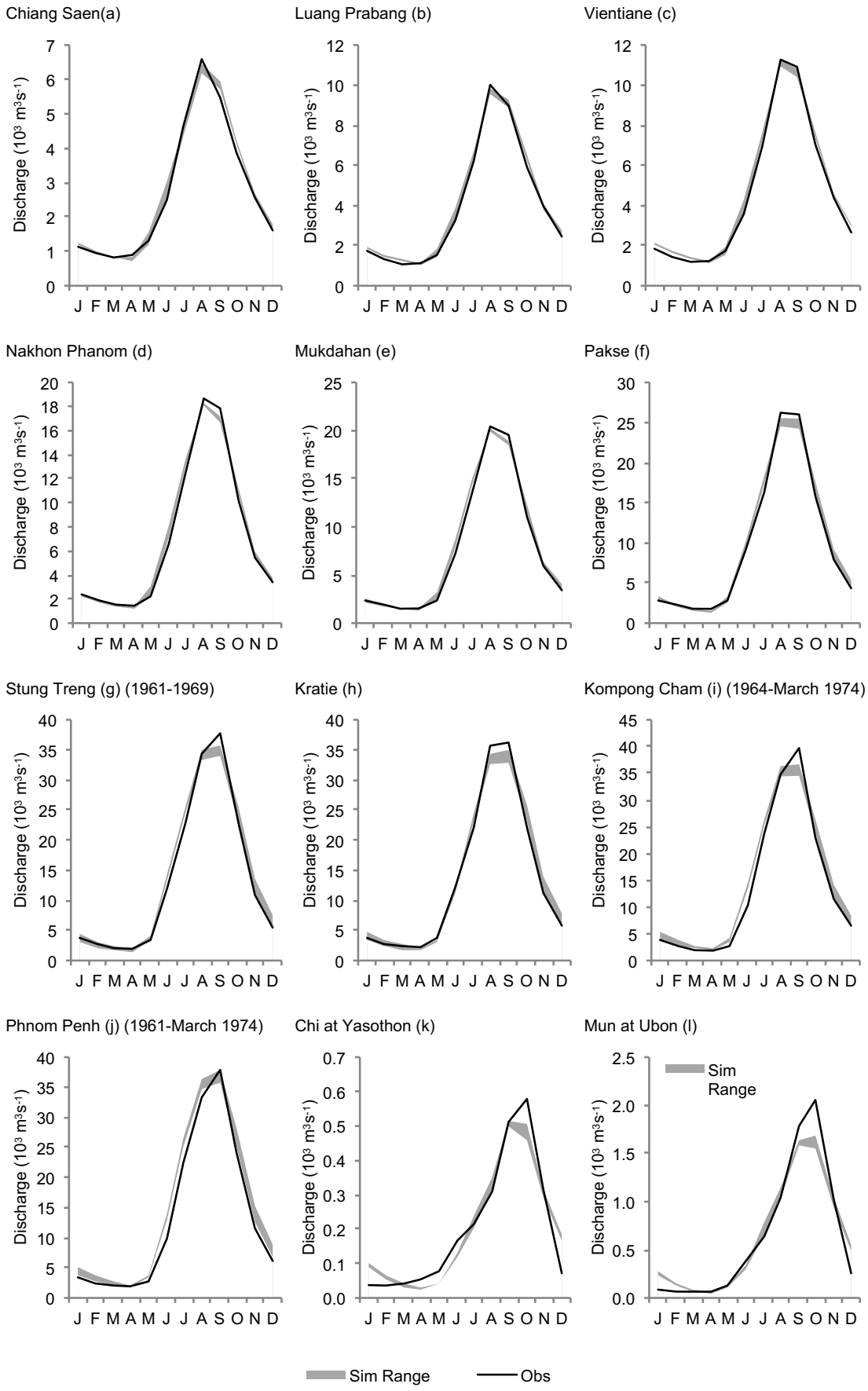

Figure 5.3. Observed and range of simulated river regimes from the six MIKE SHE models for all 12 gauging stations within the Mekong catchment for the calibration period (1961–1990 unless indicated otherwise). (Note different y-axis scales.)

Table 5.3. Range of model performance statistics from the six MIKE SHE models for twelve gauging stations within the Mekong catchment for the calibration (1961–1990 unless stated otherwise) and validation (1991–1998 unless stated otherwise) periods. NSE and r are based on mean monthly discharges.

Station	Period	Dv (%)+		NSE*		r#
Chiang Saen (a)	Cal	0.86 to 2.86	☆☆☆☆☆	0.88 to 0.90	☆☆☆☆☆	0.94 to 0.95
	Val (1/91–6/97)	-7.60 to -3.55	☆☆☆☆/ ☆☆☆☆☆	0.77 to 0.79	☆☆☆☆	0.88 to 0.90
Luang Prabang (b)	Cal	0.94 to 4.95	☆☆☆☆☆	0.89 to 0.91	☆☆☆☆☆	0.94 to 0.95
	Val (1/91–12/97)	-2.90 to 0.68	☆☆☆☆☆	0.82 to 0.84	☆☆☆☆	0.91 to 0.92
Vientiane (c)	Cal	3.03 to 4.62	☆☆☆☆☆	0.90 to 0.92	☆☆☆☆☆	0.95 to 0.96
	Val (1/91–12/96)	0.00 to 3.60	☆☆☆☆☆	0.89 to 0.90	☆☆☆☆☆	0.94 to 0.95
Nakhon Phanom (d)	Cal	0.69 to 3.85	☆☆☆☆☆	0.90 to 0.92	☆☆☆☆☆	0.95 to 0.96
	Val (1/91–11/95)	-4.22 to 0.18	☆☆☆☆☆	0.89 to 0.91	☆☆☆☆☆	0.95 (all six)
Mukdahan (e)	Cal	0.31 to 4.12	☆☆☆☆☆	0.90 to 0.91	☆☆☆☆☆	0.95 to 0.96
	Val (1/91–12/95)	-0.49 to 3.33	☆☆☆☆☆	0.91 to 0.92	☆☆☆☆☆	0.96 (all six)
Pakse (f)	Cal	-2.44 to 3.82	☆☆☆☆☆	0.90 to 0.91	☆☆☆☆☆	0.95 (all six)
	Val	-1.48 to 4.72	☆☆☆☆☆	0.88 to 0.90	☆☆☆☆☆	0.94 to 0.95
Stung Treng (g)	Cal (1/61–12/69)	-0.78 to 6.84	☆☆☆☆☆/ ☆☆☆☆	0.93 to 0.94	☆☆☆☆☆	0.96 to 0.97
	Val (1/91–12/93)	-16.41 to -8.00	☆☆☆/ ☆☆☆☆☆	0.86 to 0.88	☆☆☆☆☆	0.94 to 0.95
Kratie (h)	Cal	-3.72 to 5.28	☆☆☆☆☆/ ☆☆☆☆	0.91 (all six)	☆☆☆☆☆	0.95 to 0.96
	Val	-3.66 to 4.18	☆☆☆☆☆	0.87 to 0.88	☆☆☆☆☆	0.93 to 0.94
Kompong Cham (i)	Cal (1/64–3/74)	1.23 to 9.89	☆☆☆☆☆/ ☆☆☆☆	0.93 (all six)	☆☆☆☆☆	0.96 to 0.97
	Val†	—		—		—
Phnom Penh (j)	Cal (1/61–3/74)	6.95 to 15.80	☆☆☆☆/ ☆☆☆	0.91 to 0.93	☆☆☆☆☆	0.97 (all six)
	Val†	—		—		—
Chi at Yasothon (k)	Cal	-1.46 to 0.68	☆☆☆☆☆	0.49 to 0.56	☆☆/☆☆☆	0.71 to 0.75
	Val (1/91–12/95)‡	9.12 to 20.16	☆☆☆☆/ ☆☆☆/☆☆	-0.39 to 0.19	☆	0.41 to 0.55
	Val (1/91–12/95)•	-13.74 to -9.78	☆☆☆/ ☆☆☆☆	0.436 to 0.548	☆☆/☆☆☆	0.676 to 0.753
Mun at Ubon (l)	Cal	-2.70 to 0.22	☆☆☆☆☆/ ☆☆☆☆	0.55 to 0.61	☆☆☆	0.74 to 0.78
	Val (1/91–12/93)‡	-3.83 to 3.25	☆☆☆☆☆	0.11 to 0.38	☆/☆☆	0.53 to 0.65
	Val (1/91–12/93)•	-30.63 to -15.79	☆☆/☆☆☆	0.533 to 0.616	☆☆☆	0.755 to 0.799

Performance indicator	Excellent ☆☆☆☆☆	Very good ☆☆☆☆	Fair ☆☆☆	Poor ☆☆	Very poor ☆
Dv	< 5%	5–10%	10–20%	20–40%	>40%
NSE	>0.85	0.65–0.85	0.50–0.65	0.20–0.50	<0.20

+ Percentage deviation in simulated mean flow from observed mean flow (Henriksen *et al.*, 2003).
* Nash–Sutcliffe coefficient (Nash and Sutcliffe, 1970). # Pearson correlation coefficient.
† Validation not possible due to absence of observations.
‡ Using UDel V1.01 precipitation. • Using UDel V1.02 precipitation for 1991–1998.

during the reasonably well-reproduced annual rise and recession. This would cause Dv to increase substantially. As in the case of the LN MIKE SHE model, calibration therefore focused on matching observed and simulated mean flow (i.e. Dv values close to 0), and hence annual contributions from these tributaries to the Mekong. Within the Chi sub-catchment, this consistently (for all six models) necessitated the use of dead storage terms within the MIKE SHE baseflow linear reservoirs (Table 5.2). A dead storage term was also consistently applied to the Mekong at Vientiane sub-catchment (linear reservoir sub-catchment 5), adjacent and to the north of the Chi sub-catchment.

As discussed for the LN model in Section 4.7.1, discharge overestimation prior to implementation of dead storage could result from elevated precipitation within the UDel dataset. In support of this, mean annual UDel precipitation totals for the Chi and Mun (1273.1 mm and 1314.5 mm, respectively), exceed reported estimates of 1000 mm or less over this region (e.g. Kite, 2001; MRC, 2010b). However, the case of the Mun is less straightforward. Use of dead storage was required in the Chi linear reservoir sub-catchment for all models. Conversely, dead storage was employed in the Mun in only four models (HM, HS, PN and PT), whilst for the remaining two (BC and LN) a precipitation lapse rate was used in order to achieve a Dv value close to that of the other models. BC and LN produce the highest PET totals over the Mun (Table 5.1; Figure 5.1; Figure 5.2). This suggests that PET is overestimated in this part of the catchment by these two methods. Nevertheless, the consistently poorer performance for all MIKE SHE models / PET methods at Yasothon and Ubon could indicate poor representativeness of the UDel precipitation data over the Khorat Plateau. The requirement for dead storage within the Mekong to Vientiane linear reservoir sub-catchment (sub-catchment 5) may also be linked to unrepresentative/elevated precipitation (see Section 4.7.1). Poorer performance on the Chi and Mun could also potentially relate to irrigation not being represented within the models. These sub-catchments contain extensive areas of irrigation, some dating back to the 1950s and 1960s (Kite, 2000; Floch and Molle, 2007).

As concluded for the LN model, the application of dead storage in these few sub-catchments is considered justified in order to match observed and simulated annual contributions to the main Mekong. Furthermore, the mean annual water balance

was assessed for all gauging stations along the main Mekong to ensure that dead storage was not an unduly large term. Change in subsurface storage (which includes both the saturated and unsaturated zones) is never more than 5% of precipitation (mean 1.5%) and 9% of actual evapotranspiration (mean 2.6%). Therefore, dead storage is a small component of the overall water balance, although it is inevitably larger in the Chi and Mun sub-catchments.

5.2.4.3. Model validation

Performance of the six MIKE SHE models for the validation period is generally good, although for some stations it is inferior to the calibration period (Table 5.3). NSE for the eight stations on the main Mekong is classified as either ''excellent'' or ''very good''. Relatively high values of *r* are achieved for these stations, although at some stations they are lower than those of the calibration period. Dv for stations on the main Mekong is generally classed as either ''excellent'' or ''very good'', although at Strung Treng (short observed records) values are classified as either ''very good'' (three PET methods) or ''fair'' (three methods). As suggested in Section 4.7.2, poorer representation of mean flows might relate to changes in land cover over time not being represented within the model. Despite these issues, performance of the six MIKE SHE models for the main Mekong still compares very favourably with previous models of the Mekong (e.g. Hapuarachchi *et al.*, 2008; Västilä *et al.*, 2010; Kingston *et al.*, 2011).

In comparison to stations on the main Mekong, model performance for the Chi and Mun tributaries is poor, although the short duration of observations (especially for Ubon) should be noted. As found previously with the LN model (Chapter 4), results are sensitive to the version of UDel precipitation employed. For all the other stations, results are based on V1.01 for 1991–1996 and V1.02 for 1997–1998 (V1.01 only extends to 1996). Use of UDel V1.01 leads to a large over estimation of discharge at Yasothon and low NSE and *r* values (Table 5.3). The latter are improved by using UDel V1.02, whilst Dv values suggest discharge underestimation (albeit by a smaller amount compared to overestimations for UDel V1.01). Similar differences are evident in results for the Mun. This adds support to the assertion that issues identified during calibration of the models for these stations may lie, at least in part,

with the meteorological data for this part of the catchment. The use of an alternative precipitation dataset (CRU) is investigated in Section 5.4 in order to assess the impact of this potential source of uncertainty.

5.2.4.4. Scenario climate

Changes (compared to the baseline) in precipitation and temperature for the 2 °C, seven GCM climate scenarios were presented and discussed in detail in Section 4.7.3.1, and so are not provided here. However, for ease of reference, baseline annual precipitation and temperature, and scenario changes (in percent for precipitation and °C for temperature) are shown for eight representative sub-catchments in Table 5.4. Table 5.5 provides percentage changes in annual PET from the baseline for the eight representative sub-catchments for each PET method and 2 °C GCM scenario. Changes in annual PET are presented graphically in Figure 5.4 for all 11 sub-catchments, with changes grouped according to GCM.

Table 5.4. Mean annual precipitation and temperature for the baseline and changes (% / °C) for the 2 °C, seven GCM climate change scenarios for eight representative SLURP sub-catchments. The inter-GCM range of changes is also shown for each sub-catchment. Shaded cells indicate negative changes compared to the baseline.

Parameter/ Scenario		Lanc. (1)	Mek. 1 (4)	Chi (5)	Mun (6)	Mek. 2 (8)	Se Kong (9)	Sre Pok (10)	Mek. 3 (11)
	Baseline (mm)	1053.4	1856.9	1273.1	1314.5	2214.6	2434.1	2056.6	1871.5
Precipitation (% change)	CCCMA	10.1	10.2	12.3	10.2	8.4	5.3	1.9	5.3
	CSIRO	-4.6	-4.5	-3.3	-2.9	-2.8	-2.8	-2.9	-1.2
	HadCM3	10.1	1.0	-0.1	-0.4	-1.1	-2.1	-4.5	-3.0
	HadGEM1	6.0	-3.7	-6.1	-4.8	-1.2	2.9	3.9	1.0
	IPSL	-5.2	-1.1	-0.1	-0.1	0.6	-0.4	1.3	-0.4
	MPI	3.6	7.1	10.2	10.3	8.8	6.6	7.7	12.2
	NCAR	8.6	9.2	5.0	3.5	1.9	3.5	3.7	5.3
	Range	15.3	14.8	18.4	15.1	11.6	9.3	12.1	15.2
	Baseline (°C)	11.2	24.3	26.8	27.2	26.0	24.7	24.3	26.9
Temperature (change, °C)	CCCMA	2.3	1.9	2.0	2.0	1.8	1.9	1.9	2.0
	CSIRO	2.7	2.3	2.3	2.2	2.1	2.0	2.0	2.1
	HadCM3	2.6	2.4	2.4	2.4	2.3	2.3	2.3	2.3
	HadGEM1	2.5	2.0	1.8	1.8	1.9	2.0	2.0	2.0
	IPSL	2.9	2.3	2.2	2.1	2.1	2.0	1.9	2.0
	MPI	2.7	2.2	2.1	2.1	2.0	2.0	2.0	2.1
	NCAR	2.4	1.9	1.9	1.8	1.8	1.7	1.7	1.7
	Range	0.6	0.6	0.6	0.6	0.5	0.3	0.4	0.4

Table 5.5. Mean annual baseline potential evapotranspiration for each PET method and changes (%) for the 2 °C, seven GCM climate change scenarios for representative sub-catchments within the Mekong catchment.

Scenario/ PET method		Lanc. (1)	Mek. 1 (4)	Chi (5)	Mun (6)	Mek. 2 (8)	Se Kong (9)	Sre Pok (10)	Mek. 3 (11)
Baseline PET (mm)	BC	1339	1923	2034	2059	2003	1944	1924	2042
	HM	779	1633	1862	1907	1778	1656	1620	1868
	HS	1131	1517	1696	1727	1565	1490	1478	1654
	LN	1767	1924	2365	2338	1814	1730	1697	1771
	PN	1112	1511	1715	1716	1586	1508	1481	1693
	PT	955	1353	1469	1489	1393	1375	1389	1576
CCCMA PET (% change)	BC	7.8	4.4	4.4	4.4	4.2	4.5	4.6	4.4
	HM	14.6	11.0	11.3	11.4	10.6	11.0	11.2	11.3
	HS	7.2	4.2	4.1	4.3	4.4	4.7	4.9	4.8
	LN	11.7	12.3	13.2	12.7	12.5	12.7	12.4	12.5
	PN	3.9	5.7	6.3	6.8	6.1	6.1	6.6	6.2
	PT	9.8	7.2	7.5	8.0	8.4	8.4	9.3	7.1
CSIRO PET (% change)	BC	9.2	5.5	5.1	5.0	4.8	4.8	4.8	4.8
	HM	17.6	13.8	13.4	13.1	12.4	12.2	12.0	12.5
	HS	10.1	8.0	6.9	6.6	7.3	7.5	7.3	7.4
	LN	14.7	15.7	15.9	15.2	15.2	14.9	14.2	14.4
	PN	10.4	11.4	10.1	9.8	9.9	9.4	8.7	9.3
	PT	11.6	10.1	9.1	9.0	10.6	10.3	9.5	8.5
HadCM3 PET (% change)	BC	8.8	5.7	5.4	5.3	5.2	5.3	5.3	5.2
	HM	16.4	14.0	13.8	13.6	13.3	13.2	13.2	13.5
	HS	7.8	5.3	5.2	5.5	6.3	6.6	7.1	7.6
	LN	12.9	13.9	13.3	13.2	14.7	14.8	14.8	15.1
	PN	1.9	7.7	7.7	8.7	8.3	8.8	10.0	10.0
	PT	9.7	7.5	6.6	7.3	7.5	8.4	9.2	7.1
HadGEM1 PET (% change)	BC	8.7	4.7	4.0	4.0	4.3	4.6	4.7	4.5
	HM	16.1	11.5	10.2	10.3	10.9	11.5	11.6	11.7
	HS	8.1	4.4	3.8	3.9	4.5	4.9	5.0	4.9
	LN	12.5	12.1	10.4	10.3	12.4	13.0	12.7	12.5
	PN	9.1	7.3	5.8	6.5	6.7	6.7	7.0	7.1
	PT	7.8	5.1	4.5	5.5	5.8	5.6	6.2	5.2
IPSL PET (% change)	BC	9.9	5.6	5.0	4.7	4.7	4.7	4.5	4.4
	HM	19.2	14.1	13.0	12.4	12.2	11.9	11.1	11.4
	HS	9.4	5.4	4.7	4.7	5.0	5.0	4.8	4.8
	LN	15.9	15.8	15.3	14.2	14.3	13.9	12.8	13.2
	PN	11.9	11.1	9.9	9.1	9.3	7.7	5.6	7.3
	PT	12.3	9.0	8.3	8.0	9.1	7.8	6.2	6.4
MPI PET (% change)	BC	9.1	5.1	4.7	4.7	4.6	4.7	4.7	4.6
	HM	17.1	12.8	12.4	12.3	11.8	11.8	11.7	12.0
	HS	8.5	5.0	4.6	4.7	4.9	5.0	5.1	5.1
	LN	13.6	13.6	13.3	12.9	13.4	13.5	13.1	13.2
	PN	9.7	7.1	6.0	6.3	5.7	5.0	4.8	5.4
	PT	11.6	6.2	5.2	5.7	6.3	5.9	5.9	4.9
NCAR PET (% change)	BC	8.1	4.4	4.2	4.1	4.0	4.0	4.0	3.8
	HM	15.1	10.8	10.6	10.5	10.1	9.9	9.8	9.8
	HS	5.3	2.8	3.7	3.8	3.8	3.4	2.9	2.7
	LN	11.3	10.9	11.1	10.7	11.4	11.1	10.7	10.3
	PN	5.5	5.2	5.3	5.6	5.1	3.8	3.8	4.4
	PT	7.1	4.4	4.7	5.4	5.9	5.1	5.5	5.2

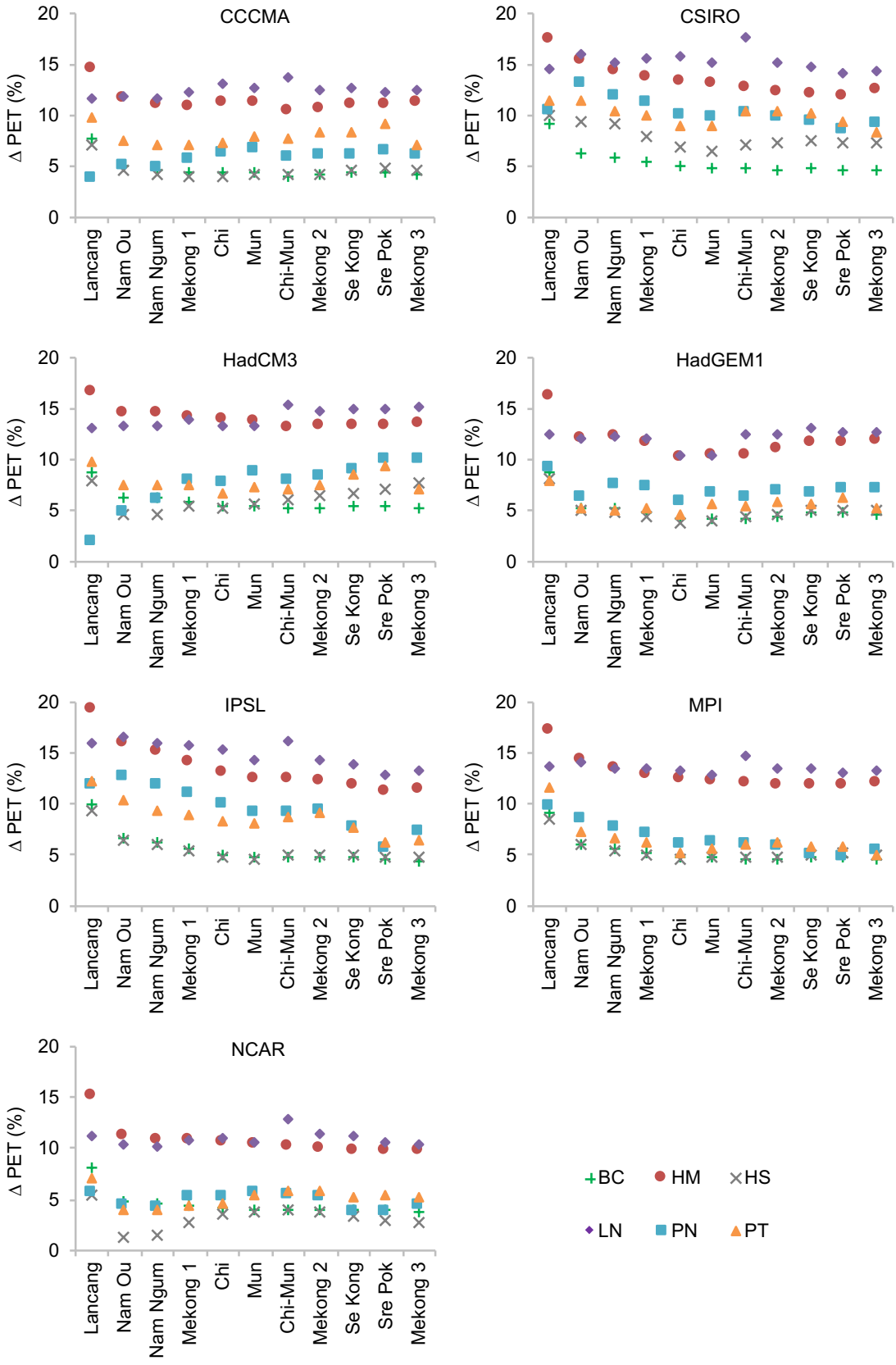

Figure 5.4. Change in annual PET (%) from the baseline for each PET method for the 2 °C, seven GCM climate change scenarios.

Mean annual PET increases for all sub-catchments for each GCM and PET method. Inter-GCM variations in changes in PET are smaller than those for precipitation. On average, the mean inter-GCM range of change in annual precipitation for the sub-catchments shown in Table 5.4 is 14.0% (range across the sub-catchments: 9.3–18.4%). For a given PET method, the corresponding mean inter-GCM range of increases in annual PET varies between 1.4% (1.2–2.1%) for BC PET and 5.9% (4.2–10.0%) for PN PET. In contrast, the mean inter-PET method range of change in annual PET for a given GCM (for the same sub-catchments) varies between 7.7% for the HadGEM1 GCM (range: 6.4–8.3%) and 9.9% for CSIRO (range: 8.3–10.7%). This demonstrates that uncertainty in the magnitude of annual PET change is often greater between different PET methods with a given GCM, than between different GCMs for a given PET method. For projected change in annual PET, choice of PET method is therefore generally a greater source of uncertainty than choice of GCM.

Of the 42 combinations of GCMs and PET methods (seven GCMs × six PET methods), the largest percentage increases in mean annual PET occur over the Lancang in 33 cases (78.6%). For the BC, HM, HS and PT methods, the largest increases occur over the Lancang across all GCMs. Increases in PET for BC, HM and HS for the more southerly sub-catchments are relatively consistent and notably lower than those for the Lancang. Across GCMs, there is some consistency in the relative order of magnitude of increase due to different PET methods. Of the 56 sub-catchment/GCM combinations in Table 5.4 (eight sub-catchments × seven GCMs), BC produces the smallest increases in mean annual PET in 31 (55.4%) followed by HS (22 instances or 39.3%). Combined, these two methods therefore account for 53 (94.6%) of the smallest increases. For the second lowest changes, the relative order is approximately reversed, with HS accounting for 30 (53.6%) and BC 19 (33.9%) sub-catchment/GCM combinations. LN is associated with most of the largest PET increases (46 or 82.1%), followed by HM (10 or 17.9%). HM and LN also account for all of the second highest increases, with the relative order being exactly reversed to that of the highest. The dominance of BC and HS in producing the lowest changes and LN and HM the highest increases is clear in Figure 5.4.

There are also consistencies in the order of magnitude of percentage increases in mean annual PET due to different GCMs. Of the 48 sub-catchment/PET method

combinations in Table 5.4 (eight sub-catchments × six PET methods), the smallest increases are associated with NCAR in 36 (75.0%). The majority of the remaining smallest increases (8 or 16.7% of the 48 combinations) are due to HadGEM1. The largest PET increases are predominantly associated with CSIRO (23 or 47.9%) and HadCM3 (18 or 37.5%).

The dominant seasonal distributions of PET through the year do not change from those of the baseline period. Monthly changes do, however, demonstrate some consistent patterns for different PET methods and GCMs. This is exemplified in Figure 5.5, which presents percentage changes in mean monthly PET for the Mekong 1 sub-catchment (selected due to its large size and central position). The four temperature-based methods (BC, HM, HS and LN) show very similar temporal changes for a given GCM, albeit with different magnitudes. Changes for BC and HS are lower than those for HM and LN (which, as noted above, produce the largest increases in mean annual PET). Changes in monthly PET for these methods for a particular GCM reflect the corresponding changes in temperature. For CCCMA and HadGEM1, changes in temperature and hence PET are characterised by the lowest intra-annual variability. The smallest gains are in March or April and they increase gradually through summer and, in particular, autumn/early winter. In contrast, CSIRO, ISPL and MPI demonstrate peak changes during the period March–May (most clearly demonstrated for CSIRO with a large change in January not repeated for the other GCMs). The smallest changes in PET occur in July–October after which they then increase. BC, HM, HS and LN PET for HadCM3 and NCAR are characterised by relatively large changes between November and February and smaller increases in the middle of the year (HS PET declines below the baseline in August for NCAR).

Changes in mean monthly PET for the two remaining methods (PN and PT – which include variables other than temperature) follow those of the temperature-based methods for much of the year. However, there are some notable differences. The largest changes are associated with a distinct June peak that, for CCCMA and IPSL, extends into July (August for CCCMA). A much smaller peak is also evident in June for PN and PT for the HadCM3 GCM, whilst the largest changes in PET for both methods for HadGEM1 is due to a similar peak in August.

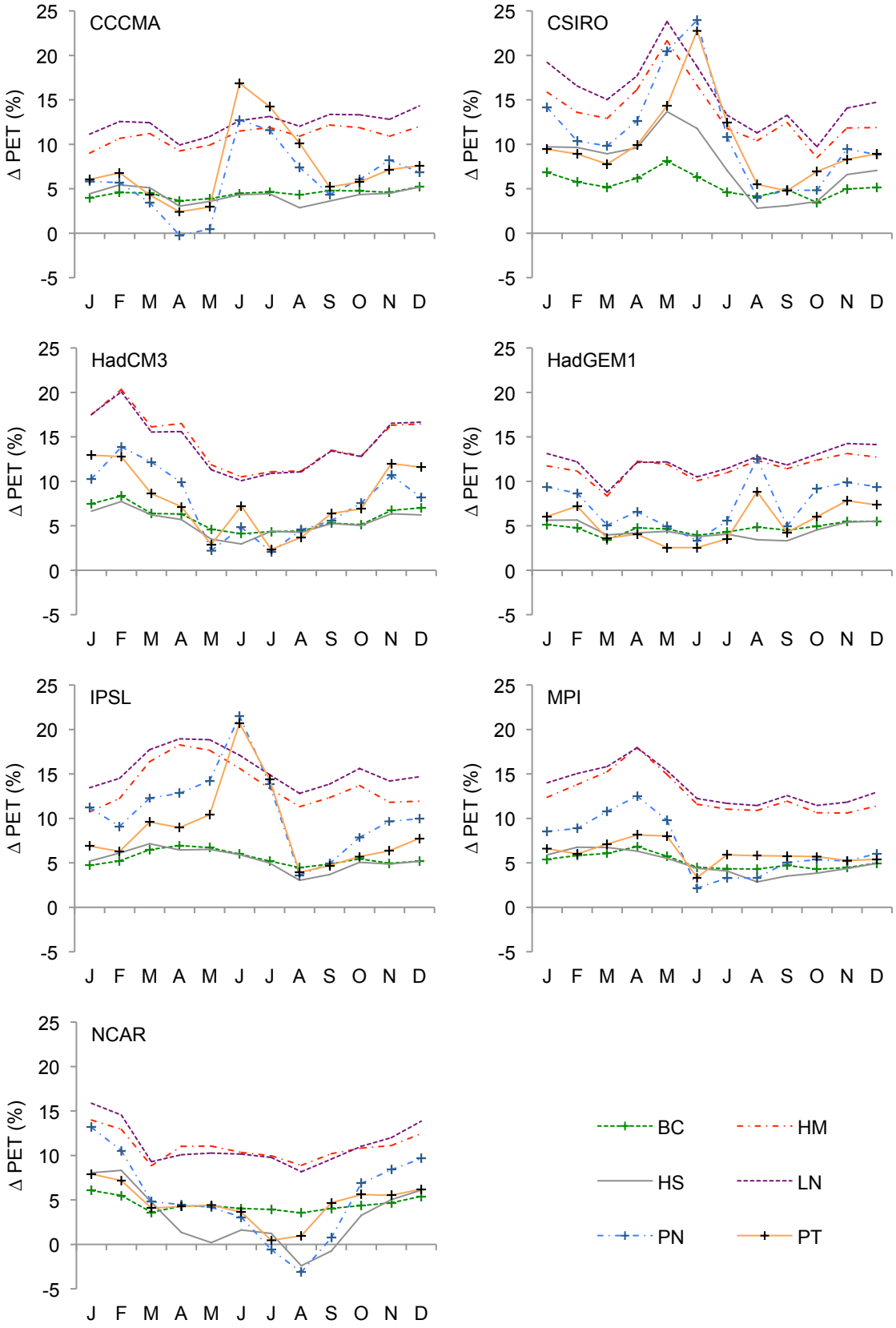

Figure 5.5. Mean monthly change (%) in PET from the baseline for the Mekong 1 sub-catchment for each PET method and GCM. Changes grouped according to GCM.

5.2.4.5. Scenario river discharge

Table 5.6 presents mean baseline discharge and percentage changes in these discharges for the six models employing different PET methods for each GCM scenario. Results are provided for eight representative gauging stations. For each station, the variability across the models in mean baseline and scenario discharges is expressed as the difference between the largest and smallest mean discharge for a given scenario (i.e. the range) as a percentage of the overall average of the mean discharges for that scenario. Changes in mean discharge for each PET method/2 °C GCM scenario are also shown in Figure 5.6 for six representative gauging stations.

The range of simulated mean discharges at each gauging stations increases for all GCMs for each PET method compared to the baseline (Table 5.6). For the baseline, the difference between the largest and smallest mean discharges at a given gauging station is, on average, 4.8% of the overall mean from the six models. The mean inter-MIKE SHE model range in mean discharge increases to between 9.7% (CCCMA) and 12.4% (HadCM3) for the GCM scenarios.

However, uncertainty associated with different GCMs is substantially greater than that due to alternative PET methods. The largest range of change in mean discharge for any gauging station on the main Mekong due to the different GCMs simulated by one of the MIKE SHE models is 37.0% (Luang Prabang, PN PET, –16.1% for IPSL to +18.9% for HadCM3). This is slightly exceeded by the 40.8% range for Ubon (BC PET, HadGEM1: –14.7%, MPI: 26.1%). The average inter-GCM range of change in mean discharge for the eight gauging stations in Table 5.6 simulated by the MIKE SHE models is 29.0% (29.2% for all 12 stations). In contrast, the largest inter-MIKE SHE model range of change in mean discharge for any gauging station (Chiang Saen) simulated for any GCM (HadCM3) is 15.6% (HM: +3.1%, PN: +18.7%). The average inter-MIKE SHE model range of change in mean annual discharge for the eight gauging stations for the seven scenarios is 8.2% (also 8.2% for all 12 gauging stations).

Table 5.6. Mean baseline discharge (m^3s^{-1}) and change from baseline mean discharge (%) for the six PET methods for each GCM at eight gauging stations. Grey shading indicates negative changes compared to the baseline. The range of mean discharges for the baseline and each GCM from the different PET methods are also indicated (% of overall mean discharge from the six models for that scenario).

Scenario	PET / Scenario	Chiang Saen (a)	Luang Prabang (b)	Vientiane (c)	Mukda-han (e)	Pakse (f)	Kratie (h)	Phnom Penh (j)	Ubon (l)
Baseline (m^3s^{-1})	BC	2767.5	4122.8	4708.8	7840.1	9823.7	12919.1	13243.5	637.6
	HM	2789.0	4135.9	4728.6	7915.4	10000.3	13390.3	13734.1	636.7
	HS	2734.7	4017.6	4699.7	7914.0	10177.8	13933.4	14325.1	637.3
	LN	2753.7	4082.6	4686.2	7626.0	9597.3	12961.7	13332.8	619.1
	PN	2766.7	4055.6	4658.0	7819.6	10143.5	13964.6	14363.5	635.6
	PT	2762.0	4177.3	4729.7	7852.7	10212.3	14127.6	14526.8	620.4
CCCMA (% change)	BC	8.6	10.6	11.6	12.9	14.4	12.7	12.6	22.0
	HM	2.7	3.7	4.6	6.9	8.0	6.7	6.6	12.5
	HS	9.0	10.7	11.5	12.6	13.7	11.8	11.7	19.4
	LN	3.4	4.2	5.0	6.8	7.8	6.2	6.1	11.1
	PN	10.6	11.3	11.6	12.0	12.4	10.6	10.5	13.8
	PT	4.1	5.4	6.2	8.3	9.1	7.7	7.7	11.7
CSIRO (% change)	BC	-19.3	-17.8	-16.7	-12.9	-11.2	-9.5	-9.2	-2.9
	HM	-25.0	-24.5	-23.3	-18.6	-17.0	-14.7	-14.4	-10.2
	HS	-19.1	-18.1	-16.7	-12.9	-11.0	-9.1	-8.8	-1.4
	LN	-25.1	-24.4	-23.5	-19.4	-18.0	-15.7	-15.4	-11.6
	PN	-18.2	-18.1	-17.1	-13.8	-12.2	-10.1	-9.8	-4.0
	PT	-20.6	-19.7	-18.7	-14.9	-13.1	-10.9	-10.7	-5.2
HadCM3 (% change)	BC	11.6	12.7	11.2	7.4	5.8	3.1	2.8	-0.5
	HM	3.1	3.8	2.6	0.4	-1.1	-3.3	-3.5	-8.8
	HS	11.7	13.0	11.3	7.5	5.7	2.7	2.5	-1.4
	LN	7.4	7.3	5.5	2.3	0.4	-2.5	-2.8	-8.3
	PN	18.7	18.9	16.6	10.6	8.0	4.4	4.1	-2.4
	PT	9.2	10.3	9.2	6.1	4.4	1.7	1.5	-2.4
HadGEM1 (% change)	BC	0.6	-0.7	-2.2	-4.7	-6.3	-4.9	-4.8	-14.7
	HM	-5.7	-7.1	-8.4	-9.9	-11.4	-9.6	-9.4	-20.6
	HS	1.0	0.1	-1.2	-3.6	-4.9	-3.2	-3.1	-12.2
	LN	-3.3	-5.9	-7.7	-9.9	-11.6	-10.0	-9.8	-20.9
	PN	0.3	-0.8	-2.0	-4.5	-6.0	-4.5	-4.4	-14.0
	PT	0.3	-0.5	-1.4	-3.8	-5.2	-3.7	-3.6	-14.0
IPSL (% change)	BC	-17.9	-14.6	-12.7	-7.8	-5.4	-4.1	-4.1	6.7
	HM	-25.3	-23.1	-21.0	-14.7	-12.2	-10.3	-10.1	-1.6
	HS	-16.4	-13.5	-11.3	-6.7	-4.5	-3.2	-3.1	5.7
	LN	-23.2	-20.6	-19.0	-14.1	-12.0	-10.4	-10.3	-3.0
	PN	-18.0	-16.1	-14.4	-9.7	-7.5	-5.6	-5.5	0.8
	PT	-20.0	-17.5	-15.7	-10.5	-8.3	-6.2	-6.1	0.1
MPI (% change)	BC	-1.4	2.0	3.7	6.7	9.7	10.6	10.8	26.1
	HM	-9.1	-6.8	-4.9	-0.4	2.5	4.1	4.3	16.7
	HS	-0.8	2.2	3.9	6.7	9.3	10.2	10.4	23.1
	LN	-6.1	-3.6	-2.1	1.1	3.7	4.8	5.0	16.7
	PN	-1.4	1.3	2.8	5.9	8.5	9.8	10.1	21.7
	PT	-5.8	-2.5	-0.8	3.5	6.3	7.9	8.2	19.7
NCAR (% change)	BC	7.8	13.4	14.2	15.1	14.3	11.8	11.7	9.5
	HM	0.7	5.2	6.1	8.4	7.8	5.8	5.8	2.4
	HS	10.7	16.4	16.7	16.9	15.7	12.7	12.5	8.9
	LN	4.7	9.6	10.1	11.2	10.2	7.4	7.2	3.1
	PN	11.5	16.3	16.4	16.3	14.8	11.9	11.7	7.1
	PT	7.8	12.7	13.0	13.9	12.6	9.9	9.8	5.3
Range of mean discharges (% of overall mean from the six models)	Baseline	2.0	3.9	1.5	3.7	6.2	8.9	9.2	2.9
	CCCMA	7.3	6.9	6.6	8.9	11.1	12.2	12.2	12.4
	CSIRO	9.2	9.2	8.9	11.3	13.8	14.5	14.4	13.6
	HadCM3	13.5	11.6	11.3	10.3	12.8	14.2	14.2	11.0
	HadGEM1	5.6	7.9	7.4	10.4	13.0	15.2	15.1	13.2
	IPSL	9.2	10.0	10.8	11.8	14.0	14.8	14.7	12.5
	MPI	7.3	8.6	8.2	9.0	11.0	12.1	12.1	10.6
	NCAR	9.3	8.0	8.9	8.7	10.7	12.0	12.0	9.0

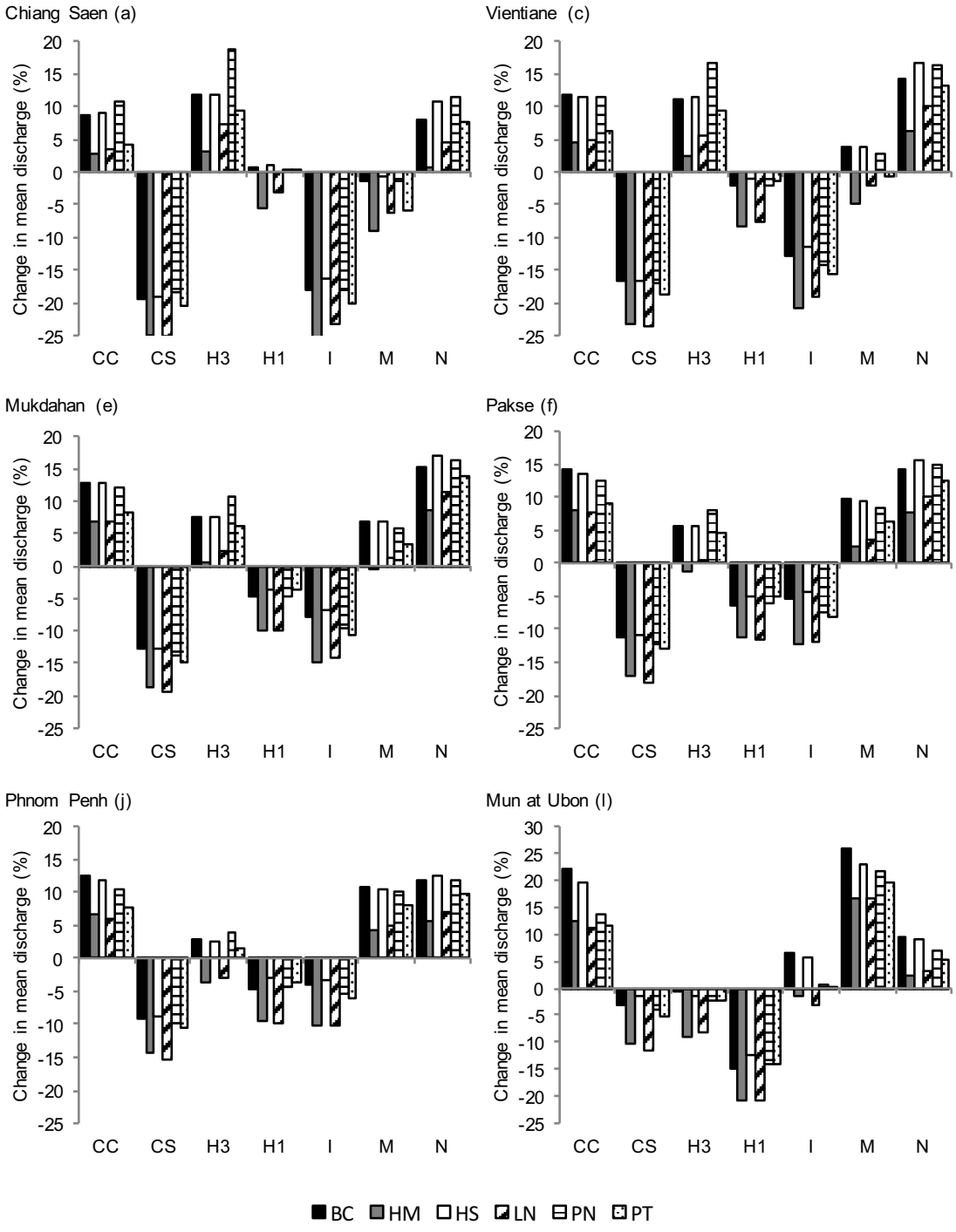

Figure 5.6. Change from baseline mean discharge for the 2 °C, seven GCM scenarios and each PET method for six gauging stations within the Mekong catchment. CC: CCCMA; CS: CSIRO; H3: HadCM3; H1: HadGEM1; I: IPSL; M: MPI; N: NCAR. (Note different y-axis scales.)

For some scenarios, direction of change in mean discharge is consistent irrespective of PET method. All MIKE SHE models simulate catchment-wide increases in mean discharge for CCCMA and NCAR. The magnitudes of increases broadly concur with the relative magnitude of changes in annual PET. Either the HM or the LN model

(largest PET increases) produces the smallest increases in discharge at all stations in Table 5.6. They are also responsible for the second smallest increases (in all but one case). Conversely, the BC and HS models (smallest PET increases), project the largest increases in mean discharge at most stations. For CCCMA, the largest increases at six stations (out of the eight in Table 5.6) are due to BC PET (the other two PN PET), whilst for NCAR, HS PET produces the largest increases at six stations (BC and PN each account for one station).

The same spatial patterns of change along the main Mekong are evident for the different PET methods for both CCCMA and NCAR. For CCCMA the magnitudes of the increases in mean discharge rise as far as Pakse and then decline due to the smaller gains in precipitation in the lower Mekong. Similarly for NCAR, discharge increases rise towards Vientiane or Mukdahan and then decline further downstream. In many cases NCAR produces the largest increases in mean discharge along the main Mekong. Conversely, increases in the mean discharge of the Mun at Ubon (and for the Chi at Yasothon) are consistently larger for CCCMA compared to NCAR due to the larger increases in precipitation over this sub-catchment for CCCMA.

Mean discharge declines at every gauging station for the CSIRO GCM for all six MIKE SHE models (Table 5.6). In all cases, the magnitude of the declines decreases in a downstream direction. The largest reductions at seven stations in Table 5.6 are due to LN PET, with HM PET accounting for the second largest reductions at these stations. This order is reversed at Luang Prabang. The HS PET MIKE SHE model projects the smallest declines in discharge at five stations, with BC PET accounting for two and PN one. BC PET is responsible for the second smallest declines in discharge at five stations, the remaining three resulting from either HS (two stations) or PN PET (one station).

For the remaining four GCMs, some uncertainty in the direction of change in mean discharge is introduced by PET method. For IPSL, mean discharge declines at all gauging stations on the main Mekong, for all PET methods. The magnitude of these declines reduces downstream. However, whilst for HM and LN discharge also declines for the Mun at Ubon (repeated for LN on the Chi at Yasothon), the other models employing alternative PET methods project relatively small increases (Table

5.6, Figure 5.6). LN and HM are associated with the largest increases in annual PET for the Mun (14.2% and 12.4%, respectively – Table 5.5). In contrast, changes in annual PET for the other methods are lower (maximum 9.1% for PN). Although the Mun experiences an overall small (0.1%) decline in annual precipitation, increases during the wet season coupled with smaller increases in PET for these four methods account for the modest increases in mean discharge.

Some uncertainty due to PET method is also evident for MPI. Annual precipitation increases in all sub-catchments, although increases are relatively small, especially upstream (e.g. the Lancang). Conversely, increases in the original LN PET are larger than those for CCCMA and NCAR, the other scenarios with catchment-wide increases in precipitation. With LN PET, mean discharge therefore declines in the upper Mekong until Vientiane and then increases. This pattern is repeated for PT PET. Larger PET increases for HM over the Lancang cause declines in Mekong discharge to extend further downstream to Mukdahan. In contrast, for BC, HS and PN, small (≤1.4%) declines in mean discharge are restricted to Chiang Saen. These PET methods result in the smallest increases in annual PET for MPI (Table 5.5). The point at which increased evapotranspiration is offset by modest increases in precipitation, leading to increased discharge, is therefore further upstream.

For HadCM3 and the LN PET model, mean discharge increases in the upper Mekong as far as Pakse. These increases decline downstream whilst below Pakse discharges decline, albeit by small amounts (Table 5.6). As discussed in Section 4.7.3.2, this pattern was attributed to the relatively large (10.1%, Table 5.4) increases in precipitation over the Lancang and smaller increases over Mekong 1 that offset elevated evapotranspiration. Further south, precipitation declines so that, in combination with higher PET, discharges decrease. The larger increases in HM PET, especially over upstream sub-catchments, cause the point at which mean discharge declines to shift upstream to between Mukdahan and Pakse (Table 5.6). In contrast, the consistently smaller increases in PET for BC, HS, PN and PT (all ≤10%, Table 5.5) cause the influence of enhanced upstream precipitation to extend throughout the catchment. Mean discharges increase along the main Mekong, although the magnitude of changes declines in a downstream direction. The particularly small increase in PN PET over the Lancang results in the largest discharge increases. The

influence of declining precipitation in the south combined with higher PET is indicated by declines in Mun discharge at Ubon. The largest reductions are due to HM and LN (larger PET increases) and the smallest from BC and HS (smallest increases in PET).

For the HadGEM1 GCM, enhanced precipitation in the upper Mekong is restricted to the two northernmost sub-catchments. For LN and HM, increases in PET (increases in annual PET over the Lancang of 12.5% and 16.1% respectively, Table 5.5) offset increases in precipitation, resulting in catchment-wide reductions in mean discharge, with the magnitude of change increasing downstream until Pakse. Modest increases in precipitation over southerly sub-catchments limit further reductions at the lowest gauging stations. In contrast, smaller PET increases for the remaining methods, combined with precipitation increases over the Lancang, cause minor (≤1.0%) increases in discharge at Chiang Saen (and Luang Prabang for HS PET), with reductions in mean discharge further downstream. For all PET methods, the largest declines in discharge on the main Mekong are at Pakse. The impact of elevated PET and lower precipitation is clearly demonstrated for the Mun at Ubon. The largest reductions in discharge result from HM and LN and the smallest from HS PET.

As an alternative way to compare PET uncertainty between methods and GCMs, changes in areal PET were considered (Figure 5.7). These were derived by weighting PET changes for each sub-catchment by the proportion these sub-catchments comprise of the total area draining to a gauging station. Areal PET for Chiang Saen and Ubon therefore correspond to changes for the Lancang and Mun sub-catchments, respectively, whilst those for Phnom Penh are based on changes over 11 upstream sub-catchments. Figure 5.7 demonstrates the strong, but not perfect, negative relationship between increase in PET and increase in discharge, as well as PET method-related uncertainty in the direction of discharge change at some gauging stations for some GCMs (Chiang Saen: HadGEM1; Phnom Penh: HadCM3; Ubon: IPSL). Greater GCM-related uncertainty is indicated by the wider range of change in mean discharge for the seven GCMs compared to those due to the different PET methods.

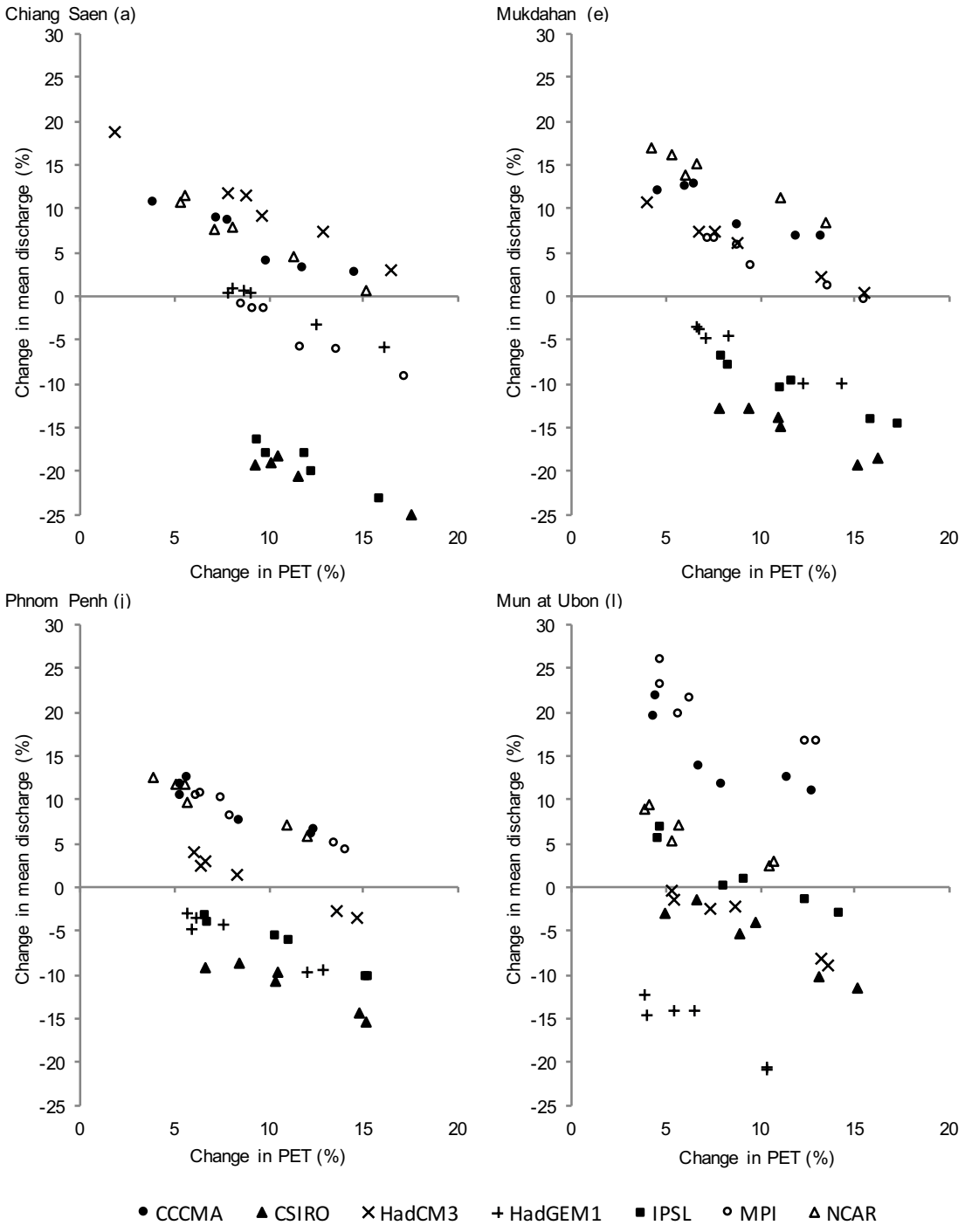

Figure 5.7. Relationship between change in mean discharge and change in weighted mean annual PET for each GCM and PET method for four gauging stations within the Mekong catchment.

Figure 5.8 presents the simulated regimes from the six MIKE SHE models under climate change, as well as the simulated range for the baseline. At a monthly resolution, greater GCM-related uncertainty compared to that associated with PET methods is further evident. For a given GCM, mean monthly discharges simulated by the different models are broadly similar and follow the patterns previously described for the LN MIKE SHE model (Section 4.7.3.2).

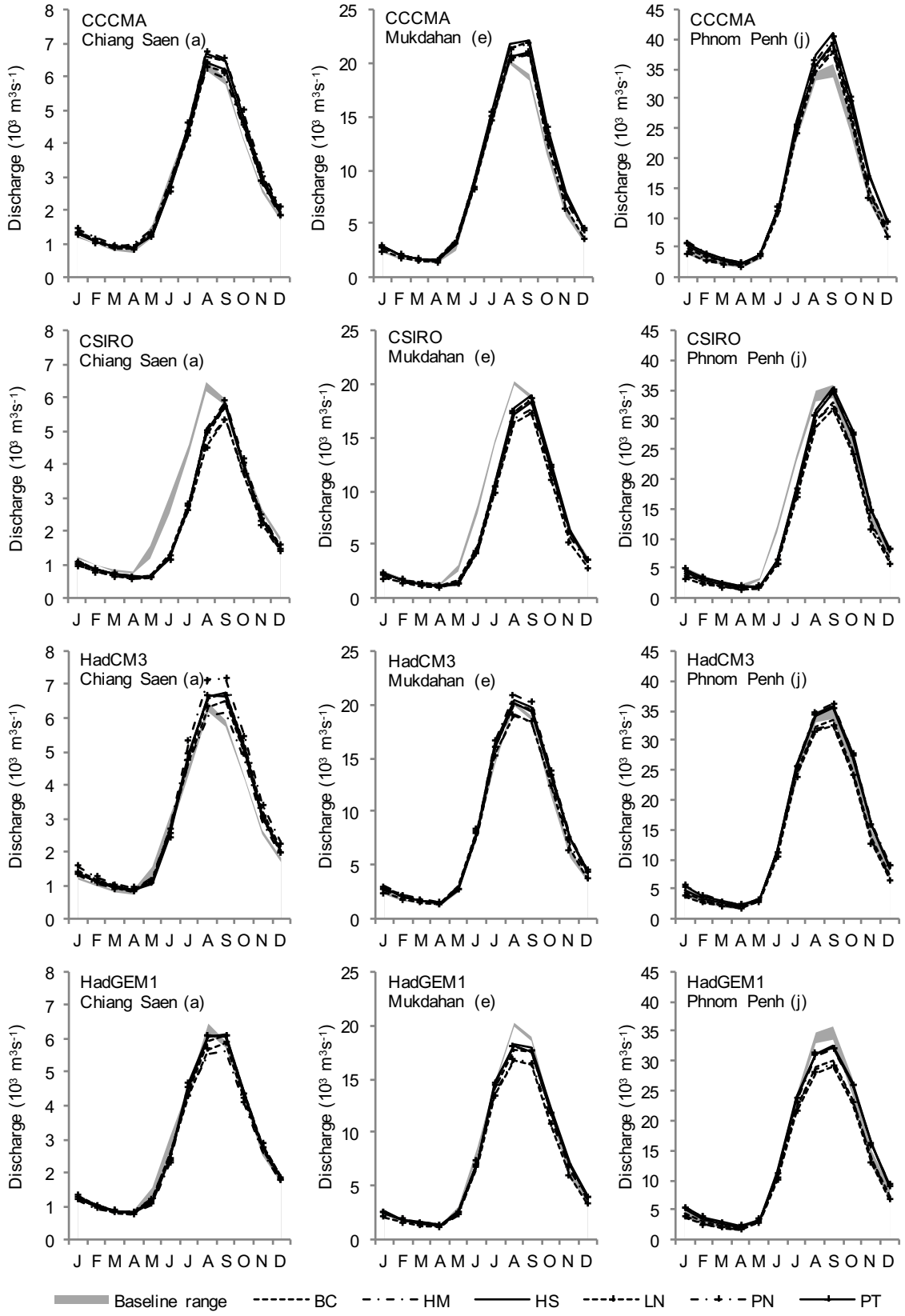

Figure 5.8. River regimes for the baseline and 2 °C, seven GCM climate change scenarios and each PET method for three gauging stations within the Mekong catchment. (Note different y-axis scales.)

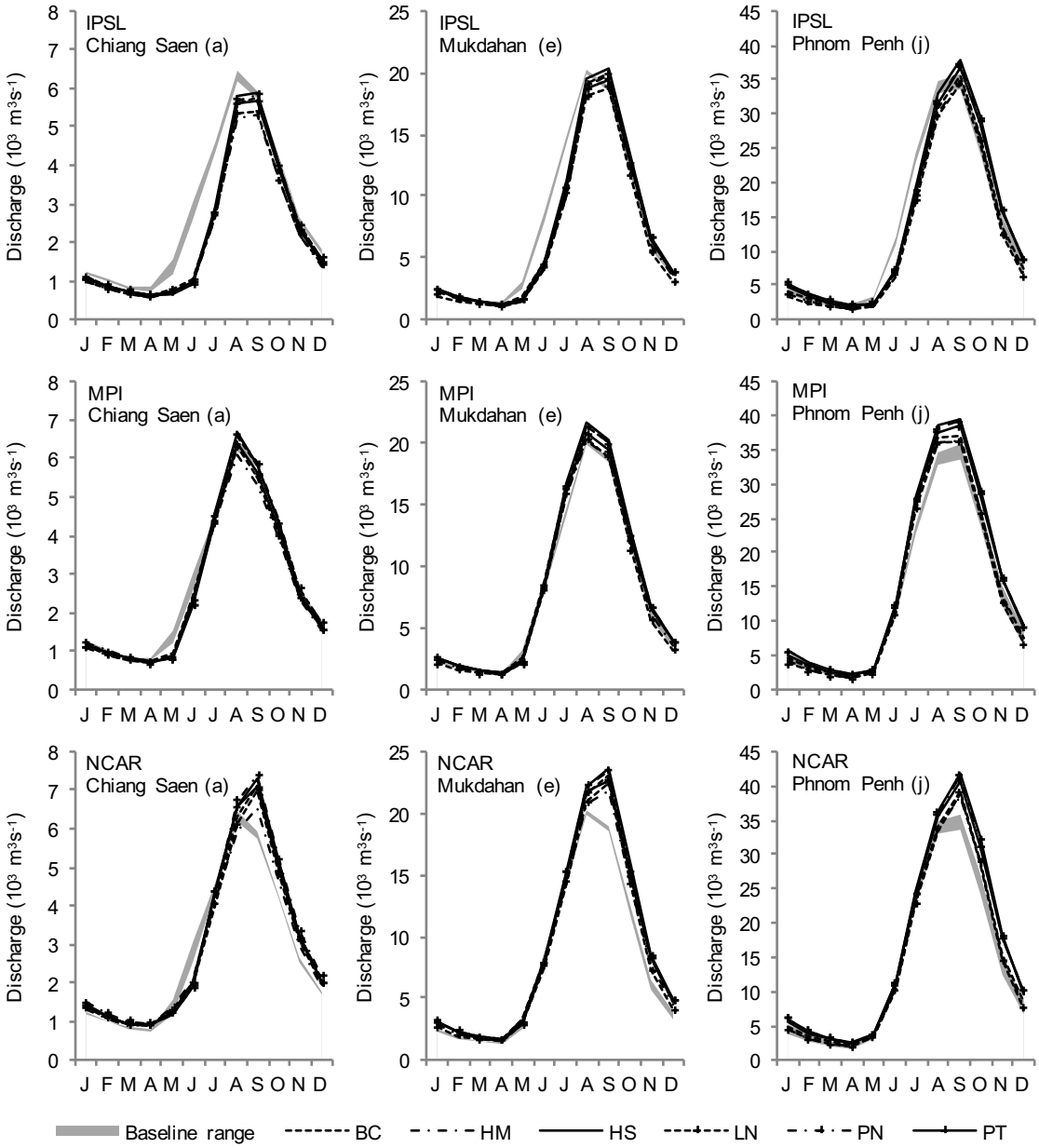

Figure 5.8 (cont.) River regimes for the baseline and 2 °C, seven GCM climate change scenarios and each PET method for three gauging stations within the Mekong catchment. (Note different y-axis scales.)

For example, for CSIRO and IPSL all six models simulate declines in the rising limb of the seasonal peak, especially further upstream. Peak discharges are delayed from August for the baseline to September. Similarly, all six models simulate this delayed peak for NCAR, but with the magnitude of the peak increasing.

The range of scenario mean monthly discharges is greater than that for the baseline. This is most apparent during the seasonal peak, although the range increases in most months. For all 12 gauging stations, the baseline inter-MIKE SHE model range

in August and September discharges, expressed as a percentage of the overall mean from the six models for the respective month, is on average 4.7% and 4.5%, respectively. In contrast, for the 2 °C GCM scenarios these ranges vary between 8.4% (MPI) and 13.6% (HadGEM1) for August and between 8.8% (CCCMA) and 11.3% (HadCM3) for September. The greatest individual change in the range of peak discharges occurs at Chiang Saen for HadCM3. Mean baseline August discharge at this station ranges between 6179.9 m^3s^{-1} (HM) and 6452.8 m^3s^{-1} (PT) (range: 272.8 m^3s^{-1} or 4.3% of the mean from the six models). This compares to a range of 1056.5 m^3s^{-1} (16.1% of the six model mean) for HadCM3. Results for individual models range between a 1.6% decrease (HM PET) to an increase of 11.1% (PN PET).

Figure 5.9 provides a clear demonstration that the pattern of change in mean monthly discharge through the year is largely unaffected by use of different PET methods. Instead, it is predominantly the magnitude of changes that is impacted by PET method, with the intra-annual change pattern for a given gauging station dominated by choice of GCM. This is evident even in cases where, for a given GCM and gauging station, the MIKE SHE models do not consistently show the same direction of change for some months of the year. For example, with the CCCMA GCM at Chiang Saen, each model shows relatively consistent percentage increases between October–December, slightly lower increases in January–March and a maximum percentage increase producing a small peak in April. The BC, PN and HS models then simulate minimum increases (≤+6.2% of baseline discharge) in May–August, whilst HM, LN and PT produce minimum increases or reductions (up to -6.4%). For September, all six models again show increases in discharge.

Table 5.7 presents projected change in monthly Q5 and Q95 discharge from the six MIKE SHE models for the same six stations as employed in Figure 5.6 for change in mean discharge. Uncertainty in the direction of change in either high or low flows, and in some cases both, is introduced for all scenarios due to the different PET methods. For some GCMs, uncertainty is only associated with either high or low flows and is restricted to parts of the catchment.

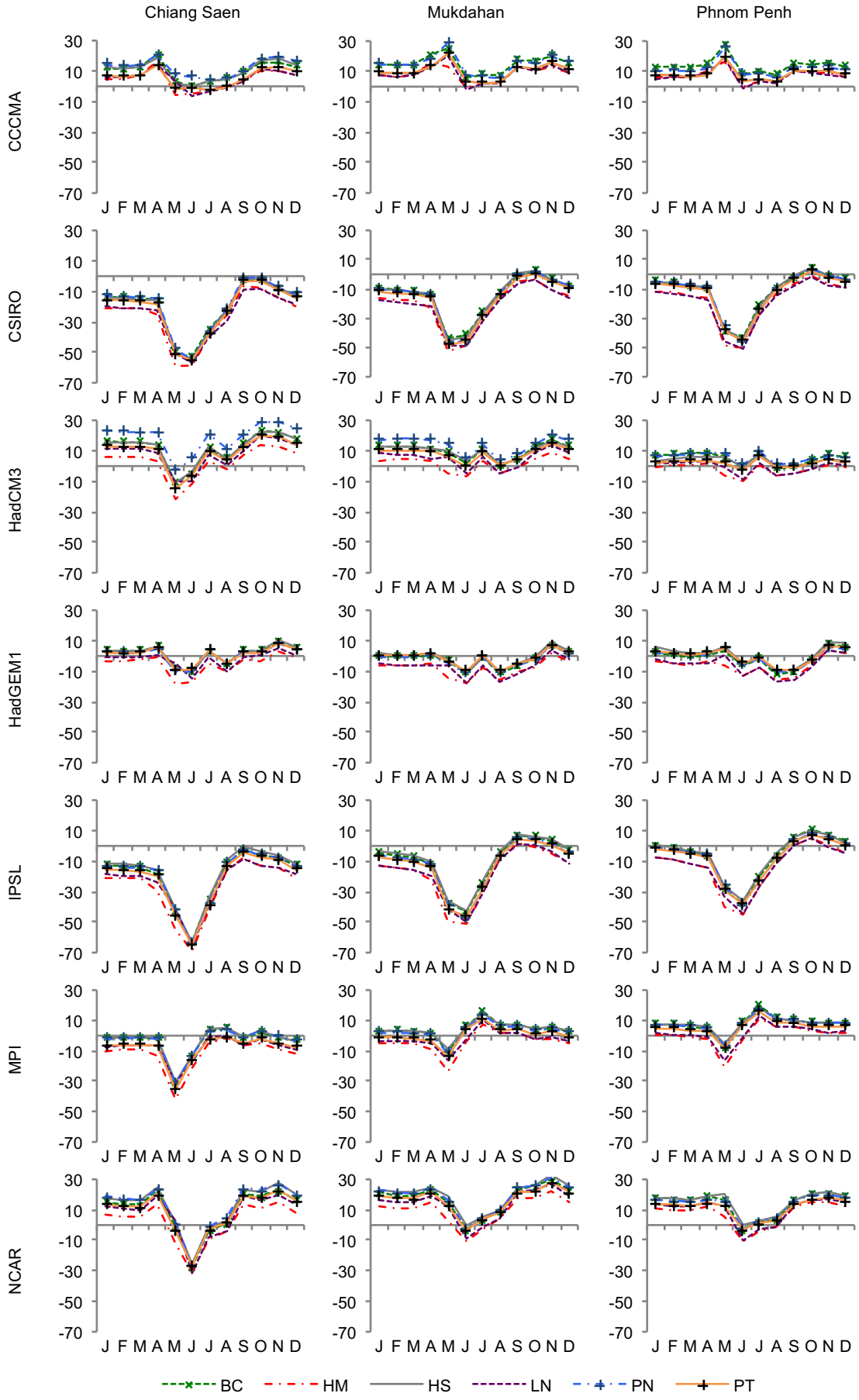

Figure 5.9. Change (%) in mean monthly discharge for the 2 °C, seven GCM climate scenarios and each PET method for three stations.

Table 5.7. Changes in Q5 and Q95 discharge (%) for the different PET methods for each GCM at six gauging stations within the Mekong catchment. (CS: Chiang Saen; Vi: Vientiane; Mu: Mukdahan; Pa: Pakse; PP: Phnom Penh; Ub: Ubon. Shaded cells indicate negative changes compared to the baseline).

		Q5						Q95					
		CS	Vi	Mu	Pa	PP	Ub	CS	Vi	Mu	Pa	PP	Ub
Scenario	**PET**	**(a)**	**(c)**	**(e)**	**(f)**	**(j)**	**(l)**	**(a)**	**(c)**	**(e)**	**(f)**	**(j)**	**(l)**
CCCMA	BC	2.9	4.9	14.8	15.6	9.9	20.9	13.8	16.8	20.5	22.0	14.7	23.8
(%	HM	-2.2	-2.0	10.3	11.3	4.5	15.7	1.8	5.6	13.5	14.1	8.7	15.2
change)	HS	3.8	2.8	14.4	15.1	9.8	18.9	12.7	12.7	18.5	15.9	12.4	26.9
	LN	-3.3	-0.9	7.9	10.8	4.8	17.3	5.8	7.5	10.9	13.2	10.0	15.7
	PN	4.5	5.0	12.7	11.2	8.1	14.8	12.4	12.2	14.6	13.8	10.1	21.6
	PT	1.0	1.3	10.5	8.8	5.1	12.7	6.6	5.4	9.9	8.6	4.7	15.6
CSIRO	BC	-11.1	-10.0	-7.5	-6.7	-6.8	3.9	-22.8	-20.1	-12.9	-10.1	-14.4	-7.9
(%	HM	-14.1	-15.1	-9.8	-10.3	-10.7	-3.3	-29.9	-28.5	-20.5	-17.8	-20.9	-14.7
change)	HS	-8.5	-10.0	-5.6	-4.7	-7.2	6.7	-22.6	-22.2	-13.6	-15.5	-17.1	-11.4
	LN	-18.2	-18.3	-15.3	-12.2	-13.4	-3.9	-29.3	-27.9	-21.5	-18.0	-19.0	-11.2
	PN	-6.0	-10.2	-6.8	-7.0	-8.3	7.6	-21.6	-21.8	-18.7	-18.5	-21.3	-14.7
	PT	-7.0	-11.2	-7.1	-7.7	-9.0	4.4	-24.5	-24.5	-19.7	-19.9	-20.8	-23.6
HadCM3	BC	11.5	8.0	2.6	1.4	-2.7	-0.3	14.6	12.7	14.6	16.7	9.4	-5.7
(%	HM	2.6	0.4	-2.5	-3.1	-6.2	-9.2	3.7	4.8	3.8	5.9	1.3	-12.3
change)	HS	11.2	5.7	2.8	1.3	-2.8	-3.5	14.1	9.9	14.3	13.7	6.4	-5.0
	LN	8.0	3.1	-3.7	-2.3	-8.6	-4.1	7.5	4.0	8.2	10.3	6.0	-6.7
	PN	16.2	10.7	4.7	3.1	0.9	-2.5	21.3	18.0	17.3	12.9	6.6	-6.9
	PT	9.7	5.3	2.0	1.5	-0.6	-2.4	11.1	9.1	10.1	7.0	1.6	-8.1
HadGEM1	BC	0.5	-3.4	-7.8	-11.0	-10.8	-10.4	0.2	-3.8	-2.0	1.8	-2.1	-14.4
(%	HM	-5.1	-8.6	-10.2	-13.2	-15.0	-15.1	-7.3	-8.6	-7.7	-5.1	-6.9	-19.8
change)	HS	1.3	-4.7	-5.9	-8.6	-9.3	-10.0	-0.4	-3.5	1.6	-0.2	0.8	-10.6
	LN	-4.1	-10.8	-13.7	-14.8	-16.7	-12.4	-5.3	-10.6	-7.2	-5.1	-5.1	-15.7
	PN	0.6	-3.0	-7.8	-10.6	-9.7	-11.3	-2.9	-3.0	-3.0	-4.4	0.3	-14.0
	PT	2.0	-2.8	-6.3	-10.0	-9.1	-11.9	-2.4	-4.3	-2.0	-3.4	0.9	-20.5
IPSL	BC	-3.7	0.1	-0.1	1.2	1.6	12.1	-23.9	-20.3	-13.0	-10.4	-10.5	0.1
(%	HM	-9.3	-8.4	-3.5	-1.7	-3.4	5.5	-32.8	-27.0	-22.9	-18.2	-17.4	-7.2
change)	HS	-2.7	-1.1	1.1	4.1	1.2	14.4	-22.6	-17.3	-11.2	-12.0	-10.9	-3.7
	LN	-11.6	-9.8	-6.7	-3.8	-4.8	9.6	-27.9	-24.9	-21.2	-18.3	-16.8	-7.7
	PN	-4.7	-2.3	-1.5	-0.4	-0.5	13.0	-24.4	-22.0	-16.9	-16.5	-13.0	-9.7
	PT	-5.4	-3.9	-2.2	-0.6	-0.8	10.2	-28.5	-23.0	-18.6	-16.1	-13.7	-14.5
MPI	BC	5.6	6.8	7.5	11.1	10.0	23.5	-5.3	-1.4	3.6	4.7	2.4	12.8
(%	HM	0.1	-1.1	2.9	5.8	4.9	16.8	-14.6	-12.2	-5.6	-3.2	-4.5	5.9
change)	HS	5.2	5.2	7.4	10.2	9.6	17.1	-3.9	-2.5	3.2	4.1	3.6	15.6
	LN	0.5	0.3	0.5	6.4	5.0	18.7	-10.0	-7.0	-7.0	-3.4	-2.1	9.6
	PN	4.2	6.8	6.4	7.9	10.1	19.7	-6.3	-5.0	-2.4	-0.6	1.1	11.5
	PT	1.2	3.6	4.6	6.5	8.1	19.6	-10.3	-10.1	-5.2	-3.5	0.1	4.0
NCAR	BC	10.0	13.8	14.7	12.2	6.5	13.6	12.9	15.9	19.1	22.3	16.1	5.4
(%	HM	3.5	6.0	10.7	9.4	2.0	7.6	2.7	7.5	10.3	10.9	9.7	-4.2
change)	HS	11.5	14.4	16.0	13.9	7.0	13.7	16.4	17.0	24.3	23.7	16.4	4.2
	LN	8.3	8.1	9.5	7.6	0.8	12.0	8.0	11.6	17.0	18.6	14.8	3.4
	PN	16.3	18.4	15.8	11.2	8.4	15.1	14.8	16.8	20.7	18.7	15.5	0.0
	PT	13.8	14.8	14.3	9.7	7.0	13.1	9.8	10.5	17.1	16.9	11.2	-4.8

Both monthly Q5 and Q95 (monthly discharges equaled or exceeded for 5% and 95% of the time, respectively) increase throughout the main Mekong for NCAR. The smallest increases are largely due to HM and LN and the largest predominantly associated with HS or PN PET. Although Q5 increases for Ubon, two models project declines in Q95, and one model projects no change. However, when looking at inter-model differences in percentage change in Q95 at Ubon, it should be noted that since simulated Q95 values at Ubon are very low (observed Q95 for the baseline is 25.4

m^3s^{-1}), inter-model differences in absolute change from the baseline for a given GCM are actually consistently very low (inter-model range in change of ≤4.3 m^3s^{-1}).

In contrast to NCAR, for the CSIRO GCM, Q5 and Q95 decline on the main Mekong for all models (largest decreases due to LN and HM). Q95 also consistently declines at Ubon, but Q5 increases for all the models except those employing HM and LN PET. Uncertainty in the direction of change in high flows for CCCMA is restricted to the top of the catchment. HM and LN project declines in Q5, albeit of small magnitude, that are contrary to increases simulated throughout the Mekong by the other models. All six models, however, project increasing low flows. The largest increases in Q95 are mostly from BC PET, followed HS and PN PET. Most of the smallest increases are due to HM and PT PET.

HadGEM1 and IPSL show a dominance of reductions in Q5 and Q95. For HadGEM1, uncertainty in the direction of change in Q5 is limited to upstream stations (Chiang Saen and Luang Prabang), with consistent reductions elsewhere. Q95 shows some uncertainty at most stations, although, as in the case of Q5, any simulated increases are minor (<2%). HM and LN project reductions in both high and low flows at all stations. Reductions in Q95 are greater with the IPSL GCM, and there is only a single case of a negligible (0.1%) increase being simulated (BC PET on the Mun at Ubon). All six MIKE SHE models produce an increase in Q5 at Ubon, whilst there is some uncertainty in the direction of change at most stations on the main Mekong.

Direction of change in Q95 for HadCM3 is consistent between MIKE SHE models - increases on the main Mekong and declines for the Mun and Chi. However, HM and LN project declines in high flows at and downstream of Mukdahan. For the other models, projected increases in Q5 extend further downstream, and at all stations in the case of the PN model. All six models project declines in high flows for the Mun. For MPI, uncertainty in the direction of change in Q5 is limited to one case at Vientiane (small reduction for HM). Elsewhere Q5 consistently increases and the magnitude of these changes tends to increase in a downstream direction. Changes in low flows vary; BC and HS project increases at and downstream of Nakhon Phanom, PN and PT project increases at and downstream of Stung Treng and

Kompong Cham, respectively, whilst HM and LN simulate declines for all gauging stations on the main Mekong. All models project increases in Mun low flows.

5.3. An assessment of the uncertainty associated with the spatial distribution of meteorological inputs

This section explores the influence of the spatial distribution of meteorological inputs within the MIKE SHE model of the Mekong upon simulated scenario results. Section 5.3.1 describes the development of two further MIKE SHE Mekong models employing alternative meteorological input distributions. Following an outline of model calibration/validation (Section 5.3.2), Section 5.3.3 outlines the generation of climate change scenario data for each of the three hydrological models for the same 2 °C, seven GCM scenarios as employed in Section 5.2 and Chapter 4. Use of these scenarios allows an evaluation of the level of uncertainty associated with the spatial distribution of meteorological inputs compared to that related to GCM uncertainty. Section 5.3.4 presents the climate scenarios and impacts of these scenarios upon simulated river flows from the three MIKE SHE models employing alternative meteorological input spatial distributions.

5.3.1. Alternative spatial distributions of meteorological inputs – model development

To define the spatial distribution of meteorological inputs, the MIKE SHE models of the Mekong described in this thesis have, up to this point, consistently employed the sub-catchments originally used in the SLURP model of the Mekong (and hence referred to as SLURP sub-catchments). As described in Section 4.2.6, this approach was employed to enable comparison of the results from MIKE SHE and the earlier SLURP model for the same climate change scenarios. However, had the initial MIKE SHE model been developed in isolation from SLURP, a more appropriate method of distributing the meteorological inputs would have instead been to use the same sub-catchments as the saturated zone linear reservoirs. Alternatively, they could be distributed according to a 0.5° × 0.5° grid, as used in the Mac.PDM.09 GHM (from which projections for the Mekong catchment were extracted in Chapter 4). Compared to the use of large sub-catchments over which inputs are spatially

averaged, this approach clearly allows for much greater spatial variability in meteorological inputs. Previous research has identified the spatial distribution of meteorological inputs, in particular precipitation, as a potential source of uncertainty in hydrological model calibration and outputs under baseline/non-scenario conditions (e.g. Mileham *et al.*, 2008; Vaze *et al.*, 2011; see Section 2.6.6.2). Assessment of the impact of this source of uncertainty on hydrological projections under climate change therefore warrants investigation.

In order to assess the spatial distribution of meteorological inputs as a source of uncertainty in river discharge projections under climate change, two additional MIKE SHE models of the Mekong were developed. These were based on the model described in the Section 5.2 that uses Penman (PN) PET. This model was selected for this part of the study over the other MIKE SHE models because Penman and Penman-based methods are widely used and recommended combination PET methods (e.g. Andréassian *et al.*, 2004; Shuttleworth, 2007). In addition, compared to the other PET methods investigated, the PN method produces mid-to low-range PET estimates for the Mekong Basin for the baseline period (Table 5.1; Figure 5.1). For clarity, the original PN MIKE SHE model will subsequently be referred to as the S-Mets model because meteorological inputs to the model are distributed according to the sub-catchments initially developed for use in the SLURP model of the Mekong (Kite, 2000; Kingston *et al.*, 2011).

The two additional models employ alternative means of spatially distributing meteorological inputs. The MIKE SHE meteorological input sub-catchments (M-Mets) model uses the MIKE SHE saturated zone linear reservoir sub-catchments (see Section 4.2.5) for distributing meteorological inputs, whilst the gridded meteorological inputs (G-Mets) model distributes the data according to a 0.5° × 0.5° grid. The three alternative spatial distributions are presented in Figure 5.10.

To provide precipitation, temperature and PET inputs for the M-Mets model employing the MIKE SHE sub-catchments to distribute meteorological inputs, the same global gridded datasets and methodology was applied as for the S-Mets model. Gridded monthly precipitation totals from the UDel precipitation dataset (Willmott and Matsuura, 2000) and monthly mean temperature data from the CRU TS 3.0

dataset (Mitchell and Jones, 2005) were spatially averaged for each of the MIKE SHE sub-catchments and stochastically disaggregated to a daily resolution using the Mac-PDM weather generator. This employed the same coefficient of variation for disaggregated daily precipitation and standard deviation of daily temperature as used for the S-Mets model, both of which were obtained from daily NCDC GSOD data (see Sections 4.2.6.1 and 4.2.6.3). Wet days data were obtained from the CRU TS 3.0 dataset (Mitchell and Jones, 2005). For the calculation of PN PET, gridded monthly data (cloud cover, mean daily minimum temperature, mean daily maximum temperature and vapour pressure) from the CRU TS 3.0 dataset (CRU TS 2.1 in the case of cloud cover) were employed. Monthly PET was evaluated for each of the MIKE SHE sub-catchments and then distributed evenly through each month.

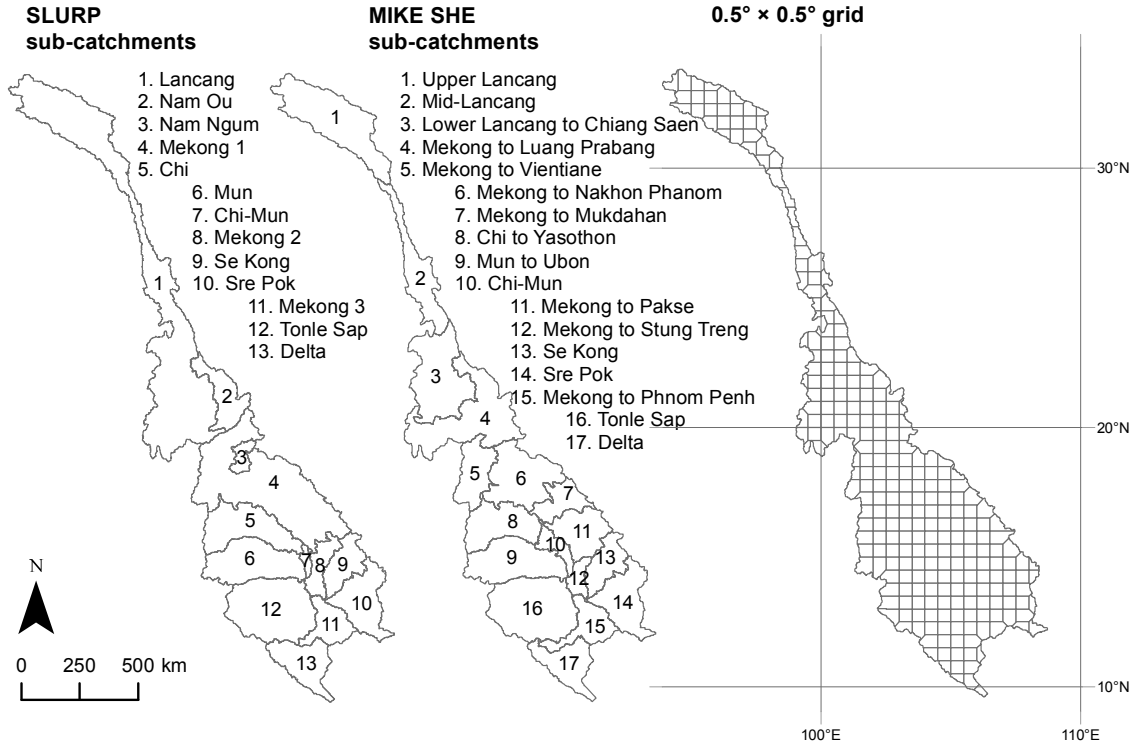

Figure 5.10. Alternative meteorological input spatial distributions for the Mekong catchment.

Attributes of the SLURP and MIKE SHE sub-catchments, including area, elevation statistics and number of CRU/UDel climate data grid cells that fall within each sub-catchment, are summarised in Table 5.8. Information is not shown for SLURP sub-catchments 12 and 13 or MIKE SHE sub-catchments 16 or 17 since these are downstream of the Phnom Penh gauging station, the most downstream point from which discharge results are extracted. This table demonstrates that the maximum

number of climate grid cells over which meteorological inputs must be spatially averaged is much greater in the case of the SLURP sub-catchments. With the MIKE SHE sub-catchments, the maximum number of climate data grid cells within a single sub-catchment is 29, for the Upper Lancang (sub-catchment 1), followed by 28, for the Mekong to Luang Prabang (sub-catchment 4). In contrast, the maximum number of grid cells within a single SLURP sub-catchment is 83 for the Lancang (sub-catchment 1), followed by 52 for Mekong 1 (sub-catchment 4).

Table 5.8. Attributes of the SLURP and MIKE SHE sub-catchments, including area, elevation statistics, and number of 0.5° × 0.5° grid CRU/UDel climate data grid cells that fall within each sub-catchment.

SLURP sub-catchment	**Area (km^2)**	**Min. elevation (masl)**	**Max. elevation (masl)**	**Median elevation (masl)**	**Number of CRU/UDel grid cells**
Lancang (1)	228,000	282	5956	1794	83
Nam Ou (2)	31,040	271	2009	930	10
Nam Ngum (3)	8,980	166	2601	1102	3
Mekong 1 (4)	158,250	96	2706	317	52
Chi (5)	56,590	103	1309	197	18
Mun (6)	61,570	97	1264	171	18
Chi-Mun (7)	4,220	107	525	147	1
Mekong 2 (8)	20,780	61	1637	144	7
Se Kong (9)	28,910	58	2100	429	9
Sre Pok (10)	48,840	63	2250	336	16
Mekong 3 (11)	28,000	7	927	97	8
MIKE SHE sub-catchment	**Area (km^2)**	**Min. elevation (masl)**	**Max. elevation (masl)**	**Median elevation (masl)**	**Number of CRU/UDel grid cells**
Upper Lancang (1)	73,870	2659	5639	4538	29
Mid-Lancang (2)	41,450	805	5956	2374	14
Lower-Lancang to Chiang Saen (3)	71,100	361	3122	1186	27
Mekong to Luang Prabang (4)	87,420	258	2195	824	28
Mekong to Vientiane (5)	34,630	149	2146	453	13
Mekong to Nakhon Phanom (6)	62,450	127	2706	234	19
Mekong to Mukdahan (7)	25,520	105	2207	224	9
Chi to Yasothon (8)	47,960	113	1309	207	16
Mun to Ubon (9)	61,270	97	1264	171	18
Chi-Mun (10)	13,270	102	535	139	3
Mekong to Pakse (11)	39,300	86	1894	205	13
Mekong to Stung Treng (12)	11,400	61	1399	112	3
Se Kong (13)	28,870	58	2100	425	9
Sre Pok (14)	48,650	63	2250	334	16
Mekong to Phnom Penh (15)	31,580	1	1471	91	10

For the G-Mets MIKE SHE model, the gridded monthly UDel precipitation and CRU temperature data covering the Mekong catchment were directly disaggregated to a daily resolution, i.e. without the requirement for prior spatial averaging. Similarly, gridded monthly PN PET was evenly temporally distributed through the month, again, without the requirement for prior spatial averaging.

5.3.2. Model calibration and validation

The model referred to as the S-Mets model in this section is the PN model described in Section 5.2, and was not altered. It therefore did not require re-calibration. However, the M-Mets and G-Mets models required calibration to achieve a similar performance for the baseline period as that achieved by the S-Mets model. The requirement for re-calibration following the specification of different meteorological data (in particular precipitation), or data with a different spatial distribution, has been reported elsewhere (e.g. Mileham *et al.*, 2008; Xu *et al.*, 2010; Vaze *et al.*, 2011).

The same calibration and validation procedures as described for the previous MIKE SHE models (Sections 4.4 and 5.2.2) were again employed. As before, the calibration parameters were the time constants of the saturated zone's baseflow reservoirs, a dead storage proportion for the baseflow reservoirs in a limited number of sub-catchments and, in sub-catchments with large elevation ranges, the precipitation lapse rate. Parameters were only adjusted where it was perceived necessary in order to achieve a similar model performance to that of the S-Mets model. Many parameters were therefore not changed. As in the case of the S-Mets model, the precipitation lapse rates within the M-Mets and G-Mets models were distributed according to the spatial extent of the MIKE SHE sub-catchments. This was deemed appropriate since the termini of these sub-catchments were made in many cases to coincide with gauging stations (e.g. Mekong to Chiang Saen, Mekong to Luang Prabang). This means that during calibration of the first, most upstream gauging station (Chiang Saen) lapse rates can be applied and adjusted over the area upstream of the station, and in the case of subsequent stations, the lapse rate can be applied and adjusted over the area between the previously calibrated and current station, and this area alone. Within the M-Mets model, temperature lapse rates over

the Lancang region (Upper Lancang and Mid-Lancang MIKE SHE sub-catchments) were also subject to calibration. In the G-Mets model, use of gridded temperature data negated the need for a temperature lapse rate since these data allowed appropriate build up and melting of snow over the upper Lancang region.

5.3.3. Simulation of climate change

For the S-Mets model, the same climate change scenarios as employed in Section 5.2 (for the PN model) were used. In the case of the M-Mets and G-Mets models, daily future climate scenario data (precipitation, temperature and PN PET with the model-appropriate spatial distribution) for a 30-year period were generated for the same 2 °C, seven GCM climate change scenarios using the gridded monthly outputs from the ClimGen spatial scenario generator. This followed the methodology described in Sections 4.5 and 5.2.3, except that data were spatially average over the MIKE SHE sub-catchments for the M-Mets models, and did not require spatial averaging for the G-Mets model. Scenario data were subsequently specified within the appropriate MIKE SHE models for climate scenario simulation.

5.3.4. Results

5.3.4.1. Baseline climate data

For the baseline period, Figure 5.11 presents the dry season (December–February), wet season (June–August) and annual UDel precipitation totals according to the SLURP sub-catchment based (S-Mets), MIKE SHE sub-catchment based (M-Mets) and gridded (G-Mets) input data for the Mekong catchment. These maps provide an indication of the different levels of spatial variability in precipitation magnitude that result from using the alternative meteorological input spatial distributions. As might be expected, the most notable differences between the S-Mets data and the two other datasets are seen over the regions of the two largest SLURP sub-catchments, the Lancang and Mekong 1 (see Figure 5.10). For example, mean annual precipitation over the Lancang SLURP sub-catchment is ~1053 mm. In contrast, over the same area, gridded mean annual precipitation totals vary between

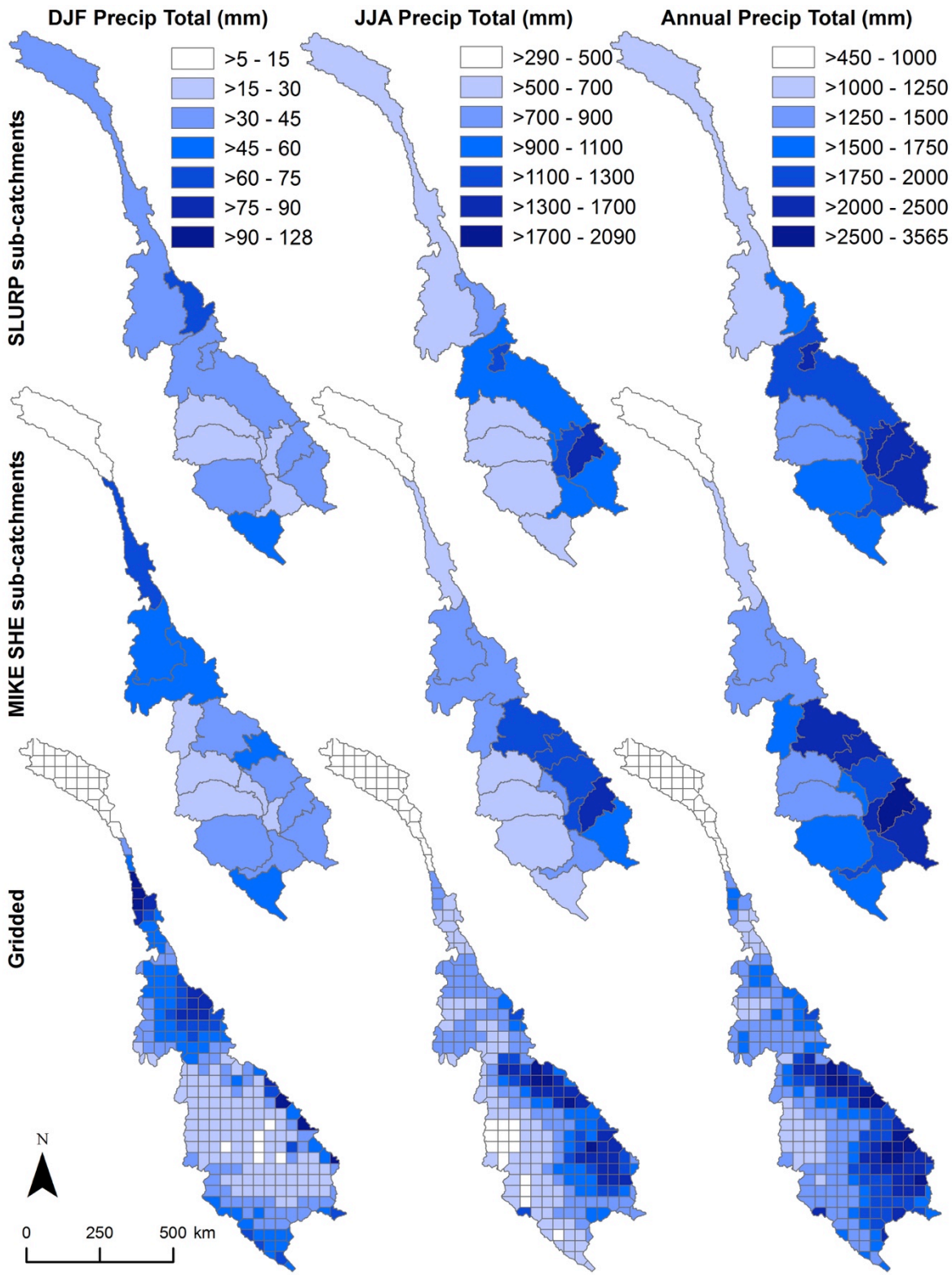

Figure 5.11. Seasonal precipitation totals for December–February (DJF; dry season) and June–August (JJA; wet season) and mean annual precipitation totals for the Mekong catchment for the period 1961–1990, according to the SLURP sub-catchment based (top), MIKE SHE sub-catchment based (middle) and gridded (bottom) data.

~450 mm and ~1645 mm. The MIKE SHE sub-catchments provide an intermediate level of spatial variability and over the same region exhibit annual precipitation totals of ~522 mm (Upper Lancang), ~1178 mm (Mid-Lancang) and >1380 mm (Lower Lancang and Mekong to Luang Prabang sub-catchments).

The S-Mets and M-Mets precipitation maps are very similar over much of the Lower Mekong (excluding the Mekong 1 SLURP sub-catchment), since the sub-catchments are generally closely aligned. At both the seasonal and annual level, the gridded data show a general increase in precipitation totals from west to east (and to the south in the case of DJF precipitation). This gradient is largely lost in the two sub-catchment averaged datasets. Within the SLURP sub-catchments, the northern part of the large Mekong 1 sub-catchment extends from the western border to the eastern border of the basin, meaning that there is no precipitation gradient over this region. In the case of the MIKE SHE sub-catchments, the SLURP Mekong 1 region is divided into four sub-catchments, allowing some variation in precipitation totals. To the south of this, in the case of both the S-Mets and M-Mets data, the division of the basin into western (e.g. Chi, Mun and Tonle Sap) and eastern (e.g. Se Kong and Sre Pok) sub-catchments means that there is a clear contrast between lower precipitation totals in the west, and higher totals in the east, but no incremental gradient as in the case of the gridded data. For a given meteorological input spatial distribution, the patterns are generally similar across the different time periods (DJF, JJA and annual precipitation totals).

Baseline temperature data are not presented here since: i) temperature is only relevant over the Lancang (only sub-catchment with snow); and ii) it was demonstrated in Chapter 4 that changes in temperature time series alone (i.e. use of scenario temperature and baseline precipitation and PET) have little impact on simulated flows.

Seasonal and annual PN PET totals for the baseline period according to the S-Mets, M-Mets and G-Mets input data are presented in Figure 5.12.

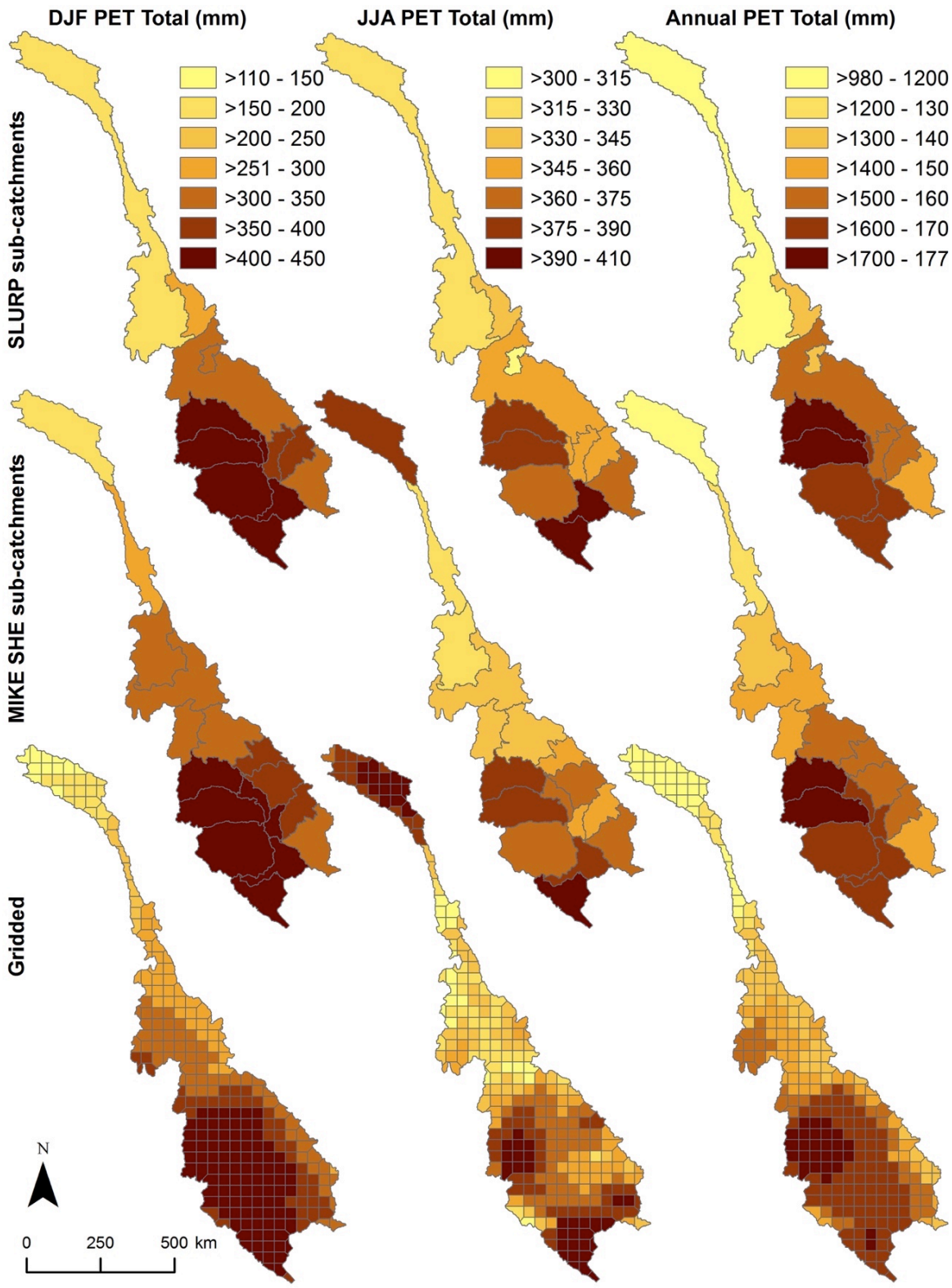

Figure 5.12. Seasonal PET totals for December–February (dry season) and June–August (wet season) and mean annual PET totals for the Mekong catchment for the period 1961–1990, according to the SLURP sub-catchment based (top), MIKE SHE sub-catchment based (middle) and gridded (bottom) data.

As with the precipitation data, the most notable differences between the S-Mets data and the other two datasets occur over the Lancang and Mekong 1 SLURP sub-catchments. For example, in the case of DJF and annual PET, the M-Mets and G-Mets data show an increase in magnitude from the Upper to Lower Lancang, whilst this region is represented by a single sub-catchment (and hence spatially uniform PET) in the case of the S-Mets data. Over the lower basin, the S-Mets and M-Mets datasets show similar patterns, again, due to the similarity in sub-catchment delineation. Westerly and southerly sub-catchments display higher seasonal and annual totals compared to easterly sub-catchments. In the case of the gridded data, there is a gradual gradient over the Lower Mekong from the southwest to the northeast, rather than a clear divide as with the sub-catchment based data.

5.3.4.2. Model calibration and validation

Through model calibration, it was possible to achieve a similar model performance to the S-Mets model (i.e. the PN MIKE SHE model from Section 5.2) in both the M-Mets and G-Mets models. This is illustrated in Figure 5.13, which presents the observed and simulated regimes from the three models for the calibration period. The validation regimes from the three models are likewise similar. Model performance statistics (Dv and NSE) for the calibration and validation periods are presented in Table 5.9. Performance indicators for the M-Mets and G-Mets models are close to those of the S-Mets model and are better in some cases.

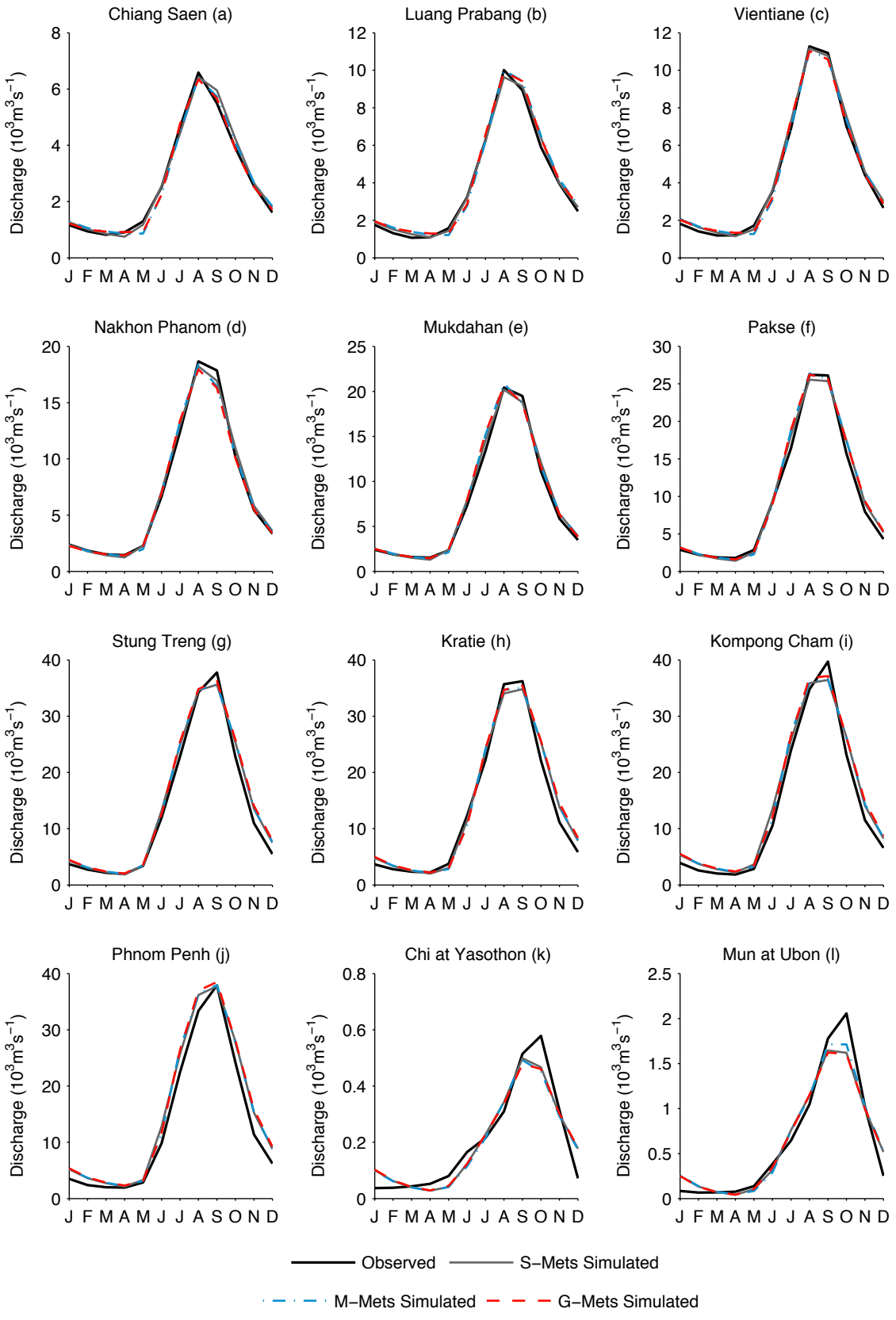

Figure 5.13. Observed and simulated regimes from the three MIKE SHE models for 12 gauging stations within the Mekong catchment for the calibration period.

Table 5.9. Model performance statistics based on mean monthly discharges from the three MIKE SHE models for twelve gauging stations within the Mekong catchment for the calibration (1961–1990 unless stated otherwise) and validation (1991–1998 unless stated otherwise) periods.

Station	Period	Dv (%)+			NSE*		
		S-Mets	M-Mets	G-Mets	S-Mets	M-Mets	G-Mets
Chiang Saen (a)	Cal	2.04 ☆☆☆☆☆	0.18 ☆☆☆☆☆	-0.92 ☆☆☆☆☆	0.90 ☆☆☆☆☆	0.92 ☆☆☆☆☆	0.93 ☆☆☆☆☆
	Val (1/91–6/97)	-7.20 ☆☆☆☆	-4.49 ☆☆☆☆☆	-7.63 ☆☆☆☆	0.79 ☆☆☆☆	0.79 ☆☆☆☆	0.81 ☆☆☆☆
Luang Prabang (b)	Cal	1.89 ☆☆☆☆☆	3.61 ☆☆☆☆☆	4.12 ☆☆☆☆☆	0.91 ☆☆☆☆☆	0.93 ☆☆☆☆☆	0.93 ☆☆☆☆☆
	Val (1/91–12/97)	-2.90 ☆☆☆☆☆	3.08 ☆☆☆☆☆	2.33 ☆☆☆☆☆	0.83 ☆☆☆☆	0.82 ☆☆☆☆	0.83 ☆☆☆☆
Vientiane (c)	Cal	3.03 ☆☆☆☆☆	0.43 ☆☆☆☆☆	0.66 ☆☆☆☆☆	0.92 ☆☆☆☆☆	0.94 ☆☆☆☆☆	0.94 ☆☆☆☆☆
	Val (1/91–12/96)	0.00 ☆☆☆☆☆	-0.38 ☆☆☆☆☆	-0.70 ☆☆☆☆☆	0.90 ☆☆☆☆☆	0.87 ☆☆☆☆☆	0.88 ☆☆☆☆☆
Nakhon Phanom (d)	Cal	0.84 ☆☆☆☆☆	-0.55 ☆☆☆☆☆	-1.52 ☆☆☆☆☆	0.92 ☆☆☆☆☆	0.93 ☆☆☆☆☆	0.94 ☆☆☆☆☆
	Val (1/91–11/95)	-4.22 ☆☆☆☆☆	-3.90 ☆☆☆☆☆	-5.25 ☆☆☆☆	0.90 ☆☆☆☆☆	0.89 ☆☆☆☆☆	0.90 ☆☆☆☆☆
Mukdahan (e)	Cal	2.86 ☆☆☆☆☆	3.74 ☆☆☆☆☆	3.78 ☆☆☆☆☆	0.91 ☆☆☆☆☆	0.93 ☆☆☆☆☆	0.93 ☆☆☆☆☆
	Val (1/91–12/95)	0.60 ☆☆☆☆☆	3.25 ☆☆☆☆☆	2.84 ☆☆☆☆☆	0.92 ☆☆☆☆☆	0.92 ☆☆☆☆☆	0.92 ☆☆☆☆☆
Pakse (f)	Cal	3.12 ☆☆☆☆☆	4.57 ☆☆☆☆☆	4.73 ☆☆☆☆☆	0.91 ☆☆☆☆☆	0.93 ☆☆☆☆☆	0.93 ☆☆☆☆☆
	Val	2.32 ☆☆☆☆☆	4.96 ☆☆☆☆☆	4.51 ☆☆☆☆☆	0.89 ☆☆☆☆☆	0.90 ☆☆☆☆☆	0.90 ☆☆☆☆☆
Stung Treng (g)	Cal (1/61–12/69)	6.11 ☆☆☆☆	6.43 ☆☆☆☆	7.86 ☆☆☆☆	0.93 ☆☆☆☆☆	0.94 ☆☆☆☆☆	0.94 ☆☆☆☆☆
	Val (1/91–12/93)	-9.53 ☆☆☆☆	-7.59 ☆☆☆☆	-6.76 ☆☆☆☆	0.88 ☆☆☆☆☆	0.90 ☆☆☆☆☆	0.90 ☆☆☆☆☆
Kratie (h)	Cal	4.07 ☆☆☆☆☆	4.57 ☆☆☆☆☆	5.84 ☆☆☆☆	0.91 ☆☆☆☆☆	0.92 ☆☆☆☆☆	0.92 ☆☆☆☆☆
	Val	2.44 ☆☆☆☆☆	3.68 ☆☆☆☆☆	4.53 ☆☆☆☆☆	0.87 ☆☆☆☆☆	0.88 ☆☆☆☆☆	0.87 ☆☆☆☆☆
Kompong Cham (i)	Cal (1/64–3/74)	9.06 ☆☆☆☆	9.06 ☆☆☆☆	9.64 ☆☆☆☆	0.93 ☆☆☆☆☆	0.94 ☆☆☆☆☆	0.94 ☆☆☆☆☆
	Val†	—	—	—	—	—	—
Phnom Penh (j)	Cal (1/61–3/74)	14.97 ☆☆☆	15.02 ☆☆☆	16.61 ☆☆☆	0.92 ☆☆☆☆☆	0.92 ☆☆☆☆☆	0.92 ☆☆☆☆☆
	Val†	—	—	—	—	—	—
Chi at Yasothon (k)	Cal	-0.56 ☆☆☆☆☆	-2.67 ☆☆☆☆☆	-1.21 ☆☆☆☆☆	0.56 ☆☆☆	0.56 ☆☆☆	0.57 ☆☆☆
	Val (1/91–12/95)	9.93 ☆☆☆☆	6.66 ☆☆☆☆	9.30 ☆☆☆☆	0.15 ☆	0.15 ☆	0.20 ☆☆
Mun at Ubon (l)	Cal	-0.11 ☆☆☆☆☆	1.86 ☆☆☆☆☆	-0.33 ☆☆☆☆☆	0.61 ☆☆☆	0.62 ☆☆☆	0.65 ☆☆☆☆
	Val (1/91–12/93)	1.28 ☆☆☆☆☆	2.01 ☆☆☆☆☆	0.76 ☆☆☆☆☆	0.34 ☆☆	0.29 ☆☆	0.38 ☆☆

Performance indicator	Excellent ☆☆☆☆☆	Very good ☆☆☆☆	Fair ☆☆☆	Poor ☆☆	Very poor ☆
Dv	< 5%	5–10%	10–20%	20–40%	>40%
NSE	>0.85	0.65–0.85	0.50–0.65	0.20–0.50	<0.20

+ Percentage deviation in simulated mean flow from observed mean flow (Henriksen *et al.*, 2003).
* Nash–Sutcliffe coefficient (Nash and Sutcliffe, 1970).
† Validation not possible due to absence of observations.

5.3.4.3. Scenario climate data

For the meteorological input data with alternative spatial distributions, changes (compared to the baseline period) in mean annual, JJA and DJF precipitation totals under the 2 °C, seven GCM scenarios are presented in Figures 5.14, 5.15 and 5.16, respectively. Use of sub-catchment based data for the baseline and scenario means that there is a uniform percentage change over each sub-catchment. These maps demonstrate how the use of sub-catchment averaged data compared to gridded data impacts the spatial pattern and variability in changes. In the majority of cases, use of sub-catchment based data does not impact the direction of change over a particular region. For example, increases in annual precipitation are seen over all grid cells and hence all sub-catchments for the CCCMA, MPI and NCAR GCMs.

However, in cases where some of the grid cells located within a sub-catchment display increases under climate change, and others show decreases, the direction of change may be altered over some areas within a sub-catchment, or little change may occur over the whole sub-catchment. For example, in the case of changes in annual precipitation projected using the CSIRO GCM, the gridded data display increases over the upper Lancang (of up to 11.6%) and decreases over the mid to lower Lancang (maximum: -11.3%). Conversely, the Lancang SLURP sub-catchment exhibits a decrease of -4.6%. A similar pattern is seen in the case of DJF and JJA precipitation with CSIRO. For changes in annual and JJA precipitation projected by the IPSL GCM, the gridded data show reductions over the western Khorat Plateau and increases over the eastern Khorat Plateau. However, spatial averaging results in little projected change (no greater than ±1%) over the Chi and Mun SLURP and MIKE SHE (except JJA precipitation over Chi) sub-catchments.

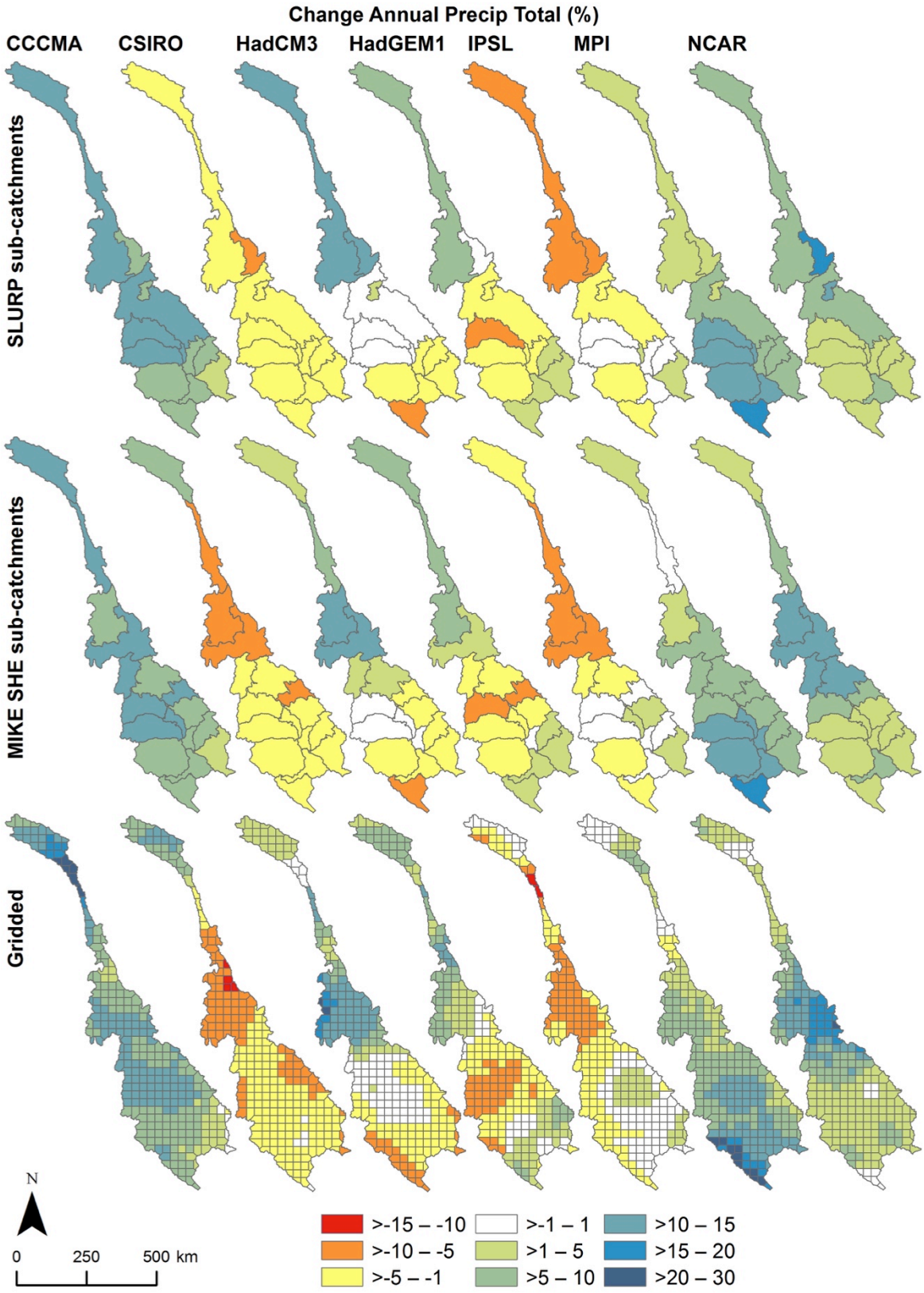

Figure 5.14. Change (%) in mean annual precipitation totals for the Mekong catchment under the 2 °C, seven GCM scenarios, according to the SLURP sub-catchment based (top), MIKE SHE sub-catchment based (middle) and gridded (bottom) data.

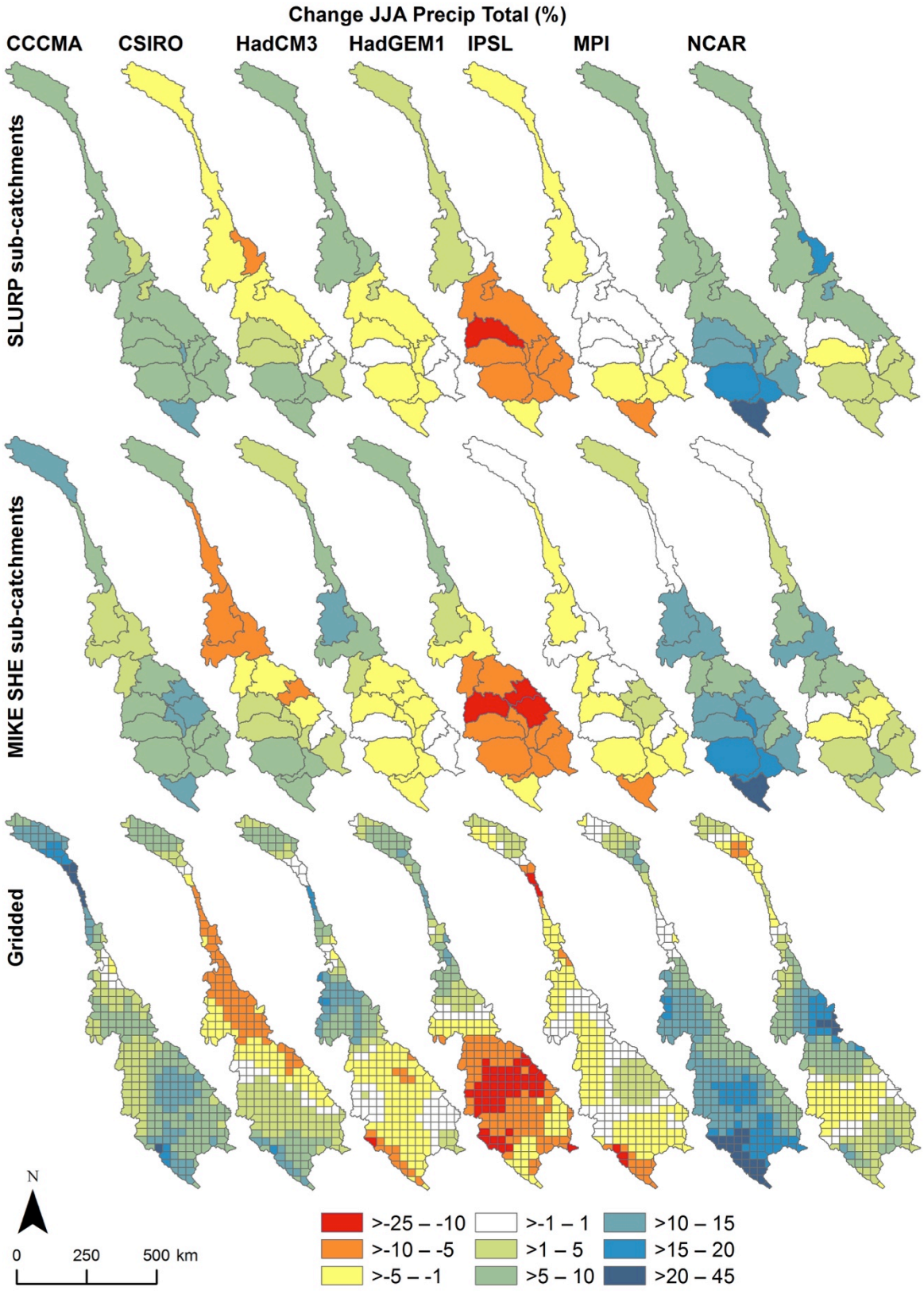

Figure 5.15. Change (%) in JJA precipitation totals for the Mekong catchment under the 2 °C, seven GCM scenarios, according to the SLURP sub-catchment based (top), MIKE SHE sub-catchment based (middle) and gridded (bottom) data.

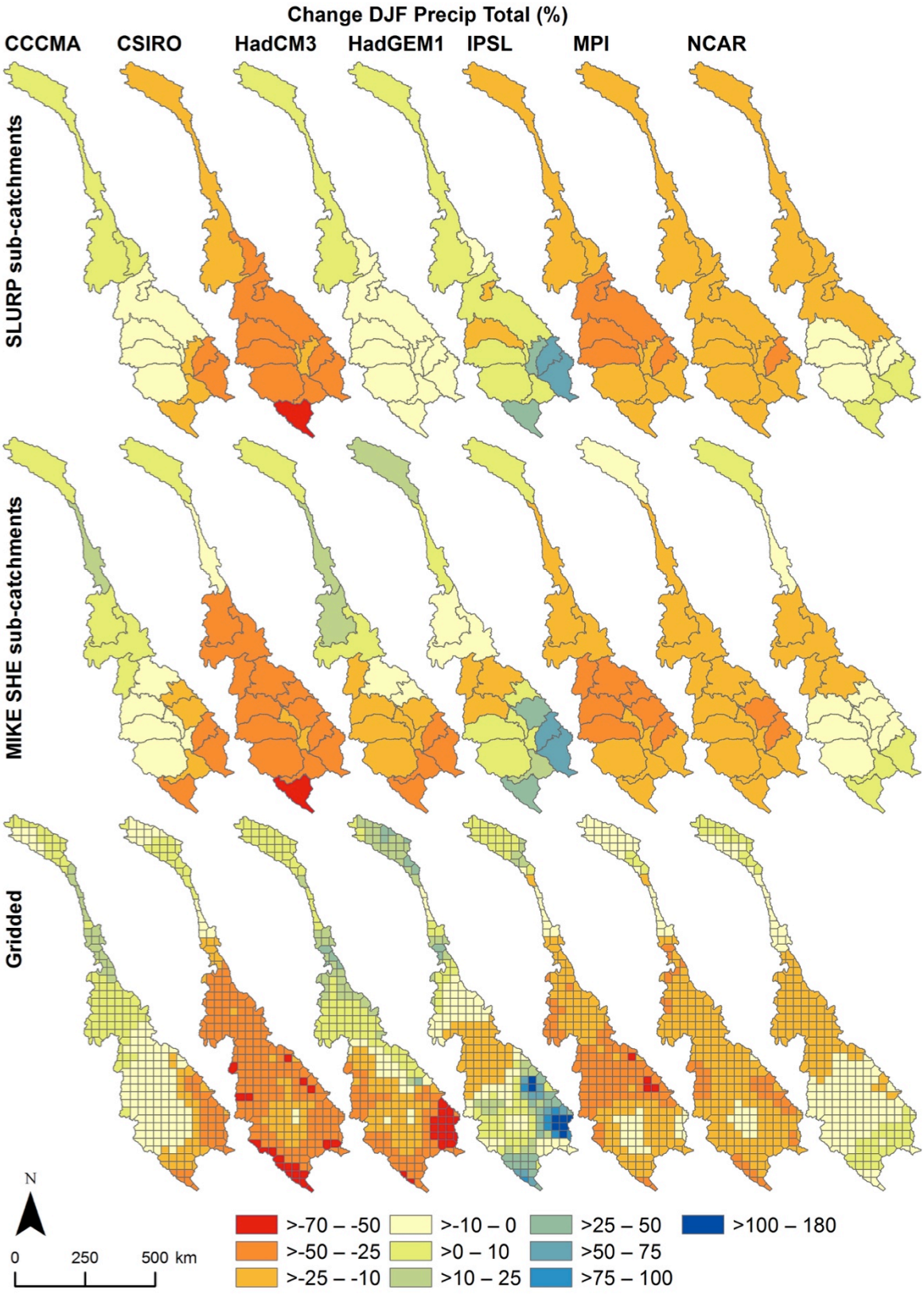

Figure 5.16. Change (%) in DJF precipitation totals for the Mekong catchment under the 2 °C, seven GCM scenarios, according to the SLURP sub-catchment based (top), MIKE SHE sub-catchment based (middle) and gridded (bottom) data.

Percentage changes (compared to the baseline period) in mean annual, JJA and DJF PET totals under the 2 °C, seven GCM scenarios are presented in Figures 5.17, 5.18 and 5.19, respectively, for the alternative meteorological input spatial distributions. It is clear from these maps that compared to the precipitation change maps, the gridded PET data show much less spatial variability in terms of the magnitude and direction of projected change. As with precipitation, for each GCM scenario, differences between the S-Mets change map and the other two change maps are generally greatest over the Lancang region. For example, for changes in JJA PET totals, the S-Mets maps show projected increases over the Lancang for all GCMs except HadCM3 (-0.9%). However, the gridded change maps for CCCMA, CSIRO and NCAR show reductions (or little change in the case of CSIRO) in PET over the upper to mid-Lancang, and increases over the mid to lower-Lancang, whilst for HadCM3, reductions are projected for the majority of grid cells falling within the Lancang region, with the greatest reductions over the mid-Lancang. The change patterns displayed in the M-Mets maps more closely match those of the gridded data. For example, for CCCMA, the M-Mets change map shows a projected decrease over the Upper Lancang, little change (-0.2%) over the Mid-Lancang and an increase over the Lower-Lancang. It is worth noting here that projected reductions in PET are not associated with the projected changes in temperature, since all grid cells show projected increases in temperature throughout the year. Instead, reductions are associated with the projected changes in cloud cover and vapour pressure.

In general, the S-Mets and M-Mets data show very similar change patterns over the Lower Mekong Basin. Although in some cases the division of the Mekong 1 SLURP sub-catchment into four MIKE SHE sub-catchments means that the latter displays slightly greater variability, the differences are generally small. For example, Mekong 1 shows a reduction of -0.2% in JJA PET with NCAR, whilst the corresponding MIKE SHE sub-catchments in this area show changes of between -1.5% to +1.7%. Regardless of spatial distribution method, increases in annual and DJF PET totals are projected throughout the Lower Mekong Basin for all seven GCMs. For the majority of grid cells and sub-catchments, increases of between 5–15% are projected. For JJA PET totals, increases are projected for all grid cells, and hence all sub-catchments, using the CCCMA, CSIRO, HadGEM1 and IPSL GCMs.

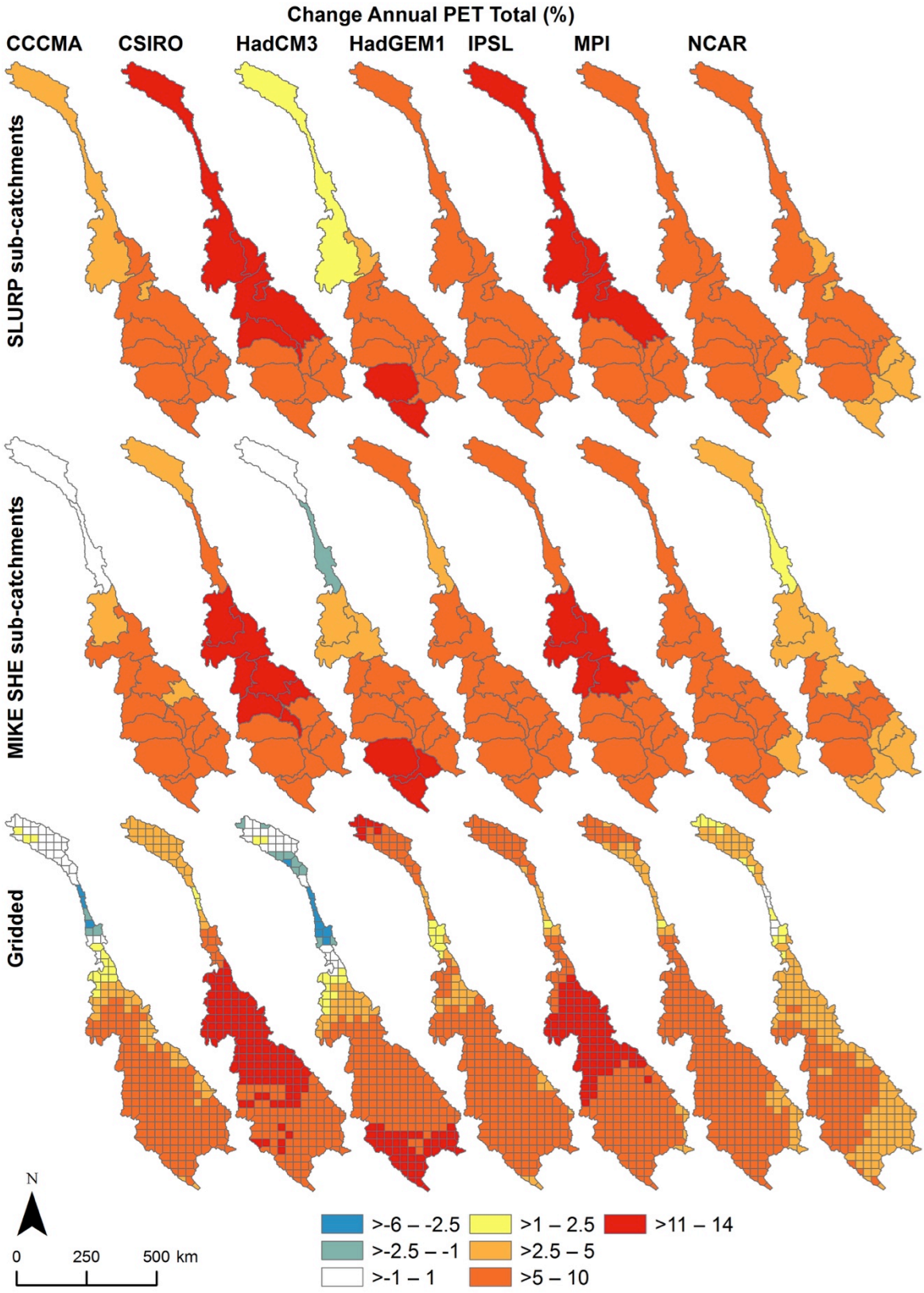

Figure 5.17. Change (%) in mean annual PET totals for the Mekong catchment under the 2 °C, seven GCM scenarios, according to the SLURP sub-catchment based (top), MIKE SHE sub-catchment based (middle) and gridded (bottom) data.

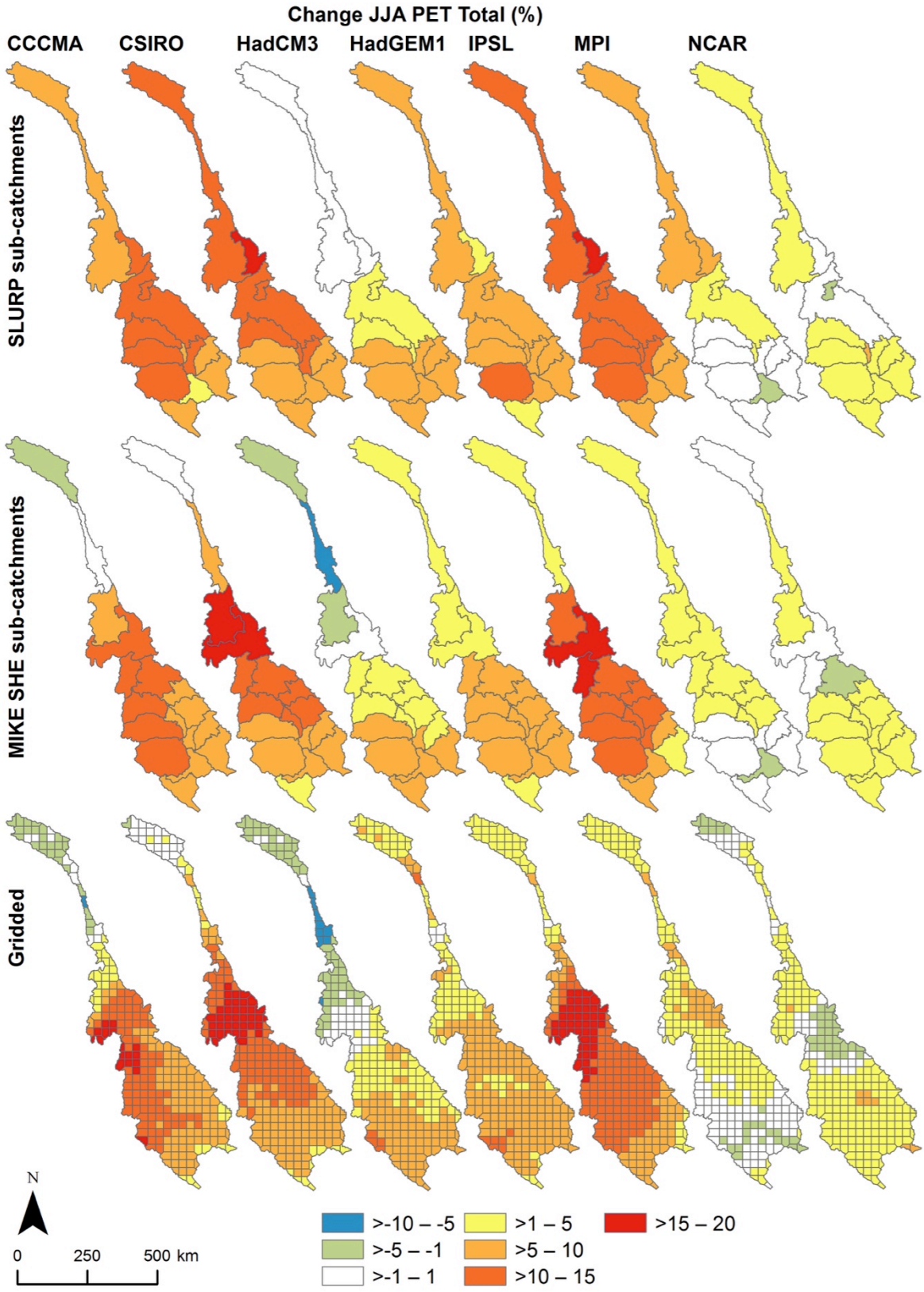

Figure 5.18. Change (%) in JJA PET totals for the Mekong catchment under the 2 °C, seven GCM scenarios, according to the SLURP sub-catchment based (top), MIKE SHE sub-catchment based (middle) and gridded (bottom) data.

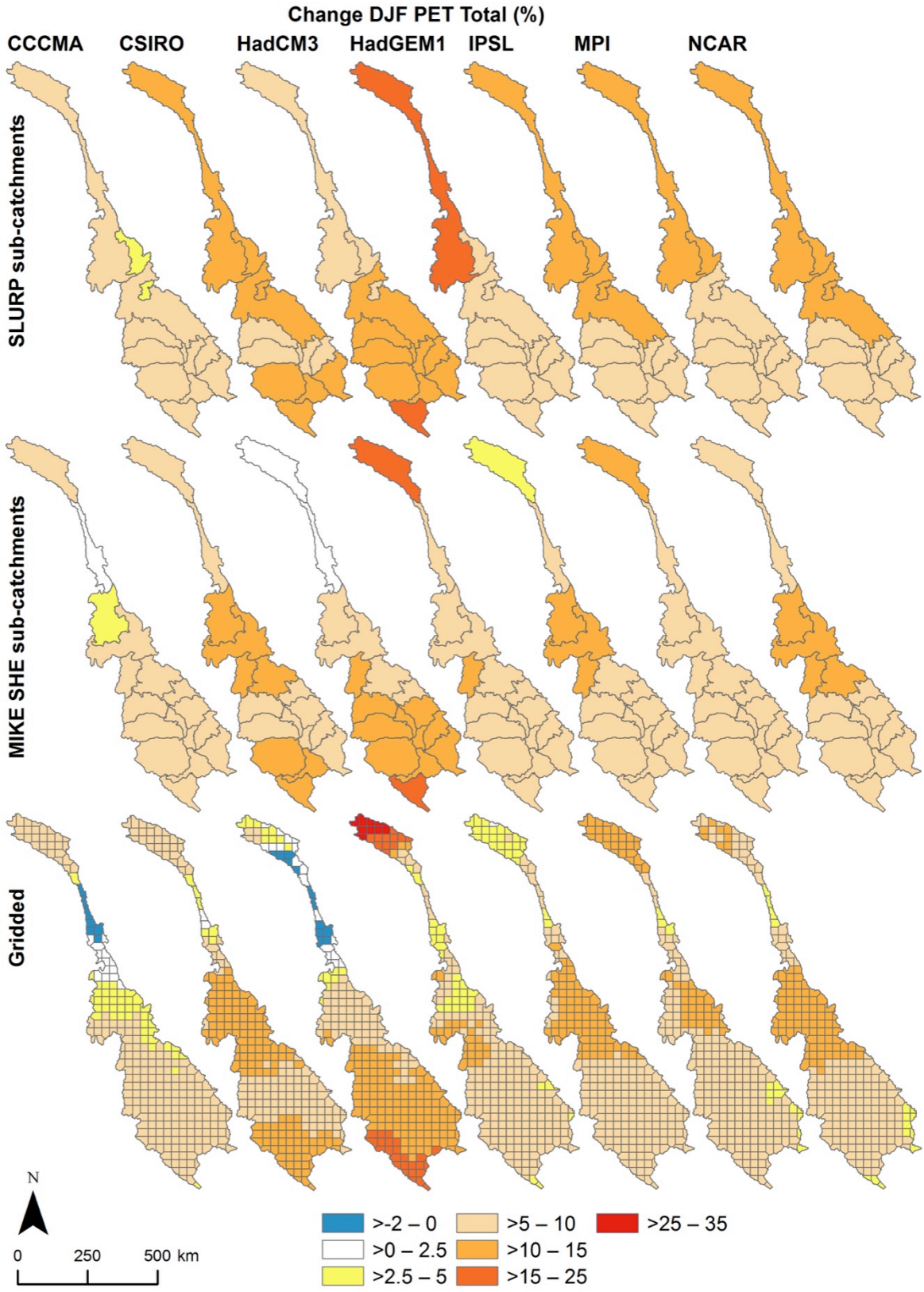

Figure 5.19. Change (%) in DJF PET totals for the Mekong catchment under the 2 °C, seven GCM scenarios, according to the SLURP sub-catchment based (top), MIKE SHE sub-catchment based (middle) and gridded (bottom) data.

5.3.4.4. Scenario river discharge

In a similar way to Table 5.6 for the models employing alternative PET methods, Table 5.10 presents mean baseline discharge and percentage changes in these discharges for each of the 2 °C scenarios for the three models with different spatial distributions of meteorological inputs. Results are provided for the same eight representative gauging stations. For each scenario/station combination, the absolute range in percentage changes simulated by the three models is also shown. At the bottom of the table, for each station, the variability across the MIKE SHE models in mean baseline and scenario discharges is expressed as the difference between the largest and smallest mean discharge for a given scenario (i.e. the range) as a percentage of the overall average of the mean discharges for that scenario. Changes in mean annual and monthly Q95 and Q5 discharges for each MIKE SHE model are shown in Figure 5.20 for four stations on the main Mekong. Changes in mean discharge for each gauging station on the main Mekong (from upstream – station a, to downstream – station j) are presented in Figure 5.21.

The pattern and magnitude of simulated changes in mean discharge is very similar across all three MIKE SHE models (Figure 5.20; Figure 5.21). Increases are consistently projected for all stations for CCCMA and NCAR, and for all stations on the main Mekong for HadCM3 (Table 5.10). For CCCMA, the absolute range of percentage changes from the three hydrological models is less than 2% at all stations except Chiang Saen (2.8%) and shows a general reduction with distance downstream, with consistent values of 0.1–0.3% between Nakhon Phanom and Phnom Penh (d–j). For NCAR, the absolute range of percentage changes across the three models is slightly larger at stations between Luang Prabang and Mukdahan (b–e), but is still low (between 2.2% and 3.8%). At other stations the range is ≤1%. A similar pattern is seen with HadCM3, with the range in percentage changes projected by the three models reaching 4.6% at Vientiane. All three models display a reduction in the magnitude of projected increases in a downstream direction from Luang Prabang onwards. In the case of all three GCMs (CCCMA, NCAR and HadCM3) on the main Mekong, simulated changes from the M-Mets and G-Mets models tend to be very similar (maximum inter-model difference of 0.4%), with the S-Mets model generally producing slightly lower increases in mean discharge.

Table 5.10. Mean baseline discharge (m^3s^{-1}) and change from baseline mean discharge (%) for the three models for each GCM at eight gauging stations. Grey shading indicates negative changes compared to the baseline. The absolute range in percentage changes for each station/scenario is also shown. The range of mean discharges for the baseline and each GCM from the different models are also indicated at the bottom (% of overall mean discharge from the three models for that scenario).

Scenario	Model / Scenario	Chiang Saen (a)	Luang Prabang (b)	Vientiane (c)	Mukda-han (e)	Pakse (f)	Kratie (h)	Phnom Penh (j)	Ubon (l)
Baseline (m^3s^{-1})	S-Mets	2766.7	4055.6	4658.0	7819.6	10143.5	13964.6	14363.5	635.6
	M-Mets	2716.3	4124.0	4540.5	7886.6	10285.9	14031.9	14396.1	648.1
	G-Mets	2686.4	4144.3	4550.8	7889.7	10302.3	14203.0	14578.7	634.2
CCCMA (% change)	S-Mets	10.6	11.3	11.6	12.0	12.4	10.6	10.5	13.8
	M-Mets	13.5	12.8	12.6	12.2	12.7	10.8	10.7	13.0
	G-Mets	13.1	12.5	12.5	12.1	12.8	10.8	10.7	13.8
	Range	2.8	1.5	1.0	0.2	0.3	0.2	0.2	0.8
CSIRO (% change)	S-Mets	-18.2	-18.1	-17.1	-13.8	-12.2	-10.1	-9.8	-4.0
	M-Mets	-16.4	-16.7	-16.2	-13.1	-11.6	-9.6	-9.3	-2.6
	G-Mets	-16.0	-16.4	-15.8	-12.9	-11.3	-9.4	-9.2	-3.6
	Range	2.3	1.7	1.3	1.0	0.9	0.7	0.6	1.4
HadCM3 (% change)	S-Mets	18.7	18.9	16.6	10.6	8.0	4.4	4.1	-2.4
	M-Mets	19.8	22.6	21.2	12.0	8.5	4.8	4.5	-2.7
	G-Mets	19.7	22.2	21.0	11.6	8.2	4.7	4.4	-2.4
	Range	1.1	3.7	4.6	1.3	0.4	0.4	0.4	0.4
HadGEM1 (% change)	S-Mets	0.3	-0.8	-2.0	-4.5	-6.0	-4.5	-4.4	-14.0
	M-Mets	6.6	4.1	2.9	-2.1	-4.3	-3.2	-3.2	-11.1
	G-Mets	6.2	4.0	3.0	-2.3	-4.3	-3.1	-3.1	-11.9
	Range	6.3	4.9	5.0	2.5	1.7	1.3	1.2	3.0
IPSL (% change)	S-Mets	-18.0	-16.1	-14.4	-9.7	-7.5	-5.6	-5.5	0.8
	M-Mets	-14.1	-13.4	-13.1	-8.3	-5.9	-4.4	-4.4	0.4
	G-Mets	-13.3	-12.4	-12.2	-7.8	-5.5	-4.1	-4.1	0.8
	Range	4.7	3.7	2.2	1.9	2.1	1.5	1.4	0.4
MPI (% change)	S-Mets	-1.4	1.3	2.8	5.9	8.5	9.8	10.1	21.7
	M-Mets	1.8	4.8	5.6	7.6	10.2	11.1	11.5	24.4
	G-Mets	1.9	4.6	5.3	7.3	9.7	10.6	10.9	21.2
	Range	3.3	3.5	2.8	1.7	1.7	1.3	1.3	3.3
NCAR (% change)	S-Mets	11.5	16.3	16.4	16.3	14.8	11.9	11.7	7.1
	M-Mets	12.4	20.0	20.1	18.5	15.0	12.3	12.1	6.7
	G-Mets	12.5	20.1	20.3	18.0	14.6	11.8	11.6	6.3
	Range	1.0	3.8	3.9	2.2	0.4	0.5	0.5	0.8
Range of mean discharges (% of overall mean from the three models)	Baseline	2.9	2.2	2.6	0.9	1.5	1.7	1.5	2.2
	CCCMA	1.4	3.3	1.7	1.0	1.8	1.9	1.7	1.5
	CSIRO	0.6	4.2	1.5	2.0	2.5	2.4	2.2	3.4
	HadCM3	2.1	4.9	1.3	2.0	1.8	2.0	1.8	1.8
	HadGEM1	4.2	6.8	2.6	3.4	3.3	3.1	2.8	5.4
	IPSL	2.8	6.4	1.3	2.9	3.8	3.2	2.9	1.8
	MPI	1.4	5.3	0.1	2.5	2.9	2.4	2.2	4.9
	NCAR	2.0	5.4	0.9	2.7	1.6	1.6	1.4	2.5

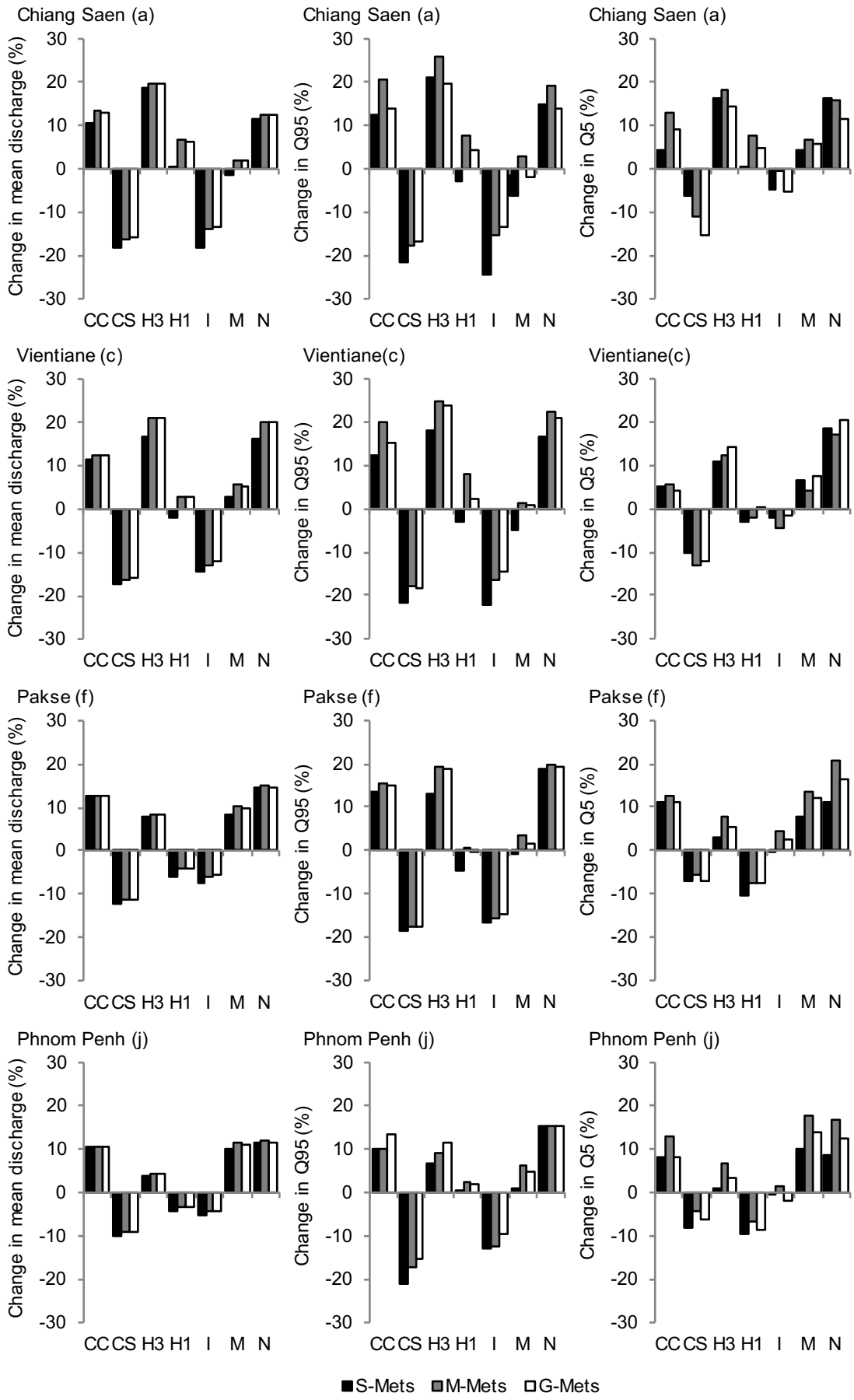

Figure 5.20. Change from baseline mean, Q5 and Q95 discharges for the 2 °C, seven GCM scenarios and each MIKE SHE model for four gauging stations. CC: CCCMA; CS: CSIRO; H3: HadCM3; H1: HadGEM1; I: IPSL; M: MPI; N: NCAR.

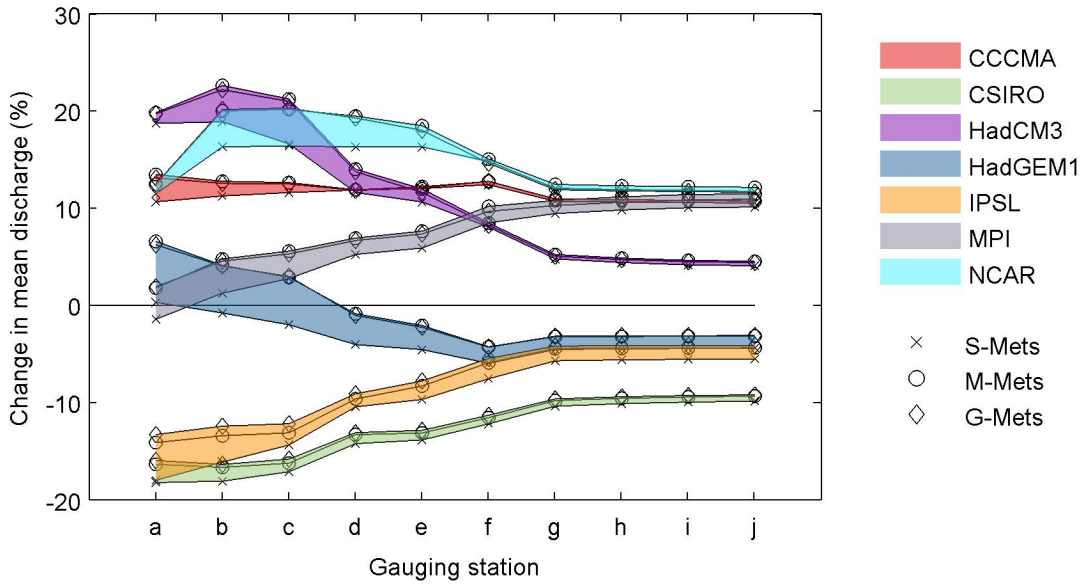

Figure 5.21. Change in mean discharge (%) for gauging stations on the main Mekong for the 2 °C, seven GCM scenarios and each MIKE SHE model (S-Mets, M-Mets and G-Mets). Shaded bands indicate the range of inter-MIKE SHE model uncertainty and enable identification of which GCM the scatter points refer to.

With the MPI GCM, the S-Mets model simulates a small (-1.4%) reduction in mean discharge at Chiang Saen, whilst the M-Mets and G-Mets models project small increases (1.8% and 1.9%, respectively). However, the inter-model range in percentage change is only 3.3%. Increases in mean discharge are projected by all three models at all other stations and the inter-model range in percentage change shows a general reduction in magnitude from Luang Prabang (3.5%) downstream.

Reductions in mean discharge are projected by all three MIKE SHE models for all stations with the CSIRO GCM, and for all stations on the main Mekong with IPSL. The magnitude of change decreases with distance downstream on the main Mekong for both GCMs with all three MIKE SHE models. The S-Mets model is consistently responsible for the greatest reductions, but inter-model differences are generally small. For CSIRO and IPSL, the range in percentage change from the three models shows a maximum of 2.3% and 4.7%, respectively, at Chiang Saen, and then a general reduction in magnitude with distance downstream until Pakse, after which inter-model differences show little variation. The inter-model ranges in percentage change at Yasothon and Ubon are consistently low (<2%).

The greatest inter-MIKE SHE model differences for change in mean discharge are seen with the HadGEM1 GCM. For the S-Mets model, an increase in mean discharge is restricted to Chiang Saen. In contrast, the M-Mets and G-Mets models, for which results are very similar, show increases down to Vientiane, and reductions for gauging stations downstream of this. The inter-model range in percentage change is 6.3% at Chiang Saen and exhibits a downstream reduction in magnitude.

For comparison, the inter-GCM range of change in mean discharge (difference between the maximum and minimum projected percentage change across the seven GCMs) for a given MIKE SHE model at given gauging station varies between 30% and 40% for stations between Chiang Saen and Mukdahan, and between 20% and 27% for stations on the main Mekong between Pakse and Phnom Penh. Across the 42 gauging station/GCM combinations (six stations × seven GCMs) in Table 5.10, the average inter-MIKE SHE model range of change in mean discharge is only 1.9%. Conversely, the average inter-GCM range of change in mean discharge across the eight stations in Table 5.10 is ~30% for each of the three MIKE SHE models. This demonstrates that for changes in mean discharge, the magnitude of GCM-related uncertainty is far greater than that associated with the spatial distribution of meteorological inputs.

Furthermore, the inter-model range of discharges expressed as a percentage of the overall mean from the three models (bottom section of Table 5.10) is, in many cases, close to (and sometimes even less than) that of the baseline. For the baseline, for the stations in Table 5.10 the difference between the largest and smallest mean discharges at a given gauging station is, on average, 1.9% of the overall mean from the three models. For the scenarios, mean inter-MIKE SHE model range in mean discharge is 1.8% for CCCMA and for the other GCMs increases to between 2.2–2.4% (CSIRO, HadCM3, and NCAR) and 3.9% (HadGEM1). This indicates that for the CCCMA GCM scenario, the level of inter-model variability is, on average, no greater than that experienced under the baseline. Although the other GCMs show increases in inter-model variability compared to the baseline at a greater number of stations, the increases are generally small. For all GCM scenarios, the greatest inter-model range of discharges (as a percentage of the overall mean from the three models) is

associated with the Luang Prabang gauging station, ranging from 3.3% (CCCMA) to 6.8% (HadGEM1). This station exhibited a range of 2.2% under baseline conditions.

Figure 5.20 demonstrates that there is generally slightly greater inter-model uncertainty associated with changes in Q95 and Q5 discharges. The average (across the seven GCMs) inter-MIKE SHE model range of percentage change in Q95 (low flows) is 7.9% at Chiang Saen (maximum of 11.0% for IPSL), 8.5% at Luang Prabang (maximum of 11.1% for HadGEM1) and between 7.0% and 3.1% at stations from Vientiane downstream to Phnom Penh. This contrasts to an average (across the seven GCMs) inter-MIKE SHE model range of percentage change in mean discharge of 3.1% at Chiang Saen (maximum: 6.3% for HadGEM1), 2.7% at Luang Prabang (maximum: 4.3% for HadGEM1) and between 3.3% and 0.8% at stations from Vientiane downstream to Phnom Penh. The average (across the seven GCMs) inter-MIKE SHE model range of percentage change in Q5 (high flows) at each station varies between 5.8% at Chiang Saen (maximum of 9.3% for CSIRO) and 1.9% (Stung Treng). This demonstrates that the uncertainty associated with the spatial distribution of meteorological inputs is greater for changes in high and low flows compared to changes in mean discharge.

However, choice of GCM remains a far greater source of uncertainty for changes in Q5 and Q95 discharges. For change in Q95, the inter-GCM range in percentage change is over 29% at all stations for all three MIKE SHE models, and above 20% for all stations for Q5. Furthermore, in the majority of cases the three MIKE SHE models project the same direction of change for a given GCM/gauging station. Exceptions include change in Q5 with HadGEM1 at Luang Prabang, where the S-Mets model projects a small decrease of -1.2% whilst the M-Mets and G-Mets models project small increases of 3.4% and 2.5%, respectively. Exceptions that can be seen in Figure 5.20 include change in Q95 at Chiang Saen and Vientiane with the MPI GCM and change in Q95 at Pakse for the HadGEM1 GCM.

5.4. An assessment of the uncertainty associated with the use of alternative baseline precipitation data

This section investigates the uncertainty in river discharge projections associated with the use of alternative precipitation data during hydrological model calibration/validation and baseline simulation. Sections 5.4.1–5.4.2 describe the development of a MIKE SHE Mekong model that employs precipitation data derived from the CRU TS 3.0 dataset, rather than the previously used UDel dataset. Section 5.4.3 then outlines the generation of climate change scenario data for the additional model for the 2 °C, seven GCM scenarios. The results section (5.3.4) presents the climate scenarios and the calibration, validation and climate change scenario results of the two MIKE SHE models that employ alternative baseline precipitation data.

5.4.1. Alternative baseline precipitation – model development

The MIKE SHE models in previous sections have all used baseline precipitation data derived from the UDel dataset (Willmott and Matsuura, 2000). To investigate the impact that use of alternative baseline precipitation data can have on calibrated model parameter values and discharge projections under climate change, a MIKE SHE model is developed that uses precipitation derived from the CRU TS 3.0 dataset (Mitchell and Jones, 2005). Whilst there are several gridded precipitation datasets available, CRU was selected because it is very widely used, was employed in most of the QUEST-GSI studies (Todd *et al.*, 2011), and, unlike many alternative datasets (see for example Lauri *et al.*, 2014), CRU covers the full 1961–1990 baseline period. Although it would potentially be interesting to explore the use of a daily dataset such as APHRODITE (Yatagai *et al.*, 2012), the ClimGen scenario outputs used throughout this chapter cannot be employed to perturb baseline data with a daily resolution.

The model that uses CRU precipitation was based on the MIKE SHE model developed in Section 5.3 that uses PN PET and employs the MIKE SHE sub-catchments for the distribution of meteorological inputs (the M-Mets model). This model was selected because it is the intermediate option between use of 0.5° × 0.5° gridded meteorological inputs and the SLURP sub-catchment averaged inputs. Furthermore, this means that the same sub-catchments are used for the meteorological inputs as

for the linear reservoir groundwater sub-catchments, which would likely have been the case if the MIKE SHE model had been developed independently from SLURP.

Daily CRU-based precipitation data for 1961–1998 were derived for the MIKE SHE meteorological input sub-catchments using the same methodology as for the UDel based data (see Sections 4.2.6.1 and 5.3.1). These alternative data were then specified within the M-Mets MIKE SHE model developed in Section 5.3. The model employing CRU-based precipitation is subsequently referred to as the CRU-precip MIKE SHE model, whilst the M-Mets MIKE SHE model that this was based on is instead referred to as the UDel-precip MIKE SHE model within this section.

5.4.2. Model calibration and validation

Specification of the CRU-based precipitation data within the MIKE SHE model necessitated model re-calibration. This was undertaken manually using the same calibration procedure and calibration parameters as described for the MIKE SHE models employing alternative meteorological input spatial distributions (see Section 5.2.2). For each gauging station, the objective was to achieve a similarly good or better level of performance as the UDel-precip MIKE SHE model. For some gauging stations (discussed further in Section 5.2.4.2), adjustment of model parameters could not achieve any notable improvement in model performance and so parameters were again left unchanged, despite model performance not being comparable to that of the UDel-precip model at some gauging stations.

5.4.3. Simulation of climate change

For simulation of climate change using the CRU-precip MIKE SHE model, the same temperature and PN PET data for the 2 °C, seven GCM scenarios as used and presented in Section 5.2 were again employed. CRU-based precipitation scenario data were generated using a delta-change approach. For each GCM scenario, mean monthly multiplicative/ratio delta factors were derived using the gridded UDel-based baseline and scenario precipitation data. These delta factors were then applied to the gridded CRU-based baseline data. As before, the monthly gridded scenario precipitation was spatially averaged at the MIKE SHE meteorological input

sub-catchment scale and disaggregated to daily resolution using the Mac-PDM weather generator. The same scenario wet days data were employed as were used for the UDel data. Although this method would not provide exactly the same scenario data as if the data had been generated using the ClimGen technique, it was deemed a suitable approach for the purposes of this uncertainty assessment. ClimGen also uses a multiplicative approach to perturb baseline data.

Scenario results from the CRU-precip MIKE SHE model are subsequently compared with scenario results previously generated by the UDel-precip MIKE SHE model (which is the M-Mets model in Section 5.3).

5.4.4. Results

5.4.4.1. Baseline precipitation

For the period 1961–1998, Figure 3.10 presents mean monthly UDel- and CRU-based SLURP sub-catchment average precipitation for four sub-catchments and Figure 3.11 displays monthly mean and mean annual UDel- and CRU-based SLURP sub-catchment average precipitation values. Figure 3.11 clearly demonstrates that the UDel-based data generally show higher annual precipitation values in the majority of years for most sub-catchments excluding the Chi and the Mun, for which values are generally similar. Furthermore, Figure 3.10 indicates that the pattern of mean monthly precipitation also sometimes differs between the two datasets.

For the baseline period of 1961–1990, Figure 5.22 presents UDel- and CRU-based MIKE SHE sub-catchment average mean monthly precipitation. Data are not shown for the smallest sub-catchment (Chi-Mun). This figure further demonstrates that the two datasets are very similar over the Khorat Plateau (Chi and Mun). UDel and CRU also show similar values over the four northernmost sub-catchments (1–4), with a maximum difference in mean monthly precipitation of 31 mm in August for the sub-catchment 4. UDel shows greater values in the majority of cases. Differences are more notable over sub-catchments 5 to 7 and are greatest during the wet season, with maximum differences, of 59 mm, 143 mm and 102 mm occurring in July for sub-catchments 5, 6 and 7, respectively. The pattern of mean monthly precipitation

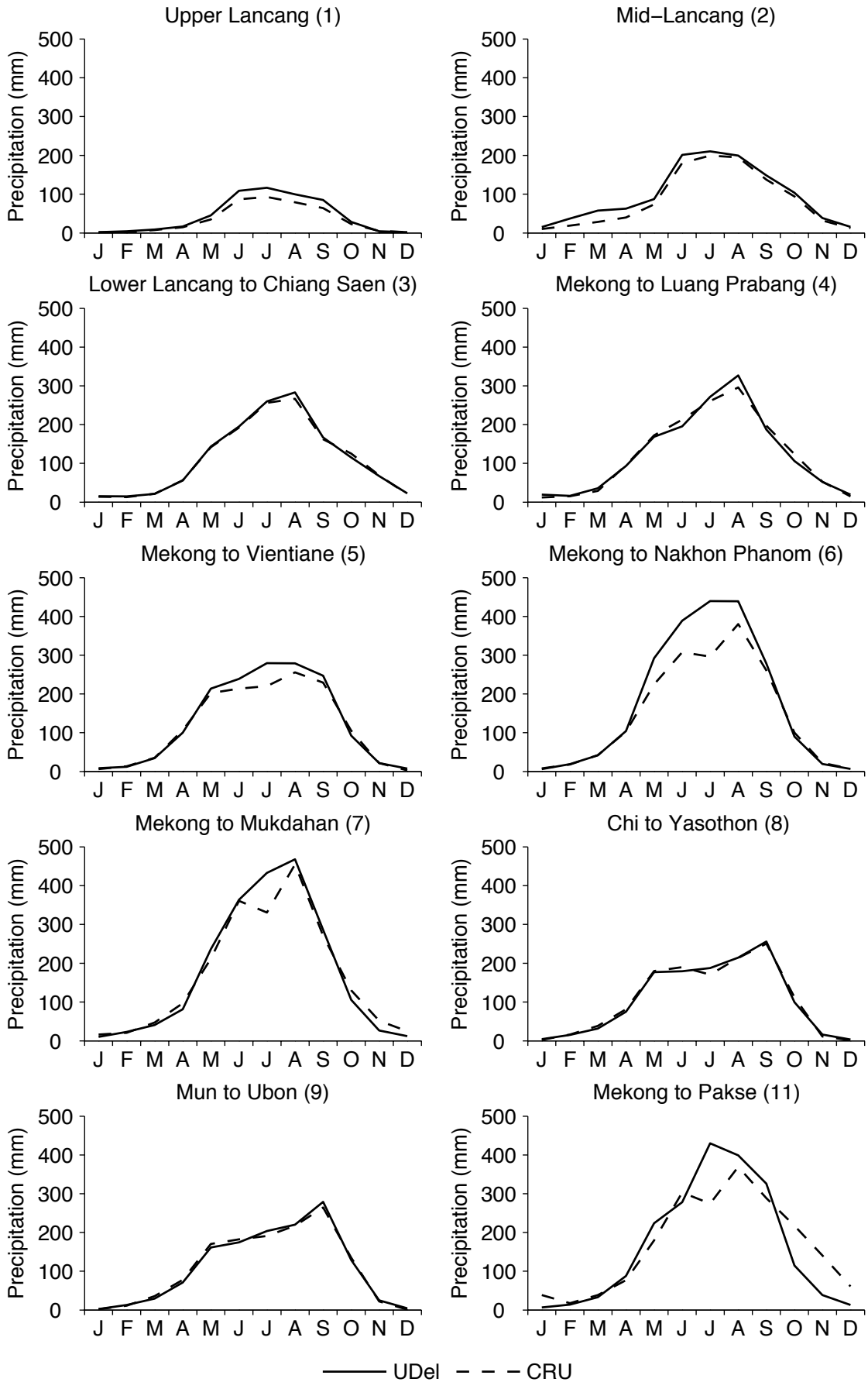

Figure 5.22. UDel- and CRU-based mean monthly precipitation for the period 1961–1990, presented for 14 MIKE SHE sub-catchments.

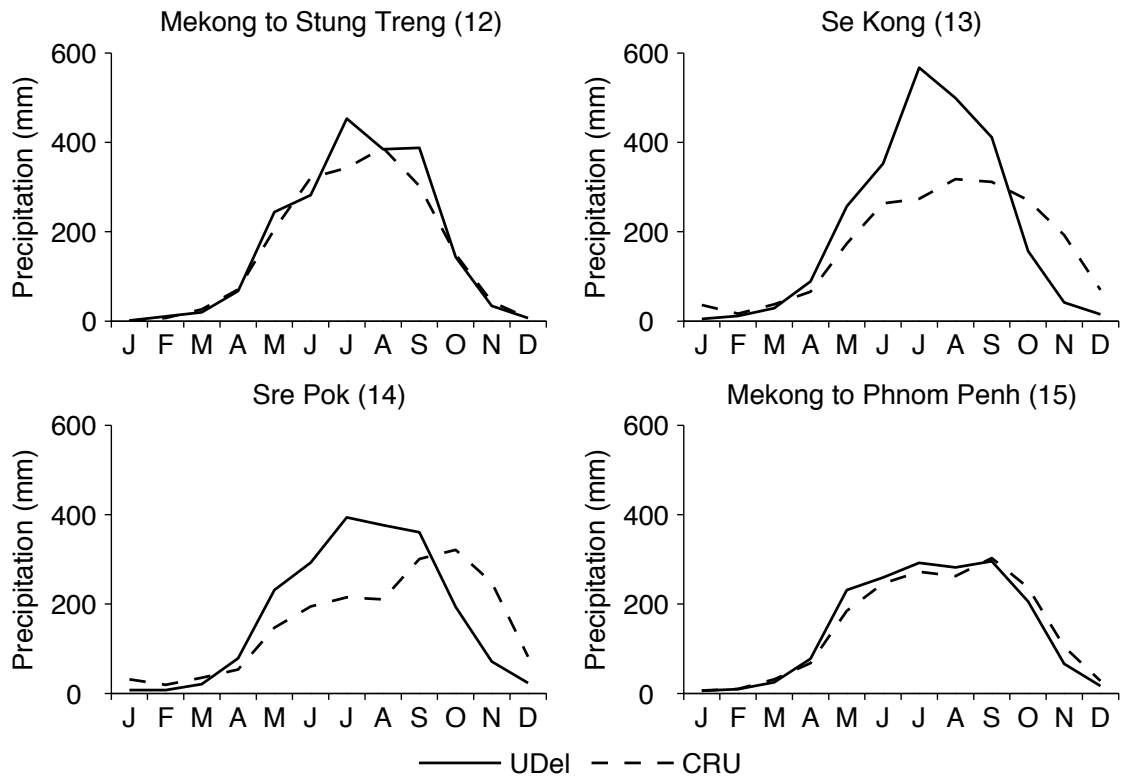

Figure 5.22. (cont.) UDel- and CRU-based mean monthly precipitation for the period 1961–1990, presented for 14 MIKE SHE sub-catchments.

for each of these sub-catchments is, however, relatively similar between UDel and CRU, although CRU shows a dip in mean monthly precipitation in July compared to June for sub-catchments 6 and 7, a pattern which is not exhibited by UDel.

Differences between UDel and CRU are most notable over the lower sub-catchments. For Mekong to Pakse, UDel shows higher values throughout July–September, with a maximum difference of 156 mm in July. In addition, peak mean monthly precipitation occurs in August with CRU, rather than July as with UDel, a pattern that is repeated for Mekong to Stung Treng. Over Se Kong and Sre Pok, the patterns of mean monthly precipitation are very different. For example, over Se Kong, UDel shows a relatively sharp peak of maximum mean monthly precipitation in July, whilst CRU displays a more dome shaped regime with precipitation totals lower by up to 293 mm in July, but higher totals than UDel by up to 151 mm in October–December. In the case of Sre Pok, CRU shows a delayed rise and peak in precipitation totals compared to UDel, with maximum mean monthly precipitation occurring in October rather than July. In July, UDel precipitation is 179 mm higher than CRU and in October, CRU is 128 mm higher than UDel. Over the Mekong to Phnom Penh sub-

catchment, UDel and CRU show a similar annual regime, although mean monthly precipitation values vary by up to 47 mm between the two datasets.

Figure 5.23 demonstrates that UDel-based mean annual precipitation values for the MIKE SHE sub-catchments for the baseline period are greater than CRU-based values for the majority of sub-catchments, although the difference for sub-catchments 4 and 9 is very small (<10 mm). The absolute difference is also less than 25 mm for sub-catchments 3, 8 and 15. Elsewhere, UDel-based values are higher by between 70 mm (Mekong to Mukdahan – sub-catchment 7) and 405 mm (Se Kong – sub-catchment 13). CRU-based values are greater than UDel-based values by 31 mm and 41 mm over sub-catchments 10 and 11, respectively.

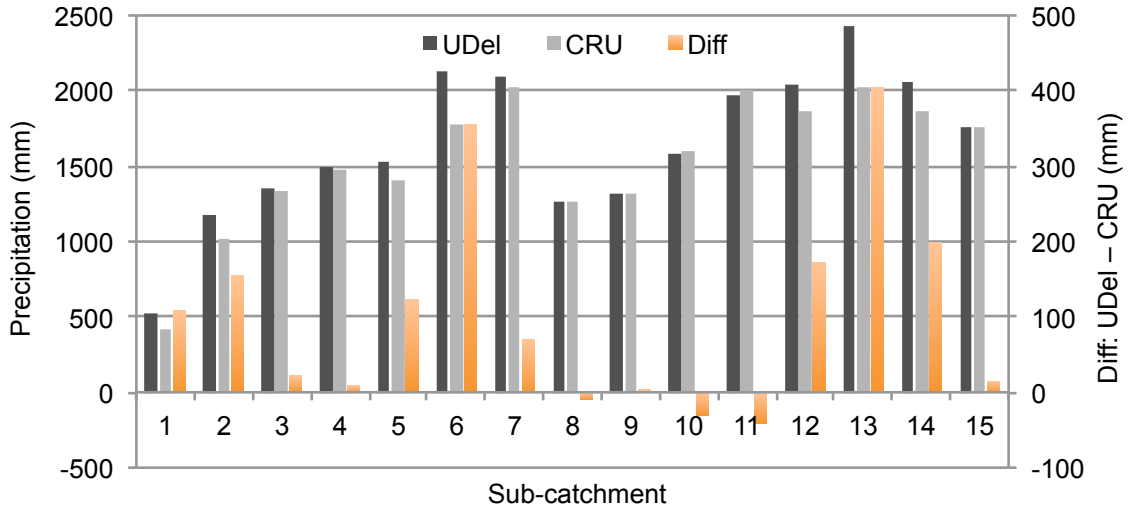

Figure 5.23. UDel- and CRU-based mean annual precipitation values (left-hand axis) and the difference (UDel minus CRU) between the two datasets (right-hand axis) for the MIKE SHE sub-catchments, for the period 1961–1990.

5.4.4.2. Model calibration and validation

For the two MIKE SHE models employing alternative precipitation data, Table 5.11 presents the optimised values for the calibration parameters. When employing CRU precipitation, higher precipitation lapse rates were required over the Lancang (sub-catchments 1–3) and Mekong to Nakhon Phanom (sub-catchment 6). This is unsurprising considering that CRU provides lower precipitation values over these sub-catchments (see Figure 5.22 and Figure 5.23). Similarly, within the CRU-precip MIKE SHE model, dead storage was not required within baseflow reservoir 2 of

Mekong to Vientiane (sub-catchment 5). This can again be explained by the lower CRU precipitation values over this sub-catchment meaning that dead storage is not required. For sub-catchments 10–15, the same parameter values as employed in the UDel-precip model were employed in the CRU-precip model. These were left unaltered as it was found that adjustment of parameters in these sub-catchments could not provide any notable improvement in model performance.

Table 5.11. Final calibration parameter values for the two MIKE SHE models employing different precipitation data. Numbers in column headings refer to the MIKE SHE linear reservoir sub-catchments identified in Figure 4.4. Grey shading indicates altered values within the CRU-precip model compared to the UDel model.

Parameter	Precip	1	2	3	4	5	6	7	8	9	11	12	13 & 14	15
Precip. lapse rate (%/100 m)	UDel	2.60	2.60	2.60	0.00	0.00	0.85	0.00	0.00	0.00	0.00	0.00	0.00	0.00
	CRU	3.55	3.55	3.55	0.00	0.00	6.15	0.00	0.00	0.00	0.00	0.00	0.00	0.00
Time constant for BR1* (days)	UDel	80	80	80	75	100	45	140	180	140	65	55	60	120
	CRU	65	65	65	80	100	45	90	140	130	65	55	60	120
Dead storage fraction for BR1	UDel	0.00	0.00	0.00	0.00	0.00	0.00	0.00	0.46	0.00	0.00	0.00	0.00	0.00
	CRU	0.00	0.00	0.00	0.00	0.00	0.00	0.00	0.46	0.00	0.00	0.00	0.00	0.00
Time constant for BR2^{+} (days)	UDel	700	650	850	550	610	160	230	380	180	100	330	285	380
	CRU	650	600	800	550	400	160	230	380	180	100	330	285	380
Dead storage fraction for BR2	UDel	0.00	0.00	0.00	0.00	0.80	0.00	0.00	0.93	0.59	0.00	0.00	0.00	0.00
	CRU	0.00	0.00	0.00	0.00	0.00	0.00	0.00	0.93	0.59	0.00	0.00	0.00	0.00

* BR1: Baseflow reservoir 1; $^{+}$ BR2: Baseflow reservoir 2

Figure 5.24 provides observed and simulated mean monthly discharges from the calibrated UDel-precip and CRU-precip MIKE SHE models. Model performance statistics for both models for the calibration period are presented in Table 5.12. At gauging stations between Chiang Saen and Pakse, the pattern of mean monthly discharges simulated by the two model generally matches that observed very well. At Chiang Saen and Luang Prabang, the two models display very similar mean monthly discharges and the values are generally close to those observed. Between Vientiane and Pakse, the CRU-precip model consistently underestimates mean monthly discharges in August and September, by between 3.9% (Vientiane in August) and 8.7% (Nakhon Phanom in September) of the corresponding observed mean monthly discharges. Although the UDel-precip model also displays lower mean monthly discharges than those observed in August and September at Vientiane, discharge is only notably underestimated in September between Nakhon Phanom and Pakse, and to a lesser extent than the CRU-precip model.

Table 5.12. Model performance statistics based on mean monthly discharges from the two MIKE SHE models for twelve gauging stations within the Mekong catchment for the calibration (1961–1990 unless stated otherwise) and validation (1991–1998 unless stated otherwise) periods.

Station	Period	Dv (%)+		NSE*		r#	
		UDel	CRU	UDel	CRU	UDel	CRU
Chiang Saen (a)	Cal	0.18 ☆☆☆☆☆	0.24 ☆☆☆☆☆	0.92 ☆☆☆☆☆	0.90 ☆☆☆☆☆	0.96	0.95
	Val (1/91–6/97)	-4.49 ☆☆☆☆☆	2.84 ☆☆☆☆☆	0.79 ☆☆☆☆	0.76 ☆☆☆☆	0.90	0.94
Luang Prabang (b)	Cal	3.61 ☆☆☆☆☆	3.59 ☆☆☆☆☆	0.93 ☆☆☆☆☆	0.90 ☆☆☆☆☆	0.96	0.95
	Val (1/91–12/97)	3.08 ☆☆☆☆☆	7.57 ☆☆☆☆	0.82 ☆☆☆☆	0.84 ☆☆☆☆	0.91	0.94
Vientiane (c)	Cal	0.43 ☆☆☆☆☆	3.12 ☆☆☆☆☆	0.94 ☆☆☆☆☆	0.90 ☆☆☆☆☆	0.97	0.95
	Val (1/91–12/96)	-0.38 ☆☆☆☆☆	4.65 ☆☆☆☆☆	0.87 ☆☆☆☆☆	0.88 ☆☆☆☆☆	0.94	0.95
Nakhon Phanom (d)	Cal	-0.55 ☆☆☆☆☆	-0.64 ☆☆☆☆☆	0.93 ☆☆☆☆☆	0.91 ☆☆☆☆☆	0.97	0.95
	Val (1/91–11/95)	-3.90 ☆☆☆☆☆	-7.60 ☆☆☆☆	0.89 ☆☆☆☆☆	0.91 ☆☆☆☆☆	0.95	0.96
Mukdahan (e)	Cal	3.74 ☆☆☆☆☆	2.87 ☆☆☆☆☆	0.93 ☆☆☆☆☆	0.90 ☆☆☆☆☆	0.97	0.95
	Val (1/91–12/95)	3.25 ☆☆☆☆☆	0.21 ☆☆☆☆☆	0.92 ☆☆☆☆☆	0.92 ☆☆☆☆☆	0.96	0.96
Pakse (f)	Cal	4.57 ☆☆☆☆☆	3.88 ☆☆☆☆☆	0.93 ☆☆☆☆☆	0.91 ☆☆☆☆☆	0.96	0.96
	Val	4.96 ☆☆☆☆☆	8.46 ☆☆☆☆	0.90 ☆☆☆☆☆	0.90 ☆☆☆☆☆	0.95	0.95
Stung Treng (g)	Cal (1/61–12/69)	6.43 ☆☆☆☆	-4.85 ☆☆☆☆☆	0.94 ☆☆☆☆☆	0.87 ☆☆☆☆☆	0.97	0.95
	Val (1/91–12/93)	-7.59 ☆☆☆☆	-2.16 ☆☆☆☆☆	0.90 ☆☆☆☆☆	0.69 ☆☆☆☆	0.95	0.84
Kratie (h)	Cal	4.57 ☆☆☆☆☆	-2.20 ☆☆☆☆☆	0.92 ☆☆☆☆☆	0.86 ☆☆☆☆☆	0.96	0.94
	Val	3.68 ☆☆☆☆☆	4.29 ☆☆☆☆☆	0.88 ☆☆☆☆☆	0.81 ☆☆☆☆	0.94	0.91
Kompong Cham (i)	Cal (1/64–3/74)	9.06 ☆☆☆☆	0.28 ☆☆☆☆☆	0.94 ☆☆☆☆☆	0.88 ☆☆☆☆☆	0.97	0.95
	Val†	—	—	—	—	—	—
Phnom Penh (j)	Cal (1/61–3/74)	15.02 ☆☆☆	5.67 ☆☆☆☆	0.92 ☆☆☆☆☆	0.89 ☆☆☆☆☆	0.97	0.95
	Val†	—	—	—	—	—	—
Chi at Yasothon (k)	Cal	-2.67 ☆☆☆☆☆	-1.72 ☆☆☆☆☆	0.56 ☆☆☆	0.59 ☆☆☆	0.75	0.77
	Val (1/91–12/95)	‡ 6.66 ☆☆☆☆☆ / • -11.24 ☆☆☆	-17.67 ☆☆☆	‡ 0.15 ☆ / • 0.54 ☆☆☆	0.62 ☆☆☆	‡ 0.52/ • 0.74	0.81
Mun at Ubon (l)	Cal	1.86 ☆☆☆☆☆	-0.51 ☆☆☆☆☆	0.62 ☆☆☆	0.71 ☆☆☆☆	0.79	0.85
	Val (1/91–12/93)	‡2.01☆☆☆☆☆/ • -14.37 ☆☆☆	-3.42 ☆☆☆☆☆	‡ 0.29 ☆☆ / • 0.59 ☆☆☆	0.86 ☆☆☆☆☆	0.56‡ • 0.78	0.94

Performance indicator	Excellent ☆☆☆☆☆	Very good ☆☆☆☆	Fair ☆☆☆	Poor ☆☆	Very poor ☆
Dv	< 5%	5–10%	10–20%	20–40%	>40%
NSE	>0.85	0.65–0.85	0.50–0.65	0.20–0.50	<0.20

+ Percentage deviation in simulated mean flow from observed mean flow (Henriksen *et al.*, 2003).
* Nash–Sutcliffe coefficient (Nash and Sutcliffe, 1970). # Pearson correlation coefficient.
† Validation not possible due to absence of observations.
‡ Using UDel V1.01 precipitation. • Using UDel V1.02 precipitation for 1991–1998.

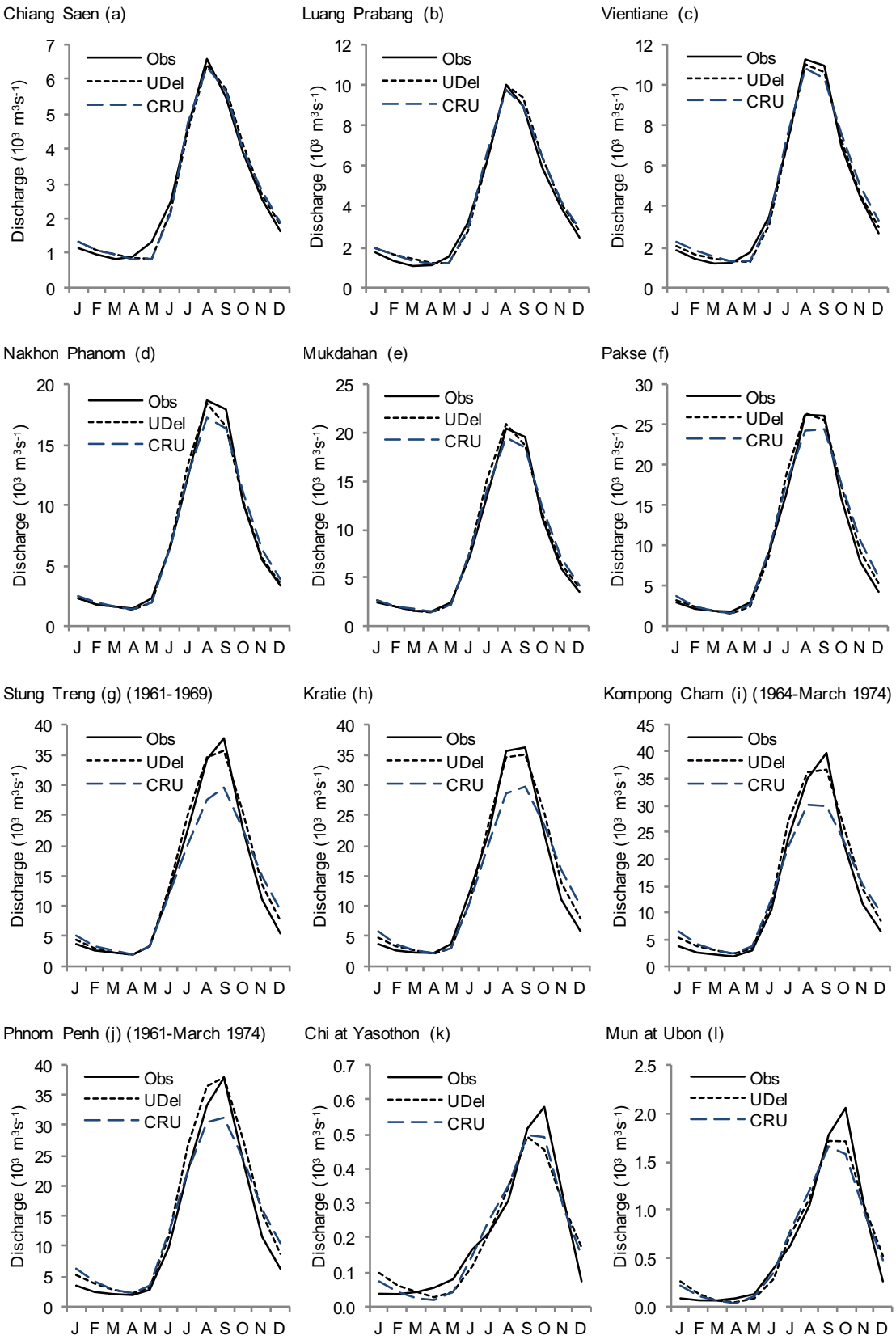

Figure 5.24. Observed and simulated river regimes from the two MIKE SHE models employing alternative precipitation, for all 12 gauging stations within the Mekong catchment for the calibration period (1961–1990 unless indicated otherwise). (Note different y-axis scales.)

This is undoubtedly due to the CRU precipitation having lower precipitation totals than UDel in the months of peak precipitation in sub-catchments 5–6, as demonstrated by mean monthly precipitation values (see Figure 5.22). As discussed above, this was partly addressed within the CRU-precip model by removing the dead storage term from sub-catchment 5 and increasing the precipitation lapse rate over sub-catchment 6. As confirmed by the model performance statistics, performance of both models at stations between Chiang Saen and Pakse for the calibration period is excellent overall, with both models achieving an NSE value of ≥0.9, a Dv of less than ±5% and an *r* value of ≥0.95 at all stations between Chiang Saen and Pakse.

For gauging stations on the main Mekong between Stung Treng and Phnom Penh, NSE values are still consistently classed as "excellent". However, NSE values for the CRU-precip model are lower than for stations further upstream (below 0.9) and are consistently lower than those of the UDel-precip model. For the same stations, Dv values for the UDel-precip model are classed as "excellent" at one station, "very good" at two and "fair" at the most downstream station (Phnom Penh: Dv of 15.02%). Positive values demonstrate than mean discharge is consistently overestimated at these stations. For the CRU-precip model, Dv is instead classed as "excellent" at three stations and "very good" at Phnom Penh.

However, the simulated regimes demonstrate that overall, the UDel-precip model better represents the observed pattern of mean monthly discharges. The UDel-precip model does show a tendency towards overestimation during the annual rise and recession and underestimation of discharge in September between Stung Treng and Kompong Cham (by up to 8%). However, the CRU-precip model shows greater overestimation during the recession and low flow period between November and March, and peak flows in August–September are notably lower than those observed (by between 8% and 25%). This is due to the CRU precipitation providing lower peak precipitation totals and higher totals in October–January compared to UDel precipitation over sub-catchments 11, 13, 14 and 15 (see Figure 5.22). As might be expected, this could not be ameliorated through adjustment of the saturated zone's time constant parameter values for these sub-catchments. Following experiments to see whether model performance could be improved, these parameter values were therefore returned to the same values as those in the UDel-precip MIKE SHE model.

The poorer representation of the annual river regimes in the CRU-precip model between Pakse and Phnom Penh provides a strong indication that the CRU-based precipitation data over sub-catchments 11 and 13–15 are less representative of the true precipitation regimes over this region.

Both the plots of simulated mean monthly discharge and the model performance statistics for the Yasothon and Ubon gauging stations indicate that performance of the two MIKE SHE models is very similar at these stations, although the CRU-precip model achieves a higher NSE classification for the Mun ("very good" instead of "fair"). As discussed previously for the UDel-precip model as well as other MIKE SHE models of the Mekong in Sections 4.7.1 and 5.2.4.2, performance at these stations is weaker than elsewhere, the cause of which can only be speculated. As with the UDel-precip model, a dead storage term was required within the baseflow reservoir 2 of the Chi and Mun groundwater sub-catchments of the CRU-precip model. The same values as in the UDel-precip model were employed, as adjustment of these parameters did not improve model performance.

Observed and simulated mean monthly discharges for the validation period are presented in Figure 5.25. Overall, both MIKE SHE models achieve a good level of performance for the validation period. Performance at some gauging stations is, however, inferior to that of the calibration period. For Chiang Saen to Vientiane, both models display a tendency toward underestimation of mean monthly discharges on the ascending limb, and overestimation of discharges on the descending limb, with the CRU-precip model showing notable overestimation in both August and September. This poorer performance is reflected in lower NSE values (Table 5.12), although these values are still good (being classed as "very good" to "excellent").

Between Nakhon Phanom and Pakse, mean monthly discharges are well represented by both models through the majority of the year, although the CRU-precip model shows greater overestimation of discharge in November to January. NSE values are consistently classified as excellent, whilst Dv is classified as "very good" to "excellent". At Stung Treng and Kratie, as well as being poorer than for the validation period, performance of the CRU-precip model is inferior to that of the UDel-precip model, as demonstrated by the NSE values (Table 5.12). As for the

calibration period, peak discharges are considerably underestimated, whilst low flows are considerably overestimated during December–March.

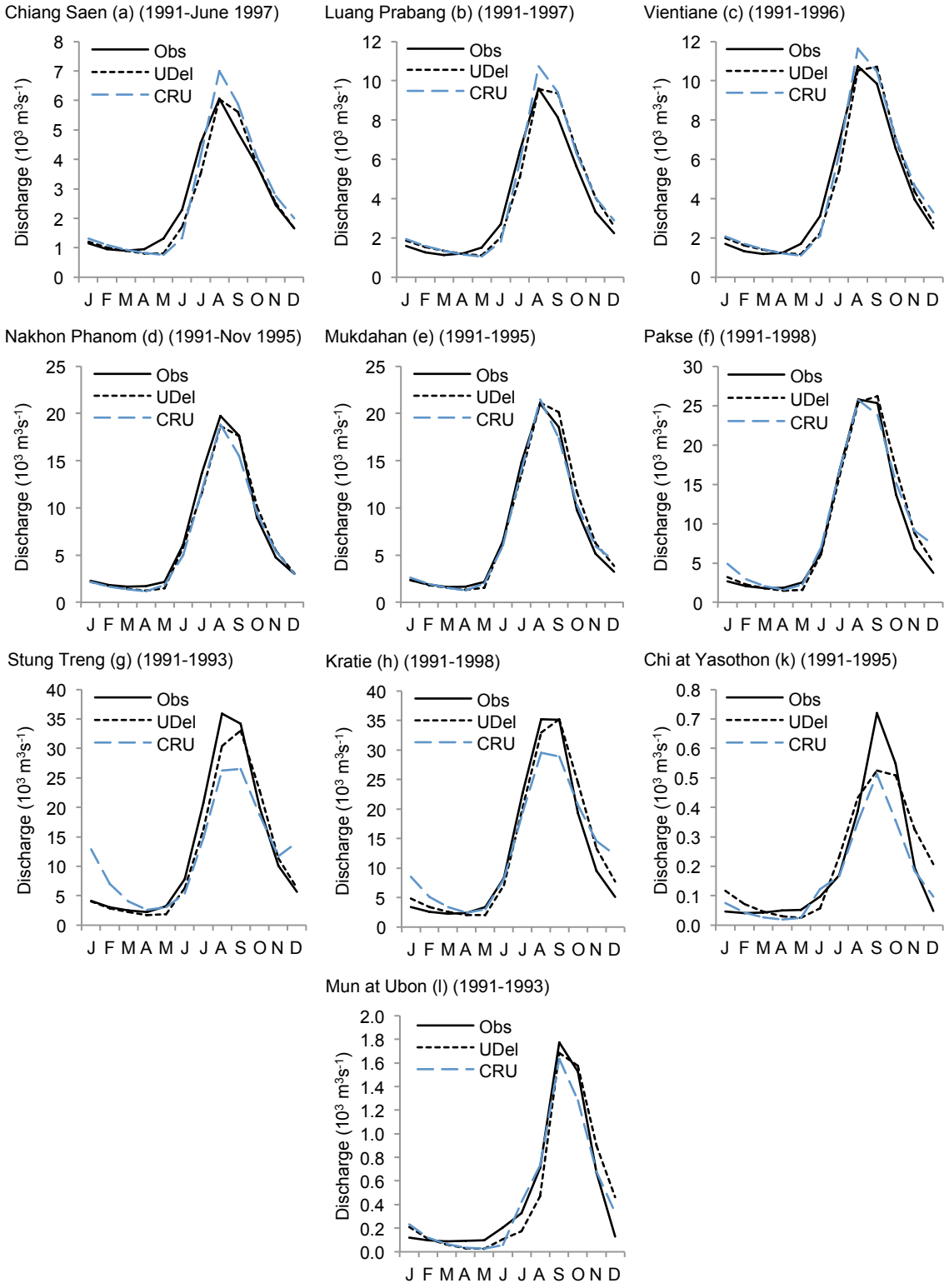

Figure 5.25. Observed and simulated river regimes from the two MIKE SHE models employing alternative precipitation, for ten gauging stations within the Mekong catchment for the validation period (1991–1998 unless indicated otherwise). (Note different y-axis scales.)

For the Chi tributary, performance of the CRU-precip model is superior to that of the UDel-precip model when employing UDel V1.01 throughout the validation period of this station, and similar to that of the UDel-precip model when employing UDel V1.02 throughout the validation period of this station (Table 5.12). The simulated regimes for the Yasothon and Ubon in Figure 5.25 are shown for UDel V1.01, although these are similar to those produced when using UDel V1.02. Both the UDel- and CRU-precip models underestimate peak discharges at Yasothon. For the Mun tributary, performance of the CRU-precip model is actually superior to that for the calibration period, as well as superior to that of the UDel-precip model, with NSE and Dv classed as excellent, and mean monthly discharges that more closely follow those observed.

Overall, despite poorer performance of the CRU-precip model over lower gauging stations on the main Mekong, both MIKE SHE models are deemed appropriate for climate change impact assessment.

5.4.4.3. Scenario precipitation

As outlined in Section 5.4.3, scenario precipitation data for input to the CRU-precip MIKE SHE models were generated using a delta-change approach. Gridded scenario CRU data were developed through perturbation of the gridded baseline CRU data using mean monthly multiplicative delta-change factors developed for each GCM using the gridded UDel-based baseline and scenario data. The gridded CRU scenario datasets were subsequently spatially averaged over the MIKE SHE meteorological input sub-catchments and stochastically disaggregated to daily resolution using the Mac-PDM weather generator.

Changes in mean monthly precipitation (in mm) for the seven GCM scenarios are presented in Figure 5.26 for the UDel- and CRU-based data. Sub-catchment 9 is representative of sub-catchments 8 and 10 (not shown), whilst sub-catchment 13 displays similar patterns to sub-catchment 14 (not shown).

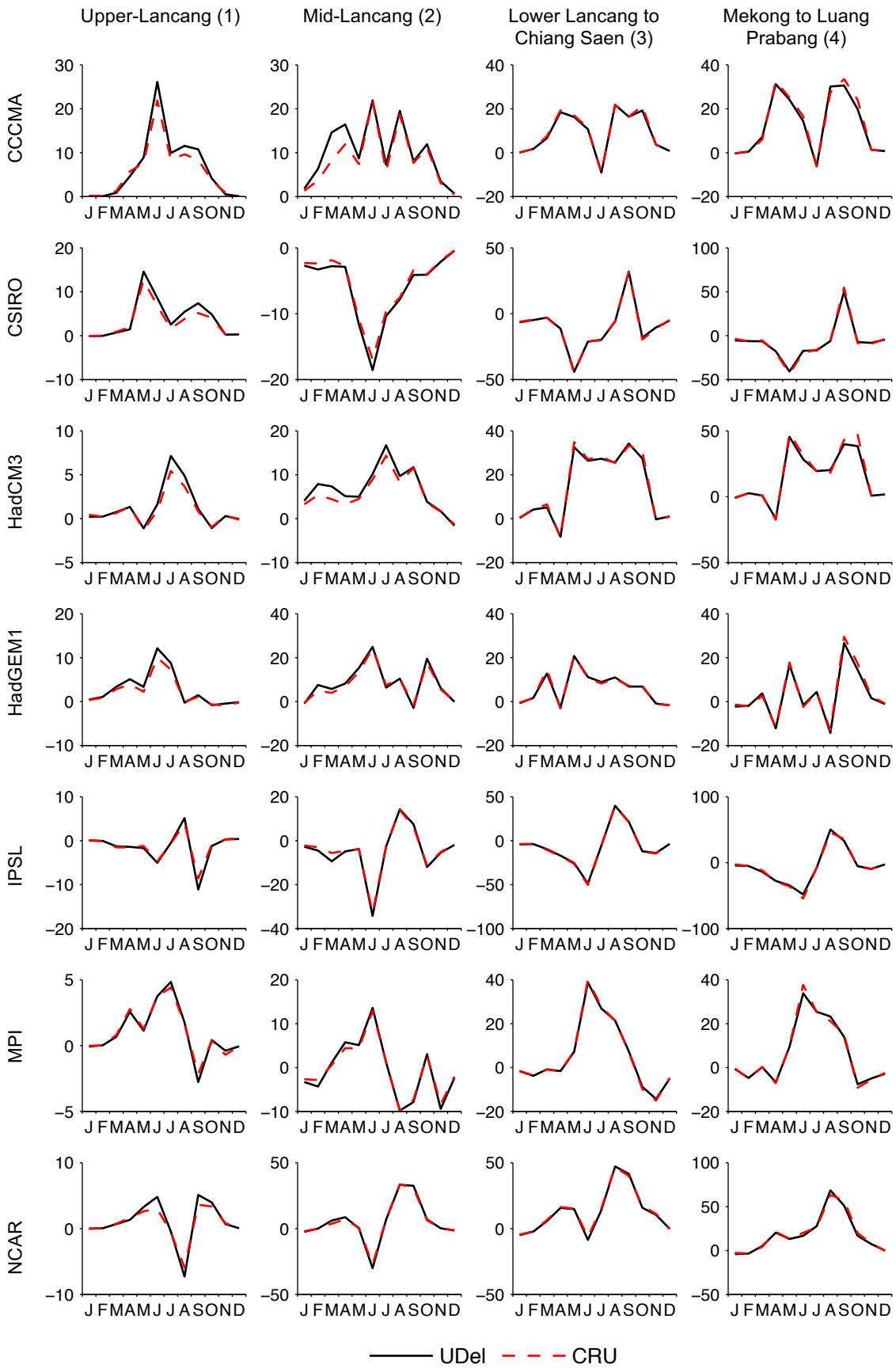

Figure 5.26. Change in mean monthly precipitation (mm for all y axes) for 12 MIKE SHE sub-catchments for the 2 °C, seven GCM climate change scenarios. (Note different y-axis scales.)

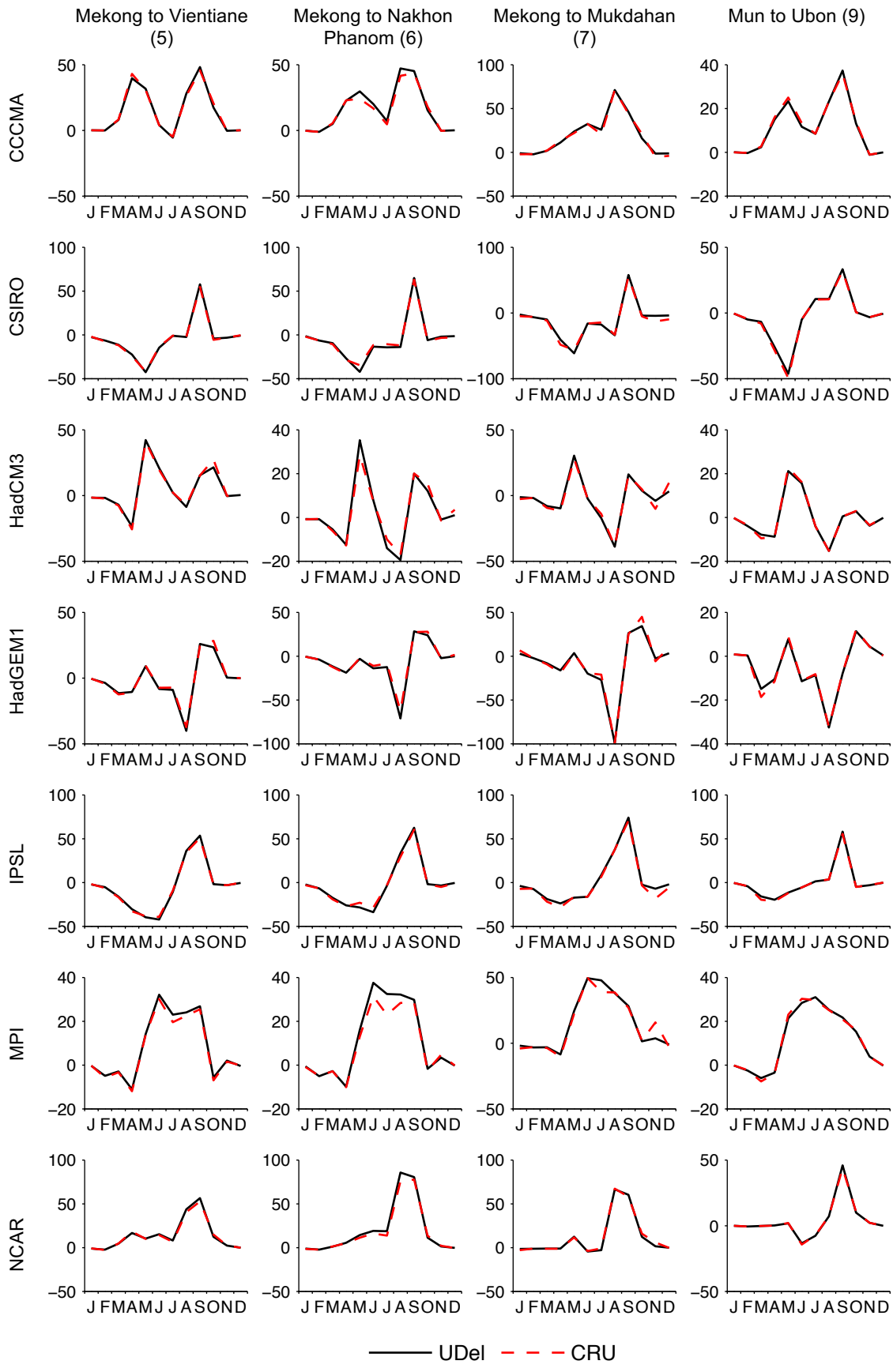

Figure 5.26. Change in mean monthly precipitation (mm for all y axes) for 12 MIKE SHE sub-catchments for the 2 °C, seven GCM climate change scenarios. (Note different y-axis scales.)

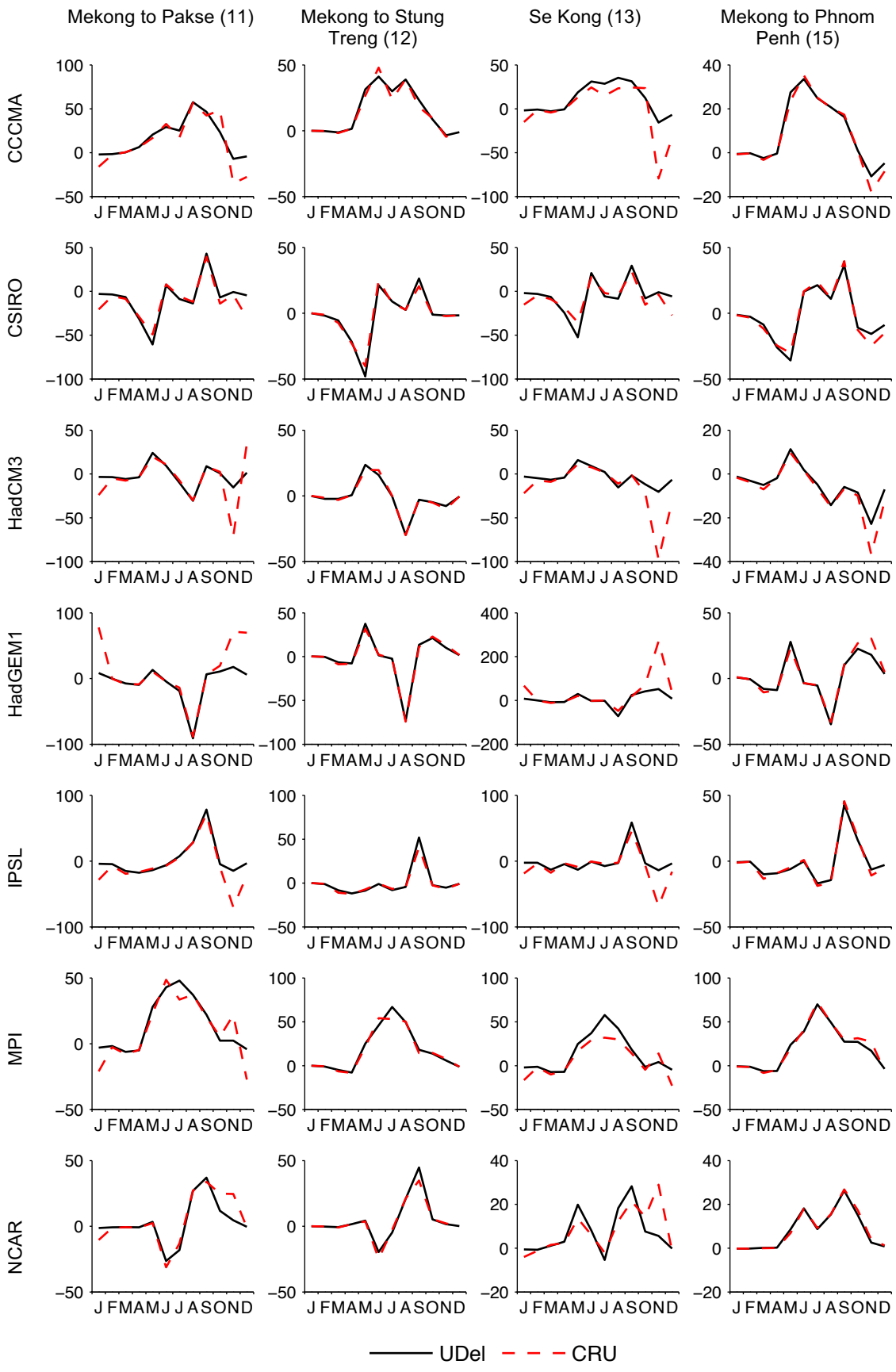

Figure 5.26. Change in mean monthly precipitation (mm for all y axes) for 12 MIKE SHE sub-catchments for the 2 °C, seven GCM climate change scenarios. (Note different y-axis scales.)

These plots demonstrate that where the UDel and CRU baseline data are very similar (see Figure 5.22), absolute scenario changes are consistently very similar between the two datasets (e.g. sub-catchments 3, 4, 5, 9 and 12). In contrast, for sub-catchments where the baseline UDel- and CRU-based mean monthly precipitation data diverge, the scenario changes for UDel and CRU show different magnitudes. For example, over the Mid-Lancang, the CRU baseline data show lower precipitation totals than UDel during February–April. As a result of using multiplicative/ratio delta-factors to derive the scenario CRU data, the CRU scenario data show lower absolute (i.e. mm) scenario changes at this time of year compared to the UDel data, since the same percentage change translates into a lower absolute (mm) change for CRU.

The most notable differences between UDel and CRU occur over lower sub-catchments (11, 13, 14 and 15) during the dry season, where CRU-based scenario changes are notably greater in magnitude, whether positive or negative. This is due to the CRU baseline data displaying higher baseline precipitation totals during the dry season (Figure 5.22). The same percentage change therefore corresponds to a greater absolute change with the CRU data.

5.4.4.4. Scenario river discharge

Similar to Tables 5.6 and 5.1 for the models employing alternative PET methods and alternative meteorological input spatial distributions, respectively, Table 5.13 presents mean baseline discharge and percentage changes in these discharges for the 2 °C scenarios for the two models that employ alternative baseline precipitation data. Results are provided for the same eight representative gauging stations. The absolute inter-model range in percentage change is again shown for each scenario/station combination. At the bottom, for each station, the inter-model range in mean baseline and scenario discharges is expressed as a percentage of the average mean discharge from the two models for that scenario. Change in mean discharge for stations on the main Mekong is also presented graphically in Figure 5.27, with changes plotted as scatter points and a shaded band indicating the inter-model range for each GCM. Changes in mean, Q95 and Q5 discharges for both MIKE SHE model are shown in Figure 5.28 for four gauging stations on the main Mekong.

Table 5.13. Mean baseline discharge (m^3s^{-1}) and change from baseline mean discharge (%) for the two models for each GCM at eight gauging stations. Grey shading indicates negative changes compared to the baseline. The absolute range in percentage change for each station/scenario is also shown. The range of mean discharge for the baseline and each GCM from the two models are also indicated at the bottom (% of overall mean discharge from the two models for that scenario).

Scenario	Precip. / Scenario	Chiang Saen (a)	Luang Prabang (b)	Vientiane (c)	Mukda-han (e)	Pakse (f)	Kratie (h)	Phnom Penh (j)	Ubon (l)
Baseline (m^3s^{-1})	UDel	2716.3	4124.0	4540.5	7886.6	10285.9	14031.9	14396.1	648.1
	CRU	2717.8	4122.9	4662.0	7820.6	10218.6	13123.3	13543.9	633.0
CCCMA (% change)	UDel	13.5	12.8	12.6	12.2	12.7	10.8	10.7	13.0
	CRU	13.2	13.9	14.2	13.7	13.6	9.5	9.5	14.0
	Range	0.2	1.2	1.6	1.5	0.9	1.3	1.3	1.0
CSIRO (% change)	UDel	-16.4	-16.7	-16.2	-13.1	-11.6	-9.6	-9.3	-2.6
	CRU	-18.8	-18.4	-17.9	-14.7	-13.3	-12.2	-11.9	-7.4
	Range	2.5	1.7	1.7	1.6	1.7	2.7	2.5	4.8
HadCM3 (% change)	UDel	19.8	22.6	21.2	12.0	8.5	4.8	4.5	-2.7
	CRU	20.9	25.4	23.7	13.8	9.2	3.0	2.5	-5.6
	Range	1.1	2.8	2.4	1.8	0.7	1.9	2.0	2.8
HadGEM1 (% change)	UDel	6.6	4.1	2.9	-2.1	-4.3	-3.2	-3.2	-11.1
	CRU	6.7	5.3	3.6	-1.6	-1.7	4.5	4.3	-13.0
	Range	0.1	1.2	0.7	0.5	2.6	7.7	7.5	2.0
IPSL (% change)	UDel	-14.1	-13.4	-13.1	-8.3	-5.9	-4.4	-4.4	0.4
	CRU	-14.7	-14.4	-14.3	-9.8	-8.5	-7.6	-7.4	-4.8
	Range	0.6	1.0	1.2	1.5	2.6	3.2	3.1	5.2
MPI (% change)	UDel	1.8	4.8	5.6	7.6	10.2	11.1	11.5	24.4
	CRU	2.8	5.6	6.5	7.9	9.9	10.8	11.4	20.1
	Range	1.0	0.9	0.9	0.2	0.3	0.3	0.0	4.4
NCAR (% change)	UDel	12.4	20.0	20.1	18.5	15.0	12.3	12.1	6.7
	CRU	14.2	22.5	22.9	20.9	16.9	14.6	14.4	3.7
	Range	1.7	2.5	2.7	2.4	1.8	2.3	2.3	3.0
Range in mean discharges (% of mean from the two models)	Baseline	0.1	0.0	2.6	0.8	0.7	6.7	6.1	2.4
	CCCMA	0.2	1.0	4.0	0.5	0.1	7.9	7.3	1.5
	CSIRO	2.9	2.1	0.6	2.7	2.6	9.7	8.9	7.4
	HadCM3	0.9	2.2	4.6	0.7	0.0	8.5	8.1	5.3
	HadGEM1	0.1	1.1	3.3	0.3	2.0	0.9	1.3	4.6
	IPSL	0.7	1.1	1.3	2.5	3.5	10.1	9.4	7.7
	MPI	1.0	0.8	3.5	0.6	0.9	7.0	6.1	5.9
	NCAR	1.6	2.0	4.9	1.2	0.9	4.7	4.1	5.2

Overall, the two MIKE SHE models display very similar results in most cases. Furthermore, Figure 5.27 demonstrates clearly that the direction and spatial pattern (i.e. from upstream – station a, to downstream – station j) in the magnitude of changes in mean discharge is predominantly driven by choice of GCM. For all gauging stations on the main Mekong down to Pakse, the two models consistently project the same direction of change in mean discharge for a given GCM. In addition, the absolute inter-MIKE SHE model range in percentage change at these stations is ≤2.8%.

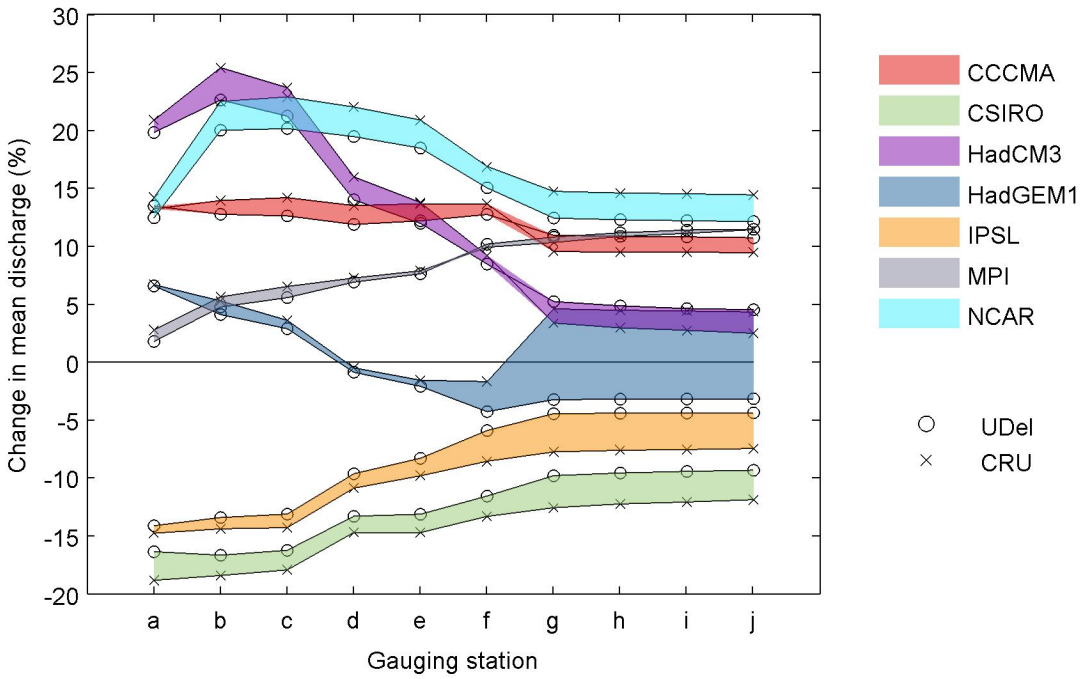

Figure 5.27. Change in mean discharge (%) for gauging stations on the main Mekong for the 2 °C, seven GCM scenarios and each MIKE SHE model employing alternative precipitation data. Shaded bands indicate the range of inter-MIKE SHE model uncertainty and enable identification of which GCM the scatter points refer to.

For stations between Stung Treng and Phnom Penh, the absolute inter-MIKE SHE model range in percentage change remains at ≤2.7% for all GCMs except HadGEM1 and IPSL. For IPSL, the absolute inter-model range in percentage change is only marginally greater, ranging between 3.1–3.3%. In contrast, the absolute range varies between 7.5–7.9% for HadGEM1. Moreover, HadGEM1 stands out as the only GCM for which the two models project a different direction of change. Whilst the UDel model shows a consistent reduction in mean discharge of 3.2% for stations between Stung Treng and Phnom Penh (stations g–j) for HadGEM1, the CRU-precip model projects increases of 4.3–4.6%. This divergence is the result of the CRU precipitation data having much greater absolute increases in precipitation (compared to the baseline) over sub-catchments 11 and 13–15 during October–January, as demonstrated in Figure 5.26. These increases in precipitation are therefore sufficient to counteract the effect of upstream reductions in precipitation and consequently discharge, as well as reductions in precipitation during parts of the year over sub-catchments 11 and 13–15. This is further illustrated in Figure 5.28, which shows that Q95 at Phnom Penh increases for both models for HadGEM1 (greater increases for the CRU-precip model), whereas Q5 decreases.

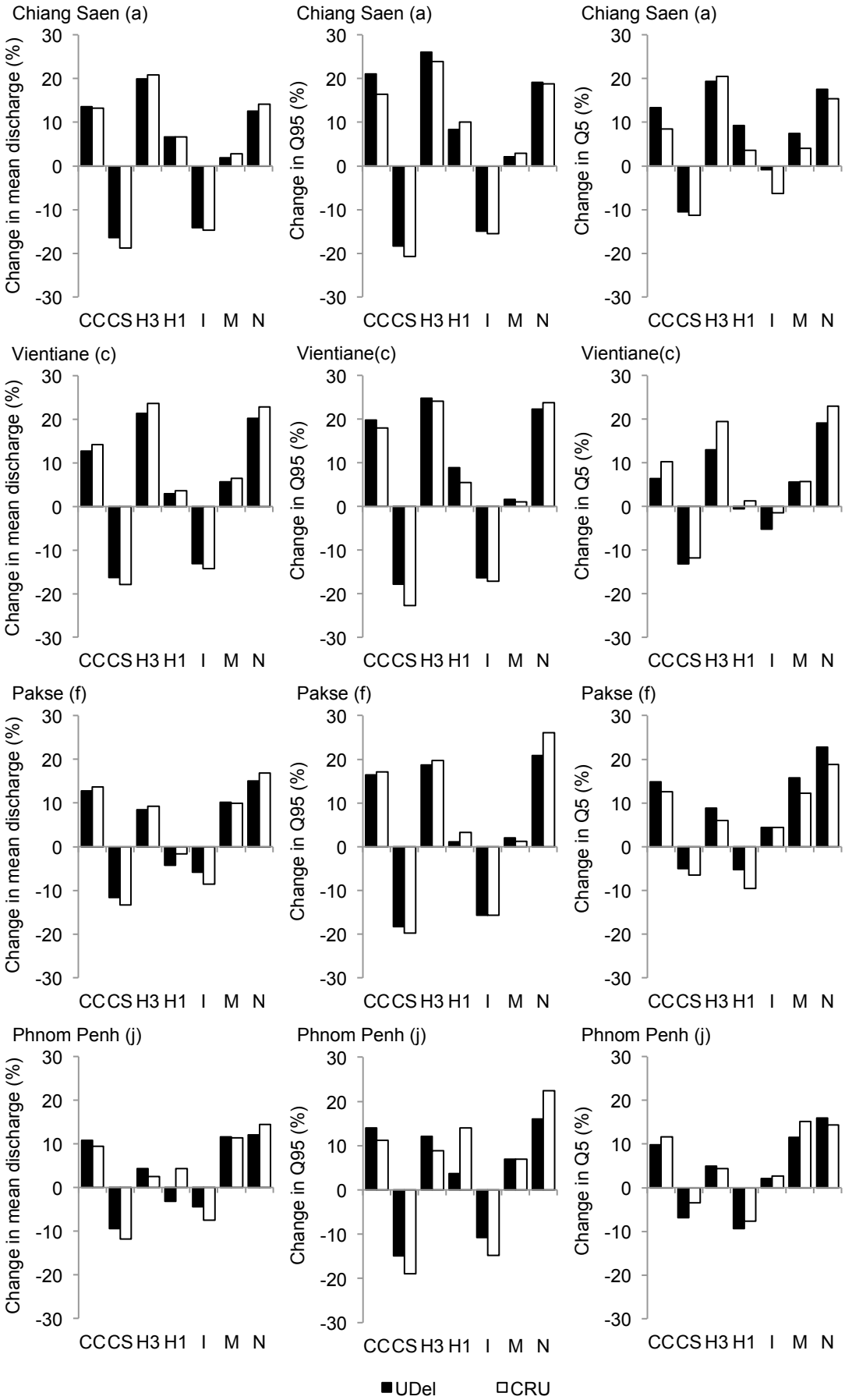

Figure 5.28. Change from baseline mean, Q5 and Q95 discharges for the 2 °C, seven GCM scenarios and each MIKE SHE model for four gauging stations.

CC: CCCMA; CS: CSIRO; H3: HadCM3; H1: HadGEM1; I: IPSL; M: MPI; N: NCAR.

Differences between the UDel- and CRU-based MIKE SHE model projections of change in mean discharge for downstream gauging stations are much less notable for other GCMs compared to HadGEM1. This is largely due to other GCMs producing lower percentage change in precipitation during October–January, leading to smaller differences (between UDel and CRU) in absolute (mm) baseline to scenario changes in precipitation. In addition, in some cases there is no consistent direction of change throughout October–January. For example, in the case of MPI over sub-catchment 11, CRU produces a greater increase in mean monthly precipitation in November, but a greater reduction in December–January. This has the effect of reducing the difference between UDel- and CRU-based precipitation changes at an annual level.

For the River Mun at Ubon and River Chi at Yasothon, the two MIKE SHE models project the same direction of change in mean discharge for a given GCM, except in the case of IPSL at Ubon, for which the UDel-precip model projects a negligible increase (0.4%) whilst the CRU-precip model produces a decrease of -4.8%. The maximum absolute inter-MIKE SHE model range of change for a given GCM is 5.2% at Ubon and 3.9% at Yasothon.

The inter-MIKE SHE model range of mean discharges expressed as a percentage of the overall mean from the two models (bottom section of Table 5.13) is, in most cases (43 out of the 56 gauging station/GCM combinations, or ~77%), larger than that of the baseline. However, the inter-model range in mean discharge often remains fairly low (e.g., <2.5% of the mean discharge from the two models in 80% of cases). For all except the HadGEM1 GCM, the largest ranges are seen at Kratie and Phnom Penh, which also display the largest range for the baseline. In the case of the HadGEM1 GCM at Kratie and Phnom Penh, the range in mean discharge (as a percentage of the mean from the two models) shows a reduction compared to the baseline. However, this is misleading, since these stations display the greatest absolute inter-model range in percentage change (see Figure 5.27). This is a result of the UDel-precip model, which simulated the higher baseline discharge of the two models, projecting a reduction in mean discharge, whilst the CRU-precip model produces an increase.

Figure 5.28 demonstrates that in most cases, the two MIKE SHE models project the same direction of change in high (Q5) and low (Q95) flows, also indicating that the intra-annual pattern of change is largely unaffected by choice of baseline precipitation. The inter-model ranges of percentage change in Q5 and Q95 are, on average, marginally larger than the range of change in mean discharge (average for mean Q: 2.0%; average for Q5: 2.6%; average for Q95: 3.3%). These values were calculated by taking the average inter-model range in percentage change from the 84 combinations of GCMs and gauging stations (7 GCMs × 12 gauging stations).

5.5. Discussion: Uncertainty associated with meteorological inputs

5.5.1. PET method-related uncertainty

The investigation of PET method-related uncertainty demonstrated considerable differences in baseline potential evapotranspiration totals (but some consistent spatial and temporal patterns) for the Mekong evaluated using six different, but widely used, PET methods. Without PET observations across the Mekong it is not possible to state whether one method (and hence MIKE SHE model) should be preferred over another (e.g. as done so by Prudhomme and Williamson, 2013). This is therefore beyond the scope of the study. It might be expected that Penman (PN) should produce most realistic results as it incorporates the most meteorological variables, but as previously noted the additional variables are typically relatively poorly observed. Furthermore, only climatological values for wind speed have been used (and so were unchanged for the calculation of scenario PN PET) and net radiation in PN (and Priestley-Taylor – PT) is derived empirically from cloud cover data. Whilst testing different PET methods for the calculation of a historical global gridded PET dataset, Sperna Weiland *et al.* (2012) demonstrated that global Penman-Monteith PET fields were in fact sensitive to both these substitutions. Although these substitutions are commonly made in large-scale impact assessments (e.g. Arnell, 2003; Kingston *et al.*, 2009; Prudhomme and Williamson, 2013), their influence on the reliability of PET calculations remains a matter for further research.

In the absence of an assessment of the reliability of each PET method, it is at least worth noting that the relative order of magnitude in baseline PET has similarities

with previous studies. For example, Kingston *et al.* (2009) showed that for much of the latitudinal range of the Mekong, PT consistently produced the lower PET totals, with Hamon (HM) producing the lowest totals over latitudes corresponding to the highest parts of the basin (over 30˚N). Excluding PET methods not included in this thesis, the highest PET for latitudes between 10–20˚N was for Blaney-Criddle (BC) and Hamon (HM).

Consistent calibration/validation procedures result in alternative parameter values for the six MIKE SHE models that act to mitigate the differences in absolute PET. The parameters modified included the precipitation lapse rates (within five to six sub-catchments) and the saturated zone dead storage terms (two to three sub-catchments only), which therefore altered the overall water balance. The linear reservoir time constants, which affect the timing of the flood pulse, were also modified. Each model simulates very similar baseline river discharge and performance is generally ‘‘excellent’’ or ‘‘very good’’. This ability to compensate for differences between PET input datasets through model calibration is consistent with previous studies (e.g. Andréassian *et al.*, 2004; Remesan and Holman, 2015).

In the simulation of GCM scenarios, the hydrological models are largely sensitive to changes between baseline and scenario PET, rather than inter-PET method differences in baseline PET. This is evident because the magnitude of simulated changes in discharge generally corresponds to the magnitude of PET changes. Alternative approaches, such as employing alternative PET data within a model calibrated using a specific PET method, should be interpreted with caution.

Inter-GCM ranges of change in PET are small in comparison to those for precipitation. Annual PET increases for all GCMs (and PET methods), whilst precipitation climate change signals vary between catchment-wide increases or decreases to spatially variable changes. The BC, HM and LN PET methods all have similar inputs (i.e. mean temperature and day length), but BC displays markedly different climate change signals to HM and LN (BC produces some of the lowest PET increases, HM and LN some of the highest). This indicates that the PET equation (i.e. the empirical formulation) itself can be just as important a source of uncertainty as the input meteorological variables. Previous research has also highlighted that PET

methods show different sensitivities to changes in climate, and that methods that employ the same input data can still produce significantly varied results (e.g. Kingston *et al.*, 2009; Bormann, 2011).

The hierarchy of changes in annual PET for a given GCM using different methods is similar to those demonstrated in other studies. Bae *et al.* (2011) showed that for a range of climate change scenarios, HS consistently produced the lowest change in PET. PT produced larger changes, with the largest due to HM. In their global analysis, Kingston *et al.* (2009) demonstrated that for the latitudinal range of the Mekong, HM also produced the largest changes in PET for five GCMs employed in the current study (CSIRO and HadGEM1 were excluded). Some of the smallest changes were associated with HS PET.

In a very insightful study, Shaw and Riha (2011) highlight that Hamon and Thornthwaite, two purely temperature based PET equations (disregarding adjustments for day length), are much more sensitive to temperature than the Oudin, Priestley-Taylor and Penman-Monteith PET equations. As with the Hargreaves-Samani method, Oudin and Priestley-Taylor have a strong dependency on radiation, which can be calculated indirectly rather than requiring a measured value. The sensitivity of HM to temperature is evident for the Mekong in Figure 5.1, since HM displays the greatest spatial variability in annual baseline PET totals (lowest totals of the six PET methods over the Lancang, the coldest sub-catchment; second highest totals over the Mekong 3 sub-catchment).

Shaw and Riha (2011) found HM to produce notably higher PET increases than PT for a climate change scenario, although the analysis was limited to June–September. Shaw and Riha (2011) argue that temperature-based PET methods have limited physical justification; they are empirical approximations of the correlation between temperature and PET and this correlation relies on the correlation between temperature and radiation (a key environmental driver of evapotranspiration). Relying on this correlation in a stationary world is not unreasonable, but 'using this correlation between [radiation] and [temperature] to predict PET in a changing climate is fundamentally flawed because [temperature] is projected to change much more than [radiation]' (Shaw and Riha, 2011: 1473). Shaw and Riha (2011) also

suggest that temperature-based equations will likely exaggerate PET in a changing climate.

In the case of the Mekong (i.e. the current study), HM and LN do appear to produce exaggerated increases in PET under climate change compared to other methods (see Figure 5.4; Figure 5.5). Conversely, BC, also a temperature-based method, produces some of the lowest increases. These findings indicate that although not all temperature-based equations will exaggerate PET in a changing climate, the use of these methods for climate change projections should be treated with caution, as recommended by Shaw and Riha (2011).

Some consistencies in the relative order of change in annual PET for the different GCMs are also common to other studies. CCCMA followed by NCAR and HadGEM1 produced the smallest increases over three sub-catchments of the Manipur River in Northeast India, around 500 km to the west of the Mekong and at the same latitude as central parts of the Lancang (Singh *et al.*, 2010). The largest increases were similarly associated with CSIRO and then HadCM3.

A notable finding is that inter-GCM differences in PET changes for a given PET method are generally smaller than differences in changes between the PET methods for a given GCM. This indicates that for future changes in PET, choice of PET method is actually a greater source of uncertainty than GCM-related uncertainty. This could have more significant implications for climate change impact assessments in some basins compared to those demonstrated here for the Mekong. For example, in regions where, for a particular scenario (e.g. a prescribed warming, SRES or RCP scenario), greater increases in temperature are projected, or where relatively small changes in precipitation are consistently projected across GCMs, the importance of PET method-related uncertainty could be greater in relation to other sources of uncertainty. Kingston *et al.* (2009) highlighted that for projections of future freshwater availability, uncertainty in the PET climate change varied regionally.

PET method-related uncertainty in simulation of Mekong river discharge under climate change is considerably less than GCM-related uncertainty (that is in turn dominated by uncertainty in precipitation). It is worth noting, however, that for

those scenarios involving a spatially variable precipitation climate change signal, PET method influences the spatial extent of increases or decreases in mean discharge. In these cases, PET specific differences in the direction of change in discharge could have important implications including variability in projected impacts for power generation from existing and planned dams, as well as environmental conditions within the river (Thompson *et al.*, 2014b). However, the intra-annual pattern of discharge changes (i.e. the pattern of changes to the river regime through the year) was largely unaffected by choice of PET method. Instead, it is the magnitude of changes that are impacted.

The magnitude of PET-method related uncertainty in simulated discharges is greater under scenario conditions compared to the baseline. Consistent with the findings of Remesan and Holman (2015), this demonstrates that it cannot be assumed that the range/magnitude of inter-hydrological model uncertainty will be the same under altered climate conditions as for calibrated baseline conditions.

The finding that the models using alternative PET methods result in some differences in scenario discharge supports the assertion that differences in the climate change discharge/runoff signals for the Mekong simulated by MIKE SHE, SLURP and Mac-PDM.09 for the same scenarios could, at least in part, be attributable to PET method (LN for MIKE SHE and SLURP, Penman–Monteith for Mac-PDM.09). However, some increases simulated by the GHM at upstream gauging stations were three to nearly six times as large as those simulated by MIKE SHE (Section 4.7.3.3). Such large increases are not simulated by any of the MIKE SHE models in this investigation. Further downstream, however, differences between MIKE SHE/SLURP and Mac-PDM.09 were comparable in magnitude to the PET-related uncertainty identified herein.

5.5.2. Uncertainty associated with the spatial distribution of meteorological inputs

The specification of alternative spatial distributions of meteorological inputs required some adjustment of model parameters within the MIKE SHE hydrological models. Following this, performance of the three models (S-Mets – SLURP sub-catchment based distribution; M-Mets – MIKE SHE sub-catchments; G-Mets – gridded meteorological inputs) was very similar. Previous studies that investigated the impact of rainfall distribution within a hydrological model also found that input-specific calibration was required (Mileham *et al.*, 2008; Xu *et al.*, 2010).

It should be acknowledged that the findings of this investigation related to spatial variability in climate projections are likely to be more relevant for large river basins. Spatial representation of meteorological inputs (particularly precipitation) can have important implications for calibration and parameterisation of hydrological models of small to medium sized catchments (Mileham *et al.*, 2008; Xu *et al.*, 2010). However, climate change signals are likely to vary by much smaller amounts over the spatial extent of such catchments. In the case of the QUEST-GSI project, for example, GCM scenario data were downscaled to a 0.5˚ × 0.5˚ grid. Catchments of 2100–3300 km^2 only occupy a handful (≤9) of such grid cells (Kingston and Taylor, 2010; Xu *et al.*, 2011). For comparison, 225 grid cell nodes (0.5˚ × 0.5˚) fall within the Mekong catchment down to Phnom Penh.

In this investigation, analysis of both the baseline meteorological inputs, and relative (%) annual and seasonal changes from the baseline under the 2˚C, seven GCM scenarios, demonstrates that use of sub-catchment averaged data inevitably leads to loss of spatial variability compared to gridded inputs. Similarly, it is unsurprising that division of the basin into a greater number of sub-catchments (and in particular breaking up the largest SLURP sub-catchments) in the case of the MIKE SHE sub-catchments provides greater spatial variability compared to those inherited from the SLURP model. More specifically, division of the S-Mets Lancang sub-catchment, which spans a large latitudinal range (~20–34˚N) into three sub-catchments for the M-Mets model allows a better representation of the latitudinal variation in baseline precipitation and PET totals (Figure 5.11 and Figure 5.12).

Likewise, division of the S-Mets Mekong 1 sub-catchment into four M-Mets sub-catchments permits greater variability from northwest to southeast over this region. For scenario changes in precipitation and PET, use of sub-catchment averaged data sometimes led to loss of variability in the projected direction of change in annual or seasonal totals over a particular region that is evident in the gridded data. However, the M-Mets spatial distribution is better able to capture differing directions of change compared to the S-Mets spatial distribution, especially over the upper, mid and lower Lancang.

Use of alternative spatial distributions of meteorological inputs did impact the magnitude of simulated changes in mean, high and low flows. For percentage changes in mean discharge, inter-model differences were greatest at upstream stations and tended to show a downstream reduction in magnitude. The maximum inter-model range of change in mean discharge was 6.3% (Chiang Saen station, HadGEM1 GCM). However, the spatial pattern of changes through the basin was largely unaffected, and is instead GCM-dependent. The magnitude of inter-hydrological model difference at a given gauging station varies between GCMs. This indicates that the impact that the differing meteorological input spatial distributions has on discharge projections depends on the nature (magnitude and spatiality) of the projected changes in climate. The results of the M-Mets and G-Mets models are consistently close. There is generally a greater magnitude of inter-model uncertainty in projected percentage changes in high (Q5) and low (Q95) flows. Again, however, the direction, magnitude and spatial pattern of changes is predominantly GCM-dependent. Unlike changes in mean discharge, inter-model differences do not show a downstream reduction in magnitude for some GCMs. Meteorological input spatial distribution only has the ability to influence the direction of change when the magnitude of change is fairly low (<5% for all three models for mean discharge and Q5; <8% for all three models for Q95). The maximum inter-model range of percentage change in Q5 and Q95 is 9.8% and 11.2%, respectively. For comparison, the inter-GCM range of change at any given station is around 20–35% for Q5, and 30–45% for Q95.

Overall, the similarity in climate change results from the three hydrological models employing alternative meteorological input spatial distributions suggests that in

this instance, the use of a sub-catchment based distribution is a fairly robust alternative to the use of gridded inputs. Use of the different spatial distributions does impact the magnitude of projected changes, but GCM-related uncertainty is much more significant for projected changes in Mekong river flows.

5.5.3. Baseline precipitation input-related uncertainty

The analysis of two (sub-catchment based) baseline precipitation datasets for the Mekong derived from different global gridded products reveals that such datasets can exhibit notable temporal and spatial differences. Calibration of some parameters within the CRU-precip model (MIKE SHE model employing CRU precipitation) allows similar model performance to the UDel-precip model at upstream gauging stations for the calibration period. Model parameters were not adjusted in downstream sub-catchments. For downstream gauging stations, although performance statistics for the CRU model were generally close to those of the UDel model, the river regimes are a poorer match to the observed, with underestimation of peak flows and overestimation in the dry season. This corresponds to patterns in the baseline precipitation regimes over some downstream sub-catchments, with CRU displaying lower peak precipitation totals and higher dry season values than UDel. Adjustment of model parameters could not compensate for these differences.

Poorer simulation of the baseline river regimes for downstream gauging stations in the CRU-precip model provides a strong indication that CRU precipitation is less representative of true baseline precipitation patterns over this region compared to UDel precipitation. Investigation of the potential causes of disparity between the two data products is beyond the scope of this study. Both data products are developed from station-based observation records. It may be that differences between the products over this region are due to the use of records from different meteorological stations (e.g. different numbers or spatial distributions of stations; Thompson *et al.*, 2016). Previous studies from this (Kingston *et al.*, 2011) and other river basins have also experienced difficulties in hydrological model calibration when employing CRU precipitation (Hughes *et al.*, 2011; Thompson *et al.*, 2016).

The delta-change method was employed to generate the scenario CRU precipitation data for the Mekong. Multiplicative delta-factors were used, which means that absolute (mm) changes from the baseline are impacted by the magnitude of baseline precipitation values. The UDel and CRU-based scenario precipitation data therefore show different absolute changes from their respective baseline. These are greater where: i) the baseline datasets show greater disparity and ii) percentage changes from the baseline are greater. Consequently, the magnitude of inter-model differences in simulated river discharges from the two MIKE SHE models varies between the different GCM scenarios and gauging stations.

On the main Mekong, the inter-MIKE SHE model range of percentage change in mean discharge for a given GCM is generally low, with values of ≤3.3% at all stations except in the case of HadGEM1. For this GCM, the inter-model difference is between 7.5–7.8% at the four most downstream gauging stations (g-j). In addition, the CRU-precip model simulates increases in mean discharge for these stations, whilst the UDel-precip model projects reductions. This is due to HadGEM1 scenario producing greater percentage changes (in this case increases) in precipitation from the baseline during the dry season, compared to the other GCMs. As discussed above, the CRU baseline precipitation data display notably higher precipitation totals during the dry season than UDel, so absolute scenario increases are higher for CRU than UDel. This is reflected in simulated changes in mean discharge and Q95 (low flows), the latter of which displays an inter-model range of change of >10–15% for stations g–j for HadGEM. The inter-model ranges in change in Q95 for the same stations are also fairly high for the NCAR GCM (7.0– 11.1%). The average inter-model range in percentage change in mean discharge across the 84 combinations of GCMs and gauging stations (7 GCMs × 12 gauging stations) is 2.0%. The equivalent values for Q5 and Q95 are 2.6% and 3.3%. The spatial pattern of changes in Q5 and Q95 through the catchment for a given GCM is largely unaffected by choice of baseline precipitation data.

This investigation demonstrates that choice of baseline precipitation data does have the potential to affect the results of hydrological climate change impact assessments. In this situation, a multiplicative delta change approach was used to perturb the baseline CRU precipitation data. The ClimGen pattern scaling technique employed

in the QUEST-GSI project also involves scaling baseline precipitation multiplicatively using patterns of change obtained from GCM outputs (Todd *et al.*, 2011). Other bias correction techniques such as local scaling and quantile-quantile mapping involve adjusting the GCM outputs instead, but rely on using baseline data to determine relationships that characterise the bias in the GCM outputs (e.g. Dobler *et al.*, 2012). As such, the potential uncertainty associated with choice of baseline precipitation data is still of relevance to assessments that use different techniques to bias-correct GCM outputs.

Accuracy of the baseline precipitation is not only important for better simulation of baseline hydrological conditions, it is also important at the climate scenario generation stage of the impact assessment modelling process. It is therefore advisable that in cases where precipitation data are suspected to be erroneous (as in the case of CRU over the lower Mekong) alternative precipitation datasets should be sought.

5.6. Summary

For Mekong river flow projections under climate change, GCM-related uncertainty is the overriding source of uncertainty out of those investigated in this chapter. Choice of GCM dominates the magnitude, direction and spatial pattern of changes in mean annual and mean monthly discharges and high and low flows. Table 5.14 summarises the MIKE SHE models used in this chapter and the magnitude of GCM-related uncertainty for percentage change in mean discharge across the seven GCMs for the 2 °C prescribed warming scenario.

Table 5.15 summarises the maximum inter-hydrological range of change in mean discharge for a single GCM, and the average across the seven GCMs, associated with choice of: i) PET method, ii) spatial distribution of meteorological inputs and iii) baseline precipitation data. The magnitude of GCM-related uncertainty (for change in mean discharge) assessed using the different MIKE SHE models does vary, but is around 20–40%, and is ~30% on average. The maximum PET related uncertainty (15.6%) is around 2.5 times smaller than the maximum GCM-related uncertainty from models 1–6 (36.9% on the main Mekong; 40.8% at Ubon). On average, GCM-

related uncertainty for change in mean discharge is ~3.5 times as large as PET method-related uncertainty. The same is true for changes in Q5 and Q95.

Uncertainty associated with the spatial distribution of meteorological inputs and choice of baseline precipitation were found to be much smaller (~4 times on average) than PET-related uncertainty, and are, on average, comparable in magnitude.

Table 5.14. Summary of MIKE SHE models developed in this Chapter. For each of these, the absolute inter–GCM range of simulated percentage change in mean discharge is provided for five stations. The average column is the average taken across all 12 gauging stations.

Model summary				**Inter-GCM range of change in mean discharge across seven GCMs for the 2 °C scenario (%)**					
Model no.	PET method	Met. Dist.	Precip.	Chiang Saen (a)	Vientiane (d)	Pakse (f)	Phnom Penh (j)	Ubon (l)	12-station average
1	BC	S-Mets	UDel	31.0	30.9	25.6	21.8	40.8	29.6
2	HM	S-Mets	UDel	28.3	29.4	25.0	21.0	37.3	27.9
3	HS	S-Mets	UDel	30.9	33.5	26.7	21.4	35.3	29.0
4	LN	S-Mets	UDel	32.5	33.6	28.1	22.5	37.6	31.0
5	PN	S-Mets	UDel	36.9	33.7	27.0	21.6	35.7	29.9
6	PT	S-Mets	UDel	29.8	31.7	25.7	20.4	33.8	27.6
7	PN	M-Mets	UDel	36.2	37.5	26.6	21.4	35.5	30.5
8	PN	G-Mets	UDel	35.7	36.8	25.9	20.9	33.0	29.6
9	PN	M-Mets	CRU	39.7	41.6	30.2	26.3	33.1	33.9

Table 5.15. Summary of uncertainty in percentage change in mean discharge associated with PET method, spatial distribution of meteorological inputs and choice of precipitation. Model numbers are from the above table.

	Maximum inter-hydrological model range of change for a single GCM for the 2 °C scenario (%)					
Models (source of uncertainty)	Chiang Saen (a)	Vientiane (d)	Pakse (f)	Phnom Penh (j)	Ubon (l)	12-station average
1–6 (PET)	15.6	14.0	9.2	7.6	10.9	10.9
5, 7, 8 (Met. spatial. dist.)	6.3	5.0	2.1	1.4	3.3	3.1
7, 9 (UDel vs. CRU precip.)	2.5	2.7	2.6	7.5	5.2	4.6
	Average inter-hydrological model range of change across the seven GCM scenarios					
1–6 (PET)	9.3	9.2	7.5	6.8	9.2	8.2
5, 7, 8 (Met. spatial. dist.)	3.1	3.0	1.1	0.8	2.7	1.9
7, 9 (UDel vs. CRU precip.)	1.0	1.6	1.5	2.7	3.3	2.0

Chapter 6

GCM-related uncertainty assessment using CMIP5 GCMs

6.1. Introduction

The scenario climate data employed in Chapters 4 and 5 represent scenarios of prescribed warming (e.g. 2 °C increase in mean global temperature, relative to the 1961–1990 baseline period) and were generated through rescaling the outputs of GCMs that took part in CMIP3 (Meehl et al., 2007a), using the ClimGen technique (Arnell and Osborn, 2006; see Section 4.5). This chapter uses climate scenario data for the Mekong catchment generated using the outputs from an ensemble of CMIP5 GCMs for one of the latest generation of scenarios, Representative Concentration Pathways (RCPs see Section 2.5.1). Additionally, a much larger number of GCMs (41) form the ensemble compared to the seven-member ensemble for the 2 °C prescribed warming scenarios used in previous chapters. This chapter therefore provides a more up-to-date assessment of the potential impacts of climate change on river discharge in the Mekong catchment and the associated GCM-related uncertainty.

Existing assessments for the Mekong have tended to employ a relatively small ensemble of GCMs (five to seven), which have been selected to either span a range of plausible global climate futures (Kingston *et al.*, 2011), or based on their historical performance in the region (e.g. Lauri *et al.*, 2012; Hoang *et al.*, 2016). It is possible that selection of a relatively small number of GCMs narrows the range of future climate, and in turn hydrological projections, and therefore reduces the magnitude of uncertainty represented by the ensemble. Although this may seem desirable, provision of a 'falsely narrow' range of projections could lead to mal-adaptation (McSweeney *et al.*, 2014: 3238). The range of projections resulting from an ensemble may be falsely narrow in the sense that plausible projections (that fall outside of the ensemble-specific range) may have been omitted through the exclusion of other GCMs.

Existing hydrological impact assessments for the Mekong are also almost exclusively based on climate projections from earlier generations of climate models and scenarios, in particular those from CMIP3 (Kingston *et al.*, 2011; Lauri *et al.*,

2012). A notable exception is Hoang *et al.* (2016), who employed an ensemble of five CMIP5 GCMs and two Representative Concentration Pathway (RCP) scenarios (RCP4.5 and RCP8.5). The five GCMs were selected based on a review of the literature on GCM performance (Sillmann *et al.*, 2013; Huang *et al.*, 2014; Hasson *et al.*, 2016), with the aim being to select GCMs better able to produce historical tropical temperature and precipitation conditions, particularly over the Mekong region. Hoang *et al.* (2016) suggest a trend towards increases in seasonal and annual river discharge. Results from their ensemble also indicate reduced uncertainty compared to earlier CMIP3-based assessments.

6.2. Hydrological model selection

The model employed in this chapter is based on the model developed in Section 5.3 (and also used in Section 5.4) that uses the MIKE SHE sub-catchments for the spatial distribution of meteorological inputs, and UDel precipitation. This was selected because it represents an intermediate level of spatial distribution, allowing greater spatial variability in meteorological inputs than the SLURP sub-catchment distribution, but reduced model execution times and meteorological data that can be more easily handled and presented than that of the MIKE SHE model with gridded climate inputs. In addition, UDel precipitation provided better model performance than CRU precipitation during model calibration/validation, particularly at downstream gauging stations (Section 5.4.4.2).

As detailed in the Section 6.3, GCM outputs for the development of climate scenario data were obtained from the KNMI (Royal Netherlands Meteorological Institute) Climate Explorer (https://climexp.knmi.nl). However, some of the climate data required for the calculation of PN (Penman) PET (e.g. cloud cover and vapour pressure data) were unavailable. Therefore, rather than PN PET, the baseline and scenario models in this chapter employ HS (Hargreaves–Samani) PET. The HS PET method was selected since it is recommended by the FAO for use in situations where there are insufficient data to calculate Penman/Penman–Monteith PET (Allen *et al.*, 1998). Following specification of HS PET data, minor calibration of the MIKE SHE model was undertaken for the calibration (1961–1990) period using the approach

adopted in the previous chapter, with the aim being to achieve model performance that was as good as that of the original model that employed PN PET.

6.3. Simulation of climate change

Projected precipitation and temperature (mean, maximum and minimum) data for the period 2040–2069 for the RCP4.5 scenario were derived using simulation outputs from 41 GCMs that participated in CMIP5, using similar techniques to those described by Ho *et al.* (2016). The RCP4.5 scenario, which represents a pathway where radiative forcing reaches 4.5 W m^{-2} in the year 2100, was selected since it is an intermediate/mid-range RCP scenario (see Section 2.5.1) and had data available for the largest number of GCMs. In addition, other studies that have selected a single illustrative RCP scenario have also used RCP4.5 (e.g. Dai, 2012; Kim and Yu, 2012; Thrasher *et al.*, 2013; Ho *et al.*, 2016; Shin *et al.*, 2016).

The delta-factor approach was employed to perturb the baseline sub-catchment averaged UDel precipitation and CRU temperature data. Monthly GCM outputs were obtained from the KNMI Climate Explorer, with the data for each sub-catchment being spatially averaged over the relevant grid cells using an in-built processing tool. Mean monthly precipitation and mean monthly mean, minimum and maximum temperature for each GCM were derived for the 1961–1990 baseline period and 2040–2069 scenario period. These values were subsequently used to calculate monthly delta factors (expressed as % for precipitation, i.e. relative change; and °C for temperature, i.e. absolute change), which were in turn used to perturb the monthly observed baseline climate data (UDel precipitation and CRU mean, minimum and maximum temperature). The monthly precipitation and mean temperature data were stochastically disaggregated to a daily resolution using the Mac-PDM.09 weather generator, using the same wet days data, coefficient of variation for daily precipitation and standard deviation of daily temperature as used to generate the daily baseline data (see description for the M-Mets model, Section 5.3.1). Hargreaves–Samani PET was re-evaluated for each GCM using the perturbed temperature data. As for the baseline period, PET values were evenly distributed throughout each month to provide daily data.

Advantages of the delta-change approach include that it is widely used, easy to implement and computationally inexpensive (Kay *et al.*, 2009; Anandhi *et al.*, 2011; Dobler *et al.*, 2012). Moreover, since it uses observed data for the baseline and for perturbing to generate scenario data, results are unaffected by GCM biases in the simulation of climate variability (Anandhi *et al.*, 2011; Teutschbein and Seibert, 2012; Ho *et al.*, 2016). However, there are also disadvantages. For example, the number of wet and dry days does not change for the future climate, the temporal sequencing of wetter/drier months and years is unaltered and months with extreme precipitation totals or temperatures are modified by the same factor as other months (Graham *et al.*, 2007a; Anandhi *et al.*, 2011; Teutschbein and Seibert, 2012). However, since changes in climate and river discharge in this investigation are analysed at a mean monthly or lower temporal resolution, with a focus on mean changes rather than on extremes or event frequency, these limitations are not considered to detract from the results presented herein.

The GCMs for which scenario data were generated are summarised in Table 6.1. The model groupings were obtained from Ho *et al.* (2016) and are based on the concept of model genealogy (Masson and Knutti, 2011; Knutti *et al.*, 2013). Different versions of the same model are grouped together, as are models from the same research centre and models that have evolved from a common ancestor or share components and code. Although all GCMs are similar in that they aim to describe the climate system, models sharing code or components are more likely to contain similar biases in terms of their omission or simplification of processes and numerical approximations, and will therefore often be similarly biased with regard to reality (Knutti *et al.*, 2013). In support of this, Masson and Knutti (2011) and Knutti *et al.* (2013) demonstrated that models with clear similarities in code and models

Table 6.1. GCMs used in this chapter. Models grouped according to genealogy.

Model name	Institution	Group name	Group no.	No. of models
CanESM2	Canadian Centre for Climate Modelling and Analysis	CanESM2	1	1
CSIRO-Mk3.6.0	Commonwealth Scientific & Industrial Research Organisation in collaboration with Queensland Climate Change Centre of Excellence	CSIRO-Mk3.6.0	2	1
FGOALS-g2	LASG, Institute of Atmospheric Physics, Chinese Academy of Sciences	FGOALS-g2	3	1
INMCM4	Institute for Numerical Mathematics	INMCM4	4	1
MRI-CGCM3	Meteorological Research Institute	MRI-CGCM3	5	1
GFDL-CM3 GFDL-ESM2G GFDL-ESM2M	NOAA Geophysical Fluid Dynamics Laboratory	GFDL	6	3
GISS-E2-H p1 GISS-E2-H p2 GISS-E2-H p3 GISS-E2-H-CC GISS-E2-R p1 GISS-E2-R p2 GISS-E2-R p3 GISS-E2-R-CC	NASA Goddard Institute for Space Studies	GISS	7	8
IPSL-CM5A-LR IPSL-CM5A-MR IPSL-CM5B-LR	Institut Pierre-Simon Laplace	IPSL	8	3
MIROC5 MIROC-ESM MIROC-ESM-CHEM	Atmosphere and Ocean Research Institute (The University of Tokyo), National Institute for Environmental Studies, and Japan Agency for Marine-Earth Science and Technology	MIROC	9	3
ACCESS1-0 ACCESS1-3	Commonwealth Scientific and Industrial Research Organisation (CSIRO) and Bureau of Meteorology (BOM), Australia	UKMO	10	5
HadGEM2-AO HadGEM2-CC HadGEM2-ES	Met Office Hadley Centre (additional HadGEM2-ES realisations contributed by Instituto Nacional de Pesquisas Espaciais)			
CMCC-CM CMCC-CMS	Centro Euro-Mediterraneo sui Cambiamenti Climatici	European	11	6
CNRM-CM5	Centre National de Recherches Météorol-ogiques/ Centre Européen de Recherche et de Formation Avancée en Calcul Scientifique			
EC-EARTH	EC-Earth consortium			
MPI-ESM-LR MPI-ESM-MR	Max-Planck-Institut für Meteorologie (Max Planck Institute for Meteorology)			
bcc-csm1-1 bcc-csm1-1-m	Beijing Climate Center, China Meteorological Administration	NCAR	12	8
BNU-ESM	College of Global Change and Earth System Science, Beijing Normal University			
CCSM4	National Center for Atmospheric Research			
CESM1-BGC CESM1-CAM5	Community Earth System Model Contributors			
FIO-ESM	The First Institute of Oceanography, SOA, China			
NorESM1-M	Norwegian Climate Centre			

developed by the same institution show much greater similarity in terms of simulated climate fields under both control (preindustrial) conditions and future scenario conditions. This means that the GCMs employed in this investigation cannot be assumed to be independent of each other. It is therefore important to take the model groupings into consideration when analysing and interpreting the ensemble climate projections and resulting hydrological projections, as the distribution of results may be biased towards the models for which there are multiple versions and the groups that contain the most models.

It is worth acknowledging that an RCP4.5 scenario set could have been developed using alternative datasets. For example, one possibility is to use data from the CORDEX (Coordinated Regional Climate Downscaling Experiment) initiative (Giorgi *et al.*, 2009; Giorgi and Gutowski, 2015), which provides downscaled RCP scenario data generated by RCMs driven with GCM outputs. However, the decision was made to employ GCM data from KNMI Climate Explorer for a number of reasons. In particular, one objective in this chapter is to compare the CMIP5 GCM results with the CMIP3 GCM results from the previous chapter. Use of GCM-RCM downscaled data would make the comparison less fair. In addition, data for Southeast Asia were available for fewer GCMs in the case of CORDEX. Furthermore, choice of RCM is in itself a notable source of uncertainty, and it was deemed counterproductive to start exploring this additional source of uncertainty in this chapter.

6.4. Results

6.4.1. Model calibration and validation

The baseline MIKE SHE model used in this chapter employs HS PET and is based on the model in Sections 5.2 and 5.3 that employed the MIKE SHE sub-catchments meteorological input spatial distribution (as opposed to SLURP sub-catchments or gridded) and PN PET. Specification of HS PET within the model required minor calibration of some parameters. Performance of the MIKE SHE model employing HS PET was assessed for the calibration (1961–1990) and validation (1991–1998) periods used in Chapters 4 and 5. As stated previously, shorter periods were employed for some stations due to data availability.

Table 6.2 presents the optimised values for the calibration parameters in sub-catchments 1–9 of both models. Parameters in the remaining sub-catchments did not require adjustment in order to achieve similar model performance. Likewise, many of the parameter values in this table are consistent between the two models.

Table 6.2. Final calibration parameter values for the two MIKE SHE models employing different PET data. Numbers in column headings refer to the MIKE SHE linear reservoir sub-catchments identified in Figure 4.4. Grey shading indicates altered values within the HS model compared to the PN model.

Parameter	PET	1	2	3	4	5	6	7	8	9
Precip. lapse rate (%/100 m)	PN	2.60	2.60	2.60	0.00	0.00	0.85	0.00	0.00	0.00
	HS	2.40	2.40	2.40	0.00	0.00	0.85	0.00	0.00	0.00
Time constant for baseflow reservoir 1 (days)	PN	80	80	80	75	100	45	140	180	140
	HS	80	80	80	60	80	45	120	180	140
Dead storage fraction for baseflow reservoir 1	PN	0.00	0.00	0.00	0.00	0.00	0.00	0.00	0.46	0.00
	HS	0.00	0.00	0.00	0.00	0.00	0.00	0.00	0.43	0.00
Time constant for baseflow reservoir 2 (days)	PN	700	650	850	550	610	160	230	380	180
	HS	650	600	800	550	400	160	230	380	180
Dead storage fraction for baseflow reservoir 2	PN	0.00	0.00	0.00	0.00	0.80	0.00	0.00	0.93	0.59
	HS	0.00	0.00	0.00	0.00	0.00	0.00	0.00	0.93	0.50

Figure 6.1 demonstrates that, overall, the simulated river regimes of the HS model match the observed closely, and are likewise similar to those of the PN model, for both the calibration and validation periods. Weaker performance for the tributary stations (Yasothon and Ubon) is repeated. Performance statistics for the HS model (not shown) are consistently very similar to those of the PN model (see Table 5.12, the model employing UDel precipitation), and indicate generally good to excellent model performance. For example, employing the same classification scheme used previously, for both models for the calibration period, Dv is classed as excellent at all stations except Kompong Cham ("very good") and Phnom Penh ("fair"). Similarly, NSE for both models is ≥0.92, and therefore classed as "excellent", at all stations on the main Mekong. NSE for Yasothon (0.61 for both models) and Ubon (0.62 and 0.61 for the PN and HS model, respectively) is classed as fair for both models. For the validation period, Dv for both models is classed as "excellent" at all stations except Stung Treng and Yasothon ("very good"). For both models, NSE is classed as "very good" at the two most upstream stations, and as "excellent" for all other stations on the main Mekong. Model performance according to NSE is "very poor" for both models at the two tributary stations (Yasothon and Ubon).

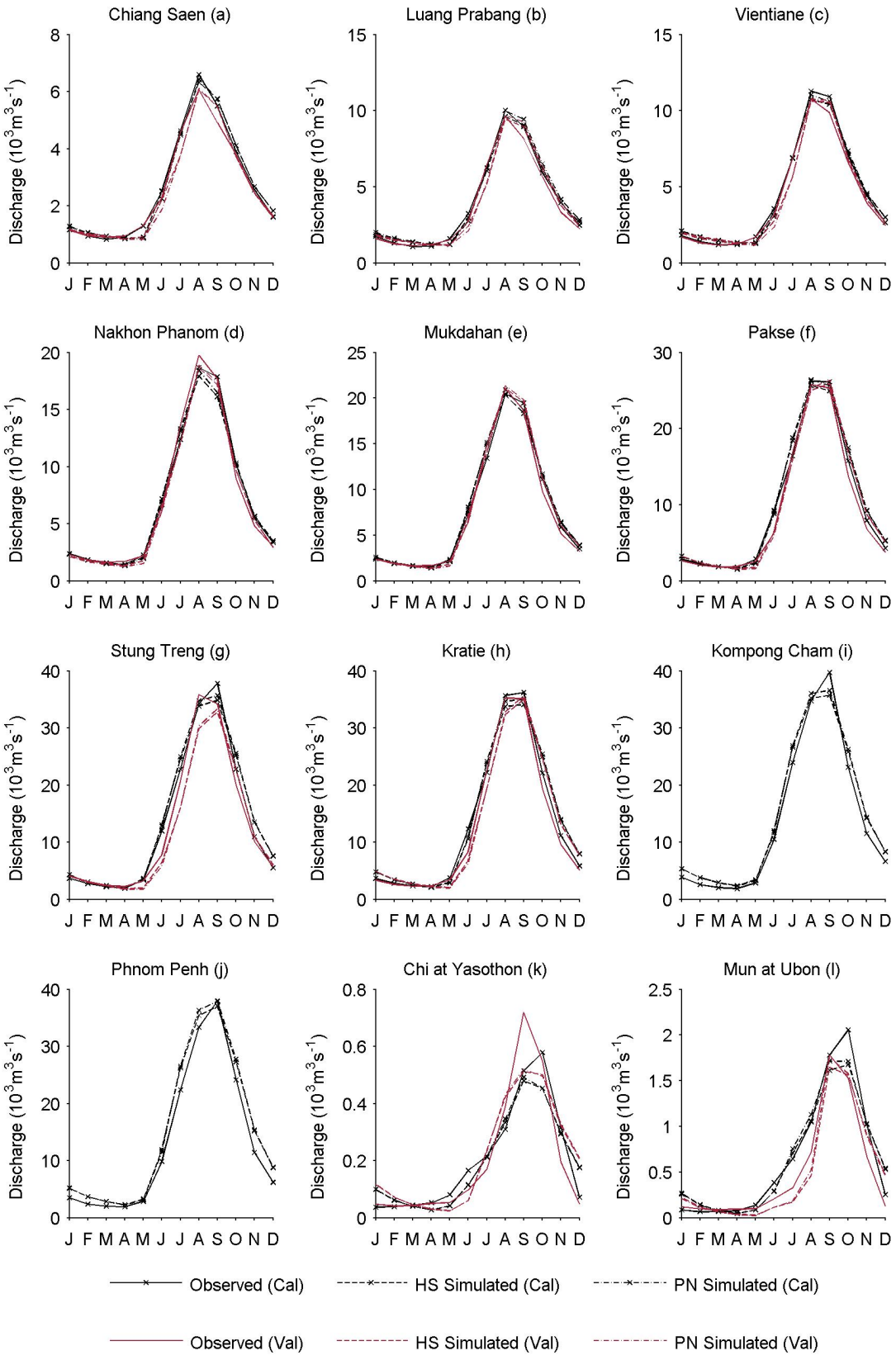

Figure 6.1. Observed and MIKE SHE simulated river regimes for the models employing HS and PN PET, for the calibration and validation periods. No validation data are presented for Kompong Cham or Phnom Penh as there are no observations for this period. (Note different y-axis scales.)

6.4.2. Changes in climate

Projected changes in climate are assessed relative to the observed baseline datasets (UDel precipitation and CRU temperature) and HS PET data calculated using CRU temperature, all for the 1961–1990 baseline period. Changes in precipitation and PET are presented first, since these are relevant throughout the catchment, whilst changes in temperature are discussed separately as these are only directly relevant within the MIKE SHE model over the upper two sub-catchments where snow accumulation and melting are relevant.

The boxplots in Figure 6.2 summarise the variability across the 41 CMIP5 GCMs in percentage change in mean annual precipitation and PET for each MIKE SHE sub-catchment for the RCP 4.5 scenario (2040–2069 time slice). This figure demonstrates that there is notable uncertainty in the direction of projected changes in annual precipitation for all but the Upper Lancang (sub-catchment 1), for which only a single GCM (CMCC-CMS) projects a negligible (<0.1%) reduction in annual precipitation. Elsewhere, the number of GCMs that project a reduction for any given sub-catchment varies between 9 (~22% of models; sub-catchment 2) and 19 (~46% of models; sub-catchment 12). Only 9 models (~22%) generate catchment-wide increases in precipitation. If outliers are included, the greatest inter-GCM range is seen over sub-catchment 1, with changes ranging between 0.0% and +41.1%, giving an inter–GCM range of change of 41.1%. If the +41.1% outlier (associated with GFDL-CM3) is excluded however, the range falls to 21.8%. Excluding all outliers (values lying more than 1.5 times the interquartile range below the 25th quartile or above the 75th quartile) results in sub-catchment 8 having the greatest inter–GCM range, with changes ranging between -14.0% and +17.0% (range: 31.1%). The mean inter–GCM range across sub-catchments 2–15 is 29.8% including outliers. The inter-quartile range, which describes the spread (range) of the middle 50% of data values, varies between 6.5% (sub-catchments 3 and 4) and 9.9% (sub–catchments 12 and 15). The middle 50% of values for each sub-catchment consistently fall within a band from -5% to +15%.

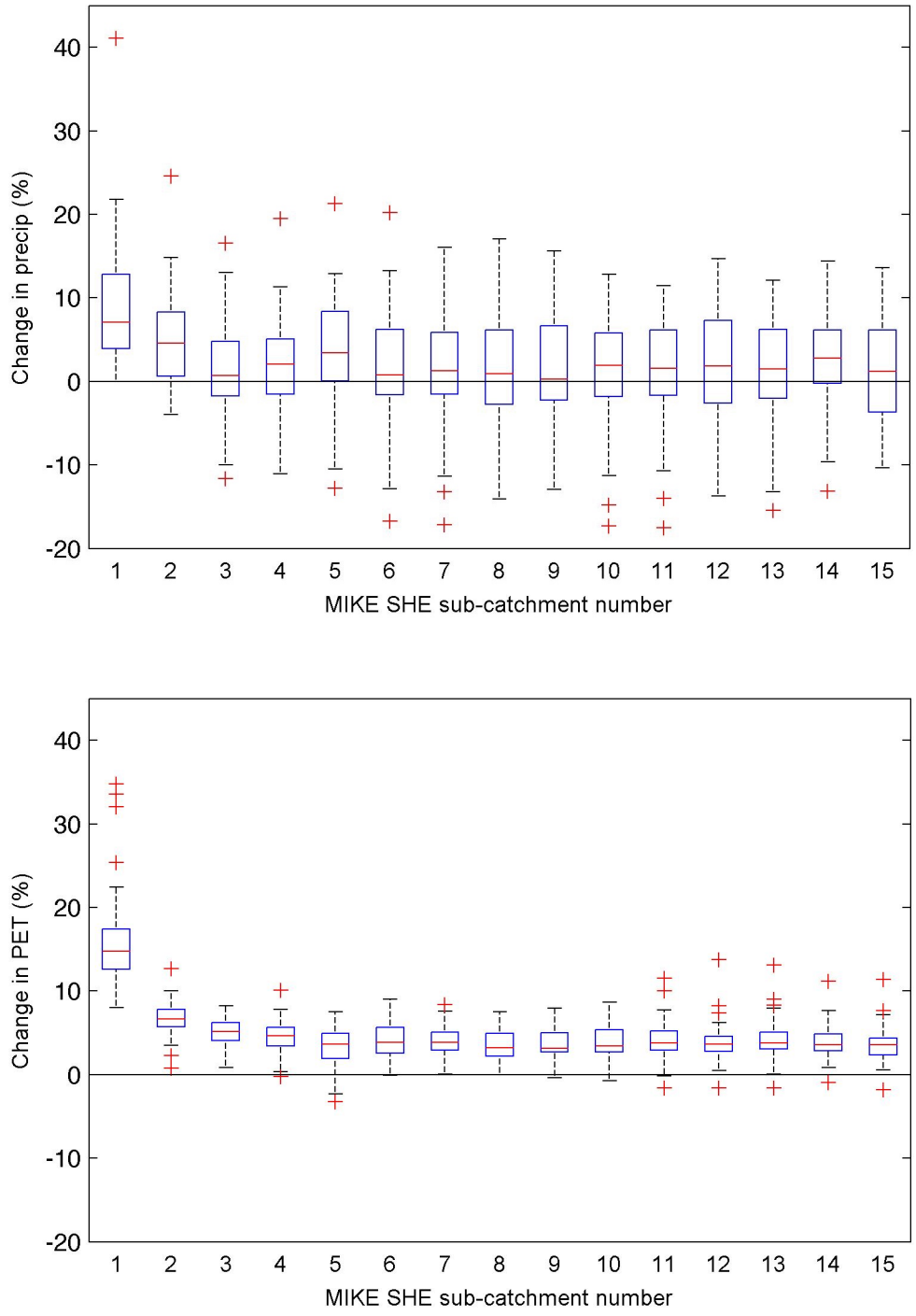

Figure 6.2. Boxplots of percentage change in mean annual precipitation (top) and PET (bottom) across the 41 GCMs for each sub-catchment. The boxplots show the median, 25th and 75th quartiles, and range of the data. Any value that lies more than 1.5 times the interquartile range below the 25th quartile or above the 75th quartile is plotted as an outlier (+).

In contrast to precipitation, the majority of GCMs project increases in annual PET across the catchment, with no more than three GCMs projecting a reduction for any given sub-catchment, and ~85% (35/41) of GCMs projecting an increase across all 15 sub-catchments. This means that only six GCMs are responsible for any projected reductions. Of these six, four of the GCMs only project a negligible to small reduction at a single sub-catchment, with reductions ranging from <0.1% to 3.3%, and one GCM projects reductions of <0.3% at four sub-catchments. INMCM4 projects a reduction for the greatest number of sub-catchments (seven), with a maximum reduction of 1.8% for sub-catchment 15.

Variability in the magnitude of projected changes in PET is also lower compared to that for precipitation. Both the greatest increases (consistently across all GCMs) and the greatest range in changes are seen over the Upper Lancang (sub-catchment 1), with a median change of +14.8%, and changes ranging from +8.0% to +34.8% (including outliers), giving an absolute range in percentage change of 26.8%. Projected changes across the remaining sub-catchments are generally lower, with less inter-GCM variability. For example, the median change varies between +3.2% (sub-catchments 8 and 9) and +6.7% (sub-catchment 2) and the average inter-GCM range of change across sub-catchments 2–15 is 10.8%, compared to a value of 29.8% for precipitation. The inter-quartile range is relatively low across all sub-catchments, with a maximum of 4.9% for sub-catchment 1, and values of 1.8–3.0% elsewhere. The middle 50% of models therefore fall within a narrow band of changes in annual PET.

Projected change in annual precipitation is presented for each individual GCM and sub-catchment in Figure 6.3, with GCMs separated into different subplots according to the groupings shown in Table 6.1. The equivalent for annual PET is presented in Figure 6.4.

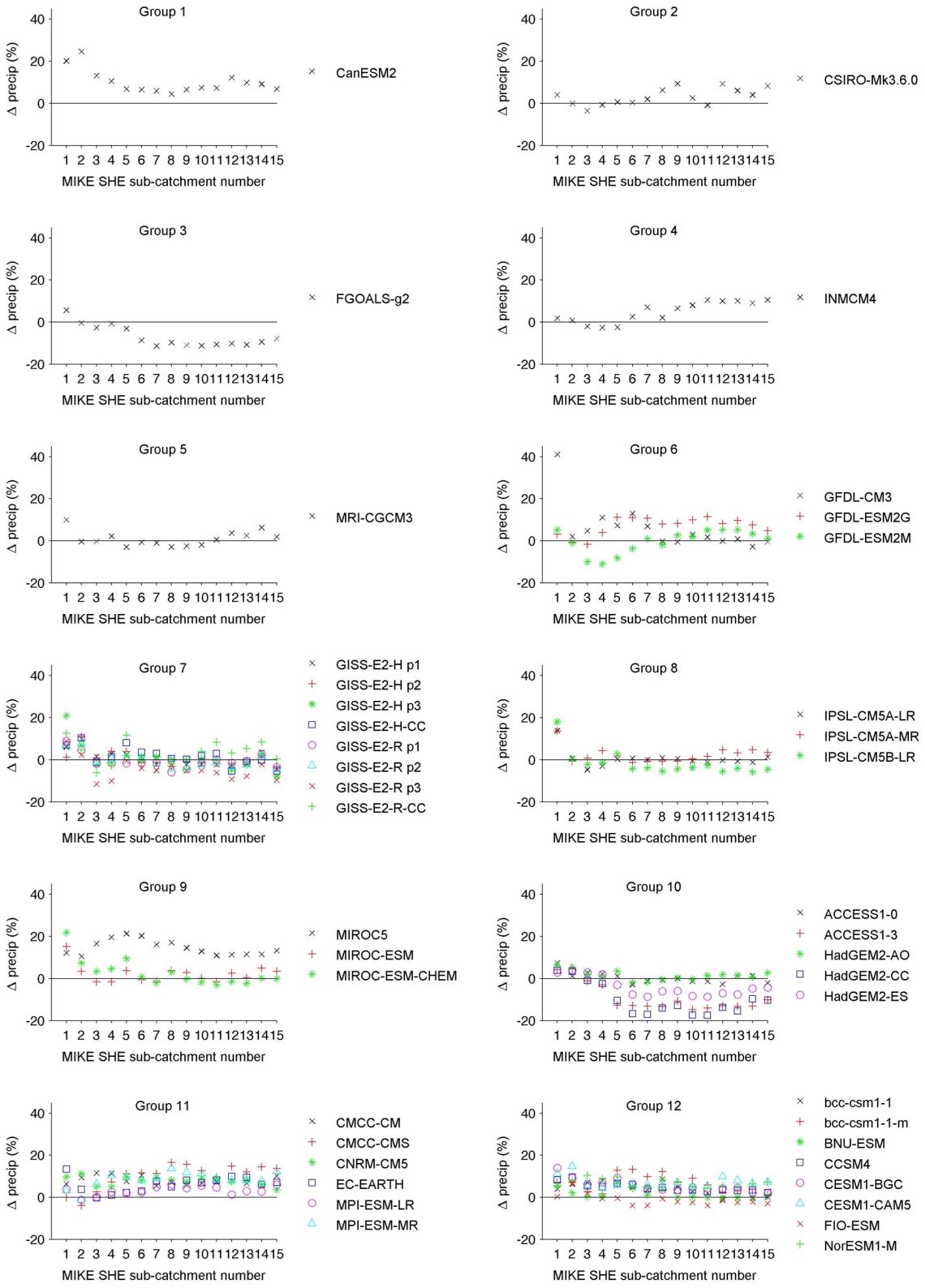

Figure 6.3. Projected percentage change in mean annual precipitation across the Mekong MIKE SHE sub-catchments. Individual subplots for each GCM group.

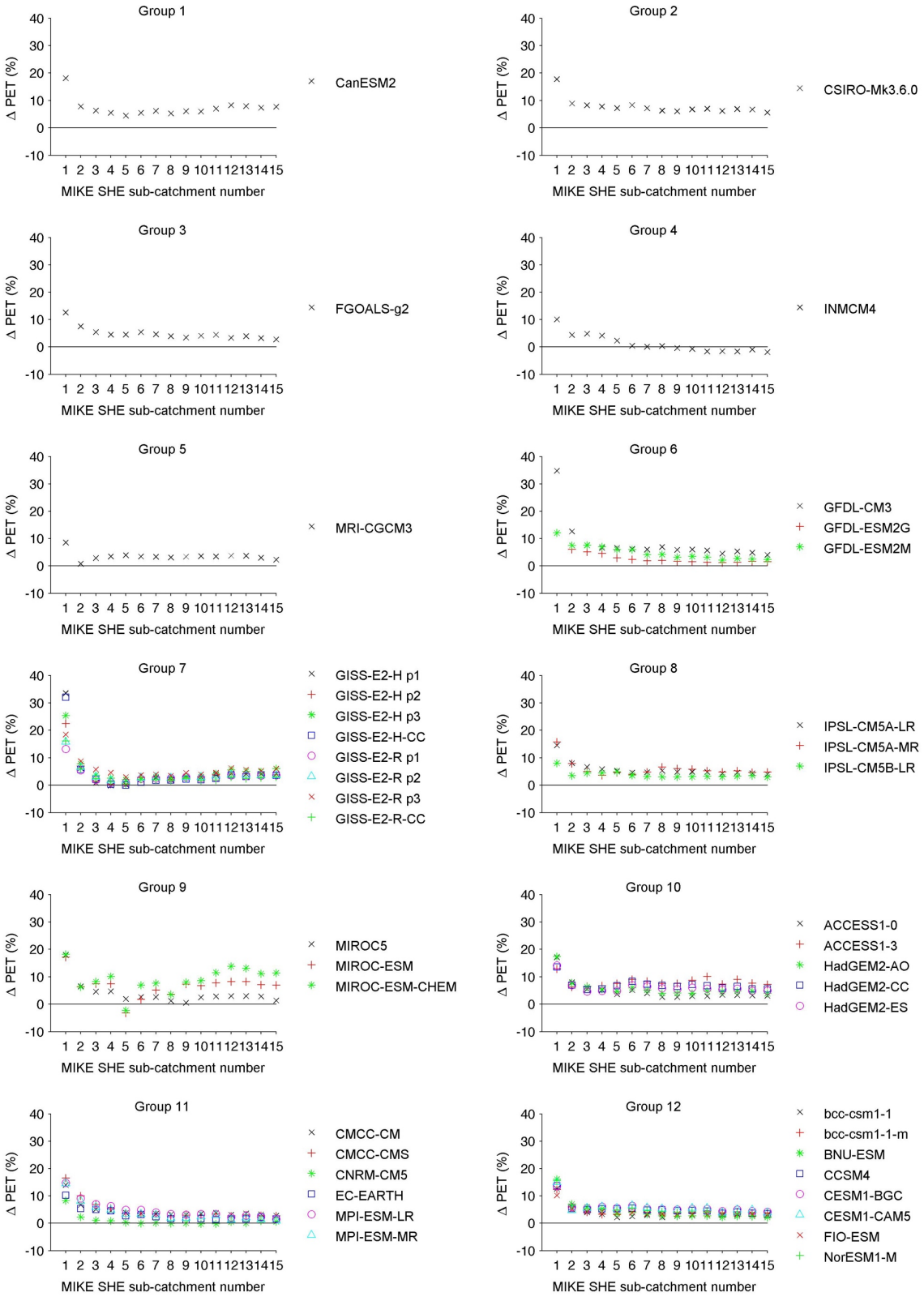

Figure 6.4. Projected percentage change in mean annual PET across the Mekong MIKE SHE sub-catchments. Individual subplots for each GCM group.

There is clearly great variation between GCMs in terms of the spatial pattern and magnitude of changes in annual precipitation (Figure 6.3). For example, whilst some models project catchment-wide increases (e.g. CanESM2 – Group 1; MIROC5 – Group 9), others produce reductions over the majority (≥8) of sub-catchments (e.g. FGOALS-g2 – Group 3; HadGEM2-CC and -ES – Group 10). Within some of the groups that contain multiple GCMs, there are some clear similarities in the spatial pattern of changes. For example, within Group 10, the greatest increases are seen over sub-catchments 1 and 2, whilst either reductions or only small increases (<3.5%) are seen over the remaining sub-catchments. However, the inter-GCM range of change within an individual group can vary considerably. For example, for Group 10, the inter–GCM range is consistently between 12–16% for sub-catchments 5–15, whilst for Group 9, it varies between 11–21% for sub-catchments 3–15.

Figure 6.4 demonstrates that, in contrast to precipitation, many of the GCMs across the different groups display a similar spatial pattern of change in annual PET, since, as described above, the largest increase is consistently seen over the Upper Lancang (sub-catchment 1). Within the groups that contain multiple GCMs, although the different models display generally similar spatial patterns, the magnitude of changes can sometimes vary notably. For example, in Groups 6 and 7 over sub-catchment 1, there is an inter-GCM range of change of 22.7% and 20.4%, respectively. In contrast, Group 9 has an inter-GCM range of <1.5% over sub-catchments 1 and 2 and displays the greatest inter-GCM ranges (between 8.3–10.9%) over sub-catchments 11–15.

Figures 6.5 and 6.6 show projected mean monthly precipitation and HS PET, respectively, for 10 representative MIKE SHE sub-catchments for each GCM, as well as the ensemble mean derived from the 41 GCMs. Observed baseline values are also shown. In the case of precipitation, there is great variability in the pattern and magnitude of projected changes through the year and, with the exception of sub-catchments 1 and 2 (where it is more clear that a majority of GCMs project increases) the direction of precipitation change has no clear majority for any season.

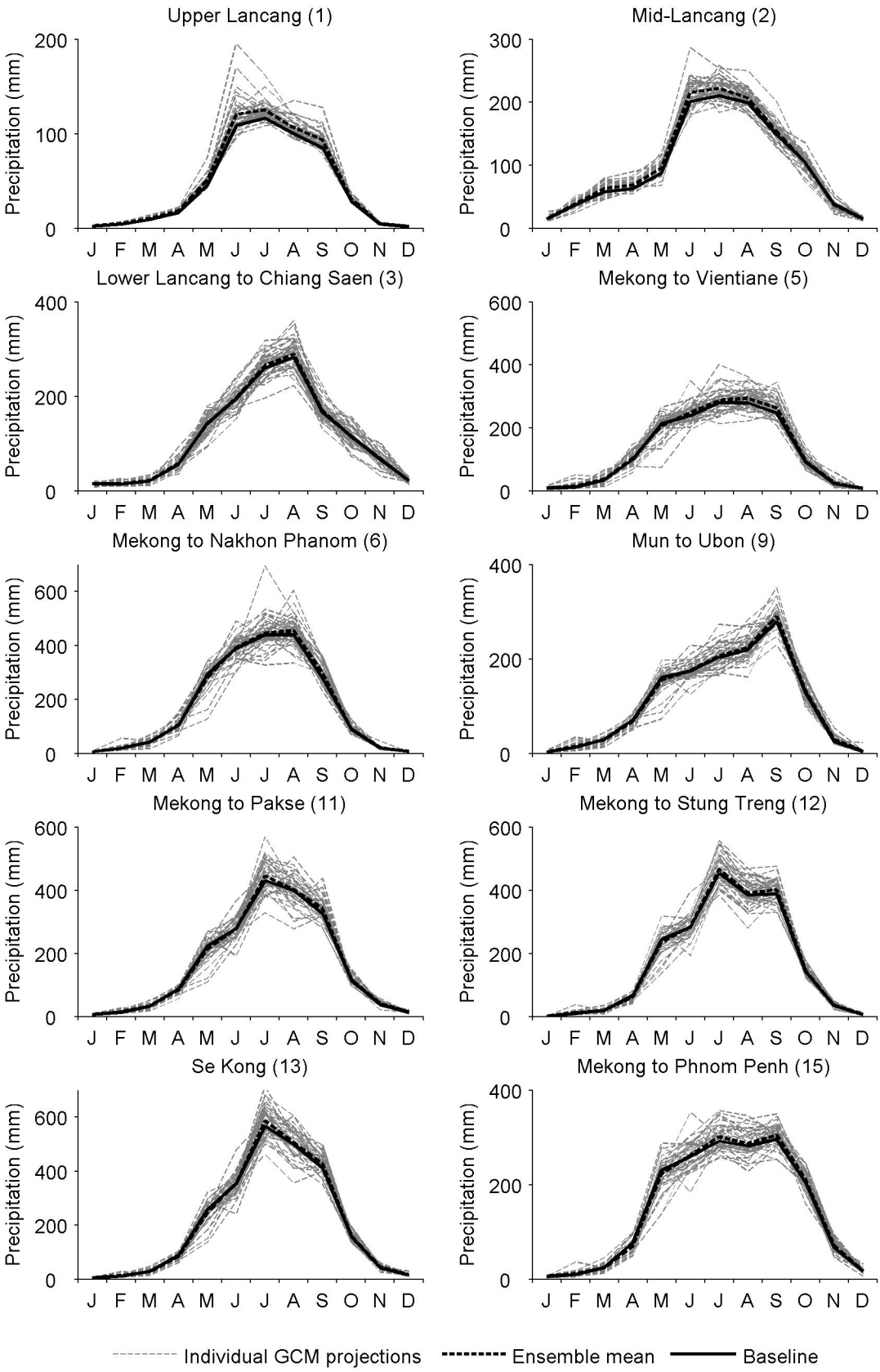

Figure 6.5. Mean monthly precipitation for 10 MIKE SHE sub-catchments for the baseline, each GCM and the ensemble mean. (Note different y-axis scales.)

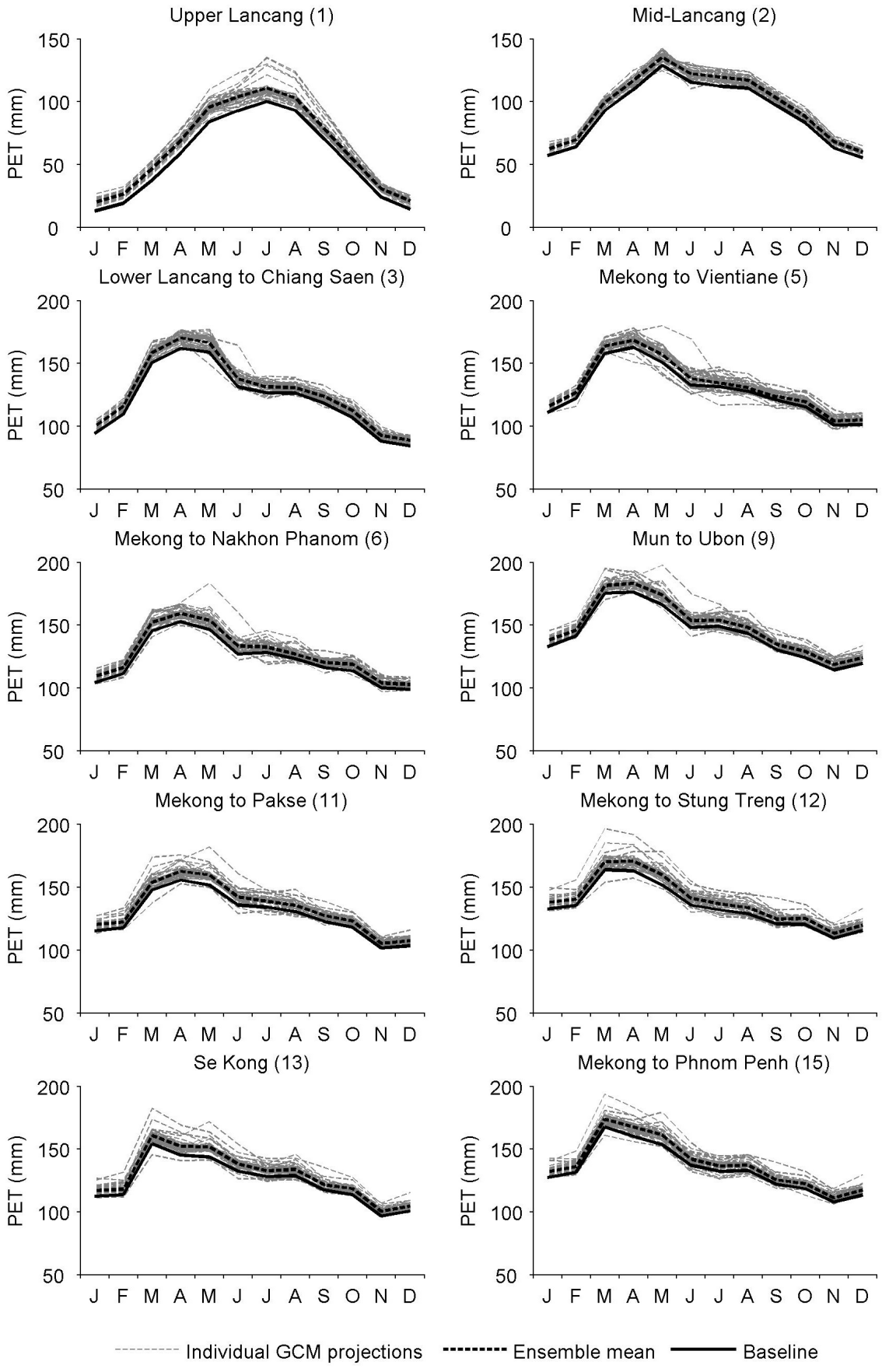

Figure 6.6. Mean monthly PET for 10 MIKE SHE sub-catchments for the baseline, each GCM and the ensemble mean. (Note different y-axis scales.)

Changes in mean monthly PET show much less variability. For each month in each sub-catchment, the majority of GCMs produce increases in PET, although some GCMs show little change or reductions of up to 11% for at least some months of the year. For any given month in any given sub-catchment, less than 32% of the 41 GCMs (i.e. never more than 13 GCMs) project a reduction in PET. Consequently, the ensemble mean increases throughout the year for all sub-catchments. Maximum mean monthly increases are seen over the Upper Lancang, with a maximum absolute increase of 35.3 mm in July (equivalent to +35.2%), and a maximum percentage increase of 104.1% in January (+13.5 mm). Where reductions in PET are projected, this is sometimes due to a projected reduction in maximum or minimum mean monthly temperature (mean monthly temperature consistently increases). Most cases, however, are associated with a reduction in the difference between the maximum and minimum mean monthly temperatures, as this difference is used in the calculation of HS PET to implicitly represent relative humidity (Samani, 2000).

Across the 15 sub-catchments, the mean inter–GCM range in absolute (mm) change in precipitation for July (one of the wettest months) is 172.8 mm. This value was derived by calculating the difference between the maximum and minimum projected change (in mm) for July for each sub-catchment, and then finding the mean of these 15 range values. July is the month with the highest mean absolute inter–GCM range. The mean inter–GCM range in percentage change for July is 52.9%. For comparison, across sub-catchments 1–15, the mean inter–GCM range in absolute (mm) change in PET for June (the month with the highest mean range) is 31.9 mm (less than a fifth of the value stated above for precipitation) and the mean inter–GCM range in percentage change for June is 24.4% (less than half the value stated for precipitation).

As noted previously, changes in mean temperature are only directly relevant within the MIKE SHE model of the Mekong over the upper catchment (sub-catchments 1 and 2). However, changes in mean, minimum and maximum temperature drive, and are therefore reflected in, projected changes in PET. Boxplots of projected change in sub-catchment based mean temperature from the 41 GCMs are presented in Figure 6.7.

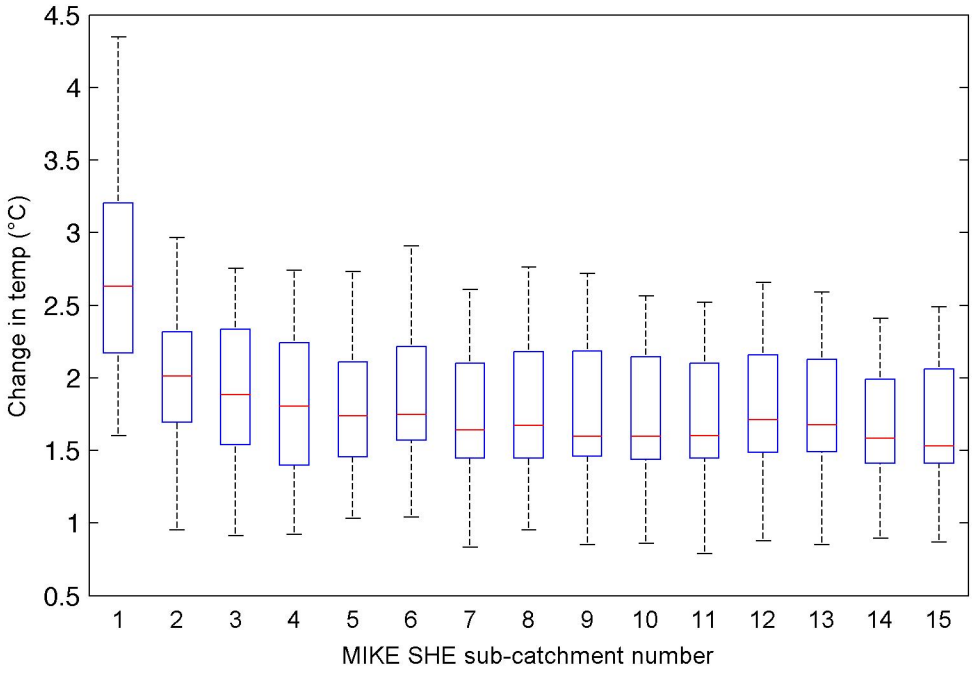

Figure 6.7. Boxplots of change in mean temperature (°C) across the 41 GCMs for each sub-catchment. The boxplots show the median, 25th and 75th quartiles, and range of the data. No values lie more than 1.5 times the interquartile range below the 25th quartile or above the 75th quartile.

Mean temperature is projected to increase across all sub-catchments. The greatest increases are projected over sub-catchment 1, with changes ranging between +1.6–4.3 °C (range: 2.7 °C) and a median change of +2.6 °C. Changes across the remaining sub-catchments are generally lower and fall between +0.8–2.9 °C, with median values of between +1.5 °C (sub-catchment 15) and +2.0 °C (sub-catchment 2). These patterns are replicated in changes in PET, where both the greatest increases and greatest inter–GCM variability are seen over sub-catchment 1, with less variability across the other sub-catchments (see Figure 6.2).

6.4.3. Changes in river flow

Throughout this section, MIKE SHE simulated river discharges for the ensemble of GCMs for the RCP4.5 scenario are compared to those simulated by MIKE SHE for the 1961–1990 baseline period. Figure 6.8 summarises the variability in projected percentage change in mean, Q5 and Q95 discharges for the 12 gauging stations.

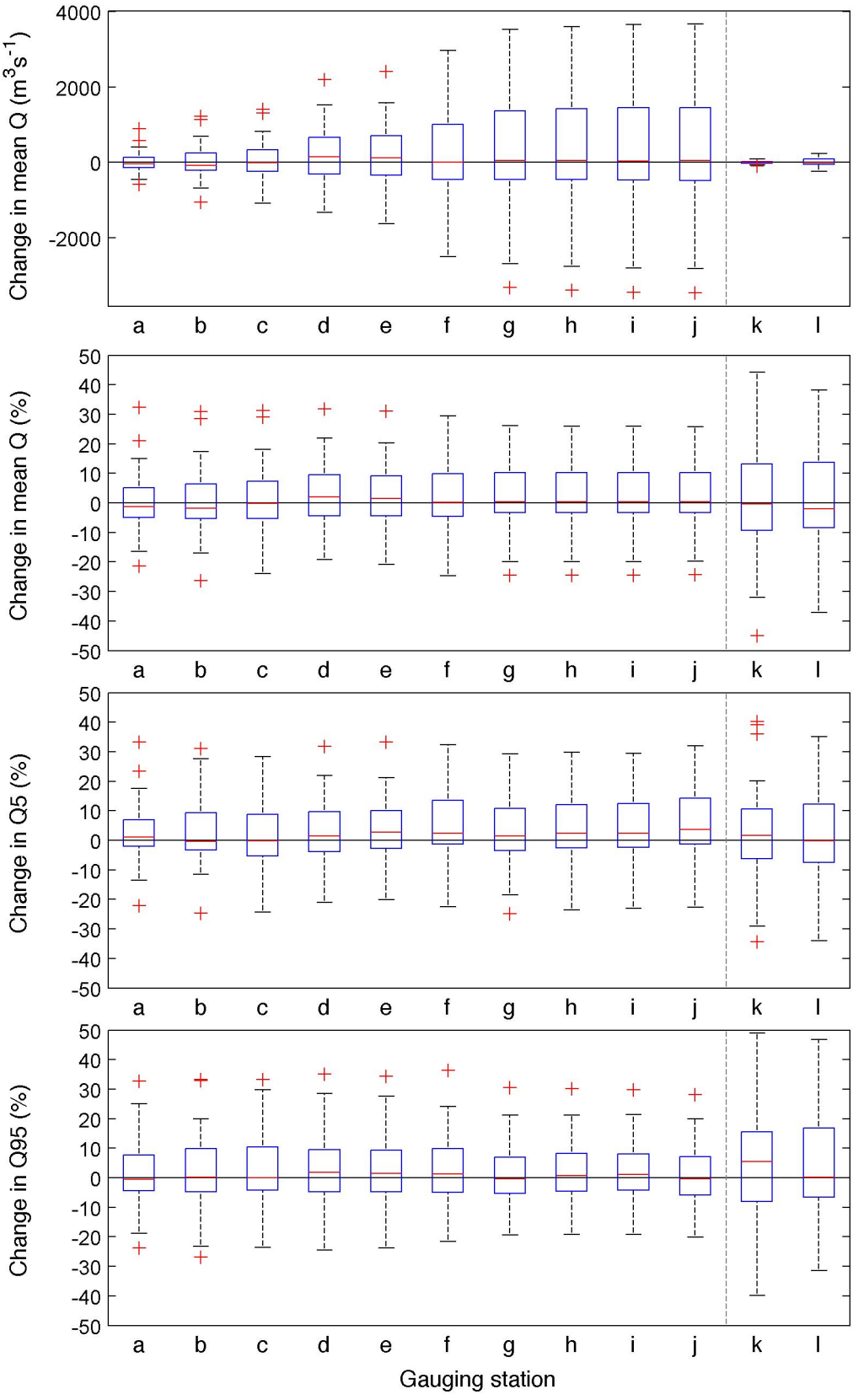

Figure 6.8. Boxplots of change in mean, Q5 and Q95 discharges across the 41 GCMs for each gauging station. The boxplots show the median, 25th and 75th quartiles, and range of the data. Any value that lies more than 1.5 times the interquartile range below the 25th quartile or above the 75th quartile is plotted as an outlier (+). Stations a to j are on the main Mekong; k and l are located on tributary branches.

Projections of mean, high (Q5) and low (Q95) discharges show great variability across the GCMs, with percentage changes (including those plotted as outliers) at each station ranging between -19% or greater (i.e. more negative) and +25% or greater. The inter-GCM range in percentage changes (for all three discharge measures) varies between 49–60% at all stations on the main Mekong (a–j), whilst the inter-quartile range for these stations varies between 9–15%. For the two tributary stations (k: Chi at Yasothon; l: Mun at Ubon), the range and inter-quartile range of percentage changes are greater (range: >68%; inter-quartile range: >15%). However, these percentage changes still equate to absolute changes that are far smaller than at any of the stations on the main Mekong, as demonstrated for mean discharges in Figure 6.8, due to discharges being markedly smaller on these tributaries.

The median change in mean and Q95 discharges at each station is frequently very close to 0 (within ±1.5%), suggesting that there is often a relatively even split between the number of GCMs that project positive and negative changes. In fact, in the case of mean discharge, nine out of 12 stations display a 20:21 or 21:20 ratio for the number of GCMs that display positive or negative changes. For Q95, this is the case for three stations, and a further six stations display a ratio of 19:22 (or vice versa). In the case of Q5, four stations display a ratio of 20:21 or 19:22 (or vice versa) and at the remaining stations, a majority of between 56.1% (23/41) and 60.1% (25/41) of GCMs project increases in Q5.

Although Figure 6.8 provides a useful summary of the variability in projected changes in mean discharges across the 41 GCMs, it does not allow the spatial pattern or magnitude of changes for individual GCMs to be discerned. Figure 6.9 displays changes in mean discharge at each of the 12 gauging stations for each GCM, with a separate subplot for each GCM group. When comparing these plots to projected changes in precipitation and PET, it is worth noting that the MIKE SHE sub-catchments in the latter do not match up from left to right with the gauging stations. For example, station a (Chiang Saen) is located at the terminus of sub-catchment 3, and stations k and l correspond to sub-catchments 8 and 9. Figure 6.10 is provided for reference.

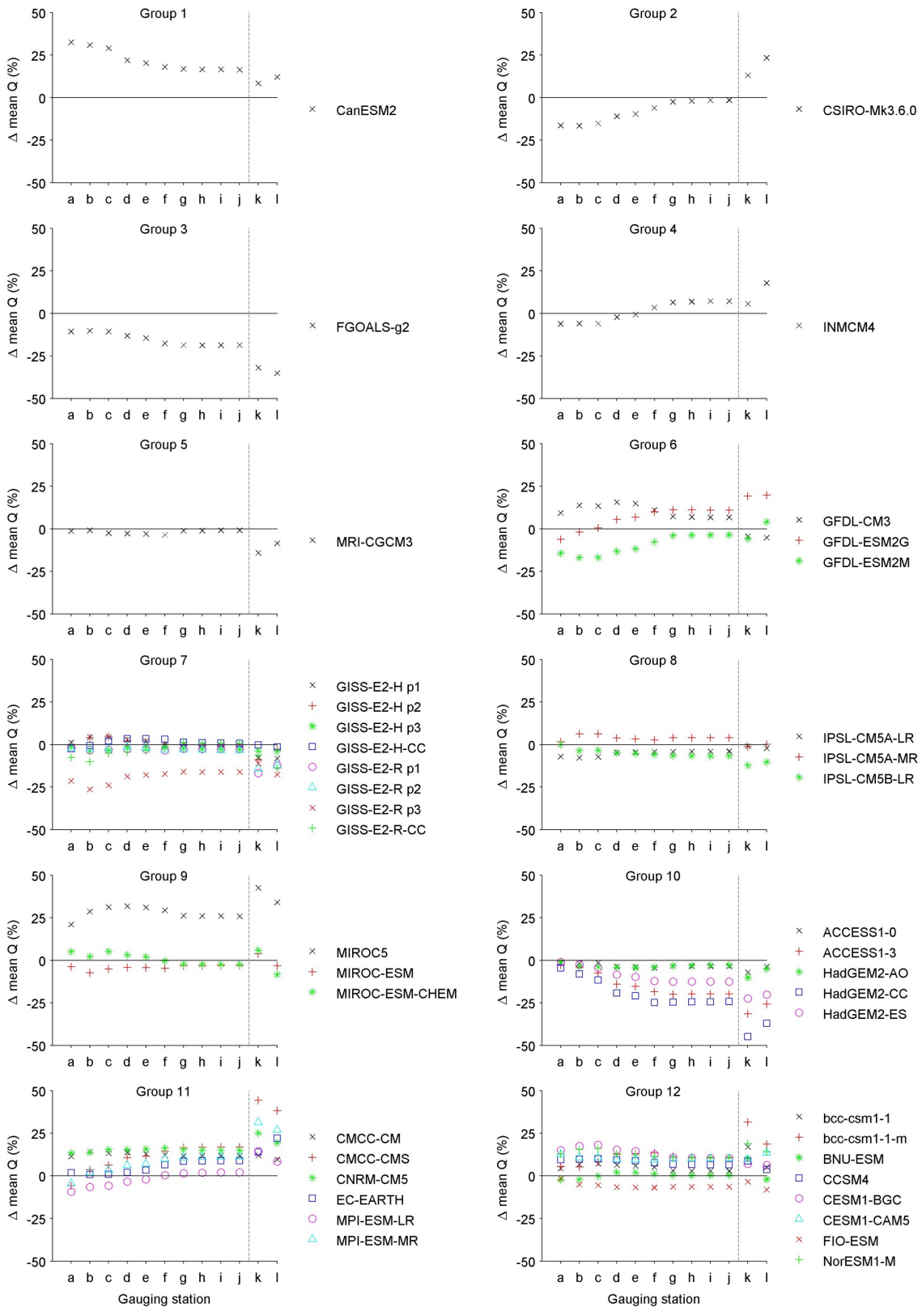

Figure 6.9. Projected percentage change in mean discharge across the 12 gauging stations (a–l). Individual subplots for each GCM group.

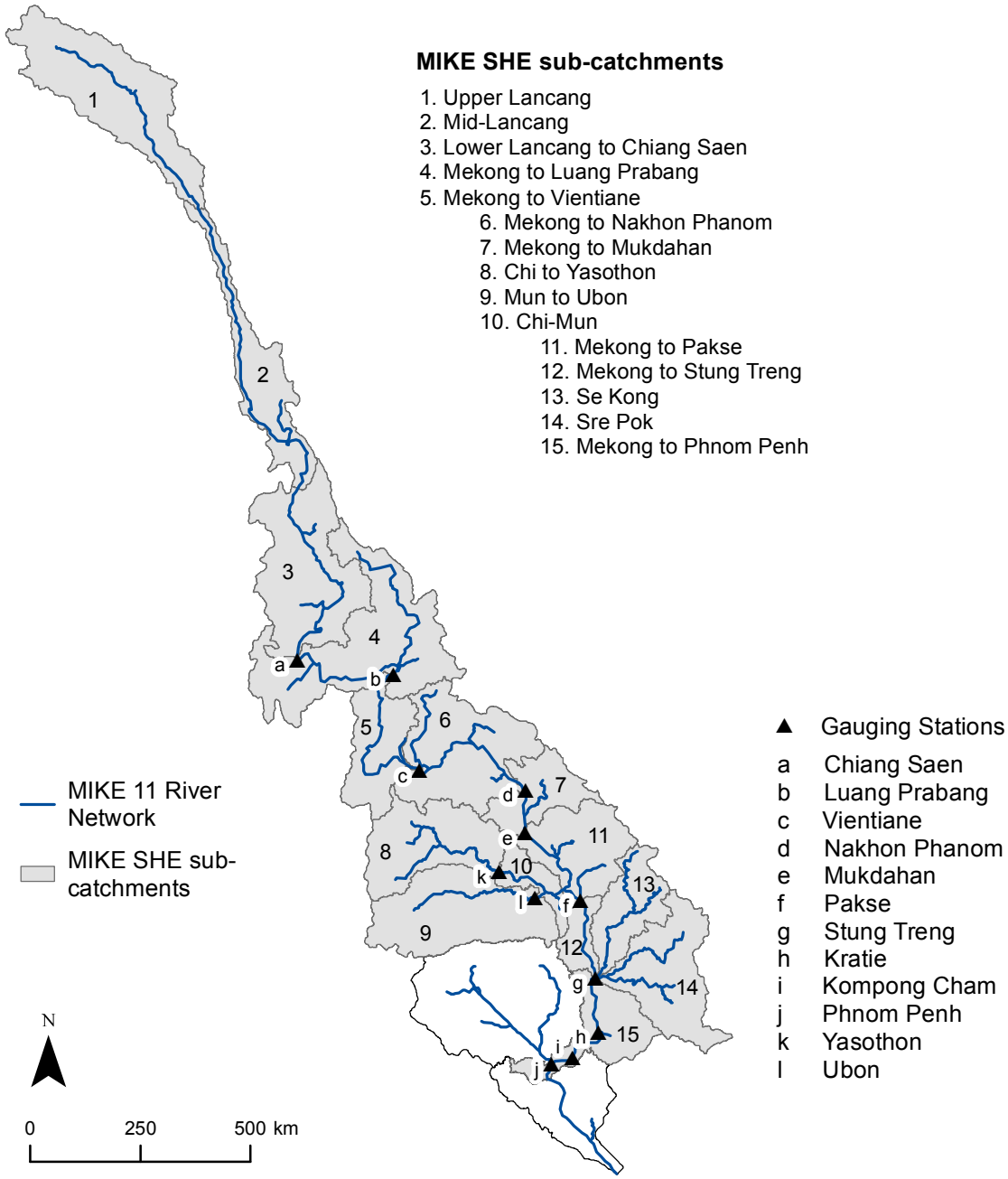

Figure 6.10. MIKE SHE sub-catchments and gauging stations on the river network.

As with mean annual precipitation, changes in mean discharge across the different GCMs show great variability in terms of the spatial pattern of the direction and magnitude of changes. For example, 11 GCMs show increases in discharge at all stations (CanESM2 – Group 1; MIROC5 – Group 9; three GCMs from Group 11, six from Group 12), and 14 show decreases at all stations (FGOALS-g2 – Group 3; MRI–CGCM3 – Group 5; four GCMs from Group 7; two GCMs Group 8; all GCMs Group 10; FIO–ESM – Group 12). The remaining 16 GCMs do not show a consistent direction of change across all stations. In terms of the spatiality in the magnitude of changes

on the main Mekong (stations a–j), some GCMs show a relatively consistent magnitude of change across all stations (e.g. CNRM-CM5 – Group 11), whereas others display greatest increases or decreases over upstream, downstream, or mid-catchment stations.

It is clear that the spatiality of the direction and magnitude of changes can largely be explained by (and is therefore largely driven by) the projected changes in precipitation (Figure 6.3), although changes in PET also play a role. For example, the GCMs that display increased mean discharge at all stations correspond to projections of increased precipitation for the majority (if not all) sub-catchments. Conversely, the GCMs that result in decreased mean discharge at all stations correspond to projections of decreased precipitation for the majority (if not all) sub-catchments.

Within some of the groups that contain multiple GCMs, there are some clear similarities in the spatial pattern of changes. For example, within Group 10, ACCESS 1-3, HadGEM2-CC and HadGEM2-ES display reductions at all stations, with an increase in the magnitude of changes in a downstream direction from stations a (Chiang Saen) to f (Pakse), and a relatively consistent change across stations f–j. Despite this similarity in the pattern of changes, the inter-GCM range in percentage change (across these three GCMs) is >10% for stations d–j. In contrast to Group 10, within Group 6, there is little similarity between the three GCMs in the spatial pattern of changes, with one (GFDL-CM3) showing reductions at the two most upstream stations (a and b) with increases further downstream that increase in magnitude down to station g, one (GFDL-ESM2G) showing increases at all stations on the main Mekong, with greatest increases in the mid-catchment (station d) and the final GCM (GFDL-ESM2M) showing decreases at all stations on the main Mekong, with greatest increases at stations b and c.

It is possible that the median projection for each station and the proportion of GCMs indicating increases or decreases could be biased due to the inclusion in some cases of multiple GCMs from the same genealogical group. To investigate this, for each of the multi-GCM groups, a mean projected change in mean discharge was derived for each station by averaging the projected changes from all of the GCMs in the relevant

group. Boxplots generated using the 12 projected changes per station (i.e. one from each group) are presented in Figure 6.11, alongside the 25th, 50th (median) and 75th percentiles of changes from all 41 GCMs for comparison (i.e. the same values as in Figure 6.8). For stations on the main Mekong, use of the group-based changes results in only a relatively small shift in the median, downwards for stations a and c–e (by between 0.6–4.2%) and upwards by up to 1.6% for the other stations. Similarly, the 25th percentiles are altered by <2% at all stations, including k and l, whilst the 75th percentile decreases by up to 3.4%.

The relatively small differences between the 25th, 50th and 75th percentiles of the 12-group set and the 41-GCM ensemble indicate that the inclusion of different versions of GCMs and GCMs from the same research group has not led to a notable bias in the median, or the spread of the middle 50% of results. Furthermore, since the 12-group set shows a loss of some outliers and shortening of some of the boxplot whiskers compared to the 41-GCM ensemble (see Figure 6.9), the 41 GCM-ensemble provides a greater range of results and therefore a more complete picture of GCM-related uncertainty.

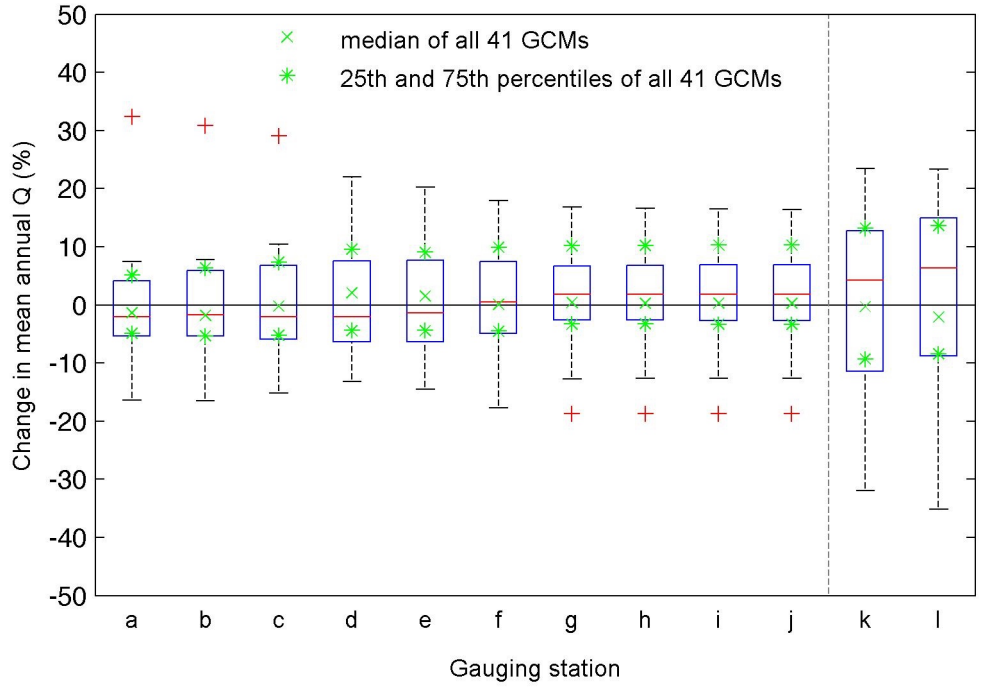

Figure 6.11. Boxplots of change (%) in mean discharges across the 12 GCM groups for each gauging station. The boxplots show the median, 25th and 75th quartiles, and range of the data. Any value that lies more than 1.5 times the interquartile range below the 25th quartile or above the 75th quartile is plotted as an outlier (+). The median, 25th and 75th percentiles of changes from all 41 GCMs are also plotted.

In addition, as exhibited by the 41-GCM ensemble, there is no clear or consistent consensus on the projected direction of change in mean discharge from the 12-group set, with a 6:6 ratio of increases:decreases at five stations, 5:7 at two, 7:5 at two and 4:8 at the three most upstream stations, equating to two thirds (66.7%) of GCMs projecting reductions. This is not dissimilar, for example, to the 63% of GCMs in the 41-member ensemble projecting a reduction in mean discharge at station a. This demonstrates that the use of multiple GCMs from the same genealogical group has not had any clear overriding impact on the direction of projected changes.

The analysis of projected changes in discharge from the 41-GCM ensemble has so far assessed changes in mean, Q5 and Q95 discharges. For eight representative gauging stations, Figure 6.12 displays the simulated river regimes (mean monthly discharges) for the 2040–2069 time slice, as well as the ensemble mean (average simulated river regime) and the baseline. Unsurprisingly (considering the projected changes in mean monthly precipitation and the results for changes in mean, Q5 and Q95 discharges), there is uncertainty in the seasonality, magnitude and direction of changes. Some GCMs display year-round increases (between four and eight GCMs at each station), some year-round decreases (3–7 GCMs at each station), and others a variable direction and pattern of change through the year. The inter-GCM ranges of absolute changes tend to be highest in June–October during the wet season, whilst the inter-GCM ranges of percentage changes tend to be highest in May–July on the ascending limb of the river regime. For example, at Pakse, the inter-GCM range in percentage change is between 40–50% throughout September–April, but over 90% in May and June.

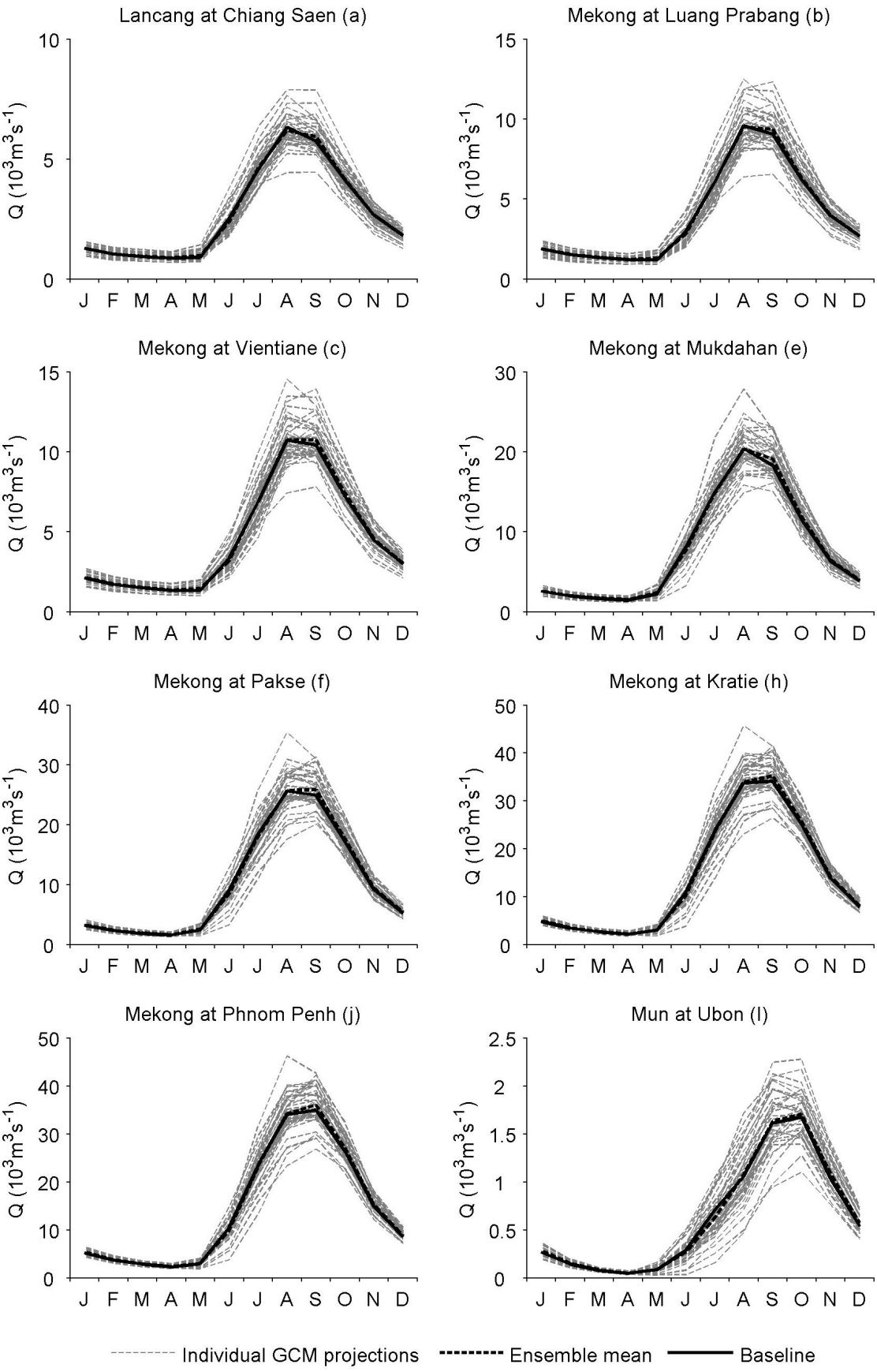

Figure 6.12. Simulated river regimes for eight gauging stations for the baseline, each GCM and the ensemble mean. (Note different y-axis scales.)

6.5. Discussion and summary: GCM-related uncertainty assessment using 41 CMIP5 GCMs versus seven CMIP3 GCMs

This chapter has furthered the investigation of GCM-related uncertainty in river flow projections under climate change, using climate outputs from 41 CMIP5 GCMs under the RCP4.5 scenario for the 2040–2069 time slice. The magnitude, seasonality and spatial pattern of simulated changes in river discharge show great variability across the GCMs, with no consensus on the direction (i.e. positive or negative) of changes. Uncertainty in the projected direction of change is dominated by uncertainty in precipitation projections. These findings are consistent with those of Chapters 4 and 5, which employed a smaller ensemble of seven CMIP3 GCMs for a scenario of 2 °C rise in global mean air temperature, relative to a 1961–1990 baseline period.

These two sets of scenarios differ considerably in the nature of their generation. For the 2 °C scenario, GCM outputs were rescaled to match 2 °C prescribed warming using the ClimGen pattern-scaling technique. They do not, therefore, relate to a specific time slice or a predefined GHG or radiative forcing scenario. In contrast, the RCP4.5 scenario, for which a 2040–2069 time slice was employed in this chapter, relates to a pathway where radiative forcing reaches 4.5 W m^{-2} in the year 2100. Therefore, although the CMIP5 GCMs are responding to the same radiative forcing, mean global warming for this time slice will vary between the GCMs due to GCM uncertainty. In addition, these scenario data were generated using the delta-factor approach. Despite the lack of direct equivalence of the two different scenario sets, it is still possible to draw some comparisons between the GCM-related uncertainty in the river flow projections from the two sets. Tables 6.3 and 6.4 provide a summary of the inter-GCM related uncertainty in the discharge projections for the RCP4.5 scenario across 41 GCMs and the 2 °C scenario across seven GCMs, respectively. Results are presented for four stations and the 12-station average. They demonstrate that the maximum and minimum projected changes, and therefore the inter-GCM range of change, in mean, Q5 and Q95 discharges are consistently greater for the RCP4.5, 41 GCM ensemble compared to the 2 °C, seven GCM ensemble. Across the 12 gauging stations, the average inter-GCM range of change for the three flow measures are around 55–60% for the former, and 30–40% for the latter. The greater

range for the CMIP5 ensemble is most probably due to the inclusion of a greater number of GCMs.

Table 6.3. Summary of projected percentage changes in mean, Q5 and Q95 discharges from 41 CMIP5 GCMs for the RCP 4.5 scenario, 2040–2069 time slice. Results are from the hydrological model employing MIKE SHE sub-catchments and HS PET.

Results from the MIKE SHE sub-catchments model employing HS PET, for the 2040–2069 RCP 4.5 scenario, from 41 GCMs						
Units for all: %		Chiang Saen (a)	Vientiane (d)	Pakse (f)	Ubon (l)	12 station average
Max. change mean Q		32.4	31.7	29.4	38.2	31.1
Min. change mean Q		-21.4	-19.2	-24.7	-37.2	-26.4
Max. change Q5		33.3	31.9	32.3	35.1	32.2
Min. change Q5		-22.1	-21.0	-22.5	-34.0	-24.7
Max. change Q95		32.8	35.0	36.3	46.8	34.9
Min. change Q95		-23.7	-24.5	-21.6	-31.5	-24.4
Inter-GCM range of change in:	Mean Q	53.8	50.9	54.1	75.4	57.5
	Q5	55.4	52.9	54.8	69.0	56.9
	Q95	56.5	59.5	57.9	78.3	59.4

Table 6.4. Summary of projected percentage changes in mean, Q5 and Q95 discharges from seven CMIP3 GCMs for the 2 °C warming scenario. Results are from the hydrological model employing MIKE SHE sub-catchments and PN PET.

Results from the MIKE SHE sub-catchments model employing PN PET, for the 2 °C prescribed warming scenario, from seven GCMs						
Units for all: %		Chiang Saen (a)	Vientiane (d)	Pakse (f)	Ubon (l)	12 station average
Max. change mean Q		19.8	21.2	15.0	24.4	17.7
Min. change mean Q		-16.4	-16.2	-11.6	-11.1	-12.8
Max. change Q5		18.2	17.1	21.0	19.2	19.0
Min. change Q5		-11.1	-13.1	-7.4	-13.3	-10.9
Max. change Q95		25.7	24.6	19.8	35.1	22.4
Min. change Q95		-17.7	-17.9	-17.6	-13.7	-16.9
Inter-GCM range of change in:	Mean Q	36.2	37.5	26.6	35.5	30.5
	Q5	29.3	30.1	28.3	32.5	29.9
	Q95	43.4	42.5	37.4	48.8	39.3

The CMIP3 GCMs included in the 2 °C, seven GCM ensemble are predecessors of some of the CMIP5 GCMs (Table 6.5). Figure 6.13 presents projected changes in mean discharge from the CMIP3 GCMs alongside projected changes from the corresponding GCM group's results for the RCP4.5 scenario. Considering that these results are for a different scenario, there are some striking similarities between the results for the CMIP3 GCMs and those from their successor GCMs, and where relevant, also other CMIP5 GCMs from the same genealogical group.

Table 6.5. Relationship between CMIP3 and CMIP5 models used in this thesis.

CMIP3 GCM	Abbreviation in Chapters 4 and 5	Successor model	GCM group number
CCCMA CGCM3.1	CCCMA	CanESM2	1
CSIRO-MK3.0	CSIRO	CSIRO-Mk3-6-0	2
HadCM3	HadCM3	HadGEM1, which is the predecessor of the HadGEM2 family	10
HadGEM1	HadGEM1	HadGEM2 family of models	10
IPSL-CM4	IPSL	IPSL-CM5A	8
MPI-ECHAM5	MPI	MPI-ESM	11
NCAR-CCSM3	NCAR	CCSM4	12

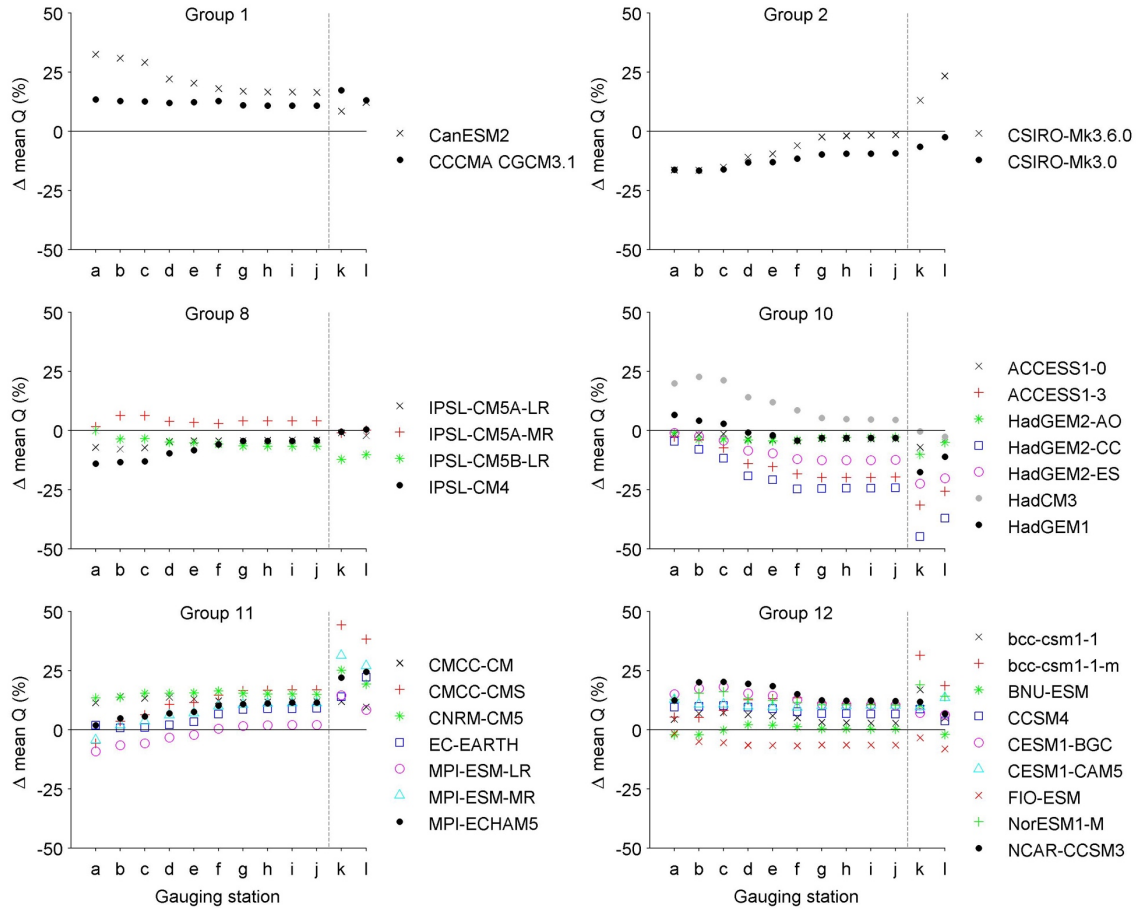

Figure 6.13. MIKE SHE projected changes in mean discharge from the CMIP3 GCMs for the 2 °C scenario, and from the CMIP5 GCMs from the corresponding GCM groups for the RCP4.5 scenario. CMIP3 GCMs are represented by filled circles (black, or grey in the case of HadCM3).

In Group 1, both GCMs show catchment-wide increases in mean discharge, although the disparity is >15% at the three most upstream gauging stations. At lower stations, the inter-GCM difference is <6%. In Group 2, both climate models result in decreases at all stations on the main Mekong, with an inter-GCM range of <4% at stations a–e

and up to 8% at downstream stations. Disparity is greater (>20%) for the two tributary stations (k and l), with the older GCM (CSIRO-Mk3.0) projecting reductions and the newer GCM increases. In Group 8, projections from the CMIP3 GCM (IPSL-CM4) display the same spatial pattern of changes as IPSL-CM5A-LR. IPSL-CM5A is an extension of IPSL-CM4, with -LR and -MR denoting the low and medium resolution versions, respectively (Dufresne *et al.*, 2013). Both HadCM3 and HadGEM1 display the same spatial pattern as the CMIP5 GCMs in Group 10. However, whilst the latter project catchment-wide reductions, with a tendency towards a great reduction with distance downstream, HadCM3 shows increases at all stations on the main Mekong, with smaller increases in a downstream direction. HadGEM1 exhibits increases for stations a-c, but at the remaining stations changes are very similar to those of HadGEM2-AO and ACCESS 1-0. MPI-ECHAM5 displays a very similar spatial pattern to the Group 11 CMIP5 GCMs. Changes in mean discharge for this earlier GCM are in the middle of the range for the CMIP5 GCMs at all stations and are closest to the results for the medium resolution version of its successor (MPI-ESM-MR). NCAR-CCM3 also displays a similar pattern to its CMIP5 counterparts in Group 12, although it displays the largest increases at the majority of stations.

There is, therefore, notable similarity in the results for the CMIP3 GCMs to those of their CMIP5 genealogical successors, despite the CMIP3 projections being generated using a different downscaling/bias-correction technique and for a different scenario type. At the same time, there are often considerable differences between the GCM groups. This supports the assertion that the greater level of observed inter-GCM uncertainty in the CMIP5 ensemble is due to the inclusion of a greater number of GCMs, meaning that the true extent of GCM-related uncertainty is sampled more fully. Furthermore, these findings strongly indicate that for the Mekong catchment, and likely the Southeast Asia region as a whole, GCM-related uncertainty (particularly in relation to precipitation projections) is the dominant source of uncertainty in hydrological projections under climate change, with scenario-related and downscaling uncertainty being less important. For regions where there is greater consensus amongst GCMs on the direction of annual and seasonal changes in precipitation, then the relative importance of other sources of uncertainty may increase.

Chapter 7
Conclusions and recommendations

7.1. Introduction

This chapter revisits the aim and objectives of this thesis and provides an outline and discussion of the key findings. Methodological recommendations for future hydrological modelling studies and potential areas of further research are also highlighted. The aim of this thesis was to assess some of the sources of uncertainty in river flow projections under climate change, focussing on the impact of some key decisions made during the hydrological modelling process. A series of objectives were formulated to achieve this aim and the Mekong River Basin, a major international catchment and the largest in Southeast Asia, was employed as a case study site. In Sections 7.2–7.5, the research objectives and the key related findings are discussed in turn. Within each of these sections is a sub-section that provides practical implications or guidelines for the design of future climate change impact assessments based on the findings of this research, as well as potential future research directions.

7.2. Review of the tools and approaches employed in hydrological climate impact assessments and sources of uncertainty introduced through the modelling process (Objective 1; Chapter 2)

Through an in-depth review of the literature, Chapter 2 successfully achieved the first objective of this thesis. In addition, this review demonstrated that GCM-related uncertainty is a key source of uncertainty and that inter- and intra-hydrological model uncertainty are relatively understudied. In particular, choice of method for the calculation of potential evapotranspiration (PET) for specification within hydrological models, spatial distribution of meteorological inputs within these models and the use of alternative baseline precipitation datasets were highlighted as potential sources of uncertainty that require further investigation. These areas were the foci of subsequent investigations undertaken within the thesis.

7.3. Assessment of inter-GCM related uncertainty (Objective 2; Chapters 4–6)

Inter-GCM related uncertainty was investigated using two sets of scenarios for the Mekong Basin. The first was based on a 2 °C increase in mean global temperature as simulated by seven CMIP3 GCMs and was previously employed in an international assessment of inter-GCM related uncertainty, which this thesis has therefore extended (Chapters 4–5). The second set of scenarios was based on the RCP4.5 scenario as simulated by 41 CMIP5 GCMs. This source of uncertainty was investigated alongside other sources, allowing evaluation of the relative magnitude of uncertainty associated with different aspects of the modelling process. GCM-related uncertainty was the greatest source of uncertainty of those investigated; choice of GCM impacts the direction, magnitude, and spatial and temporal distribution of projected changes in river flow within the Mekong Basin. For the Mekong, inter-GCM differences are largely driven by differences in precipitation, with much less inter-GCM uncertainty being associated with projections of temperature and hence PET. Furthermore, the inclusion of a greater number of GCMs in the CMIP5 ensemble led to a more robust assessment of GCM-related uncertainty and consequently an expanded envelope of uncertainty. For the 2 °C, seven GCM ensemble, the average inter-GCM range of change in mean discharge across the 12 gauging stations used in the impact assessments was ~30% (for the different MIKE SHE models), compared to 57.5% for the 41 GCM ensemble for the RCP4.5 scenario.

Comparison of Mekong river flow projections simulated by the same hydrological model using the CMIP3 and CMIP5 GCM ensembles is a unique aspect of this research. A notable finding is that, despite the use of a different scenario type (2 °C prescribed warming versus RCP4.5) and downscaling method (ClimGen pattern-scaling versus the delta-change approach), projected changes in mean discharge from the CMIP3 GCMs display similar spatial patterns and magnitudes of change in mean discharge to their more recent CMIP5 counterparts. This is because GCMs evolve gradually and successive versions of the same climate model contain largely the same components and parameterisations, with modifications only being made to some aspects of the model (Masson and Knutti, 2011; Knutti *et al.*, 2013). These findings demonstrate that advances in climate modelling have, so far, been unable

to reduce inter-GCM related uncertainty in hydrological projections for the Mekong catchment. This is consistent with the findings of Knutti and Sedláček (2012), who demonstrated that climate model spread (in terms of temperature and precipitation changes) across the global surface has not changed much between CMIP3 and CMIP5 models. In other words, there is a lack of convergence in climate projections from CMIP5 compared to CMIP3.

In Chapter 6, the 41 CMIP5 GCMs were allocated to 12 groups (established by Ho *et al.*, 2016) based on the concept of model genealogy (Masson and Knutti, 2011; Knutti *et al.*, 2013). A key finding was that GCMs from the same genealogical group tended to result in similar spatial patterns of change in mean discharge, but the magnitudes of change sometimes varied notably. However, analysis involving the generation of mean change in mean discharge for each of the GCM groups indicated that use of multiple GCMs from the same group did not bias the distribution of results. The 12-group set does not provide greater consensus on the direction of discharge changes. Ho *et al.* (2016), who identified the GCM groupings employed herein, used the same 41 GCM ensemble to assess climate change impacts on the Tocantins-Araguaia Basin in Brazil. They also investigated whether grouping and weighting GCMs based on their genealogy impacted discharge projections. In line with the current study, they found that conclusions drawn from the group-based re-analysis did not differ much from those drawn from the 41 GCM ensemble. Thompson *et al.* (2017) obtained similar findings for West Africa's Upper Niger Basin. Although aggregating results according to model genealogy might lead to a (perhaps small) reduction in the spread of results, this is not a robust method for constraining GCM-related uncertainty (see also Ho *et al.*, 2016). As discussed by Arnell (2011), a number of studies have shown that weighting GCMs differently or excluding poor GCMs may have relatively little effect on the range of estimated climate change impacts (e.g. Brekke *et al.*, 2008; Chiew *et al.*, 2009; Weigel *et al.*, 2010). Furthermore, such methods may actually lead to equally plausible projections being removed (e.g. through the averaging process).

Recommendations based on this research and future research directions

In line with previous research (e.g. Prudhomme and Davies, 2009b; Todd *et al.*, 2011; Ho *et al.*, 2016), this study has highlighted the importance of employing an ensemble of GCMs when undertaking hydrological climate change impact assessments. An ensemble approach is necessary in order to provide a more robust evaluation of the potential impacts. This is particularly important for basins, such as the Mekong, that are located in regions (in this case Southeast Asia) where there is no consensus amongst GCMs on projected changes in annual or seasonal precipitation. Unsurprisingly, the more GCMs included within an ensemble, the more fully GCM-related uncertainty is likely to be sampled.

In addition, findings based on the CMIP5 ensemble indicate that studies that employ multi-model ensembles should consider model genealogy when selecting GCMs for inclusion within an ensemble and when interpreting ensemble results. This is because, as emphasized by Masson and Knutti (2011) and Knutti *et al.* (2013), there are strong similarities (in terms of both model code and simulated outputs) between GCMs developed at the same research institution and between GCMs that share model components or code. This means that impact assessment results could potentially be biased by use of an ensemble that contains multiple GCMs from the same genealogical group or only a few of these groups. In Chapter 6, an ensemble of 41 GCMs (from 12 genealogical groups) were employed, and use of multiple GCMs from the same group did not bias the results. However, similarity between river discharge projections for GCMs from the same group indicates that care should be taken when selecting GCMs for inclusion within an ensemble, especially when a smaller number of GCMs are to be employed.

It would be desirable if the magnitude of GCM-related uncertainty could be robustly constrained, through, for example, a review of the literature, in order to identify a relatively smaller number of the best GCMs in terms of model performance under historical conditions, and so considerably restrict the size of the ensemble. However, this poses a significant challenge. As summarised by Hasson *et al.* (2016), identification of the best GCMs to include in an ensemble is itself subject to uncertainties, owing to: 1) the diversity of skill metrics employed to assess GCM

performance; 2) sample size of the GCM simulations analysed and the inclusion of different GCMs in different studies; and 3) choice of observational datasets against which GCM performance is evaluated. Whether the assessment scale is regional (e.g. Su *et al.*, 2013), multi-regional (e.g. McSweeney *et al.*, 2014) or at the river basin scale (e.g. Hasson *et al.*, 2016; Lutz *et al.*, 2016) will also impact the results. Furthermore, better performance of GCMs over the historical period does not guarantee better performance under future climate conditions (Tebaldi and Knutti, 2007; Arnell, 2011; McSweeney *et al.*, 2014; Hasson *et al.*, 2016). Selecting a small number of GCMs may therefore exclude plausible climate scenarios, therefore giving a falsely narrow range of hydrological projections and an underestimation of GCM-related uncertainty (see, for example, Hughes *et al.*, 2011).

An alternative approach to the identification of a relatively small number of the "best" GCMs may be to use a larger ensemble of GCMs, but with the aim being to exclude those GCMs that perform particularly poorly. McSweeney *et al.* (2014) illustrate a novel approach for the selection of a GCM ensemble for use in regional climate change assessments. They exclude a GCM if it fails to simulate a large-scale process that is a significant driver of the climate of a region of interest, such as monsoonal circulations. Their rationale is that such a significant shortcoming would mean that the GCM is unlikely to realistically capture how global climate change will manifest itself over the region. However, their study also aimed to capture the maximum possible range of changes in mean temperature and precipitation for their regions of interest (see also Lutz *et al.*, 2016). It was not their intention to select an ensemble that produced a reduced range of future climate projections and in only a few cases did they eliminate poorly performing models that were outliers affecting the range of outcomes. Both the selection of better or best GCMs and the identification of poorer or even implausible GCMs is subject to multiple uncertainties and subjective choices (Sillmann *et al.*, 2013; McSweeney *et al.*, 2014; Hasson *et al.*, 2016; Lutz *et al.*, 2016). Strategically eliminating GCMs from the ensemble used herein is beyond the scope of this study. There is clearly, however, potential for future studies to further investigate the impacts on scenario river discharge projections of excluding GCMs from climate change ensembles based on a range of different criteria.

7.4. Assessment of uncertainty associated with the use of alternative hydrological model codes (Objective 3; Chapter 4)

River flow/runoff projections from the quasi-physically based, distributed MIKE SHE model were compared with those from the conceptual, semi-distributed SLURP model and the Mac-PDM.09 global hydrological model. Two scenario sets were employed: the 2 °C, seven GCM scenario set and the 1–6 °C HadCM3 scenario set. Inter-hydrological model-related uncertainty was notable; it influenced the magnitude and temporal distribution of runoff changes through the year, but in most cases the three hydrological models simulated the same direction of change in mean discharge for a given GCM scenario. Where increases in mean discharge/runoff were projected, Mac–PDM.09 consistently produced the greatest changes. Inter-model differences were greatest at the most upstream gauging station and showed a downstream reduction in magnitude. Inter-model differences for change in mean discharge were relatively small between the two catchment models that had been specifically developed and calibrated for the Mekong (MIKE SHE and SLURP), but there were still some notable differences in the intra-annual patterns of change at the most upstream gauging station.

Under the 1–6 °C HadCM3 scenarios, the magnitude of inter-hydrological model uncertainty increased with prescribed warming. At downstream stations, the models (in particular MacPDM.09) displayed different directions and patterns of change at both a mean annual and mean monthly resolution, although the magnitude of inter-model uncertainty was much smaller compared to upstream stations. Inter-hydrological model differences are likely attributed to alternative model structures and process representations, and the lack of catchment-specific calibration of Mac-PDM.09 for the Mekong. Use of a different PET method in this model may also be a contributing factor, but cannot explain the largest inter-model differences (discussed further below). Exclusion of this model from the assessment leads to a greatly reduced magnitude of inter-hydrological model uncertainty for change in mean discharge and mean monthly discharge.

Recommendations based on this research

Choice of hydrological model code has the potential to impact the magnitude and spatial or temporal pattern of hydrological changes for a given GCM/climate scenario. This indicates that use of an ensemble of hydrological models may provide a more robust assessment of potential hydrological impacts of climate change. However, it is recognised that the development of multiple hydrological models of an individual catchment imposes potentially large resource / expertise demands. This may account for the relatively small number of studies such as this one that have investigated this aspect of uncertainty. Hydrological model-related uncertainty may, however, be constrained or reduced through comprehensive catchment-specific calibration. In addition, whilst GHMs are an extremely useful tool for impact assessments at a global or regional scale, caution should be exercised when applying them at the catchment or sub-catchment scale, especially when they have not been validated against observed records.

Another recommendation that has emerged from the results of this research is that when undertaking hydrological climate change impact assessments for large basins, or at a regional level, it is desirable to use distributed approaches and analyse both projected climate and projected hydrological changes in a distributed manner. In particular, assessment of projected changes in river discharge for a single gauging station located at the downstream end of a catchment should not be used as an indicator of change for the catchment as a whole. Instead, discharge changes should be assessed at multiple points in the catchment. As this research has shown, changes can show great spatial variability. This has implications for water resources and ecological responses that could otherwise not be appreciated (e.g. Thompson *et al.*, 2014b). In addition, the magnitude and nature of different sources of uncertainty can vary spatially.

7.5. Assessment of sources of uncertainty associated with meteorological inputs to the hydrological model (Objectives 4 to 6; Chapter 5)

The investigations in Chapter 5 demonstrated that decisions made by the modeller during hydrological model development, such as choice of PET method, baseline

precipitation input data and spatial distribution of meteorological inputs, impact model calibration and parameterisation. Adjustment of parameter values during model calibration can often compensate for varied meteorological input spatial distributions or differences between alternative baseline precipitation or PET input datasets. This enables the different model builds to display very similar performance for the calibration and validation periods. However, use of the resulting models for impact assessment will give varied outputs, with the level of variability dependent upon the model element under consideration. For the assessments in Chapter 5, the 2 °C, seven GCM scenario set was consistently employed. In some cases, inter-model variability in the projected river flows under scenario conditions was greater than that shown under the baseline conditions. It is important to emphasize that in this study the overriding cause of the inter-model differences in scenario outputs is not the result of model parameterisation, as discussed below. Although the effects of all three meteorological considerations on scenario discharges are smaller than choice of GCM, they do have the potential to expand the overall envelope of uncertainty.

7.5.1. Assessment of PET method-related uncertainty (Objective 4; Chapter 5)

PET method-related uncertainty was investigated through the development (including method-specific calibration) of six MIKE SHE models employing alternative PET methods. Despite considerable inter-method differences in baseline PET in terms of magnitude (and sometimes also seasonality), the six models displayed very similar performance against observations following calibration.

Use of different PET methods for the same climate scenario resulted in different magnitudes of PET change at an annual and intra-annual resolution, as well as varied spatial patterns of change through the catchment. A key finding was that inter-GCM differences in scenario changes in PET were smaller than inter-PET method differences for a given GCM scenario. This indicates that choice of PET method is a greater source of uncertainty in projections of PET than choice of GCM. This is consistent with results presented by Kingston *et al.* (2009).

Inter-hydrological model differences in scenario results due to the use of different PET methods were notable and consistently greater than inter-model differences for the baseline. Moreover, the inter-hydrological model differences were largely consistent with (i.e. could be explained by) the varied changes in PET compared to the baseline from the alternative PET methods. In other words, the magnitude of change in discharge was conditioned by choice of PET method for baseline and scenario calculation. In general, in cases where increases in river discharge were projected under climate change, PET methods that displayed larger increases in PET resulted in smaller increases in discharge. Conversely, in cases where reductions in discharge were simulated, PET methods that produced larger increases in PET led to larger reductions in discharge. Where projected changes in discharge (e.g. mean discharge or high or low flows) were small, choice of PET method could sometimes influence the projected direction of change. Of course, the relationship between projected changes in annual PET and annual discharge is made more complex due to a range of factors, such as intra-annual difference in PET changes and at a given gauging station, the competing influence of upstream changes in discharge that are propagated downstream, and local changes in runoff generation. The correspondence between changes in PET and changes in discharge shows that it is the influence of calculation method on scenario changes in PET that causes the inter-model differences in scenario projections, not model parameterisation.

Overall, however, GCM-related uncertainty for change in mean discharge and high (Q5) and low (Q95) flows is on average 3.5 times greater than PET method-related uncertainty. Choice of GCM has an overriding influence on the direction and spatial and temporal pattern of discharge projections in the Mekong. Compared to inter-hydrological model uncertainty, PET-related uncertainty was of a similar magnitude to inter-model differences between MIKE SHE and SLURP, and between the Mac-PDM.09 GHM and either of the two catchment hydrological models (CHMs) at downstream stations. However, at the most upstream station, differences between the GHM and either CHM for change in mean discharge were more than two times greater than the maximum PET-related disparity. Differences between the GHM and the two CHMs may therefore be partly, but not entirely, due to the use of a different PET method (Penman-Monteith) in the GHM compared to the CHMs (Linacre PET).

Recommendations based on this research and future research directions

Choice of PET-method remains an understudied source of uncertainty in hydrological projections under climate change. Analysis for the Mekong could be extended by the application of additional PET methods. This would most likely reveal an expanded envelope of uncertainty, but would not help constrain the level of PET method-related uncertainty in river flow projections. Further research is required to assess the suitability of different PET methods for estimating PET under a changing climate. As argued by Shaw and Riha (2011), good performance of a PET method under historical climate conditions cannot necessarily be assumed to be an indicator of future accuracy in a changing climate. A better understanding of which PET methods are most suitable, both for different regions and under a changing climate, would help constrain the uncertainty associated with PET projections.

7.5.2. Assessment of the impact of meteorological input spatial distribution (Objective 5; Chapter 5)

Three MIKE SHE models of the Mekong were developed using alternative meteorological input spatial distributions. The S-Mets model employed a sub-catchment based distribution with 11 sub-catchments upstream of Phnom Penh gauging station, including two sub-catchments that were particularly large (>150,000 km^2). The M-Mets distribution had 15 sub-catchments, with a maximum area of 87,420 km^2. The G-Mets model employed a 0.5° × 0.5° grid. Input-specific calibration was undertaken. Unsurprisingly, analysis of climate inputs to the three models demonstrated that the gridded inputs provided the greatest spatial variability in baseline data and scenario climate changes. The M-Mets distribution captured greater spatial variability compared to the S-Mets distribution over specific regions where smaller sub-catchments were employed in the M-Mets distribution.

Use of alternative spatial distributions of meteorological inputs had some impact on the magnitude of simulated discharge changes, with slightly greater uncertainty associated with high and low flows compared to mean discharge. The magnitude of inter-hydrological model difference at a given gauging station varies between GCMs.

This indicates that the impact that the differing spatial distributions has on discharge projections depends on the nature (magnitude and spatiality) of the projected changes in climate. The magnitude of uncertainty for change in mean discharge is relatively low and is, on average, ~4 times smaller than that associated with PET method. The results of the M-Mets and G-Mets models were generally close. The spatial pattern and direction of discharge changes for a given GCM is largely unaffected by meteorological input spatial distribution within the hydrological model.

Recommendations based on this research

In this investigation, uncertainty in river flow projections under climate change associated with meteorological input spatial distribution (within the hydrological model) is small compared to other sources of uncertainty, such as GCM and PET method-related uncertainty. This finding suggests that only a small proportion of the differences between MIKE SHE/SLURP (sub-catchment based data) and Mac-PDM.09 (gridded data) could potentially be attributed to the spatial distribution of their meteorological inputs. In this study, the spatial averaging of gridded meteorological data to provide sub-catchment based data appears to be a robust alternative to the direct use of gridded data. However, if this approach is to be used, it is recommended that climate data for the basin of interest should first be analysed to assess any key spatial variations, in order to inform an appropriate sub-catchment distribution. Sub-catchment based data files are much easier to handle and the analysis and presentation of these data is much simpler compared to gridded data. Moreover, some semi-distributed hydrological models, such as SLURP, require sub-catchment based data, precluding the direct application of gridded meteorological inputs.

7.5.3. Assessment of uncertainty associated with the use of alternative baseline precipitation data (Objective 6; Chapter 5)

Uncertainty associated with meteorological input spatial distribution and choice of baseline precipitation are of a comparable magnitude; both are much smaller than PET method and GCM-related uncertainty. In the case of baseline precipitation input

uncertainty, the dominant cause of varied hydrological projections for the same GCM scenario relates to the perturbation of the baseline data (to generate scenario data) using a multiplicative (i.e. percentage based) approach. Use of a multiplicative approach for the perturbation of baseline precipitation data is a common approach, whether a relatively simple delta-change approach is adopted (e.g. Minville *et al.*, 2008; Dobler *et al.*, 2012; Ho *et al.*, 2016), or whether an alternative such as the ClimGen pattern scaling technique is employed (Todd *et al.*, 2011). However, a multiplicative approach means that the magnitudes of absolute changes are impacted by the choice of baseline precipitation data. Throughout most of the Mekong catchment, choice of baseline precipitation from the two datasets (UDel and CRU) only had a fairly small impact on simulated changes in mean, high and low flows. However, over downstream sub-catchments where the baseline data showed greater divergence during the dry season, scenario discharges were notably affected in the case of a GCM that projected larger percentage changes in precipitation during the dry season. Model parameter values within the relevant downstream sub-catchments were in fact the same in the two models, as adjustment of model parameters was unable to compensate for the less representative nature of the CRU data. Model parameterisation therefore did not play a role in the inter-model uncertainty at downstream stations. This demonstrates that choice of baseline precipitation data has the potential to influence scenario changes in precipitation and consequently discharge, and is therefore a source of uncertainty. This finding may also be relevant to cases where alternative bias correction techniques are employed, such as local scaling and quantile-quantile mapping, since these rely on using baseline data to characterise the bias in the GCM outputs (e.g. Dobler *et al.*, 2012).

Recommendations based on this research and future research directions

In this study, it was clear that one precipitation dataset (UDel) was more representative of the true seasonal patterns in precipitation over the downstream sub-catchments, as the other, less representative dataset (CRU) led to significant underestimation of peak mean monthly discharges and overestimation of dry season discharges. In situations such as this, where a precipitation dataset is found to be unrepresentative, alternative precipitation datasets should ideally be sought.

Alternatively, correction of the baseline precipitation data could be explored. Of course, it may not always be clear which datasets are most representative. These findings support the recommendation of Remesan and Holman (2015) that modellers should be aware of the potential implications that choice of baseline data can have on simulated future impacts, particularly in situations where there is considerable uncertainty in the observed meteorological datasets.

Analysis of precipitation input uncertainty could be extended for the Mekong by investigating the use of additional precipitation datasets. In particular, it would be interesting to explore the use of daily (or even sub-daily) resolution precipitation data. This would also allow the analysis of discharge projections at a higher temporal resolution than used herein. Use of daily precipitation could not be compared alongside UDel and CRU in Chapter 5 since, as discussed in Section 5.3.1, daily resolution climate data cannot be directly perturbed using the ClimGen scenario outputs employed in Chapter 4 and 5, which have a monthly resolution. Similarly, the delta-change approach used in Chapter 6 cannot be used for directly perturbing daily data. Perturbation of daily baseline data would therefore require the use of alternative bias correction / downscaling techniques. In order to compare multiple daily datasets, a different baseline period would also need to be used, since many potential datasets do not start until much later than 1961. Lauri *et al.* (2014) compared the use of five publicly available gridded precipitation datasets for baseline hydrological modelling of the Mekong. All had a daily or higher (3 h or 6 h) temporal resolution. However, four of these do not cover the baseline period used herein (1961–1990). The exception is APHRODITE, which has a 0.25° × 0.25° grid and daily resolution, unlike CRU and UDel which have a 0.5° × 0.5° spatial resolution and are monthly datasets (necessitating the use of a weather generator for disaggregation to daily data).

7.5.4. Uncertainty associated with meteorological inputs to the hydrological model: concluding discussion

Decisions made during model development related to meteorological inputs have the ability to impact scenario results under climate change. MIKE SHE models with different PET inputs or spatial distributions performed similarly under baseline

conditions following model calibration. In the case of alternative precipitation data, the CRU precipitation data was presumed more erroneous over downstream stations and model parameters over downstream sub-catchments were left consistent between the two models. The model employing CRU precipitation therefore displayed weaker performance compared to the model employing UDel. In this investigation, choice of PET method was found to be a much greater source of uncertainty in discharge projections compared to choice of meteorological input spatial distribution or baseline precipitation (e.g. ~4 times larger on average for change in mean discharge).

The fact that multiple model set-ups were able to achieve an acceptable and relatively similar level of performance illustrates the issue of equifinality (see Sections 2.6.2 and 2.6.5). Within the context of scenario modelling, discussions of equifinality often focus on the potential for different model set-ups (e.g. with different structures or parameter values) to respond differently under scenario conditions. This study highlights a slightly different issue arising from model equifinality, namely that decisions made during model set-up can actually go on to influence the scenario changes in PET (dependent on choice of PET method) or precipitation (dependent on baseline precipitation) or the spatial distribution of changes in climate (dependent on meteorological input spatial distribution) before the scenario climate data are even run through the model. This is an interesting concept that warrants further investigation in future studies.

It is worth recognising that varied parameterisation between the MIKE SHE models might have played a small role in contributing to the observed inter-model uncertainty in scenario discharges. However, in the case of PET and precipitation, the dominant cause of inter-model differences in scenarios projections was the variation in baseline-to-scenario changes in PET and precipitation, respectively. This was evident from the correspondence between scenario changes in PET or precipitation and scenario changes is discharge. Furthermore, parameter values in the two models employing alternative baseline precipitation data were consistent over downstream catchments where the greatest inter-model scenario differences were observed. This demonstrates that model parameterisation was not a contributing factor to uncertainty in this instance. In the case of meteorological

input spatial distribution, the dominant cause of inter-model scenario differences is most likely due to the varied spatial distributions of meteorological changes.

The issue of parameter equifinality and uncertainty could be investigated further. For example, which parameters are subject to calibration is in part down to the subjective choices of the modeller. In this study, the baseflow linear reservoir time constants were subject to calibration as these are conceptual parameters and could not be based on values from the modelling literature. When model inputs were changed, these were again subject to manual calibration in order to modify the general shape of the hydrograph. Other key parameters in some sub-catchments were the precipitation lapse rate and dead storage proportion (only applied to a small number of linear reservoirs). The former was applied to address the perceived underestimation of precipitation in mountainous areas, whilst the dead storage (only applied to two sub-catchments) was theorised to be required due to water abstractions that were otherwise not represented within the model, or due to elevated precipitation within the input data over these regions. It is of course possible that different parameters could have been selected for calibration. For example, although vegetation root depths are not commonly subject to calibration, they could be modified to alter the water balance as they affect the depth to which evapotranspiration from the unsaturated zone can occur. Alternatively, crop coefficients could have been applied to modify PET according to land cover type. This could have then been used as a calibration term in response to varied baseline inputs (e.g. PET). On the other hand, irrigation could potentially be represented within the model, although it would likely be difficult to obtain reliable data on which to base this. Further investigations could therefore be undertaken to assess how differently models with alternative set-ups and parameterisations respond under scenarios of climate change, and in doing so provide an indication of the associated model structure and parameterisation uncertainty.

Whether using the same set of calibration parameters as used herein, or different sets, parameter equifinality could be explored using automatic calibration techniques to find a range of acceptable model parameterisations to subsequently use during scenario simulation. It seems unlikely, however, that the broad conclusions related to uncertainty in the meteorological inputs would be affected.

In the case of PET method-related uncertainty, for example, scenario changes in discharge would still be conditioned by scenario changes in PET relative to baseline PET, with PET methods producing larger increases in PET resulting in smaller increases in mean discharge under climate change, or larger reductions.

7.6. Multiple drivers of change in the Mekong Basin and future research directions

This thesis has focused on assessing specific sources of uncertainty in projecting the potential impacts of climate change on river flows in the Mekong Basin. However, the water resources (both surface and groundwater) of the Mekong Basin have been and will continue to be subject to multiple drivers of change. As discussed in Section 3.9, these include the construction and operation of dams, land cover change and rising water abstractions for domestic, industrial and agricultural purposes (Pech and Sunada, 2008; MRC, 2010b; Grumbine *et al.*, 2012; Räsänen *et al.*, 2012). These are in turn driven by factors such as population growth and socioeconomic development. Water resources management strategies will themselves be influenced by expected and emerging impacts of climate change (MRC, 2010b), making adaptation response an additional layer of uncertainty. Assessing the cumulative impacts of different drivers of change is a complex challenge facing both the Mekong (Pech and Sunada, 2008; MRC, 2010b; Grumbine *et al.*, 2012) and water resources worldwide (Bates *et al.*, 2008).

The MIKE SHE models developed for this thesis could be applied in further impact and uncertainty assessments for the Mekong. They could, for example, be used to assess the potential impacts of land cover change on Mekong river flows. Deforestation in the Mekong catchment and the wider region of Southeast Asia is being driven by increasing demand for agricultural and forest products (MRC, 2010b; Stibig *et al.*, 2014). However, it is likely that to provide a robust assessment, irrigation would need to be incorporated within the model under both baseline and future conditions. Expansion of irrigation is expected in the future, which will increase water demand and abstractions from the Mekong (Pech and Sunada, 2008; Kirby and Mainuddin, 2009). Ty *et al.* (2012) investigated the potential impacts of land cover changes in the Sre Pok catchment (a tributary of the Mekong) using a

hydrological model. A notable finding was that although deforestation in favour of agriculture and urbanization causes an increase in simulated surface runoff, this is outweighed by the projected increase in irrigation water demand.

The role of existing and planned dams in modifying Mekong River flows was excluded from the assessments undertaken in this thesis. This was justifiable from a methodological point of view as it allowed specific sources of uncertainty in the climate impact assessment process to be investigated. In addition, the major existing dams in the basin were built after the calibration period and so did not affect model calibration. The largest hydropower projects are located in the Upper Mekong Basin on the Lancang (in China) and more mainstream dams have been planned for both the Upper and Lower Basin, with some now under construction (see Section 3.9.3). Current dams in the basin have been identified as having impacted the Mekong's river flows (e.g. Lu *et al.*, 2014), with Räsänen *et al.* (2017) reporting considerable modifications to river discharge since 2011. Dam operations are therefore another significant driver of change and source of uncertainty in future Mekong river flows. The inclusion of dams within the MIKE SHE/MIKE 11 model of the Mekong is therefore a further avenue of potential research.

It is clear that whilst the current study focussed on assessing specific sources of uncertainty that were inherent in the climate impact assessment process, studies seeking to fully explore potential future changes in Mekong river flows will need to take multiple drivers of change into account. These include climate change, land cover change, dam operations and water abstractions for irrigation.

One limitation of the Mekong MIKE SHE models' current set up is that the saturated zone is modelled using a conceptual linear reservoir method. This method is computationally efficient, has greatly reduced data requirements and is adequate when the focus is on simulating river flows. However, it means that the model cannot be used to assess impacts of climatic or other changes on groundwaters (beyond perhaps very broad statements regarding storage volumes over large areas). Groundwater is used to supplement surface water supplies and is an important source of domestic water supply in some rural areas (Johnston and Kummu, 2012). According to Johnston and Kummu (2012) and Johnston and

Smakhtin (2014), none of the hydrological models developed for the Mekong have a working groundwater model. MIKE SHE and other models from the DHI suite are capable of physically-based modelling of groundwater. However, there is a lack of groundwater data for the Mekong region and obtaining the necessary data to build and calibrate a physically-based, distributed groundwater model for such a large basin (or even parts of the basin) would require a major research program (Johnston and Kummu, 2012; Johnston and Smakhtin, 2014).

7.7. Wider considerations: climate impacts and adaptation

The vital environmental and socio-economic importance of water resources means that there is a strong impetus to assess the potential hydrological impacts of climate change. The approach used in this thesis, whereby impacts are investigated by driving a hydrological model (or multiple hydrological models) with climate projections derived from GCMs, is commonly employed. This approach is also used for other sectors, such as agriculture, with the exception that different types of impact models are employed, such as crop models (e.g. Alexandrov *et al.*, 2002; Olesen *et al.*, 2007). However, as described in Section 2.3, uncertainty is introduced at each stage of this impact assessment process, resulting in a cascade of uncertainty (Wilby and Dessai, 2010). This can lead to potentially high levels of uncertainty in the resulting projections.

Nevertheless, such assessments and the identification and characterisation of different sources of uncertainty are vital areas of research. Uncertainty exploration can identify knowledge gaps and areas where further research could possibly lead to reduced uncertainty. In the case of water resources, model-based assessments can improve our understanding of how changes in climate may impact hydrological processes. Furthermore, they have the potential to help inform water management decisions and adaptation planning (Todd *et al.*, 2011; Velázquez *et al.*, 2013). Climate impact assessments, both on water resources and other sectors, can indicate the scale of adaptation required (Falloon *et al.*, 2014). Within this context, adaptation refers to the process of adjustment to human systems/activities in response to actual or expected effects of climate change, in order to limit negative impacts or exploit beneficial opportunities (IPCC, 2012). Adaptation strategies

include both 'hard' infrastructural measures (e.g. dams, flood barriers) and 'soft' measures such as ecosystem-based adaptation, institutional and regulatory reform, financial tools and effective early warning systems for hazards such as floods (Wilby and Dessai, 2010; Lal *et al.*, 2012; Bastakoti *et al.*, 2013; Jiménez Cisneros *et al.*, 2014).

It is important to acknowledge, however, that the development of robust water resources management decisions and climate adaptation strategies in general (i.e. related to other sectors) requires a variety of approaches (Wilby and Dessai, 2010; AGWA, 2013). The approach outlined above and used herein has been described as a 'top-down' approach to risk assessment for adaptation, as climate scenarios are identified first and then translated into local impacts (i.e. in this case on river flows), which can then inform adaptation measures (Dessai and Hulme, 2004; Carter *et al.*, 2007; Wilby and Dessai, 2010; Lal *et al.*, 2012; AGWA, 2013). In contrast, 'bottom-up' approaches focus on identifying and understanding current vulnerabilities of society to climate variability, so that measures can be identified that improve resilience to climate variability and change (Dessai and Hulme, 2004; Carter *et al.*, 2007; Kwadijk *et al.*, 2010; Wilby and Dessai, 2010; Pielke *et al.*, 2012). Such strategies can be taken independently of climate and impact projections. Alternatively, modelling approaches can contribute to the formulation of bottom-up vulnerability-based strategies, as well as the appraisal of different adaptation options (Kwadijk *et al.*, 2010; Wilby and Dessai, 2010; Ranger *et al.*, 2013). This can provide robust decision-making despite the uncertainty associated with impact projections.

Currently, many modelling based impact and uncertainty assessments (both in relation to water resources and other sectors) are undertaken in relative isolation from policy and decision-makers and other stakeholders. Such research undoubtedly contributes to the body of research and does reach policy and decision-makers through dissemination activities such as the IPCC reports (e.g. IPCC, 2012, 2013). However, it would be beneficial if a larger proportion of model-based assessment activities were undertaken within a context of collaboration or close communication with policy-makers, decision-makers and stakeholders. This would facilitate the development of model-based impact assessments that contribute to

bottom-up strategies and provide outputs that are more directly useful to adaptation planning (Dilling and Lemos, 2011; Falloon *et al.*, 2014). Furthermore, this could help tailor uncertainty description to focus on key factors that are of particular utility (Falloon *et al.*, 2014). Overall though, the best progress is likely to be made through the continued use of a variety of approaches.

In the case of the Mekong Basin, which provides the focus of the current study, such collaboration with policy-makers, decision-makers and stakeholders could benefit future extensions to the work. Communications with the most relevant stakeholders could most effectively be established through the Mekong River Commission (MRC). The MRC is an intergovernmental organisation founded in 1995 to coordinate sustainable water resources planning in the Lower Mekong Basin (Jacobs, 2002; MRC, 2010b). The activities of the MRC include the promotion of information sharing between different organisations within the Mekong's riparian nations through stakeholder forums and workshops (MRC, 2016). These mechanisms could facilitate the formulation of new scenarios that could be simulated using the MIKE SHE Mekong models developed in this thesis. They could also guide how uncertainty in projections of future hydrological conditions can most usefully be communicated to end-users. This could include which river flow indicators (e.g. Q5, Q95 or other indicators) are of most interest and practical use to different decision-makers.

7.8. Contribution to knowledge – concluding review

This thesis as a whole makes a distinct and significant contribution to knowledge. It has integrated a systematic and structured quantitative evaluation of some specific sources of uncertainty into a collective assessment of these aspects of uncertainty in modelling the impacts of climate change on basin hydrology.

Whilst contributions to knowledge are made throughout the thesis, the conclusions and recommendations provided in this chapter clearly demonstrate the practical implications of this research. This thesis does, of course, build on previous research. It is, however, distinct from previous studies. In particular, in using the CMIP3 climate projections from the QUEST-GSI project and the related river flow projections from the earlier SLURP (Kingston *et al.*, 2011) and Mac-PDM.09 (Gosling

et al., 2011) models, it has developed upon these earlier works. There are multiple aspects that make this thesis distinct from these studies though. For example, several additional sources of uncertainty have been investigated herein, namely those associated with the meteorological inputs to the MIKE SHE models, allowing a comparative analysis of the different sources. In addition, whereas Kingston *et al.* (2011) only calibrated and analysed the results of SLURP at three stations, 12 stations were used herein (including stations further downstream), providing greater understanding of the spatial variation in discharge projections and associated uncertainty for the Mekong.

Similarly, Gosling *et al.* (2011) only compared results from SLURP and MacPDM.09 at a single downstream station, whereas projections were compared between the three hydrological models (two CHMs and one GHM) at up to five stations (only three available for SLURP) herein. Key findings from this analysis that could not be drawn from the earlier study included that the two catchment models displayed more similar results compared to the GHM, and that relative inter-model (particularly CHM–GHM) differences were considerably greater at upstream stations and displayed a downstream reduction in magnitude. A greater magnitude of CHM–GHM uncertainty was therefore revealed herein. As highlighted in the literature review, a relatively small proportion of hydrological impact assessments use multiple hydrological models or structures. This thesis contributes to the body of work on this aspect of uncertainty.

Another original aspect of this thesis compared to both the QUEST-GSI papers and other existing hydrological impact assessments for the Mekong is the use in Chapter 6 of a large ensemble of 41 GCMs from the CMIP5 generation. In contrast, previous studies have employed either a single GCM or a small ensemble of GCMs, and have for the most part employed earlier generations of GCMs (see Section 6.1). This thesis has therefore complemented earlier research with a more up-to-date and comprehensive analysis of GCM-related uncertainty for the Mekong. As highlighted above, comparison of the CMIP3 and CMIP5-based discharge projections for the Mekong from the same hydrological model is another original contribution to knowledge.

The insights into meteorological input related uncertainty provided by this research are a particularly significant contribution to knowledge. The sources of uncertainty investigated were specifically selected because a review of the literature discovered that these were understudied sources of uncertainty. In the case of PET and baseline precipitation, for example, more studies have investigated this source of uncertainty under baseline conditions, whilst comparatively few have looked at the implications for simulated hydrological projections under climate change (as discussed in Chapter 2). Kingston *et al.* (2009) presented differences between six PET methods in PET climate change signals on a global basis, but did not undertake hydrological modelling to assess the impacts on simulated discharges. Some model-based climate impact assessments have used different PET methods without re-calibrating the model (e.g. Bae *et al.*, 2011). Remesan and Holman (2015) explored the use of two different baseline precipitation datasets and three reference evapotranspiration (ETo) methods and how these impacted river flows under scenario climate conditions. However, their study did not explicitly investigate how use of the varied baseline datasets impacted scenario changes in precipitation or PET. This demonstrates that a distinct contribution of this thesis is that the impacts of choice of baseline meteorological input dataset or distribution upon scenario meteorological changes were explicitly assessed.

In addition to the conclusions and recommendations summarised within this chapter, additional contributions to knowledge are made throughout this thesis. For example, the literature review may be useful for anyone wishing to gain an overview of the hydrological climate change impact assessment process, or anyone interested in any of the specific sources of uncertainty focused upon herein, such as PET-related uncertainty. Similarly, the chapter on the Mekong may be useful for anyone wishing to have an overview of the spatial variation of key hydrologically relevant characteristics of the catchment.

Finally, it is worth recognising explicitly that the nature and magnitude of different sources of uncertainty in climate impact assessments are likely to vary from one investigation to another, for example, depending on the specific basin of interest, the region it falls within, the hydrological models employed or input datasets used.

Nevertheless, this study draws attention to several understudied sources of uncertainty and provides results against which future studies can be compared.

7.9. Conclusion

Hydrological models are extremely valuable tools for increasing our understanding of hydrological processes, both generally and within a catchment-specific context. They are particularly useful for undertaking what-if scenario modelling to assess the potential impacts of a wide variety of scenario types on freshwater resources. It is, however, widely recognised that uncertainty is introduced at each stage of the modelling process. Identifying and quantifying the different sources of uncertainty is an essential aspect of hydrological modelling research.

This thesis investigated sources of uncertainty related to the modelling of river flow projections under climate change, using the Mekong River Basin as a case study catchment. Of the sources of potential uncertainty explored, choice of GCM was found to be dominant. However, other sources, such as choice of hydrological model code or structure, PET method and choice of baseline meteorological inputs and their spatial distribution should not be ignored. These sources of uncertainty contribute to the overall envelope of uncertainty. In terms of change in mean discharge using a seven GCM ensemble for a prescribed 2 °C increase in global mean temperature, inter-GCM related uncertainty (average range of change: ~30%) was found to be ~3.5 times greater than PET method-related uncertainty on average (based on the use of six different PET methods). Uncertainty for change in mean discharge associated with choice of spatial distribution of meteorological inputs (assessed using three spatial distributions) and baseline precipitation (using two alternative datasets) were found to be comparable in magnitude, and ~4 times smaller than PET-related uncertainty on average. GCM-related uncertainty assessed using 41 GCMs for the RCP4.5 scenario is nearly twice as large that revealed using the 2 °C, seven GCM ensemble. Although these relative magnitudes are based on changes in mean discharge, they are also indicative of the relative impact of different sources of uncertainty on changes in Q5 and Q95. Further research is required to increase our understanding of how other decisions made during the modelling process can impact scenario results.

References

Abbott, M.B., Bathurst, J.C., Cunge, J.A., O'Connell, P.E. and Rasmussen, J. (1986a) 'An introduction to the European hydrological system – Système Hydrologique Europeén, SHE, 1: History and philosophy of a physically-based distributed modelling system', *Journal of Hydrology*, 87, 45–59.

Abbott, M.B., Bathurst, J.C., Cunge, J.A., O'Connell, P.E. and Rasmussen, J. (1986b) 'An introduction to the European hydrological system – Système Hydrologique Europeén, SHE, 2: Structure of a physically-based distributed modelling system', *Journal of Hydrology*, 87, 61–77.

Adamson, P. and Bird, J. (2010) 'The Mekong: A Drought-prone Tropical Environment?', *International Journal of Water Resources Development*, 26, 579–594.

Adamson, P.T. (2006) *An Evaluation of Landuse and Climate Change on the Recent Historical Regime of the Mekong,* Vientiane: Mekong River Commission.

AGWA (2013) *Caveat Adaptor: The Best Use of Climate Model Simulations for Climate Adaptation & Freshwater Management, White Paper 1,* World Bank and Stockholm International Water Institute.

Ajami, N.K., Gupta, H., Wagener, T. and Sorooshian, S. (2004) 'Calibration of a semi-distributed hydrologic model for streamflow estimation along a river system', *Journal of Hydrology*, 298, 112–135.

Alcamo, J., Flörke, M. and Märker, M. (2007) 'Future long-term changes in global water resources driven by socio-economic and climatic changes', *Hydrological Sciences Journal*, 52, 247–275.

Alexandrov, V., Eitzinger, J., Cajic , V. and Oberforster, M. (2002) 'Potential impact of climate change on selected agricultural crops in north–eastern Austria', *Global Change Biology*, 8, 372–389.

Allen, R.G., Pereira, L.S., Raes, D. and Smith, M. (1998) *Crop evapotranspiration - Guidelines for computing crop water requirements - FAO Irrigation and drainage paper 56,* Rome: FAO.

Allen, R.G., Pereira, L.S., Smith, M., Raes, D. and Wright, J.L. (2005) 'FAO-56 Dual Crop Coefficient Method for Estimating Evaporation from Soil and Application Extensions', *Journal of Irrigation and Drainage Engineering*, 131, 2–13.

Anandhi, A., Frei, A., Pierson, D.C., Schneiderman, E.M., Zion, M.S., Lounsbury, D. and Matonse, A.H. (2011) 'Examination of change factor methodologies for climate change impact assessment', *Water Resources Research*, 47, W03501.

Andersen, J., Dybkjaer, G., Jensen, K.H., Refsgaard, J.C. and Rasmussen, K. (2002a) 'Use of remotely sensed precipitation and leaf area index in a distributed hydrological model', *Journal of Hydrology*, 34–50.

Andersen, J., Refsgaard, J.C. and Jensen, K.H. (2001) 'Distributed hydrological modelling of the Senegal River Basin – model construction and validation', *Journal of Hydrology*, 247, 200–214.

Andersen, J., Sandholt, I., Jensen, K.H., Refsgaard, J.C. and Gupta, H. (2002b) 'Perspectives in using a remotely sensed dryness index in distributed hydrological models at the river-basin scale', *Hydrological Processes*, 16, 2973–2987.

Anderson, J.R., Hardy, E.E., Roach, J.T. and Witmer, R.E. (1976) *A Land Use And Land Cover Classification System For Use With Remote Sensor Data. Geological Survey Professional Paper 964,* Washington: United States Geological Survey.

Anderson, M.P. and Woessner, W., W. (1992) 'The role of the postaudit in model validation', *Advances in Water Resources*, 15, 167–173.

Andréassian, V., Perrin, C. and Michel, C. (2004) 'Impact of imperfect potential evapotranspiration knowledge on the efficiency and parameters of watershed models', *Journal of Hydrology*, 286, 19–35.

Apaydin, H., Anli, A.S. and Ozturk, A. (2006) 'The temporal transferability of calibrated parameters of a hydrological model', *Ecological Modelling*, 195, 307–317.

Arnell, N.W. (1999) 'A simple water balance model for the simulation of streamflow over a large geographic domain', *Journal of Hydrology*, 217, 314–335.

Arnell, N.W. (2003) 'Effects of IPCC SRES* emissions scenarios on river runoff: A global perspective', *Hydrology and Earth System Sciences*, 7, 619–641.

Arnell, N.W. (2004) 'Climate change and global water resources: SRES emissions and socio-economic scenarios', *Global Environmental Change*, 14, 31–52.

Arnell, N.W. (2011) 'Uncertainty in the relationship between climate forcing and hydrological response in UK catchments', *Hydrology and Earth System Sciences*, 15, 897–912.

Arnell, N.W. and Gosling, S.N. (2013) 'The impacts of climate change on river flow regimes at the global scale', *Journal of Hydrology*, 486, 351–364.

Arnell, N.W. and Osborn, T.J. (2006) *Interfacing climate and impacts models in integrated assessment modelling. Tyndall Centre Technical Report 52,* Southampton and Norwich: Tyndall Centre for Climate Change Research.

Arnell, N.W. and Reynard, N.S. (1996) 'The effects of climate change due to global warming on river flows in Great Britain', *Journal of Hydrology*, 183, 397–424.

Arnold, J.G., Srinivasan, R., Mutiah, R.S. and Wiliams, J.R. (1998) 'Large area hydrologic modeling and assessment Part I: Model development', *Journal of the American Water Resources Association*, 34, 73–89.

Aronica, G.T. and Candela, A. (2007) 'Derivation of flood frequency curves in poorly gauged Mediterranean catchments using a simple stochastic hydrological rainfall-runoff model', *Journal of Hydrology*, 347, 132–142.

Ascough, J.C., Maier, H.R., Ravalico, J.K. and Strudley, M.W. (2008) 'Future research challenges for incorporation of uncertainty in environmental and ecological decision-making', *Ecological Modelling*, 219, 383–399.

Bae, D.-H., Jung, I.-W. and Lettenmaier, D.P. (2011) 'Hydrologic uncertainties in climate change from IPCC AR4 GCM simulations of the Chungju Basin, Korea', *Journal of Hydrology*, 401, 90–105.

Bastakoti, R.C., Gupta, J., Babel, M.S. and van Dijk, M.P. (2013) 'Climate risks and adaptation strategies in the Lower Mekong River basin', *Regional Environmental Change*, 14, 207–219.

Bastola, S., Murphy, C. and Sweeney, J. (2011) 'The role of hydrological modelling uncertainties in climate change impact assessments of Irish river catchments', *Advances in Water Resources*, 34, 562–576.

Bates, B.C., Kundzewicz, Z.W., Wu, S. and Palutikof, J.P., (eds.) (2008) *Climate Change and Water. Technical Paper of the Intergovernmental Panel on Climate Change,* Geneva: IPCC Secretariat.

Bergström, S. (1995) 'The HBV model', In: Singh, V.P. (ed.) *Computer Models of Watershed Hydrology*, Highlands Ranch, Colorado: Water Resources Publications, 443–476.

Bernard, S. and De Koninck, R. (1996) 'The retreat of the forest in Southeast Asia: A cartographic assessment', *Singapore Journal of Tropical Geography*, 17, 1–14.

Beven, K. (1989) 'Changing ideas in hydrology – The case of physicaly-based model', *Journal of Hydrology*, 105, 157–172.

Beven, K. (1993) 'Prophecy, reality and uncertainty in distributed hydrological modelling', *Advances in Water Resources*, 16, 41–51.

Beven, K. (1996) 'A discussion of distributed hydrological modelling', In: Abbott, M.B. and Refsgaard, J.C. (eds.) *Distributed Hydrological Modelling*, Dordrecht: Kluwer Academic, 255–278.

Beven, K. (2001) 'Calibration, Validation and Equifinality in Hydrological Modelling: A Continuing Discussion', In: Anderson, M.G. and Bates, P.D. (eds.) *Model Validation: Perspectives in Hydrological Science*, Chichester: John Wiley & Sons, 43–55.

Beven, K. (2002) 'Towards a coherent philosophy for modelling the environment', *Proceedings of the Royal Society A: Mathematical, Physical and Engineering Sciences*, 458, 2465–2484.

Beven, K. (2006) 'A manifesto for the equifinality thesis', *Journal of Hydrology*, 320, 18–36.

Beven, K. (2012) *Rainfall-Runoff Modelling: The Primer*, 2nd Edition, Chichester: John Wiley & Sons.

Beven, K. and Binley, A. (1992) 'The future of distributed models: Model calibration and uncertainty prediction', *Hydrological Processes*, 6, 279–298.

Beven, K. and Freer, J. (2001a) 'A dynamic TOPMODEL', *Hydrological Processes*, 15, 1993–2011.

Beven, K. and Freer, J. (2001b) 'Equifnality, data assimilation, and uncertainty estimation in mechanistic modelling of complex environmental systems using the GLUE methodology', *Journal of Hydrology*, 249, 11–29.

Beven, K.J. and Kirkby, M.J. (1976) *Towards a simple physically based variable contributing model of catchment hydrology, Working Paper 154,* School of Geography, University of Leeds.

Beven, K.J. and Kirkby, M.J. (1979) 'A physically based, variable contributing area model of basin hydrology', *Hydrological Sciences Bulletin*, 24, 43–69.

Beven, K.J., Lamb, R., Quinn, P., Romanowicz, R. and Freer, J. (1995) 'TOPMODEL', In: Singh, V.P. (ed.) *Computer Models of Watershed Hydrology*, Highlands Ranch, Colorado: Water Resources Publications, 627–668.

Biftu, G.H. and Gan, T.Y. (2001) 'Semi-distributed, physically based, hydrologic modeling of the Paddle River Basin, Alberta, using remotely sensed data', *Journal of Hydrology*, 244, 137–156.

Blaney, H.F. and Criddle, W.D. (1950) *Determining water requirements in irrigated areas from climatological and irrigation data. Technical Paper no. 96,* Washington, DC: U.S. Department of Agriculture, Soil Conservation Service.

Blöschl, G. and Sivapalan, M. (1995) 'Scale issues in hydrological modelling: A review', *Hydrological Processes*, 9, 251–290.

Bonheur, N. and Lane, B.D. (2002) 'Natural resources management for human security in Cambodia's Tonle Sap Biosphere Reserve', *Environmental Science & Policy*, 5, 33–41.

Booij, M.J. (2005) 'Impact of climate change on river flooding assessed with different spatial model resolutions', *Journal of Hydrology*, 303, 176–198.

Bormann, H. (2011) 'Sensitivity analysis of 18 different potential evapotranspiration models to observed climatic change at German climate stations', *Climatic Change*, 104, 729–753.

Brekke, L.D., Dettinger, M.D., Maurer, E.P. and Anderson, M. (2008) 'Significance of model credibility in estimating climate projection distributions for regional hydroclimatological risk assessments', *Climatic Change*, 89, 371–394.

Breuer, L., Huisman, J.A., Willems, P., Bormann, H., Bronstert, A., Croke, B.F.W., Frede, H.G., Gräff, T., Hubrechts, L., Jakeman, A.J., Kite, G., Lanini, J., Leavesley, G., Lettenmaier, D.P., Lindström, G., Seibert, J., Sivapalan, M. and Viney, N.R.

(2009) 'Assessing the impact of land use change on hydrology by ensemble modeling (LUCHEM). I: Model intercomparison with current land use', *Advances in Water Resources*, 32, 129–146.

Brouwer, C. and Heibloem, M. (1986) *Irrigation Water Management: Irrigation Water Needs, Irrigation Water Management Training Manual 3,* Rome: FAO.

Brown, A.E., Zhang, L., McMahon, T.A., Western, A.W. and Vertessy, R.A. (2005) 'A review of paired catchment studies for determining changes in water yield resulting from alterations in vegetation', *Journal of Hydrology*, 310, 28–61.

Bruijnzeel, L.A. (2004) 'Hydrological functions of tropical forests: not seeing the soil for the trees?', *Agriculture, Ecosystems & Environment*, 104, 185–228.

Burke, S. (2004) 'Decision-Support Systems for Managing Water Resources', In: Wainwright, J. and Mulligan, M. (eds.) *Environmental Modelling: Finding Simplicity in Complexity*, Chichester: John Wiley & Sons, 273-276.

Burnash, R.J.C. (1995) 'The NWS river forecast system-catchment modeling', In: Singh, V.P. (ed.) *Computer Models of Watershed Hydrology*, Highlands Ranch, Colorado: Water Resources Publications, 311–366.

Burnash, R.J.E., Ferral, R.L. and McGuire, R.A. (1984) *A Generalised Streamflow Simulation System,* Sacramento: Joint Federal-State River Forecast Centre.

Butts, M.B., Payne, J.T., Kristensen, M. and Madsen, H. (2004) 'An evaluation of the impact of model structure on hydrological modelling uncertainty for streamflow simulation', *Journal of Hydrology*, 298, 242–266.

Buytaert, W., Célleri, R. and Timbe, L. (2009) 'Predicting climate change impacts on water resources in the tropical Andes: The effects of GCM uncertainty', *Geophysical Research Letters*, 36, L07406.

Carter, T.R., Jones, R.N., Lu, X., Bhadwal, S., Conde, C., Mearns, L.O., O'Neill, B.C., Rounsevell, M.D.A. and Zurek, M.B. (2007) 'New Assessment Methods and the Characterisation of Future Conditions', In: Parry, M.L., Canziani, O.F., Palutikof, J.P., van der Linden, P.J. and Hanson, C.E. (eds.) *Climate Change 2007: Impacts, Adaptation and Vulnerability. Contribution of Working Group II to the Fourth Assessment Report of the Intergovernmental Panel on Climate Change*, Cambridge: Cambridge University Press.

Carter, T.R., Parry, M.L., Harasawa, H. and Nishioka, S. (1994) *Technical Guidelines for Assessing Climate Change Impacts and Adaptations. Intergovernmental Panel on Climate Change Working Group II,* University College London, UK and Center for Global Environmental Research, Japan.

Chiew, F.H.S., Teng, J., Vaze, J. and Kirono, D.G.C. (2009) 'Influence of global climate model selection on runoff impact assessment', *Journal of Hydrology*, 379, 172–180.

Choi, W. and Deal, B.M. (2008) 'Assessing hydrological impact of potential land use change through hydrological and land use change modeling for the

Kishwaukee River basin (USA)', *Journal of Environmental Management*, 88, 1119–1130.

Chow, V.T. (1959) *Open Channel Hydraulics*, New York: McGraw-Hill.

Clapp, R.B. and Hornberger, G.M. (1978) 'Empirical equations for some soil hydraulic properties', *Water Resources Research*, 14, 601–604.

Cochrane, T.A., Arias, M.E. and Piman, T. (2014) 'Historical impact of water infrastructure on water levels of the Mekong River and the Tonle Sap system', *Hydrology and Earth System Sciences*, 18, 4529–4541.

Collins, M., Knutti, R., Arblaster, J., Dufresne, J.-L., Fichefet, T., Friedlingstein, P., Gao, X., Gutowski, W.J., Johns, T., Krinner, G., Shongwe, M., Tebaldi, C., Weaver, A.J. and Wehner, M. (2013) 'Long-term Climate Change: Projections, Commitments and Irreversibility', In: Stocker, T.F., Qin, D., Plattner, G.-K., Tignor, M., Allen, S.K., Boschung, J., Nauels, A., Xia, Y., Bex, V. and Midgley, P.M. (eds.) *Climate Change 2013: The Physical Science Basis. Contribution of Working Group I to the Fifth Assessment Report of the Intergovernmental Panel on Climate Change*, Cambridge: Cambridge University Press, 1029–1136.

Cosslett, T.L. and Cosslett, P.D. (2014) *Water Resources and Food Security in the Vietnam Mekong Delta*, Cham: Springer.

Costa-Cabral, M.C., Richey, J.E., Goteti, G., Lettenmaier, D.P., Feldkötter, C. and Snidvongs, A. (2008) 'Landscape structure and use, climate, and water movement in the Mekong River basin', *Hydrological Processes*, 22, 1731–1746.

Cramer, W., Bondeau, A., Woodward, F.I., Prentice, C., Betts, R.A., Brovkin, V., Cox, P.M., Fisher, V., Foley, J.A., Friend, A.D., Kucharik, C., Lomas, M.R., Ramankutty, N., Sitch, S., Smith, B., White, A. and Young-Molling, C. (2001) ' Global response of terrestrial ecosystem structure and function to CO_2 and climate change: Results from six dynamic global vegetation models', *Global Change Biology*, 7, 357–373.

Crawford, N.H. and Linsley, R.K. (1966) *Digital Simulation in Hydrology. Stanford Watershed Model IV, Technical Report No. 39,* Stanford: Department for Civil Engineering, University of Stanford.

Crosbie, R.S., Dawes, W.R., Charles, S.P., Mpelasoka, F.S., Aryal, S., Barron, O. and Summerell, G.K. (2011) 'Differences in future recharge estimates due to GCMs, downscaling methods and hydrological models', *Geophysical Research Letters*, 38, L11406.

Dai, A. (2012) 'Increasing drought under global warming in observations and models', *Nature Climate Change*, 3, 52–58.

Dai, Z., Li, C., Trettin, C., Sun, G., Amatya, D. and Li, H. (2010) 'Bi-criteria evaluation of the MIKE SHE model for a forested watershed on the South Carolina coastal plain', *Hydrology and Earth System Sciences*, 14, 1033–1046.

Dent, M.C., Shulze, R.E. and Angus, G.R. (1988) *Crop water requirements, deficits and water yield for irrigation planning in southern Africa. Report 118/1/88,* Pietermaritzburg, South Africa: University of Natal.

Dessai, A. and Hulme, M. (2004) 'Does climate adaptation policy need probabilities?', *Climate Policy*, 4.

DHI (2009) *MIKE SHE Technical Reference,* Hørsholm: DHI Water and Environment.

DHI-WE (2009a) *MIKE 11: A modelling system for Rivers and Channels – User Guide,* Hørsholm: DHI Water and Environment.

DHI-WE (2009b) *MIKE SHE User Manual. Volume 2: Reference Guide,* Hørsholm: DHI Water and Environment.

Dilling, L. and Lemos, M.C. (2011) 'Creating usable science: Opportunities and constraints for climate knowledge use and their implications for science policy', *Global Environmental Change*, 21, 680–689.

Dobler, C., Hagemann, S., Wilby, R.L. and Stötter, J. (2012) 'Quantifying different sources of uncertainty in hydrological projections in an Alpine watershed', *Hydrology and Earth System Sciences*, 16, 4343–4360.

Döll, P., Berkhoff, K., Bormann, H., Fohrer, N., Gerten, D., Hagemann, S. and Krol, M. (2008) 'Advances and visions in large-scale hydrological modelling- findings from the 11th Workshop on Large-Scale Hydrological Modelling', *Advances in Geosciences*, 18, 51–61.

Douglas-Mankin, K.R., Srinivasan, R. and Arnold, J.G. (2010) 'Soil and Water Assessment Tool (SWAT) model: Current development and applications', *Transactions of the American Society of Agricultural and Biological Engineers*, 53, 1423–1431.

Duan, Q., Sorooshian, S. and Gupta, V. (1992) 'Effective and Efficient Global Optimization for Conceptual Rainfall-Runoff models', *Water Resources Research*, 28, 1015–1031.

Duan, Q.Y., Gupta, V.K. and Sorooshian, S. (1993) 'Shuffled complex evolution approach for effective and efficient global minimization', *Journal of Optimization Theory and Applications*, 76, 501–521.

Dubus, I.G., Brown, C.D. and Beulke, S. (2003) 'Sources of uncertainty in pesticide fate modelling', *The Science of the Total Environment*, 317, 53–72.

Duethmann, D., Zimmer, J., Gafurov, A., Güntner, A., Kriegel, D., Merz, B. and Vorogushyn, S. (2013) 'Evaluation of areal precipitation estimates based on downscaled reanalysis and station data by hydrological modelling', *Hydrology and Earth System Sciences*, 17, 2415–2434.

Dufresne, J.L., Foujols, M.A., Denvil, S., Caubel, A., Marti, O., Aumont, O., Balkanski, Y., Bekki, S., Bellenger, H., Benshila, R., Bony, S., Bopp, L., Braconnot, P., Brockmann, P., Cadule, P., Cheruy, F., Codron, F., Cozic, A., Cugnet, D., de Noblet, N., Duvel, J.P., Ethé, C., Fairhead, L., Fichefet, T., Flavoni, S.,

Friedlingstein, P., Grandpeix, J.Y., Guez, L., Guilyardi, E., Hauglustaine, D., Hourdin, F., Idelkadi, A., Ghattas, J., Joussaume, S., Kageyama, M., Krinner, G., Labetoulle, S., Lahellec, A., Lefebvre, M.P., Lefevre, F., Levy, C., Li, Z.X., Lloyd, J., Lott, F., Madec, G., Mancip, M., Marchand, M., Masson, S., Meurdesoif, Y., Mignot, J., Musat, I., Parouty, S., Polcher, J., Rio, C., Schulz, M., Swingedouw, D., Szopa, S., Talandier, C., Terray, P., Viovy, N. and Vuichard, N. (2013) 'Climate change projections using the IPSL-CM5 Earth System Model: from CMIP3 to CMIP5', *Climate Dynamics*, 40, 2123–2165.

Dugan, P.J., Barlow, C., Agostinho, A.A., Baran, E., Cada, G.F., Chen, D., Cowx, I.G., Ferguson, J.W., Jutagate, T., Mallen-Cooper, M., Marmulla, G., Nestler, J., Petrere, M., Welcomme, R.L. and Winemiller, K.O. (2010) 'Fish Migration, Dams, and Loss of Ecosystem Services in the Mekong Basin', *Ambio*, 39, 344–348.

Eastham, J., Mpelasoka, F., Mainuddin, M., Ticehurst, C., Dyce, P., Hodgson, G., Ali, R. and Kirby, M. (2008) *Mekong River Basin Water Resources Assessment: Impacts of Climate Change. Water for a Healthy Country National Research Flagship Report,* Canberra: CSIRO.

El-Nasr, A.A., Arnold, J.G., Feyen, J. and Berlamont, J. (2005) 'Modelling the hydrology of a catchment using a distributed and a semi-distributed model', *Hydrological Processes*, 19, 573–587.

El-Sadek, A., Bleiweiss, M., Shukla, M., Guldan, S. and Fernald, A. (2011) 'Alternative climate data sources for distributed hydrological modelling on a daily time step', *Hydrological Processes*, 25, 1542–1557.

Ewen, J., Parkin, G. and O'Connell, P.E. (2000) 'SHETRAN: Distributed river basin flow and transport modelling system', *Journal of Hydrologic Engineering*, 5, 250–258.

Falloon, P., Challinor, A., Dessai, S., Hoang, L., Johnson, J. and Koehler, A.-K. (2014) 'Ensembles and uncertainty in climate change impacts', *Frontiers in Environmental Science*, 2.

Fan, H., He, D. and Wang, H. (2015) 'Environmental consequences of damming the mainstream Lancang-Mekong River: A review', *Earth-Science Reviews*, 146, 77–91.

FAO (1998) *Digital Soil Map of the World and Derived Soil Properties*, Rome: Food and Agriculture Organization of the United Nations.

FAO (2000) *FRA 2000: Forest Cover Mapping & Monitoring with NOAA-AVHRR & Other Coarse Resolution Sensors,* Rome: Food and Agriculture Organization of the United Nations.

FAO (2003) *The Digital Soil Map of the World. Food and Agriculture Organization of the United Nations. Version 3.6,* Rome: Land and Water Development Division, FAO.

FAO (2012) *Irrigation in Southern and Eastern Asia in figures. AQUASTAT Survey – 2011. FAO Water Reports 37,* Rome: Food and Agricultural Organization of the United Nations.

FAO (2016) *AQUASTAT Main Database. Food and Agriculture Organization of the United Nations (FAO)* [Online] Available from: http://www.fao.org/nr/water/aquastat/data/query/index.html?lang=en [Accessed 14th October 2017].

FAO-Unesco (1974a) *Soil Map of the World, 1:5 000 000. Volume I: Legend,* Paris: United Nations Educational, Scientific and Cultural Organization.

FAO-Unesco (1974b) *Soil Map of the World, 1:5 000 000. Volume IX: Southeast Asia,* Paris: United Nations Educational, Scientific and Cultural Organization.

Feyen, I., Vázquez, R., Christiaens, K., Sels, O. and Feyen, J. (2000) 'Application of a distributed physically-based hydrological model to a medium size catchment', *Hydrology and Earth System Sciences*, 4, 47–63.

Feyen, J. and Vázquez Zambrano, R.l.F. (2011) 'Modeling hydrological consequences of climate and land use change - Progress and Challenges', *Maskana*, 2, 83–100.

Flato, G., Marotzke, J., Abiodun, B., Braconnot, P., Chou, S.C., Collins, W., Cox, P., Driouech, F., Emori, S., Eyring, V., Forest, C., Gleckler, P., Guilyardi, E., Jakob, C., Kattsov, V., Reason, C. and Rummukainen, M. (2013) 'Evaluation of Climate Models', In: Stocker, T.F., Qin, D., Plattner, G.-K., Tignor, M., Allen, S.K., Boschung, J., Nauels, A., Xia, Y., Bex, V. and Midgley, P.M. (eds.) *Climate Change 2013: The Physical Science Basis. Contribution of Working Group I to the Fifth Assessment Report of the Intergovernmental Panel on Climate Change*, Cambridge: Cambridge University Press, 741–866.

Floch, P. and Molle, F. (2007) *Marshalling Water Resources: A Chronology of Irrigation Development in the Chi-Mun River Basin, Northeast Thailand,* Colombo: CGIAR Challenge Program on Water and Food.

Floch, P. and Molle, F. (2009) *Water Traps: The Elusive Quest for Water Storage in the Chi- Mun River Basin, Thailand. Working Paper. Mekong Program on Water, Environment and Resilience (M-POWER),* University of Natural Resources and Applied Life Sciences, Institut de Recherche pour le Développement, Chiang Mai, Thailand.

Fontaine, T.A., Cruickshank, T.S., Arnold, J.G. and Hotchkiss, R.H. (2002) 'Development of a snowfall-snowmelt routine for mountainous terrain for the soil water assessment tool (SWAT)', *Journal of Hydrology*, 262, 209–223.

Frei, C., Christensen, J.H., Déqué, M., Jacob, D., Jones, R.G. and Vidale, P.L. (2003) 'Daily precipitation statistics in regional climate models: Evaluation and intercomparison for the European Alps', *Journal of Geophysical Research*, 108(D3), 4124.

Frei, C. and Schär, C. (1998) 'A precipitation climatology of the Alps from high-resolution rain-gauge observations', *International Journal of Climatology*, 18, 873–900.

French, J.R. (2010) 'Critical perspectives on the evaluation and optimization of complex numerical models of estuary hydrodynamics and sediment dynamics', *Earth Surface Processes and Landforms*, 35, 174–189.

Gao, Q.-z., Wan, Y.-f., Xu, H.-m., Li, Y., Jiangcun, W.-z. and Borjigidai, A. (2010) 'Alpine grassland degradation index and its response to recent climate variability in Northern Tibet, China', *Quaternary International*, 226, 143–150.

Garbrecht, J. and Martz, L.W. (1997) *TOPAZ Version 1.20: An Automated Digital Landscape Analysis Tool for Topographic Evaluation, Drainage Identification, Watershed Segmentation and Subcatchment Parameterization – Overview. Report number GRL 97–2,* El Reno: USDA Grazinglands Research Laboratory, Agricultural Research Service.

García, A., Sainz, A., Revilla, J.A., Álvarez, C., Juanes, J.A. and Puente, A. (2008) 'Surface water resources assessment in scarcely gauged basins in the north of Spain', *Journal of Hydrology*, 356, 312–326.

Gasca Tucker, D.L. and Acreman, M.A. (2000) 'Modelling ditch water levels on the Pevensey Levels wetland, a lowland wet grassland wetland in East Sussex, UK', *Physics and Chemistry of the Earth (B)*, 25, 593–597.

Giorgi, F. and Gutowski, W.J. (2015) 'Regional Dynamical Downscaling and the CORDEX Initiative', *Annual Review of Environment and Resources*, 40, 467-490.

Giorgi, F., Jones, C. and Asrar, G. (2009) 'Addressing climate information needs at the regional level: the CORDEX framework', *WMO Bulletin*, 58, 175–183.

Gleick, P.H. (1989) 'Climate change, hydrology and water resources', *Reviews of Geophysics*, 27, 329–344.

Goderniaux, P., Brouyère, S., Fowler, H.J., Blenkinsop, S., Therrien, R., Orban, P. and Dassargues, A. (2009) 'Large scale surface–subsurface hydrological model to assess climate change impacts on groundwater reserves', *Journal of Hydrology*, 373, 122–138.

Gosling, S.N. (2013) 'The likelihood and potential impact of future change in the large-scale climate-earth system on ecosystem services', *Environmental Science & Policy*, 27, S15–S31.

Gosling, S.N. and Arnell, N.W. (2011) 'Simulating current global river runoff with a global hydrological model: model revisions, validation, and sensitivity analysis', *Hydrological Processes*, 25, 1129–1145.

Gosling, S.N. and Arnell, N.W. (2016) 'A global assessment of the impact of climate change on water scarcity', *Climatic Change*, 134, 371–385.

Gosling, S.N., Bretherton, D., Haines, K. and Arnell, N.W. (2010) 'Global hydrology modelling and uncertainty: running multiple ensembles with a campus grid', *Philosophical transactions. Series A, Mathematical, physical, and engineering sciences*, 368, 4005–4021.

Gosling, S.N., Lowe, J.A., McGregor, G.R., Pelling, M. and Malamud, B.D. (2009) 'Associations between elevated atmospheric temperature and human mortality: a critical review of the literature', *Climatic Change*, 92, 299–341.

Gosling, S.N., Taylor, R.G., Arnell, N.W. and Todd, M.C. (2011) 'A comparative analysis of projected impacts of climate change on river runoff from global and catchment-scale hydrological models', *Hydrology and Earth System Sciences*, 15, 279–294.

Goteti, G. and Lettenmaier, D.P. (2001) *Effects of Streamflow Regulation and Land Cover Change on the Hydrology of the Mekong River Basin. Water Resources Series. Technical Report No. 169,* Washington: Department of Civil Engineering University of Washington.

Graham, D.N. and Butts, M.B. (2005) 'Flexible integrated watershed modeling with MIKE SHE', In: Singh, V.P. and Frevert, D.K. (eds.) *Watershed Models*, Boca Raton: CRC Press, 245–272.

Graham, L.P., Andréasson, J. and Carlsson, B. (2007a) 'Assessing climate change impacts on hydrology from an ensemble of regional climate models, model scales and linking methods – a case study on the Lule River basin', *Climatic Change*, 81, 293–307.

Graham, L.P., Hagemann, S., Jaun, S. and Beniston, M. (2007b) 'On interpreting hydrological change from regional climate models', *Climatic Change*, 81, 97–122.

Grayson, R. and Blöschl, G. (2000) 'Spatial Modelling of Catchment Dynamics', In: Grayson, R. and Blöschl, G. (eds.) *Spatial Patterns in Catchment Hydrology: Observations and Modelling*, Cambridge: Cambridge University Press, 51–81.

Grayson, R.B., Moore, I.D. and McMahon, T.A. (1992) 'Physically based hydrological modelling 1. A terrain-based model for investigative purposes', *Water Resources Research*, 28, 2639–2658.

Grumbine, R.E., Dore, J. and Xu, J. (2012) 'Mekong hydropower: drivers of change and governance challenges', *Frontiers in Ecology and the Environment*, 10, 91–98.

Gupta, A., Hock, L., Xiaojing, H. and Ping, C. (2002) 'Evaluation of part of the Mekong River using satellite imagery', *Geomorphology*, 44, 221–239.

Gupta, H.V., Sorooshian, S. and Yapo, P.O. (1998) 'Toward improved calibration of hydrologic models: Multiple and noncommensurable measures of information', *Water Resources Research*, 34, 751–763.

Haddeland, I., Clark, D.B., Franssen, W., Ludwig, F., Voß, F., Arnell, N.W., Bertrand, N., Best, M., Folwell, S., Gerten, D., Gomes, S., Gosling, S.N., Hagemann, S.,

Hanasaki, N., Harding, R., Heinke, J., Kabat, P., Koirala, S., Oki, T., Polcher, J., Stacke, T., Viterbo, P., Weedon, G.P. and Yeh, P. (2011) 'Multimodel Estimate of the Global Terrestrial Water Balance: Setup and First Results', *Journal of Hydrometeorology*, 12, 869–884.

Haddeland, I., Lettenmaier, D.P. and Skaugen, T. (2006) 'Effects of irrigation on the water and energy balances of the Colorado and Mekong river basins', *Journal of Hydrology*, 324, 210–223.

Hagemann, S., Chen, C., Clark, D.B., Folwell, S., Gosling, S.N., Haddeland, I., Hanasaki, N., Heinke, J., Ludwig, F., Voss, F. and Wiltshire, A.J. (2013) 'Climate change impact on available water resources obtained using multiple global climate and hydrology models', *Earth System Dynamics*, 4, 129–144.

Hamon, W.R. (1963) 'Computation of direct runoff amounts from storm rainfall', In: *International Association of Scientific Hydrology Publication 63*, 52–62.

Hapuarachchi, H.A.P., Takeuchi, K., Zhou, M., Kiem, A.S., Georgievski, M., Magome, J. and Ishidaira, H. (2008) 'Investigation of the Mekong River basin hydrology for 1980–2000 using the YHyM', *Hydrological Processes*, 22, 1246–1256.

Harbaugh, A.W. (2005) *MODFLOW-2005, The US Geological Survey Modular Ground-water Model—The Ground Water Flow Process,* US Geological Survey Techniques and Methods 6-A16.

Harbaugh, A.W., Banta, E.R., Hill, M.C. and McDonald, M.G. (2000) *MODFLOW-2000, the US geological survey modular ground-water model – user guide to modularization concepts and the ground-water flow process,* US Geological Survey Open-File Report 00-92.

Hargreaves, G.H. and Samani, Z.A. (1982) 'Estimating potential evapotranspiration. Technical note', *Journal of the Irrigation and Drainage Division - ASCE*, 108, 225–230.

Harris, I., Jones, P.D., Osborn, T.J. and Lister, D.H. (2014) 'Updated high-resolution grids of monthly climatic observations - the CRU TS3.10 Dataset', *International Journal of Climatology*, 34, 623–642.

Hasson, S.u., Pascale, S., Lucarini, V. and Böhner, J. (2016) 'Seasonal cycle of precipitation over major river basins in South and Southeast Asia: A review of the CMIP5 climate models data for present climate and future climate projections', *Atmospheric Research*, 180, 42–63.

Havnø, K., Madsen, M.N. and Dørge, J. (1995) 'MIKE 11 – A generalized river modelling package', In: Singh, V.P. (ed.) *Computer Models of Watershed Hydrology*, Highlands Ranch, Colorado: Water Resources Publications, 733–782.

Hawkins, E. (2014) *The Cadcade of Uncertainty in Climate Projections* [Online] Available from: http://www.climate-lab-book.ac.uk/2014/cascade-of-uncertainty/ [Accessed 14 July 2015].

Hay, L.E., Wilby, R.L. and Leavesley, G.H. (2000) 'A comparison of delta change and downscaled GC< scnearios for three mountainous basins in the United States', *Journal of the American Water Resources Association*, 36, 387–397.

Hayhoe, K., Cayan, D., Field, C.B., Frumhoff, P.C., Maurer, E.P., Miller, N.L., Moser, S.C., Schneider, S.H., Cahill, K.N., Cleland, E.E., Dale, L., Drapek, R., Hanemann, R.M., Kalkstein, L.S., Lenihan, J., Lunch, C.K., Neilson, R.P., Sheridan, S.C. and Verville, J.H. (2004) 'Emissions pathways, climate change, and impacts on California', *PNAS*, 101, 12422–12427.

Henriksen, H.J., Troldborg, L., Højberg, A.L. and Refsgaard, J.C. (2008) 'Assessment of exploitable groundwater resources of Denmark by use of ensemble resource indicators and a numerical groundwater–surface water model', *Journal of Hydrology*, 348, 224–240.

Henriksen, H.J., Troldborg, L., Nyegaard, P., Sonnenborg, T.O., Refsgaard, J.C. and Madsen, B. (2003) 'Methodology for construction, calibration and validation of a national hydrological model for Denmark', *Journal of Hydrology*, 280, 52–71.

Ho, J.T., Thompson, J.R. and Brierley, C. (2016) 'Projections of hydrology in the Tocantins-Araguaia Basin, Brazil: uncertainty assessment using the CMIP5 ensemble', *Hydrological Sciences Journal*, 61, 551–567.

Hoa, L.T.V., Shigeko, H., Nhan, N.H. and Cong, T.T. (2008) 'Infrastructure effects on floods in the Mekong River Delta in Vietnam', *Hydrological Processes*, 22, 1359–1372.

Hoang, L.P., Lauri, H., Kummu, M., Koponen, J., van Vliet, M.T.H., Supit, I., Leemans, R., Kabat, P. and Ludwig, F. (2016) 'Mekong River flow and hydrological extremes under climate change', *Hydrology and Earth System Sciences*, 20, 3027–3041.

Hortle, K.G. (2007) *Consumption and the yield of fish and other aquatic animals from the Lower Mekong Basin. MRC Technical Paper No.16,* Vientiane: Mekong River Commission.

House, A.R., Thompson, J.R., Sorensen, J.P.R., Roberts, C. and Acreman, M.C. (2015) 'Modelling groundwater/surface-water interaction in a managed riparian chalk valley wetland', *Hydrological Processes*, Author Manuscript Online.

Houze, R., A. (2012) 'Orographic effects on precipitating clouds', *Reviews of Geophysics*, 50, RG1001.

Huang, Y., Wang, F., Li, Y. and Cai, T. (2014) 'Multi-model ensemble simulation and projection in the climate change in the Mekong River Basin. Part I: temperature', *Environmental Monitoring and Assessment*, 186, 7513–7523.

Hughes, D.A., Kingston, D.G. and Todd, M.C. (2011) 'Uncertainty in water resources availability in the Okavango River basin as a result of climate change', *Hydrology and Earth System Sciences*, 15, 931–941.

Huntington, T.G. (2006) 'Evidence for intensification of the global water cycle: Review and synthesis', *Journal of Hydrology*, 319, 83–95.

Immerzeel, W.W., Beek, L.P.H., Konz, M., Shrestha, A.B. and Bierkens, M.F.P. (2012a) 'Hydrological response to climate change in a glacierized catchment in the Himalayas', *Climatic Change*, 110, 721–736.

Immerzeel, W.W., Droogers, P., de Jong, S.M. and Bierkens, M.F.P. (2009) 'Large-scale monitoring of snow cover and runoff simulation in Himalayan river basins using remote sensing', *Remote Sensing of Environment*, 113, 40–49.

Immerzeel, W.W., Pellicciotti, F. and Shrestha, A.B. (2012b) 'Glaciers as a Proxy to Quantify the Spatial Distribution of Precipitation in the Hunza Basin', *Mountain Research and Development*, 32, 30–38.

Institute of Hydrology (1988) *Investigation of Dry Season Flows. Water Balance Study Phase 3. Report to the Interim Committee for Coordination of Investigations of the Lower Mekong Basin,* Wallingford: Institute of Hydrology.

International Rivers (2017) *A dangerous trajectory for the MekongRiver: Update on the status of the Mekong Mainstream Dams,* Berkeley: International Rivers.

IPCC (2000) *IPCC Special Report. Emisions Scenarios. Summary for Policymakers. A Special Report of IPCC Working Group III,* Intergovernmental Panel on Climate Change.

IPCC (2007) 'Summary for Policymakers', In: Solomon, S., Qin, D., Manning, M., Chen, Z., Marquis, M., Averyt, K.B., Tignor, M. and Miller, H.L. (eds.) *Climate Change 2007: The Physical Science Basis. Contribution of Working Group I to the Fourth Assessment Report of the Intergovernmental Panel on Climate Change*, Cambridge: Cambridge University Press.

IPCC (2012) 'Summary for Policymakers', In: Field, C.B., Barros, V., Stocker, T.F., Qin, D., Dokken, D.J., Ebi, K.L., Mastrandrea, M.D., Mach, K.J., Plattner, G.-K., Allen, S.K., Tignor, M. and Midgley, P.M. (eds.) *Managing the Risks of Extreme Events and Disasters to Advance Climate Change Adaptation. A Special Report of Working Groups I and II of the Intergovernmental Panel on Climate Change*, Cambridge and New York: Cambridge University Press.

IPCC (2013) 'Summary for Policymakers', In: Stocker, T.F., Qin, D., Plattner, G.-K., Tignor, M., Allen, S.K., Boschung, J., Nauels, A., Xia, Y., Bex, V. and Midgley, P.M. (eds.) *Climate Change 2013: The Physical Science Basis. Contribution of Working Group I to the Fifth Assessment Report of the Intergovernmental Panel on Climate Change*, Cambridge: Cambridge University Press, 3–32.

Jackson, C.R., Meister, R. and Prudhomme, C. (2011) 'Modelling the effects of climate change and its uncertainty on UK Chalk groundwater resources from an ensemble of global climate model projections', *Journal of Hydrology*, 399, 12–28.

Jackson, R.B., Canadell, J., Ehleringer, J.R., Mooney, H.A., Sala, O.E. and Schulze, E.D. (1996) 'A global analysis for root distribitions for terrestrial biomes', *Oecologia*, 108, 389–411.

Jacobs, J.W. (2002) 'The Mekong River Commission: transboundary water resources planning and regional security', *The Geographical Journal*, 168, 354–364.

Jakeman, A.J., Littlewood, L.G. and Whitehead, P.G. (1990) 'Computation of the instantaneous unit hydrograph and identifiable component flows with application to two small upland catchments', *Journal of Hydrology*, 275–300.

Ji, X. and Luo, Y. (2013) 'The influence of precipitation and temperature input schemes on hydrological simulations of a snow and glacier melt dominated basin in Northwest China', *Hydrology and Earth System Sciences Discussions*, 10, 807–853.

Jiang, S., Ren, L., Hong, Y., Yong, B., Yang, X., Yuan, F. and Ma, M. (2012) 'Comprehensive evaluation of multi-satellite precipitation products with a dense rain gauge network and optimally merging their simulated hydrological flows using the Bayesian model averaging method', *Journal of Hydrology*, 452–453, 213–225.

Jiang, T., Chen, Y.D., Xu, C.-y., Chen, X., Chen, X. and Singh, V.P. (2007) 'Comparison of hydrological impacts of climate change simulated by six hydrological models in the Dongjiang Basin, South China', *Journal of Hydrology*, 336, 316–333.

Jiménez Cisneros, B.E., Oki, T., Arnell, N.W., Benito, G., Cogley, J.G., Döll, P., Jiang, T. and Mwakalila, S.S. (2014) 'Freshwater Resources', In: Field, C.B., Barros, V.R., Dokken, D.J., Mach, K.J., Mastrandrea, M.D., Bilir, T.E., Chatterjee, M., Ebi, K.L., Estrada, Y.O., Genova, R.C., Girma, B., Kissel, E.S., Levy, A.N., MacCracken, S., Mastrandrea, P.R. and White, L.L. (eds.) *Climate Change 2014: Impacts, Adaptation, and Vulnerability. Part A: Global and Sectoral Aspects. Contribution of Working Group II to the Fifth Assessment Report of the Intergovernmental Panel on Climate Change*, Cambridge and New York: Cambridge University Press, 229–269.

Johnston, R. and Kummu, M. (2012) 'Water Resource Models in the Mekong Basin: A Review', *Water Resources Management*, 26, 429–455.

Johnston, R., Lacombe, G., Hoanh, C.T., Noble, A., Pavelic, P., Smakhtin, V., Suhardiman, D., Kam, S.P. and Choo, P.S. (2010) *Climate change, water and agriculture in the Greater Mekong Subregion. IWMI Research Report 136,* Colombo: International Water Management Institute.

Johnston, R. and Smakhtin, V. (2014) 'Hydrological Modeling of Large River Basins: How Much is Enough?', *Water Resources Management*, 28, 2695–2730.

Jones, J.A.A. (1997) *Global Hydrology: Processes, Resources and Environmental Management*, Harlow: Longman.

Kay, A.L. and Davies, H.N. (2008) 'Calculating potential evaporation from climate model data: A source of uncertainty for hydrological climate change impacts', *Journal of Hydrology*, 358, 221–239.

Kay, A.L., Davies, H.N., Bell, V.A. and Jones, R.G. (2009) 'Comparison of uncertainty sources for climate change impacts: flood frequency in England', *Climatic Change*, 92, 41–63.

Kiem, A.S., Geogievsky, M.V., Hapuarachchi, H.P., Ishidaira, H. and Takeuchi, K. (2005) 'Relationship between ENSO and snow covered area in the Mekong and Yellow River basins', In: Franks, S.W., Wagener, T., Bøgh, E., Bastidas, L., Nobre, C. and Galvão, C.O. (eds.) *Regional Hydrological Impacts of Climate Change – Hydroclimatic Variability. IAHS Publ. 296*, Wallingford, 255–264.

Kiem, A.S., Ishidaira, H., Hapuarachchi, H.P., Zhou, M.C., Hirabayashi, Y. and Takeuchi, K. (2008) 'Future hydroclimatology of the Mekong River basin simulated using the high-resolution Japan Meteorological Agency (JMA) AGCM', *Hydrological Processes*, 22, 1382–1394.

Kim, S.T. and Yu, J.-Y. (2012) 'The two types of ENSO in CMIP5 models', *Geophysical Research Letters*, 39, L11704.

Kingston, D.G. and Taylor, R.G. (2010) 'Sources of uncertainty in climate change impacts on river discharge and groundwater in a headwater catchment of the Upper Nile Basin, Uganda', *Hydrology and Earth System Sciences*, 14, 1297–1308.

Kingston, D.G., Thompson, J.R. and Kite, G. (2010) 'Uncertainty in climate change projections of discharge for the Mekong River Basin', *Hydrology and Earth System Sciences Discussions*, 7, 5991–6024.

Kingston, D.G., Thompson, J.R. and Kite, G. (2011) 'Uncertainty in climate change projections of discharge for the Mekong River Basin', *Hydrology and Earth System Sciences*, 15, 1459–1471.

Kingston, D.G., Todd, M.C., Taylor, R.G., Thompson, J.R. and Arnell, N.W. (2009) 'Uncertainty in the estimation of potential evapotranspiration under climate change', *Geophysical Research Letters*, 36, L20403.

Kirby, C., Newson, M. and Gilman, K. (1991) *Plynlimon Research: The first two decades,* Wallingford: Institute of Hydrology.

Kirby, M. and Mainuddin, M. (2009) 'Water and agricultural productivity in the Lower Mekong Basin: trends and future prospects', *Water International*, 34, 134–143.

Kirtman, B., Power, S.B., Adedoyin, J.A., Boer, G.J., Bojariu, R., Camilloni, I., Doblas-Reyes, F.J., Fiore, A.M., Kimoto, M., Meehl, G.A., Prather, M., Sarr, A., Schär, C., Sutton, R., van Oldenborgh, G.J., Vecchi, G. and Wang, H.J. (2013) 'Near-term Climate Change: Projections and Predictability', In: Stocker, T.F., Qin, D., Plattner, G.-K., Tignor, M., Allen, S.K., Boschung, J., Nauels, A., Xia, Y., Bex, V. and Midgley, P.M. (eds.) *Climate Change 2013: The Physical Science Basis. Contribution of Working Group I to the Fifth Assessment Report of the Intergovernmental Panel on Climate Change*, Cambridge and New York: Cambridge University Press, 953–1028.

Kite, G. (1995) 'The SLURP model', In: Singh, V.P. (ed.) *Computer Models of Watershed Hydrology*, Highlands Ranch, Colorado: Water Resources Publications, 521–562.

Kite, G. (2000) *Developing a Hydrological Model for the Mekong Basin: Impacts of Basin Development on Fisheries Productivity. Working Paper 2,* Colombo: International Water Management Institute.

Kite, G. (2001) 'Modelling the Mekong: hydrological simulation for environmental impact studies', *Journal of Hydrology*, 253, 1–13.

Kite, G. (2007) *Manual for the SLURP Hydrological Model*, HydroLogic-Solutions.

Kite, G.W., Dalton, A. and Dion, K. (1994) 'Simulation of streamflow in a macroscale watershed using general circulation model data', *Water Resources Research*, 30, 1547–1559.

Kite, G.W. and Pietroniro, A. (1996) 'Remote sensing applications in hydrological modelling', *Hydrological Sciences Journal*, 41, 563–591.

Kite, G.W. and Spence, C.D. (1994) *Land Cover, NDVI, LAI and Evapotranspiration in Hydrological Modelling,* Canada: National Hydrology Research Institute.

Klemeš, V. (1986) 'Operational testing of hydrological simulation models', *Hydrological Sciences Journal*, 31, 13–24.

Knutti, R., Masson, D. and Gettelman, A. (2013) 'Climate model genealogy: Generation CMIP5 and how we got there', *Geophysical Research Letters*, 40, 1194–1199.

Knutti, R. and Sedláček, J. (2012) 'Robustness and uncertainties in the new CMIP5 climate model projections', *Nature Climate Change*, 3, 369–373.

Konikow, L.F. and Bredehoeft, J.D. (1992) 'Ground-water models cannot be validated', *Advances in Water Resources*, 15, 75–83.

Krause, P., Boyle, D.P. and Bäse, F. (2005) 'Comparison of different efficiency criteria for hydrological model assessment', *Advances in Geosciences*, 5, 89–97.

Kummu, M., Lu, X.X., Wang, J.J. and Varis, O. (2010) 'Basin-wide sediment trapping efficiency of emerging reservoirs along the Mekong', *Geomorphology*, 119, 181–197.

Kummu, M., Sarkkula, J., Koponen, J. and Nikula, J. (2006) 'Ecosystem Management of the Tonle Sap Lake: An Integrated Modelling Approach', *International Journal of Water Resources Development*, 22, 497–519.

Kuntiyawichai, K. (2012) *Interactions between land use and flood management in the Chi River Basin*, PhD Thesis, Wageningen University, Wageningen University.

Kwadijk, J.C.J., Haasnoot, M., Mulder, J.P.M., Hoogvliet, M.M.C., Jeuken, A.B.M., van der Krogt, R.A.A., van Oostrom, N.G.C., Schelfhout, H.A., van Velzen, E.H., van Waveren, H. and de Wit, M.J.M. (2010) 'Using adaptation tipping points to prepare for climate change and sea level rise: a case study in the Netherlands', *Wiley Interdisciplinary Reviews: Climate Change*, 1, 729–740.

Lacombe, G., Pierret, A., Hoanh, C.T., Sengtaheuanghoung, O. and Noble, A.D. (2010) 'Conflict, migration and land-cover changes in Indochina: a hydrological assessment', *Ecohydrology*, 3, 382–391.

Laizé, C.L.R., Acreman, M.C., Schneider, C., Dunbar, M.J., Houghton-Carr, H.A., Flörke, M. and Hannah, D.M. (2014) 'Projected Flow Alteration and Ecological Risk for Pan-European Rivers', *River Research and Applications*, 30, 299–314.

Lal, P.N., Mitchell, T., Aldunce, P., Auld, H., Mechler, R., Miyan, A., Romano, L.E. and Zakaria, S. (2012) 'National systems for managing the risks from climate extremes and disasters', In: Field, C.B., Barros, V., Stocker, T.F., Qin, D., Dokken, D.J., Ebi, K.L., Mastrandrea, M.D., Mach, K.J., Plattner, G.-K., Allen, S.K., Tignor, M. and Midgley, P.M. (eds.) *Managing the Risks of Extreme Events and Disasters to Advance Climate Change Adaptation. A Special Report of Working Groups I and II of the Intergovernmental Panel on Climate Change (IPCC)*, Cambridge and New York: Cambridge University Press, 339–392.

Lamb, R., Beven, K. and Myrabø, S. (2000) 'Shallow Groundwater Response at Minifelt', In: Grayson, R. and Blöschl, G. (eds.) *Spatial Patterns in Catchment Hydrology: Observations and Modelling*, Cambridge: Cambridge University Press, 272–303.

Lauri, H., de Moel, H., Ward, P.J., Räsänen, T.A., Keskinen, M. and Kummu, M. (2012) 'Future changes in Mekong River hydrology: impact of climate change and reservoir operation on discharge', *Hydrology and Earth System Sciences Discussions*, 9, 6569–6614.

Lauri, H., Räsänen, T.A. and Kummu, M. (2014) 'Using reanalysis and remotely sensed temperature and precipitation data for hydrological modelling in monsoon climate: Mekong River case study', *Journal of Hydrometeorology*, 15, 1532–1545.

Leenders, E.E. and Woo, M.-k. (2002) 'Modeling a two-layer flow system at the subarctic, subalpine tree line during snowmelt', *Water Resources Research*, 38, 20-21–20-28.

Legates, D.R. and McCabe, G.J. (1999) 'Evaluating the use of "goodness-of-fit" measures in hydrologic and hydroclimatic model validation', *Water Resources Research*, 35, 233–241.

Legates, D.R. and Willmott, C., J. (1990) 'Mean seasonal and spatial variability in gauge-corrected, global precipitation', *International Journal of Climatology*, 10, 111–127.

Li, S. and He, D. (2008) 'Water Level Response to Hydropower Development in the Upper Mekong River', *AMBIO: A Journal of the Human Environment*, 37, 170–176.

Linacre, E.T. (1977) 'A simple formula for estimating evaporation rates in various climates, using temperature data alone', *Agricultural Meteorology*, 18, 409–424.

Lindstöm, G., Johansson, B., Persson, M., Gardelin, M. and Bergström, S. (1997) 'Development and test of the distributed HBV-96 hydrological model', *Journal of Hydrology*, 201, 272–288.

Liu, Y. and Gupta, H.V. (2007) 'Uncertainty in hydrologic modeling: Toward an integrated data assimilation framework', *Water Resources Research*, 43, W07401.

Loucks, D.P. and van Beek, E. (2005) *Water Resources Systems Planning and Management: An Introduction to Methods, Models and Applications*, Paris: United Nations Educational, Scientific and Cultural Organization.

Lu, J., Sun, G., McNulty, S.G. and Amatya, D.M. (2005) 'A comparison of six potential evapotranspiration methods for regional use in the southeastern United States', *Journal of the American Water Resources Association*, 41, 621–633.

Lu, X.X., Li, S., Kummu, M., Padawangi, R. and Wang, J.J. (2014) 'Observed changes in the water flow at Chiang Saen in the lower Mekong: Impacts of Chinese dams?', *Quaternary International*, 336, 145–157.

Lu, X.X. and Siew, R.Y. (2006) 'Water discharge and sediment flux changes over the past decades in the Lower Mekong River: possible impacts of the Chinese dams', *Hydrology and Earth System Sciences*, 10, 181–195.

Ludwig, R., May, I., Turcotte, R., Vescovi, L., Braun, M., Cyr, J.-F., Fortin, L.-G., Chaumont, D., Biner, S., Chartier, I., Caya, D. and Mauser, W. (2009) 'The role of hydrological model complexity and uncertainty in climate change impact assessment', *Advances in Geosciences*, 21, 63–71.

Luo, Y., Arnold, J., Liu, S., Wang, X. and Chen, X. (2013) 'Inclusion of glacier processes for distributed hydrological modeling at basin scale with application to a watershed in Tianshan Mountains, northwest China', *Journal of Hydrology*, 477, 72–85.

Lutz, A.F., ter Maat, H.W., Biemans, H., Shrestha, A.B., Wester, P. and Immerzeel, W.W. (2016) 'Selecting representative climate models for climate change impact studies: an advanced envelope-based selection approach', *International Journal of Climatology*, 36, 3988–4005.

Madsen, H. (2003) 'Parameter estimation in distributed hydrological catchment modelling using automatic calibration with multiple objectives', *Advances in Water Resources*, 26, 205–216.

Madsen, H. and Jacobsen, T. (2001) 'Automatic calibration of the MIKE SHE integrated hydrological modelling system', In: *4th DHI Software Conference*, *6–8 June, 2001*, *Scanticon Conference Centre, Helsingør, Denmark*, Hørsholm: DHI.

Marshall, T.J., Holmes, J.W. and Rose, C.W. (1996) *Soil Physics*, 3rd Edition, Cambridge: Cambridge University Press.

Masood, M., Yeh, P.J.F., Hanasaki, N. and Takeuchi, K. (2015) 'Model study of the impacts of future climate change on the hydrology of Ganges–Brahmaputra–Meghna basin', *Hydrology and Earth System Sciences*, 19, 747–770.

Masson, D. and Knutti, R. (2011) 'Climate model genealogy', *Geophysical Research Letters*, 38, L08703.

Matott, L.S., Babendreier, J.E. and Purucker, S.T. (2009) 'Evaluating uncertainty in integrated environmental models: A review of concepts and tools', *Water Resources Research*, 45, W06421.

Maurer, E.P. and Duffy, P.B. (2005) 'Uncertainty in projections of streamflow changes due to climate change in California', *Geophysical Research Letters*, 32, L03704.

McCartney, M.P. and Acreman, M.C. (2009) 'Wetlands and Water Resources', In: Maltby, E. and Barker, T. (eds.) *The Wetlands Handbook*, Chichester: Wiley-Blackwell.

McDonald, M.G. and Harbaugh, A.W. (1988) *A modular three- dimensional finite difference ground-water flow model,* US Geological Survey Techniques of Water Resources Investigations, 06-A1.

McGuffie, K. and Henderson-Sellers, A. (2005) *A Climate Modelling Primer*, 3rd Edition, Chichester: John Wiley & Sons.

McMichael, C.E. and Hope, A.S. (2007) 'Predicting streamflow response to fire-induced landcover change: implications of parameter uncertainty in the MIKE SHE model', *Journal of Environmental Management*, 84, 245–256.

McMichael, C.E., Hope, A.S. and Loaiciga, H.A. (2006) 'Distributed hydrological modelling in California semi-arid shrublands: MIKE SHE model calibration and uncertainty estimation', *Journal of Hydrology*, 317, 307–324.

McMillan, H., Jackson, B., Clark, M., Kavetski, D. and Woods, R. (2011) 'Rainfall uncertainty in hydrological modelling: An evaluation of multiplicative error models', *Journal of Hydrology*, 400, 83–94.

McSweeney, C.F., Jones, R.G., Lee, R.W. and Rowell, D.P. (2014) 'Selecting CMIP5 GCMs for downscaling over multiple regions', *Climate Dynamics*, 44, 3237–3260.

Mearns, L.O., Giorgi, F., Whetton, P., Pabon, D., Hulme, M. and Lal, M. (2003) *Guidelines for Use of Climate Scenarios Developed from Regional Climate Model Experiments, IPCC-TGICA Report* [Online] Available from: http://www.ipcc-data.org/guidelines/dgm_no1_v1_10-2003.pdf [Accessed 15 December 2014].

Meehl, G.A., Covey, C., Delworth, T., Latif, M., McAvaney, B., Mitchell, J.F.B., Stouffer, R.J. and Taylor, K.E. (2007a) 'THE WCRP CMIP3 Multimodel Dataset: A New Era in Climate Change Research', *Bulletin of the American Meteorological Society*, 88, 1383–1394.

Meehl, G.A., Covey, C., McAvaney, B., Latif, M. and Stouffer, R.J. (2005) 'Overview of the Coupled Model Intercomparison Project', *Bulletin of the American Meteorological Society*, 86, 89–93.

Meehl, G.A., Stocker, T.F., Collins, W.D., Friedlingstein, P., Gaye, A.T., Gregory, J.M., Kitoh, A., Knutti, R., Murphy, J.M., Noda, A., Raper, S.C.B., Watterson, I.G., Weaver, A.J. and Zhao, Z.-C. (2007b) 'Global climate projections', In: Solomon, S., Qin, D., Manning, M., Chen, Z., Marquis, M., Averyt, K.B., Tignor, M. and Miller, H.L. (eds.) *Climate Change 2007: The Physical Science Basis. Contribution of Working Group I to the Fourth Assessment Report of the Intergovernmental Panel on Climate Change*, Cambridge: Cambridge University Press, 747–845.

Mileham, L., Taylor, R., Thompson, J., Todd, M. and Tindimugaya, C. (2008) 'Impact of rainfall distribution on the parameterisation of a soil-moisture balance model of groundwater recharge in equatorial Africa', *Journal of Hydrology*, 359, 46–58.

Millennium Ecosystem Assessment (2005) *Ecosystems and Human Well-being: Wetlands and Water. Synthesis.,* Washington, DC: World Resources Institute.

Minville, M., Brissette, F. and Leconte, R. (2008) 'Uncertainty of the impact of climate change on the hydrology of a nordic watershed', *Journal of Hydrology*, 358, 70–83.

Mitchell, T.D. (2003) 'Pattern scaling: An examination of the accuracy of the technique for describing future climates', *Climatic Change*, 60, 217–242.

Mitchell, T.D. and Jones, P.D. (2005) 'An improved method of constructing a database of monthly climate observations and associated high-resolution grids', *Journal of Climatology*, 25, 693–712.

Moriasi, D.N., Arnold, J.G., Van Liew, M.W., Bingner, R.L., Harmel, R.D. and Veith, T.L. (2007) 'Model evaluation guidelines for systematic quantification of accuracy in watershed simulations', *Transactions of the American Society of Agricultural and Biological Engineers*, 50, 885–900.

Moss, R.H., Edmonds, J.A., Hibbard, K.A., Manning, M.R., Rose, S.K., van Vuuren, D.P., Carter, T.R., Emori, S., Kainuma, M., Kram, T., Meehl, G.A., Mitchell, J.F., Nakicenovic, N., Riahi, K., Smith, S.J., Stouffer, R.J., Thomson, A.M., Weyant, J.P. and Wilbanks, T.J. (2010) 'The next generation of scenarios for climate change research and assessment', *Nature*, 463, 747–756.

MRC (2003) *State of the basin report 2003: Executive Summary,* Phnom Penh: Mekong River Comission.

MRC (2005a) *The MRC Basin Development Plan. Regional Sector Overviews. BDP Library Volume 14 November 2002 Revised September 2005,* Vientiane: Mekong River Commission.

MRC (2005b) *Overview of the Hydrology of the Mekong Basin,* Vientiane: Mekong River Commission.

MRC (2010a) *Intergrated Water Resources Management-based Basin Development Strategy for the Lower Mekong Basin,* Vientiane: Mekong River Commission.

MRC (2010b) *State of the Basin Report: 2010,* Vientiane: Mekong River Commission.

MRC (2011) *Strategic Plan: 2011-2015,* Mekong River Commission.

MRC (2016) *Integrated Water Resources Management-based Basin Development Strategy For the Lower Mekong Basin: 2016–2020,* Phnom Penh and Vientiane: Mekong River Commission.

Mulligan, M. (2004) 'Modelling catchment hydrology', In: Wainwright, J. and Mulligan, M. (eds.) *Environmental Modelling: Finding Simplicity in Complexity*, Chichester: John Wiley & Sons, 107–119.

Mulligan, M. and Wainwright, J. (2004) 'Modelling and Model Building', In: Wainwright, J. and Mulligan, M. (eds.) *Environmental Modelling: Finding Simplicity in Complexity*, Chichester: John Wiley & Sons, 7–73.

Murphy, J.M., Sexton, D.M.H., Jenkins, G.J., Boorman, P.M., Booth, B.B.B., Brown, C.C., Clark, R.T., Collins, M., Harris, G.R., Kendon, E.J., Betts, R.A., Brown, S.J., Howard, T.P., Humphrey, K.A., McCarthy, M.P., McDonald, R.E., Stephens, A., Wallace, C., Warren, R., Wilby, R. and Wood, R.A. (2009) *UK Climate Projections Science Report: Climate change projections,* Exeter: Met Office Hadley Centre.

Muzik, I. (1996) 'Lumped Modeling and GIS in Flood Prediction', In: Singh, V.P. and Fiorentino, M. (eds.) *Geographical Information Systems in Hydrology*, Dordrecht: Kluwer Academic, 269–301.

Myhre, G., Shindell, D., Bréon, F.-M., Collins, W., Fuglestvedt, J., Huang, J., Koch, D., Lamarque, J.-F., Lee, D., Mendoza, B., Nakajima, T., Robock, A., Stephens, G., Takemura, T. and Zhang, H. (2013) 'Anthropogenic and Natural Radiative Forcing', In: Stocker, T.F., Qin, D., Plattner, G.-K., Tignor, M., Allen, S.K., Boschung, J., Nauels, A., Xia, Y., Bex, V. and Midgley, P.M. (eds.) *Climate Change 2013: The Physical Science Basis. Contribution of Working Group I to the Fifth Assessment Report of the Intergovernmental Panel on Climate Change*, Cambridge: Cambridge University Press, 659–740.

Najafi, M.R., Moradkhani, H. and Jung, I.W. (2011) 'Assessing the uncertainties of hydrologic model selection in climate change impact studies', *Hydrological Processes*, 25, 2814–2826.

Nakićenović, N., Alcamo, J., Davis, G., de Vries, B., Fenhann, J., Gaffin, S., Gregory, K., Griibler, A., Jung, T.Y., Kram, T., La Rovere, E.L., Michaelis, L., Mori, S., Morita, T., Pepper, W., Pitcher, H., Price, L., Riahi, K., Roehrl, A., Rogner, H.-H., Sankovski, A., Schlesinger, M., Shukla, P., Smith, S., Swart, R., van Rooijen, S., Victor, N. and Dadi, Z. (2000) *Special Report on Emissions Scenarios, A Special Report of Working Group III of the Intergovernmental Panel on Climate Change*, Cambridge: Cambridge University Press.

Nash, I.E. and Sutcliffe, I.V. (1970) 'River flow forecasting through conceptual models', *Journal of Hydrology*, 10, 282–290.

New, M., Hulme, M. and Jones, P. (1999) 'Representing Twentieth-Century Space–Time Climate Variability. Part I: Development of a 1961–90 Mean Monthly Terrestrial Climatology', *Journal of Climate*, 12, 829–856.

Ngigi, S.N., Savenije, H.H.G. and Gichuki, F.N. (2007) 'Land use changes and hydrological impacts related to up-scaling of rainwater harvesting and management in upper Ewaso Ng'iro river basin, Kenya', *Land Use Policy*, 24, 129–140.

Nijssen, B., O'Donnel, G.M., Hamlet, A.F. and Lettenmaier, D.P. (2001) 'Hydrological sensitivity of global rivers to climate change', *Climatic Change*, 50, 143–175.

Nóbrega, M.T., Collischonn, W., Tucci, C.E.M. and Paz, A.R. (2011) 'Uncertainty in climate change impacts on water resources in the Rio Grande Basin, Brazil', *Hydrology and Earth System Sciences*, 15, 585–595.

Nobuhiro, T., Shimizu, A., Kabeya, N., Tamai, K., Ito, E., Araki, M., Kubota, T., Tsuboyama, Y. and Chann, S. (2008) 'Evapotranspiration during the late rainy season and middle of the dry season in the watershed of an evergreen forest area, central Cambodia', *Hydrological Processes*, 22, 1281–1289.

Norman, D.W. and Dixon, J. (1995) *Sustainable dryland cropping in relation to soil productivity - FAO soils bulletin 72,* Rome: Food and Agriculture Organization of the United Nations.

O'Connell, E., Ewen, J., O'Donnell, G. and Quinn, P. (2007) 'Is there a link between agricultual land-use management and flooding?', *Hydrology and Earth System Sciences*, 11, 96–107.

Olesen, J.E., Carter, T.R., Díaz-Ambrona, C.H., Fronzek, S., Heidmann, T., Hickler, T., Holt, T., Minguez, M.I., Morales, P., Palutikof, J.P., Quemada, M., Ruiz-Ramos, M., Rubæk, G.H., Sau, F., Smith, B. and Sykes, M.T. (2007) 'Uncertainties in projected impacts of climate change on European agriculture and terrestrial ecosystems based on scenarios from regional climate models', *Climatic Change*, 81, 123–143.

Oreskes, N., Shrader-Frechette, K. and Belitz, K. (1994) 'Verification, Validation, and Confirmation of Numerical Models in the Earth Sciences', *Science*, 263, 641-646.

Osborn, T.J. (2009) *A user guide for ClimGen: A flexible tool for generating monthly climate data sets and scenarios,* Norwich: Climatic Research Unit, School of Environmental Sciences, University of East Anglia.

Oudin, L., Hervieu, F., Michel, C., Perrin, C., Andréassian, V., Anctil, F. and Loumagne, C. (2005a) 'Which potential evapotranspiration input for a lumped rainfall–runoff model? Part 2—Towards a simple and efficient potential evapotranspiration model for rainfall–runoff modelling', *Journal of Hydrology*, 303, 290–306.

Oudin, L., Michel, C. and Anctil, F. (2005b) 'Which potential evapotranspiration input for a lumped rainfall-runoff model? Part 1—Can rainfall-runoff models

effectively handle detailed potential evapotranspiration inputs?', *Journal of Hydrology*, 303, 275–289.

Ouyang, Y., Higman, J. and Hatten, J. (2011) 'Estimation of dynamic load of mercury in a river with BASINS-HSPF model', *Journal of Soils and Sediments*, 12, 207–216.

Pappenberger, F. and Beven, K.J. (2006) 'Ignorance is bliss: Or seven reasons not to use uncertainty analysis', *Water Resources Research*, 42, n/a-n/a.

Patil, S.D., Wigington, P.J., Leibowitz, S.G., Sproles, E.A. and Comeleo, R.L. (2014) 'How does spatial variability of climate affect catchment streamflow predictions?', *Journal of Hydrology*, 517, 135-145.

Pech, S. and Sunada, K. (2008) 'Population Growth and Natural-Resources Pressures in the Mekong River Basin', *Ambio*, 37, 219–224.

Penman, H.L. (1948) 'Natural evaporation from open water, bare soil and grass', *Proceedings of the Royal Society A: Mathematical, Physical and Engineering Sciences*, 193, 120–145.

Penny, D. (2008) 'The Mekong at Climatic Crossroads: Lessons from the Geological Past', *AMBIO: A Journal of the Human Environment*, 37, 164–169.

Peterson, T.C. and Vose, R.S. (1997) 'An overview of the Global Historical Climatology Network temperature database', *Bulletin of the American Meteorological Society*, 78, 2837–2849.

Pielke, R.A.S., Wilby, R., Niyogi, D., Hossain, F., Dairuku, K., Adegoke, J., Kallos, G., Seastedt, T. and Suding, K. (2012) 'Dealing With Complexity and Extreme Events Using a Bottom-Up, Resource-Based Vulnerability Perspective', *Extreme events and natural hazards: the complexity perspective. Geophysical Monograph Series*, 196, 345–359.

Piman, T., Lennaerts, T. and Southalack, P. (2013) 'Assessment of hydrological changes in the lower Mekong Basin from Basin-Wide development scenarios', *Hydrological Processes*, 27, 2115–2125.

Postel, S. and Richter, B. (2003) *Rivers for Life: Managing Water for People and Nature*, Island Press.

Poulin, A., Brissette, F., Leconte, R., Arsenault, R. and Malo, J.-S. (2011) 'Uncertainty of hydrological modelling in climate change impact studies in a Canadian, snow-dominated river basin', *Journal of Hydrology*, 409, 626–636.

Praskievicz, S. and Chang, H. (2009) 'A review of hydrological modelling of basin-scale climate change and urban development impacts', *Progress in Physical Geography*, 33, 650–671.

Priestley, C.H.B. and Taylor, R.J. (1972) 'On the assessment of surface heat fluxes and evaporation using large-scale parameters', *Monthly Weather Review*, 100, 81–92.

Prudhomme, C. and Davies, H. (2009a) 'Assessing uncertainties in climate change impact analyses on the river flow regimes in the UK. Part 1: baseline climate', *Climatic Change*, 93, 177–195.

Prudhomme, C. and Davies, H. (2009b) 'Assessing uncertainties in climate change impact analyses on the river flow regimes in the UK. Part 2: future climate', *Climatic Change*, 93, 197–222.

Prudhomme, C., Jakob, D. and Svensson, C. (2003) 'Uncertainty and climate change impact on the flood regime of small UK catchments', *Journal of Hydrology*, 277, 1–23.

Prudhomme, C., Reynard, N. and Crooks, S. (2002) 'Downscaling of global climate models for flood frequency analysis: where are we now?', *Hydrological Processes*, 16, 1137–1150.

Prudhomme, C. and Williamson, J. (2013) 'Derivation of RCM-driven potential evapotranspiration for hydrological climate change impact analysis in Great Britain: a comparison of methods and associated uncertainty in future projections', *Hydrology and Earth System Sciences*, 17, 1365–1377.

Quinton, J.N. (2004) 'Erosion and sediment transport', In: Wainwright, J. and Mulligan, M. (eds.) *Environmental Modelling: Finding Simplicity in Complexity*, Chichester: John Wiley & Sons, 187–196.

Randall, D.A., Wood, R.A., Bony, S., Colman, R., Fichefet, T., Fyfe, J., Kattsov, V., Pitman, A., Shukla, J., Srinivasan, J., Stouffer, R.J., A., S. and Taylor, K.E. (2007) 'Climate models and their evaluation', In: Solomon, S., Qin, D., Manning, M., Chen, Z., Marquis, M., Averyt, K.B., Tignor, M. and Miller, H.L. (eds.) *Climate Change 2007: Impacts, Adaptation and Vulnerability. Contribution of Working Group II to the Fourth Assessment Report of the Intergovernmental Panel on Climate Change*, Cambridge: Cambridge University Press, 589–662.

Ranger, N., Reeder, T. and Lowe, J. (2013) 'Addressing 'deep' uncertainty over long-term climate in major infrastructure projects: four innovations of the Thames Estuary 2100 Project', *EURO Journal on Decision Processes*, 1, 233–262.

Räsänen, T.A., Koponen, J., Lauri, H. and Kummu, M. (2012) 'Downstream Hydrological Impacts of Hydropower Development in the Upper Mekong Basin', *Water Resources Management*, 26, 3495–3513.

Räsänen, T.A., Someth, P., Lauri, H., Koponen, J., Sarkkula, J. and Kummu, M. (2017) 'Observed river discharge changes due to hydropower operations in the Upper Mekong Basin', *Journal of Hydrology*, 545, 28–41.

Refsgaard, J.C. (1996) 'Terminology, Modelling Protocol and Classification of Hydrological Model Codes', In: Abbott, M.B. and Refsgaard, J.C. (eds.) *Distributed Hydrological Modelling*, Dordrecht: Kluwer Academic, 17–39.

Refsgaard, J.C. (1997) 'Parameterisation, calibration and validation of distributed hydrological models', *Journal of Hydrology*, 198, 69–97.

Refsgaard, J.C. (2000) 'Towards a Formal Approach to Calibration and Validation of Models Using Spatial Data', In: Grayson, R. and Blöschl, G. (eds.) *Spatial Patterns in Catchment Hydrology: Observations and Modelling*, Cambridge: Cambridge University Press, 329–354.

Refsgaard, J.C. (2007) *Hydrological Modelling and River Basin Management*, Doctoral Thesis, University of Copenhagen.

Refsgaard, J.C. and Henriksen, H.J. (2004) 'Modelling guidelines––terminology and guiding principles', *Advances in Water Resources*, 27, 71–82.

Refsgaard, J.C. and Storm, B. (1995) 'MIKE SHE', In: Singh, V.P. (ed.) *Computer Models of Watershed Hydrology*, Highlands Ranch, Colorado: Water Resources Publications, 809–846.

Refsgaard, J.C., Storm, B. and Clausen, T. (2010) 'Système Hydrologique Europeén (SHE): review and perspectives after 30 years development in distributed physically-based hydrological modelling', *Hydrology Research*, 41, 355–377.

Refsgaard, J.C., Storm, B. and Refsgaard, A. (1995) 'Recent developments of the Système Hydrologique Européen (SHE) towards the MIKE SHE', In: *Modelling and Management of Sustainable Basin-scale Water Resource Systems Symposium Proceedings*, *July 1995*, *Boulder*, 427–434, IAHS Publ. no. 231.

Refsgaard, J.C., van der Sluijs, J.P., Brown, J. and van der Keur, P. (2006) 'A framework for dealing with uncertainty due to model structure error', *Advances in Water Resources*, 29, 1586–1597.

Remesan, R. and Holman, I.P. (2015) 'Effect of baseline meteorological data selection on hydrological modelling of climate change scenarios', *Journal of Hydrology*, 528, 631–642.

Richter, B.D., Baumgartner, J.V., Wigington, R. and Braun, D.P. (1997) 'How much water does a river need?', *Freshwater Biology*, 37, 231–249.

Ringler, C., von Braun, J. and Rosegrant, M.W. (2004) 'Water Policy Analysis for the Mekong River Basin', *Water International*, 29, 30–42.

Robinson, M. (1998) '30 years of forest hydrology changes at Coalburn: water balance and extreme flows', *Hydrology and Earth System Sciences*, 2, 233–238.

Rochester, R.E.L. (2010) *Uncertainty in Hydrological Modelling: A Case Study in the Tern Catchment, Shropshire, UK*, PhD Thesis, University College London, London.

Rodda, J.C. (1967) 'The rainfall measurement problem', In: *Proceedings of the IASH General Assembly*, *Bern*: IASH, 215–231.

Roe, G., H. (2005) 'Orographic precipitation', *Annual Review of Earth and Planetary Sciences*, 33, 645–671.

Rundel, P.W. (2009) 'Vegetation in the Mekong Basin', In: Campbell, I. (ed.) *The Mekong: Biophysical Environment of an International River Basin*, New York: Elsevier, 53–76.

Running, S.W., Nemani, R.R., Peterson, D.L., Band, L.E., Potts, D.F., Pierce, L.L. and Spanner, M.A. (1989) 'Mapping regional forest evapotranspiration and photosynthesis by coupling satellite data with ecosystem simulation', *Ecology*, 70, 1090–1101.

Rust, W., Corstanje, R., Holman, I.P. and Milne, A.E. (2014) 'Detecting land use and land management influences on catchment hydrology by modelling and wavelets', *Journal of Hydrology*, 517, 378–389.

Sahoo, G.B., Ray, C. and De Carlo, E.H. (2006) 'Calibration and validation of a physically distributed hydrological model, MIKE SHE, to predict streamflow at high frequency in a flashy mountainous Hawaii stream', *Journal of Hydrology*, 327, 94–109.

Samani, Z. (2000) 'Estimating Solar Radiation and Evapotranspiration Using Minimum Climatological Data', *Journal of Irrigation and Drainage Engineering*, 126, 265–267.

Saraswat, D. and Pai, N. (2011) 'Spatially distributed hydrological modelling in the Illinois River drainage area, Arkansas, using SWAT', In: Shukla, M.K. (ed.) *Soil Hydrology, Land Use and Agriculture: Measurement and Modelling*, Wallingford: CAB International, 196–210.

Sarkkula, J., Keskinen, M., Koponen, J., Kummu, M., Richey, J.E. and Varis, O. (2009) 'Hydropower in the Mekong Region: What Are the Likely Impacts upon Fisheries?', In: Molle, F., Foran, T. and Käkönen, M. (eds.) *Contested waterscapes in the Mekong Region: Hydropower, Livelihoods and Governance*, London: Earthscan, 227–252.

Savoskul, O.S. and Smakhtin, V. (2013a) *Glacier Systems and Seasonal Snow Cover in Six Major Asian River Basins: Hydrological Role under Changing Climate. IWMI Research Report 150,* Colombo, Sri Lanka: International Water Management Institute (IWMI).

Savoskul, O.S. and Smakhtin, V. (2013b) *Glacier Systems and Seasonal Snow Cover in Six Major Asian River Basins: Water Storage Properties under Changing Climate. IWMI Research Report 149,* Colombo, Sri Lanka: International Water Management Institute (IWMI).

Schneider, S.H. (1983) 'CO_2, Climate and Society: A Brief Overview', In: Chen, R., Boulding, E. and Schneider, S. (eds.) *Social Science Research and Climate Change: An Interdisciplinary Appraisal*, Dordrecht: D. Reidel, 9–15.

Schulze, R. (1989) *ACRU: Background, Concepts and Theory. Report 35,* Pietermaritzburg, South Africa: Agricultural Catchments Research Unit, Department of Agricultural Engineering, University of Natal.

Schuol, J. and Abbaspour, K.C. (2006) 'Calibration and uncertainty issues of a hydrological model (SWAT) applied to West Africa', *Advances in Geosciences*, 9, 137–143.

Sevruk, B. (1996) 'Adjustment of tipping-bucket precipitation gauge measurements', *Atmospheric Research*, 42, 237–246.

Sevruk, B., Ondrás, M. and Chvíla, B. (2009) 'The WMO precipitation measurement intercomparisons', *Atmospheric Research*, 92, 376–380.

Shaw, S.B. and Riha, S.J. (2011) 'Assessing temperature-based PET equations under a changing climate in temperate, deciduous forests', *Hydrological Processes*, 25, 1466–1478.

Shin, M.-J., Eum, H.-I., Kim, C.-S. and Jung, I.-W. (2016) 'Alteration of hydrologic indicators for Korean catchments under CMIP5 climate projections', *Hydrological Processes*, 30, 4517–4542.

Shopea, N. (2003) *Station Profiles of Water Quality Monitoring Network in Cambodia: MRC Water Quality Monitoring Station Network Review,* Phnom Penh: Mekong River Commission.

Shuttleworth, W.J. (1993) 'Evaporation', In: Maidment, D.R. (ed.) *Handbook of Hydrology*, New York: McGraw-Hill, 4.1–4.53.

Shuttleworth, W.J. (2007) 'Putting the 'vap' into evaporation', *Hydrology and Earth System Sciences*, 11, 201–244.

Siebert, S., Döll, P. and Hoogeveen, J. (2002) *Global Map of Irrigated Areas Version 2.1.,* Center for Environmental Systems Research, University of Kassel, Germany /Food and Agriculture Organization of the United Nations, Rome, Italy.

Silberstein, R.P. (2006) 'Hydrological models are so good, do we still need data?', *Environmental Modelling & Software*, 21, 1340–1352.

Sillmann, J., Kharin, V.V., Zhang, X., Zwiers, F.W. and Bronaugh, D. (2013) 'Climate extremes indices in the CMIP5 multimodel ensemble: Part 1. Model evaluation in the present climate', *Journal of Geophysical Research: Atmospheres*, 118, 1716–1733.

Singh, C.R., Thompson, J.R., French, J.R., Kingston, D.G. and Mackay, A.W. (2010) 'Modelling the impact of prescribed global warming on runoff from headwater catchments of the Irrawaddy River and their implications for the water level regime of Loktak Lake, northeast India', *Hydrology and Earth System Sciences*, 14, 1745–1765.

Singh, C.R., Thompson, J.R., Kingston, D.G. and French, J.R. (2011) 'Modelling water-level options for ecosystem services and assessment of climate change: Loktak Lake, northeast India', *Hydrological Sciences Journal*, 56, 1518–1542.

Singh, V.P. and Frevert, D.K. (2002) 'Mathematical modeling of watershed hydrology', In: Singh, V.P. and Frevert, D.K. (eds.) *Mathematical Models of*

Large Watershed Hydrology, Highlands Ranch, Colorado: Water Resources Publications.

Singh, V.P. and Woolhiser, D.A. (2002) 'Mathematical modeling of watershed hydrology', *Journal of Hydrologic Engineering*, 7, 270 – 292.

Smerdon, B.D., Allen, D.M., Grasby, S.E. and Berg, M.A. (2009) 'An approach for predicting groundwater recharge in mountainous watersheds', *Journal of Hydrology*, 365, 156–172.

Sokhem, P. and Sunada, K. (2006) 'The Governance of the Tonle Sap Lake, Cambodia: Integration of Local, National and International Levels', *International Journal of Water Resources Development*, 22, 399–416.

Sperna Weiland, F.C., Tisseuil, C., Dürr, H.H., Vrac, M. and van Beek, L.P.H. (2012) 'Selecting the optimal method to calculate daily global reference potential evaporation from CFSR reanalysis data for application in a hydrological model study', *Hydrology and Earth System Sciences*, 16, 983–1000.

Stakhiv, E.Z. (1997) 'Policy implications of climate change impacts on water resources management', *Water Policy*, 1, 159–175.

Stibig, H.J., Achard, F., Carboni, S., Raši, R. and Miettinen, J. (2014) 'Change in tropical forest cover of Southeast Asia from 1990 to 2010', *Biogeosciences*, 11, 247–258.

Stisen, S., Jensen, K.H., Sandholt, I. and Grimes, D.I.F. (2008) 'A remote sensing driven distributed hydrological model of the Senegal River basin', *Journal of Hydrology*, 354, 131–148.

Stisen, S. and Sandholt, I. (2010) 'Evaluation of remote-sensing-based rainfall products through predictive capability in hydrological runoff modelling', *Hydrological Processes*, 24, 879–891.

Stocker, T.F., Qin, D., Plattner, G.-K., Alexander, L.V., Allen, S.K., Bindoff, N.L., Bréon, F.-M., Church, J.A., Cubasch, U., Emori, S., Forster, P., Friedlingstein, P., Gillett, N., Gregory, J.M., Hartmann, D.L., Jansen, E., Kirtman, B., Knutti, R., Krishna Kumar, K., Lemke, P., Marotzke, J., Masson-Delmotte, V., Meehl, G.A., Mokhov, I.I., Piao, S., Ramaswamy, V., Randall, D., Rhein, M., Rojas, M., Sabine, C., Shindell, D., Talley, L.D., Vaughan, D.G. and Xie, S.-P. (2013) 'Technical Summary', In: Stocker, T.F., Qin, D., Plattner, G.-K., Tignor, M., Allen, S.K., Boschung, J., Nauels, A., Xia, Y., Bex, V. and Midgley, P.M. (eds.) *Climate Change 2013: The Physical Science Basis. Contribution of Working Group I to the Fifth Assessment Report of the Intergovernmental Panel on Climate Change*, Cambridge: Cambridge University Press, 33–116.

Storm, B. and Refsgaard, A. (1996) 'Distributed physically‐based modelling of the entire land phase of the hydrological cycle', In: Abbott, M.B. and Refsgaard, J.C. (eds.) *Distributed Hydrological Modelling*, Dordrecht: Kluwer Academic, 55–69.

Su, F., Duan, X., Chen, D., Hao, Z. and Cuo, L. (2013) 'Evaluation of the Global Climate Models in the CMIP5 over the Tibetan Plateau', *Journal of Climate*, 26, 3187–3208.

Su, F., Hong, Y. and Lettenmaier, D.P. (2008) 'Evaluation of TRMM Multisatellite Precipitation Analysis (TMPA) and its utility in hydrologic prediction in the La Plata basin', *Journal of Hydrometeorology*, 9, 622–640.

Su, M., Stolte, W.J. and van der Kamp, G. (2000) 'Modelling Canadian prairie wetland hydrology using a semi-distributed streamflow model', *Hydrological Processes*, 2405–2422.

Sugawara, M. (1995) 'Tank model', In: Singh, V.P. (ed.) *Computer Models of Watershed Hydrology*, Highlands Ranch, Colorado: Water Resources Publications, 165–214.

Sultana, Z. and Coulibaly, P. (2011) 'Distributed modelling of future changes in hydrological processes of Spencer Creek watershed', *Hydrological Processes*, 25, 1254–1270.

Taylor, K.E., Stouffer, R.J. and Meehl, G.A. (2012) 'An Overview of CMIP5 and the Experiment Design', *Bulletin of the American Meteorological Society*, 93, 485–498.

Tebaldi, C. and Knutti, R. (2007) 'The use of the multi-model ensemble in probabilistic climate projections', *Philosophical Transactions A Mathematical Physical and Engineering Sciences*, 365, 2053-2075.

Teutschbein, C. and Seibert, J. (2012) 'Bias correction of regional climate model simulations for hydrological climate-change impact studies: Review and evaluation of different methods', *Journal of Hydrology*, 456–457, 12–29.

Thanapakpawin, P., Richey, J., Thomas, D., Rodda, S., Campbell, B. and Logsdon, M. (2007) 'Effects of landuse change on the hydrologic regime of the Mae Chaem river basin, NW Thailand', *Journal of Hydrology*, 334, 215–230.

Thompson, J.R. (2004) 'Simulation of Wetland Water-Level Manipulation Using Coupled Hydrological/Hydraulic Modeling', *Physical Geography*, 25, 39–67.

Thompson, J.R. (2012) 'Modelling the impacts of climate change on upland catchments in southwest Scotland using MIKE SHE and the UKCP09 probabilistic projections', *Hydrology Research*, 43, 507–530.

Thompson, J.R., Crawley, A. and Kingston, D.G. (2016) 'GCM-related uncertainty for river flows and inundation under climate change: the Inner Niger Delta', *Hydrological Sciences Journal*, 61, 2325–2347.

Thompson, J.R., Crawley, A. and Kingston, D.G. (2017) 'Future river flows and flood extent in the Upper Niger and Inner Niger Delta: GCM-related uncertainty using the CMIP5 ensemble', *Hydrological Sciences Journal*, 62, 2239–2265.

Thompson, J.R., Gavin, H., Refsgaard, A., Refstrup Sørenson, H. and Gowing, D.J. (2009) 'Modelling the hydrological impacts of climate change on UK lowland wet grassland', *Wetlands Ecology and Management*, 17, 503–523.

Thompson, J.R., Green, A.J. and Kingston, D.G. (2014a) 'Potential evapotranspiration-related uncertainty in climate change impacts on river flow: An assessment for the Mekong River basin', *Journal of Hydrology*, 510, 259–279.

Thompson, J.R., Green, A.J., Kingston, D.G. and Gosling, S.N. (2013) 'Assessment of uncertainty in river flow projections for the Mekong River using multiple GCMs and hydrological models', *Journal of Hydrology*, 486, 1–30.

Thompson, J.R. and Hollis, G.E. (1995) 'Hydrological modelling and the sustainable development of the Hadejia-Nguru Wetlands, Nigeria', *Hydrological Sciences*, 40, 97–116.

Thompson, J.R., Laizé, C.L.R., Green, A.J., Acreman, M.C. and Kingston, D.G. (2014b) 'Climate change uncertainty in environmental flows for the Mekong River', *Hydrological Sciences Journal*, 59, 935–954.

Thompson, J.R., Refstrup Sørenson, H., Gavin, H. and Refsgaard, A. (2004) 'Application of the coupled MIKE SHE/MIKE 11 modelling system to a lowland wet grassland in southeast England', *Journal of Hydrology*, 293, 151–179.

Thorne, R. (2011) 'Uncertainty in the impacts of projected climate change on the hydrology of a subarctic environment: Liard River Basin', *Hydrology and Earth System Sciences*, 15, 1483–1492.

Thrasher, B., Xiong, J., Wang, W., Melton, F., Michaelis, A. and Nemani, R. (2013) 'Downscaled climate projections suitable for resource management', *Eos, Transactions, American Geophysical Union*, 94, 321–323.

Todd, M.C., Taylor, R.G., Osborn, T.J., Kingston, D.G., Arnell, N.W. and Gosling, S.N. (2011) 'Uncertainty in climate change impacts on basin-scale freshwater resources – preface to the special issue: the QUEST-GSI methodology and synthesis of results', *Hydrology and Earth System Sciences*, 15, 1035–1046.

Ty, T.V., Sunada, K., Ichikawa, Y. and Oishi, S. (2012) 'Scenario-based Impact Assessment of Land Use/Cover and Climate Changes on Water Resources and Demand: A Case Study in the Srepok River Basin, Vietnam—Cambodia', *Water Resources Management*, 26, 1387–1407.

UNEP (2006) *Snidvongs, A. and Teng, S-K. Mekong River, GIWA Regional Assessment 55,* Kalmar, Sweden: University of Kalmar.

UNEP (2010) *Blue harvest: Inland Fisheries as an Ecosystem Service,* Penang, Malaysia: WorldFish Center.

University of Washington (2009) *Virtual Mekong Basin. Geology of the Mekong Basin.* [Online] Available from: http://vmb.ocean.washington.edu/story/Geology+of+the+Mekong+Basin.

USGS (1996) *Global 30 Arc-Second Elevation (GTOPO30)* [Online] Available from: https://lta.cr.usgs.gov/GTOPO30 [Accessed 16 January 2014].

USGS (1997) *Global Land Cover Characterization Version 1.2* [Online] Available from: http://edc2.usgs.gov/glcc/glcc_version1.php - Global [Accessed 20 January 2014].

van der Linden, S. and Woo, M.-k. (2003a) 'Application of hydrological models with increasing complexity to subarctic catchments', *Journal of Hydrology*, 270, 145–157.

van der Linden, S. and Woo, M.-k. (2003b) 'Transferability of hydrological model parameters between basins in data-sparse areas, subarctic Canada', *Journal of Hydrology*, 270, 182–194.

van Vuuren, D.P., Edmonds, J., Kainuma, M., Riahi, K., Thomson, A., Hibbard, K., Hurtt, G.C., Kram, T., Krey, V., Lamarque, J.-F., Masui, T., Meinshausen, M., Nakicenovic, N., Smith, S.J. and Rose, S.K. (2011) 'The representative concentration pathways: an overview', *Climatic Change*, 109, 5–31.

Vansteenkiste, T., Tavakoli, M., Ntegeka, V., De Smedt, F., Batelaan, O., Pereira, F. and Willems, P. (2014) 'Intercomparison of hydrological model structures and calibration approaches in climate scenario impact projections', *Journal of Hydrology*, 519, 743–755.

Västilä, K., Kummu, M., Sangmanee, C. and Chinvanno, S. (2010) 'Modelling climate change impacts on the flood pulse in the Lower Mekong floodplains', *Journal of Water and Climate Change*, 1, 67–86.

Vaze, J., Post, D.A., Chiew, F.H.S., Perraud, J.-M., Teng, J. and Viney, N.R. (2011) 'Conceptual Rainfall–Runoff Model Performance with Different Spatial Rainfall Inputs', *Journal of Hydrometeorology*, 12, 1100–1112.

Vaze, J. and Teng, J. (2007) 'Impact of DEM resolution on topographic indices and hydrological modelling results', In: Oxley, L. and Kulasiri, D. (eds.) *MODSIM 2007 International Congress on Modelling and Simulation. Modelling and Simulation Society of Australia and New Zealand*, *December 2007*, 74–80.

Vázquez, R.F. and Feyen, J. (2003) 'Effect of potential evapotranspiration estimates on effective parameters and performance of the MIKE SHE-code applied to a medium-size catchment', *Journal of Hydrology*, 270, 309–327.

Vázquez, R.F. and Feyen, J. (2007) 'Assessment of the effects of DEM gridding on the predictions of basin runoff using MIKE SHE and a modelling resolution of 600m', *Journal of Hydrology*, 334, 73–87.

Vázquez, R.F., Feyen, L., Feyen, J. and Refsgaard, J.C. (2002) 'Effect of grid size on effective parameters and model performance of the MIKE-SHE code', *Hydrological Processes*, 16, 355–372.

Velázquez, J.A., Schmid, J., Ricard, S., Muerth, M.J., Gauvin St-Denis, B., Minville, M., Chaumont, D., Caya, D., Ludwig, R. and Turcotte, R. (2013) 'An ensemble approach to assess hydrological models' contribution to uncertainties in the

analysis of climate change impact on water resources', *Hydrology and Earth System Sciences*, 17, 565–578.

Verma, S.C. (1982) 'Modified Horton's infiltration equation', *Journal of Hydrology*, 58, 383–388.

Vieux, B.E. (2004) *Distributed Hydrologic Modeling Using GIS*, Dordrecht: Kluwer Academic.

Villarini, G., Mandapaka, P.V., Krajewski, W.F. and Moore, R.J. (2008) 'Rainfall and sampling uncertainties: A rain gauge perspective', *Journal of Geophysical Research*, 113, D11102.

von Storch, H., Hewitson, B. and Mearns, L. (2000) 'Empirical Downscaling Techniques', In: Iversen, T. and Høiskar, B.A.K. (eds.) *Regional climate development under global warming. General Technical Report No. 4. Conf. Proceedings RegClim Spring Meeting*, *8–9 May*, *Jevnaker, Torbjørnrud, Norway*, 29–46.

Vörösmarty, C.J., Federer, C.A. and Schloss, A.L. (1998) 'Potential evaporation functions compared on US watersheds: Possible implications for global-scale water balance and terrestrial ecosystem modeling', *Journal of Hydrology*, 207, 147–169.

Vose, R.S., Schmoyer, R.L., Steurer, P.M., Peterson, T.C., Heim, R., Karl, T.R. and Eischeid, J. (1992) *The Global Historical Climatology Network: Long-term monthly temperature, precipitation, sea level pressure, and station pressure data. Environmental Sciences Division Publication No. 3912. ORNL/CDIAC-53,* Oak Ridge: Oak Ridge National Laboratory.

Wagener, T., Boyle, D.P., Lees, M.J., Wheater, H.S., Gupta, H.V. and Sorooshian, S. (2001) 'A framework for development and application of hydrological models', *Hydrology and Earth System Sciences*, 5, 13–26.

Wagener, T., McIntyre, N., Lees, M.J., Wheater, H.S. and Gupta, H.V. (2003) 'Towards reduced uncertainty in conceptual rainfall-runoff modelling: Dynamic identifiability analysis', *Hydrological Processes*, 17, 455–476.

Wang, J.J., Lu, X.X. and Kummu, M. (2011) 'Sediment load estimates and variations in the Lower Mekong River', *River Research and Applications*, 27, 33–46.

Ward, R.C. and Robinson, M. (2000) *Principles of Hydrology*, London: McGraw‐Hill.

Weigel, A.P., Knutti, R., Liniger, M.A. and Appenzeller, C. (2010) 'Risks of Model Weighting in Multimodel Climate Projections', *Journal of Climate*, 23, 4175–4191.

Wijesekara, G.N., Farjad, B., Gupta, A., Qiao, Y., Delaney, P. and Marceau, D.J. (2014) 'A comprehensive land-use/hydrological modeling system for scenario simulations in the Elbow River watershed, Alberta, Canada', *Environmental management*, 53, 357–381.

Wijesekara, G.N., Gupta, A., Valeo, C., Hasbani, J.G., Qiao, Y., Delaney, P. and Marceau, D.J. (2012) 'Assessing the impact of future land-use changes on hydrological processes in the Elbow River watershed in southern Alberta, Canada', *Journal of Hydrology*, 412-413, 220–232.

Wilby, R.L., Charles, S.P., Zorita, E., Timbal, B., Whetton, P. and Mearns, L.O. (2004) *Guidelines for Use of Climate Scenarios Developed from Statistical Downscaling Methods, IPCC-TGICA Report* [Online] Available from: http://www.ipcc-data.org/guidelines/dgm_no2_v1_09_2004.pdf [Accessed 15 December 2014].

Wilby, R.L. and Dessai, S. (2010) 'Robust adaptation to climate change', *Weather*, 65, 180–185.

Wilby, R.L. and Harris, I. (2006) 'A framework for assessing uncertainties in climate change impacts: Low-flow scenarios for the River Thames, UK', *Water Resources Research*, 42, W02419.

Wilk, J., Andersson, L. and Plermkamon, V. (2001) 'Hydrological impacts of forest conversion to agriculture in a large river basin in northeast Thailand', *Hydrological Processes*, 15, 2729–2748.

Willmott, C.J. and Matsuura, K. (2000) *Terrestrial Air Temperature and Precipitation: Monthly and Annual Time Series (1950 - 1996) Version 1.01* [Online] Available from: http://climate.geog.udel.edu/~climate/html_pages/README.ghcn_ts.html [Accessed 27 January 2013].

Winchell, M., Gupta, H.V. and Sorooshian, S. (1998) 'On the simulation of infiltration- and saturation-excess runoff using radar-based rainfall estimates: Effects of algorithm uncertainty and pixel aggregation', *Water Resources Research*, 34, 2655–2670.

WMO (2008) *Guide to Hydrological Practices. Volume I: Hydrology – From Measurement to Hydrological Information. Sixth edition. WMO-No. 168,* Geneva.

Xu, C.-y., Widén, E. and Halldin, S. (2005) 'Modelling Hydrological Consequences of Climate Change—Progress and Challenges', *Advances in Atmospheric Sciences*, 22, 789–797.

Xu, H., Taylor, R.G., Kingston, D.G., Jiang, T., Thompson, J.R. and Todd, M.C. (2010) 'Hydrological modeling of River Xiangxi using SWAT2005: A comparison of model parameterizations using station and gridded meteorological observations', *Quaternary International*, 226, 54–59.

Xu, H., Taylor, R.G. and Xu, Y. (2011) 'Quantifying uncertainty in the impacts of climate change on river discharge in sub-catchments of the Yangtze and Yellow River Basins, China', *Hydrology and Earth System Sciences*, 15, 333–344.

Xue, X., Hong, Y., Limaye, A.S., Gourley, J.J., Huffman, G.J., Khan, S.I., Dorji, C. and Chen, S. (2013) 'Statistical and hydrological evaluation of TRMM-based Multi-

satellite Precipitation Analysis over the Wangchu Basin of Bhutan: Are the latest satellite precipitation products 3B42V7 ready for use in ungauged basins?', *Journal of Hydrology*, 499, 91–99.

Yan, J. and Smith, K.R. (1994) 'Simulation of integrated surface water and ground water systems – model formulation', *Water Resources Bulletin*, 30, 879–890.

Yatagai, A., Kamiguchi, K., Arakawa, O., Hamada, A., Yasutomi, N. and Kitoh, A. (2012) 'APHRODITE: Constructing a Long-Term Daily Gridded Precipitation Dataset for Asia Based on a Dense Network of Rain Gauges', *Bulletin of the American Meteorological Society*, 93, 1401–1415.

Young, C.P., Chotai, A. and Beven, K.J. (2004) 'Data-Based Mechanistic Modelling and the Simplification of Environmental Systems', In: Wainwright, J. and Mulligan, M. (eds.) *Environmental Modelling: Finding Simplicity in Complexity*, Chichester: John Wiley & Sons, 371–388.

Yu, M., Chen, X., Li, L., Bao, A. and Paix, M.J.d.l. (2011) 'Streamflow Simulation by SWAT Using Different Precipitation Sources in Large Arid Basins with Scarce Raingauges', *Water Resources Management*, 25, 2669–2681.

Zeng, X., Kundzewicz, Z.W., Zhou, J. and Su, B. (2012) 'Discharge projection in the Yangtze River basin under different emission scenarios based on the artificial neural networks', *Quaternary International*, 282, 113–121.

Zhao, F.F., Zhang, L., Chiew, F.H.S. and Vaze, J. (2011) 'The effect of spatial rainfall variability on streamflow prediction for a south-eastern Australian catchment', In: *19th International Congress on Modelling and Simulation*, *12–16 December 2011*, *Perth, Australia*, 3684–3690.

Zhou, M.C., Ishidaira, H., Hapuarachchi, H.P., Magome, J., Kiem, A.S. and Takeuchi, K. (2006) 'Estimating potential evapotranspiration using Shuttleworth–Wallace model and NOAA-AVHRR NDVI data to feed a distributed hydrological model over the Mekong River basin', *Journal of Hydrology*, 327, 151–173.

Zierl, B. and Bugmann, H. (2005) 'Global change impacts on hydrological processes in Alpine catchments', *Water Resources Research*, 41, W02028.

Ziv, G., Baran, E., Nam, S., Rodríguez-Iturbe, I. and Levin, S.A. (2012) 'Trading-off fish biodiversity, food security, and hydropower in the Mekong River Basin', *PNAS*, 109, 5609–5614.

List of copyright permissions for figures/tables

Figure 2.10. Republished with permission of Taylor and Francis Group LLC Books from Graham and Butts (2005); permission conveyed through Copyright Clearance Center, Inc.

Figure 2.11. Republished with permission of Taylor and Francis Group LLC Books from Graham and Butts (2005); permission conveyed through Copyright Clearance Center, Inc.

Figure 2.13. Republished with permission of John Wiley and Sons from Gosling and Arnell (2011).

Figure 2.14. Reprinted from Vázquez and Feyen (2003), with permission from Elsevier.

Figure 2.15. Reproduced with permission of John Wiley and Sons from Kingston *et al.* (2009).

Figure 2.16. Reprinted from Kay and Davies (2008), with permission from Elsevier.

Figure 2.17. Reprinted from Kay and Davies (2008), with permission from Elsevier.

Table 3.4. Reprinted from Adamson and Bird (2010), with permission from Taylor and Francis.

Figure 3.8. Reprinted from Immerzeel *et al.* (2009), with permission from Elsevier.

Figure 3.22. Reproduced with permission of John Wiley and Sons from Bernard and De Koninck (1996).

Figure 3.24. Reproduced with permission of John Wiley and Sons from Lacombe *et al.* (2010).

Figure 3.26. Reprinted from Räsänen *et al.* (2017), with permission from Elsevier.